



**HAL**  
open science

# 4D seismic data analysis and processing for underground monitoring: time-lapse, continuous-time and real-time

Julien Cotton

## ► To cite this version:

Julien Cotton. 4D seismic data analysis and processing for underground monitoring: time-lapse, continuous-time and real-time. Environmental Engineering. Université Paris sciences et lettres, 2019. English. NNT : 2019PSLEM023 . tel-02466422

**HAL Id: tel-02466422**

**<https://pastel.hal.science/tel-02466422>**

Submitted on 4 Feb 2020

**HAL** is a multi-disciplinary open access archive for the deposit and dissemination of scientific research documents, whether they are published or not. The documents may come from teaching and research institutions in France or abroad, or from public or private research centers.

L'archive ouverte pluridisciplinaire **HAL**, est destinée au dépôt et à la diffusion de documents scientifiques de niveau recherche, publiés ou non, émanant des établissements d'enseignement et de recherche français ou étrangers, des laboratoires publics ou privés.



**THÈSE DE DOCTORAT**  
**DE L'UNIVERSITÉ PSL**

Préparée à MINES ParisTech

**4D seismic data analysis and processing for underground  
monitoring: time-lapse, continuous-time and real-time**

**Analyse et traitement de données sismiques pour la surveillance  
du sous-sol**

Soutenue par

**Julien COTTON**

Le 19 Juin 2019

Ecole doctorale n° 398

**GRNE - Géosciences  
Ressources Naturelles et  
Environnement**

Spécialité

**Géosciences et géoingénierie**

Composition du jury :

Donatienne, LEPAROUX Directrice de recherche, IFSTTAR	<i>Présidente</i>
Michel, DIETRICH Directeur de recherche, CNRS ISTerre	<i>Rapporteur</i>
Adnand, BITRI Docteur, ingénieur de recherche, BRGM	<i>Examineur</i>
Eric, FORGUES Docteur, ingénieur de recherche, CGG	<i>Examineur</i>
Michel, DABAS HDR, chargé de recherche, ENS CNRS	<i>Examineur</i>
Hervé, CHAURIS Professeur, MINES ParisTech	<i>Directeur de thèse</i>
Jean-Luc, MARI Expert, IFPEN	<i>Invité</i>



# Préambule

L'exploration sismique consiste à provoquer des secousses dans le sol à l'aide de sources impulsives (air gun, explosif, chute de poids) ou vibratoires (camions vibreurs) et à enregistrer à l'aide de capteurs (hydrophones, géophones, accéléromètres, fibres optiques) l'ensemble du champ d'ondes (en particulier les ondes réfléchies ou réfractées sur les couches géologiques). L'exploration sismique est fréquemment surnommé l'échographie du sous-sol. Le traitement des enregistrements consiste à augmenter le rapport signal sur bruit et à mettre en forme l'information pour créer une image du sous-sol. De cette façon, on accède à l'identification et à la caractérisation des couches géologiques situées à différentes profondeurs. En sismique réflexion, la profondeur de pénétration dans le sol ( $z$ ) peut atteindre une dizaine de kilomètres. Les acquisitions sismiques récentes mettent en jeu des milliers de capteurs et de sources (Pecholcs et al. 2010; Meunier et al. 2008) qui sont déployés sur plusieurs milliers de kilomètres carrés, sur terre et en mer. Ces opérations nécessitent des efforts logistiques importants pour organiser des camps de base (souvent isolés en plein cœur des déserts) mais aussi pour acheminer les équipements (câbles, laboratoire d'enregistrement, éléments mécaniques, éléments informatiques) ou encore positionner rigoureusement sources et capteurs et bien sûr synchroniser les enregistrements sismiques. Les acquisitions récentes produisent communément plusieurs millions d'enregistrements générant des *centaines de téraoctets de données par mission*. Lorsque les sources et les capteurs sont déployés sur une seule ligne ( $x$ ) à la surface du sol (ou de l'océan), on parle d'une image 2D ( $x,z$ ). Par extension, on parle d'une image 3D lorsque les sources et les capteurs sont déployés sur une surface ( $x,y$ ). L'imagerie 3D ( $x,y,z$ ) permet naturellement de caractériser plus précisément les structures géologiques et leurs extensions à condition d'avoir une bonne couverture, ce qui représente une information importante pour l'exploration pétrolière.

Les réservoirs de pétrole et de gaz conventionnels s'exploitent sur plusieurs décennies. Ils sont d'abord exploités en récupération primaire par simple déplétion et, en fonction du type de gisement, on n'atteint des taux de récupérations de l'ordre de 5 à 25%. Quand, à mesure de son exploitation par déplétion, la pression du réservoir chute, des méthodes de récupérations dites secondaires sont mises en œuvre pour augmenter le taux de récupération. Cela consiste à ré-augmenter la pression du gisement en y injectant de l'eau et/ou du gaz comme le dioxyde de carbone par exemple. Le taux de récupération

total peut alors monter jusqu'à environ 45%. Au final, même dans les meilleurs réservoirs, plus de la moitié du pétrole reste ainsi prisonnier du sous-sol. Pour caractériser l'évolution de ces réservoirs au cours du temps (t), on utilise *la surveillance sismique 4D* (x,y,z,t) qui consiste à répéter une acquisition 3D sur un même champ pétrolier (Lumley, 2001; Johnston, 2013). On parle généralement de sismique 4D conventionnelle lorsque l'on répète l'acquisition tous les 2 à 5 ans voire plus lorsque les réservoirs évoluent lentement au cours de leur production. En sismique 4D conventionnelle, le principal challenge consiste à acquérir les données sismiques successives dans des conditions identiques afin que les différences observées sur les images soient effectivement liées à l'évolution du réservoir et non pas *aux erreurs de répétition des acquisitions*. En pratique, les conditions d'acquisitions ne sont jamais strictement identiques. Les variations de mesures d'une acquisition à l'autre représentent de grandes difficultés pour l'analyse de ces données (Calvert, 2005).

Les réservoirs non conventionnels demandent des efforts de production particuliers pour extraire les hydrocarbures. Ces réservoirs d'huiles lourdes, moins fluides, ne peuvent pas être produits uniquement en utilisant des pompes classiques telles que celles largement utilisées au Moyen Orient par exemple. Pour exploiter les huiles lourdes, les compagnies pétrolières ont recours à *l'injection de vapeur*. La vapeur injectée dans le réservoir réchauffe l'huile lourde et augmente ainsi sa fluidité, facilitant finalement la production. La génération de vapeur et son injection dans le réservoir représentent une source de coûts significative et nécessitent une attention particulière afin d'éviter des fuites vers la surface ou des connections entre puits injecteurs et puits producteurs. Dans ce contexte de production, le réservoir et les fluides injectés dans les couches géologiques peuvent évoluer rapidement. Il est donc souhaitable de surveiller les effets de la production de manière *beaucoup plus fréquente* qu'en sismique 4D conventionnelle : on parle d'une acquisition par jour voire même d'une acquisition toutes les 6 heures. Il s'agit alors de sismique 4D continue. Celle-ci utilise des sources et des capteurs spécifiquement conçus pour être enterrés de façon permanente (Meunier et al., 2001; Forgues et al., 2011; Hornman et al., 2012). Par rapport à la sismique 4D conventionnelle, un effort supplémentaire est mis en œuvre pour que les conditions d'acquisition soient identiques : il n'y a pas de différences dans la géométrie d'acquisition, les effets météorologiques sont négligeables et le couplage, la signature des sources, la sensibilité des capteurs sont constants. Grâce à une excellente *répétabilité* (Schisselé et al., 2009), *la sismique 4D continue* est utilisée pour

caractériser *des variations rapides et de faibles amplitudes* au sein des réservoirs non-conventionnels (Cotton et al., 2013).

Les travaux présentés ici s'inscrivent dans le suivi permanent (en temps continu) de l'évolution d'un réservoir ainsi que dans l'imagerie en temps réel de jeux de données massives.



# Preamble

Seismic exploration consists in producing acoustic waves from the Earth surface and in listening to the signal's echoes generated by the subsurface. Acoustic waves are generated using impulsive sources (air gun, explosive, weight loss) or oscillating sources (vibrating trucks). The emitted signal is modified through the propagation within the Earth, usually reflected (or refracted) by the geological layer and finally recorded using multiples sensors (hydrophones, geophones, accelerometers, optical fibers). Seismic exploration is often compared to echography. Seismic processing aims at increasing the signal-to-noise ratio and formatting the information to create an image of the subsoil. After having processed the seismic data, we access to the precise identification and characterization of the geological layers. The resolution is related to the central frequency of the recorded signal. In seismic reflection, the penetration depth ( $z$ ) can reach ten kilometers. Recent seismic acquisitions involve numerous sensors and sources (Pechols et al., 2010; Meunier et al., 2008) deployed over thousands of square kilometers either onshore (land seismic) or offshore (marine seismic). Seismic operations require considerable logistical efforts to organize isolated basecamp (often in desert environment), to transport tons of equipment including cables, spare mechanical and computer elements but also to achieve acceptable source and sensor positioning as well as sharp recording synchronization. Recent acquisitions commonly produce several million records that generate *hundreds of terabytes of data per seismic project*. When the sources and sensors are deployed on a single line ( $x$ ) at the surface of the ground (or at sea level, for marine seismic), we refer to a 2D image ( $x, z$ ). By extension, we refer to a 3D image when the sources and the sensors are deployed on a surface ( $x, y$ ). 3D imaging ( $x, y, z$ ) allows to characterize geological structures and their extensions more precisely than in 2D mode. When the acquisition coverage is sufficient, 3D seismic naturally brings out additional important information for oil exploration as it enables to understand spatially the structure of complex reservoirs.

Conventional oil and gas reservoirs operate over several decades. They evolve slowly during their production. During a primary stage, the reservoirs are commonly produced by using natural depletion. The reservoir pressure progressively decreases. At this stage, the production rate does not exceed 25% of the total resources in place. When the pressure becomes too low for primary oil recovery, secondary methods are often used to increase artificially the reservoir pressure. Generally, it consists in injecting water or

gas (like carbon dioxide). The recovery rate can reach in this case 45%. In most of the cases, even for very good reservoirs, more than a half of the oil remains in place. To characterize the evolution of these reservoirs over time ( $t$ ), *4D seismic monitoring* ( $x$ ,  $y$ ,  $z$ , and  $t$ ) is now commonly used. This consists in repeating a 3D acquisition on the same oil field (Lumley, 2001; Johnston, 2013). We usually refer to conventional 4D seismic when we repeat the acquisition every 2 to 5 years or more. In conventional 4D seismic, the main challenge is to acquire successive seismic data under identical conditions so that the differences observed in the images are effectively related to the evolution of the reservoir and not to *variations in the seismic experiment*. In practice, the conditions are never strictly identical. This represents the greatest challenge for the processing and for the analysis of these data (Calvert, 2005).

Unconventional reservoirs require special production efforts to extract hydrocarbons. These heavy oil reservoirs, less fluid, cannot be produced using conventional pumps such as those widely used in the Middle East for example. To exploit heavy oils, oil companies use *steam or gas injection*. The steam injected into the reservoir warms the heavy oil and thus increases its fluidity, ultimately facilitating production. The generation of steam and its injection into the reservoir represent a significant cost source and require special attention. In this production context, the reservoir and the overlying geological layers can evolve rapidly. It is therefore essential to monitor the effects of production *much more frequently* than in conventional 4D seismic; we talk about an acquisition every day, or even every 6 hours. With such a calendar resolution, we refer to time-continuous 4D active seismic imaging. Continuous 4D uses sources and sensors specifically designed to be permanently buried (Meunier et al., 2001; Forgues et al., 2011; Hornman et al., 2012). Compared to conventional 4D seismic, an additional effort is made to ensure that the acquisition conditions are identical: there are no differences in the acquisition geometry, the weather effects are negligible and the coupling, the signature of the sources as well as the sensitivity of the sensors are constant. Thanks to excellent repeatability (Schissel  et al., 2009); *continuous 4D seismic* is used to characterize *rapid variations with small amplitudes* within unconventional reservoirs (Cotton et al., 2013).

The present study is related to permanent reservoir monitoring (in continuous time) as well as to massive seismic dataset real-time imaging.

# Acknowledgements

I am very thankful to people who served, challenged, encouraged, and supported me throughout my academic program both at Paris Sciences & Lettres (PSL) Research University and at the University of Grenoble-Alps (UGA).

My sincere appreciation especially goes to my advisors, Pr. Chauris Hervé and Dr. Forgues Eric for their guidance in my work and giving me the opportunity to participate in remarkable research projects at MINES-ParisTech and at CGG. Appreciation is also extended to Pr. Mari Jean-Luc of IFPEN and Dr. Lacombe Céline of CGG for their support and comments.

I express my gratitude to Kees Hornman from Shell for his fertile contribution to this work and his general strong interest in and support for this project. I am grateful to Yves Lafet, and Thierry Coleou for their support and advices. I also thank Shell Global Solutions International and NAM for their permission to present this work.

I am highly indebted to Mr. Meunier Julien, Mr. Bianchi Thomas of CGG for their time and sharing of knowledge.

I am also very grateful to the CGG's Seismic Monitoring Solution team, Mrs. Michou Laurene, Dr. Berron Cécile, Dr. Duret Florian, Dr. Estelle Rebel and Dr. De Cacqueray Benoit who had contributed to this work.

I would also like to take this opportunity to thank the CGG's seismic acquisition R&D team, Mrs. Berthaud Anne, Mr. Castor Kaelig, Mr. Hardouin Paul and Mr. Tayart de Borms Brice, Mr. Rondeleux Baptiste and Mr. Herrmann Philippe for their friendship and support.

Finally yet importantly, I thank my family who encourage me during all my studies. I take this opportunity to express my love to Marie-Laure who believes in me and supports me every day.



# Contents

1. Introduction.....	16
2. Historical review of time-lapse seismic.....	24
2.1 Introduction.....	26
2.2 4D Marine.....	26
2.2.1 Draugen field (Norway).....	29
2.2.2 Gullfaks field (Norway).....	30
2.2.3 Girassol field (Angola).....	31
2.2.4 Marlim Field (Brazil).....	33
2.2.5 Conclusion on the 4D Marine case.....	34
2.3 Marine Permanent Reservoir Monitoring (PRM).....	34
2.3.1 Sea-floor receiver cables: OBC.....	35
2.3.2 Valhall OBC PRM (Norway).....	37
2.3.3 Ekofisk OBC PRM (Norway).....	39
2.3.4 Sea-floor receiver nodes: OBN.....	40
2.3.5 Atlantis OBN PRM (Gulf of Mexico).....	41
2.3.6 Mars OBN PRM (Gulf of Mexico).....	42
2.3.7 Conclusion on the Marine PRM case.....	43
2.4 4D Land.....	44
2.4.1 Holt Field (Texas).....	44
2.4.2 Carbonates 4D pilot (Abu Dhabi).....	47
2.4.3 Fazenda Alvorada (Brazil).....	48
2.4.4 Ratqa (North Kuwait).....	49
2.4.5 Conclusion on the 4D Land case.....	50
2.5 Onshore continuous seismic monitoring: SeisMovie.....	50

2.5.1 Peace River PAD32 continuous seismic monitoring (Canada).....	52
2.5.2 Schoonebeek continuous seismic monitoring (The Netherlands).....	53
2.5.3 Peace River 2015 (Canada).....	55
2.5.4 Conclusion on continuous land seismic monitoring.....	56
2.6 Discussion on optimal 4D.....	57
2.7 Conclusion.....	61
<b>3. Deghosting of continuous-time seismic data.....</b>	<b>64</b>
3.1 Introduction.....	65
3.2 Steam injection seismic monitoring in Schoonebeek.....	67
3.3 Acquisition and data quality.....	69
3.4 Ghost waves in continuous seismic monitoring.....	71
3.4.1 S-P converted ghost waves.....	73
3.4.2 Receiver ghosts.....	76
3.4.3 Source ghosts.....	82
3.5 Repeatability improvement.....	87
3.6 Travel time and amplitude variation.....	88
3.7 Discussion.....	93
3.8 Conclusion.....	93
<b>4. 4D velocity and impedance in real-time.....</b>	<b>94</b>
4.1 Introduction.....	96
4.2 4D Velocity Analysis.....	98
4.3 M-NMO correction.....	98
4.3.1 Strategy for time-lapse velocity estimation.....	100
4.3.2 Simple illustration.....	101
4.4 Application to a 2D/4D synthetic dataset.....	104
4.4.1 Forward modelling.....	104

4.4.2 Time-lapse velocity analysis .....	106
4.4.3 Velocity conversion.....	107
4.5 Application to continuous seismic monitoring real data.....	108
4.5.1 Acquisition and pre-processing .....	108
4.5.2 Velocity variations .....	110
4.5.3 Impedance variations .....	115
4.5.4 Steam monitoring .....	117
4.6 Discussion .....	122
4.7 Conclusion.....	123
<b>5. Real-time PSTM: TeraMig .....</b>	<b>124</b>
5.1 Introduction .....	126
5.2 Kirchhoff migration .....	127
5.3 TeraMig.....	130
5.4 Computational cost.....	135
5.5 Network and IT design .....	136
5.6 TeraMig workflow.....	137
5.7 Results.....	138
5.8 Conclusion.....	147
<b>6. Conclusion and perspectives .....</b>	<b>148</b>
6.1 Conclusion.....	150
6.2 Perspectives .....	151
<b>References.....</b>	<b>154</b>
<b>List of figures.....</b>	<b>172</b>

Appendix 1 .....	182
Simultaneous active and passive seismic monitoring of steam-assisted heavy oil production .	182
Appendix 2.....	184
Continuous Land Seismic Monitoring of Thermal EOR in the Netherlands.....	184
Appendix 3.....	186
Permanent, continuous & unmanned 4D seismic monitoring: Peace River case study.....	186
Appendix 4.....	188
An optimal source for continuous monitoring .....	188
Appendix 5.....	190
Method for time-lapse wave separation .....	190
Appendix 6.....	192
Plural depth seismic deghosting method and system .....	192
Appendix 7.....	194
Volumetric and non-volumetric sources-based seismic survey and method .....	194
Appendix 8.....	196
Methods and systems for monitoring a subsurface formation with a land active streamer .....	196
Appendix 9.....	198
Seismic migration using an indexed matrix .....	198

## List of acronyms

2D	Two dimension seismic	OBC	Ocean Bottom Cable
3D	Three dimension seismic	OBN	Ocean Bottom Node
4D	Four dimension seismic	OWC	Oil Water Contact
CMP	Common Midpoint	PRM	Permanent Reservoir Monitoring
CSS	Cyclic Steam Stimulation	PSDM	Pre-Stack Depth Migration
DS <sup>3</sup>	(DSSS) Distance Separated Simultaneous Shooting	PVT	Pressure Volume Temperature
EOR	Enhanced Oil Recovery	RMS	Root Mean Square
FK	Frequency Wave number	ROV	Remotely Operated underwater Vehicle
i4D	Intelligent 4D seismic	SAGD	Steam Assisted Gravity Drainage
IOR	Improved Oil Recovery	STOIP	Stock-Tank Oil Initially in Place
ISS	Independent Simultaneous Sweeping	VSP	Vertical Seismic Profile
M-NMO	Modified Normal Move Out	WAZ	Wide Azimuth
NMO	Normal Move Out		
NRMS	Normalized Root Mean Square		
PSTM	Pre-Stack Time Migration		



# 1. Introduction

---

La sismique 3D est largement utilisée dans l'industrie pétrolière. Cette méthode fournit des informations sur les structures géologiques et peut être utilisée pour construire des modèles de réservoir. Cependant, les propriétés dérivées des données sismiques 3D ne sont que statiques: nous ne pouvons pas évaluer ce qui change avec le temps.

La sismique 4D, quant à elle, bénéficie d'une dimension temporelle, ce qui permet d'analyser des modifications dans le réservoir. Un projet sismique 4D comprend plusieurs campagnes 3D (ou 2D) sur le même champ à différentes étapes de la production. Une campagne initiale est de préférence acquise avant le début de la production. Plus tard, une nouvelle campagne est acquise. Les différences entre les ensembles de données sont ensuite extraites et analysées. En mesurant les changements résultants de la production, on peut comprendre l'évolution du réservoir dans le temps, en particulier son comportement pendant la production.

---



3D seismic is widely used in the oil industry. It provides information about geological structures and can be used to build reservoir models. However, the properties derived from 3D seismic data are only statics: we cannot assess what is changing with time. Adding a time dimension to 3D data (or to 2D data), hence doing 4D seismic allows the measurement and the analysis of changes in the reservoir. A 4D seismic project includes multiple 3D (or 2D) surveys over the same field at different stages of production. An initial survey (base survey) is preferably acquired before the beginning of the production. Later, a new survey (called a monitor) is acquired. The differences between the dataset are then extracted and analysed. By measuring changes resulting from production, time-lapse seismic techniques can contribute to reservoir management and further field development (Koster et al., 2000; Kloosterman et al., 2003). The processing and the interpretation of the seismic differences aims at understanding the changes in the reservoir over time, particularly its behaviour during production. The ability to monitor the behaviour of a reservoir during its production allows engineers to evaluate changes in the subsurface beyond the limited narrow windows provided by monitoring wells (Figure 1).

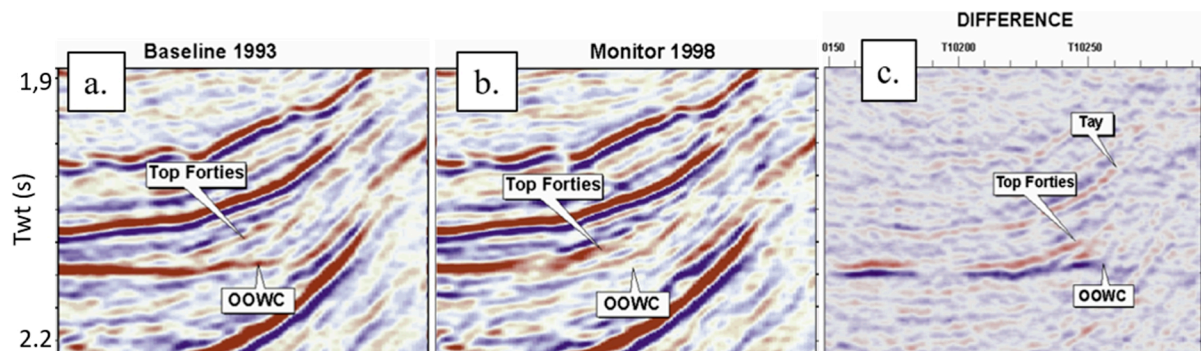


Figure 1: A well-known illustration of a 4D study conducted in Gannet C field, North sea central grabben. The Gannet C has a ring-shaped closure around a central salt dome. There is a 120-mthick oil rim under a gas cap. 1993 Baseline (a), 1998 monitor (b) and the differences (c). Illustration from Koster et al., (2000).

The additional information provided by 4D seismic has a real value in optimizing the recovery of remaining reserves (El Ouair and Strønen, 2006). Improving recovery rates by a few percent or extending production for a few years can indeed have crucial business impacts (Osdal and Alsos, 2010). With maturing basins and ever deeper and more complex frontiers, the importance of extending reservoirs lifetimes and of maximizing recovery from producing fields has never been greater. Hydrocarbon exploration and development went through several step-change technologies during the

last decades and time-lapse (or 4D) is a seismic method whose value is now recognised. Optimal 4D would be highly repeatable (Calvert, 2005; Pevzner et al., 2011; Roach et al., 2015), affordable, versatile, scalable (Smit et al., 2006; Hatchell et al., 2013) and should help reservoir engineers to take decisions in real-time (Mateeva et al., 2015). We first propose to review the evolution and the diversification of the 4D seismic methods worldwide (Chapter 2). Within many case studies, from dynamic onshore acquisition conditions toward permanent reservoir monitoring system, we will emphasise the success and the operational difficulties behind successive seismic data acquisition and the consequences on the repeatability of the measurements. This “journey toward optimal 4D” will be completed by brief presentations of some 4D continuous seismic case studies in which I participated.

Repeatability: is there a limit? We will then consider the high repeatability of onshore continuous-time seismic: in theory, such a system and method should enable to reach a perfect repeatability (Meunier et al. 2001; Schissel  et al., 2009). However, some wave propagation considerations may be necessary to understand and to reduce the residual variation “4D noises” observed on the successive seismic records (Bianchi et al., 2005). This part will be the opportunity to detail the steam injection monitoring experiment performed in Schoonebeek (The Netherlands). We will focus on the data pre-processing that was required for the detection of small and rapid changes during the continuous-time monitoring (Chapter 3). By reducing the 4D noises caused by fluctuating ghost waves, the pre-processing has significantly improved the seismic repeatability (Figure 2). The pre-processing was thus essential to detect reservoir related variations.

Enhancing the repeatability is definitively important but is not sufficient. The capability to achieve a near real-time turnaround enabling rapid reservoir management response to the 4D observations is also considered key in 4D seismic; this is particularly true when acquiring daily 4D data with a continuous seismic monitoring system. In this part (Chapter 4), we will propose and discuss a rapid, robust and automatic workflow to estimate velocity and acoustic impedance changes occurring in the reservoir (Figure 3).

Finally, the previous discussion about real-time processing and decision will introduce a more general context. Indeed, 2D and 3D projects have some conceptual similarities with 4D projects: the 4D-geophysicist compare the monitor with the reference baseline like the field-geophysicist compare the newly acquired shot-point to

a reference one. However, with blended acquisitions techniques like ISS (Howe et al., 2008), DS<sup>3</sup> (Bouska, 2009), with single sensor and single source, shot-to-shot comparison becomes more and more difficult and even not meaningful at all. In this last part (Chapter 5), we will describe a brand new approach called TeraMig (Cotton et al., 2016) for automated field quality control in the migrated domain.

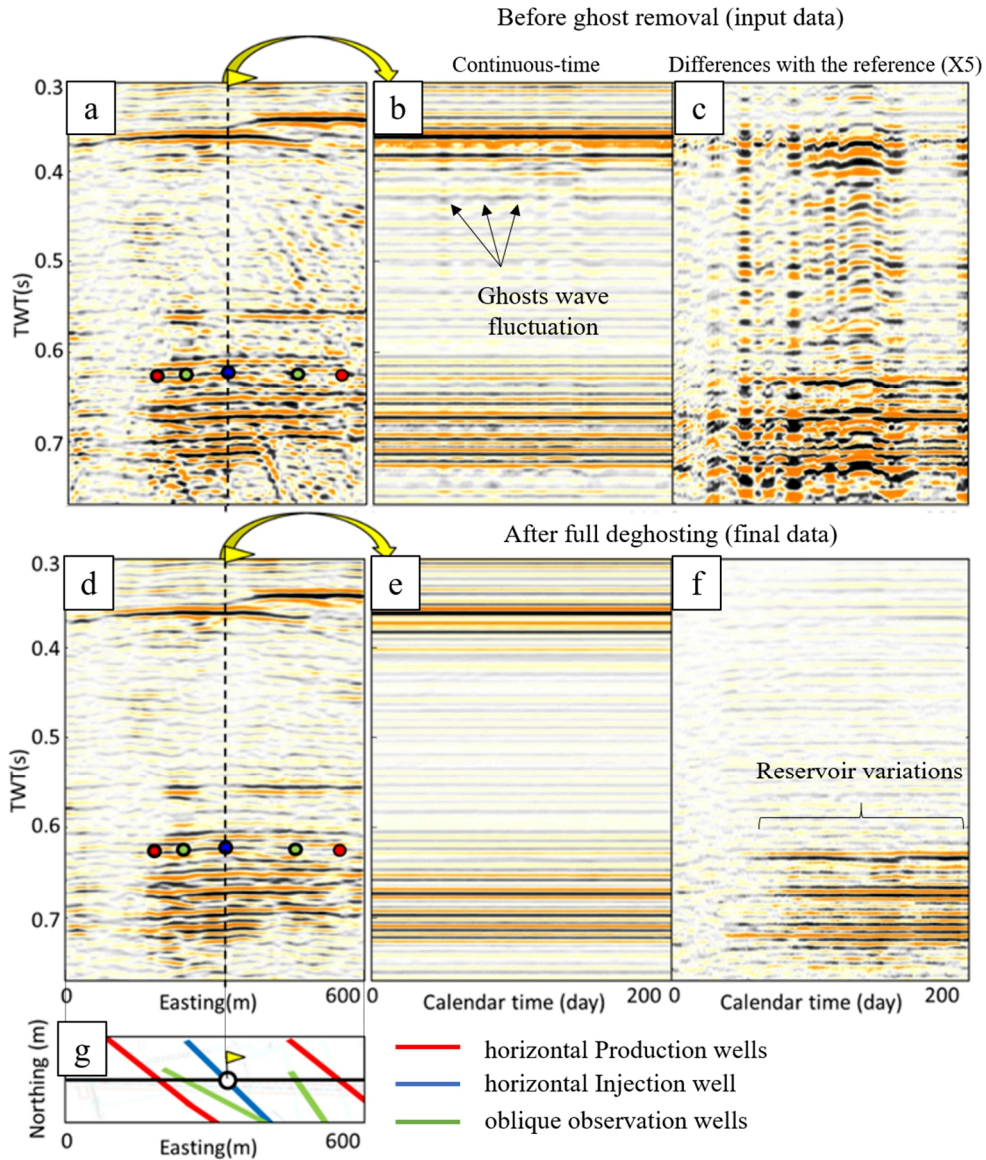


Figure 2: Data quality and repeatability comparison in different domains. The data without any ghost removal (top) and ghost attenuation (bottom). We display a stacked sections (left) as well as the calendar evolution of the stack section's center bin (middle). The selected centre bin is at the position of the injection well. The middle panel consists of one trace per day. The right panel is obtained by subtracting a reference to each daily records. The residue is then multiplied by a factor 5.

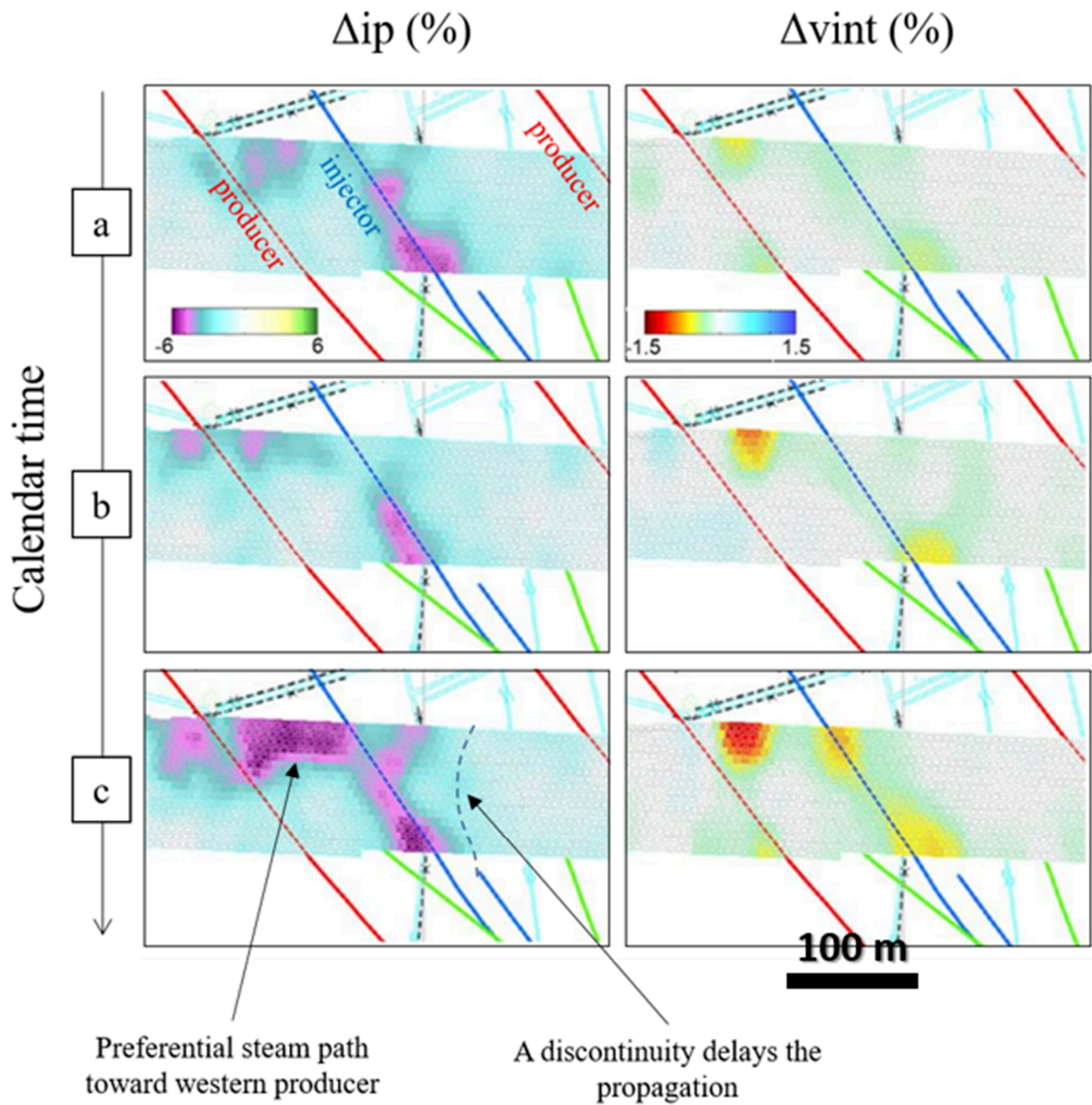


Figure 3: Acoustic impedance variation maps (left) and interval velocity variation (right) for a) August, b) October and c) December. The injection well is in blue and the two producers are in red. These maps are obtained in Chapter 4 and represent one of the main results.

This PhD thesis relates to the following references:

- GEOPHYSICS:

Cotton, J., H. Chauris, E. Forgues and P. Hardouin, 2018, Time-lapse velocity analysis—Application to onshore continuous reservoir monitoring. *GEOPHYSICS*, **83**(3), B105-B117

- EAGE and SEG expanded abstracts

Cotton, J., E. Forgues and J. C. Hornman, 2012, Land seismic reservoir monitoring: Where is the steam going? *SEG Technical Program Expanded Abstracts 2012* (pp. 1-5). Society of Exploration Geophysicists.

Cotton, J. and E. Forgues, 2012, Dual-depth hydrophones for ghost reduction in 4D land monitoring, *SEG Technical Program Expanded Abstracts 2012*, Society of Exploration Geophysicists, 1-5.

Cotton, J., L. Michou and E. Forgues, 2013, Continuous land seismic reservoir monitoring of thermal EOR in the Netherlands. In *IOR 2013-17th European Symposium on Improved Oil Recovery*.

Cotton, J., M. Beilles, S. Mahrooqi, J. Shorter et al., 2016, Automated and Real-time Field PSTM - How to QC More Efficiently 10 Billion Traces Today and More Tomorrow: 78th EAGE Conference and Exhibition, Amsterdam, 2016, Amsterdam, Netherlands, doi: 10.3997/2214-4609.201600983

- PATENTS

Cotton J. and T. Bianchi, 2013, Method for time lapse wave separation, U. S. Patent 13/766,213

Cotton, J., 2015, Plural depth seismic de-ghosting method and system. U.S. Patent Application No 14/338,696.

Cotton, J. and E. Forgues, 2017, Seismic migration using an indexed matrix. U.S. Patent Application No 15/503,773.

Cotton, J. and F-X. Grésillon, 2017, Methods and systems for monitoring a subsurface formation with a land active streamer. U.S. Patent Application No 15/120,205.



## 2. Historical review of time-lapse seismic

---

De nos jours, la sismique 4D est une méthode reconnue dans le monde entier. Elle est employée en mer et à terre.

En mer, les études 4D marines sont mises en œuvre dans des conditions dynamiques (courants, vents, marées). D'importants efforts d'ingénierie sont déployés pour repositionner et stabiliser le dispositif d'acquisition afin de reproduire les mesures sismiques d'une campagne à l'autre. L'utilisation de capteurs fixes au fond de l'océan permet d'améliorer sensiblement la répétabilité. Cependant, le repositionnement de la source qui est toujours opérée depuis la surface, reste le maillon faible.

A terre, le repositionnement ne représente plus un défi en 4D terrestre. Cependant, la plus grande difficulté concerne la proche surface. En effet, les variations de la couche superficielle soumise aux intempéries, la présence d'hétérogénéités, de karsts ou encore le couplage des sources et des récepteurs au sol sont autant de défis en terme de répétabilité.

---



## 2.1 Introduction

The additional information provided by 4D seismic has a real value in optimizing the recovery of remaining reserves (El Ouair and Strønen, 2006). Improving recovery rates by a few percent or extending production for a few years can indeed have crucial business impacts (Osdal and Alsos, 2010). With maturing basins and ever deeper and more complex frontiers, the importance of extending reservoirs lifetimes and of maximizing recovery from producing fields has never been greater. Hydrocarbon exploration and development went through several step-change technologies during the last decades and time-lapse (or 4D) is a seismic method whose value is now recognised. Optimal 4D would be highly repeatable (Calvert, 2005; Pevzner et al., 2011; Roach et al., 2015), affordable, versatile, scalable (Smit et al., 2006; Hatchell et al., 2013) and should help reservoir engineers to take decisions in real-time (Mateeva et al., 2015).

We propose to review the evolution and the diversification of the 4D seismic methods worldwide. Within many case studies, from dynamic onshore acquisition conditions toward permanent reservoir monitoring system, we will emphasise the success and the operational difficulties behind successive seismic data acquisition and the consequences on the repeatability of the measurements. This “journey toward optimal 4D” will be completed by brief presentations of some 4D continuous seismic case studies in which I participated.

## 2.2 4D Marine

Marine surveys are acquired under dynamic conditions, with both the sources and the receiver in motion. In 4D, these variations from one vintage to another become important, as differences due to the acquisition may hide the differences induced by the changes in the reservoir. In the industry, efforts are made to ensure the repeatability of the acquisition. The perfect 4D monitor survey is a precise reproduction of the acquisition of the baseline survey. This involves repeating source and receiver positions and matching environmental conditions such as tide state and currents. Variations in water temperature and salinity may be seasonal so planning to shoot at the same period of the year may also be necessary. This would be in an ideal world. Yet, Johann et al.,

(2006) relate a challenging operation plan conducted during the acquisition of the Marlim Project (Brazil):

*“The shooting plan was to have the “Pride” shoot with 10, 6 km-long cables and spaced 50 m apart. This would be possible for approximately 2/3rds of the survey area. The final phase would be shot in a two-boat mode using the “Geco Tau” as the source vessel and the “Pride” reducing its cable length to 3 km. The seismic recording started on November 2004, when a strong southerly current was encountered which reached 2.2 knots and caused 17.5 degrees of streamer feathering (e.g. the lateral deviation of a streamer away from the towing direction because of a water current). During the first two weeks of November, the weather worsened and halted seismic acquisition (gale force 7 to 9). On the last weeks of November, the weather improved enough to resume the acquisition. Further high currents were experienced causing up to 29 degrees of feather and making turns difficult. During the turns, the tail buoys often crossed because of these high currents, but the crew was able to steer them apart.”*

*Johann et al. (2006)*

Multi-vessel operations can play a range of important roles in the context of 4D acquisition. In cases of extreme strong perpendicular currents, multi-vessel operations can be performed to improve the repeatability of long offsets. The use of a separate source vessel and shorter streamers allows long offsets to be acquired more accurately and with greater repeatability than with a single vessel in these conditions.

Monitor survey over-specification (compared to a reference baseline survey), meaning using more streamers and forming a wider spread (Figure 4) can extend the base-monitor common illumination area and thus may contribute to the repeatability improvement Johnston et al., (2013). Modern processing techniques can then take advantage of this higher-density data to decimate to common dataset or to interpolate the data for optimum repeatability (Abma and Kabir, 2006; Trad, 2009).

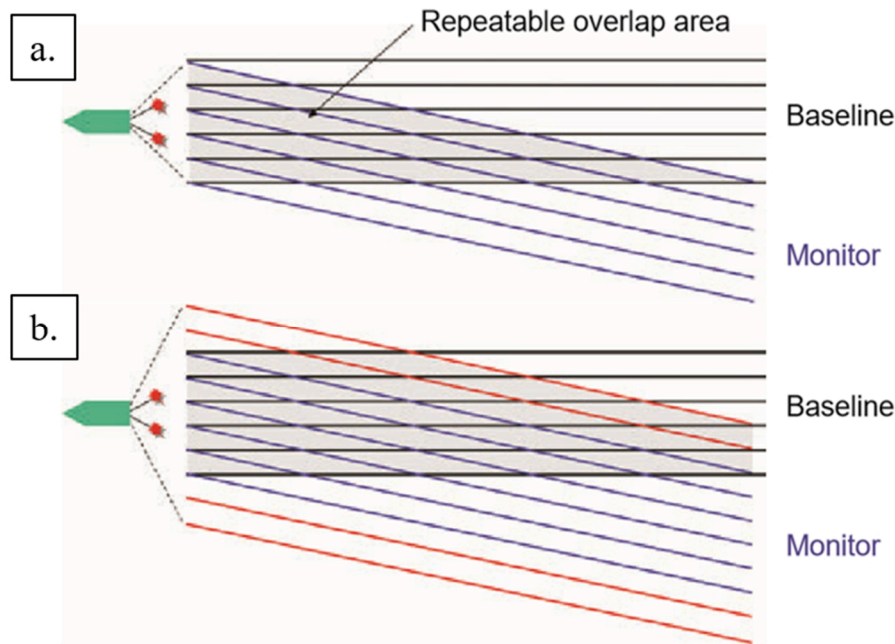


Figure 4: Reduction of the repeatable overlap area in the case of streamers feathering between the baseline and a monitor survey (a). Monitor over-specification (b) using 10 streamers instead of 6 increases the repeatable overlap area. Illustration from [Johnston et al., \(2013\)](#).

The effect of currents on streamer geometry can be anticipated during survey planning. Current models including meteorological and satellite data are used to predict currents, and therefore streamer feathering. In addition, Acoustic Doppler Current Profiling (ADCP) is used to measure the actual current ahead of the streamers and calibrate the current prediction model ([Buddery, 1991](#)). This information is often integrated to manage the vessel steering to address the large-scale effects caused by currents.

In addition, acoustic array are used to fine-tune the positioning. These provide a more precise knowledge of the streamer position so that steering devices can maintain the desired streamer geometry more accurately. As an example, Sercel's Nautilus system combines streamer steering and acoustic positioning functions into a single device (Figure 5). Solid streamers offer several clear benefits for 4D recording as well. First, solid streamers are quieter than fluid-filled ones, resulting in an improved signal-to-noise ratio. This has a great importance when targeting weak 4D seismic differences. Second, solid streamers offer improved consistency of positioning and depth control

thus improving the repeatability of the full wave field including primaries, multiples and receiver ghosts.

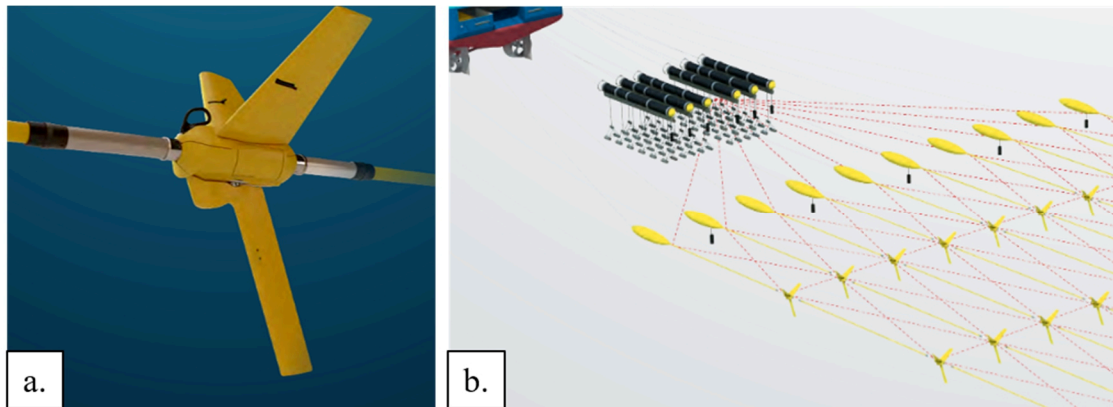


Figure 5: Illustration of cable control with birds (a). Acoustic transceivers are spread along the streamer and eventually on air gun sub-array, head buoys and tail buoys (b). Illustration courtesy of Sercel.

### 2.2.1 Draugen field (Norway)

The Draugen 4D seismic project is a successful 4D marine project conducted in the 1990's. The field is located offshore Norway (Figure 6) where the water column reaches around 250 m. The reservoir consists of an elongated anticline comprising Jurassic sands located at approximately 1.5 km depth. The production was around  $2 \cdot 10^5$  b/day in the mid 1990's.

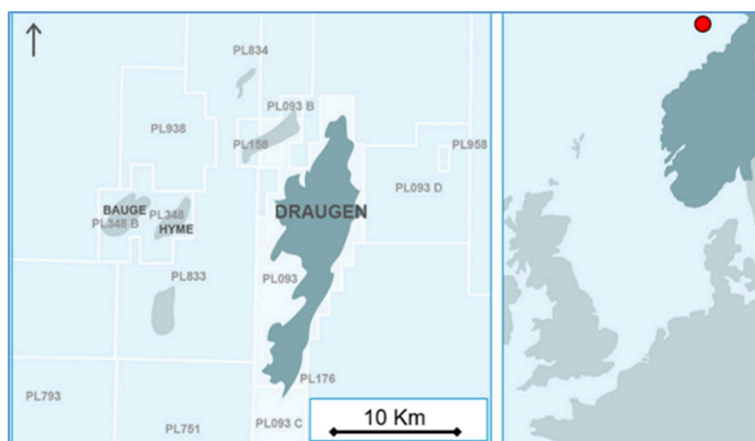


Figure 6: Draugen field location and extension.

To improve the oil production, the main strategy was to sweep the oil by water, from the north and from the south requiring drilling additional wells. However, there were uncertainties concerning the presence of aquifers, faults and fractures that could stop or slow down the oil migration. The seismic project is composed of four monitor surveys and one baseline each acquired using 3D towed streamer acquisition. The baseline was acquired in 1990 and the first monitor was acquired in 1998. Offset and azimuth range were kept as similar as possible but the number of streamer, their spacing and the receiver group interval had changed with respect to the industry standard technology development. Despite those differences, the time-lapse seismic data quality was very good (Gabriels et al., 1999; Koster, 2000; Calvert, 2005) as illustrated in Figure 7.

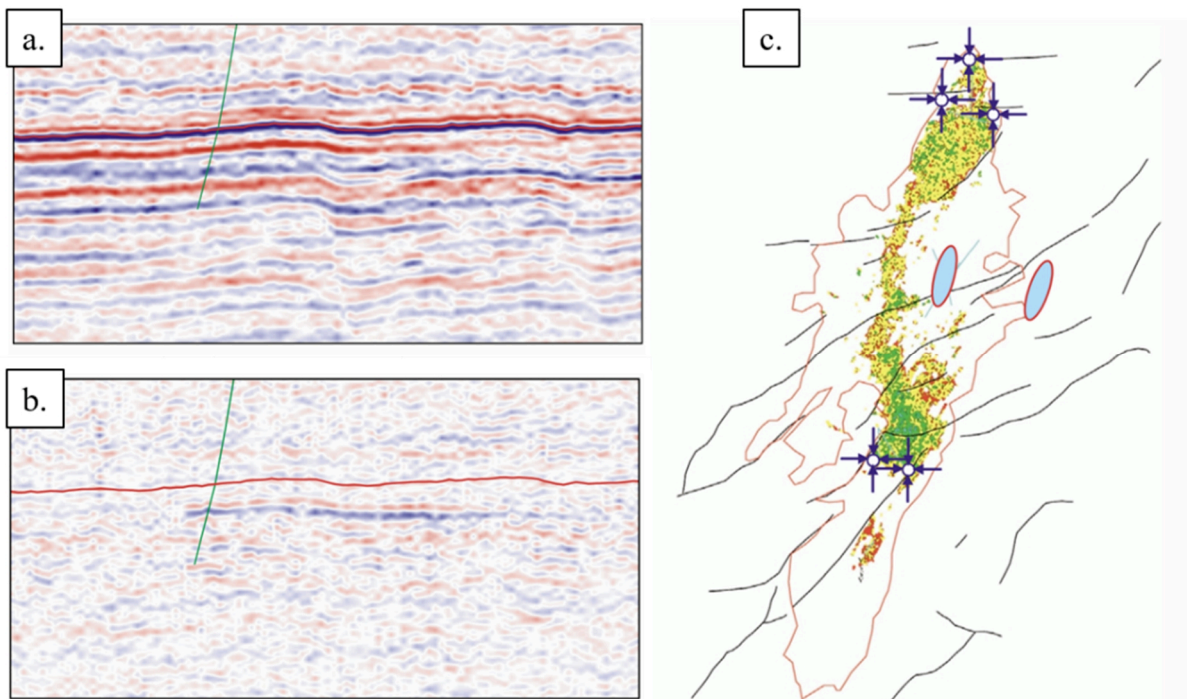


Figure 7: Section through Draugen monitor volume (a) and through the difference volume (b). Amplitude map extracted from the difference volume (c) showing the major faults (in black) and the interpreted extent of the original oil water contact OOWC (in red). From Koster et al. (2000).

### 2.2.2 Gullfaks field (Norway)

This Norwegian field was discovered in 1978. In the area of the field, the water depth is around 200 m. The reservoir is composed of Jurassic and Upper Triassic

sandstone formations located in tilted blocks and in horst structures. The field reached peak production in 2001 at  $1.8 \cdot 10^5$  b/day.

4D seismic takes a prime part in an increased oil recovery (IOR) program that aims at recovering about 70 % of the estimated reserves and directly contributes to the positioning of 19 positive wells (El Ouair and Strønen, 2006). Significant changes in seismic amplitudes were observed between 1985 and 1999 revealing a substantial depletion of the oil due to production (the oil substitution by water decreases the seismic reflection amplitude). In Gullfaks, A perfect match between the time-lapse seismic data and the repeated saturation logs was observed. Consequently, time-lapse seismic data can be used with confidence to map the drainage pattern in between the existing wells (Figure 8).

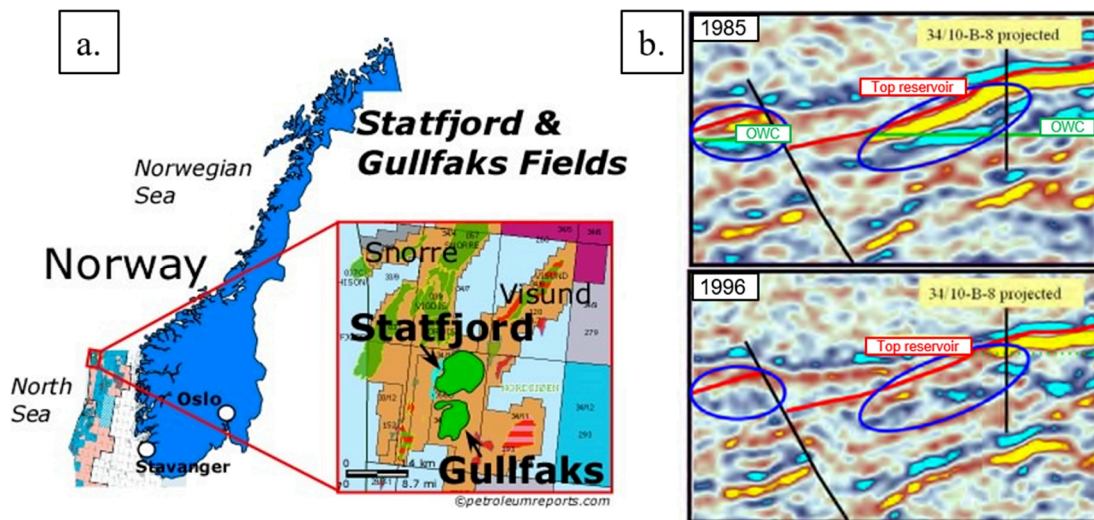


Figure 8: Location map of the Gullfaks field (a), courtesy of petroleumreports.com. Time-lapse seismic data obtained in 1985 and in 1996 (b) show the reduction of the oil water contact. From El Ouair and Strønen, 2006.

### 2.2.3 Girassol field (Angola)

The Girassol field is a complex and faulted turbidite field located deep offshore Angola. The reservoir is composed of Oligocene channel and sand extending over an  $18 \times 10$  km area. A conventional 3D survey, acquired and processed by PGS in 1996 was used to site the first appraisal wells in this field. A 400 square kilometres base 3D High Resolution (HR) seismic survey (6.25 m by 12.5 m bin size) was acquired between mid-August and October 1999 by CGG (Beydoun et al., 2002; Lefeuvre et al., 2003). Field

development started in 2000 and the first oil was produced in December 2001. 4D HR seismic was planned from the very beginning of the development with the aim to monitor the gas bubble extent.

The first 3D HR monitor was acquired in December 2002 (after one year of production and six months after starting of the gas injection). A second monitor survey was shot in 2004. For the reservoir modelling of the Girassol field, 4D seismic has been used to update the reservoir model in order to better locate the injected gas cap. The 4D processing and interpretation allowed exploiting some essential 4D information very soon after acquisition (Jourdan et al., 2006; Gonzalez-Carballo et al., 2006). After the field-monitoring strategy, a third 4D seismic monitor was acquired in 2008, covering Girassol, Jasmin, Rosa and Dalia fields (Figure 9).

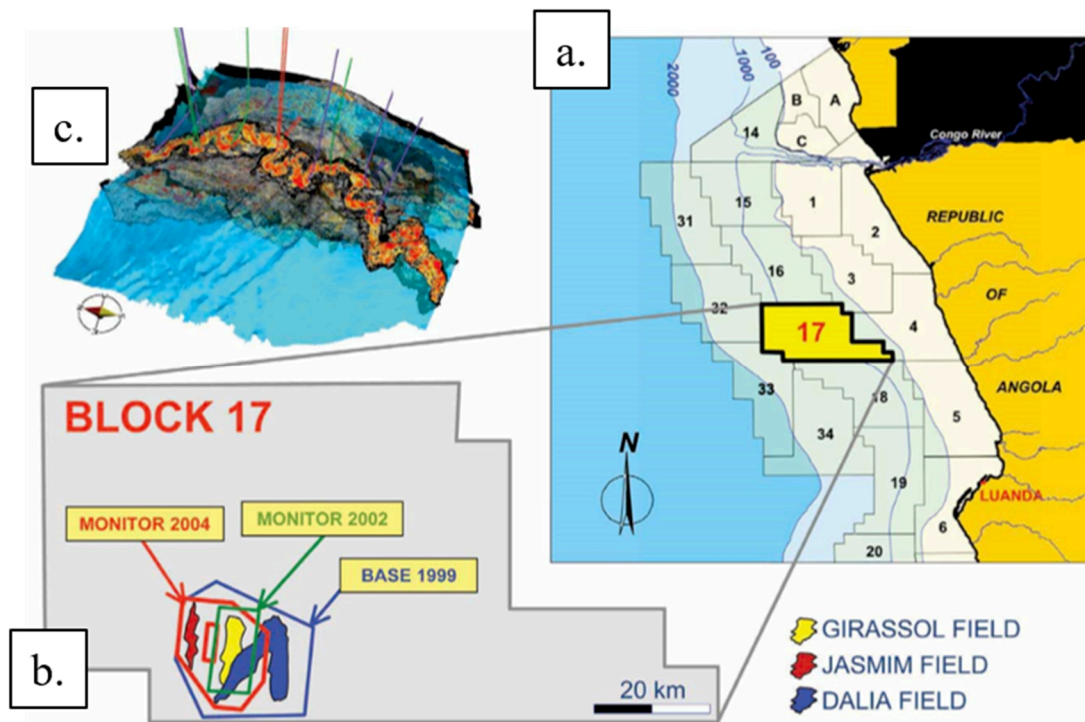


Figure 9: Map of the Angolan offshore (a), with location of the exploration blocks. The southwest of the block 17 has been covered by three HR seismic surveys: one baseline in 1999 on Girassol, Jasmin and Dali fields: one seismic monitor in 2002 on Girassol and one seismic monitor in 2004 on Girassol and Jasmin (b). The fields consist of several channel-levee and sheet complexes, separated by mud turbidites, on a turtleback structure (c). The reservoir driving mechanism is water and gas injection. From [Gonzales-Carballo et al., \(2006\)](#).

## 2.2.4 Marlim Field (Brazil)

The Campos basin (Figure 10) has a marine current condition different from that on the North Sea and West Africa. Consequently, the degree of repeatability in Marlim Complex project was low compared to other 4D projects (Johann et al., 2006).

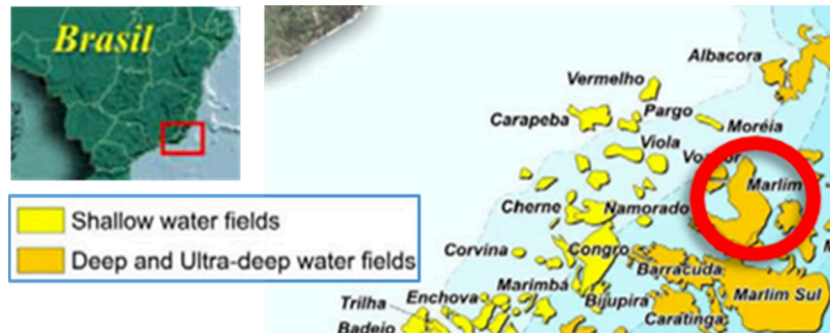


Figure 10: Marlim location map, from Bruhn et al. (2008), modified.

Three seismic surveys cover the Marlim Field. The first one was acquired in 1986 (appraisal context), the others, in 1997 and in 2005. The most recent survey was acquired using WesternGeco's Q-Marine acquisition system and was specifically acquired for reservoir monitoring and characterization purposes (Ribeiro et al., 2005, Oliveira et al., 2007). Sansonowski et al., (2007) remarkably describe the operational issues as well as the processing and interpretation challenges for this project (Figure 11).

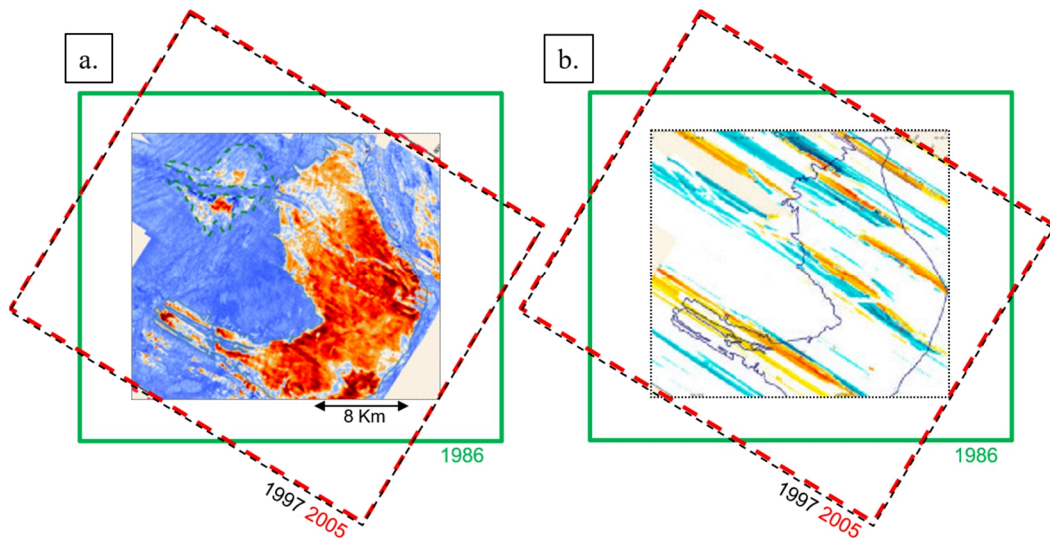


Figure 11: Amplitude map of Marlim 1997 data (a) with the polygon of the acquisitions of 1986 (green), 1997 (dashed black) and 2005 (dashed red). Azimuth map differences (b) higher and lower than 20 degrees during the acquisition of the 2005 dataset. From Sansonowski et al., (2007), modified.

### 2.2.5 Conclusion on the 4D Marine case

Up to the 2000's, most of the marine 4D surveys have been performed using streamers while it is now established that it is the least suitable technique for 4D application (a 10° feathering occurs during marine acquisition resulting in more than 600 m of common midpoint mispositioning on a 6000 m cable). The effect of mispositioning depends on apparent velocity (Meunier and Herculin, 2003). It is small on fast velocities, large on slow velocities. For this reason, it cannot be compensated for by application of a 1-D matching filter. The compensating merits of streamers are availability, cost, familiarity, and uniform source-and-receiver coupling.

## 2.3 Marine Permanent Reservoir Monitoring (PRM)

The improvement of the repeatability (more exactly the detectability of weak 4D signals) and the high cost of frequent monitor surveys motivated the industry to develop Permanent Reservoir Monitor (PRM) systems. A PRM system includes ocean bottom seismic sensors and electrical or optical communication technology. The cables are located on the seafloor (or trenched) so that the receiver positions do not change. Calvert (2005) summarizes the difficulties encountered in almost all 4D studies and pilots.

Table 1: Some cause of non-repeatability in 4D seismic (From Calvert, 2005).

Categories	Factors likely to affect repeatability
Acquisition-geometry differences	Sail-line orientation and heading Source-receiver spacing Streamer feathering Source and receiver depths Coverage influenced by obstructions
Near-surface conditions	Variations in statics Receiver coupling
Environment	Sea level Sea state and swell noise Water temperature Salinity Groundwater level
Noise	Ambient noise Shot-generated noise Residual multiples
Geology	Shallow gas Steep dips Fault shadows Producing reservoirs

Initial PRM installation costs may be high; however, if frequent repeat surveys are needed to monitor the reservoir (Grandi et al., 2013), then permanently installed receivers become cost effective. Caldwell et al., (2015) make a convincing case for the economic success of the Valhall installation in the North Sea in terms of increased oil recovered that is attributable to the PRM seismic data (see 2.3.2 for more details).

PRM presents various advantages over conventional 4D in mitigating the causes of non-repeatability and must therefore lead to a better 4D sensitivity: permanent receivers (and permanent sources, in some cases) are much more stable than re-deployable receivers or moving sources.

### 2.3.1 Sea-floor receiver cables: OBC

The main problem with streamer 4D acquisition is overcome using ocean bottom fixed receivers. With permanent Ocean Bottom Cables (OBC), the geometry problems are fixed on the receiver side; however, the repositioning of the source becomes the remaining weakest link (Figure 12).



Figure 12: Ocean Bottom Cable seismic operation with the Sercel SeaRay 428. The SeaRay encompasses three orthogonally oriented, digital accelerometers and a hydrophone to form a single four component (4C) receiver. Courtesy of Sercel.

British Petroleum is considered as pioneer in permanent OBC monitoring. During the last decades, Statoil, ConocoPhillips, Petrobras and Shell have been highly active in developing PRM techniques.

Table 2: Chronology of PRM trials and implementations (From Bett, 2012).

Year	km	Operator	Region	Field
1995	30	BP, Shell	N Sea	Foinaven
2002	8	ConocoPhillips	N Sea	Ekofisk
2003	120	BP	N Sea	Valhall
2004	10	Shell	GoM	Mars
2006	40	BP	N Sea	Clair
2007	120	BP	Caspian	CARSP
2007	1	Multiple	N Sea	Tjeldbergodden
2008	4	ConocoPhillips	N Sea	Ekofisk
2008	1	Multiple	N Sea	Tjeldbergodden
2009	25	Statoil	N Sea	Snorre
2010	200	ConocoPhillips	N Sea	Ekofisk
2012	30	Petrobras	Brazil	Jubarte
2013	90	Shell	Brazil	BC-10
2013	260	Statoil	N Sea	Snorre Phase I
2014	165	Statoil	N Sea	Grane
2015	230	Statoil	N Sea	Snorre Phase II

Many studies demonstrate the benefits of the method compared to streamers (Cooper et al., 1999; Barkved et al., 2004; Eriksrud, 2014):

- 1) Frequent surveys costs are lower despite of a high initial investment.
- 2) Wide azimuth, multi-component surveys are achievable.
- 3) Passive listening and interferometry can be performed on demand.
- 4) The array is flexible and can be used for dense shooting or quick low-fold surveys in order to monitor rapid changes.

The most-mentioned disadvantage for permanent OBC is the initial cost, which must be balanced against benefits. The cost of 100 km of four components (4C, three orthogonal geophones and a hydrophone) OBC may be as much as the cost of a well. However, the cost may be recovered many times over, by increased production or by saving wells.

*“Time-lapse seismic is playing an important role in reservoir management on the Norne, Stær and Svale oil fields. The total value of the 4D data is estimated to 4.3*

*billion NOK. The keys to the success has been a strong focus on the whole value chain from acquisition, processing, 4D interpretation and reservoir management. The importance of a good quality base survey, and frequent monitoring surveys have been clearly demonstrated.”*

*B Osdal and T Alsos (Statoil), 72nd EAGE Conference & Exhibition*

### 2.3.2 Valhall OBC PRM (Norway)

The Valhall field is located in the southern part of the Norwegian North Sea at a water depth of 70 m (Figure 13). It is operated by BP Norge AS and has been on production since 1982. The field is a highly porous, low-permeability Cretaceous chalk reservoir at a depth of about 2400 m. The reservoir thickness varies from 10 to 60 m and covers an area of more than 50 km<sup>2</sup>. The PRM system is one of the world’s largest permanently installed seismic array. Each receiver has three orthogonal components geophones and a hydrophone. The distance between receivers is 50 m, and the nominal distance between the parallel cables is 300 m. Eleven surveys have been acquired between 2003 and 2009, each having around 50 000 shot points on a 50 × 50 m grid. The error between the theoretical and the actual shot point position is close to zero, with standard deviation of 4–5 m. In good weather, a complete survey is shot in less than three weeks. During acquisition, the recording is triggered by the source vessel. Between surveys, the system records data continuously for passive monitoring analysis such as ambient noise surface wave tomography (Landes et al., 2009; Mordret et al., 2013). A direct, high-bandwidth connection between the Valhall field and Stavanger enables to perform real-time quality control and processing during acquisition. Van Gestel et al., (2008) describe a simple, automated workflow to transform the very high volume of data into products optimized for business real time decisions (Figure 14).

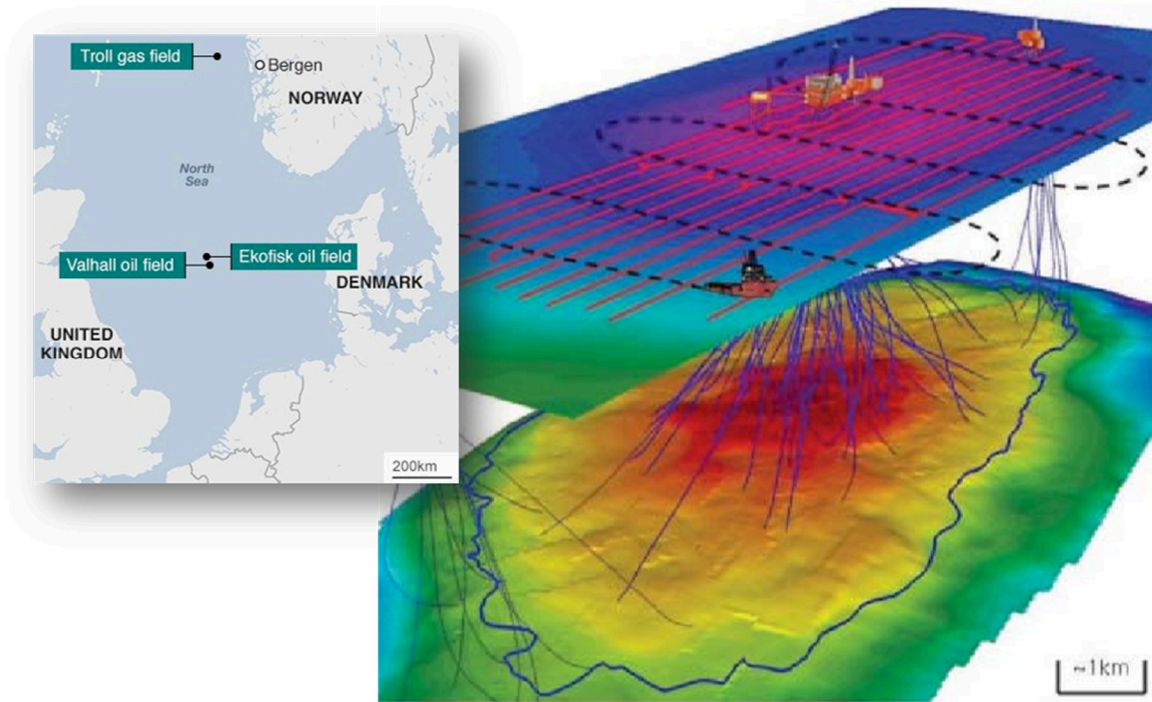


Figure 13: Overview of the Valhall Field showing the layout of the geophone array at the sea floor (red lines), the top of the reservoir, the outline of the field (dark blue) line and the wells (thin blue lines). From [Van Gestel et al., \(2008\)](#).

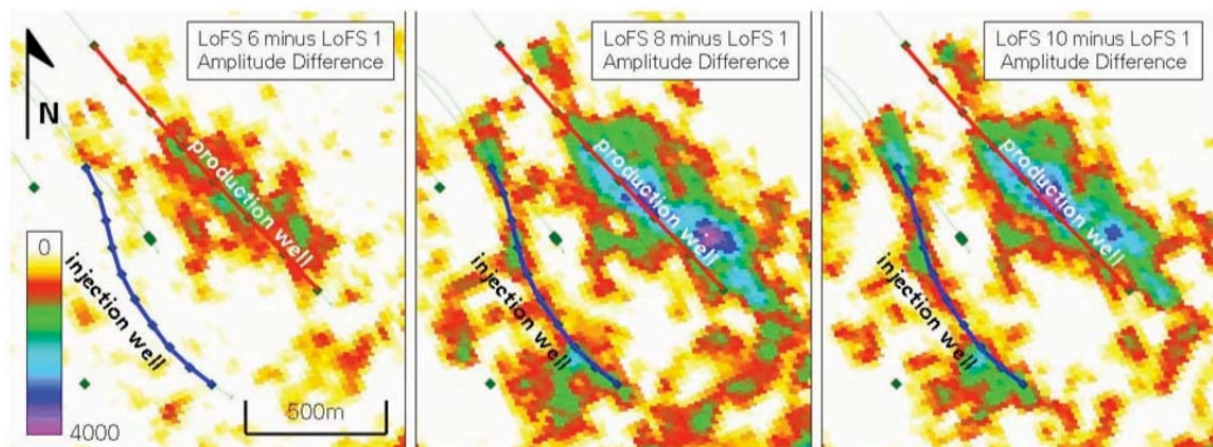


Figure 14: The acoustic impedance difference responses (thickness of amplitudes) for LoFS surveys 6, 8, and 10, all related back to LoFS survey 1. The figure shows the response of the water injector (in blue) and the nearby producer (in red). LoFS 6 was the last survey before injection started so no response is observed around the injection well. From [van Gestel et al., \(2008\)](#).

### 2.3.3 Ekofisk OBC PRM (Norway)

The PRM system installed at Ekofisk (southern part of the North Sea) was a technology revolution for fibre-optic sensing (Eriksrud, 2010). While 4D towed streamer surveys were in extensive use at Ekofisk from 1999 to 2008, it was concluded in 2005 that installing a permanent seabed system would be a better strategy (Folstad et al., 2011).

The installation of the fibre-optic system was successfully completed in October 2010 (Nakstad et al., 2011). The system consists of 200 km seismic cables (trenched at ~ 1.5 m below the seabed) covering a seabed area of 60 km<sup>2</sup> (Figure 15).



Figure 15: Seismic cable network installed at Ekofisk and overlaid with the map of the city of Paris. From Eriksrud et al. (2014).

A key factor in designing this set-up has been to achieve a rapid turnaround to enable rapid reservoir management response to the 4D observations (Buizard et al., 2013). As a result, the 4D processing was completed in less than four weeks. This results in the opportunity to interpret 4D data with a quite short delay and assist in identifying

production risks and prioritizing well interventions (Figure 16). The turnaround time affects the value of 4D data for well operations and reservoir management when rapid changes might occur in the reservoir.

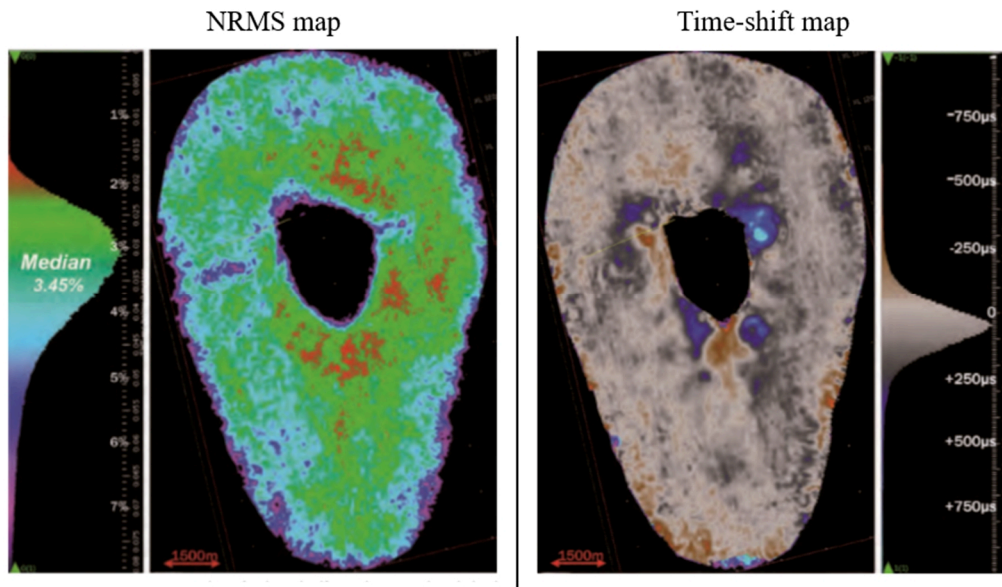


Figure 16: NRMS map (Left) computed on final stacks (from the second and third Ekofisk survey) in a 2500 – 3500 m/s window. The two surveys were acquired 4.5 months apart. The black area in the centre of the map corresponds to the seismic obscured area, which is due to an overburden gas cloud. Top reservoir time-shift map (right) computed on final stacks (from the second and third Ekofisk survey). From [Buizard et al., \(2013\)](#).

#### 2.3.4 Sea-floor receiver nodes: OBN

An alternative to OBC 4D monitoring is the use of Ocean Bottom Nodes (OBN). Individual 4C nodes (Figure 17) are deployed on the sea floor using Remotely Operated underwater Vehicles (ROV). An OBN is an autonomous recording device with a self-contained recording system, clock and battery. As there is no connection with the surface, there is no limitation on length of the receiver line, no downtime due to telemetry/power line failures and no lost time associated with moving of the recording vessel. As the OBN are not constrained by any cable, it offers more flexibility than OBC for the acquisition survey design:

- 1) Nodes can be deployed around infrastructure without interference.
- 2) Nodes can be placed more isotropically on the seabed.

- 3) Nodes offer wide-offset and wide-azimuth geometry that can be designed to illuminate structures under complex overburdens (Figure 17)



Figure 17: The evolution of deep-water nodes. Three deep-water ocean bottom nodes displayed to scale which have decreased in size over time, directly affecting ROV deployment efficiency. From [Bunting and Moses, \(2016\)](#).

After early development by Statoil in the 1990s, the first seismic reflection ocean bottom node survey was acquired in 2004 over Pemex’s Cantarell Field in the Gulf of Mexico. Ocean bottom node surveys are also very repeatable, making them very suitable for 4D seismic analysis ([Berg and Anderson, 2008](#)).

The NRMS ratio ([Kragh and Christie, 2002](#)) expresses the normalized average change in seismic amplitudes between baseline and monitor, is a common quantitative statistic to measure seismic repeatability. When measured outside the producing reservoir zone, a small background NRMS value indicates a well-repeated survey. Repeated deep-water OBN surveys in the Gulf of Mexico report characteristic background NRMS values of 5% at Atlantis (see paragraph 2.3.5) and 6% at Mars basin (see paragraph 2.3.6).

### 2.3.5 Atlantis OBN PRM (Gulf of Mexico)

The Atlantis Field sits about 300 km south of the Louisiana coast in the Gulf of Mexico with around 2100 m of water. It began production in October 2007 from Middle

Miocene turbidite reservoirs that lie about 5200 m below sea level. The geology in this area includes salt bodies with numerous salt fingers. So far, the seismic imaging has been challenging (Roberts et al., 2011). The primary objective of the 2005 first OBN survey was to obtain a consistent, high-quality image of the subsalt portion of the reservoir. This survey was the world's first large-scale deepwater autonomous nodes survey (Beudoin and Ross, 2007). OBN technology allows highly repeatable time-lapse seismic operations. Moreover, it offers a solution to overcome the challenges brought by surface and subsea installations. Therefore, in 2009 a monitor survey was acquired (Reasnor et al., 2010). The time-lapse data had excellent repeatability. Van Gestel et al., (2013) demonstrated clearly the depletion signature of the field within the time shift map (Figure 18).

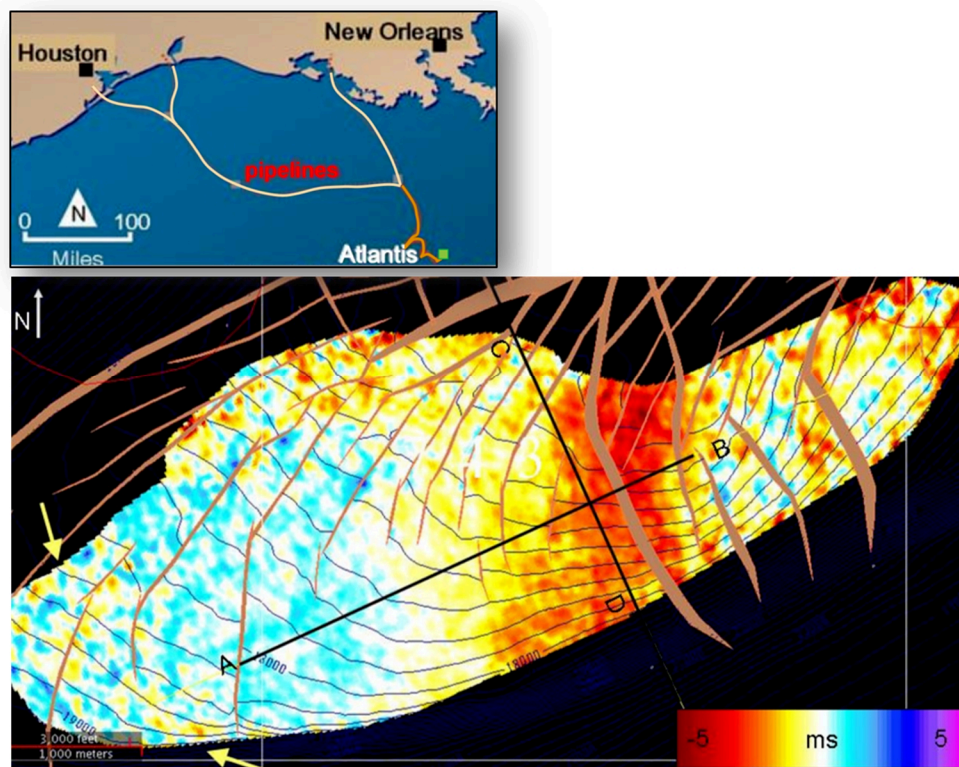


Figure 18: Map of the Atlantis field (top). An average time shift map (bottom) above the reservoir. Brown faults and depth structure of top reservoir are overlain. Yellow arrows indicate the area dominated by multiple. From Van Gestel et al., (2013).

### 2.3.6 Mars OBN PRM (Gulf of Mexico)

Shell acquired two OBN survey in the Mars basin: one in 2007 and the other in 2010. The purpose of these surveys was both illumination of deep sub-salt exploration target as well as time lapse monitoring of the shallower Mars reservoir. The 2007 survey

was acquired with Z3000 Fairfield Nodal deployed on a hexagonal 400 m grid. In 2007, the source depth was 12 meters to ensure the low-frequency illumination of the subsalt targets. In 2010, the source depth was reduced to 10 meters to obtain higher frequencies for the shallow above-salt reservoirs. The quality of the data and the processing applied led to a high repeatability with a NRMS of around 6%. On the 2010 amplitude map, the original oil water contact (OWC) has been highlighted. On the difference map, [Stopin et al., \(2011\)](#) observe the OWC in 2007 as well as the signal related to water coning effect observed near the down dip well (Figure 19).

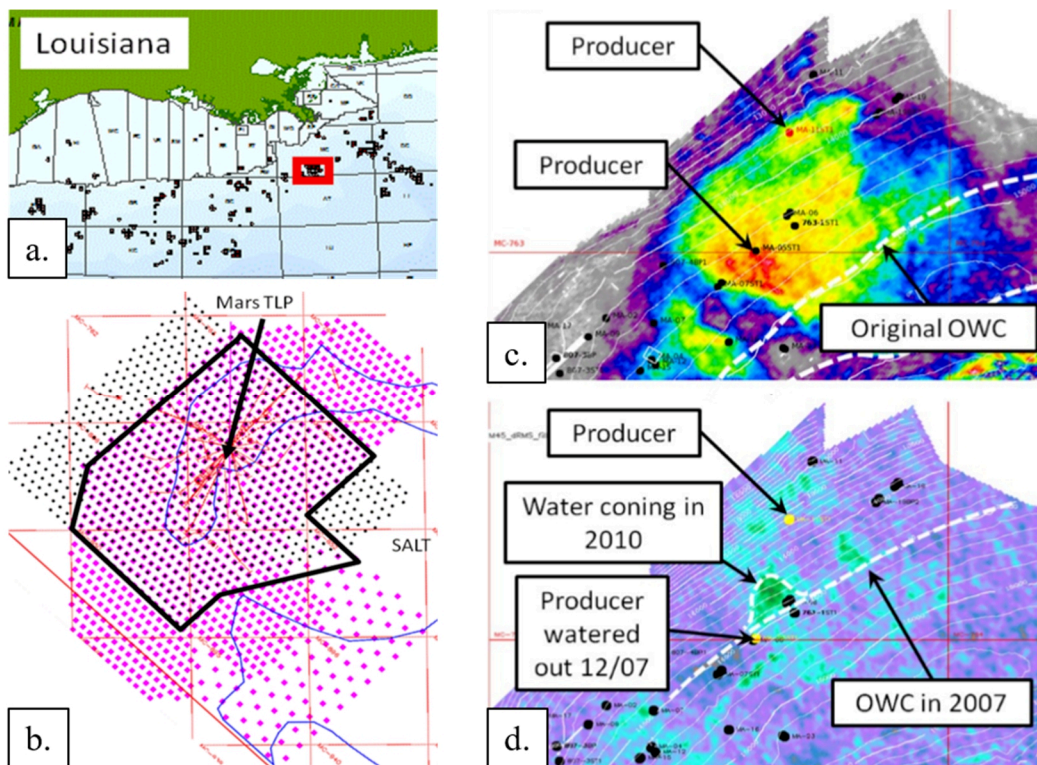


Figure 19: The Mars field location map (a). Node positions (b) for the 2007 and 2010 surveys respectively depicted by black and pink squares. The black polygon outlines the common node positions area. Amplitude map of the reservoir for the 2010 dataset (c) and amplitude differences (d) between 2010 and 2007. From [Stopin et al., \(2011\)](#).

### 2.3.7 Conclusion on the Marine PRM case

PRM presents various advantages over conventional streamer marine 4D in mitigating the causes of non-repeatability and must therefore lead to a better 4D sensitivity. Moreover, frequent surveys costs are lower despite of a high initial

investment. As the receiver spread is fixed, wide azimuth surveys are achievable and passive listening can be performed on demand. Like Marine PRM, land acquisition is achieved with a fixed receiver spread. 4D land should present all the advantage of Marine PRM; however, we will see in the next part that the 4D Land challenges are rather different.

## 2.4 4D Land

4D land project challenges are different from the 4D marine ones. Although repeatability of source and receiver locations are easier to achieve, the variations caused by changes in the weathering near-surface layer can be higher than the ones observed at the reservoir. Careful planning of the initial baseline survey and a consideration of the expected changes in both the response of the reservoir and the near surface are critical to ensure that a usable 4D signature is obtained. Positioning accuracy, and therefore repeatability has been considerably improved by the use of Differential GPS positioning systems. Actual coordinates are recorded more accurately and integrated navigation systems ensure that receivers and sources are deployed as close to the pre-defined targets as possible. The move to high-density and wide-azimuth land acquisition geometries, particularly with single-source single-receiver configurations, has great benefits for land 4D. The use of point source and point receivers results in more consistent and repeatable responses and removes unwanted array effects, which create azimuthally varying attenuation. In particular, 4D processing benefits from higher-resolution statics corrections and velocity models as well as more effective noise attenuation using 3D algorithms.

As for the marine case, we propose to review the successes and the challenges behind 4D Land operation within several case studies worldwide.

### 2.4.1 Holt Field (Texas)

One of the first 4D seismic surveys was conducted in 1982 on the Holt reservoir (northern Texas). This 4D study consists of three explosive surveys acquired over a year in order to monitor fire-flooding Enhanced Oil Recovery (EOR) process. The fire influx in a first well changes the bitumen into coke and distillates. Away, the high temperatures

cause the softening of the bitumen. The distillate-bitumen mix, less viscous, forms a fluid that can be extracted at multiple production wells. The coke remains burning, so the process can continue by injecting oxygen in the first well. The Holt sand reservoir is at around 500 m depth and is 12 meters thick. It is covered by a 2.5 m cap layer of limestone included in a thick layer of shale. The reservoir comprises heterogeneities such as thin fractured sand layers influencing the EOR process.

The acquisition survey is composed of 182 single geophones buried at 6 meters into the ground. The geophone spacing is 6 meters and the source spacing is 12 meters. The shots are fired at 23 m depth with 2.5 kg of dynamite along crossing lines. Buried sources and receivers eliminate the airwaves, reduce the other source-generated noises and preserve the signal from being affected by weathering layer variations. The maximum fold is 16 (Figure 20). Special precautions are taken to repeat the acquisition in the same conditions. The data is recorded at one millisecond and the bandwidth is 50-320 Hz.

For this case study, [Greaves and Fulp, \(1987\)](#) concludes that reflection seismic surveying can be used to monitor the EOR process as the fire-flood was detected and its propagation, direction and extend were determined. Moreover, the 4D seismic surveys were used to estimate the net burn reservoir volume. In this study, the seismic observations were confirmed by the monitoring wells. The best indicator of combustion may be the seismic amplitude attenuation emphasizing a combination of both high-temperature rock alteration and pore fluid changes (Figure 21). Subtraction of baseline seismic data to each monitor shows changed seismic responses related to active reservoir processes.

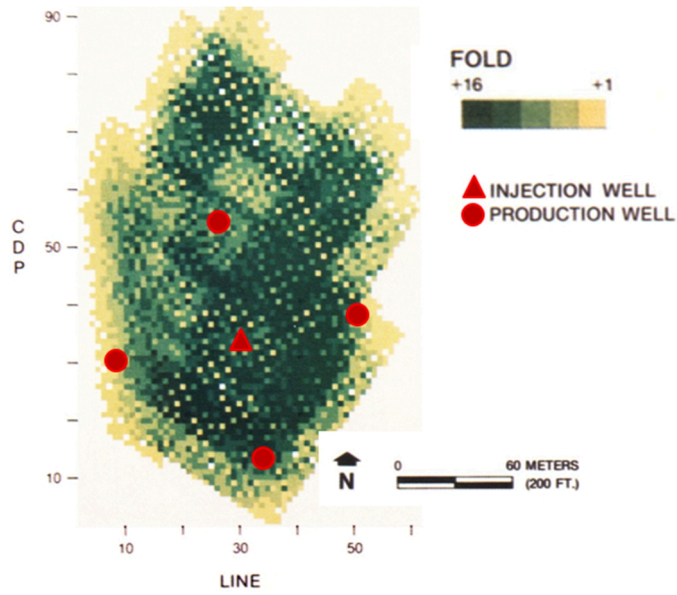


Figure 20: CDP fold distribution of the seismic surveys. Each CDP bin covers a 3 by 3 meters area. From Greaves and Fulp, (1987).

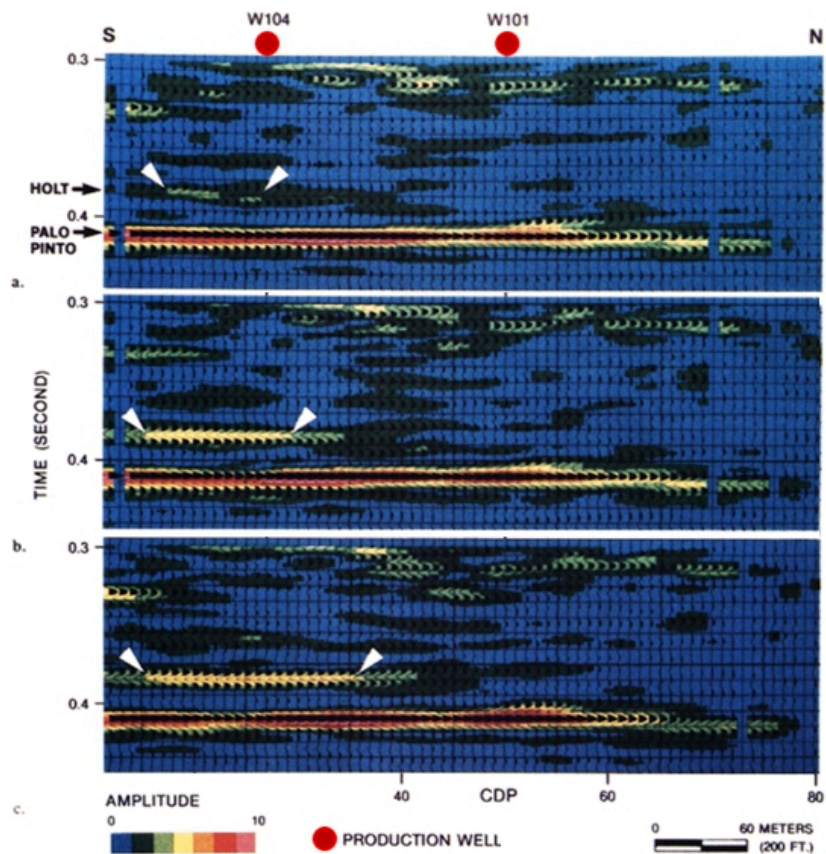


Figure 21: The evolution of the seismic response: pre-burn stage (top), mid-burn stage (middle) and post-burn stage (bottom). A color scale representing the envelope amplitude overlies the reflection wiggle traces. A bright spot was created at the top of the Holt sandstone at the mid-burn stage. From Greaves and Fulp, (1987).

### 2.4.2 Carbonates 4D pilot (Abu Dhabi)

There are only a few examples of 4D studies in the Middle East. Two reasons at least may explain this. First, the stress sensitivity of the carbonate rocks is known to be less than the one of the clastic rocks (Kleiss et al., 2000; Sun et al., 2006; Vega et al., 2007; Chen et al., 2008; Sharma et al., 2013). Second, subsurface conditions including weathering layers heterogeneities and climatic changes affecting it, may be such that achieving an acceptable repeatability remains difficult with conventional seismic. Despite of this, Soroka et al., (2005) and Al-Jenaibi et al., (2006) describe a 4D pilot conducted by ADCO from an onshore upper Cretaceous carbonate field in Abu Dhabi. The main objective of the 4D pilot was to determine whether saturation changes could be observed in carbonates reservoir (Figure 22).

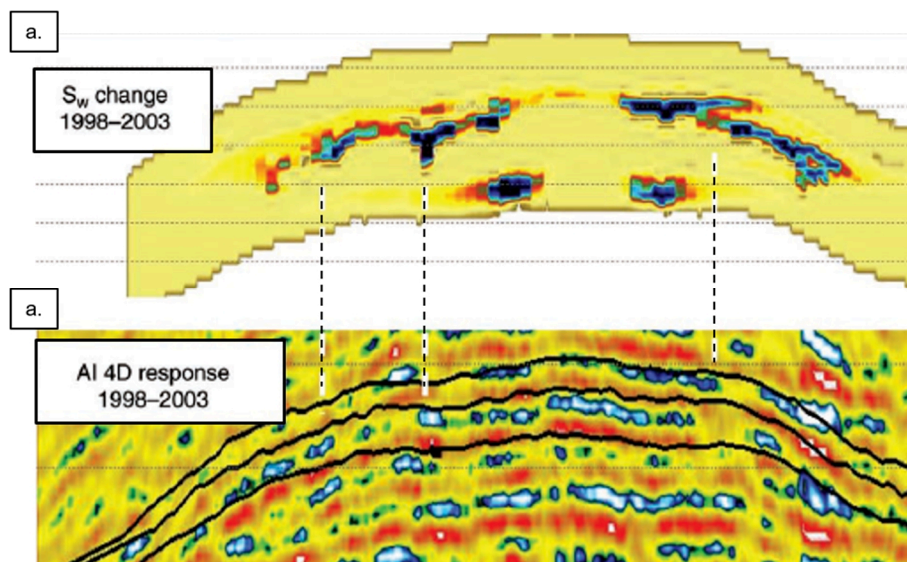


Figure 22: Acoustic impedance (bottom) compared with the saturation changes in the simulation model (top), showing some example of good agreement. From Al-Jenaibi et al., (2006).

The field selected for the 4D pilot covers an onshore area of 12 by 30 km in a sand dune and sabkha surface environment. The reservoir is Cretaceous and is at an approximate depth of 2400 m, with a thickness of 50 m. A detailed description of the Cretaceous interval in that region can be found in Strohmenger et al., (2006). Efforts were made to repeat the original base survey as closely as possible. Only the source sweep length changes between the base (16 seconds) and the monitor (8 seconds). Some original source and receiver position have not been repeated because of new surface infrastructures created during the project.

### 2.4.3 Fazenda Alvorada (Brazil)

Schinelli et al., (2006) describe a challenging 4D pilot conducted in the field of Fazenda Alvorada for steam-assisted EOR. The field was discovered in 1984 in the Northeast compartment of the Reconcavo Basin. It is formed by three sloping blocks separated by SE-NW normal faults. The main oil reservoirs consist of sandstones belonging to the Agua Grande, Itaparica and Sergi formations. The baseline survey was acquired in September 1995 using light explosives sources (150 g) and geophones both superficially buried at 6 m depth. The first seismic campaign was initially planned to be recorded two months before the start of the steam injection. Unfortunately, the injection started more than 4 years after the baseline acquisition for operational and equipment reasons. The monitor seismic was performed a year later in December 2000. Schinelli et al., (2006) observe quite large differences between the two raw record dataset (Figure 23) and believe that some of them may be related with variations on surface conditions or operational procedures.

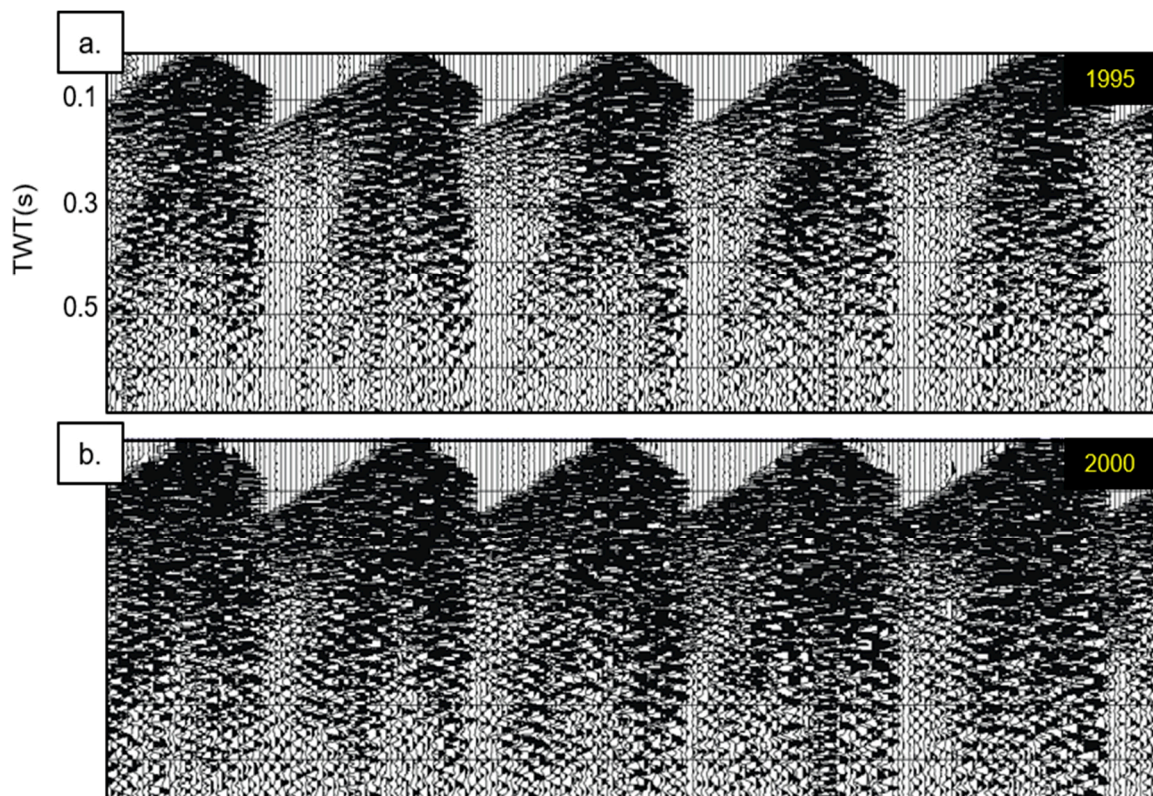


Figure 23: Group of records from the base (above) and monitor (below) surveys. Notice the difference in the signal-to-noise ratio, ground roll and energy. From Schinelli et al., (2006).

#### 2.4.4 Ratqa (North Kuwait)

El-Emam et al., (2018) describe a successful case study conducted in Ratqa for shallow heavy oil reservoir in North Kuwait (the average depth of the reservoir is between 100 and 225 m). The reservoirs consist of multiple individual layers deposited in a fluvial environment (unconsolidated, alternating sandstones, clays and silts). Cyclic Steam Stimulation (CSS) is used to enhance the oil recovery. The 4D study consisted of a baseline survey and a monitor survey separated by 39 days. Simultaneous acquisition of surface seismic and a 3D VSP enables the calibration of the 4D surface seismic for inversion and reservoir characterization. Due to the shallow target, the acquisition geometry was very dense with a staggered 8 m by 8 m source grid and an 8 m by 4 m receiver grid. This results in a 2 m by 2 m bin size with a nominal fold of 968. A viscoelastic fluid substitution model was therefore implemented, and the frequency dependent rock physics model was then calibrated to Pressure Volume Temperature (PVT) data, elastic properties of well logs, VSP, and seismic data at selective frequencies. The rock physics model developed for heavy oil can translate the acoustic impedance variation into seismically predicted temperature variation at the time of baseline and monitor seismic surveys (Figure 24). The observed seismic anomalies were well correlated to production activities (Bagheri et al., 2018).

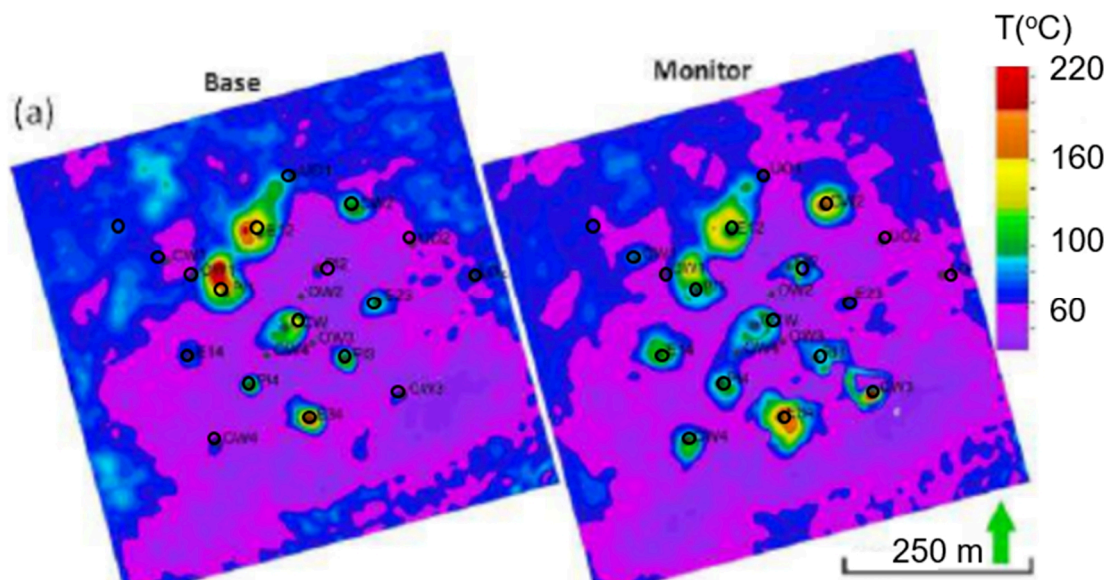


Figure 24: Average, seismically derived temperature maps in the upper sand interval reservoir for the base (left) and for the monitor (right). From El-Emam et al., (2018).

### 2.4.5 Conclusion on the 4D Land case

4D land case studies successes in highlighting substantial reservoir variations occurring on the long term. Rapid and small reservoir changes are still challenging to obtain from the surface since the variations in the weathering near-surface layer can be higher than the ones observed at the reservoir on a daily basis. Moreover, repeating frequent 4D survey would not be feasible in land. This would require having a seismic crew on demand to perform daily surveys. In addition, the extensive surface infrastructure and operations around operating fields would interfere with the seismic acquisitions. In the next part, we will describe a system that is suitable for the detection of rapid and small reservoir changes: SeisMovie.

## 2.5 Onshore continuous seismic monitoring: SeisMovie

In order to achieve frequent or even continuous reservoir monitoring onshore, CGG has developed, in collaboration with Gaz de France (now ENGIE) and Institut Français du Pétrole, a solution based on sparse and permanent sources and buried receivers: SeisMovie (Meunier et al., 2001). The SeisMovie system was initially designed for geological gas-storage applications (Mari et al., 2011) that require frequent and accurate observation to follow the gas saturation and to map the extent of the gas bubble during storage operations. Since then, numerous SeisMovie projects have been conducted in the last decades with different applications such as IOR (Improved Oil Recovery) and EOR (Enhanced Oil Recovery) monitoring (Table 3).

Table 3: Chronology of the SeisMovie projects

<b>Project</b>	<b>Country</b>	<b>Company</b>	<b>Year</b>	<b>Source</b>	<b>Src Nb</b>	<b>comment</b>
Cere la ronde	France	Gaz-de-France	2000	surface	1	Pilot
Saint Clair	France	Gaz-de-France	2004	buried/surface	2	Pilot
Surmont	Canada	Total ConocoPhillips	2006	buried	1	EOR SAGD
Peace River	Canada	Shell	2009	buried	9	EOR SAGD
Miranga	Brazil	Petrobras	2011	buried	2	Pilot
Schoonebeek 2D	The Netherland	Shell	2012	buried	12	EOR GASD
Uthmaniya	Saudi	Saudi Aramco	2012	buried/surface	2	Pilot
Schoonebeek 3D	The Netherland	Shell	2014	buried	36	EOR GASD
Peace River	Canada	Shell	2015	buried	49	EOR GASD

The system has progressively evolved from surface to buried sources and receivers. A major step in this evolution was the introduction of a patented buried piezoelectric dipole source (Meunier, 2004). The piezoelectric source is well suited for permanent installation and has a very stable source signature that further contributes to the repeatability of the system (Figure 25).

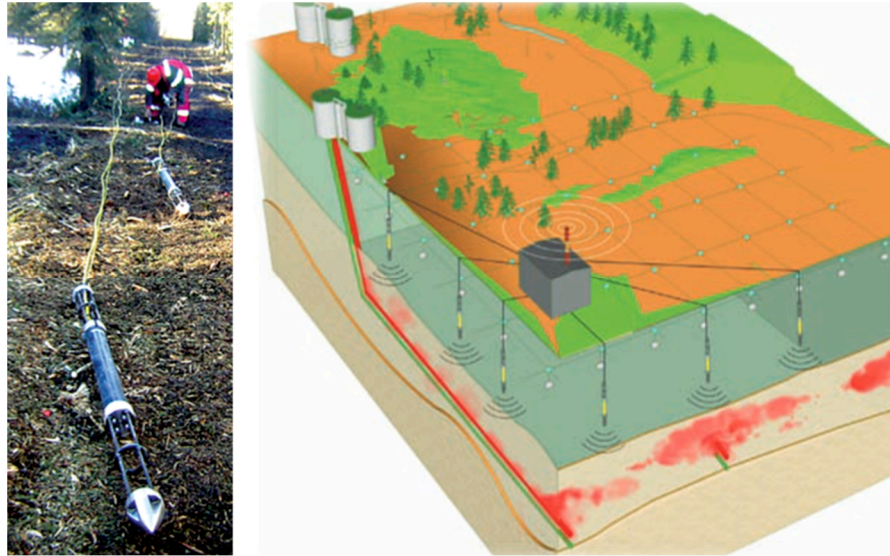


Figure 25: SeisMovie piezoelectric sources (left). A schematic SeisMovie installation for a SAGD heavy oil production operation (right). Buried piezo-electric sources are shown in yellow along with a network of buried receiver arrays. The autonomous system works 24 hrs a day, recording and pre-processing data on site before transmitting it back to the office for analysis. (Courtesy of CGG)

Using a permanent buried installation ensures excellent 4D repeatability and coupling. By placing both the sources and sensors below the weathering layer, SeisMovie eliminates near-surface variations. These features enable the system to provide unparalleled sensitivity and capture small and rapid reservoir variations, which conventional 4D techniques fail to resolve.

*“Continuous 4D seismic data have been acquired at Pad 31 in Peace River since Q2 of 2014. The 4D data quality are exceptional and have demonstrated the capability to detect production effects having signals that are much weaker than most thermal EOR signals. This indicates sufficient sensitivity for onshore monitoring of non-thermal EOR techniques such as chemical and water flooding. The data suggest significant modifications to reservoir management procedures.”*

*La folett, Jon R. (SHELL Int. E&P Inc.), 2015.*

### 2.5.1 Peace River PAD32 continuous seismic monitoring (Canada)

Shell's first deployment of SeisMovie technology took place in 2009 in Peace River (Alberta), where one-half of a production Pad 32 was monitored. The system comprised nine buried SeisMovie sources and an array of buried geophones. The recording operated during 90 days as expected. During the recording, steam injection and oil production were ongoing. For this project, [Forgues et al., \(2011\)](#) describe the simultaneous measurement of both the seismic signal (active part) and the microseismic events (passive part). Data processing was challenging because of time varying ghost causing negative time shifts (blue) in the South of the survey (Figure 26). Even though time-lapse reservoir-related variations were observed near the injector in the North, they could not be compared quantitatively against other deployed seismic methods. Key insights of this project were: first, strong enough time-varying ghosts affected the primary 4D signal, especially in the south part, second, a better data quality can be achieved using buried hydrophones, compared to geophones ([Forgues and Schisselé, 2010](#)). The detailed case study is available in the appendixes.

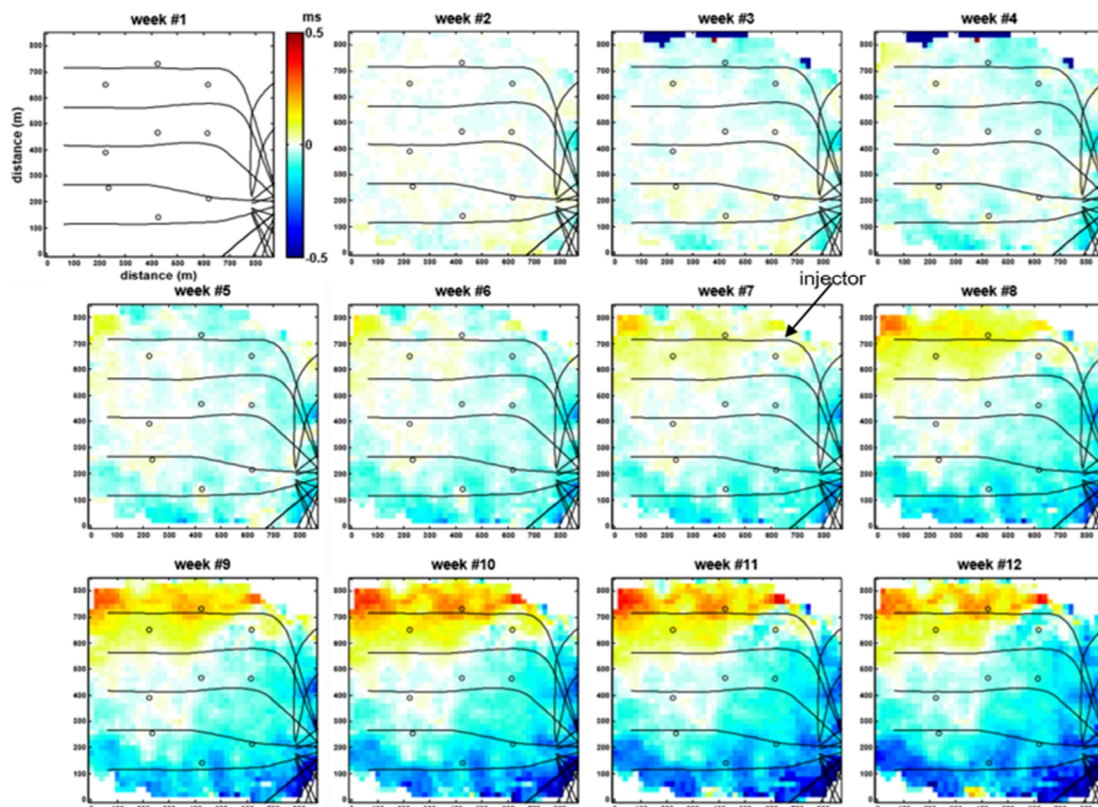


Figure 26: Location of Peace River (top). Weekly 4D time-shifts below the reservoir (bottom). The steam is injected in the northern well. [From Forgues et al., \(2011\)](#).

### 2.5.2 Schoonebeek continuous seismic monitoring (The Netherlands)

The Schoonebeek viscous oil field has a STOIP (Stock-Tank Oil Initially in Place) of 1-bln barrels. It is situated in the northeast of The Netherlands. The sandstone reservoir is about 20 m thick at about 650 m depth with a porosity of 30%. After 50 years of cold production, the field has entered a second phase of development using thermal EOR (steam injection). A Gravity-Assisted Steam Drive (GASD) technique ensures the oil (19% wax) recovery using horizontal injectors and producers.

The technical objective of the SeisMovie project was to establish whether changes in the reservoir can be monitored and if so to determine the lateral extent and the thickness of the steam chest. The swath is located above and perpendicular to an injector well, two producer wells and two observations wells. After a successful yearlong 2D permanent seismic reservoir monitoring trial (Hornman and Van Popta, 2012), a 3D swath of SeisMovie sources and detectors was installed, with a subsurface coverage of 800 m x 160 m. The fold was very low with a maximum of eight in the area of injection (Figure 27).

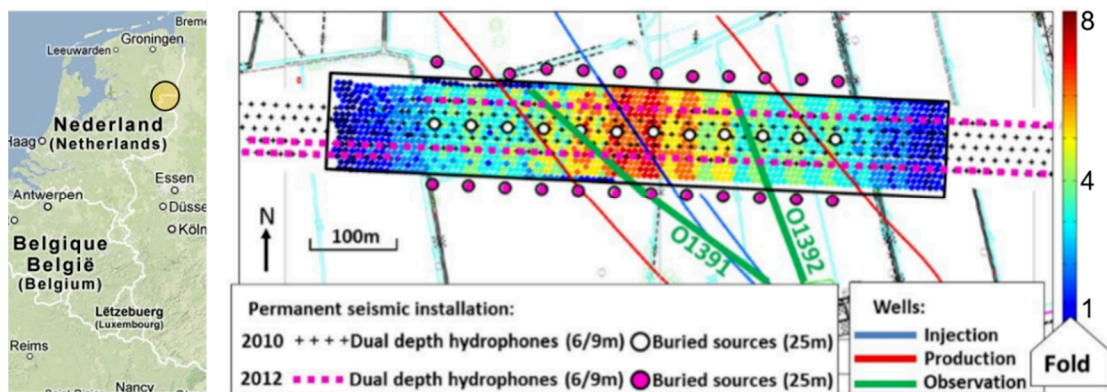


Figure 27: Schoonebeek location (left). Map showing the equipment procured for both the initial 2010 2D survey and added in 2012 to enable 3D monitoring (right). The coloured dots represent the imaging bins with the associated fold. From Cotton et al., (2013).

The dominant problems for onshore time-lapse are caused by near-surface variations between base and monitor surveys (Pevzner, 2011) so there is a need for a specific processing strategy (Chapter 3). By removing both the seasonally varying source and receiver-ghosts (Cotton and Forgues, 2012). It was then possible to follow the expansion of the steam/heat front with unprecedented detail. The detection of small and rapid changes is definitively challenging in 4D land. Thanks to an appropriate

deghosting strategy that will be detailed in Chapter 3, Cotton et al., (2013) show that the very high sensitivity of the SeisMovie system allows for the detection and mapping of weak changes within the reservoir on a daily basis as illustrated in Figure 28 (6  $\mu$ s time shift and a 0.1% amplitude variation per day). The values obtained from seismic monitoring fit the pressure variations measured at observation and production wells assisting engineers to assess 3D reservoir changes beyond the restricted monitoring well 1D windows. The detailed case study is available in the appendixes. Michou et al., (2013) and Zwartjes et al., (2015) performed 4D inversion on both the continuous 2D and 3D seismic monitoring data in order to quantify the lateral and vertical expansion of the steam chest on a daily basis. 4D inversion results not only point out that the inversion enables to quantify the 4D effects in terms of P-impedance variations, but also greatly improves the vertical location of these events.

*“By taking measures in acquisition and processing (see Chapter 3), time shifts can be measured from surface with a precision and accuracy of a fraction of a millisecond, corresponding with pressure changes of less than 10 bars.”*

*J.C. Hornmann (SHELL Global solutions int.), 2012.*

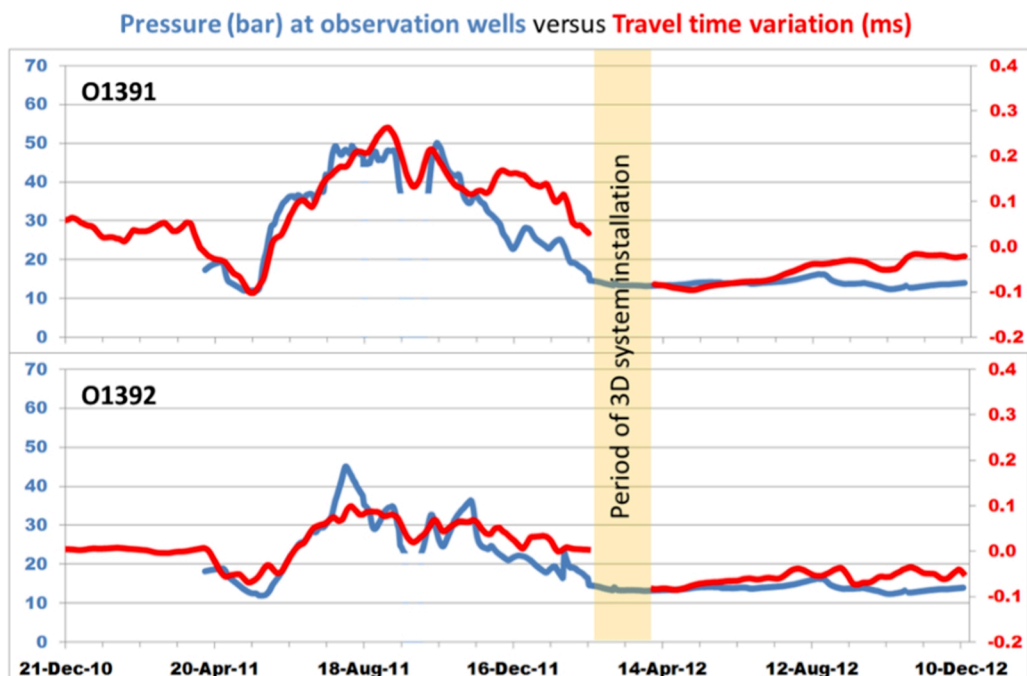


Figure 28: Comparison of travel time variations and pressure measured at both observation wells O1391 on the west (top graph) and O1392 on the west (bottom graph). From Cotton et al. (2013).

### 2.5.3 Peace River 2015 (Canada)

Shell's largest onshore PRM to date was installed in the beginning of 2014 at Peace River Pad 31 (Lopez et al., 2015). The system covers a full pad and operates without interruption for 2 years since May 2014. Peace River Pad 31 was originally drilled in 2001 as a collection of tuning-fork horizontal wells for Cyclic Steam Stimulation (CSS).

After six CSS cycles, the pad was converted to a horizontal steam drive, where alternating wells inject while the others produce. During the seismic monitoring, a new production scheme was tested. Six new horizontal wells were drilled at the top of the reservoir for steam injection. The previously installed other wells were all used for production. The SeisMovie system has been monitoring "cold" production for five months. Then, steam injection started by the end of 2014 (Figure 29) and was accurately detected (Figure 30).

The Pad 31 system comprises 49 SeisMovie source locations and approximately 1500 hydrophone locations. Five of the source locations and 49 of the receiver locations contain vertical source/detector arrays for seasonally varying ghost reduction. The processing workflow has been automated for daily delivery (Berron et al., 2015), although much work continues on the workflow to reduce noise and boost signal. The detailed case study is available in the appendixes.

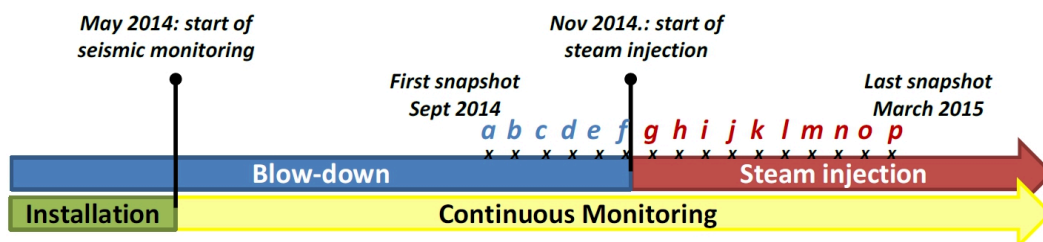


Figure 29: Calendar time line of reservoir production in Peace River 31. From Berron et al. (2015).

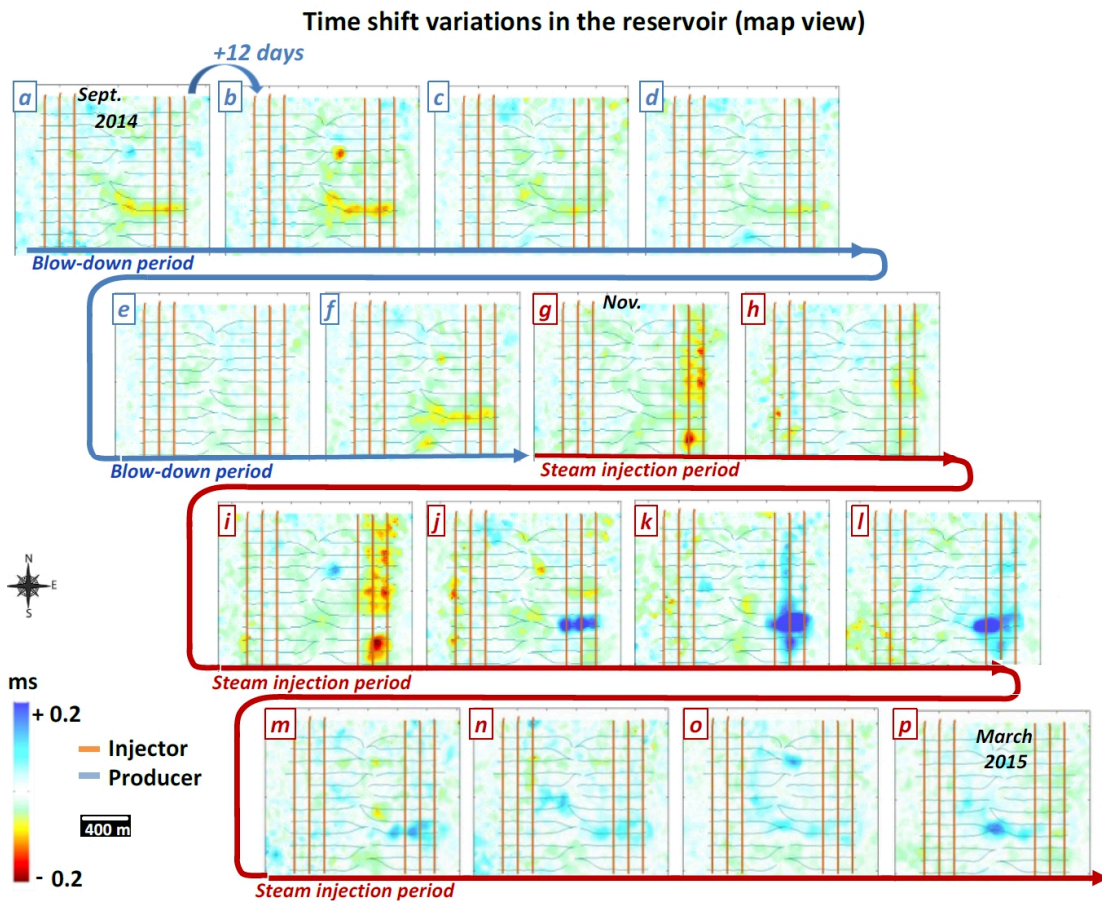


Figure 30: Time shift variations at reservoir level over seven months. Snapshots are taken every 12 days. Baseline is sliding and is taken 12 days before monitor. From Berron et al., (2015).

#### 2.5.4 Conclusion on continuous land seismic monitoring

4D Land continuous seismic monitoring is highly repeatable as both the receivers and the sources are placed below the weathering layer. This should in principle offer perfect data for detecting 4D effects (Schisselé et al., 2009; Berron et al., 2012; Shulakova et al., 2015). In practice, processing is still needed because part of the emitted signal travels through the weathering layer (Bianchi et al., 2005; Cotton and Forgues, 2012). After a reflection or a conversion near the Earth surface (affected by climatic changes), the ghosts are reverberated, interfering with the primary reflection and ultimately affecting the repeatability and thus the 4D signal.

We will thus focus on the data pre-processing that was required for the detection of small and rapid changes during the continuous-time monitoring (Chapter 3).

## 2.6 Discussion on optimal 4D

Optimal 4D would ideally be repeatable, affordable, versatile, scalable and should help reservoir engineers to take production decisions in real-time. Having a versatile and scalable solution would simplify the operations. An affordable system would reduce the costs and thus would have a direct and calculable financial impact.

The sparse OBC concept, as proposed by [Calvert and Wills, \(2003\)](#), addresses the high up-front costs of a permanent OBC system and the long acquisition and processing turnaround times of both streamer and (high density) permanent OBC 4D surveys. The term “sparse” is used here to indicate a minimal number of receiver sensors on the seafloor and a minimal shooting effort. A sparse monitoring system is based on acquisition and processing of low fold but highly repeatable seismic data. The best possible ray path repeatability is the most essential element of any sparse 4D system.

[Smit et al., \(2006\)](#) tested the concept on the Valhall Field. The purpose was to assess the 4D content of a sparse OBC dataset. The 4D content of both the sparse and the high-density dataset are then compared. At the target level, the nominal fold of the sparse dataset reaches 10 whereas it is more than 400 on high-density data sets. The results of this test shows that a low-fold data set may be acceptable for time-shift measurements (Figure 31).

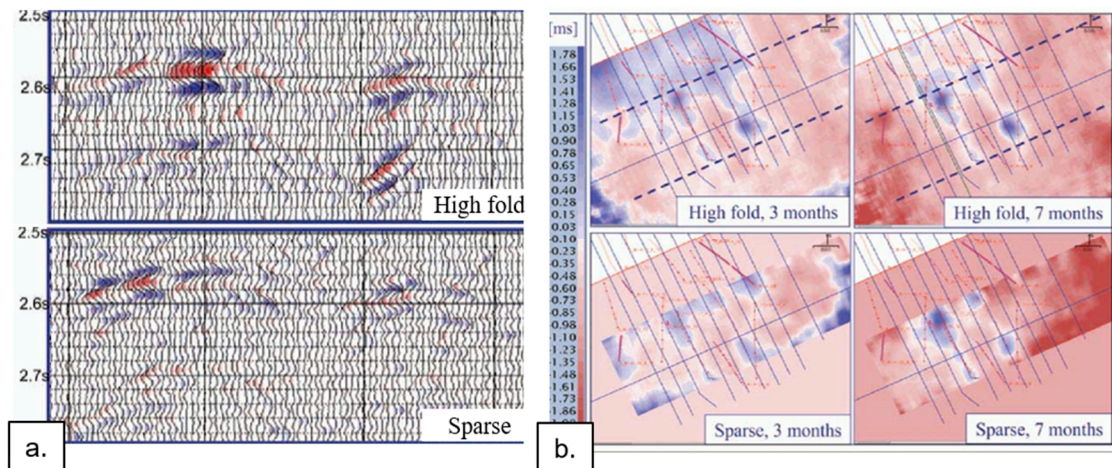


Figure 31: Comparison of 4D amplitudes on sparse and high-fold data, highlighting relative amplitude differences (a). Comparison of 4D time shifts (b) on sparse and high-density data, after three and seven months of production. The dashed lines in the top figures correspond to the areal extent of the sparse data set. [From Smit et al., \(2006\)](#).

Wang and Hatchell, (2013) conducted an interesting study on the effects of receiver density; positioning and repeatability for OBN seismic data acquired in deep water Gulf of Mexico. The results show that although receiver decimation gradually degrades the data quality, 4D noise stays at a relatively low level when the number of receivers is reduced by a factor of two. As a comparison, non-repeated receiver positions make much larger impact on the data quality (Figure 32).

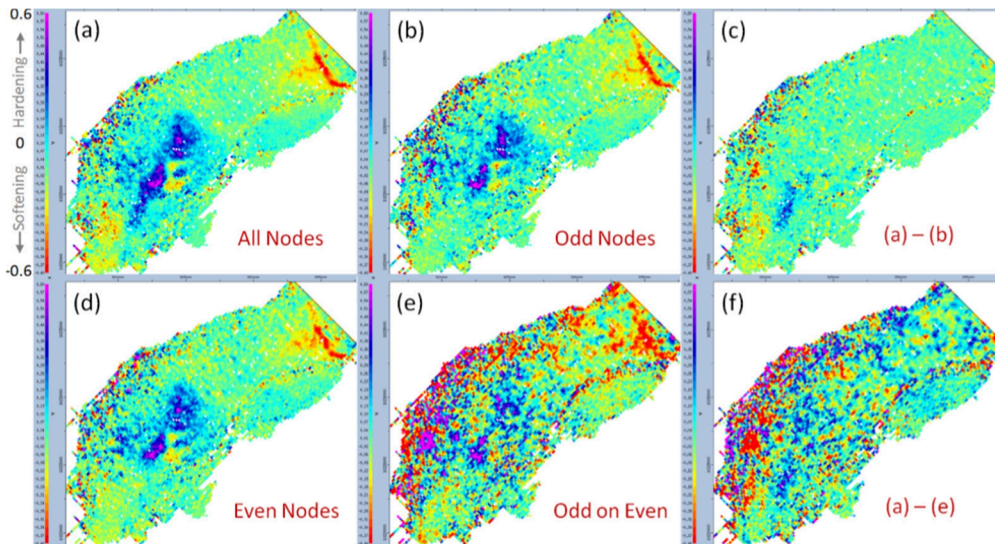


Figure 32: Normalized differential RMS maps calculated using different datasets. From Wang and Hatchell, (2013).

Hatchell et al., (2013) describes the concept of Instantaneous 4D (i4D) which aims at acquiring frequent, short turnaround and low-cost 4D survey to target a particular injection well (Figure 33). The concept enables monitoring of fast reservoir changes such as those occurring near water injection wells. The i4D does not replace conventional full-field 4D monitoring but is rather designed to fill in the interval between long-term conventional surveys and short-term monitoring needs (Figure 34).

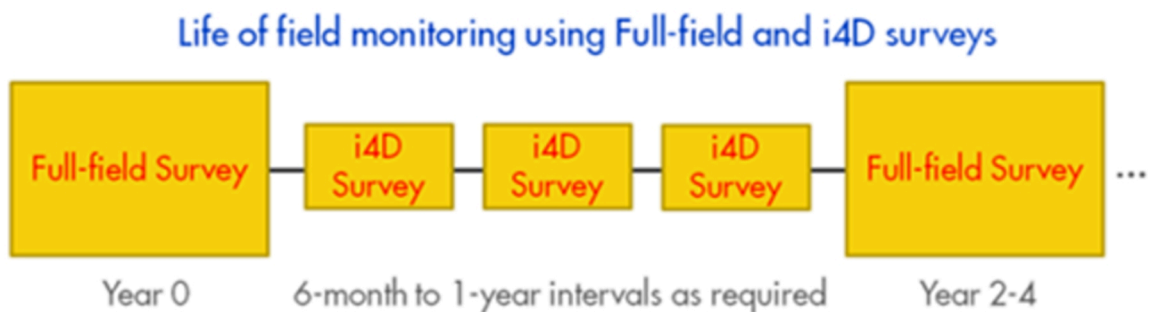


Figure 33: The concept of i4D. From Hatchell et al., (2013).

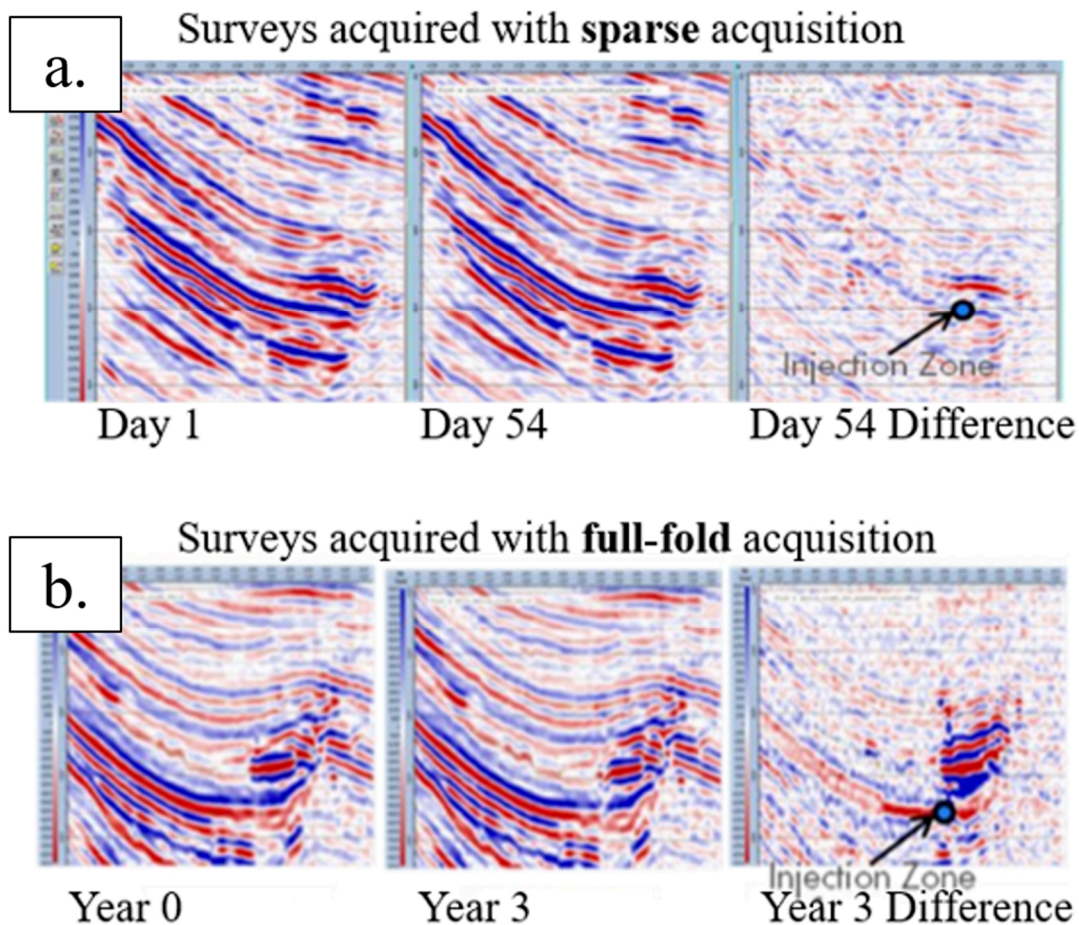


Figure 34: 4D data acquired over a water injection well using a sparse acquisition system using 16 OBN and 8 shot lines (a). 4D data acquired over the same water injection well using the full-fold OBN surveys acquired 3 years apart (b). [From Hatchell et al., \(2013\)](#).

We conduct decimation tests on the Schoonebeek case study introduced in the paragraph 2.5.2 in order to assess if reliable 4D attributes (time-shift and amplitude variation) would have been detected with a sparser SeisMovie survey design. Note that with only 36 sources positions, 333 receivers positions and a maximum fold of 8 (Figure 27), the original SeisMovie design is already sparse; nevertheless, a sparser acquisition appears interesting as it would reduce drastically the project costs (drilling, equipment). Figure 35 illustrates the decimation tests conducted on the Schoonebeek project. Note that the decimation tests are done subsequently on the fully processed dataset (processing described in Chapter 3) using the design illustrated in (Figure 35a). If the processing steps were done independently (each from input raw decimated dataset), then the results may have been even more degraded.

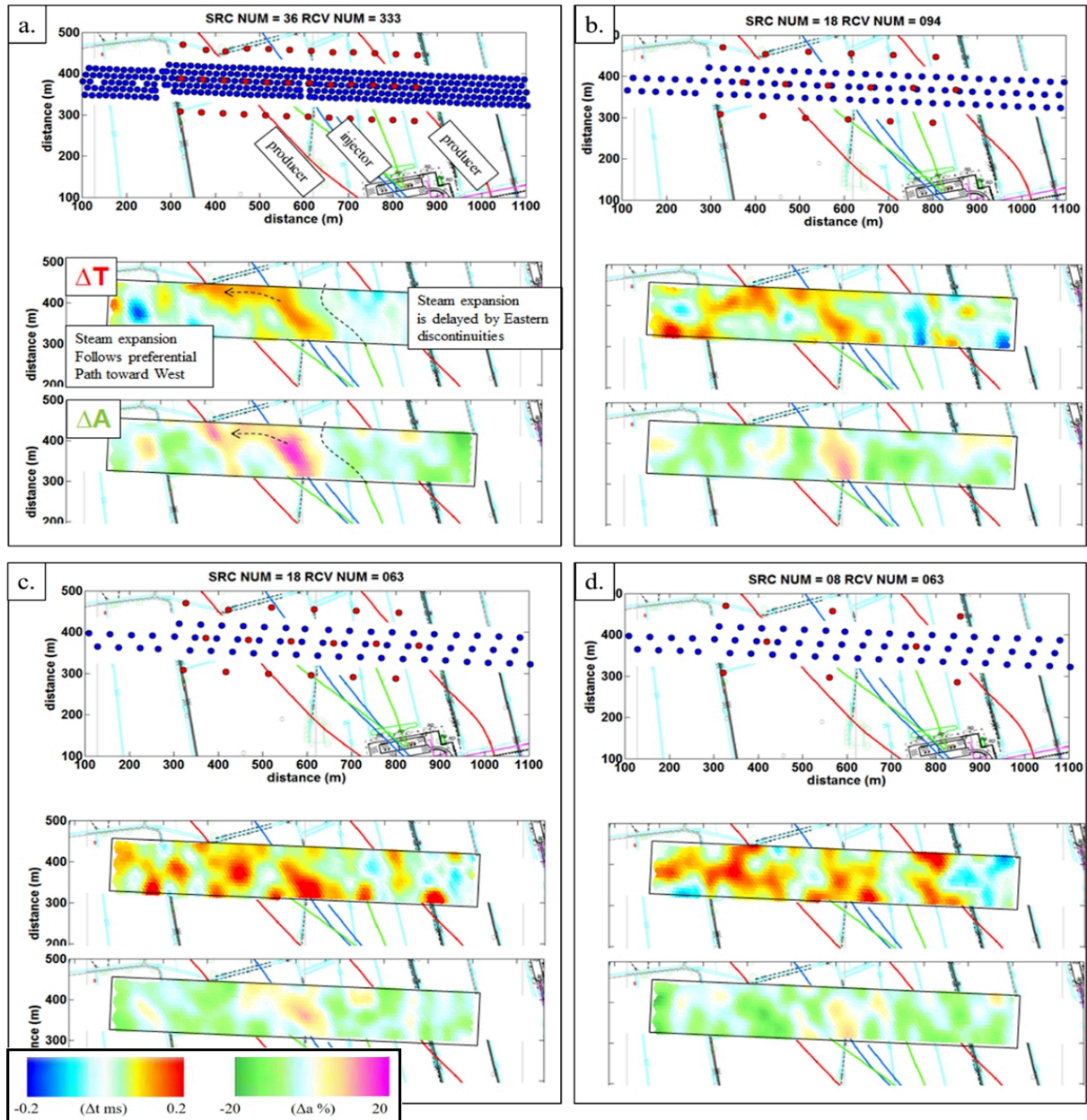


Figure 35: Decimation tests conduct on the Schoonebeek project. The original monitoring survey design (a) with the time-shift and amplitude variations maps. A first decimation test with 2 times less sources and  $\sim 3$  times less sensors (b). A second decimation test with 2 times less sources and  $\sim 5$  times less sensors (c). A third decimation test with only 8 sources and 63 sensors (d).

The decimation tests shows that the interpretation of both the travel time and the amplitude variation becomes difficult with very sparse acquisition design. This is particularly true when looking at small and rapid reservoir variations. Therefore, questions about versatility, flexibility and cost reductions remain open. Moreover, having an affordable, versatile and scalable 4D monitoring would be useless without

repeatability and real-time. Repeatability and real-time are thus essential and fundamental in 4D.

To solve the equation, the industry will probably have to move from conventional sensors to fiber-optic sensing (Hornman et al., 2013; Mateeva et al., 2014). For the near future, we foresee that optimal land 4D will include existing technologies. Among others, a good candidate to optimal Land 4D would be a combination of buried fiber-optic cables and permanent SeisMovie sources (or like) to follow rapid and low amplitude variations on a daily/weekly basis. In addition, on-demand surface “dense carpet-shooting” and the virtual source method (Bakulin et al., 2007) could be performed to monitor longer-term reservoir variations as well as background velocity and seismic horizons calibration.

## 2.7 Conclusion

Considering factors affecting the repeatability, acquisition and geometry differences may be among the most challenging. Up to the 2000’s, most of the marine 4D surveys have been performed using streamers while it is now established that it is the least suitable technique for 4D application. The main problem with streamer 4D acquisition (dynamic conditions) is overcome using fixed receivers. With Permanent Reservoir Monitoring (PRM), the geometry problems are fixed on the receiver side and the repositioning of the source becomes the remaining weakest link. Even if PRM has never totally replace streamer 4D acquisition, the PRM market has rapidly extended worldwide almost immediately after the first pilots.

Replicating survey-to-survey source and receiver positions is not that challenging in 4D Land. In appearances, ones could think that 4D land operations would be much easier to achieve. This would be true forgetting anything about the near surface variations as well as both the source and the sensor ground coupling. Indeed, subsurface conditions including weathering layers heterogeneities and climatic changes affecting it, may be such that achieving an acceptable repeatability remains difficult with conventional seismic.

To increase sensitivity and therefore applicability of seismic monitoring to a broad range of IOR/EOR methods any many environments, the seismic sources and

detectors should be operated below the changing near surface and strategies must be envisaged to suppress the time-varying ghosts that contaminate the time-lapse signals (Chapter 3).

Beyond exploration, the most important role for geophysics in the oil and gas industry is to influence field operations, so that the value of existing assets is fully realized. The recent trend in time-lapse seismic has been toward very frequent reservoir monitoring and real-time processing workflows, with the aspiration to optimize both near- and long-term field management. Long-term management does not actually need real-time processing like near-term does. In order to influence production decisions, advanced 4D attributes like P-velocity and impedance variation should indeed be computed and communicated rapidly with reservoir engineers (Chapter 4).

Finally, the previous discussion about real-time processing and decision will introduce a more general context. Indeed, 2D and 3D projects have some conceptual similarities with 4D projects: like the 4D geophysicist compare the monitor with the reference baseline, the field geophysicist compare the newly acquired shot-point to a reference one. In the last part (Chapter 5), we will describe a brand new approach called TeraMig (Cotton *et al.*, 2016) for automated field quality control in the migrated domain.



### 3. Deghosting of continuous-time seismic data

---

Les réservoirs non conventionnels demandent des efforts de production particuliers pour extraire les hydrocarbures. Ces réservoirs d’huiles lourdes, moins fluides, ne peuvent pas être produits uniquement en utilisant des pompes classiques telles que celles largement utilisées au Moyen Orient par exemple. Pour exploiter les huiles lourdes, les compagnies pétrolières ont recours à l’injection de vapeur. La vapeur injectée dans le réservoir réchauffe l’huile lourde et augmente ainsi sa fluidité, facilitant finalement la production. La génération de vapeur et son injection dans le réservoir représentent une source de coûts significative et nécessitent une attention particulière afin d’éviter des fuites vers la surface ou des connections entre puits injecteurs et puits producteurs. Dans ce contexte de production, le réservoir et les fluides injectés dans les couches géologiques peuvent évoluer rapidement. Il est donc souhaitable de surveiller les effets de la production de manière beaucoup plus fréquente qu’en sismique 4D conventionnelle : on parle d’une acquisition par jour voire même d’une acquisition toutes les 6 heures. Il s’agit alors de sismique 4D continue.

Un système de surveillance continue a été installé pour Shell dans le nord-est des Pays-Bas afin d'étudier l'évolution d'un réservoir pendant la phase d'injection de vapeur. Le système consiste en un ensemble de sources et de capteurs enterrés sous la couche superficielle pour s'affranchir des variations de surface (saisonnalité, météorologie, cycle diurne-nocturne) et minimiser l'empreinte environnementale. Ainsi, le système devrait en principe offrir des données parfaitement répétables.

Toutefois, une partie du champs d'ondes émis est transmise vers la couche superficielle. Après une réflexion ou une conversion au voisinage de la surface, ces ondes, les « fantômes », interfèrent avec les réflexions primaires issues du réservoir. On enregistre donc une combinaison d'ondes d'origine différentes : les primaires, portant l'information de l'évolution du réservoir et les « fantômes », dont les fluctuations sont liées aux variations de proche surface. La séparation des primaires et des « fantômes » est donc essentielle pour assurer la fiabilité de la surveillance.

En mettant en œuvre une stratégie de séparation appropriée, les réflexions primaires ont pu être isolées et des variations de temps de trajet ont été mesurées avec une précision d'une fraction de milliseconde, correspondant à des variations de pression au réservoir inférieures à 10 bars. Ainsi, le système d'acquisition permanent a permis de suivre de très petites variations des propriétés physiques du réservoir dans les domaines spatial et calendaire.

### 3.1 Introduction

The reduction of ghost waves is one of the main challenges in marine seismic as any free-surface reflections (water-air interface) reverse the polarity of the P-waves. The reverberation creates notches in the frequency spectrum and thus degrades significantly the data quality and resolution. Since the mid 1980's, numerous efforts were conducted to reduce the ghost both at the acquisition and at the processing stages. On the receiver side, [Parrack \(1976\)](#) introduces early the over/under streamer method (using two levels of pressure sensor). [Berni \(1985\)](#) and [Robertsson et al. \(2004\)](#) study and patented the combination of pressure and vertical particle motion sensors in streamer. [Soubaras and Dowle \(2010\)](#) proposed another approach with variable depth streamers. On the source side, multiple-level airguns ([Egan et al., 2007](#); [Cambois et al., 2009](#)) and synchronization ([Sablon et al., 2013](#)) concepts were also intensely studied.

Onshore, the ghost is almost inexistent in surface 2D/3D seismic. However, it becomes an issue when either the sources or the sensors are buried below the Earth surface. As an example, [Balch et al. \(1982\)](#) describes some near-surface reverberations and ghost effects occurring in Vertical Seismic Profile (VSP) data. Recently, a new type of acquisition has been proposed, where both sources and receivers are buried ([Meunier et al., 2001](#); [Forgues et al., 2006](#); [Hornman et al., 2012](#)). This should in principle offer perfect data for detecting 4D effects ([Schisselé et al., 2009](#); [Berron et al., 2012](#); [Shulakova et al., 2015](#)). In practice, processing is still needed because a part of the emitted signal travels through the weathering layer ([Bianchi et al., 2005](#); [Cotton and Forgues, 2012](#)). After a reflection or a conversion near the Earth surface (affected by climatic changes), the ghosts are reverberated, interfering with the primary reflection and ultimately affecting the repeatability and thus the 4D signal.

Based on marine concepts, several ways can be investigated to reduce the ghost in permanent buried acquisition. On the receiver side, we could either use dual sensors at the same location (geophone and hydrophone) or use the concept of multi-level sensors and sources. Those concepts have some weaknesses: it involves the multiplication of the equipment; it has a non-negligible impact on the drilling operations as well as on the logistic (storage, transport). To counterbalance this, we propose a deghosting methodology that takes advantages of the high redundancy in the time-lapse dimension. The full deghosting becomes possible having only a few vertical arrays distributed over the permanent acquisition spread.

We first detail the steam injection monitoring experiment performed in Schoonebeek (The Netherlands). We then describe the acquisition design and its particularities. Finally, we will focus on the data pre-processing and particularly on the receiver and source deghosting. We prove that with a careful pre-processing, time shifts can be measured from surface with a precision and accuracy of a fraction of a millisecond, corresponding with pressure changes of less than 10 bars.

### 3.2 Steam injection seismic monitoring in Schoonebeek

The Schoonebeek field is located in the northeast of the Netherlands and is operated by SHELL. With a STOIP (Stock-Tank Oil Initially in Place) of 1 billion bbls, the medium heavy-oil reservoir is about 20 m thick and is located at 650 m depth with an average porosity of 30%. Between 1948 and 1996, the oil (160 cP at 40°C, 25 API, 19% wax) was produced with thermal EOR in vertical wells. Recently, the production strategy has been revised: Gravity-Assisted Steam Drive (GASD) using horizontal injectors and producers have replaced the previous EOR (Enhanced Oil Recovery) production using vertical wells.

Reservoir engineers are interested in knowing how the steam spreads from the injector to the neighbouring producers. The pump rate could then be adjusted to optimize reservoir production. The steam, injected at low pressure, is expected to rise to the top of the reservoir, spread horizontally, and finally condense. Hot water then diffuses downward through the reservoir by gravity, heating the oil and improving its mobility. According to [Hornman et al., \(2012\)](#), a 3-m sub-seismic fault may delay the steam expansion by three years as shown in Figure 36 by an example of asymmetrical steam chest development.

In April 2011, an onshore continuous seismic monitoring system has been installed in order to daily monitor the expansion of the steam chamber. The system operated 24 hours a day and 7 days a week during 21 months from April 2011 to December 2012 (Figure 37).

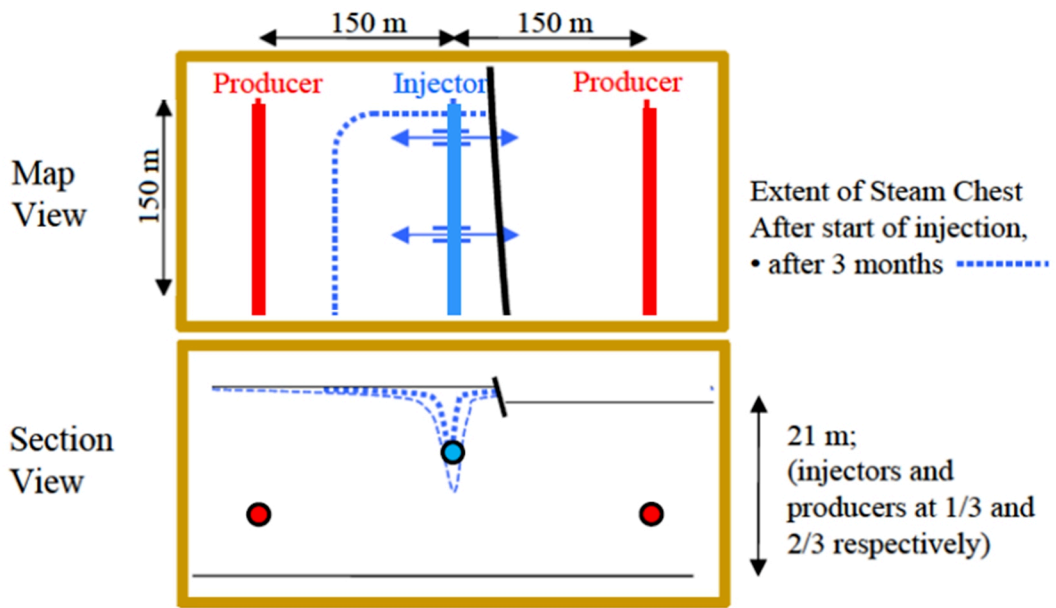


Figure 36: Asymmetric expansions of the steam chest due to the small fault throw. From Hornman et al., (2012).

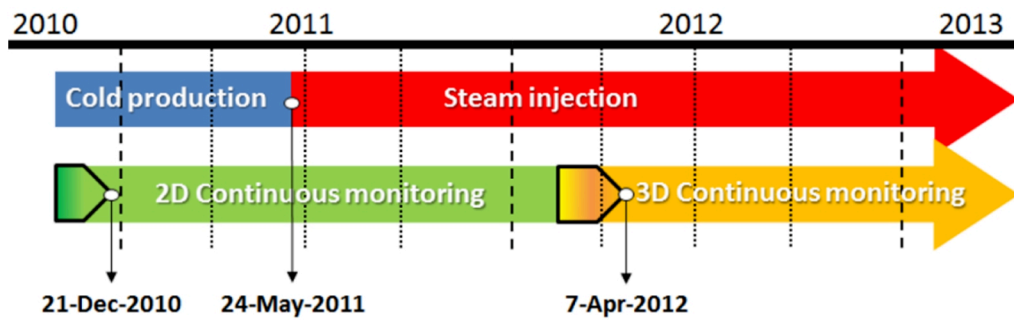


Figure 37: Permanent seismic monitoring time schedule covering the transition period between cold production and steam injection. Black triangles represent the system installation period. The monitoring includes an initial 2D phase that was then extended to 3D.

### 3.3 Acquisition and data quality

A permanent buried monitoring installation ensures excellent seismic repeatability, as well as having a minimum impact on surrounding farming activities and on the environment (Figure 38).



Figure 38: Aerial photos of the monitoring area. Top: Trenches during installation. Bottom: Four months later during continuous monitoring.

The permanent installation consists of 36 piezoelectric seismic sources buried in cemented borehole. The source typical displacement is very small  $16 \mu\text{m}$  and its instantaneous energy as well (36000 J/h). Unlike explosives, the SeisMovie piezoelectric source is highly repeatable because it does not damage the medium in which it is coupled. As a comparison, 1 g of explosive delivers 4000 J. At the end of a day, the energy delivered by the piezoelectric is equivalent to 216 g of explosive.

A detailed description of the piezoelectric source including tests, its evolution and improvement is given in the appendixes.

The signal is recorded by five sensor lines, each comprising 69 sensor positions. At each receiver position, we had two hydrophone at 6 m and at 9 m depth. Geophone were additionally installed at 9 m for the centre receiver line. The emitted signal covers a 5-185 Hz band over six hours. A daily summed shot point is shown in Figure 39. The zero-offset reservoir reflection arrives at 625 milliseconds.

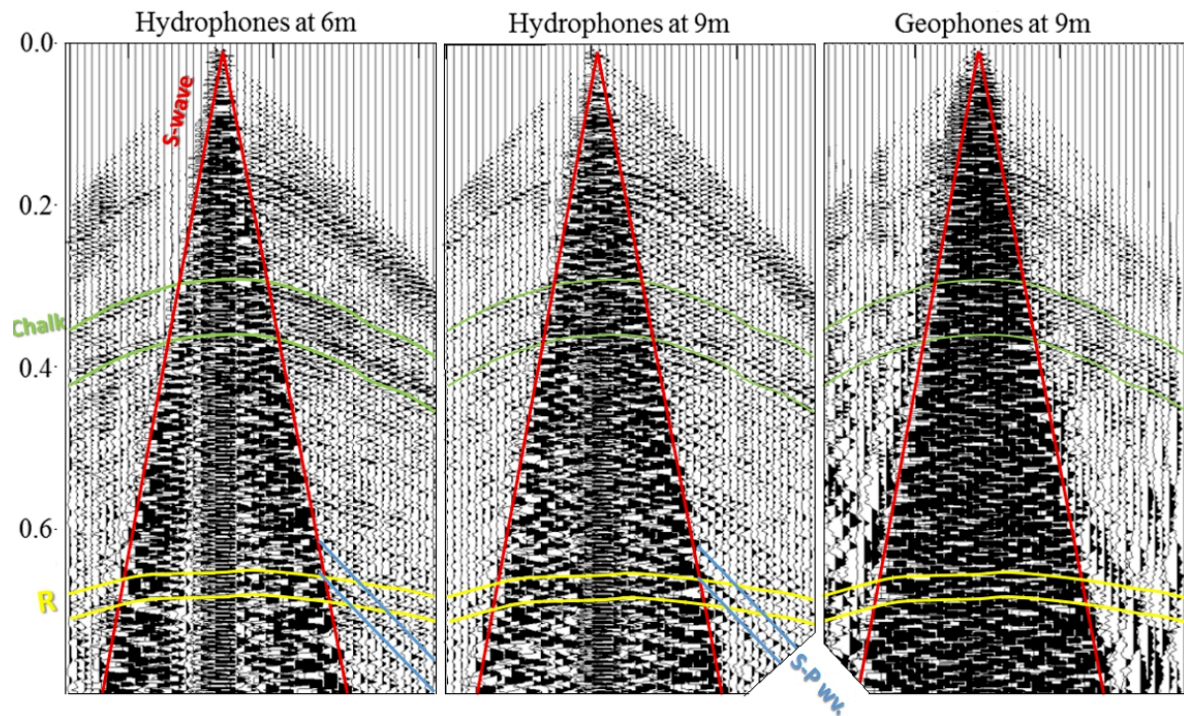


Figure 39: A SeisMovie shot point recorded by 3 sensor lines: hydrophones at 6 m and 9 m depth (left and middle) and geophones at 9 m depth (right). The S-wave (red) is visible on the near offset. The chalk reflection (green) appears at 0.4 s. The reservoir (yellow) is around 0.65 s. S-P converted waves (blue) are visible on the hydrophones only. Geophones are noisier than hydrophones in this application.

The energetic shear wave cone generated by the source hides the near offsets and was consequently muted. As a result, at the reservoir level, the contributing offset extends only from 250 to 800 meters and the stacking fold ranks from 4 to 8 in the useful part of the spread covering the injection and the production wells (Figure 40). This very low fold is counter-balanced by good data quality and high repeatability provided by the buried sources and receivers under the weathering layer.

The permanent monitoring system was located above three horizontal wells: a central injector (in blue) surrounded by two producers (in red). Furthermore, two deviated observation wells (in green) continuously measured the temperature and the pressure at 2 locations within the reservoir level.

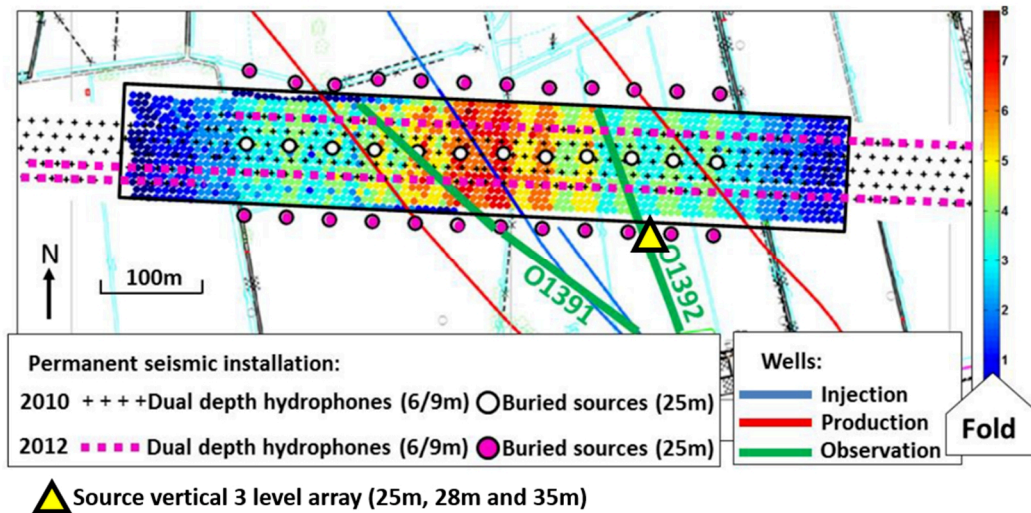


Figure 40: Map showing the equipment used for both the initial 2010 2D survey and its extension in 2012 to enable 3D monitoring. The coloured dots represent the imaging bins with associated fold. Blue line: injector well; Red line: production wells and Green line: observation wells. We have dual depth hydrophones (6 and 9 m) in any sensor positions. Geophones are collocated with hydrophones at 9 m only for the centre receiver line. A 3 level source vertical array (yellow triangle) is located in the southeast of the spread.

### 3.4 Ghost waves in continuous seismic monitoring

We consider the continuous acquisition scheme depicted in Figure 41 that represents a typical source-receiver couple in the case study. For simplification, we consider only three types of wave: the primary waves in green, the receiver ghost in blue and the source ghost in red. The SP converted ghost wave is symbolized by orange line.

On one hand, the primary waves are highly repeatable as they propagate directly downward to the reservoir then upward to the sensor without travelling in the weathering layer. Note that this would not be the case for surface monitoring. On other hand, the propagation of the ghosts that has travelled in the weathering layer is modified by any climatic, seasonal, diurnal and nocturnal changes affecting the weathering layer properties.

We will first discuss the fluctuation of the S-P ghost and propose a way to attenuate it (see paragraph 3.4.1). Then we will detail the receiver ghost attenuation using the two levels of sensors (see paragraph 3.4.2). Finally, we will propose a way to mitigate the source ghost thanks to the high sampling in the calendar time domain (see paragraph 3.4.3).

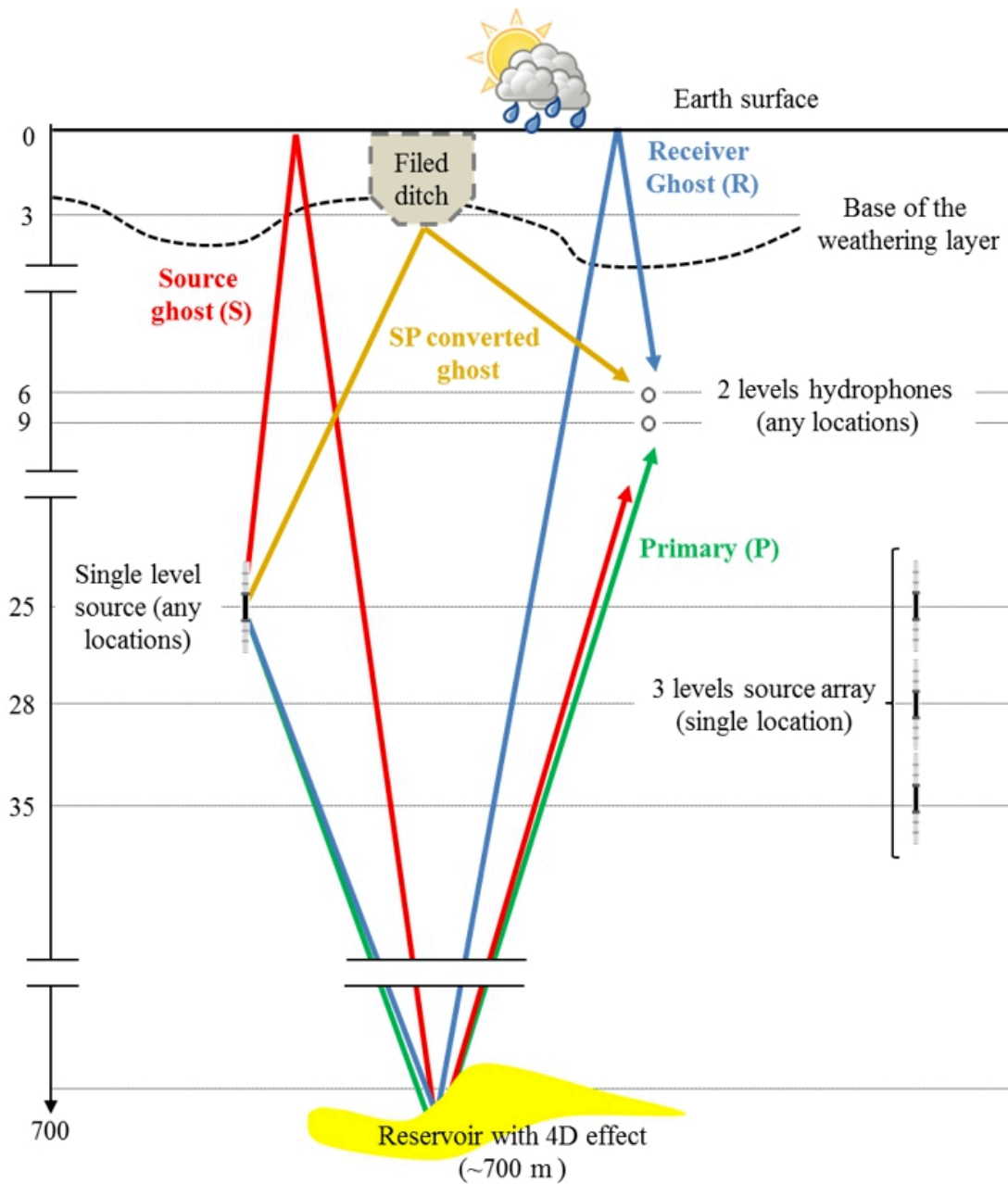


Figure 41: Ghost waves in continuous seismic monitoring: source ghost (red), receiver ghost (blue) and S-P converted ghost (orange). All varying ghosts interfere with the primary waves (green).

### 3.4.1 S-P converted ghost waves

Primary reflections at the reservoir interfere with energetic and low apparent velocity waves interpreted as S-P converted waves (Hornman et al, 2012). S-wave generated by the sources propagate up to the surface and are then converted into P-waves when reaching near-surface heterogeneities (like filled ditches in our case). These waves are then back scattered to the sensors with a quite horizontal incidence. Geophones are less sensitive to those waves compared to hydrophone. In this particular case, it might be due to a complex combination of P-wave particles motions and rays incidences.

S-P converted ghosts fluctuate with respect to seasonal changes (soil moisture, frost and ground temperature) and can be considered as 4D noise for reservoir monitoring. It has been observed that variations of the S-P converted ghost are finely correlated with the surface temperature with values of  $0.2 \text{ ms}/^{\circ}\text{C}$  and  $1.7 \text{ \%}/^{\circ}\text{C}$  for time shift and amplitude respectively (Figure 42).

As the apparent velocity of those waves differs significantly from the one observed for the primary, we use a high-resolution, amplitude preserving radon transform filter (Herrmann et al., 2000) to attenuate it. The filter was applied independently on each daily shot point with the same parameters. The result of the Radon filter is depicted in Figure 43. The S-P ghost waves have a low apparent velocity compared to the primary as illustrated on the NMO corrected shot point. Moreover, those waves fluctuate within the calendar time. This is visible by displaying a recorded trace per day (Calendar trace gather). This is emphasized when looking at the calendar trace variations that is obtained by subtracting a reference trace (the stack of the first week) to each daily traces. On the contrary, we see that the primary chalk reflection is stable.

The variations of the S-P ghost are very high and are correlated with the surface temperature ( $0.2 \text{ ms}/^{\circ}\text{C}$ ). By comparison, the reservoir variations are less than a fraction of a millisecond, corresponding with pressure changes of less than 10 bars (see paragraph 3.6). Without the attenuation of the S-P, the monitoring would have been invalid.

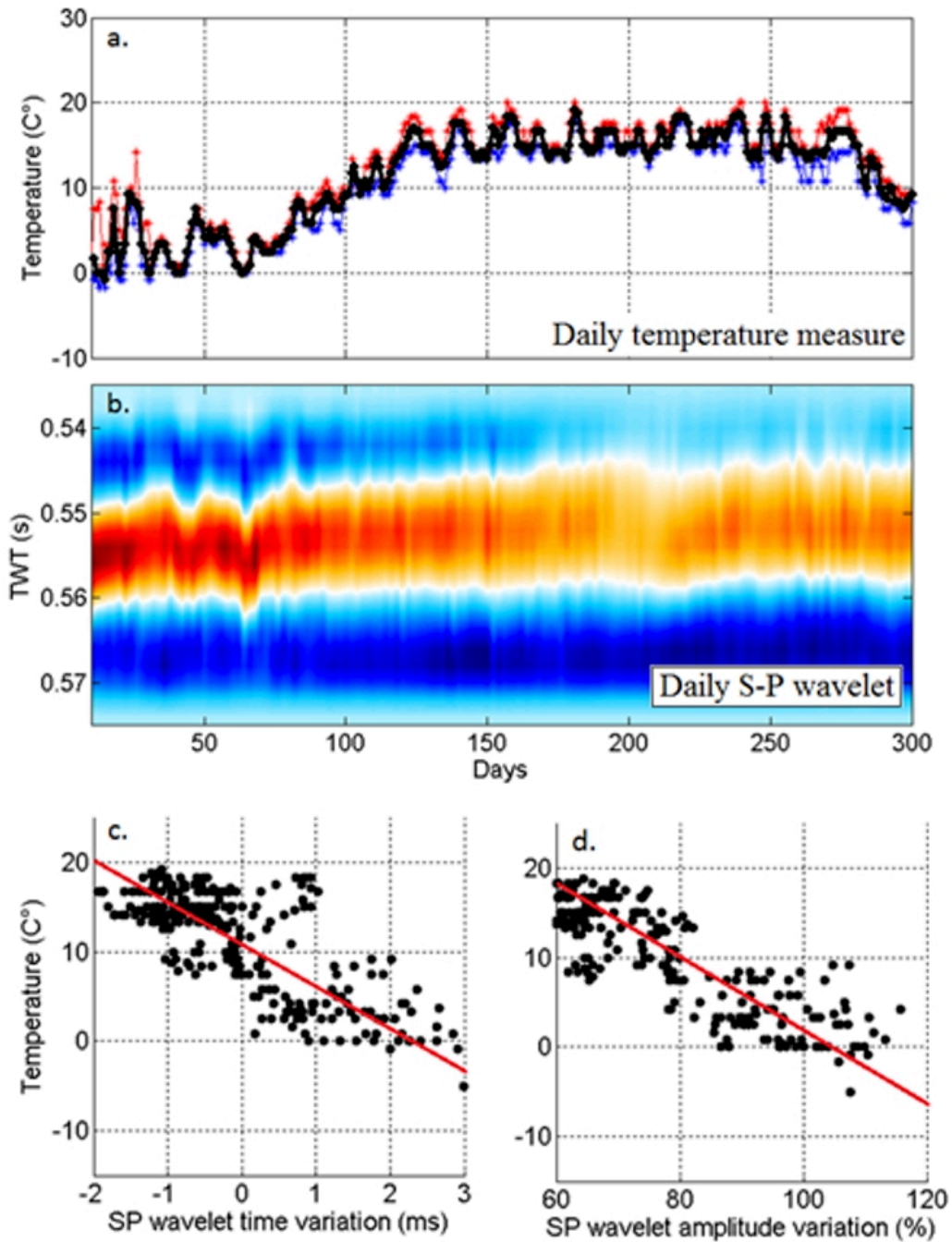


Figure 42: S-P converted ghost fluctuation over calendar time. Top: ambient surface temperature, middle: S-P converted wavelet over the calendar time. Bottom left cross plot between S-P ghost time shifts and temperature. Bottom right: cross plot between and S-P ghost amplitude variation.

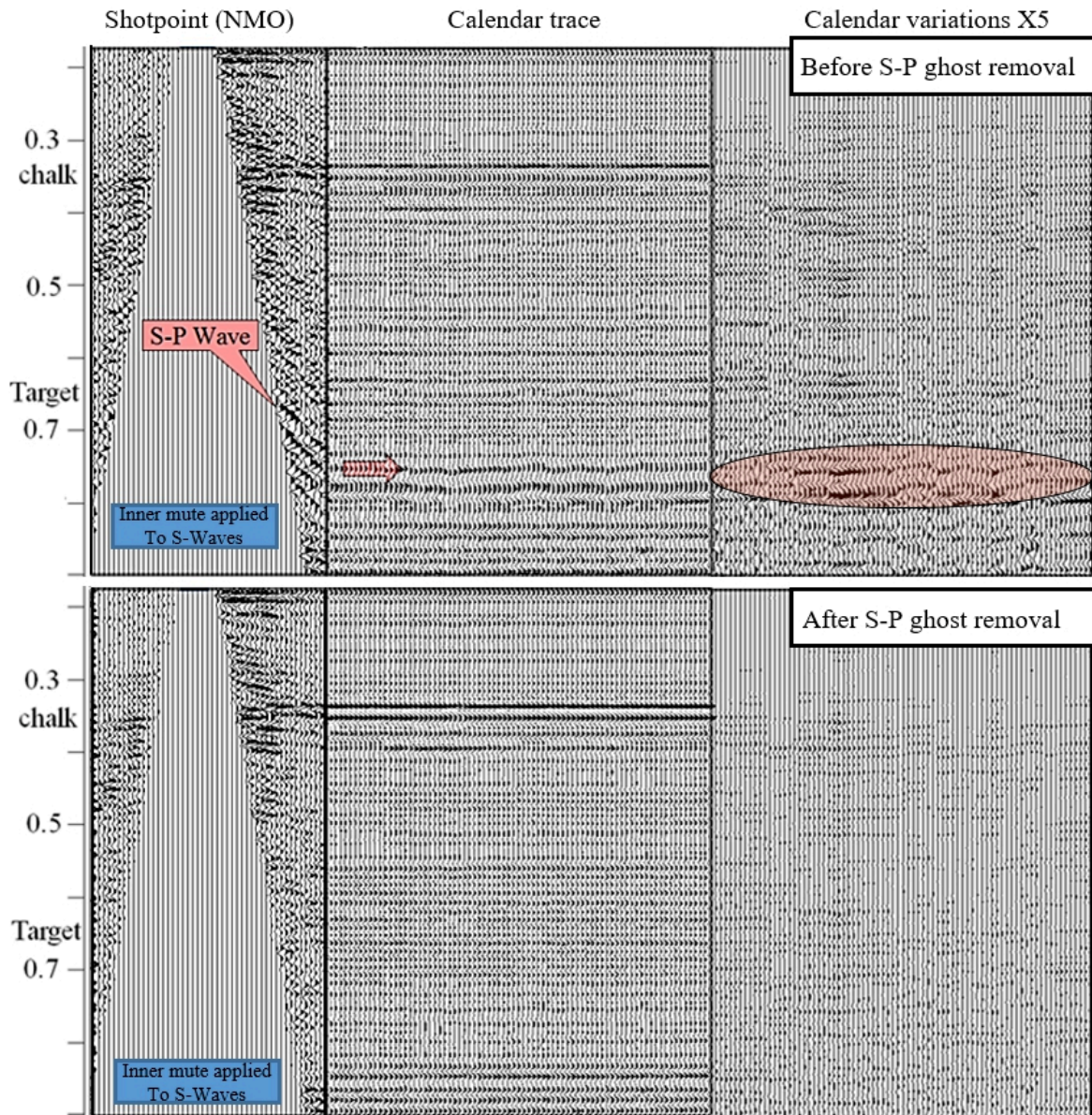


Figure 43: The reduction of the S-P ghost wave. Top: input data before S-P ghost wave attenuation. Bottom: After S-P ghost wave attenuation using a HR Radon filter. Left: Shot point with NMO applied. Middle: repeated record over calendar time (1 trace par day over several months). Right: Calendar variation obtain by subtracting the stack of the first 7 traces (1 week) to each daily trace. The obtained differences are multiplied by a factor 5.

We now consider the ghost at the receiver side.

### 3.4.2 Receiver ghosts

In marine, several methods have been proposed to derive wavefield separation operators, each having its own advantages and weaknesses (Sønneland et al., 1986; Bell and Cox, 1988; Monk, 1990; Posthumus, 1993). In this part, we present the methodology behind source and receiver ghost attenuation in continuous seismic monitoring. Later, we will show how the presented full de-ghosting workflow improves further the repeatability and thus enhances the detectability of small and rapid changes occurring in the reservoir. The full deghosting workflow implies at least three steps summarized in Figure 44:

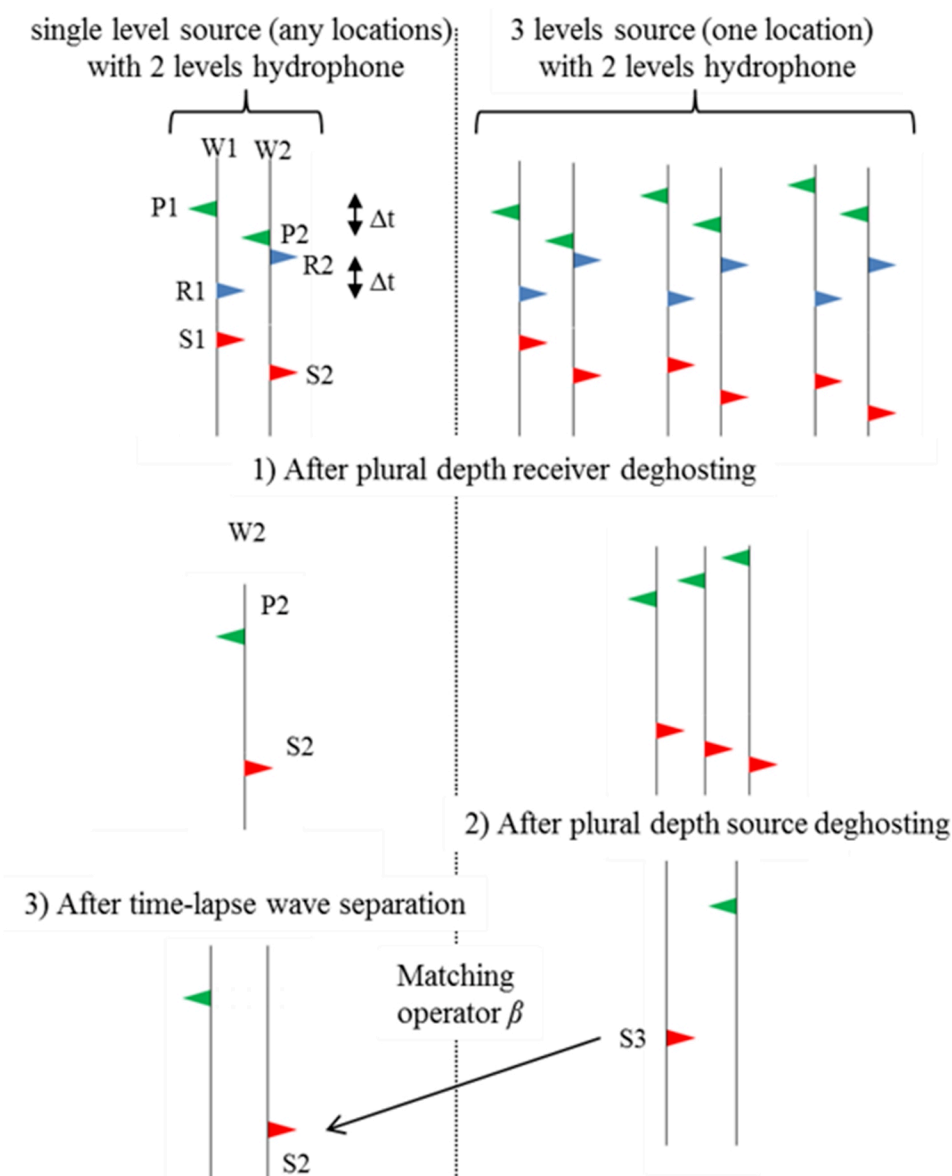


Figure 44: The full deghosting workflow applied in continuous seismic monitoring.

We assume the propagation of plane, normally incident primary, receiver and source ghosts. Onshore, this hypothesis is acceptable as a velocity gradient is often observed in the shallow subsoil resulting in the verticality of the ray paths. We assume as well no absorption between the two levels, which is a reasonable approximation when the depth difference is of an order of a few meters in a consolidated media. Consequently, the relationship between primaries and ghosts waves at the two levels of sensors becomes simple and depends only on a phase term  $\tau$ . We note:

$$\tau_{(f,\Delta z,v)} = e^{-i2\pi f \frac{\Delta z}{v}} . \quad (1)$$

In Equation 1,  $\tau$  varies as a function of the frequency ( $f$ ) and on both the velocity of the media ( $v$ ) and on the depth difference ( $\Delta z$ ) between the two level. We note  $W_1$  and  $W_2$  the recorded wavefield recorded at a first level (shallowest) and at a second level (deepest). The recorded wavefield encompasses the primaries, noted  $P$ , the receiver ghost, noted  $R$  and the source ghost  $S$ . We note:

$$W_{1(f)} = P_{1(f)} + R_{1(f)} + S_{1(f)} , \quad (2)$$

$$W_{2(f)} = P_{2(f)} + R_{2(f)} + S_{2(f)} . \quad (3)$$

We assume no attenuation between the two levels of sensors and we consider plane, normally incident waves. In this case, a simple phase shift allows expressing  $P_1$ ,  $R_1$  and  $S_1$  as a function of  $P_2$ ,  $R_2$  and  $S_2$ . We can write:

$$W_{1(f)} = \frac{1}{\tau_{(f,\Delta z,v)}} P_{2(f)} + \tau_{(f,\Delta z,v)} R_{2(f)} + \frac{1}{\tau_{(f,\Delta z,v)}} S_{2(f)} , \quad (4)$$

$$W_{2(f)} = P_{2(f)} + R_{2(f)} + S_{2(f)} . \quad (5)$$

We first derive the receiver ghost at the deepest level. We multiply Equation 4 by the term  $\tau_{(f,\Delta z,v)}$ , then we can write:

$$\tau_{(f,\Delta z,v)} W_{1(f)} = P_{2(f)} + \tau_{(f,\Delta z,v)}^2 R_{2(f)} + S_{2(f)} . \quad (6)$$

We subtract Equation 5 by Equation 6. We obtain:

$$W_{2(f)} - \tau_{(f,\Delta z,v)} W_{1(f)} = R_{2(f)} - \tau_{(f,\Delta z,v)}^2 R_{2(f)}. \quad (7)$$

By factorising Equation 7, it becomes:

$$W_{2(f)} - \tau_{(f,\Delta z,v)} W_{1(f)} = (1 - \tau_{(f,\Delta z,v)}^2) R_{2(f)}. \quad (8)$$

Then, the expression of the receiver ghost is:

$$R_{2(f)} = \frac{1}{(1 - \tau_{(f,\Delta z,v)}^2)} (W_{2(f)} - \tau_{(f,\Delta z,v)} W_{1(f)}). \quad (9)$$

We now consider the expression of the primaries. We multiply Equation 4 by the term  $\frac{1}{\tau_{(f,\Delta z,v)}}$ . We obtain:

$$\frac{1}{\tau_{(f,\Delta z,v)}} W_{1(f)} = \frac{1}{\tau_{(f,\Delta z,v)}^2} P_{2(f)} + R_{2(f)} + \frac{1}{\tau_{(f,\Delta z,v)}} S_{2(f)}. \quad (10)$$

We subtract Equation 5 by Equation 10. We obtain:

$$W_{2(f)} - \frac{1}{\tau_{(f,\Delta z,v)}} W_{1(f)} = P_{2(f)} - \frac{1}{\tau_{(f,\Delta z,v)}^2} P_{2(f)} + S_{2(f)} - \frac{1}{\tau_{(f,\Delta z,v)}} S_{2(f)}. \quad (11)$$

By factorising Equation 11, it becomes:

$$W_{2(f)} - \frac{1}{\tau_{(f,\Delta z,v)}} W_{1(f)} = \left(1 - \frac{1}{\tau_{(f,\Delta z,v)}^2}\right) (P_{2(f)} + S_{2(f)}). \quad (12)$$

Then, the expression of the primary is:

$$P_{2(f)} = \frac{1}{1 - \frac{1}{\tau_{(f,\Delta z,v)}^2}} \left( W_{2(f)} - \frac{1}{\tau_{(f,\Delta z,v)}} W_{1(f)} \right) - S_{2(f)}. \quad (13)$$

In Equation 9 and in Equation 13,  $W_2$ ,  $W_1$ ,  $R_2$ ,  $P_2$  and  $S_2$  are all expressed in the frequency domain. Note that  $\tau$  does not vary with the calendar time because the two levels of sensors are both below the weathering layer. Equations 9 and 13 cannot be solved correctly when it exists a  $k \in \mathbb{N}$  such that:

$$f = \left( \frac{v}{2\Delta z} \right) k. \quad (14)$$

The last condition allows us to predict the particular frequencies that will not be separated correctly. An appropriate choice in sensor depth difference according to the consolidated velocity of the media will moves the inconsistent frequencies to the edges of the useful bandwidth as seen in Table 4.

Table 4: Numerical application of Equation 14 giving the first ( $k=1$ ) inconsistent frequency for several couples of velocities and depth differences between the levels of the vertical array.

$k = 1$	$v = 1000\text{m/s}$	$v = 1500\text{m/s}$	$v = 2500\text{m/s}$
$\Delta z = 3\text{m}$	$f = 166.6667 \text{ Hz}$	$f = 250 \text{ Hz}$	$f = 416.6667 \text{ Hz}$
$\Delta z = 6\text{m}$	$f = 83.3333 \text{ Hz}$	$f = 125 \text{ Hz}$	$f = 208.3333 \text{ Hz}$

We first test the approach on two synthetic traces. We compare the proposed method, called the cross-deghosting with a basic processing that consist in stacking the two records after having aligned the primaries with a simple time shift (Figure 45). With two levels of sensors (Figure 45a), the cross deghosting allows to separate perfectly the receiver ghost (Figure 45d). As a result, the source ghost is suppressed and it remains only the primary and the source ghost in the output trace (Figure 45c). On the contrary, the basic subsequent time alignment and stack cannot separate the ghost. By doing so, it attenuates the ghost but we then observe two ghost residues on the output trace (Figure 45b). The cross-deghosting method thus appears more efficient.

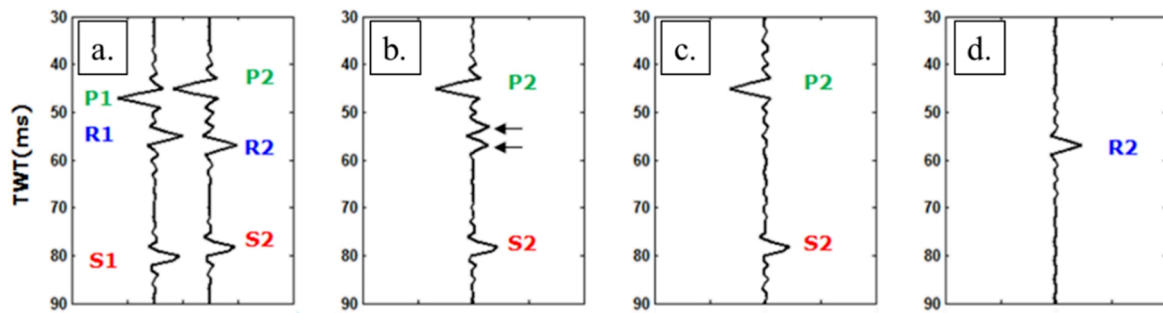


Figure 45: Illustration of the receiver ghost and primary separation. The input seismic records at the 2 levels of sensor (a). The subsequent application of the primary alignment and stack (b). Black arrows figure out the ghost residues. The application of the deghosting (c) as expressed in Equation 13 and the estimated ghost (d) as expressed in Equation 9.

The methodology is then tested on synthetic daily records in which we introduce some variations. For two levels of sensors, we generate two primary reflections and the associated receiver ghosts. The ghosts vary with the changes occurring in the weathering layer. The first primary represents a reflection above the reservoir and is constant within the calendar time. The second primary represents the reservoir reflection showing an amplitude increase within the calendar time. The reservoir is noted “R” and it is indicated by a yellow arrow in Figure 46. The ghost and primary separation is not complete using the subsequent time alignment and stack method (Figure 46a) while it is perfect using the cross-deghosting approach with the exact velocity between the two level of sensors (Figure 46b).

We evaluate the effect of an error in the velocity estimation (Figure 46c and Figure 46d). With a 10% velocity error, the cross-deghosting result is still acceptable but not perfect (a ghost leakage is visible in the primary estimation). Random noise addition is as well tested and the results are illustrated in Figure 46e. The proposed cross-deghosting approach is thus quite robust to velocity approximations and to random noise.

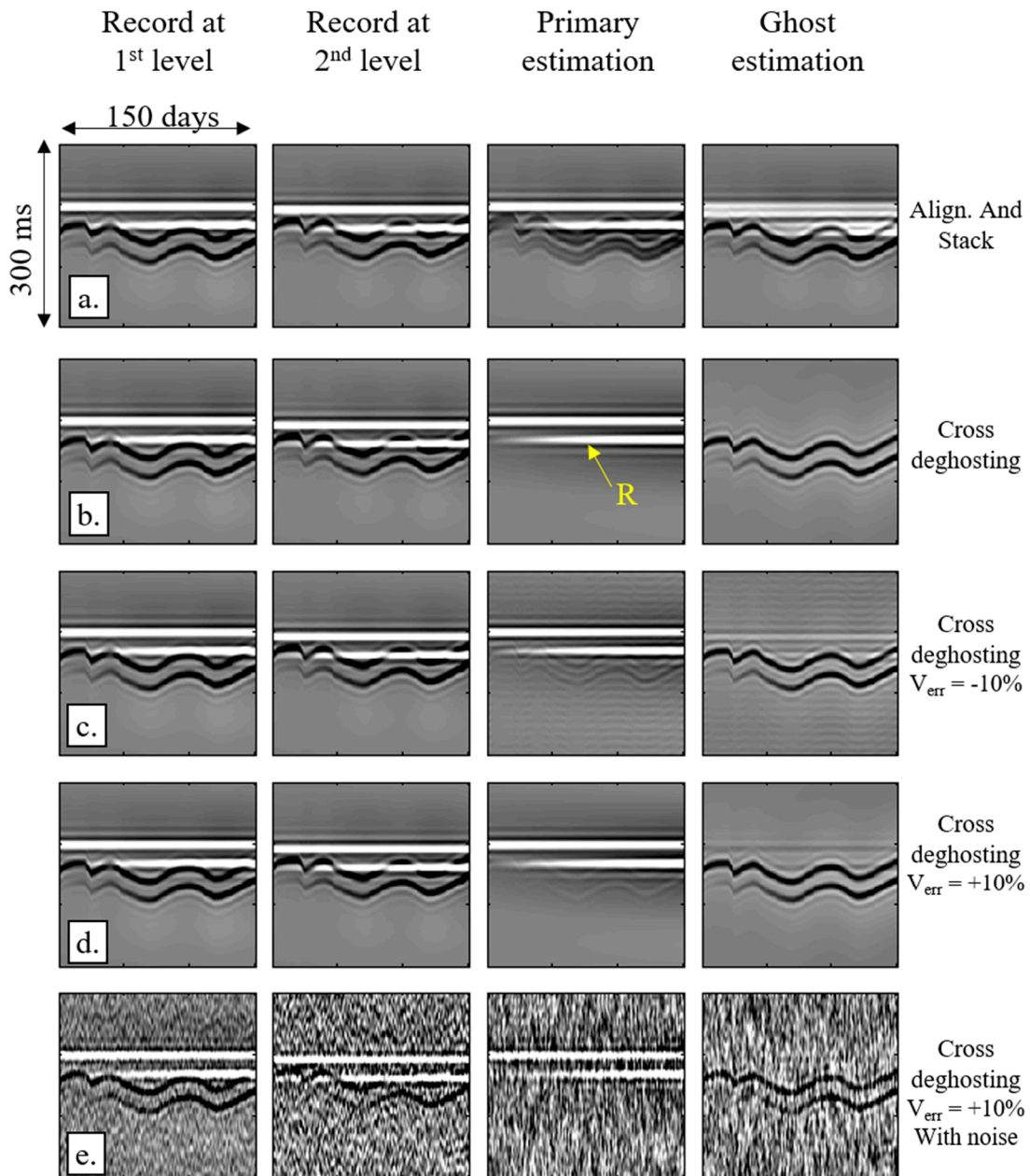


Figure 46: illustration of the cross deghosting on daily synthetic dataset (b) with a perfect ghost and primary separation and its comparison with the subsequent time alignment and stack method showing high primary and ghost leakage (a). The velocity error effect on the cross deghosting (c and d) and the random noise addition effect (e).

We applied the cross-deghosting methodology on the real dataset. To evaluate the improvement provided by the different processing steps on the receiver side, we analyse the repeatability in a 40-millisecond time window above the reservoir (Figure 47). Predictability is sensitive to the length of the correlation window and to the number of lags in the correlations, so absolute numbers are not meaningful (Kragh and Christie, 2002). Nevertheless, predictability gives a relative idea of the seismic repeatability improvement

with the different processing steps. The S-P converted ghost wave attenuation and the dual sensor deghosting lead to a significant enhancement in the seismic repeatability as both NRMS and predictability are improved.

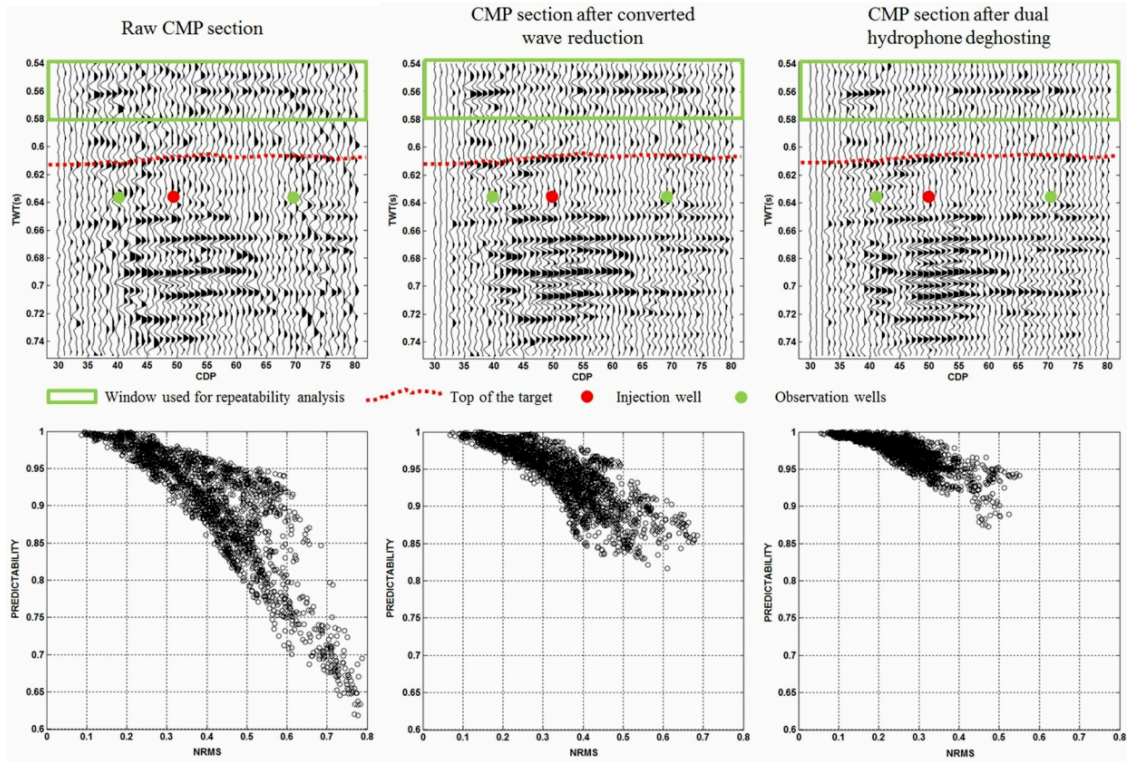


Figure 47: Effect of the S-P converted ghost and receiver ghost attenuation on the CMP stack (top) and on the repeatability metrics (bottom). The subsequent reduction of the S-P converted ghost (middle) and receiver ghost (right) improves significantly the repeatability of the data.

In Equation 13 and in Figure 45c we note that the expression of the uncontaminated primary  $P_2$  alone requires the estimation of the source ghost  $S_2$ . The estimation of  $S_2$  is described in the next part.

### 3.4.3 Source ghosts

In this part, we assume that the receiver ghost has been previously removed using the dual sensors cross-deghosting. The cross-deghosting strategy described previously is applicable as well at the source vertical array thus; the source ghost and the primary separation can be performed. However, contrary to the receivers that have two levels of sensor at any positions, the only vertical source array is located on the edge of the survey. A novel strategy to attenuate the source ghost at any source position is proposed. The strategy includes two steps:

- 1) The estimation of the source ghost at the vertical array using the cross-deghosting
- 2) The reduction of the source ghost using the concept of time-lapse wave separation (Cotton and Bianchi, 2013).

The cross-deghosting strategy applied to the source vertical array (figured out by a yellow triangle on the acquisition map Figure 40) enables to separate very well the primary and the source ghost as illustrated in Figure 48. The estimated source ghost at the vertical array is then used to reduce the source ghost at other source position having only a single source.

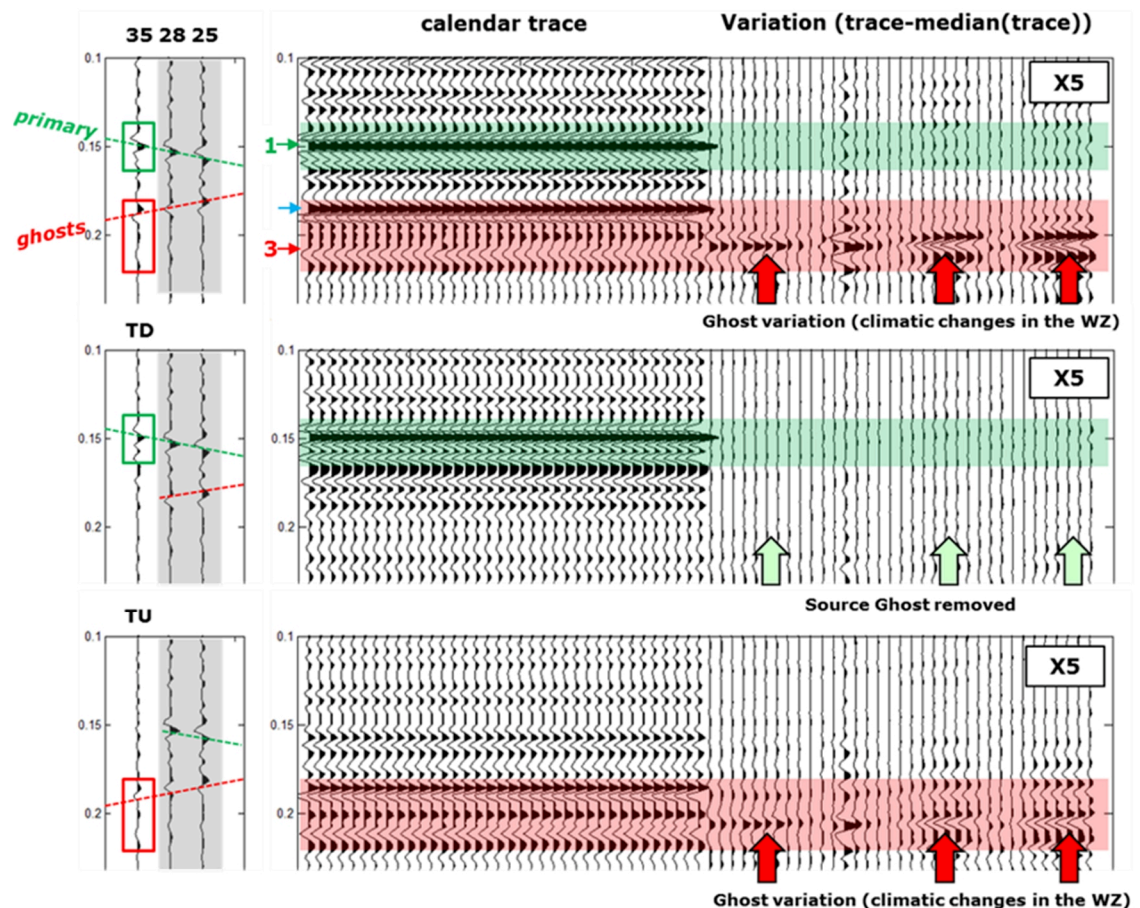


Figure 48: Illustration of the cross deghosting at the vertical array of sources. On the input records (top), we observe upgoing and downgoing primaries and ghost (top, left). In the calendar time (top, right), The primary (green window) is constant whereas the ghost (red window) varies with the weathering layer changes. After cross deghosting (middle and bottom), the primaries and the ghost are isolated.

The concept of time-lapse wave separation is based on the assumption that a constant operator (constant with calendar time) can match a time-lapse variation model (the source

ghost estimated at the vertical array) to a given time-lapse variation record. The constant operator can be found by the resolution of a linear inverse problem in the frequency-calendar-time domain. We note:

$$\delta W_{(c,f)} = \delta S_{(c,f)} + \delta P_{(c,f)}, \quad (15)$$

$$\delta W_{(c,f)} = \alpha_{(f)} \cdot \delta S m_{(c,f)} + \delta P_{(c,f)}. \quad (16)$$

In Equation 15 and 16,  $W_{(c,f)}$  represents the time-lapse record defined in the calendar-time-frequency domain noted  $c$  and  $f$ . Its time-lapse derivative  $\delta W_{(c,f)}$  represents the 4D variations. In the same way,  $\delta P_{(c,f)}$  and  $\delta S_{(c,f)}$  represents respectively the primary and ghost waves 4D variations comprised in  $\delta W_{(c,f)}$ . The source ghost variation model (estimated with the source vertical array) is noted  $\delta S m_{(c,f)}$ . Finally,  $\alpha_{(f)}$  expresses the matching operator that is constant in the calendar-time domain. We first assume that the primaries are constant with the calendar time, then  $\delta P_{(c,f)} = 0$ . This is exclusively the case when no reservoir 4D effect are expected, then the Equation 16 becomes:

$$\delta S_{(c,f)} = \alpha_{(f)} \cdot \delta S m_{(c,f)}. \quad (17)$$

In this case, the expression of the matching operator is:

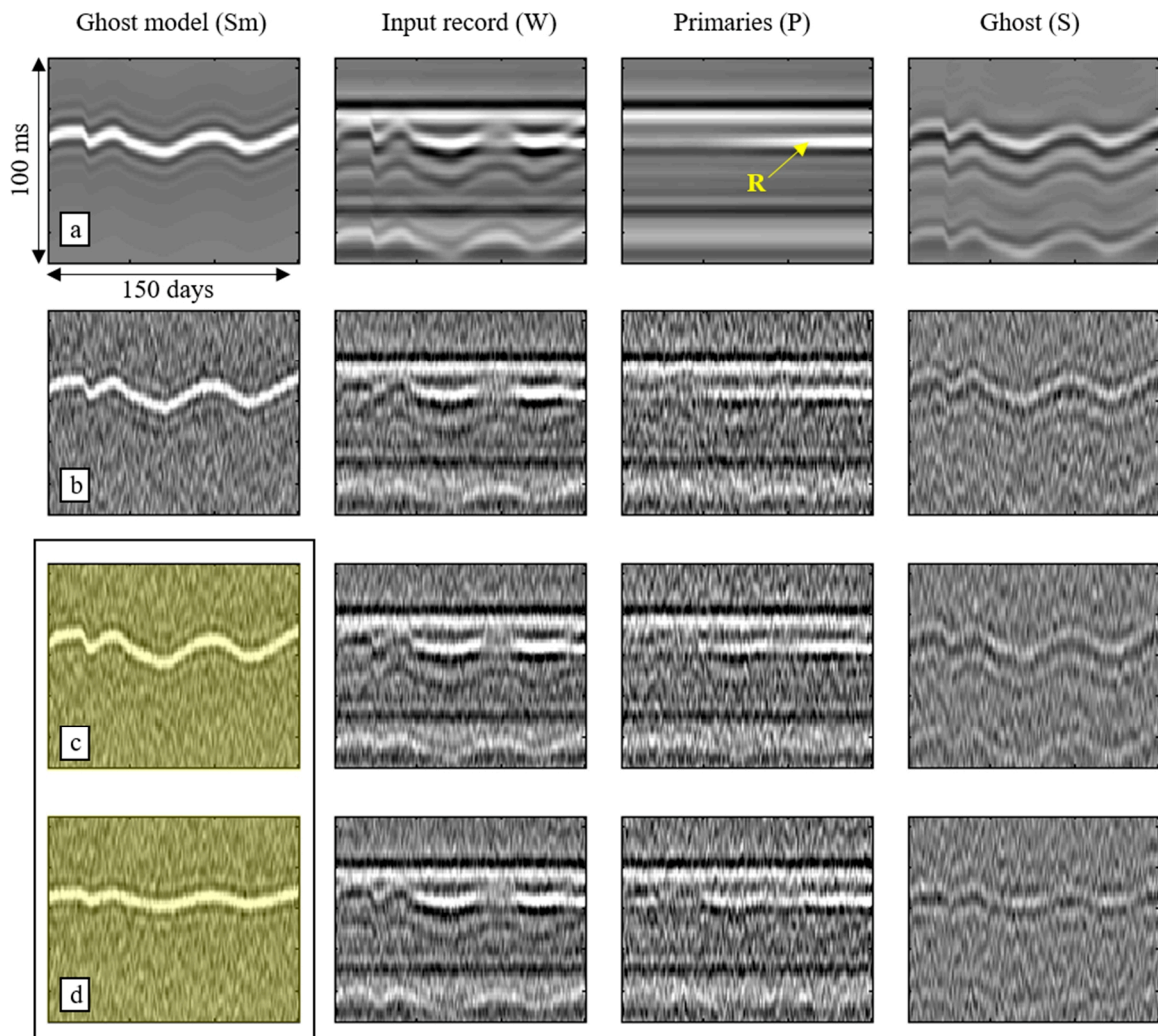
$$\alpha_{(f)} = \frac{[\delta S m_{(c,f)}]^T \delta S_{(c,f)}}{[\delta S m_{(c,f)}]^T \delta S m_{(c,f)}}. \quad (18)$$

In practice,  $\delta P_{(c,f)} = 0$  is too restrictive. However, during certain periods, we could reasonably assume that  $\delta P_{(c,f)} \ll \delta S_{(c,f)}$  and  $\delta P_{(c,f)} \ll \delta S m_{(c,f)}$ . In this is the case, we can write:

$$\alpha_{(f)} = \frac{[\delta S m_{(c,f)}]^T \delta W_{(c,f)}}{[\delta S m_{(c,f)}]^T \delta S m_{(c,f)}} \quad (19)$$

We tested the methodology on synthetic data. We generate daily traces containing fluctuating source ghosts and primary waves. A first primary wave (located above the reservoir) is constant within calendar time while the second is affected by reservoir variation. We generate as well a daily source ghost model that would be obtained by applying the cross-deghosting method on a distant vertical source array. The daily traces and the daily source ghost model are not at the same position; however, having the daily source ghost model, we

find a constant operator that matches its variation to the ones observed on the distant daily traces. The proposed method works perfectly assuming that both the source ghost model and the current source ghost (comprised in a distant daily trace) vary in the same way (Figure 49a). Moreover, the approach is quite robust to noise (Figure 49b). Figure 49c and Figure 49d are interesting: in these tests, the source ghost model variations are different from the current ghost ones (comprised in the distant daily trace). These two cases show that the time-lapse wave attenuation is reasonably efficient.



In those 2 panels ghost model variations do not match exactly the ones in the input records

Figure 49: Illustration of the time-lapse wave separation. The process applied to the synthetic dataset without noise (a) and with noise (b). The process applied with some bias introduced in the ghost model (c and d).

The time-lapse wave separation method was then applied to the real data. As in Figure 49c and Figure 49d, the source ghost attenuation is not perfect (some residues still appear in

the calendar variations after time-lapse wave separation); however, the global and significant improvement for all sources reveals that the calendar ghost variations were quite comparable for all sources. The granted patent describing the time-lapse wave separation method is also available in the appendixes.

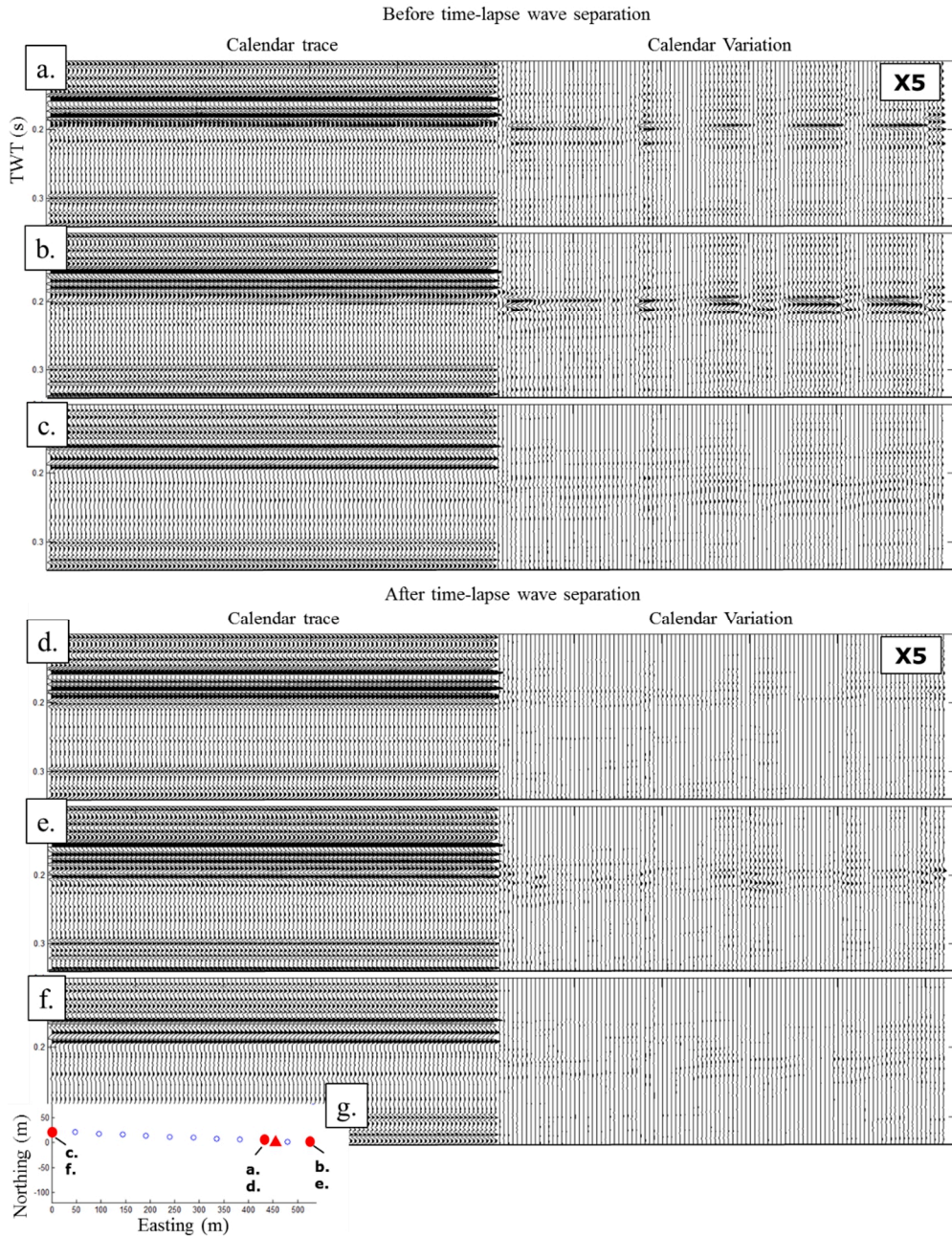


Figure 50: Application of the time-lapse wave separation on several sources located in different places over the survey (a to f) as showed in the map (g). Before processing (top) and after processing (bottom). The reduction of the source ghost further improves the repeatability as seen on the calendar variations (right).

### 3.5 Repeatability improvement

The repeatability improvement brought by the full deghosting workflow can be represented as the reduction of the time-lapse differential energy above the reservoir as illustrated in Figure 51 and Figure 52. Without any processing, the fluctuation of the ghost are visible on the calendar trace gather (Figure 51b). The variation panel (Figure 51c) emphasizes the fact that the reservoir-related variations appearing below 0.7 s are completely hidden by the fluctuation of the ghost. After full deghosting (Figure 52f), the reservoir-related variations appears quite clearly opening the door on precise 4D attribute measurement.

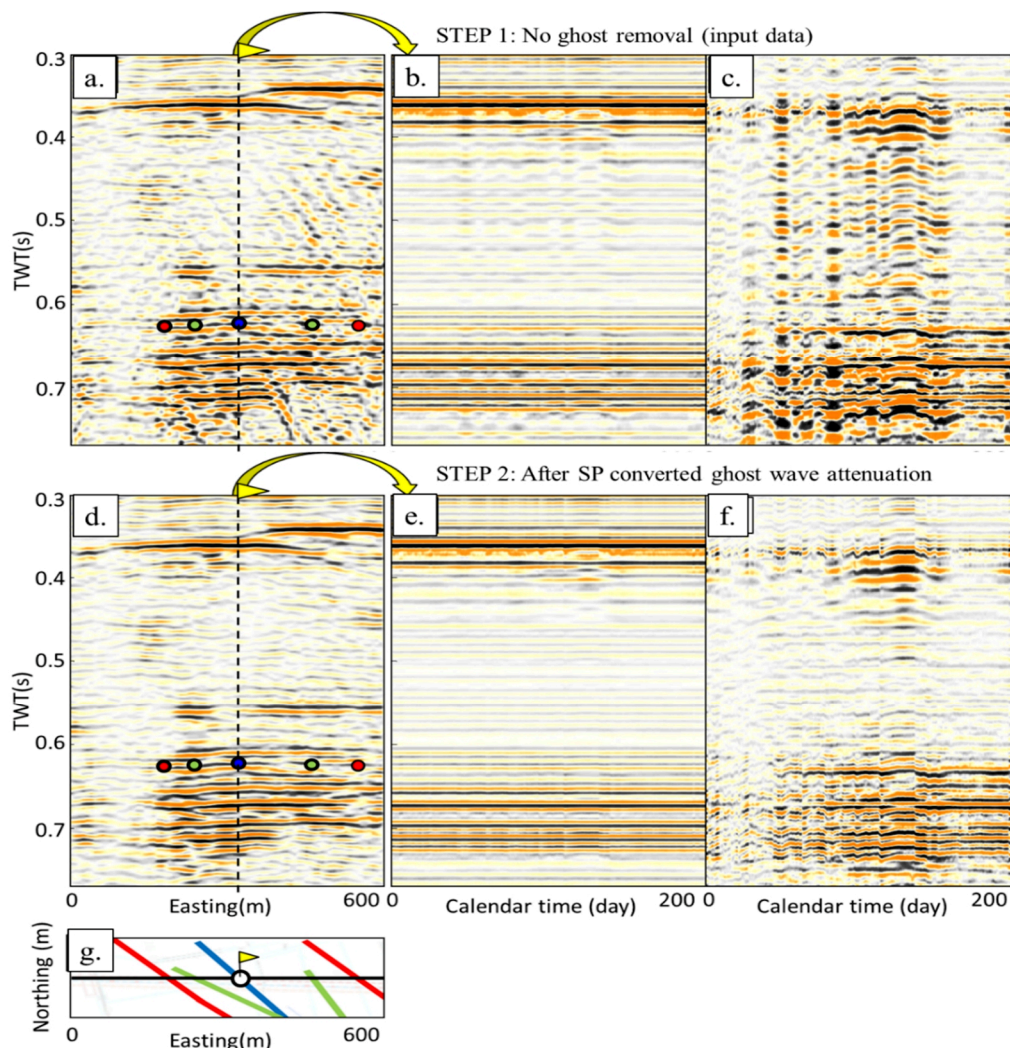


Figure 51: Data quality and repeatability comparison in different domain. The data without any ghost removal (top) and with the S-P converted ghost attenuation (bottom). We display a stacked sections (left) as well as the calendar evolution of the stack section's center bin (middle). The selected centre bin is right at the position of the injection well. The middle panel consists of one trace per day and its relative calendar variations (right). The right panel is obtained by subtracting a reference to each daily records. The residue is then multiplied by a factor 5. The reference is obtained by averaging the first month of the acquisition.

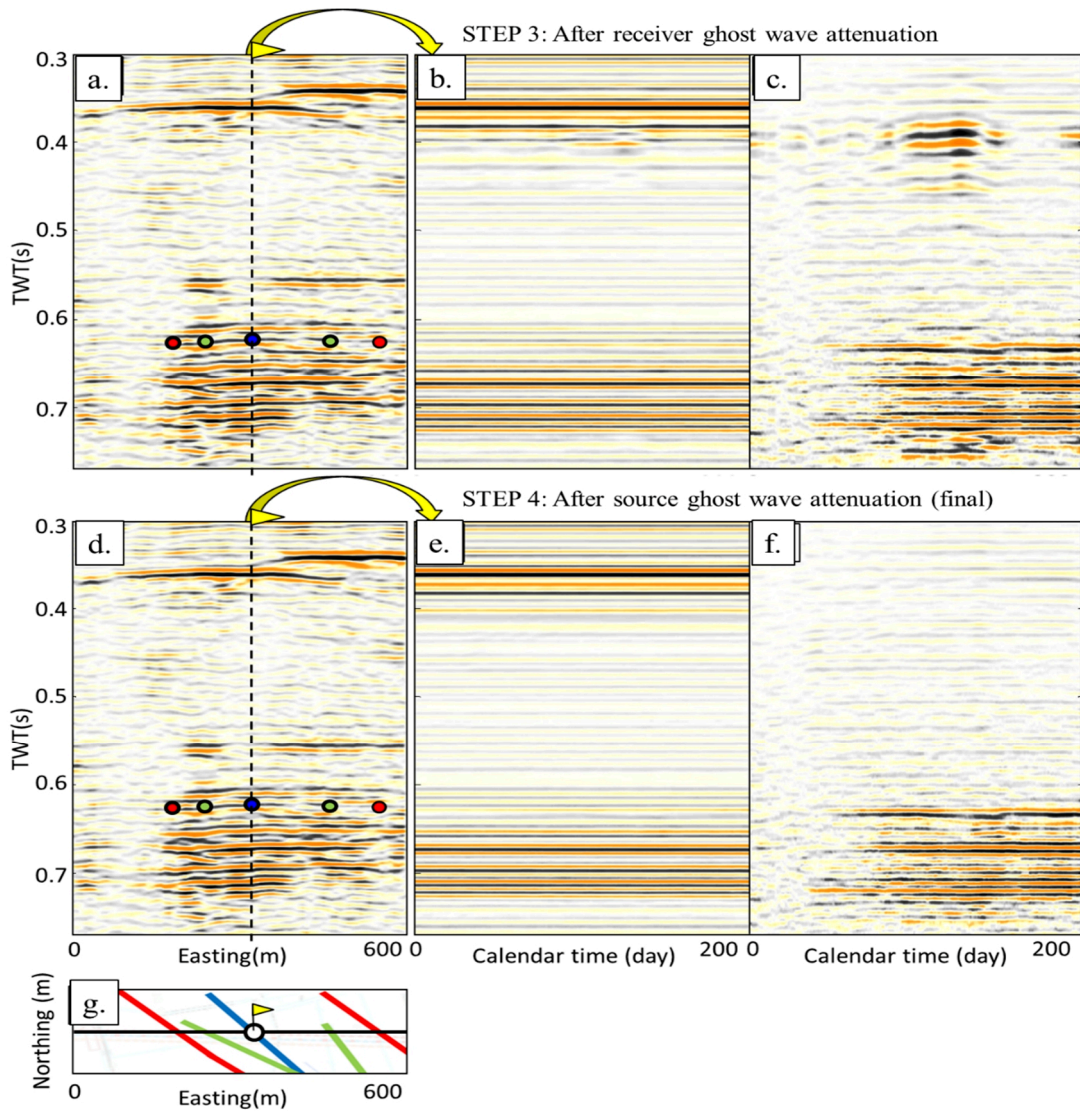


Figure 52: Same as for Figure 51 but for the receiver ghost attenuation using the cross-deghosting (top) and with the attenuation of the source ghost using the time-lapse wave separation (bottom).

### 3.6 Travel time and amplitude variation

Travel time and amplitude variations are obtained using cross-correlation with a reference dataset on a post-stack migration image. The lengths of the correlation windows are 100 and 20 milliseconds respectively for the travel times and for the amplitudes. A common method to estimate travel time delays in a cross-correlation is to fit a parabola with three points: the apparent maximum of the cross-correlation and its two neighbors. The maximum of this fitted parabola can then be found, indicating a subsample estimate of the delay. For

the travel time variation, we estimate the time corresponding to the maximum of the parabola fitted to the cross-correlation. For the amplitude variation, we did a ratio between the maximum of the parabola fitted to the cross-correlation and the maximum of the parabola fitted to the reference autocorrelation.

At the injector, the seismic attributes are compared to the injection steam rate (Figure 53a). The steam injection started on May 9th, 2011, and the full injection started around May 24th, 2011. This graphical comparison highlights that the fact that the steam injection and interruptions are detected almost instantaneously on the time shift (red curve) and with some delay on the amplitude variation (green curve). There is virtually no change above the reservoir (light curves). The time shifts occur very rapidly, following the steam injection rate. These travel time variations can be interpreted as essentially pressure change effects. Near the injector, three months after the start of steam injection, the maximum observed cumulative variation in amplitude and time shift are 10% and 0.4 milliseconds respectively (by comparison, the recording sample interval is 1 ms). During the same period, the average calculated daily time shift variations are about 6 microseconds and the daily amplitude variations are about 0.1%.

In Figure 53b, we see a good correlation between the travel time variations and the pressure measured at the two observation wells. Between April and December 2011, pressure effects were detected on both observation wells O1391 and O1392, each located 80 and 160 meters from the injector. Between April and December 2012, almost no pressure effects were detected at the observation wells, while the steam injection rate and the travel time variation at the injector were both rising.

The 3D monitoring system is required to understand and map the complex path of the steam propagation following the injection period. To visualize the daily evolution of the amplitude variations, a 4D movie was produced. Figure 54 shows four maps at different dates. The travel time variations were measured below the reservoir at 675 milliseconds and the amplitude variations were measured in the reservoir at 625 milliseconds. On the amplitude variation maps (left column), we see that the steam propagates from the injector well (blue) to the western production well (red) passing north of the western observation well O1391 (green). No significant variations are observed on the east side of the injector well. Figure 55 shows snap shots of the 4D movie computed during the injection. The 3D yellow “blob” is the 7% iso amplitude variation compared to May 2012. It represents the spatial and calendar

amplitude spreading due to steam injection. Figure 56 recaps the interpretations and conclusions made by SHELL.

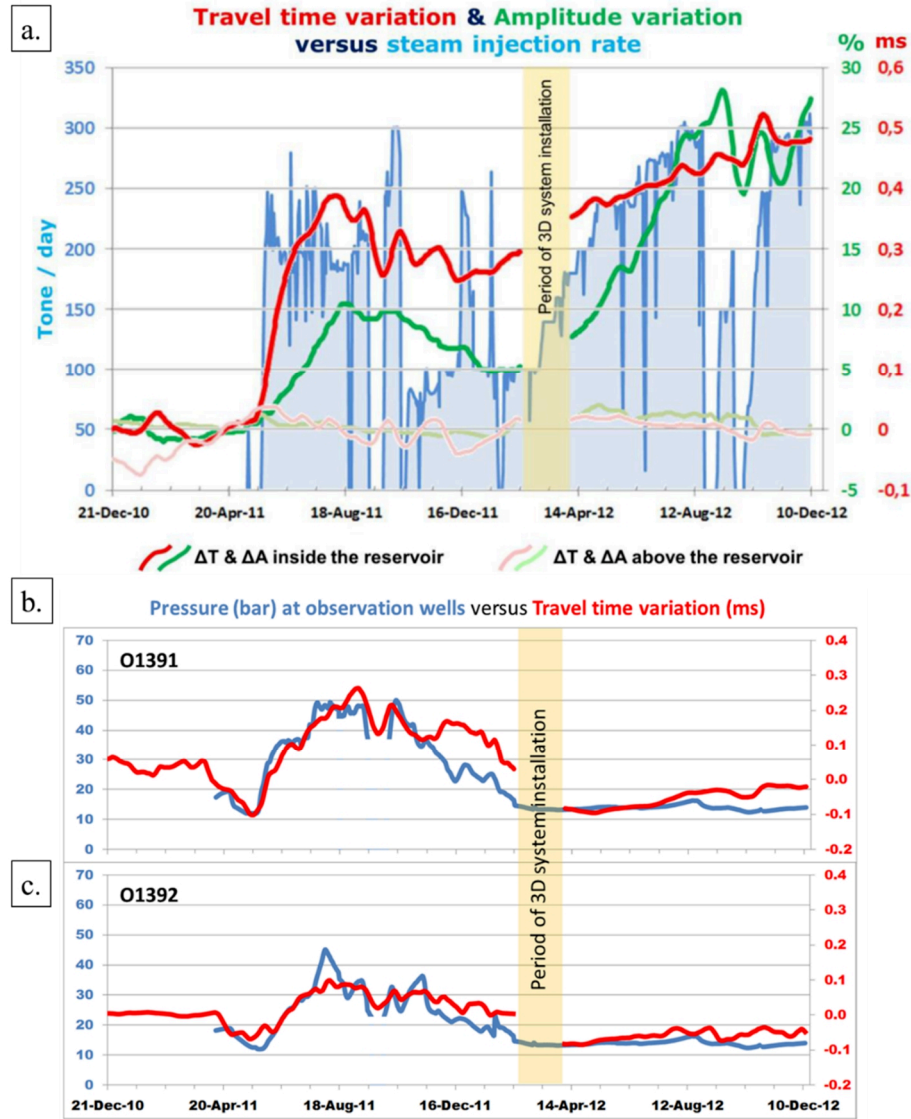


Figure 53: At the injection well (a), the steam injection rate (blue) is correlated with the seismic travel time shift below the reservoir (red curve) and with amplitude measured in the reservoir (green curve). Above the reservoir, the time shift and the amplitude variations (light red and light green) are very stable. Comparison between the travel time variations and pressure measured at both observation wells (b) and (c). The well O1391 is located on the east and the well O1392 is located on the west.

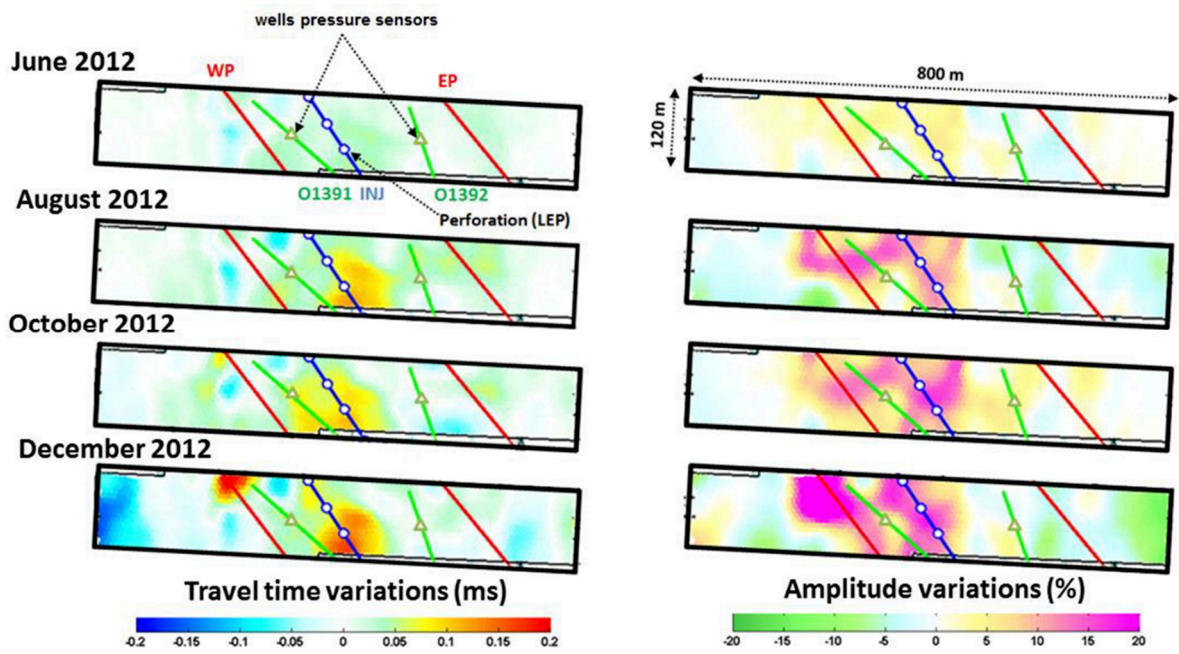


Figure 54 : Travel time variations below the reservoir (Left) and amplitude variations in the reservoir (Right) at different dates. The east part of the reservoir is clearly not swept by the steam.

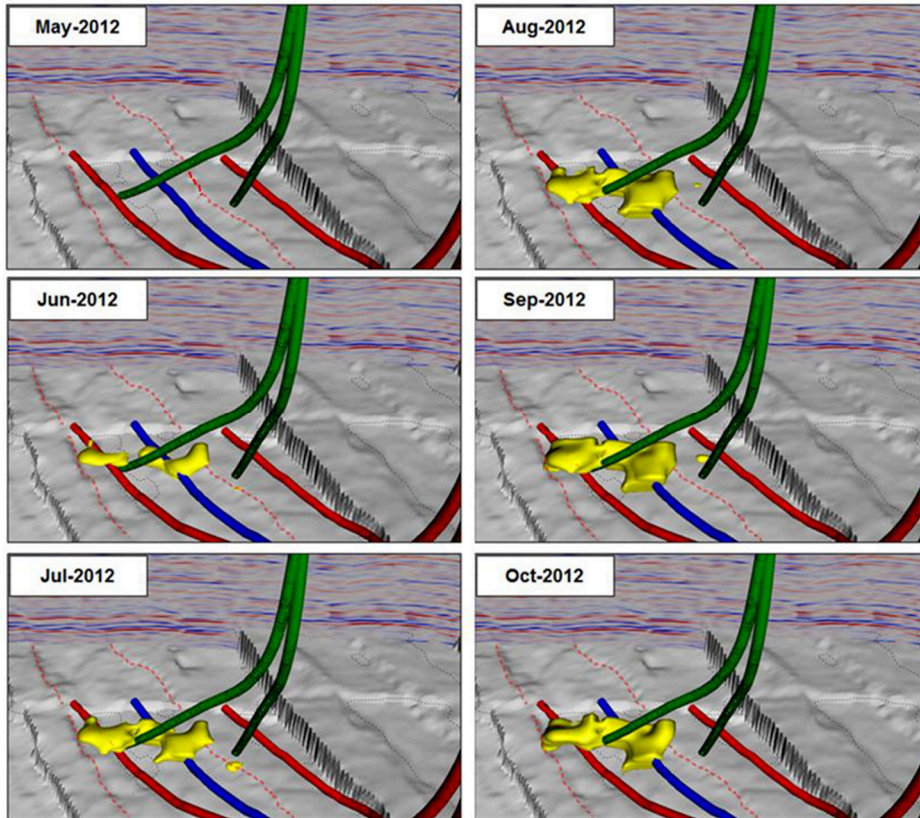


Figure 55: Evolution of the 7% iso amplitude volume over calendar time.

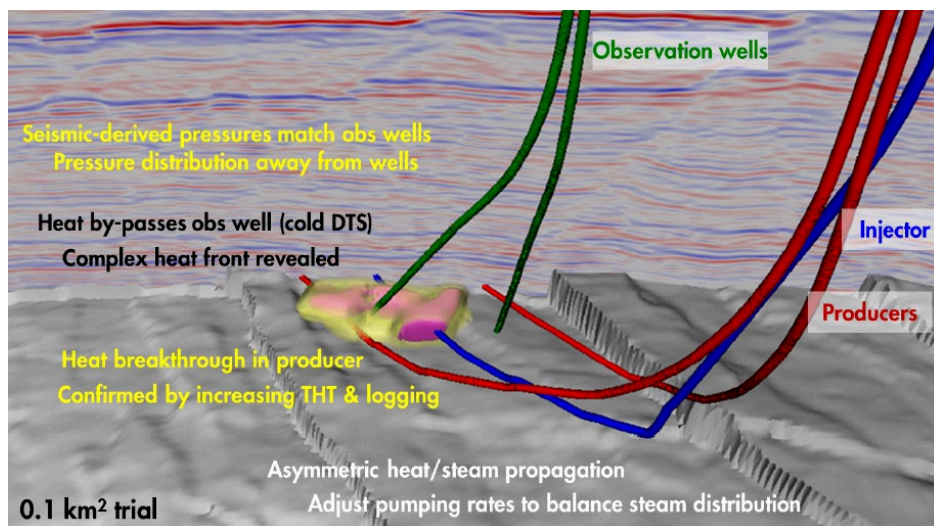


Figure 56: Interpretation and conclusions made by SHELL. Courtesy of SHELL

### 3.7 Discussion

For the dual depth cross deghosting, it implies to double the equipment in the field that can be costly for permanent reservoir monitoring. We could envisage having some sparse arrays of sensors (and/or source) combined with dense single level sensors and to use the time-lapse wave separation. This would be efficient if the variations of the ghost's waves are relatively regional; otherwise, the deghosting would not be straightforward. For the time-lapse wave separation, the choice of the calendar period to estimate the matching operator is critical. During this period, the reservoir variation and the ghost variation must be uncorrelated: This seems obvious; however, the worst case appears when slow reservoir injections or productions are done in parallel with seasonal climatic changes trend. In this case, it would be complicated to estimate the required matching operator.

Discussions exists on pre-migration versus post-migration deghosting. In fact, there are no restrictions to perform the presented deghosting workflow after migration. This requires migrating separately each level separately to get a migrated cube by level. By doing so, the deghosting process would be facilitated; the migration images would be in a common migration grid. The amplitude variations obtained by cross-correlation give a cumulative effect of the steam over the whole reservoir thickness but do not allow us to distinguish the 4D effects between the top and the base of the reservoir. The next step would be quantitative validation of the P-impedance and P-velocity variations evolution that would open the door to the interpretation it in terms of fluid or temperature variations (see chapter 4).

### 3.8 Conclusion

In studies where buried hydrophones give a good seismic response, we have shown that the use of dual-depth hydrophones is an interesting solution for handling the receiver ghost attenuation in land seismic monitoring. Accurate sampling in the time-lapse domain enables us to use specific 4D filtering techniques with a specific calendar variation to remove unwanted waves, which interfere with the real 4D signal coming from the reservoir. We have shown that when using a continuous seismic acquisition system with both calendar variation filtering and ghost attenuation using dual-depth hydrophones, we have significantly improved the seismic repeatability in terms of NRMS and predictability. This improvement in 4D acquisition and processing sequence opens the door for very precise measurements of small 4D signals on a daily basis.

## 4. 4D velocity and impedance in real-time

---

En sismique 4D, le modèle de vitesse utilisé pour l'imagerie et la caractérisation du réservoir peut changer à mesure que la production du réservoir progresse. Cela est particulièrement vrai pour les réservoirs de pétrole lourd stimulés par injection de vapeur. Dans le contexte d'acquisitions sismiques permanentes et continues, les analyses de vitesse classiques se révèlent être inadéquates en raison d'une faible couverture et d'un échantillonnage irrégulier en offset.

Dans ce chapitre, nous introduisons une version modifiée de la migration temps « pré-stack » (M-PSTM) pour détecter les changements de vitesse liés à la stimulation du réservoir. Les variations de vitesse sont obtenues par corrélation croisée entre les données journalières et les données de référence (la moyenne du premier mois d'acquisition). La méthode est d'abord testée sur des données synthétiques. Elle est ensuite appliquée aux données réelles (décrit au chapitre précédent) et révèle comment la vapeur se propage dans le temps au sein du réservoir.

---



This chapter is essentially related to a GEOPHYSICS paper that is available under the following reference:

Cotton, J., H. Chauris, E. Forgues and P. Hardouin, 2018, Time-lapse velocity analysis—Application to onshore continuous reservoir monitoring. *GEOPHYSICS*, **83**(3), B105-B117.

## 4.1 Introduction

Time-lapse imaging with active seismic reflection-related methods consists of acquiring, processing and analyzing a number of data sets recorded in succession at the same location (Lumley, 2001; Calvert, 2005; Johnston, 2013). The objective is to better understand potential changes in subsurface properties. Time-lapse seismic is playing an increasingly important role in reservoir monitoring. In conjunction with well data, it can improve the understanding of the reservoir behavior and optimize hydrocarbon recovery. Typical oil and gas reservoirs have a lifespan of many years and evolve slowly over their productive life; new surveys on an annual basis are appropriate for 4D seismic monitoring of conventional reservoirs. Many successful applications have been reported in different contexts (Goodway, 2014): heavy oil exploitation with steam injection (Behrens et al., 1998), CO<sub>2</sub> injection for storage or enhanced oil recovery (EOR) (Eiken et al., 2011; Bergmann et al., 2014; White et al., 2015), thermal field management with cross wells (Lee et al., 1995; Mathisen et al., 1995), and hydraulic fracturing (Groenenboom and Fokkema, 1998; Willis et al., 2007). A large number of references are available in Roach et al., (2015) and in Vasco et al., (2015). We report here three main challenges (e.g. Lumley, 2001):

- 1) Repeatability between two surveys is important to be able to distinguish between ambient noise and 4D signals. In practice, data processing cannot necessarily correct for imperfect repeatability (Rennie et al., 1997).
- 2) The images of the subsurface obtained after having processed different surveys are poorly sampled over the calendar time: usually, acquisitions are repeated every six months or over longer periods. The majority of heavy oil reservoirs in Canada are produced using in-situ enhanced recovery techniques, steam-assisted production being the most popular method (Prats, 1969). In this case, the characteristics of the reservoir can significantly vary over a few weeks: this means there is a need to monitor production effects on a daily

or weekly basis (Cabolo<sup>va</sup> et al., 2014; Mateeva et al., 2015; La Follet et al., 2015; Barker and Xue, 2016).

- 3) Seismic 4D effects may affect both pore pressure and saturation within the reservoir (Landrø, 2001; Cole et al., 2002; Landrø et al., 2003; Vasco, 2004). It is difficult to distinguish between these two effects. One solution is to introduce additional *a priori* information (Witsker et al., 2014).

To enhance the repeatability, current practice is to deploy permanent sensors (van Gestel et al., 2008; Roach et al., 2015). However, the sources are not necessarily identical between two surveys. Recently, a new type of acquisition has been proposed, where both sources and receivers are buried (Meunier et al., 2001; Forgues et al., 2006; Hornman et al., 2012; Cotton et al., 2013; Berron et al. 2015; White et al., 2015). This should in principle offer high-quality data for detecting 4D effects (Schissel<sup>é</sup> et al., 2009). In practice, processing is still needed (Bianchi et al., 2005) since part of the emitted signal travels through the near-surface weathering layer. After a reflection or conversion in the vicinity of the Earth's surface affected by climatic changes, ghosts waves are recorded by the buried sensors and may interfere with the primary 4D signal. Careful removal of multiples as well as ghost reduction workflows using appropriate survey designs are proposed to preserve 4D signals in land seismic monitoring (Cotton and Forgues, 2012). With buried sources and receivers, the number of sources and sensors is currently limited, resulting in a sparse low-fold narrow-offset acquisition. The objective here is to understand how velocity changes can be captured over the calendar time in the context of sparse acquisitions.

The paper is organized as follows: we first describe the methodology for capturing velocity changes over time. The main idea is to cross-correlate time-migrated gathers corresponding to the monitor and base surveys. For this, we propose a modified prestack time migration scheme. The approach is first illustrated on a synthetic data set, and then on a real onshore data set from the Netherlands in the context of steam injection. Both data sets have low-fold coverage but a dense sampling over calendar time.

## 4.2 4D Velocity Analysis

Conventional 4D analysis based on a Normal Move-Out scheme (4D-NMO) consists in first determining the optimal velocity model for the baseline for which the associated move-out correction provides an optimal stack. The same correction is then applied to other surveys: residual move-out corrections are associated with 4D effects (Calvert, 2005). Conventional NMO correction does not modify the arrival times at zero offset. However, these arrival times differ from one acquisition to the next as the velocity model changes over the calendar time. We propose here a modified NMO (M-NMO) correction that considers this effect. For an updated velocity model, the M-NMO correction matches the arrival times of the current data set to the times of the baseline data set. We first describe the M-NMO principle and the main hypothesis behind it. In the next sections, we illustrate the differences between the NMO and M-NMO approaches on a basic example, before presenting applications on both a synthetic and a real data set.

## 4.3 M-NMO correction

Let  $c$  be the calendar time. Typically, a new vintage can be acquired on a daily basis (Bianchi et al., 2005; Forgues et al., 2006; Schisselé et al., 2009). We consider a locally 1D Earth model, consisting of  $N$  interfaces at depth  $z_k$ , with  $k$  varying between 1 and  $N$ , associated to interval velocities  $v_{int}^k$  and thicknesses  $e_k = z_k - z_{k-1}$ . For each interface  $k$ , we define the mean velocity  $v_{avg}^k$ , controlling the zero-offset travel time, and the RMS velocity  $v_{rms}^k$ , acting on the curvature of the wave-front. The standard definitions are found in many reference books (e.g. Lavergne, 1986; Sherif and Geldart, 1995).

$$v_{avg}^k = \frac{\sum_{i=1}^k e_i}{\sum_{i=1}^k \frac{e_i}{v_{int}^i}}, \quad (20)$$

$$v_{rms}^k = \sqrt{\frac{\sum_{i=1}^k e_i v_{int}^i}{\sum_{i=1}^k \frac{e_i}{v_{int}^i}}}. \quad (21)$$

In the remaining part, we omit the reference to  $k$  in the velocity notations. We consider seismic amplitudes  $d(x, t; c)$ , corresponding to the pressure field recorded at the receiver

position, for a fixed mid-point position, where  $x$  is the offset distance and  $t$  the travel time. The calendar time  $c$  plays a particular role and indicates that new amplitudes are frequently recorded over calendar  $c$  axis. The application of the NMO correction distorts the gather and leads to a new data set  $d_{NMO}(x, t; c)$  defined as:

$$d_{NMO}(x, t; c) = d \left( x, \sqrt{t^2 + \frac{x^2}{v_{rms}^2(c)}}; c \right). \quad (22)$$

For an optimal  $v_{rms}$  correction, the selected interface should be flat in the  $d_{NMO}$  panel. If we consider the zero-offset trace, the conventional NMO correction does not modify the original gather and we should have  $d_{NMO}(x=0, t; c) = d(x=0, t; c)$ . However in a 4D context,  $d(x=0, t; c)$  is expected to be different from  $d_{NMO}(x=0, t; c)$  as the velocities are modified between the base and monitor surveys, typically within the reservoir. To obtain a zero-offset trace less sensitive to the calendar  $c$ , we propose a modified NMO approach (M-NMO) that takes into account both the modification of the zero-offset travel time and the reflection curvature. The main hypothesis behind the M-NMO considers that geological interface depths do not change over the calendar time, whereas the interval velocities may vary. The application of the M-NMO to  $d(x=0, t; c)$  reads

$$d_{M-NMO}(x, t; c) = d \left( x, \frac{v_{rms}(0)}{v_{rms}(c)} \sqrt{\beta^2 t^2 + \frac{x^2}{v_{rms}^2(0)}}; c \right), \quad (23)$$

with,

$$\beta(c) = \frac{v_{avg}(0) v_{rms}(c)}{v_{avg}(c) v_{rms}(0)}. \quad (24)$$

We first analyze the properties of the M-NMO correction. Then we consider the simplification  $\beta=1$ . It is an important step, as the M-NMO would otherwise depend on both the average and RMS velocities: in that case, we would have to directly determine the interval velocities. We indicate the strategy for determining the optimal RMS and interval velocities in the context of time-lapse imaging. We finally quantify the errors introduced by the simplification on  $\beta$ . If one introduces the ratio  $v_{rms}(0)/v_{rms}(c)$  inside the square root in Equation 23, the M-NMO correction reads

$$d_{M-NMO}(x, t; c) = d \left( x, \sqrt{\left( \frac{v_{avg}(0)}{v_{avg}(c)} t \right)^2 + \frac{x^2}{v_{rms}^2(c)}}; c \right). \quad (25)$$

The term associated to the offset  $x$  and controlling the curvature is still  $v_{rms}(c)$  as in the conventional NMO correction (Equation 22). However, the zero-offset trace is now modified. Let us consider a fixed interface at depth  $z$ , associated to the average velocity  $v_{avg}(c)$  for the monitor survey. The zero-offset travel time corresponds to  $\tau(c)=2z/v_{avg}(c)$ . That interface after M-NMO correction will be positioned around  $t$  such that  $(v_{avg}(0)/v_{avg}(c))t=\tau(c)$ . If the depth  $z$  of the interface does not depend on the calendar time, the focusing appears for the same time, whatever the calendar time. It means that under the assumption of fixed interface depth, the optimal velocity model can simultaneously corrects for the normal move-out variation and the zero-offset time-shift.

### 4.3.1 Strategy for time-lapse velocity estimation

The M-NMO correction described previously is used to perform a velocity scan. In practice, we further simplify the M-NMO by considering  $\beta(c)=1$  in Equation 23. The main reason is that we do not want to consider at the same time average and RMS velocities. Note that by definition,  $\beta(c)=1$  and  $d_{M-NMO}(x, t; c=0)=d_{NMO}(x, t; c=0)$ . We investigate in the next section the impact of such simplification.

We apply the M-NMO correction to the current data gather and we subsequently stack it within an offset range. The optimal velocity is obtained when the arrival times of the current stacked data match the arrival times of the stacked baseline. The matching is estimated through the picking of the cross-correlation between the M-NMO stacked baseline and the M-NMO stacked current data set. The interval velocity can be subsequently derived from the RMS velocity using Dix's formula (Dix, 1952). The 4D time-lapse velocity analysis reads:

$$v_{rms_{optim}}(t; c) = \operatorname{argmax}_{v_{rms_{scan}(c)}} \left( \int_x d_{M-NMO}(x, t; 0) dx \otimes \int_x d_{M-NMO}(x, t; c) dx \right). \quad (26)$$

where  $\otimes$  denotes the cross-correlation term.

We summarize the strategy and the two hypotheses behind the proposed method. With the M-NMO approach, the optimal velocity model both focuses the gathers and preserves the zero-offset time whatever the calendar time. In practice, this offers a new way of estimating

the velocity changes: here, the velocity model will be estimated by minimizing the phase of the cross-correlation between the baseline stacks corresponding to calendar time  $c=0$  and the different time-lapse seismic data sets  $c$ . The same strategy is extended in a straightforward way to prestack time migration (PSTM) and modified M-PSTM as for the NMO correction.

The underlying hypotheses are two-fold. The M-NMO is applicable if we consider that geological interfaces depths do not change over calendar time; only interval velocities may vary. Secondly, the ratio  $\beta$  is set to 1: only the RMS velocities are considered and later converted to interval velocities.

### 4.3.2 Simple illustration

We illustrate the differences between NMO and M-NMO on a simple 2D synthetic data set containing a single reflector with homogeneous velocity above it. The data set is generated by ray tracing. In the reference model for initial calendar time  $c=0$ , the corrected gather  $d_{M-NMO}(x, t; c=0)=d_{NMO}(x, t; c=0)$ , using the correct RMS velocity model, displays a horizontal event (Figure 57, left panel). For the new data set acquired at  $c=n$ , the NMO correction (Equation 22) leads to different gathers  $d_{NMO}(x, t; c=0)$  with different move-outs, depending on the RMS velocity values. The optimal focusing is obtained for a velocity perturbation of +3.4% compared to the reference velocity value. In each case, the zero-offset trace  $d_{NMO}(x=0, t; c=0)$  remains identical (Figure 57, top panels). With the modified M-NMO correction (Equation 23) and with the same RMS velocity scan, the optimal focusing for  $d_{M-NMO}(x, t; c=n)$  is still obtained for the same velocity perturbation of +3.4% (Figure 57, bottom panels). However, the zero-offset trace  $d_{M-NMO}(x=0, t; c=n)$  also depends on the velocity.

The NMO and M-NMO approaches lead to the same result. However, due to sparse offset definition and low fold (and thus poor S/N) as in the real data set, we prefer to propose first summing the gathers over offsets and then correlating the stacks corresponding to calendar times  $c=0$  and  $c=n$ . The minimum phase cross-correlation is obtained for the correct velocity perturbation only in the M-NMO case. We numerically investigate the consequences of setting the ratio  $\beta$  to 1. The velocity model consists of 27 interfaces every 25 m. We simulate six models, for which the interval velocities vary from -0.75 to 0.75% above the reservoir and from -1.5 to 1.5 % within the reservoir (Figure 58a).

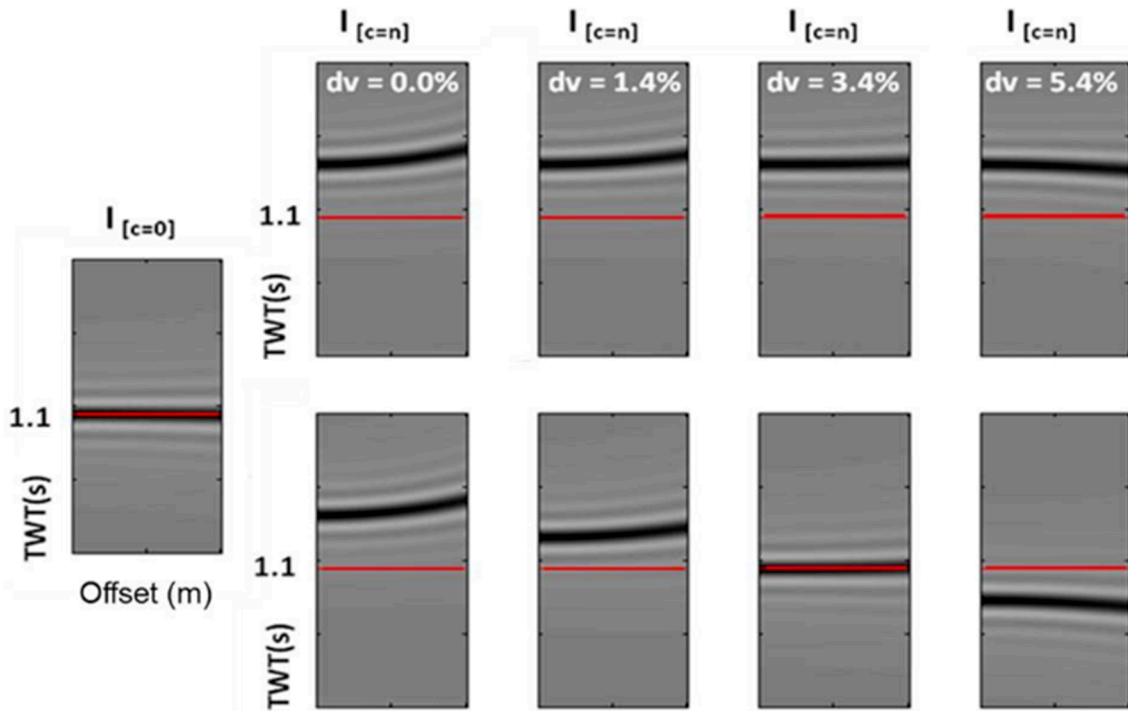


Figure 57: Moveout corrected gathers and the illustration of the differences between the NMO and the M-NMO on a simple 2D synthetic data set. Left: NMO correction in  $v(0)$  on the base line; top: NMO corrections for different velocity perturbations applied to the monitor line; bottom: same as for top, but with the M-NMO correction. The M-NMO corrects simultaneously the event curvature and the time-shifts.

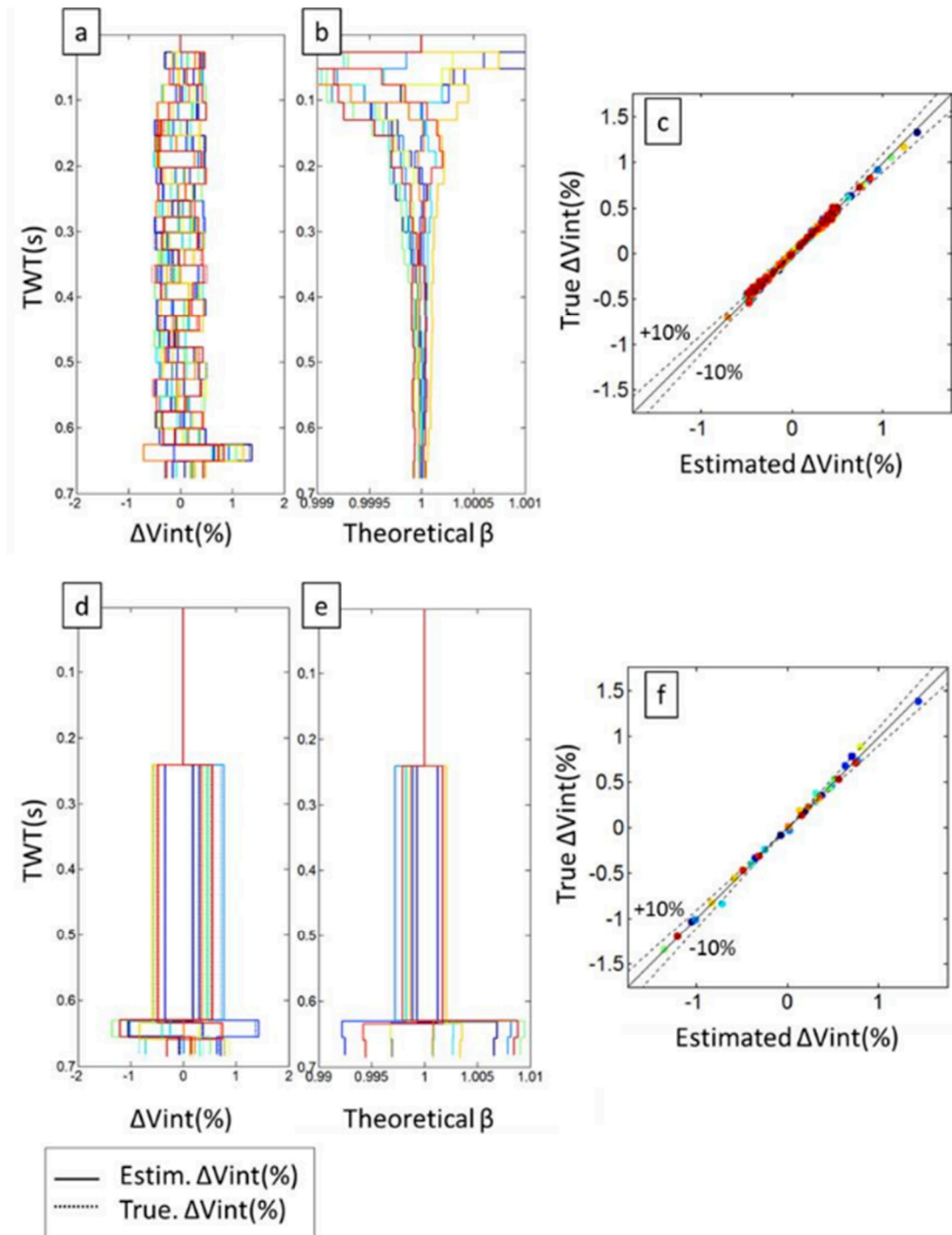


Figure 58: Exact (solid line) and estimated (dotted line) interval velocity perturbations for each horizon (a and d), theoretical beta values (b and e), and one compare to the other (c and f). The images (a-c) correspond to random perturbations above the reservoir, while the images (d-f) to biased deviations between the monitor and the base. All estimated values are contained within the 10% error range indicated by dotted lines (c and f).

The dotted and dashed lines represent the true and estimated interval velocity perturbations for a given calendar time. The velocity estimation follows the M-NMO strategy and includes the hypothesis  $\beta=1$ . A 10% error is introduced in the estimation of the interval velocity perturbation (Figure 58b). Typical interval velocity variations during a month are 0.5%. This means that the proposed estimation scheme would give variations between 0.45 and 0.55%. These are acceptable values in the time-lapse seismic imaging context described here.

## 4.4 Application to a 2D/4D synthetic dataset

### 4.4.1 Forward modelling

We apply the methodology on a 2D/4D synthetic dataset with the same characteristics as the ones of the real data set analyzed in the next section. The original model consists of flat interfaces (Figure 59). The variations in both the reflection and the transmission coefficients with respect to the incidence angles (AVA) are modeled according to the elastic properties of the medium based on the Zoeppritz equations.

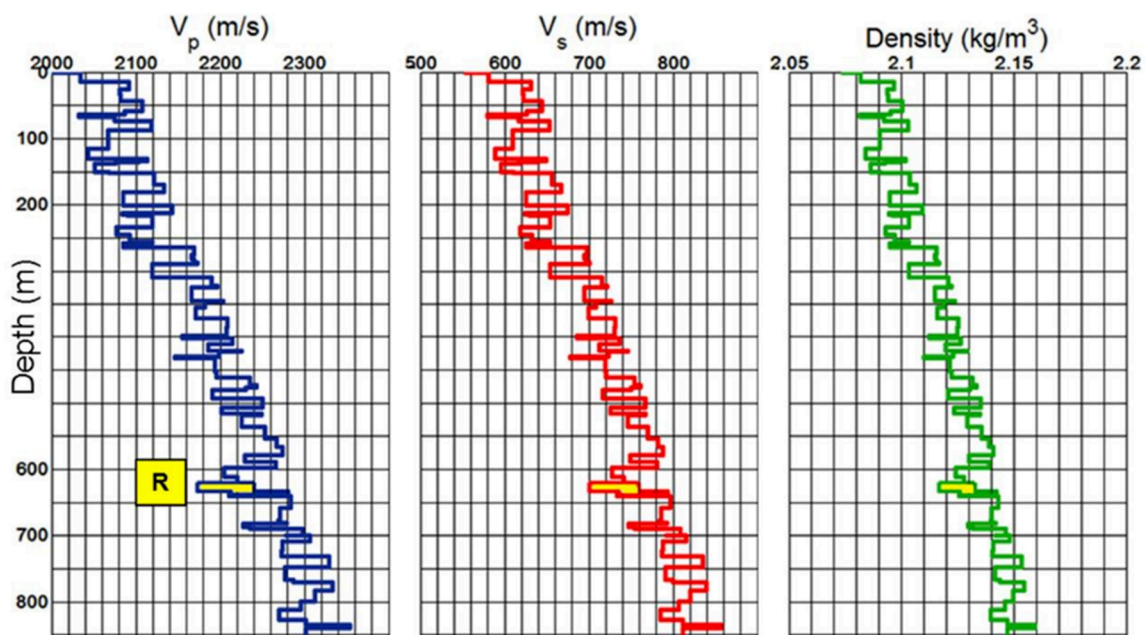


Figure 59: Elastic parameters used to generate the synthetic data set a)  $V_p$ , b)  $V_s$  and c) density models. The 4D variations are localized within the 20 m-thick reservoir.

For the construction of a realistic model, we use Castagna's relationship (water-saturated clastic silicate rocks) to estimate the shear velocity ( $V_s$ ) and Gardner rule to obtain

the density. We compute two data sets for a 3% compressional velocity ( $V_p$ ) increase within a 20-m thick reservoir located at a 620 m depth.

We generate dense seismic gather (Figure 60, Figure 60b and Figure 60c) that are subsequently decimated to obtain sparse, low-fold and aliased seismic gathers (Figure 60d, Figure 60e and Figure 60f). Without noise, the baseline seismic data set (Figure 60a and Figure 60d) aims at representing the summation of a month of repeated acquisition (the stack of 30 consecutive acquisitions) while, in the middle (Figure 60b and Figure 60e), the noisy gather illustrates a daily acquisition. The direct differences between the baseline and the daily data set reveal the noise as well as the amplitude variations at the reservoir interface and the cumulative kinematic variations below the reservoir.

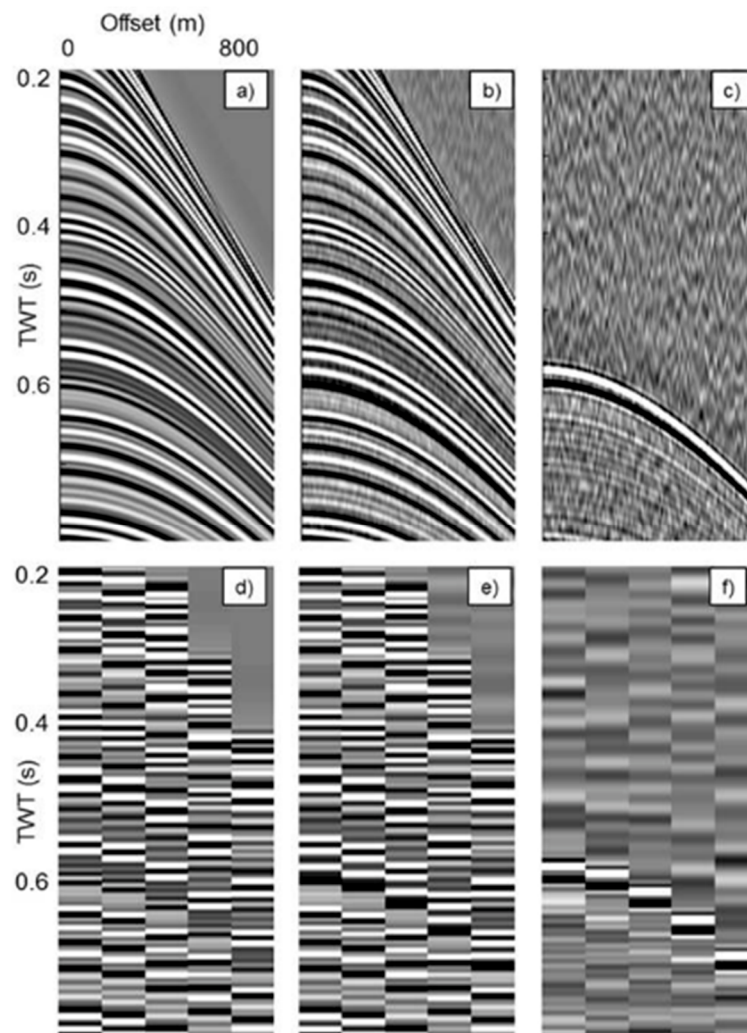


Figure 60: Synthetic data sets (left: base, middle: monitor, right: differences) associated to macro bins ( $48 \times 48 \text{ m}^2$ , top) and to standard bins ( $8 \times 8 \text{ m}^2$ ). In practice, b and c are not available and a is obtained by locally averaging the input data set.

#### 4.4.2 Time-lapse velocity analysis

To determine the background (reference) velocity model  $v(0)$ , we consider the baseline dense gathers (Figure 60a). In the real case study, the baseline dense gathers are obtained by stacking one month of acquisition and by averaging the data over larger bins (spatial macro-binning), typically  $48 \times 48 \text{ m}^2$ . This results in a finer offset sampling as well as in a better signal to-noise ratio; however, we lose both spatial and calendar resolution. This is suitable for building a smooth reference background velocity model but not satisfactory for the detection of localized and rapid reservoir velocity changes.  $v(0)$  is obtained by optimizing the stack (Figure 61a). The first option for determining the velocity perturbation would be to optimize the stack for the monitor survey (Figure 61b and Figure 62b—d). In practice, the stack is only partly improved whereas the velocity perturbations vary around 0.5%. The expected velocity perturbations are small and the semblance value is not discriminative as only limited offsets are available, here up to 800 m. We prefer to follow the alternative strategy (Figure 61c and Figure 62e—g). With the modified M-NMO, the cross-correlation between the base and monitor surveys is more sensitive to small velocity perturbations. We display the travel time shifts corresponding to the maximum cross-correlation (Figure 62f) as well as the associated velocity perturbation (Figure 62g). After velocity updating, the travel-time shifts are reduced and the velocity variations are essentially located below the reservoir.

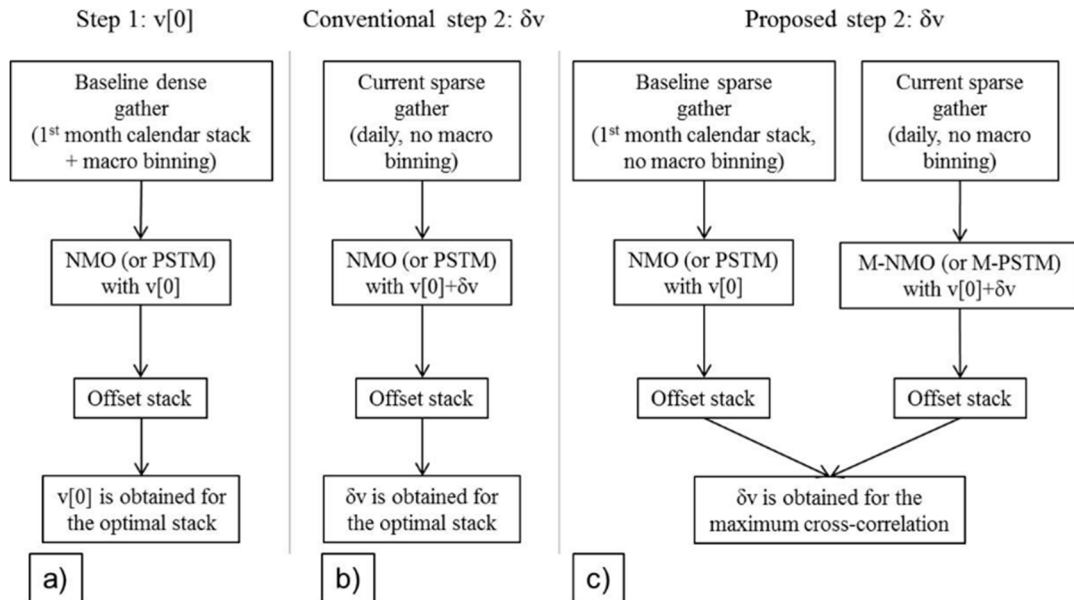


Figure 61: Workflows to determine  $v(0)$  (left) and  $v(c)$  with the moveout analysis (middle) and with the M-NMO (or M-PSTM) and cross-correlation approach (right).

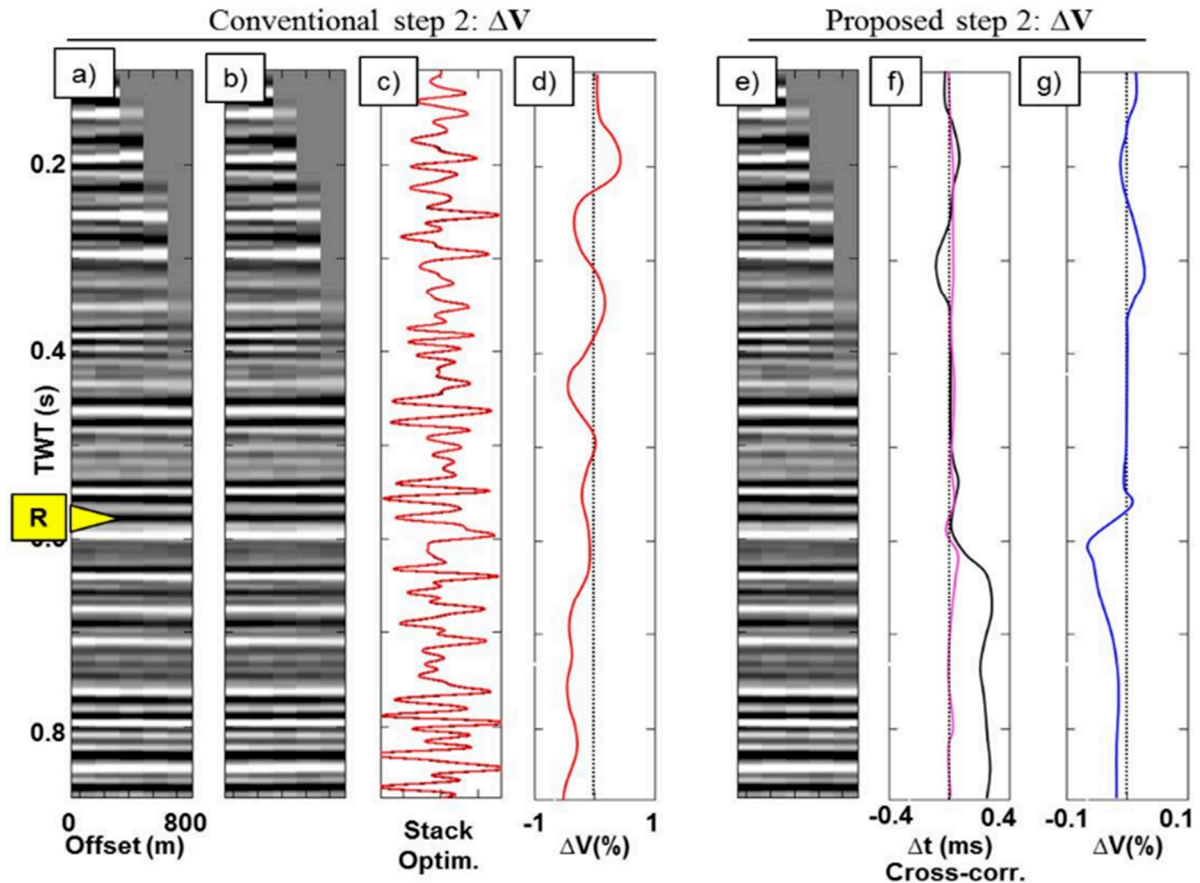


Figure 62: Comparison between the conventional approach based on maximizing the stack (b-d) and the M-NMO and cross-correlation approach (e-g). The gather (a) is obtained by applying a NMO correction in  $v(t)$ . For (b), the NMO correction is designed in  $v(c)$ . The optimal velocity model (d) is the one maximizing the stack. In both cases (red and blue lines, c), the stacks are almost superimposed due to limited offset. The M-NMO gather (e) looks similar, but the cross-correlation is able to detect subtle velocity variations (g). The time shifts corresponding to the maximum value of the cross-correlation are reduced in  $v(c)$  (black and purple curves, f).

#### 4.4.3 Velocity conversion

Many approaches are proposed to estimate accurately interval velocity in complex geological environments (Clapp et al., 1998; Clapp, 2001; Valenciano et al., 2004). The Dix equation states the nonlinear relationship between root mean-square (RMS) velocity and interval velocity (Dix, 1952). After conversion, the main interval velocity perturbation is located around the reservoir (Figure 63). The shallower velocity anomaly (Figure 62g) is not visible in terms of interval velocity perturbation as it has a smoother behavior. The amplitude of the inverted interval velocity model is inversely proportional to the selected thickness of the layers (Figure 63b and Figure 63c). We conclude from the analysis on synthetic data that

the cross-correlation approach is more sensitive than the semblance method for detecting small velocity changes. This is because the proposed approach modifies the position of the events as depth migration would do, allowing a direct comparison through cross-correlation between the base and the monitor surveys. The main hypothesis behind this is that the interface positions remain fixed over time.

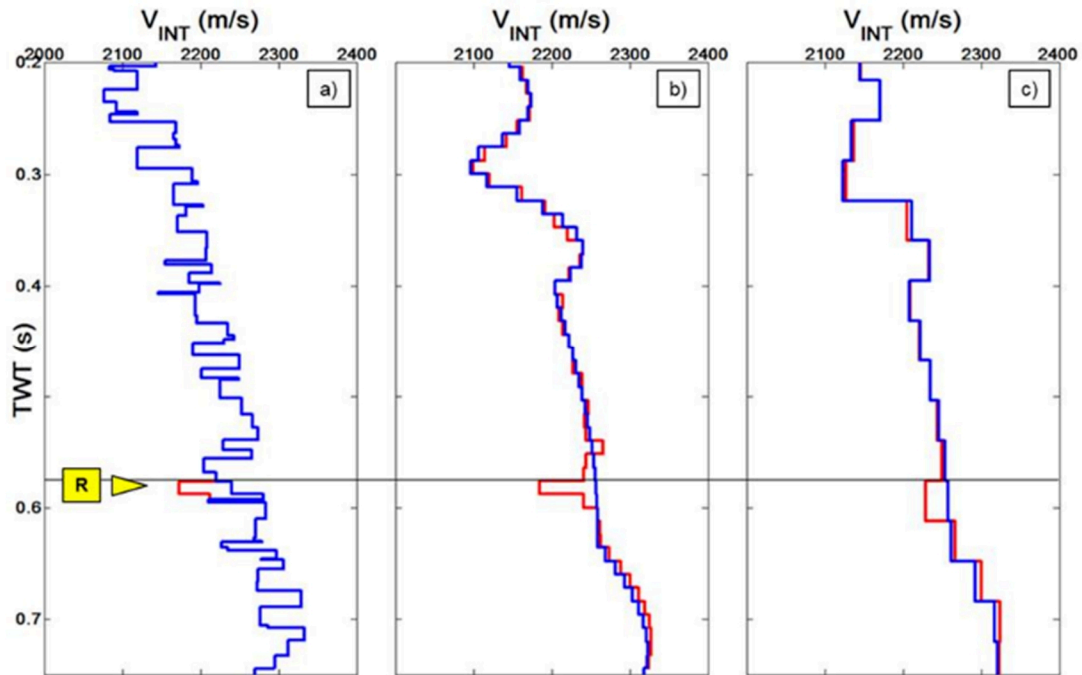


Figure 63: Interval velocity models (blue: reference, red: perturbation) for a) the exact model, b) and c) the inverted interval velocity models, for thicknesses equal to 14 ms and 42 ms, respectively.

## 4.5 Application to continuous seismic monitoring real data

### 4.5.1 Acquisition and pre-processing

We apply the methodology on Schoonebeek continuous reservoir monitoring described in Chapter 3. The preprocessing, previously described is quickly reminded here:

- 1) mute of the near offset shear wave cone,
- 2) attenuation of the near-surface converted waves using a linear high-resolution Radon transform performed on shot point gathers,
- 3) receiver ghost attenuation by cross-deghosting using two level (over/under) hydrophones,
- 4) source ghost attenuation using the time-lapse wave separation.

In the proposed method, we recommend removing the ghost waves prior to the velocity scan as we update the velocity by cross-correlating a daily data set with a baseline survey. By doing so, we ensure that the velocity updates are linked to the reservoir changes and not to ghost variations. The relatively limited number of sources and sensors in continuous seismic monitoring results in a narrow illumination range with a poor offset sampling and a low fold thus leading to sparse common mid-point trace gathers. In order to illustrate how difficult it is to identify the reservoir reflection in the real data, we arbitrarily gathered real seismic records to build two common mid-points (CMP) having different bin sizes (Figure 64).

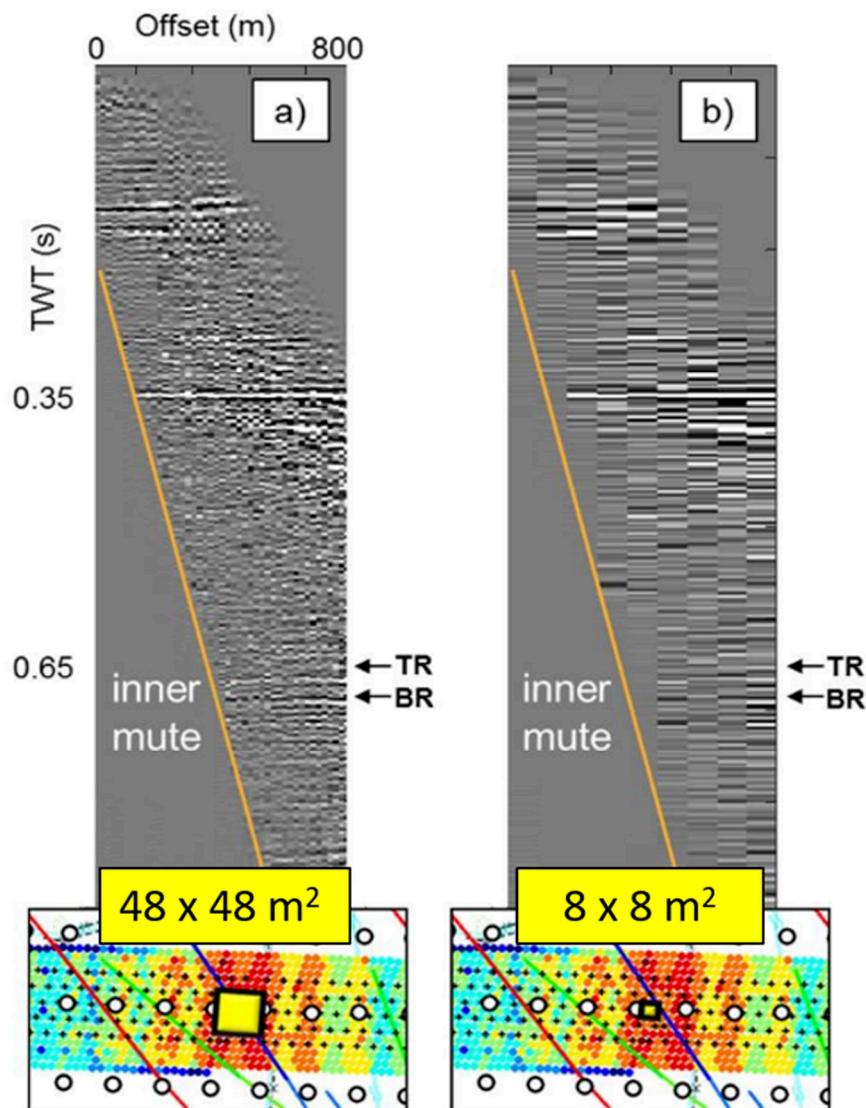


Figure 64: Illustration of the macro-binning (NMO corrected gathers): a 48x48 m<sup>2</sup> macro bin (a) and a 8x8 m<sup>2</sup> nominal size bin (b). The two arrows indicate the base (BR) and top (TR) reservoir

These two CMP are located at the same geographical point, in the middle of the acquisition survey, at the location of the injection well. With the large  $48 \times 48 \text{ m}^2$  bin, the reflection at the reservoir can be identified (Figure 64a). It becomes much more hazardous to recognize the reservoir reflection with the nominal bin size of  $8 \times 8 \text{ m}^2$  (Figure 64b), which is the one that we have to work with to obtain a sufficient spatial resolution for the detection of the steam chamber.

#### 4.5.2 Velocity variations

As for the synthetic data set, we used the approach described in Figure 61. We estimate the background velocity by optimizing the stack using a baseline dataset (over a month of acquisition and  $48 \times 48 \text{ m}^2$  trace gathering). By doing so, we obtain a smooth background velocity  $v(0)$ . Macro bins of  $48 \times 48 \text{ m}^2$  mitigate both the sparse offset definition and the low-fold aspects. Macro bins are used to obtain a reference and smooth background velocity model but are not adequate to detect small-scale and rapid velocity changes within the reservoir. For the velocity update, we rely on both the  $8 \times 8 \text{ m}^2$  baseline (one month of acquisition is stacked) and the daily monitor data. We perform the M-PSTM velocity scan as described in Figure 61c. In the center of the acquisition, at the injection well position, we display the calendar differences (one trace per day) between the month baseline and the numerous daily monitors after PSTM and M-PSTM. We show the differences obtained without any velocity update (Figure 65) and with the velocity updates obtained using the M-PSTM approach.

There are almost no time-lapse effects above the reservoir, showing the high repeatability of the data obtained after careful ghost wave reduction. The residual energy is visible at the reservoir level and below. The M-PSTM in the updated velocity model aims at reducing the residual energy below the reservoir by describing both the kinematic effect and the time shift at zero-offset resulting in a time alignment of the repeated traces.

Figure 66 illustrates both the imaging results (4D differences, in the top) and the associated velocity update (bottom) obtained for the same section located in the north of the survey. We compare the results obtained without updating the velocity model (left) with the ones obtained by updating the velocity model by stack optimization (middle) and by using the proposed M-PSTM velocity analysis (right).

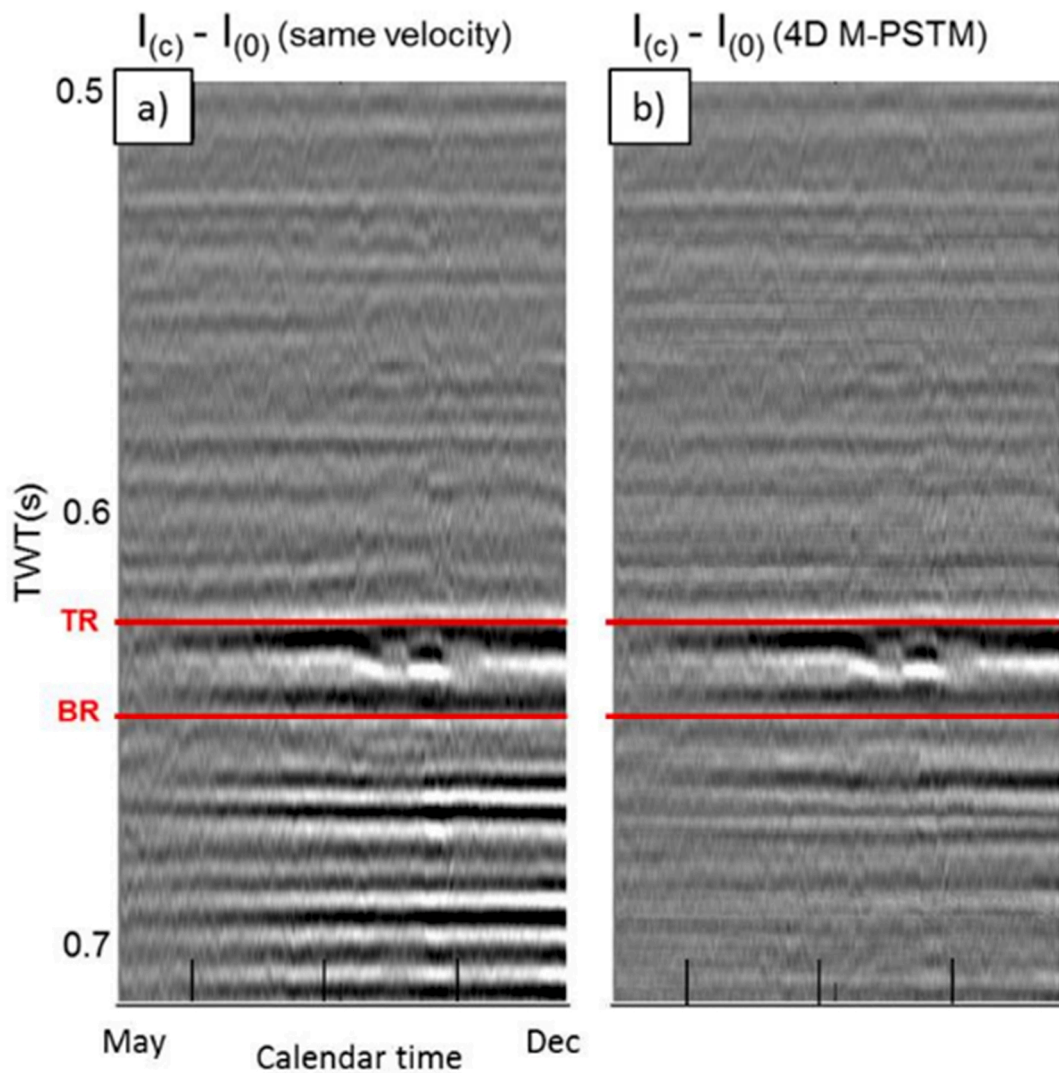


Figure 65: Calendar differences with the baseline (stack of May) at the injection well a) without updating the velocity model and b) with a velocity model update using the M-PSTM approach.

As for the synthetic case, the stack optimization is highly unstable (Figure 66e), resulting in some spiky imaging artefacts observed between 0.3 and 0.4 s as well as below the reservoir (Figure 66b). On the contrary, the proposed 4D M-PSTM time-lapse velocity analysis approach shows more stable results (Figure 66f) with a slight decrease in the RMS velocity directly below the injection well. Moreover, the M-PSTM approach explains both the move-out and the zero-offset time shift resulting in a time-aligned image (Figure 66c).

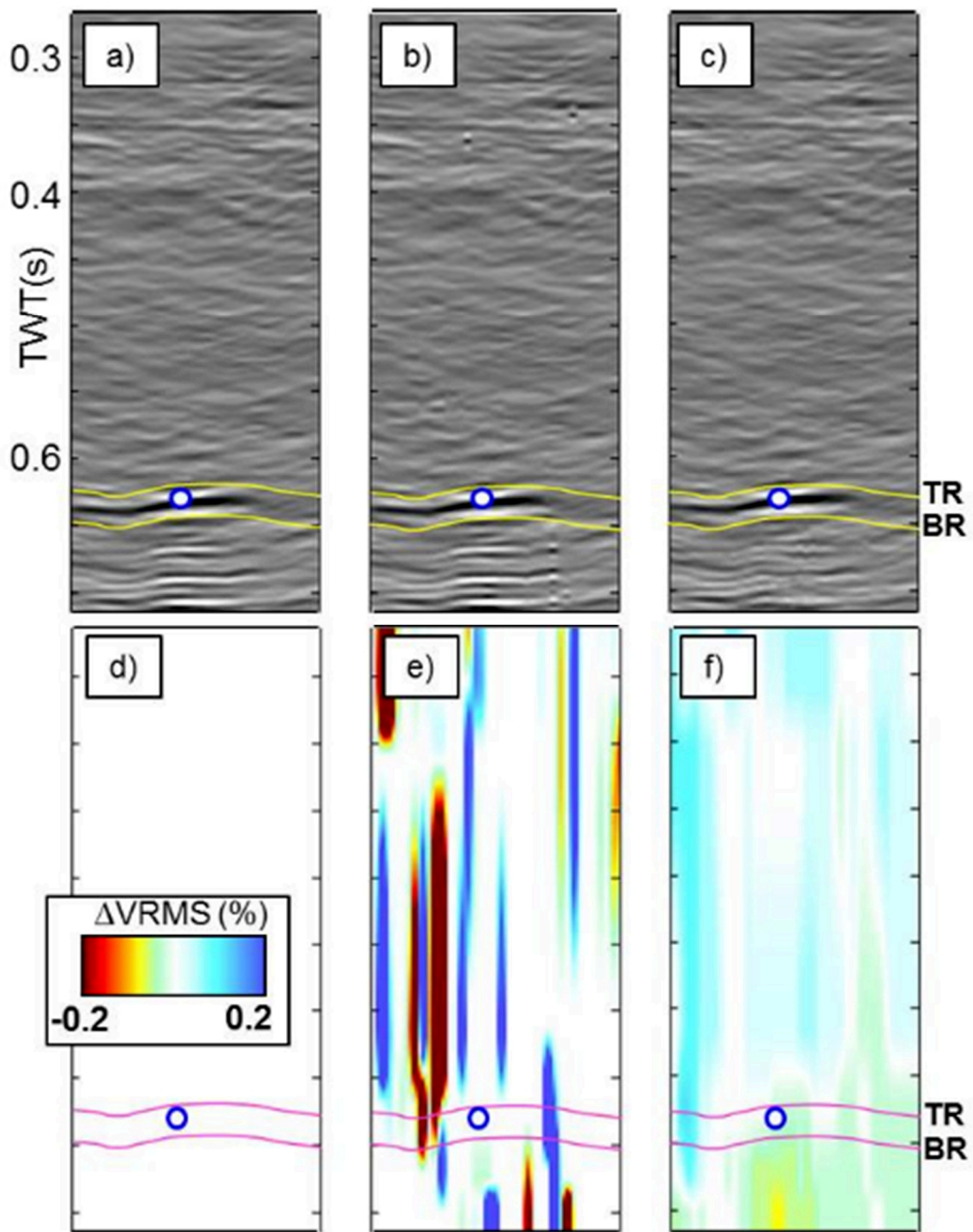


Figure 66: Top: Northern section differences (15th April 2012 and 28th July 2012) without updating the velocity model (a), with updating the velocity model by stack optimization (b) and with velocity updating using the M-PSTM approach (c). Bottom: the velocity variations: no variation (d), variations obtained by stack optimization (e) and variations obtained with the proposed 4D M-PSTM approach (f).

4D interval velocities are obtained with the Dix conversion formula from the RMS velocity (Dix, 1952) (Figure 67 and Figure 68). The crucial element is to provide an estimation of the layer time thicknesses using available horizons for this survey. The available horizons are depicted in red in Figure 67 and Figure 68 while the other horizons (in black) are interpolated linearly in the two-way-time dimension. The RMS to interval velocity conversion aims at focusing the velocity variation around the injection well (Figure 68b). We observe that the interval velocity change is localized inside the reservoir with a 1.5% variation whereas the RMS velocity change is localized at the reservoir and below with smaller values (0.1%). The conversion is therefore essential to localize more precisely the 4D effects.

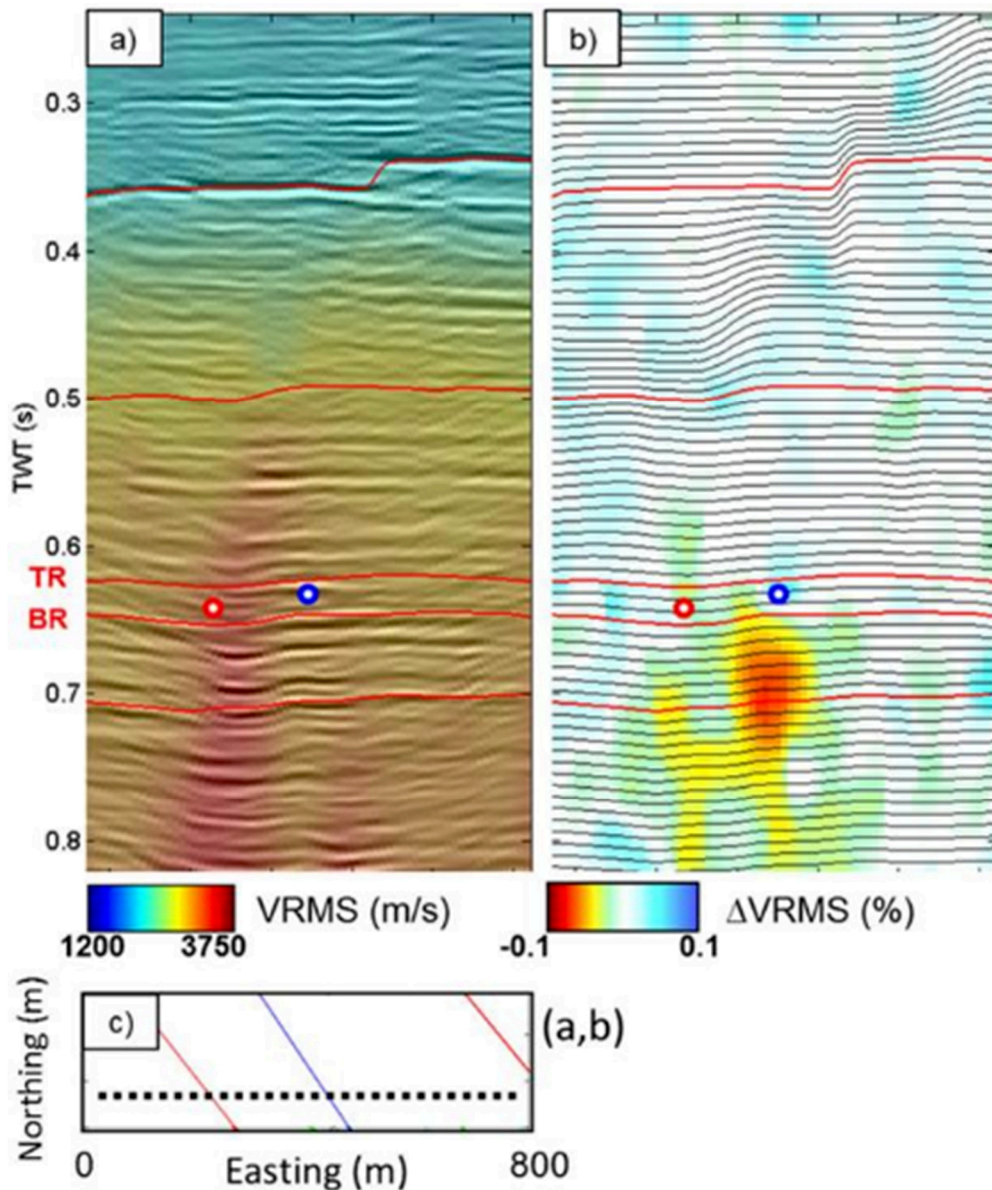


Figure 67: a) Migrated image section in the southern part (background grey scale) for 15th April 2012 and the RMS velocities model; b) the variation percentages (15th April to 28th July) with the horizons and c), the location map.

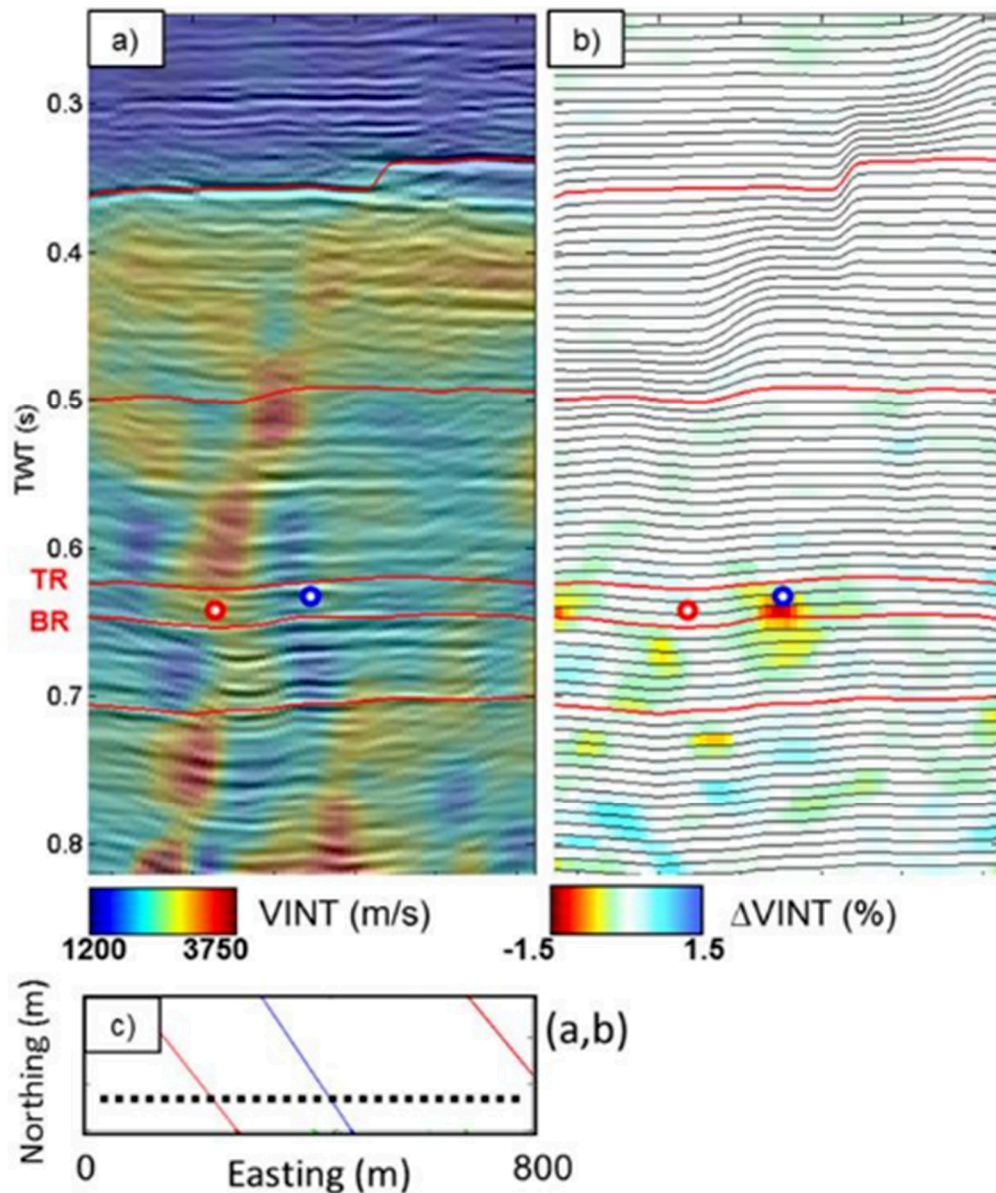


Figure 68: Same as Figure 67, but for the interval velocity models.

We then compare the interval velocity obtained with the proposed 4D M-PSTM approach with the P-wave velocity from log data at the observation well (Figure 69a). Log data including  $V_p$  and impedances refer to a slanted observation well that crosses the seismic volume between 0.610 and 0.630 s TWT. At the injection well location, the reservoir is located between 0.620 and 0.640 s TWT (Figure 69b and 69c). We observe a decrease in the 4D interval velocity down to 1 % around the position of the injection well.

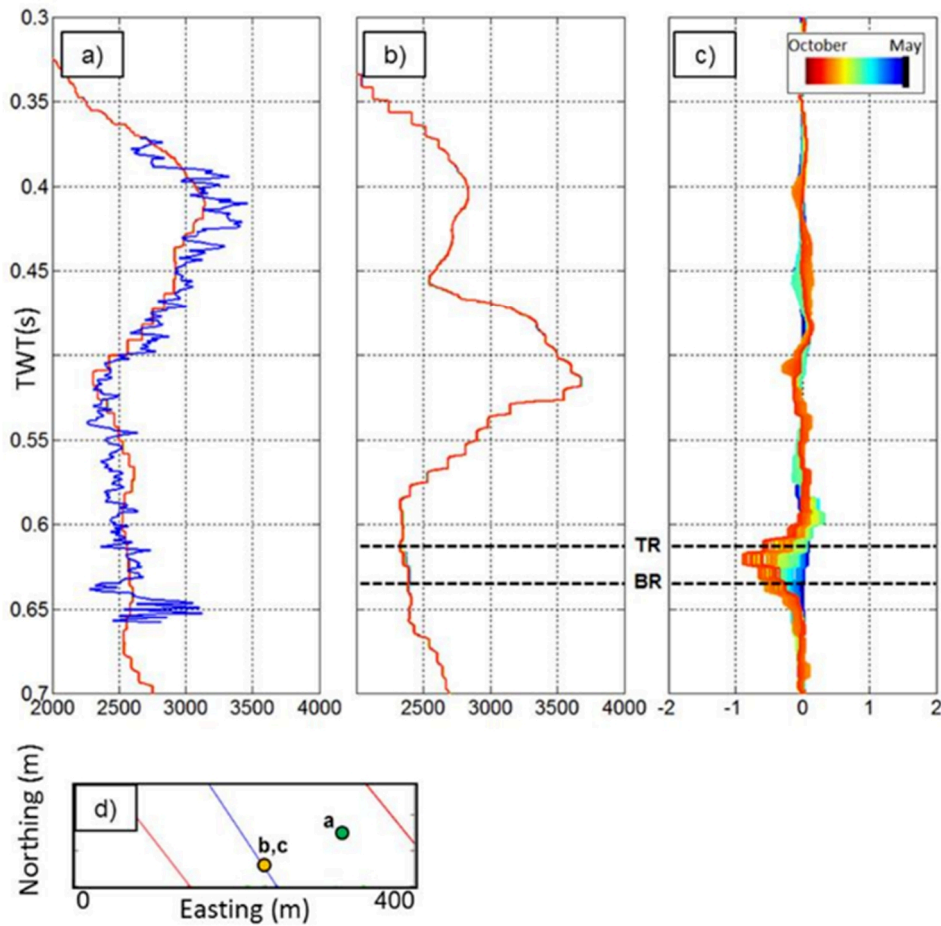


Figure 69: a) 4D interval velocities (in red, with blocky aspect) compared to  $V_p$  given at the observation well in blue. b) 4D interval velocities at the injection well and c) the corresponding variations.

### 4.5.3 Impedance variations

The final imaging residuals after time-lapse velocity analysis are essentially related to impedance variations. In order to retrieve the impedance, Waters (1987) indicated that band-limited impedance generation is equivalent to the application of a -90 degree phase rotation and a high-cut filter of 6 decibels per octave to a zero-phase migration seismic data. Alternatives have been proposed by Ferguson and Margrave (1996). A complete description of the band-limited acoustic impedance work is also available in Simm and Bacon (2014). In this study, the band-limited acoustic impedances and relative variations are obtained by integrating the migrated image that is initially zero-phase. For the present case study, we estimate impedances following these steps: (1) we integrate the zero-phase seismic traces. (2) At the target level, we compare the integrated seismic trace and the impedance log that is filtered by the 10-160 Hz seismic bandwidth. We find a unique scalar that matches the amplitudes of the seismic trace to the amplitudes of the log (Figure 70a). As the well is

oblique (deviated), the matching between the log data and the seismic trace only makes sense at target level (in grey). (3) We take the 10-Hz low-pass filtered impedance log (Figure 70b) and we add it to the integrated and matched seismic trace (Figure 70a) to obtain an estimation of the impedance (Figure 70c). (4) We integrate the whole imaging volume and we apply the same amplitude scalar (the one found in step 2). We then add the same 10-Hz low-pass filtered impedance log to the volume. Seismic data are combined with available well log data. The combination of the log and the band-limited acoustic impedance obtained with the seismic is visible on a section in Figure 71. The vertical resolution of the impedance variation is very high around 5 ms (Figure 71b).

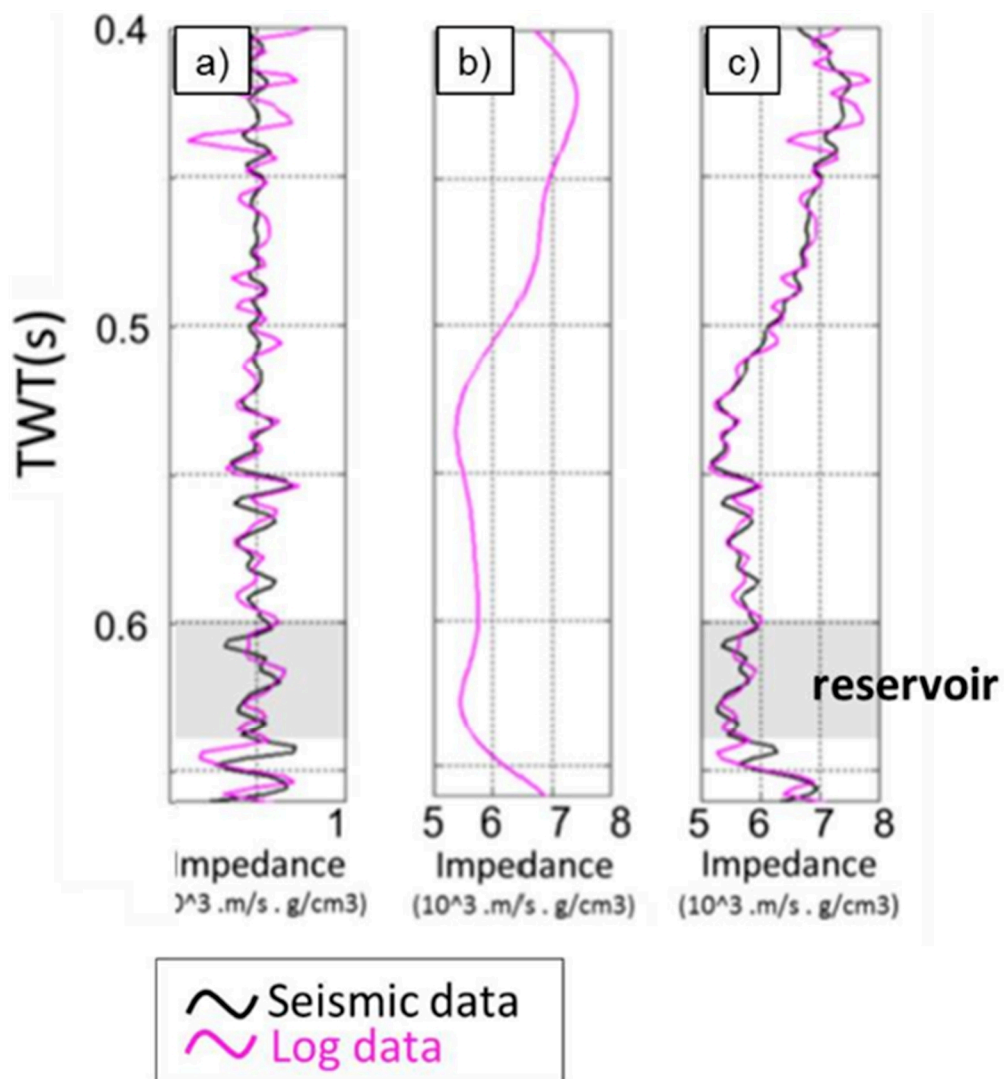


Figure 70: Seismic trace at the observation well a) after calibration to fit the impedance log values in purple. b), the low-frequency part of the log (< 10 Hz). c) Estimation of the impedance.

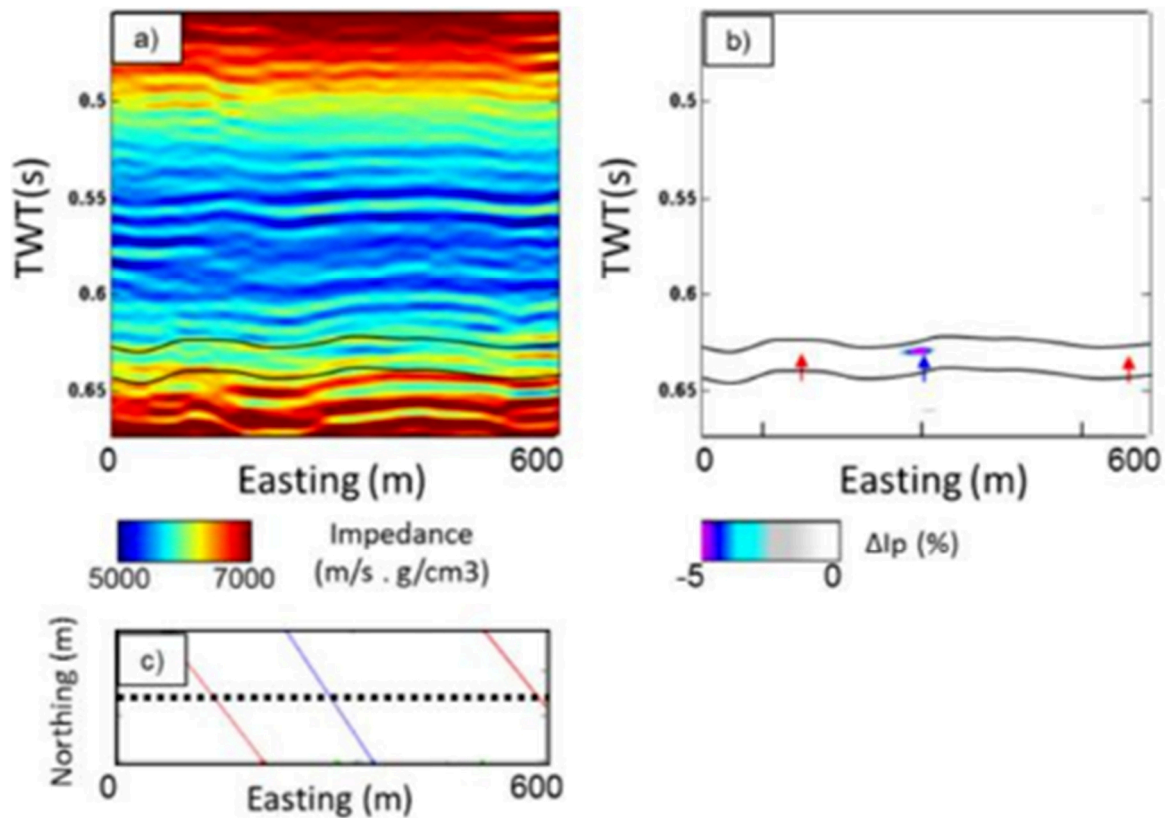


Figure 71: a) Acoustic impedance section obtained by combining well data and seismic section for the 15th of April 2012 and b) impedance variations between the 15th of April and the 28th of July 2012 (b). In (b), the arrows show the well positions (blue: injector, red: producers). c) Location map.

#### 4.5.4 Steam monitoring

The Gravity-Assisted Steam Flood is typically run with two horizontal production wells located on both sides (~150 m) of a center horizontal steam injector. A general description of the field context and of the expected reservoir behavior due to steam injection is given in [Hornman et al., \(2012\)](#) and [Zwartjes et al., \(2015\)](#). Essentially, the low pressure steams injected at a 650 m deep is expected to rise to the top of the 20 m thick reservoir, spread horizontally and then condense. Hot water should then penetrate the reservoir, heating the oil and improving its mobility. The reservoir engineer are interested in knowing how the steam spreads from the injector to the neighboring producers as the pump rate can be changed in order to optimize the reservoir sweep. Moreover, it offers a way of controlling the asymmetric development of the steam front development in the reservoir.

The main 4D observation of the seismic monitoring is that the steam front moves preferentially from the injector to the western producer along a narrow path, rather than spreading uniformly from injector to both producers. A “barrier” prevents the steam from propagating to the eastern side towards the other producer.

The calendar evolution of impedance variations and interval velocity variations in the reservoir is shown from June to December with a two-month interval (Figure 72 and Figure 73). The reference baseline for computation is taken in May. The results are consistent with the measurements of the two observation wells that never detected the expected rise in temperature during the monitoring. A year after the end of the seismic monitoring, the western observation well detects the rise in temperature and pressure, confirming that the steam reached this part (Zwartjes et al., 2015), and also indicating that the steam was absent in those areas during the monitoring.

We observe a fair correlation between the injection data and the seismic attribute ( $\Delta I_p$  and  $\Delta V_{int}$ , Figure 74); we recognize the two notches in the injection rate curve that indicate a temporary halt in the injection. These declines in injection are detected with a one-month delay on the interval velocity variation curve and with a two-month delay on the impedance curve. A similar seismic differential reaction time was also observed for travel time and amplitude variations as a function of the injection rate (Cotton et al., 2013).

Temperature petroelastic model forecast (Zwartjes et al., 2015) state that a temperature increase from 40°C to 240°C should correspond approximately to a 10% P-wave velocity decrease. We measured smaller velocity decreases compared to the petroelastic prevision. Nevertheless, this is expected as the monitoring period (from May to December 2012) started a year after the beginning of the steam injection. In this case, the reservoir may have reached a high temperature earlier. Moreover, Kato et al., (2008) show that for bitumen sand, P- and S-wave velocities have an unusual behavior. Both  $V_p$  and  $V_s$  first decrease rapidly when the temperature rises to a transition temperature (50 °C). Then  $V_p$  continues to decrease but slowly follows the Gassmann prediction slope. In the present case study, a year after the steam injection began; the temperature may have reached the transition temperature at least close to the injector, explaining the small velocity decrease.

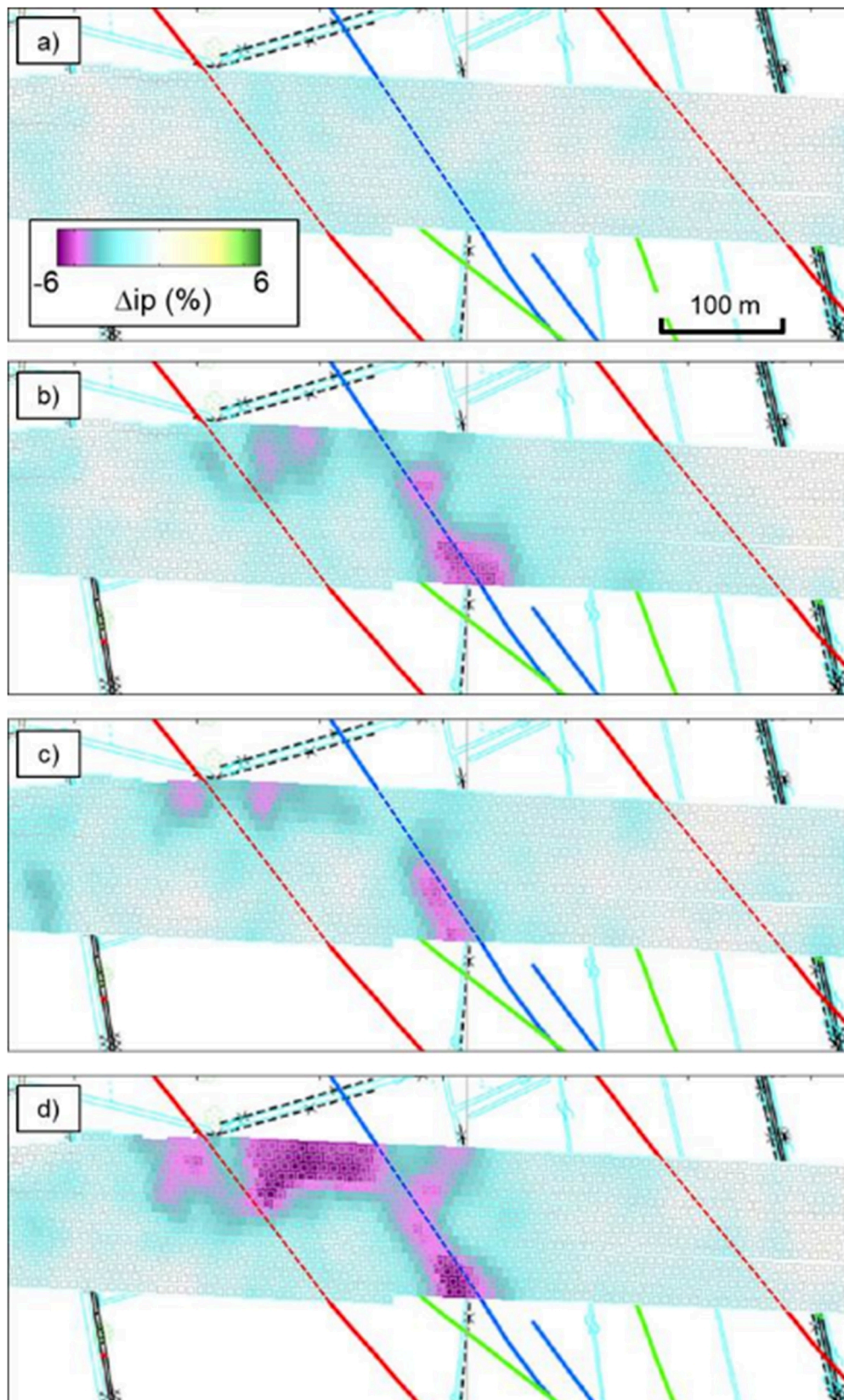


Figure 72: Acoustic impedance variation maps for a) June, b) August, c) October and d) December. The injection well is in blue and the two producers are in red.

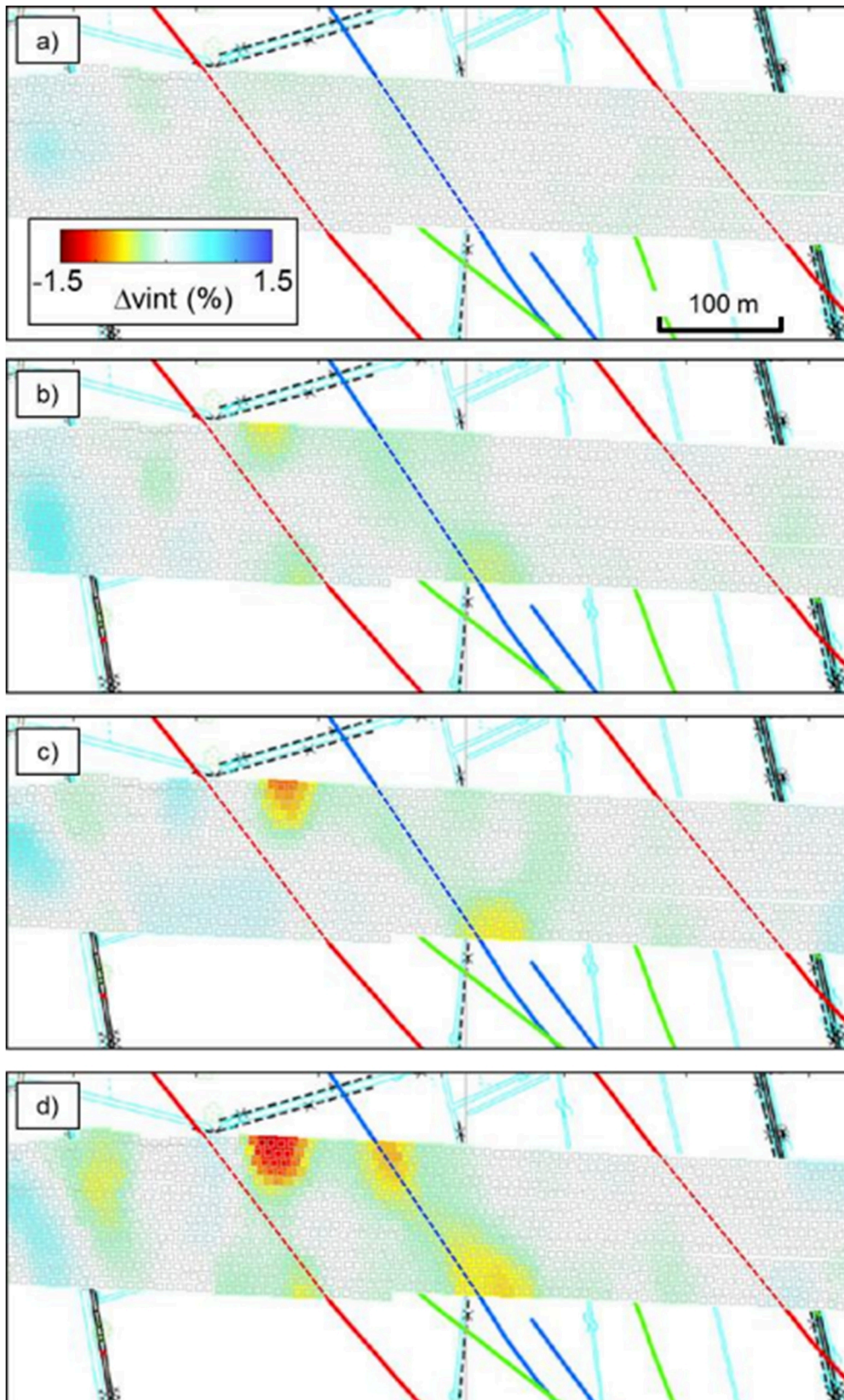


Figure 73: Same as for Figure 72, but for the interval velocity variations.

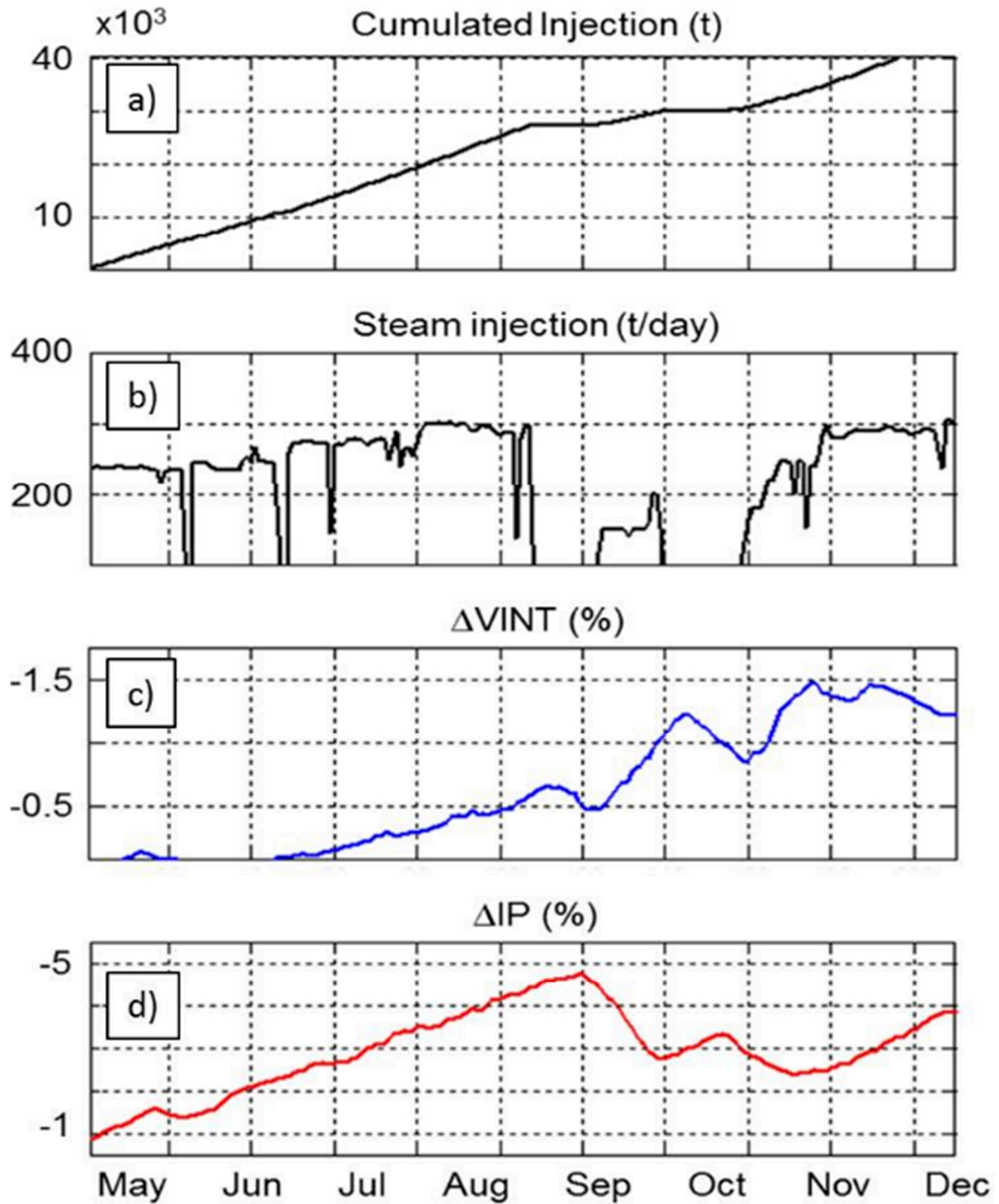


Figure 74: a) and b): cumulated and steam injection, c) the interval velocity variations, and d) the impedance variations at the steam injection well.

## 4.6 Discussion

The ultimate goal of such a seismic monitoring would be to determine temperature, water-saturation and pressure changes within the reservoir. For most of the conventional 4D seismic data, this would be possible by estimating both P- and S-wave velocities as well as the density and having a petro-elastic model (PEM). 4D petro-elastic inversion is known to be the industry standard to estimate it, however, it would require a sufficient number of angle stack images that are not available in this present onshore continuous seismic case study. For this reason, former works were able to provide only impedance variations performing 4D acoustic inversion (Michou et al., 2013; Zwartjes et al., 2015). With the proposed methodology, we confirm the former impedance variations results as well as providing additional information about velocity changes.

Absolute acoustic impedance and P-wave velocity variations estimation is still challenging: the impedance estimation is limited by the seismic frequency and the interval velocity depends on the thickness of the layers. We consider no modification in the reservoir layer thicknesses as proposed by Barker and Xue (2016), assuming that steam diffuses inside the reservoir without modifying its boundaries. As a consequence, we measure the average effect of the steam within given hypothetical layers. The steam chest thickness could be a few meters (Hornman et al., 2012) at the injector and possibly less than a meter at the edges of the steam chamber implying that we are probably underestimating the absolute changes in both velocity and impedance variations.

To quantify the velocity variations in the reservoir, we proposed the 4D M-PSTM approach that computes velocity variations highlighting thermal changes in the reservoir. The 4D M-PSTM data sets are then free from velocity effects. The only remaining effect relating to density perturbation due to the steam saturation can be estimated by a subsequent 4D inversion.

When steam is injected to modify reservoir properties, the velocity model varies from one day to the next. With continuous acquisition, we have proposed an approach where residuals are minimized (delay in the cross-correlation with a baseline survey), offering the possibility to monitor every day the evolution of interval velocity perturbation versus impedance perturbation at different locations. This is a fast 4D qualitative reservoir characterization technique that is able to detect subtle velocity changes and can subsequently be used to validate reservoir models or facilitate the convergence of petro-elastic inversions.

The daily acquisition rate implies the need to conduct fast data processing. The estimated travel-time shifts are small (up to 0.4 ms) compared to the acquisition time sampling interval (2 ms), meaning that careful pre-processing is needed. In the context evaluated here with simple geology, the proposed 4D M-PSTM is sufficient to extract qualitative information. For more complex settings, Full Waveform Inversion, e.g. (Tarantola, 1986) or wave-equation MVA techniques, e.g. (Shragge and Lumley, 2013), would be needed. However, these techniques do not yet deliver real-time output for 3D data sets acquired every day. This may be the case in the future as the number of shots is relatively small and a good reference background model is known. The conversion from RMS to interval velocities is still challenging for a quantitative analysis. Here, we arbitrarily fixed the layer thickness. The resulting values are essentially proportional to the chosen thickness. Limited-frequency bandwidth is combined with available well log data but it is not always easy to extrapolate further away from the well locations.

## 4.7 Conclusion

For sparse seismic data with permanent buried sources and receivers, we have proposed a way to benefit from continuous monitoring. For each calendar acquisition, a new RMS velocity model is determined. It then becomes possible to spatially monitor steam fronts. Time shifts related to kinematic perturbations are automatically corrected. The methodology has been applied to an onshore 4D data set with daily acquisitions over a period of six months. The main limitation in the time-lapse analysis proposed here is the assumption that the interface positions do not vary over time, whereas the interval velocities may change. With denser sources and receivers, residual travel-times could be picked and used for updating the velocity model. In the future, the ray-based approach should be replaced by a wave-equation strategy to better take into account the limited-frequency aspect of the data.

## 5. Real-time PSTM: TeraMig

---

Les projets 2D/3D présentent certaines similitudes conceptuelles avec les projets 4D. En 4D, Le géophysicien compare les données courantes aux données de référence issues d'une acquisition passée. En 2D et en 3D, et particulièrement sur le terrain, le géophysicien compare les enregistrements issus du point de tir le plus récent à ceux issus d'un point de tir de référence. Dans ce dernier cas, le rôle du géophysicien consiste à vérifier la cohérence des données en temps réel pendant la période d'acquisition. Quelque part, il s'agit également d'une question de répétabilité.

Afin de réaliser le contrôle qualité des données en temps réel, nous proposons une méthode innovante (TeraMig) qui effectue automatiquement la migration temps « pré-stack » sur le terrain. Cette méthode facilite le travail de contrôle qualité. De plus, elle permet dès l'étape d'acquisition de fournir une image sismique de qualité pouvant être utilisée comme volume initial pour le début des travaux d'interprétation.

---



## 5.1 Introduction

Real-time acquisition quality control faces new and real challenges. In the Middle East, the data quantities to be controlled in the field have increased exponentially over the last decade (Pecholcs et al., 2010). This trend is particularly true in the case of ‘mega-crew’, blended, single-sensor, high density, and wide-azimuth acquisitions (Shabrawi et al., 2005; Meunier et al. 2008). In other parts of the world, seismic exploration is carried out in unconventional areas (rainforest, foothills) where acquisition conditions are challenging (Munoz et al. 2015). For these acquisitions, the ability to control the data quality in real-time is considered key. In other strategic exploration areas, unstable geopolitical conditions make it hazardous to have quality control staff permanently in the field.

Pre-stack time migration (PSTM) is still considered as a final product as it is generally performed in a processing center once the whole dataset become available at the end of the acquisition. Among time processing workflows, the PSTM is known to be computer time-consuming. It still indeed requires a certain time to be fully performed, even the best-clustered computer system. In some recent land massive dataset, it would require months of intensive computing to achieve a full PSTM: this is the case for the most recent blended dataset acquired for Apache in Egypt.

In some operations, fast track processing is applied in the field after a block of seismic data is collected. However, acquiring a block of seismic data may take several weeks, and processing the data may take up to a week, even when post-stack migration techniques are used. As a result, there is a substantial time delay between acquiring raw seismic data in the field and producing analyses or images using migrated seismic data.

Faced with these challenges, we propose a new quality control tool that performs real-time pre-stack time migration (PSTM) in the field autonomously and automatically taking into account the global quality of the seismic data during the acquisition. The goal of the real-time field PSTM is not to replace the end-product PSTM but is rather to provide an intermediate product that could be used to QC the data quality in the field and to start earlier the interpretation.

The main ingredient is the Kirchhoff migration, formulated as a matrix multiplication (section 5.2), where the input vector is a newly acquired trace and the output result is the migrated trace. We describe the computational cost (section 5.3) and present some results (section 5.4) obtained in a real time situation during an acquisition in the Middle East.

## 5.2 Kirchhoff migration

Most of the migration algorithms were implemented 50 years ago when the best computer clusters were 10 times less powerful than a present single laptop. In the early 1970's, some careful approximations were required to perform a migration within reasonable time. Among others, the most popular approximation was the time migration. Time migration is always incorrect as it assumes that the diffraction shape is purely hyperbolic (locally 1D) and as it does not take into account ray curving at velocity boundaries except in the case of curved ray PSTM, as proposed by [Levin \(2003\)](#). However, time migration is quite fast and is robust to velocity model errors contrary to depth migration. Further, errors in the shallow velocity model have very limited impact on the imaging of the deeper structures. Moreover, a time migrated section can be easily compared to a CMP stack sections that is an advantage for field implementation as the CMP stack is still commonly used in the field.

Among time migrations methods, FK migration ([Stolt, 1978](#)) would be a good candidate for real-time implementation as it is one of the fastest migration methods. FK migration works perfectly for constant velocity and would have an interesting application for onboard real-time water bottom migration (i.e. anti-multiple model building). However, FK migration is restricted to constant velocity migration. To overcome the constant velocity restriction, [Beasley et al. \(1988\)](#) propose to manage time-variant velocity by cascading the FK migration and by partitioning the velocity field. This method brings promising results but induces many careful interpolations of the migrations operators that have been investigated by many authors ([Harlan 1982 and 1983](#); [Popovici et al., 1993](#); [Lin et al., 1993](#); [Blondel and Muir, 1993](#)). Finally, FK migration would be less flexible than Kirchhoff migration because of the numerous interpolation and regularization issues.

[Claerbout \(1985\)](#) uses the harbor example to describe the principles of migration. In this example, a wavefront comes across a breached storm barrier with a plane incidence (the wave front is parallel to the barrier) as illustrated in Figure 75a. The hole in the barrier acts as a Huygens's secondary source and induces a semicircular wave front that is propagating in the direction of the shore (Figure 75b). Suppose that the hole in the barrier position is unknown and that we want to locate it; we would lay out a receiver cable along the shore to record the approaching wave front (Figure 75c). The response in the  $x - t$  plane is the diffraction hyperbola. The apex of the diffraction hyperbola gives the position of the hole in the barrier (Figure 75d).

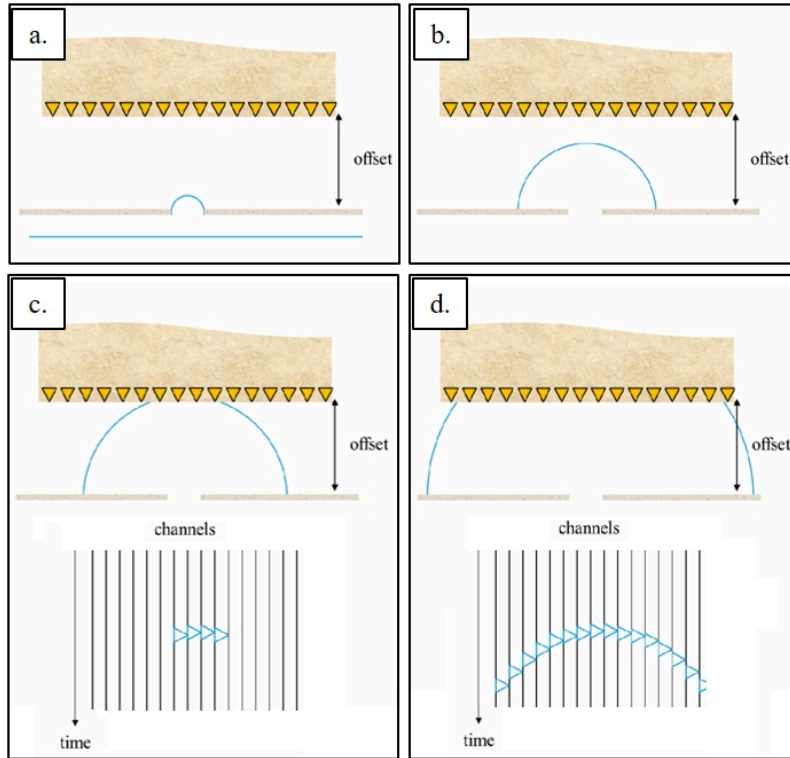


Figure 75: The harbour experiment showing a diffraction hyperbola. From Claerbout (1985), modified. (illustration done for a TeraMig lecture given at CGG-University)

The second illustration (Figure 76) is closer to what is happening in seismic exploration. A wave is generated at the Earth surface. It induces a semicircular wave front that is propagating in the subsurface. The direct wave is propagating to the sensors. When the wave front comes across a subsurface heterogeneity, it acts as a secondary source inducing a circular wave front.

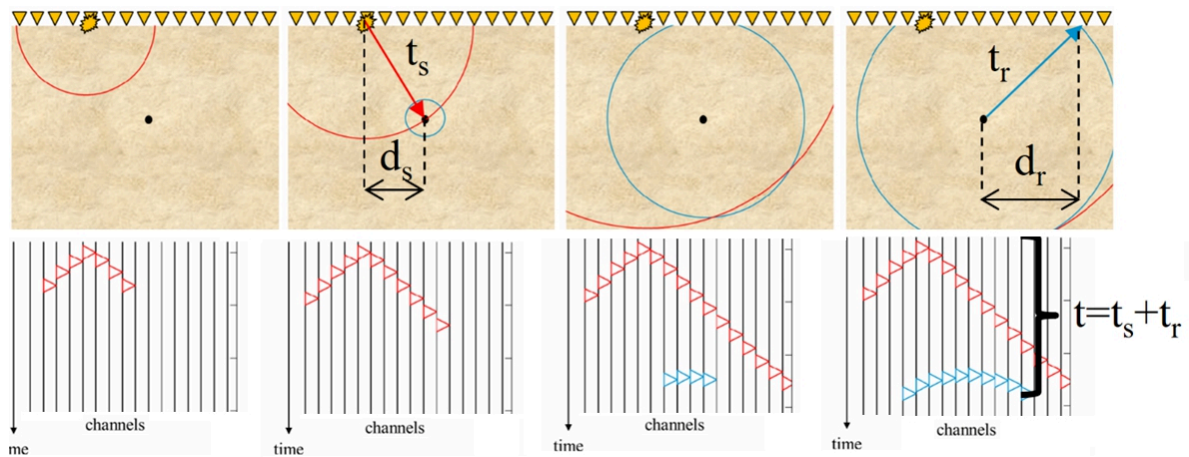


Figure 76: Diffraction in a seismic experiment. (illustration done for a TeraMig lecture given at CGG-University)

Part of the wave front is propagating downward (transmitted wave front) while the other part is propagating upward (reflected wave front). The position of the heterogeneity is at the apex of the diffraction hyperbola. At each sensors, the recorded propagation travel time is the sum of both the source-to-heterogeneity and the heterogeneity-to-receiver travel times (Figure 77).

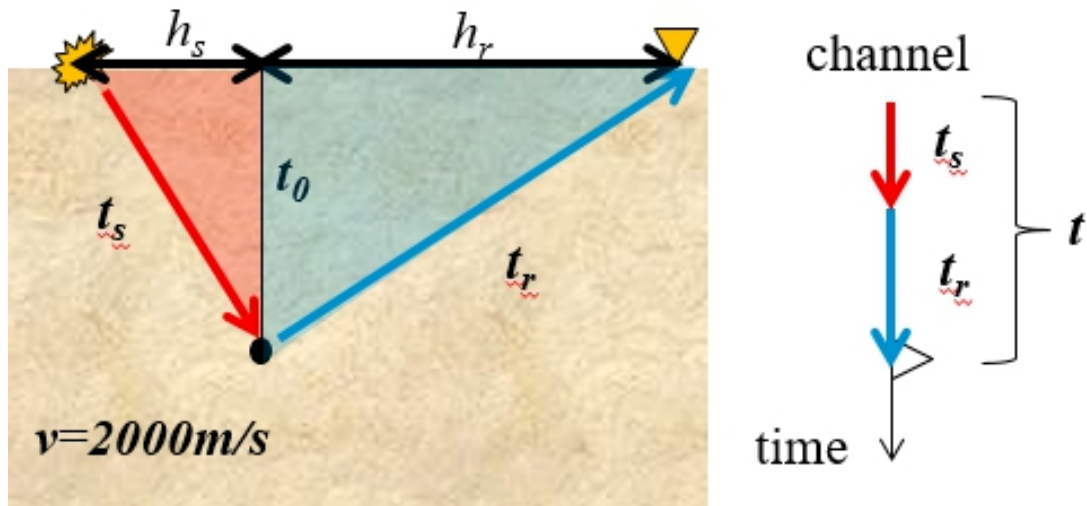


Figure 77: Illustration of the double square root equation that define the direct Kirchhoff migration. (illustration done for a TeraMig lecture given at CGG-University)

In any locations, the total travel time equation reads:

$$t(h_s, h_r, v) = \sqrt{t_0^2 + \left(\frac{h_s}{v}\right)^2} + \sqrt{t_0^2 + \left(\frac{h_r}{v}\right)^2}, \quad (27)$$

where  $t_0$  is the two-way-time at zero offset,  $h_s$  and  $h_r$  are the surface projection of the distance source-to-heterogeneity and heterogeneity-to-receiver,  $v$  is the wave propagation velocity inside the medium. The diffraction curve can thus be modeled and the travel time surface is known as “Cheops’ pyramid” (Figure 78). The result of the seismic amplitude summation over the pyramidal surface is finally placed at its apex. Reflectors in the subsurface can be visualized as being made up of many points that act as Huygens’ secondary sources.

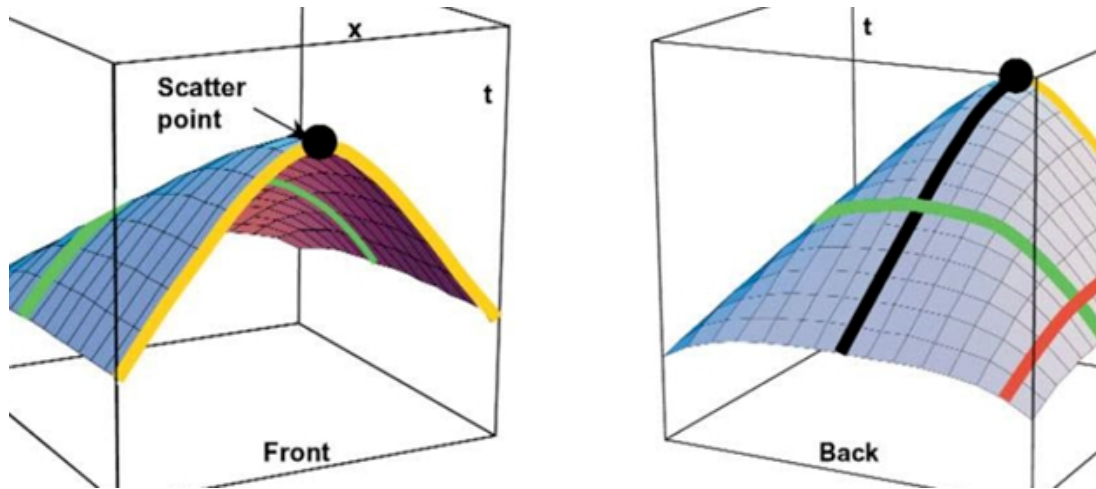


Figure 78: Cheops' pyramid illustrating the diffraction surface in 3D seismic (yellow: zero-offset diffraction; green: common-offset diffraction; Black: common-midpoint at the scatter point location; red: common-midpoint away from the scatter). (Courtesy of CGG-University)

### 5.3 TeraMig

The diffraction summation that incorporates the obliquity, spherical spreading and wavelet shaping factors is called the Kirchhoff migration. The relation between the migrated and the input data can be expressed as follow:

$$d_{Mig}(x, y, t) = \varphi * \iint_{s,r} d \left( s, r, \sqrt{\frac{t^2}{4} + \frac{h_s(x, y)^2}{v(x, y, t)^2}} + \sqrt{\frac{t^2}{4} + \frac{h_r(x, y)^2}{v(x, y, t)^2}} \right) ds dr, \quad (28)$$

where the asterisk denotes a convolution operator. The filter  $\varphi$  corresponds to the time derivative of the measured wavefield, which yields the 90-degree phase shift and adjustment of the amplitude spectrum. For 2-D migration, the half-derivative of the wavefield is used. In Equation 28,  $h_s(x, y)$  and  $h_r(x, y)$  respectively represent the source-to-image and the receiver-to-image distances projected at the Earth surface. Equation 28 is quite simple; however, note that the distances should be computed for every imaging positions and every source-receiver couples. In the case of billions of traces to be used for the imaging of millions of positions, the distance computation becomes challenging by itself. The velocity varies spatially with  $x$  and  $y$  as well as with the time  $t$ . A velocity model defined for e.g. 3000 time samples and millions of imaging position would be memory consuming. One could consider a sparse definition of the velocity says every kilometers; however, this would lead to

interpolation challenges. In TeraMig, we assume a 1D velocity varying only with time and we propose to compute the migration operator for theoretical discretized  $x$  and  $y$  positions. The advantage is that the computation can be done without any real data and thus can be achieved before the acquisition. By doing so, Equation 28 can be reformulated as a matrix vector product when the indexes matrix, noted  $M$ , is pre-computed:

$$d_{Mig} = \varphi * \sum M d \quad (29)$$

The indexes of the migration operator represents the time delays that have to be applied to the input trace (shift up) to be in place before the summation. In practice, the time delays are divided by a sample interval meaning that the shift is always an integer number of samples. Prior to the shift, the input data is oversampled to a desired accuracy. When seismic data are processed, we first compute both the source-to-image and the receiver-to-image distances projected at the Earth surface as in Figure 79.

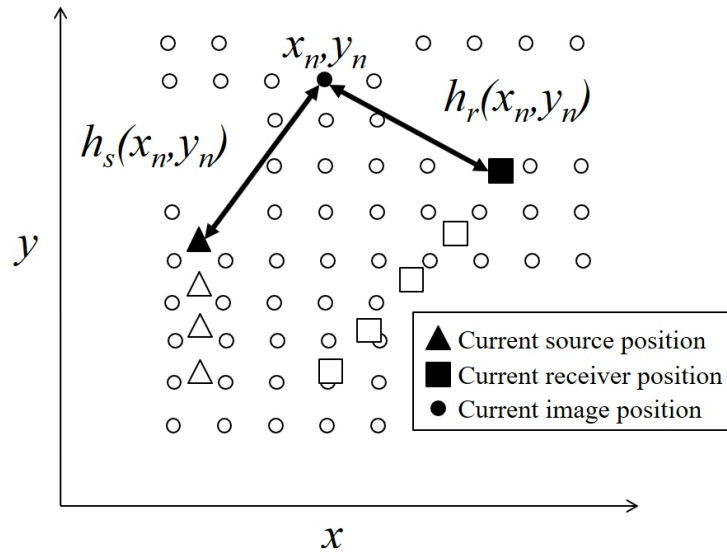


Figure 79: source-to-image and receiver-to-image computation

Once the distances are calculated, we find the corresponding cell in the pre-computed index matrix containing the shift to be applied at any times as illustrated in Figure 80. In practice, the image positions are regrouped in spatial tiles so that the distance computation is optimized. By doing so, we do not need to compute the distances for all the image points comprised in the whole survey. We first select the required tiles as illustrated in Figure 81, then we compute the distances as illustrated previously. Once the tiles are selected, we use an atomic multithreading algorithm that is comprised in the open MP library of the programming language C. By combining the tiling and the multithreading, the distance computation becomes achievable in reasonable times.

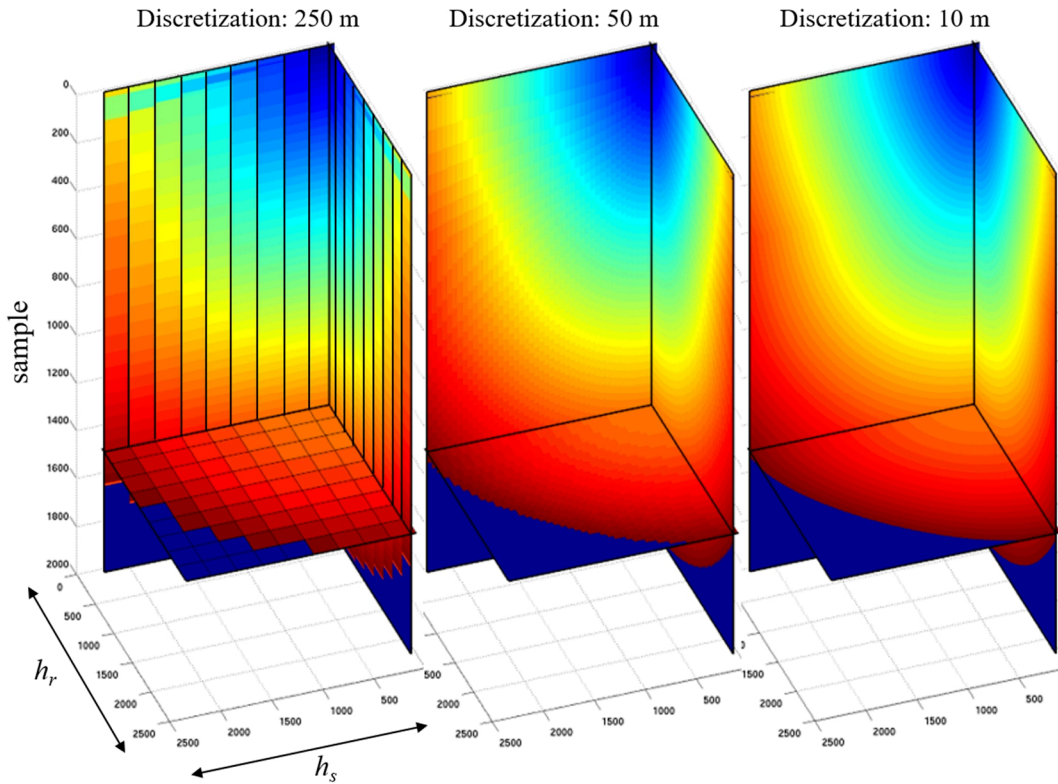


Figure 80: Representation of the TeraMig indexes and of the spatial discretization: 250 m that is never used in practice (left), 50 m (middle) and 10 m (right).

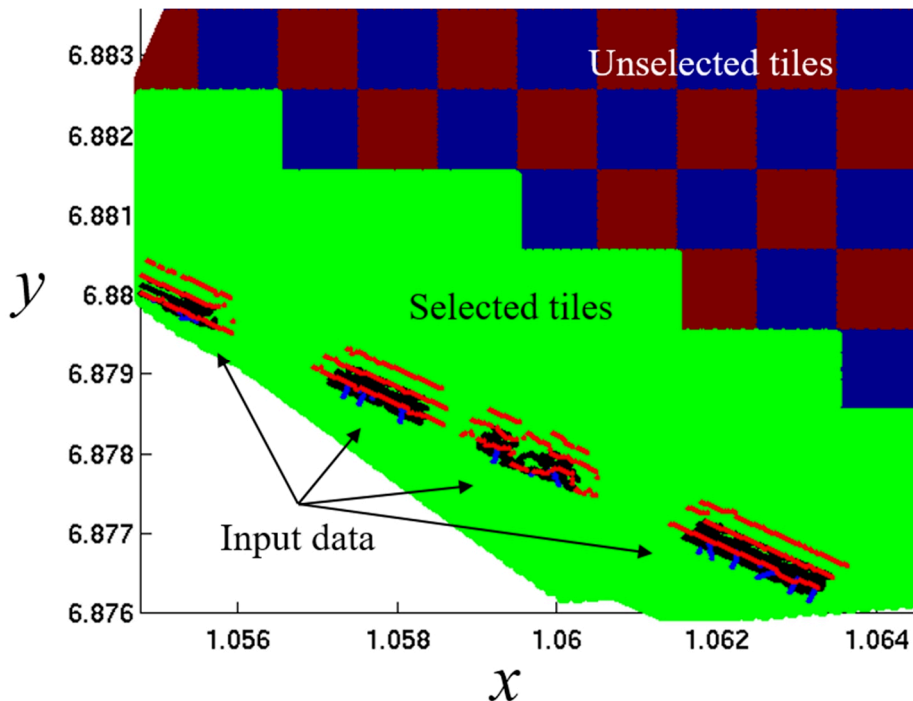


Figure 81: Illustration of the tile selection in TeraMig. Each tile comprises numerous imaging positions.

The TeraMig algorithm results are compared to the ones obtained with a reference algorithm comprised in the CGG Geovation<sup>TM</sup> software suite (TIKIM). Figure 82 shows the

PSTM image of a unique trace for different source-receiver offsets. The two algorithm gives very close results validating the TeraMig PSTM algorithm. The slight differences between the two are mainly due to the spatial discretization process in TeraMig.

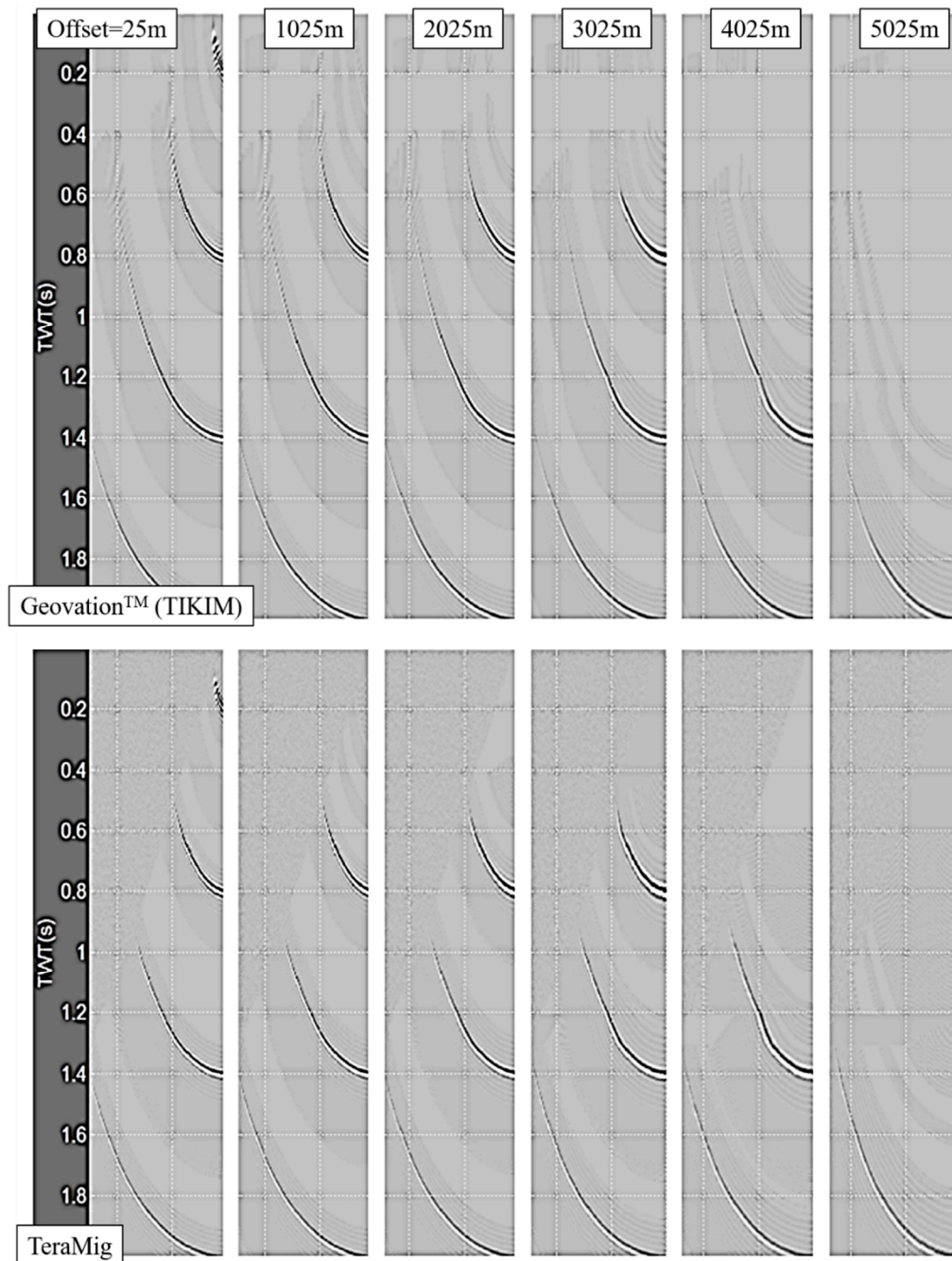


Figure 82: Comparison between a reference PSTM algorithm (TIKIM) in Geovation™ (top) and TeraMig (bottom). Each panel represents a common offset migration from 25 m (left) to 5025 m (right). The results are very close validating the TeraMig algorithm for field QC PSTM.

As expressed in Equation 29, The Kirchhoff migration acts as a de-noising filter as it stacks numerous samples of input data (Figure 83). This is valuable for field QC as

acquisition inconsistencies would be better highlighted on clean data than on noisy data (GPS datum change, sweep change, block overlapping). Moreover, this summation will mitigate as well most of the blending noise and should attenuate the ground-roll (except in the ground-roll apexes).

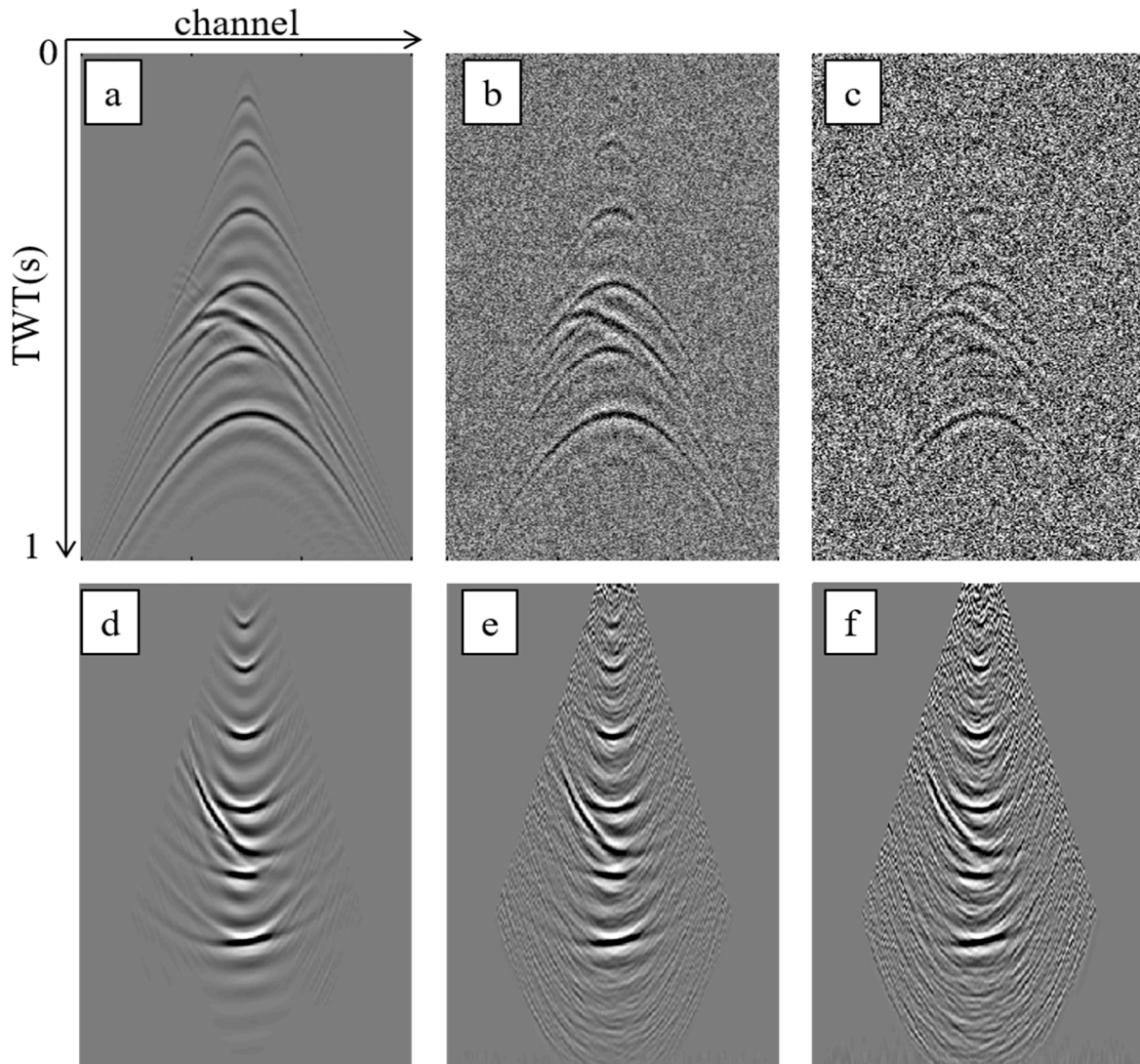


Figure 83: Illustration of the noise reduction in the image domain after migration. Before migration (top), we show synthetic input data without noise (a) and with an increasing noise level (b and c). The reflections becomes somewhere hidden by the noise (c). After migration (bottom), the noise level is significantly attenuated. Even for the noisier synthetic input record (c), the reflections appears clearly after migration (f).

## 5.4 Computational cost

As opposed to the post-acquisition PSTM carried out by high-qualified processors in the time-pressured processing center, we have somewhere plenty of time to run the PSTM in the field. The only challenging constraint is to be able to follow the acquisition and thus to do not accumulate PSTM processing delay during the operations. In other term, we must follow the real-time of the acquisition cycle to be able to perform QC, to analysis the data and ultimately to take decisions and to make corrective actions during acquisitions. This is illustrated in Figure 84.

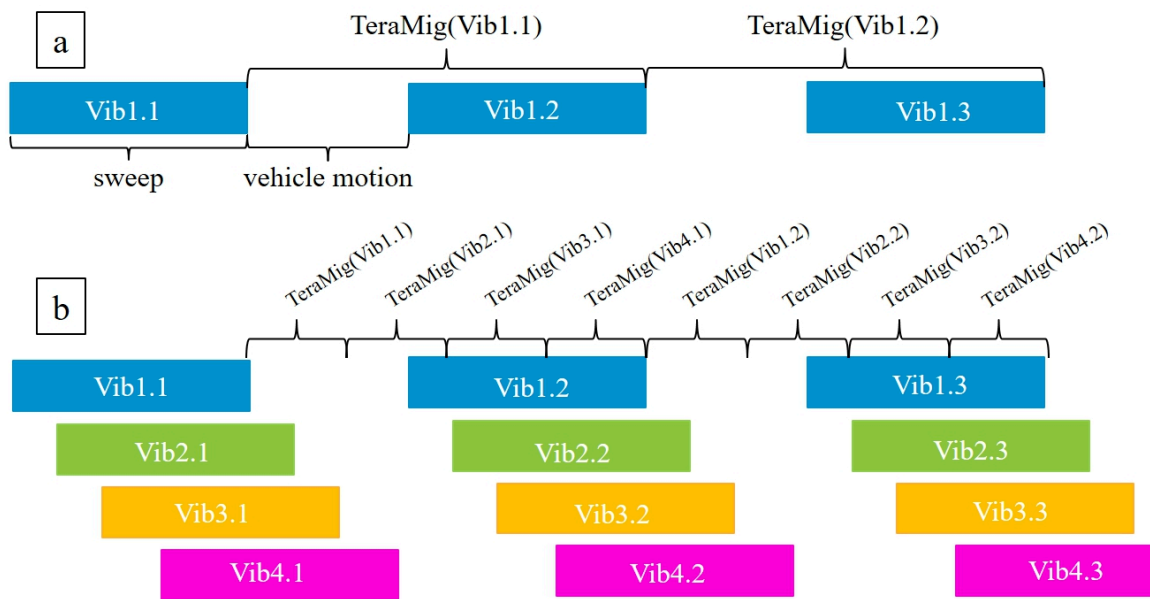


Figure 84: The acquisition cycles and the maximum time-slots for TeraMig processing. A conventional acquisition with a single vibrator (a). A more advanced productivity using the slip-sweep method (b). The TeraMig time slots can be significantly reduced.

Despite of the real-time constraint, we can use the whole acquisition period (commonly several months) to achieve the whole PSTM cube. This allows us to use a reduced computational effort, sized to follow the acquisition production cycle that is typically less than 5 seconds using high productivity techniques like slip-sweep, DS<sup>3</sup>, ISS, unconstrained acquisition. Hence, the total computational effort for real-time field PSTM is spread over the whole acquisition period (Figure 85) and is thus achievable using simple, standard (and low-cost) computers.

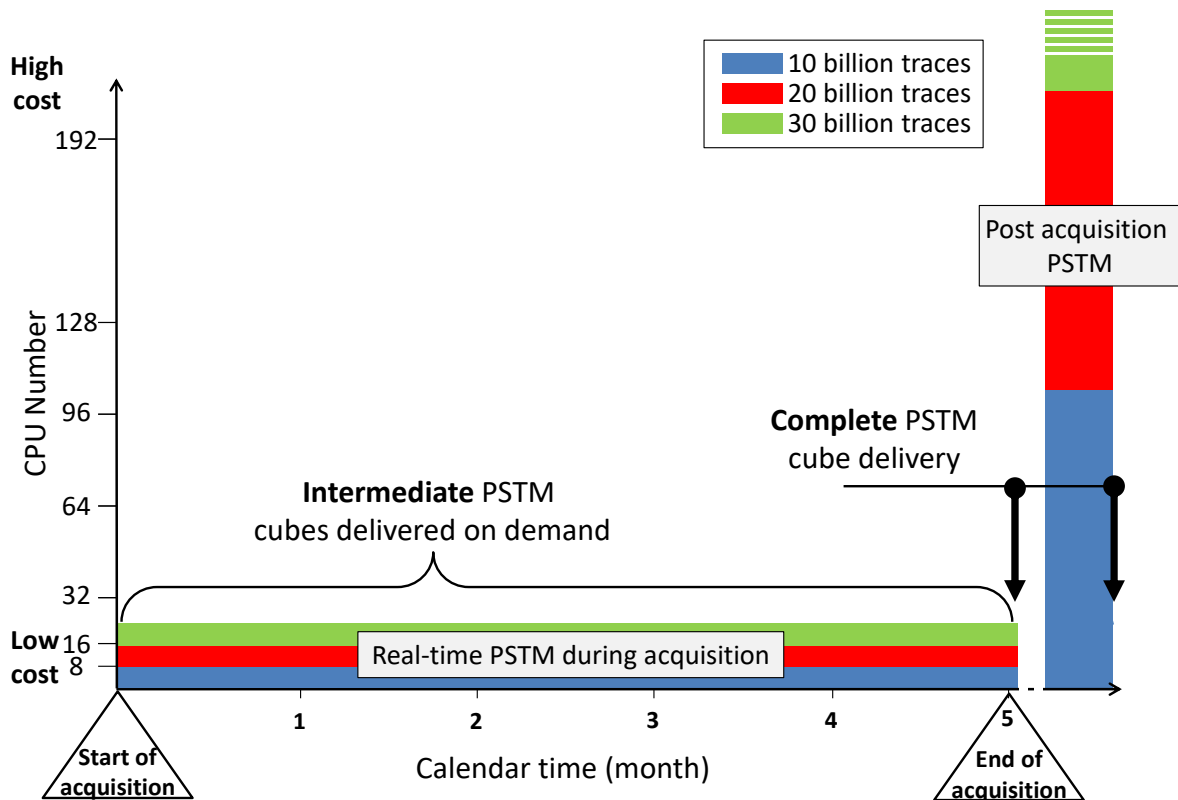


Figure 85: Comparison of the computational efforts between real-time field PSTM and post-acquisition PSTM. Computational effort is represented by the surface of the coloured rectangles that is equal to computing time multiplied by number of CPUs.

## 5.5 Network and IT design

Seismic surveys are often carried out far away from the processing centers. Expensive and limited satellite connections remain inadequate to transfer the huge amounts of raw VP data. When the field location is not relatively close to the processing office, tape transfer by physical ways (truck or air shipment) from the field to a processing agency is considered as an issue (Duncan et al., 1997). Finally, data transmission would not be feasible in our case study and in most of the Middle East acquisitions (time constrain, cost and HSE). This explains why the proposed system is implemented in the field. Moreover, as the PSTM is done automatically in the field, the field geophysicist in charge of the data quality control can continuously control the updated field PSTM cube (Figure 86a).

The proposed system is designed to send samples of the field PSTM cube to a processing center (Figure 86b). In this case study, the satellite connection is extremely limited and only established once daily within a short, underutilized time window at night.

This connection is nonetheless sufficient for transmitting inlines, crosslines, and even several time-slices on a daily basis. This enables the project staff in the processing center to remotely follow the building of the field PSTM cube during acquisition on a daily basis.

In the processing center, the data received daily is automatically organized and displayed in a report file (pdf format). It is then automatically sent worldwide to the end users via intranet or internet so that they can follow the building of the field PSTM cube while acquisition is ongoing (Figure 86c).

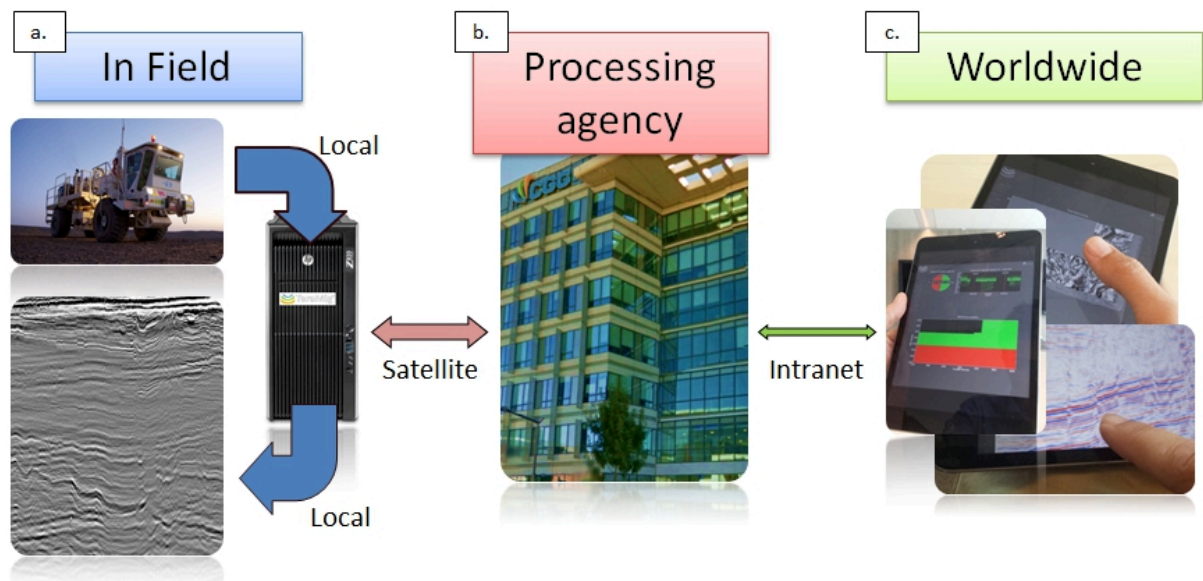


Figure 86: Real-time Field PSTM network: « TeraMig Everywhere »

## 5.6 TeraMig workflow

TeraMig is designed to deal with raw acquisition data in real-time meaning that numerous integrity checks must be done when considering billions of seismic records representing hundreds of terabytes per project. Figure 87 summarizes the TeraMig workflow. On the dedicated TeraMig computer, a file manager (running on a single thread) continuously cross-examines the distant raw data storage bay and its own log information. Each new file that is not in the log is immediately loaded. This may appear simple; however, even this simple step requires careful coding and data organization procedures (millions of shot point files will be stored in the bay at the end of the acquisition and millions of lines may compose the text log file). The file manager checks as well the data integrity (seismic headers, sampling interval, total number of traces in the file, number of dead traces, average RMS). Then it

applies the elevation statics (and eventually other basic processing like amplitude equalization or spherical divergence compensation). Additionally, the file manager does some selections (auxiliary traces and spurious traces are flagged in the log and are not stored in the local hard disk). When a raw seismic file contains too many anomalous traces, the file manager immediately alerts the field QC geophysicist and flag the shot point file with a bad status in the log (the field QC geophysicist has the possibility to modify this threshold to e.g. 5 % of anomalous traces). Note that the file manager must be faster than the TeraMig main processing (the one that performs the PSTM on multi threads).

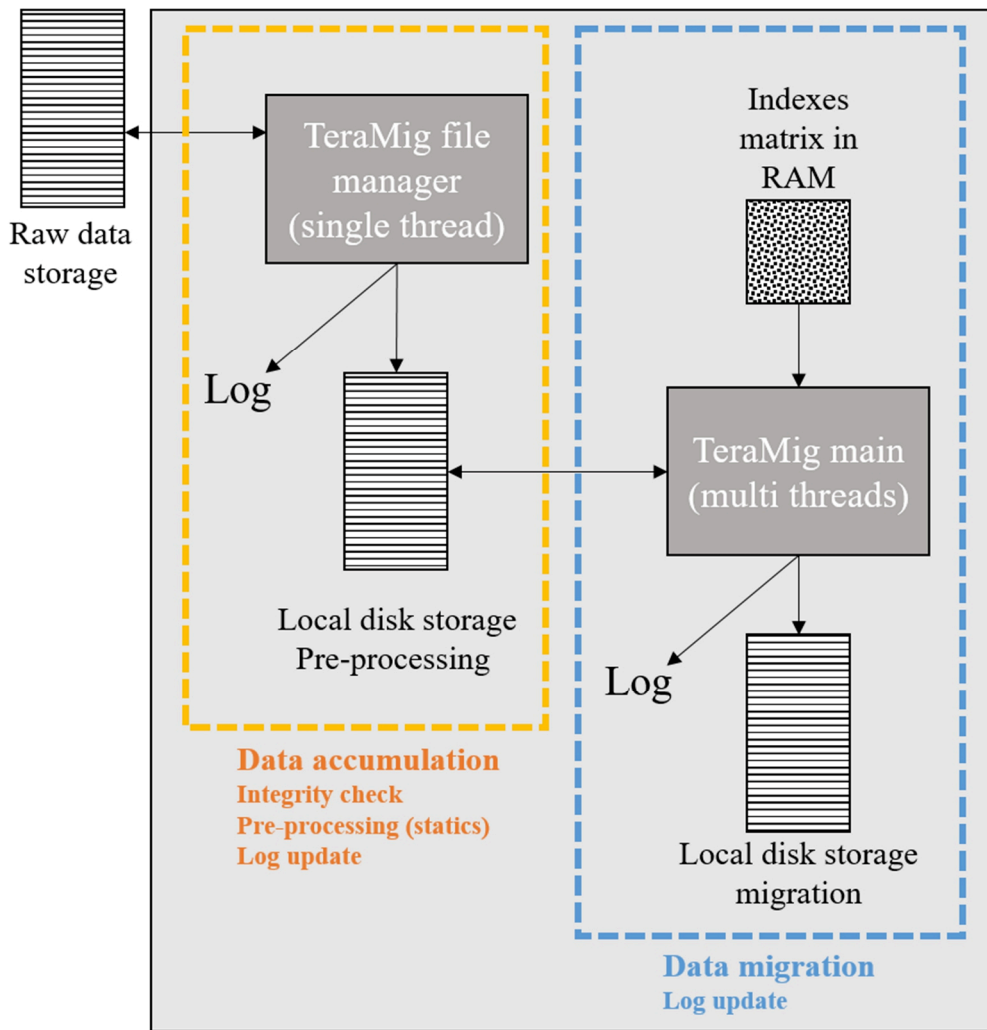


Figure 87: The TeraMig workflow.

## 5.7 Results

The dedicated computer processed the raw VP data with only one intervention needed to reboot subsequent to a seismic crew global power down. The application proved

remarkably stable given that it operated autonomously 24/7 during the five months of acquisition. The real-time field PSTM migrated around one million VPs representing more than 10 billion traces.

In this case study, we used one desktop computer powered by 8 cores, each cadenced at 3 GHz. The computer had 32 GB of RAM. With this quite light computer capacity, we have been able to process an average of 15,000 VPs per day (approximately one VP processed every five seconds) that was sufficient to follow the real-time seismic acquisition cycle (Figure 88).

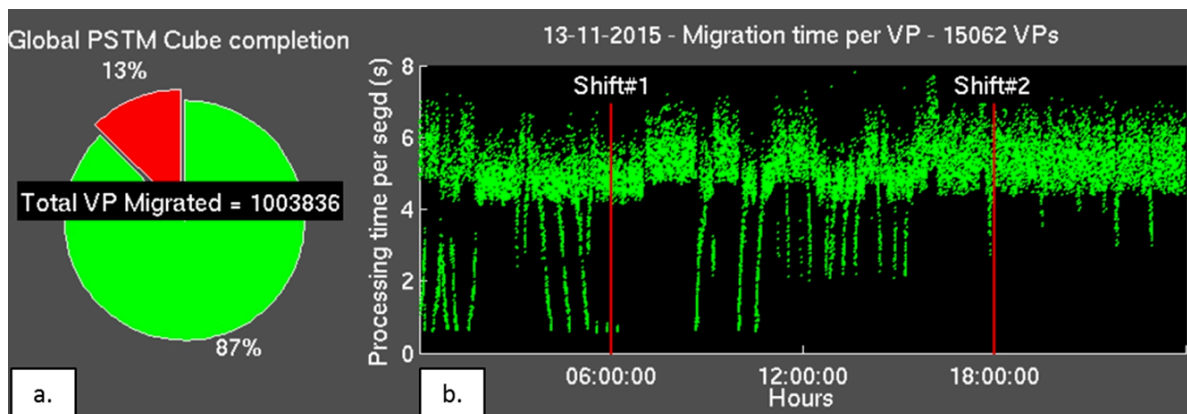


Figure 88: Operational results as of 13 November (extract of the automated daily reports).

Figure 88a and Figure 88b are part of a typical daily reports sent to the end users. In Figure 88a, the pie chart shows the status of the field PSTM cube completion as well as the total count of processed VPs up to a given day. In Figure 88b, we show the processing of the VPs as a function of the time during the production day. The duration of the processing per VP is not constant but depends on its maximum offset, its position compared to the PSTM cube (edge effects), and the number of active channels selected.

We compare the real-time field PSTM and the conventional field stack that is produced weekly by the quality control geophysicist in the field (Figure 89).

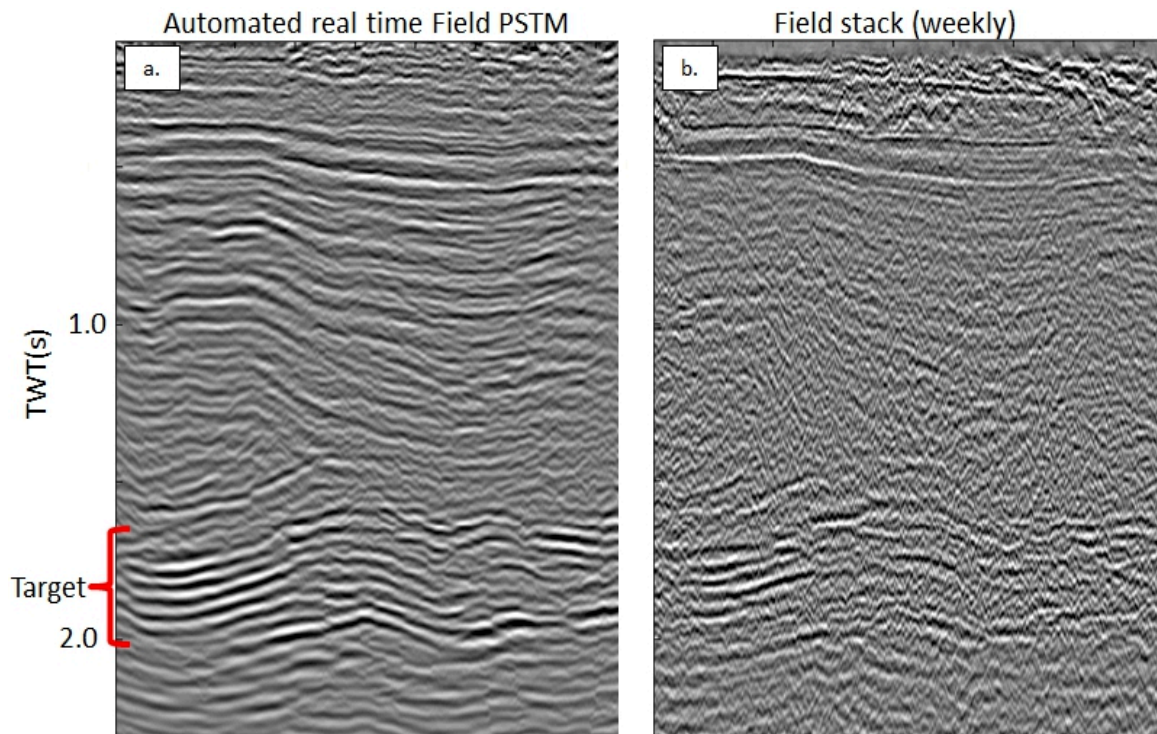


Figure 89: Comparison of the seismic images obtained during the acquisition: automated real-time field PSTM (a) and field stack (b).

The field stack pre-conditioning embeds elevation statics, random noise attenuation, ground-roll filtering, amplitude equalization, predictive deconvolution, normal move-out, and stretch mute adjustment. By comparison, the proposed automated real-time field PSTM pre-conditioning is composed of only two steps: automatic high-energy noisy-trace detection and edition and elevation statics. Compared to the field stack, the real-time field PSTM has improved continuity and shows better imaging of the deep structures including faults and anticlines. PSTM is naturally a very good de-noising technique.

We then compare the real-time field PSTM with a post-stack time migration following the end of the acquisition (Figure 90).

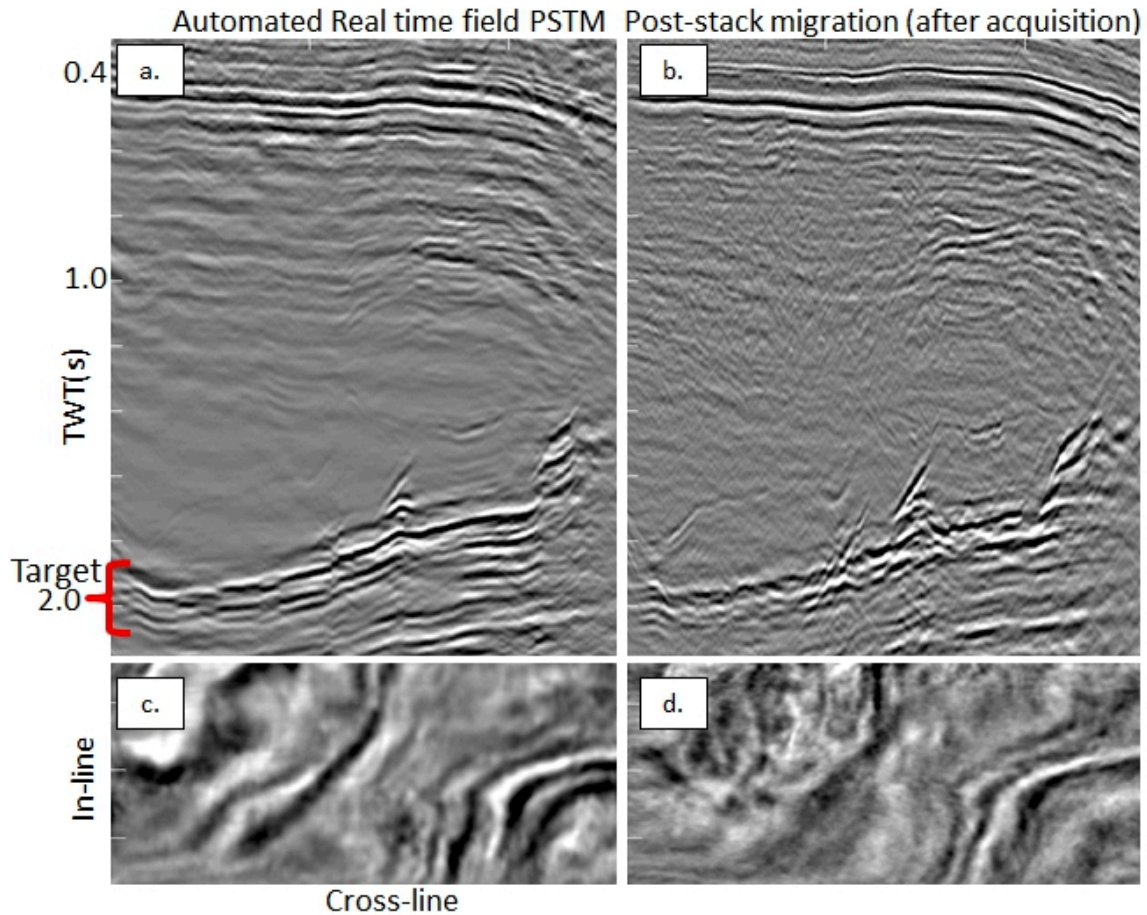


Figure 90: Real-time field PSTM, (a) and (c), and the post-stack time migration, (b) and (d). Inline sections are displayed in (a) and (b). Time-slices at 2 seconds are shown in (c) and (d).

The post-stack time migration pre-conditioning embedded all the processing steps used in the field stack. Firstly, we observe that the two images are consistent despite different pre-conditionings. However for the deep events (below 2 seconds), including the target, the imaging quality is better on the real-time field PSTM both in terms of continuity and fault definition. This can be explained by the efficiency of the compared technique (pre-stack migration vs. post-stack migration) and the pre-migration de-noising used to obtain the field stack (and the post-stack migration). Perhaps the pre-stack de-noising, particularly the ground-roll filtering, was too harsh. This is sometimes the case when applying ground roll filtering and only looking at shot point gathers (and not migrated data). As a result, the ground roll filtering may have affected primary diffractions as well. Note that the shallow data quality is better on the post-stack migration. This is explained by a better fine-tuning of the stretch mute used in the field stack (and the post-stack migration).

Figure 91, Figure 92, Figure 93 and Figure 94 show the advancement of the PSTM cube during the acquisition. With TeraMig, the cube is migrated automatically and in real-time in the field. It allows early structural interpretation and data quality assessment. We foresee this new method as a step change in the quality control in the field.

*"Bigger, faster, better is the trend for land wide azimuth surveys. With crews' channel counts measured in the high tens of thousands, one would expect that obtaining a 3D imaged volume from the acquired seismic data would take much longer than before. Remarkably, TeraMig provides a real time imaged volume as acquisition progresses. This represents a huge leap forward in providing the client with an early seismic product that can be used as an initial volume for the start of interpretation work. With TeraMig, the interpretation of a survey can now begin weeks, instead of many months, after the start of acquisition and be complete a week after the end of acquisition. Information from this interpretation can then be transferred and adjusted to subsequent volumes as seismic imaging continues.*

*As a real example, I have followed the impressive TeraMig results on Block C of Petroleum Development Oman's RTQ WAZ survey. We are processing this dataset for PDO in Muscat. The first imaged product from the processing Centre is expected to be available to PDO just over two months after the final TeraMig volume has completed."*

*Richard Cramp, Processing Supervisor at PDO Centre*

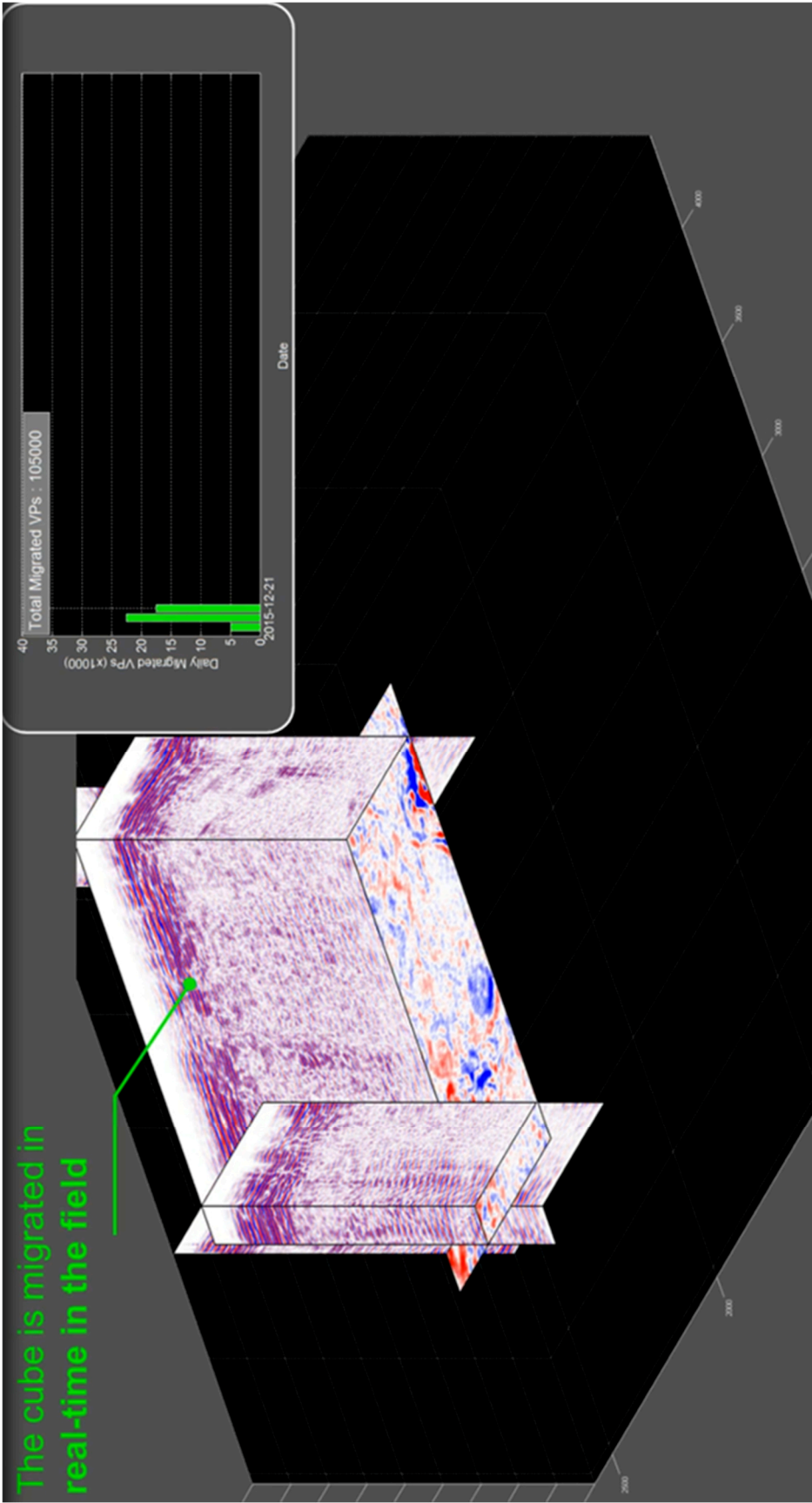


Figure 91: The PSTM cube advancement: 21/12/2015

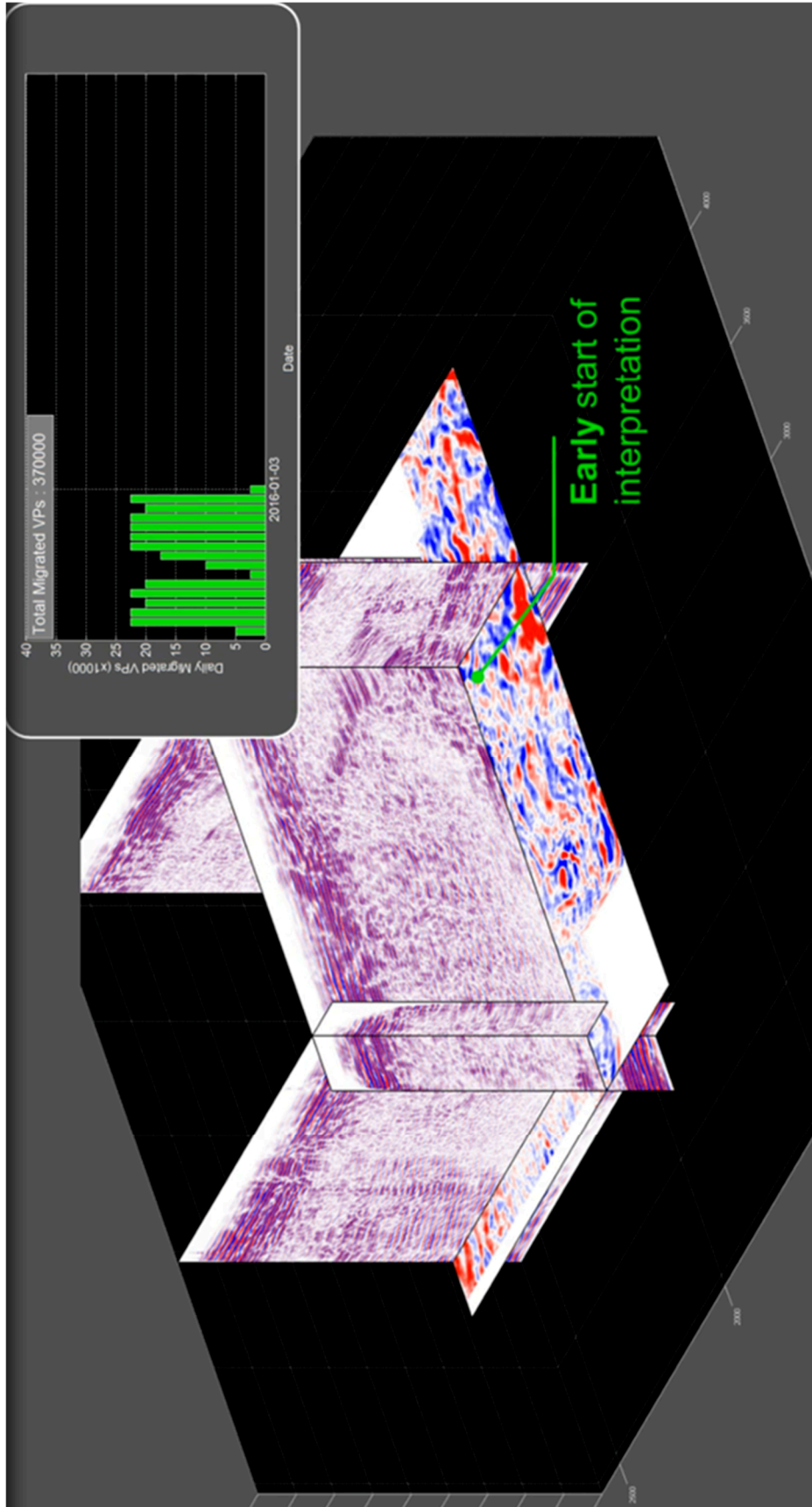


Figure 92: The PSTM cube advancement: 03/01/2015



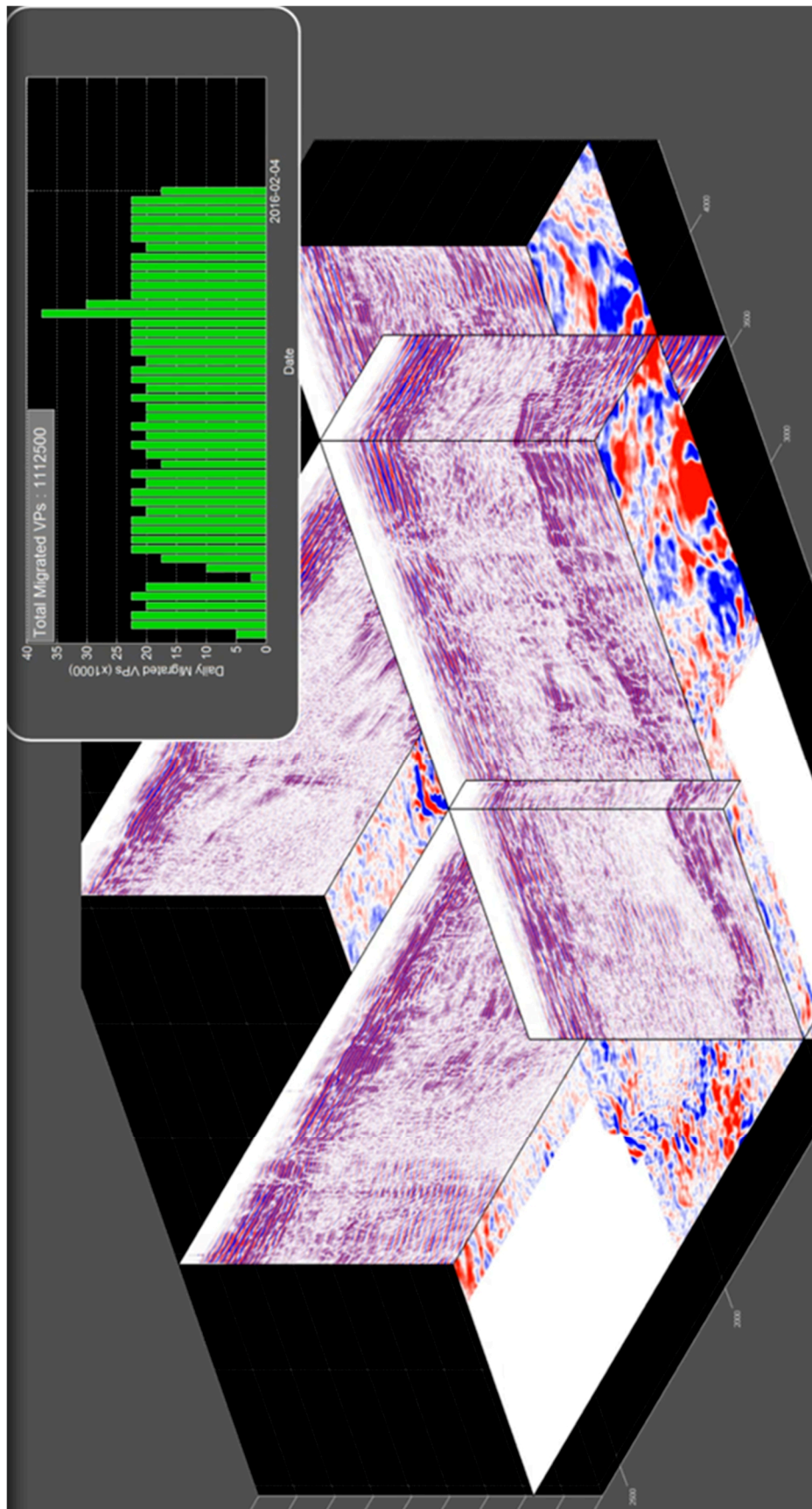


Figure 94: The PSTM Cube advancement: 04/02/2015

## 5.8 Conclusion

In this part, we demonstrated that true real-time field PSTM is achievable in the case of massive 3D WAZ data, even with limited computer capacity and without extra staffing. The proposed system opens a window on new aspects of quality control in the imaging domain. As well as being an operational success, this first test shows that we can get high-quality results with basic data pre-conditioning. The real-time image allows us to estimate the multiple content, statics issues, and velocity model imperfections. By knowing where to concentrate efforts in terms of processing, we have already gained a significant advantage that allows us to achieve more advanced processing in the seismic imaging center.

## 6. Conclusion and perspectives



## 6.1 Conclusion

Time-lapse (or 4D) is a seismic method whose value is now recognised worldwide. 4D Marine surveys are acquired under dynamic conditions and significant engineering efforts have been made to stabilize the sources and the streamers paths during replicated seismic operations. Marine permanent reservoir monitoring fixes the repositioning challenge on the receiver side; however, the source repositioning becomes the remaining weakest link.

In 4D Land, the weathering layer variations, the presence of superficial heterogeneities, the source and the receiver ground coupling are many repeatability challenges. Therefore, performing continuous seismic monitoring with both buried receivers and buried sources appears interesting.

Continuous seismic monitoring should in principle offer perfect data for detecting small and rapid reservoir variations; however, fluctuating near-surface ghost waves interfere with the primary reflections. By implementing a suitable deghosting strategy, reservoir time shifts have been measured with a precision and accuracy of a fraction of a millisecond, corresponding with pressure changes of less than 10 bars.

The most important role for geophysics in the oil and gas industry is to influence field operations, so that the value of existing assets is fully realized. The recent trend in time-lapse seismic has been toward very frequent reservoir monitoring and real-time processing workflows. For continuous seismic monitoring using sparse buried sources and receivers, we have proposed a way to estimate velocity and impedance variation in near real-time. It then becomes possible to spatially monitor steam fronts and to take production decisions.

2D and 3D projects have some conceptual similarities with 4D projects: like the 4D geophysicist compare the monitor with the reference baseline, the field geophysicist compare the newly acquired shot-point to a reference one. The most important role for the field geophysicist is to check the data consistency in real-time during the acquisition time. Somewhere, it is a question of repeatability as well. In order to fulfil the data quality control of massive data in real-time, we have proposed an innovative method TeraMig that performs the PSTM automatically in the field. This represents as well a significant leap forward in providing the client with an early seismic product that can be used as an initial volume for the start of the interpretation work.

## 6.2 Perspectives

Optimal 4D would ideally be repeatable, affordable, versatile, scalable and should help reservoir engineers to take production decisions in real-time. Having a versatile and scalable solution would simplify the operations. An affordable system would reduce the costs and thus would have a direct and calculable financial impact. However, having an affordable, versatile and scalable 4D monitoring would be useless without repeatability and real-time. Repeatability and real-time are thus essential and fundamental in 4D. Questions about versatility, flexibility and cost reductions remains open. To solve the equation, the industry will probably have to move from conventional sensors to fiber-optic sensing ([Hornman et al., 2013](#); [Mateeva et al., 2014](#)). For the near future, we foresee that optimal land 4D will include existing technologies. Among others, a good candidate to optimal Land 4D would be a combination of buried fiber-optic cables and permanent SeisMovie sources (or like) to follow rapid and low amplitude variations on a daily/weekly basis. In addition, on-demand surface “dense carpet-shooting” and the virtual source method ([Bakulin et al., 2007](#)) could be performed to monitor longer-term reservoir variations as well as background velocity and seismic horizons calibration.

For the dual depth cross-deghosting, it implies to double the equipment in the field that can be costly for permanent reservoir monitoring. We could envisage having some sparse arrays of sensors (and/or source) combined with dense single level sensors and to use the time-lapse wave separation. This would be efficient if the variations of the ghost’s waves are relatively regional; otherwise, the deghosting would not be straightforward. For the time-lapse wave separation, the choice of the calendar period to estimate the matching operator is critical. During this period, the reservoir variation and the ghost variation must be uncorrelated: This seems obvious; however, the worst case appears when slow reservoir injections or productions are done in parallel with seasonal climatic changes trend. In this case, it would be complicated to estimate the required matching operator. Perspectives exist on pre-migration versus post-migration deghosting. In fact, there are no restrictions to perform the presented deghosting workflow after migration. This requires migrating separately each level separately to get a migrated cube by level. By doing so, the deghosting process would be facilitated; the migration images would be in a common migration grid.

The proposed 4D M-PSTM appears sufficient to extract qualitative information (4D velocities and 4D impedance) in a simple geological context. For more complex settings, Full Waveform Inversion, e.g. (Tarantola, 1986) or wave-equation MVA techniques, e.g. (Shragge and Lumley, 2013), would be needed. However, these techniques do not yet deliver real-time output for 3D data sets acquired every day. This may be the case in the future as computing resources increase.

Concerning TeraMig, the 1D velocity model is currently the main limitation and a velocity approximation has an impact on the quality of the full stack image. This is accentuated when stacking together near and very far offsets traces; however, the impact on the stack is less significant considering similar offsets. Offset classes PSTM is possible with TeraMig. In this case, the output migrated gathers would appear under or over corrected therefore a subsequent application of a “residual” 3D velocity correction to align the gather can be a good perspective. Even if this could not be considered as a true 3D PSTM, it could be used to build a “first hint” migration velocity model. Finally, many applications could be envisaged. In Marine, TeraMig could easily be used to deliver images of the ocean bottom using a constant velocity (e.g. 1500 m/s). Having such migrated images would indeed be valuable to build ocean bottom multiple models.



## References

- Abma, R. and N. Kabir, 2006, 3D interpolation of irregular data with a POCS algorithm. *Geophysics*, **71**(6), E91-E97.
- Al-Jenaibi, M., W. L. Soroka, A. Jeelani, A. Baker, H. H. Hafez, E. B. Kleiss and P. D. Melville, 2006. 4D seismic monitors fluid changes over time in a carbonate reservoir. In Abu Dhabi International Petroleum Exhibition and Conference. Society of Petroleum Engineers, doi: 10.2118/100479-MS.
- Bagheri, M. A., M. Paydayesh and S. Al-Ballam, 2018, Monitoring of Steam Injection in a Heavy Oil Reservoir by Integration of Production and 4D Seismic Data. 80th EAGE Conference and Exhibition 2018, doi: 10.3997/2214-4609.201800984.
- Bakulin, A., A. Mateeva, K. Mehta, P. Jorgensen, J. Ferrandis, I. S. Herhold and J. Lopez, 2007, Virtual source applications to imaging and reservoir monitoring. *The Leading Edge*, **26**(6), 732-740.
- Balch, A. H., M. W. Lee, J. J. Miller and R. T. Ryder, 1982, The use of vertical seismic profiles in seismic investigations of the earth, *Geophysics*, **47**(6), 906-918.
- Barker, T., and Y. Xue, 2016, Inversion of continuous 4D seismic attributes to reveal daily reservoir changes: SEG Technical Program Expanded Abstracts, 5527—5531. doi: 10.1190/segam2016-13866468.1
- Barkved, O., J. Kommedal, and L. Thomsen, 2004, The role of multi-component seismic data in developing the Valhall field, Norway, 66th Annual International Conference and Exhibition, EAGE, Expanded Abstracts, E040.
- Beasley, C. J., W. Lynn, K. Larner and H. Nguyen, 1988: Cascaded fk migration: Removing the restrictions on depth-varying velocity. *Geophysics*, **53**(7), 881-893.

Beaudoin, G., and A. A. Ross, 2007, Field design and operation of a novel deepwater, wide-azimuth node seismic survey: *The Leading Edge*, **26**(4), 494–503, doi:10.1190/1.2723213

Beaudoin, G., M. Reasnor, M. Pfister, and G. Openshaw, 2010, First wide-azimuth, time-lapse seismic acquisition using ocean bottom seismic nodes at the Atlantis Field, Gulf of Mexico, 72nd Annual Conference and Exhibition, EAGE, Extended Abstracts, B029.

Behrens, R., M. MacLeod, T. Tran, and A. Alimi, 1998, Incorporating seismic attribute maps in 3D reservoir models: *SPE Reservoir Evaluation & Engineering*, **1**(2), 122–126, doi: 10.2118/36499-PA.

Bell, D. W. and V. VD. Cox, 1988, U.S. Patent No. 4794573, Washington, DC: U.S. Patent and Trademark Office.

Berg E. & B. Anderson, 2008, Autonomous Nodes for Time Lapse Reservoir Seismic – An Alternative to Permanent Seabed Arrays – Gulf Coast SPE Conference, Houston.

Bergmann, P., A. Kashubin, M. Ivandic, S. Lüth, and C. Juhlin, 2014, Time-lapse difference static correction using prestack cross-correlations: 4D seismic image enhancement case from Ketzin: *Geophysics*, **79**(6), B243—B252, doi: 10.1190/geo2013-0422.1.

Berni, A. J., 1985, Marine seismic system, U.S. Patent No. 4520467. Washington, DC: U.S. Patent and Trademark Office.

Berron, C., E. Forgues, A. Bakulin, R. Burnstad and M. Jervis, 2012, Effects of complex near surface on 4D acquisition with buried source and receiver. *SEG Technical Program Expanded Abstracts 2012*, Society of Exploration Geophysicists, pp. 1-5.

Berron, C., L. Michou, B. D. Cacqueray, F. Duret, J. Cotton & E. Forgues, 2015, Permanent, continuous & unmanned 4D seismic monitoring: Peace River case study,

SEG Technical Program Expanded Abstracts 2015, Society of Exploration Geophysicists, 5419-5423, doi: 10.1190/segam2015-5813292.1.

Bett, M., 2012, The Value of PRM in Enabling High Payback IOR, PESA News Resources, 44-45.

Beydoun, W., Y. Kerdraon, F. Lefeuvre, J. P. Bancelin, S. Medina, and B. Bleines, 2002, Benefits of a 3DHR survey for Girassol Field appraisal and development, Angola, *The Leading Edge*, **21**(11), 1152-1155, doi: 10.1190/1.1523744.

Bianchi, T., J. Meunier, P. Lanfranchi, F. Huguet and J. Bruneau, 2005, Acquisition and processing challenges in continuous active reservoir monitoring. In second EAGE North African/Mediterranean Petroleum & Geosciences Conference & Exhibition.

Blondel, P and F. Muir, 1993: Parallel computing exhumes slow Fourier transform in Stolt migration: *SEP-79*, 265–268.

Bouska, J., 2010, Distance separated simultaneous sweeping, for fast, clean, vibroseis acquisition. *Geophysical Prospecting*, **58**(1), 123-153.

Bruhn, C. H. L., A. Pinto, and P. R. S. Johann, 2008, Main challenges and uncertainties for oil production from turbidite reservoirs in deep water Campos Basin, Brazil: Presented at AAPG International Conference and Exhibition

Buddery, D. L. (1991). U.S. Patent No. 5,050,133. Washington, DC: U.S. Patent and Trademark Office.

Buizard, S., A. Bertrand, K. M. Nielsen, S. de Pierrepont, A. Grandi, H. Hoeber, G. Oexnevad and A. Gresillaud, 2013, Ekofisk Life of Field Seismic – 4D Processing, 75th EAGE Conference & Exhibition Extended Abstracts, TU 0802.

Bunting, T. & J. Moses, 2016, The transformation of seabed seismic, *First Break*, **34**, 59–64.

Cabolova, A., J. L. Lopez, and P. Wills, 2014, Benefits of frequent seismic monitoring and computer simulations in thermal EOR projects: 84th Annual International Meeting, SEG, Expanded Abstracts, 3513–3517, doi: 10.1190/segam2014-0160.1

Caldwell, J., Koudelka, E., Nesteroff, K., Price, R. and Zhang, P., 2015, Seismic permanent reservoir monitoring (PRM) – a growing market. *First Break*, **33**(11), 65-73.

Calvert, R., 2005, Insights and methods for 4D reservoir monitoring and characterization: SEG/EAGE Distinguished Instructor Short Course, ISBN: 978-1-56080-128-3, doi: 10.1190/1.9781560801696

Calvert, R. W. & P. Wills, 2003, The case for 4D monitoring with sparse OBC. In 65th EAGE Conference & Exhibition.

Cambois, G., A. Long, G. Parkes, T. Lundsten, A. Mattsson and E. Fromyr, 2009, Multi-level airgun array: A simple and effective way to enhance the low frequency content of marine seismic data, SEG Technical Program Expanded Abstracts 2009 Society of Exploration Geophysicists, pp. 152-156.

Chen, G., K. Wrobel, A. Tiwari, J. Zhang, M. Payne, W. L. Soroka, ... and A. A. Sultan, 2008, 4D Seismic in Carbonates: From Rock Physics to Field Examples. In International Petroleum Technology Conference. International Petroleum Technology Conference, doi: 10.2523/12065-MS

Claerbout, J. F. (1985), *Imaging the earth's interior (Vol. 1)*. Oxford: Blackwell scientific publications.

Clapp, R. G., P. Sava J. F. and Claerbout, 1998, Interval velocity estimation with a null-space: *SEP*.97, 147.156.

Clapp, R. G., 2001, geologically constrained migration velocity analysis: Ph.D. thesis, Stanford University.

Cole, S., D. Lumley, M. Meadows, and A. Tura, 2002, Pressure and saturation inversion of 4D seismic data by rock physics forward modelling: SEG Technical Program Expanded Abstracts, 2475—2478, doi: 10.1190/1.1817221.

Cooper, M., P. Westwater, E. Thorogood, P. Kristiansen, & P. Christie, 1999, Foinaven Active Reservoir Management: Towed streamer and buried sea-bed detectors in deep water for 4D seismic, SEG Technical Program Expanded Abstracts 1999, Society of Exploration Geophysicists, 1632-1635.

Cotton, J., & E. Forgues, 2012, Dual-depth hydrophones for ghost reduction in 4D land monitoring, SEG Technical Program Expanded Abstracts 2012, Society of Exploration Geophysicists, 1-5.

Cotton, J., E. Forgues, and J. Meunier, 2013, Continuous Land Seismic Reservoir Monitoring of Thermal EOR in the Netherlands: 75th EAGE Conference and Exhibition, doi: 10.3997/2214-4609.20130426.

Cotton J. and T. Bianchi, 2013, Method for time lapse wave separation, U. S. Patent 13/766,213

Cotton, J., M. Beilles, S. Mahrooqi, J. Shorter et al., 2016, Automated and Real-time Field PSTM - How to QC More Efficiently 10 Billion Traces Today and More Tomorrow: 78th EAGE Conference and Exhibition, Amsterdam, 2016, Amsterdam, Netherlands, doi: 10.3997/2214-4609.201600983

Dix, C. H., 1952, Seismic prospecting for oil: Harper & Brothers, New York.

Duncan, P. M., E.B. Gardner and D.C. Nester, 1997: 3-D seismic imaging in real-time: What's stopping us?, *The Leading Edge*, **16**(10), 1402-1409.

Egan, M., K. G. El-Kasseh and N. Moldoveanu, 2007, Full deghosting of OBC data with over/under source acquisition. SEG Technical Program Expanded Abstracts 2007, Society of Exploration Geophysicists, pp. 31-35.

Eiken, O., P. Ringrose, C. Hermanrud, B. Nazarian, T. A. Torp, and L. Høier, 2011, Lessons learned from 14 years of CCS operations: Sleipner, In Salah and Snøhvit: *Energy Procedia*, **4**, 5541–5548, doi: 10.1016/j.egypro.2011.02.541.

El-Emam, A., J. Al-Jenaie, H. Bayri, W. Zahran, and C. Koeninger, 2018, Imaging of 4D seismic during steam injection for shallow heavy oil reservoir in North Kuwait. *SEG Technical Program Expanded Abstracts 2018*, pp. 5268-5272. Society of Exploration Geophysicists, doi: 10.1190/segam2018-2995307.1

El Ouair, Y and L. K. Strønen, 2006, Value creation from 4D seismic at the Gullfaks Field: achievements and new challenges, *SEG Technical Program Expanded Abstracts*, 3250-3254, doi: 10.1190/1.2370206.

Eriksrud, M., 2010, Towards the optical seismic era in reservoir monitoring, *First Break*, **28**(6), 105-111.

Eriksrud, M., 2014, Seabed permanent reservoir monitoring (PRM)—A valid 4D seismic technology for fields in the North Sea, *First Break*, **32**(5), 67-73.

Ferguson, R. J. and G. F. Margrave, 1996, a simple algorithm for band-limited impedance inversion: *CREWES Research Report 8*, 1–10.

Folstad, P.G., H. Haugvaldstad and G. Jeangeot, 2011, Ekofisk PRM – The technical case for this brand new installation. *EAGE Workshop on Permanent Reservoir Monitoring (PRM) – Using Seismic Data*, Extended Abstracts, 10198.

Forgues, E., J. Meunier and C. Hubans, 2006, Steam Injection Seismic Monitoring Experiment. In *Geomodel 2006-8th EAGE science and applied research conference on oil and gas geological exploration and development*.

Forgues, E. & E. Schisselé, 2010, Benefits of hydrophones for land seismic monitoring, *72nd EAGE Conference and Exhibition, Expanded Abstracts B (Vol. 34)*.

Forgues, E., E. Schisselé and J. Cotton, 2011, Simultaneous active and passive seismic monitoring of steam-assisted heavy oil production: The Leading Edge, **30**(11), 1288-1294, doi: 10.1190/1.3663401.

Gabriels, P. W., N. A. Horvei, J. K. Koster, A. Onstein, and R. Staples, 1999, Time lapse seismic monitoring of the Draugen field, SEG Technical Program Expanded Abstracts, 2035-2037, doi: 10.1190/1.1820970.

Gonzalez-Carballo, A., P.-Y. Guyonnet, B. Levallois, A. Veillerette and R. Deboiasne, 2006, 4D monitoring in Angola and its impact on reservoir understanding and economics, The Leading Edge, **25**(9), 1150-1159, doi: 10.1190/1.2349820.

Goodway, B., 2014, Introduction to this special section: 4D: The Leading Edge, **33**(2), 130–133, doi: 10.1190/tle33020130.1.

Grandi, A., B. Lyngnes and N. Haller, 2013, Reservoir management through frequent seismic monitoring at Ekofisk field, 75th EAGE Conference & Exhibition Extended Abstracts, TH 1409.

Greaves, R.J. and T.J. Fulp, 1987, Three-dimensional seismic monitoring of an enhanced oil recovery process. *Geophysics*, **52**(9), 1175–1187, doi: 10.1190/1.1442381.

Groenenboom, J., and J. T. Fokkema, 1998, Monitoring the width of hydraulic fractures with acoustic waves: *Geophysics*, **63**(1), 139—148, doi: 10.1190/1.1444306.

Harlan, W. S., 1982: Avoiding interpolation artifacts in Stolt migration: SEP–30, 103–110.

Harlan, W. S., 1983, linear properties of Stolt migration and diffraction: SEP–35, 181–184.

Hatchell, P., K. Wang, J. Lopez, J. Stammeijer, and M. Davidson, 2013, Instantaneous 4D Seismic (i4D) for water injection monitoring. EAGE Annual Meeting, Extended Abstracts.

Herrmann, P., T. Mojesky, M. Magesan and P. Hugonnet, 2000, De-aliased, high-resolution Radon transforms. SEG Technical Program Expanded Abstracts (pp. 1953-1956). Society of Exploration Geophysicists.

Hornman, J. C., J. van Popta, C. Didraga, and H. Dijkerman, 2012, Continuous monitoring of thermal EOR at Schoonebeek for Intelligent Reservoir Management: SPE Intelligent Energy International, 150215.

Hornman, K., B. Kuvshinov, P. Zwartjes, and A. Franzen, 2013, Field trial of a broadside-sensitive distributed acoustic sensing cable for surface seismic: 75th Conference & Exhibition, EAGE, Extended Abstracts, doi: 10.3997/2214-4609.20130383.

Howe, D., M. Foster, T. Allen, B. Taylor and I. Jack, 2008, Independent simultaneous sweeping – a method to increase the productivity of land seismic crews: 78<sup>th</sup> Annual International Meeting, SEG, Expanded Abstracts, 2826-2830.

Johann, P. R. S., E. A. Thedy, F.A. Gomes and M. C. Schinelli, 2006, 4D seismic in Brazil: Experiences in reservoir monitoring. In Offshore Technology Conference. Offshore Technology Conference.

Johnston, D. H., 2013, Practical applications of time-lapse seismic data: SEG/EAGE Distinguished Instructor Short Course, ISBN: 978-1-56080-307-2, doi: 10.1190/1.9781560803126.

Jourdan, J.A., F. Lefeuvre, and D. Dubucq, 2006, Integration of 4D seismic into the dynamic model: Girassol, deep offshore Angola, First break, 4(24), 51-58, doi: 10.3997/1365-2397.2006010

Kato, A., S. Onozuka, and T. Nakayama, 2008, Elastic property changes in bitumen reservoir during steam injection: The Leading Edge, 27(9), 1124–1131, doi: 10.1190/1.2978974.

Kleiss, E., P. Melville, A. B. Al-Jeelani, S. Al-Menhali, H. H. Hafez, C. A. Modavi and B. Blonk, 2000, The feasibility of using time-lapse 3D seismic to monitor

fluid displacements in an Abu Dhabi onshore oil field. In Abu Dhabi International Petroleum Exhibition and Conference. Society of Petroleum Engineers, doi: 10.2118/68190-MS

Kloosterman, H. J., R. S. Kelly, J. Stammeijer, M. Hartung, J. van Waarde and C. Chajeki, 2003, Successful application of time-lapse seismic data in Shell Expro's Gannet field, Central North sea, *Petroleum Geoscience*, **9**(1), 25-34, doi: 10.1144/1354-079302-513.

Koster, K., P. Gabriels, M. Hartung, J. Verbeek, G. Deinum, and R. Staples, 2000, Time-lapse seismic surveys in the North Sea and their business impact: The Leading Edge, **19**(3), 286-293, doi: 10.1190/1.1438594

Kragh, E. and Christie, P., 2002, Seismic repeatability, normalized rms, and predictability. *The Leading Edge*, **21**(7), 640-647.

La Follett, J. R., P. Wills, J. L. Lopez, J. K. Przybysz-Jarnut and M. van Lokven, 2015, Continuous seismic reservoir monitoring at Peace River: Initial results and interpretation: 85th Annual International Meeting, SEG, Expanded Abstracts, 5440–5444, doi: 10.1190/segam2015-5883275.1

Landes, M., N. M. Shapiro, S. Singh & R. Johnston, 2009, Studying shallow seafloor structure based on correlations of continuous seismic records. SEG Technical Program Expanded Abstracts 2009, Society of Exploration Geophysicists, 1693-1697.

Landrø, M., 2001, Discrimination between pressure and fluid saturation changes from time-lapse seismic data: *Geophysics*, **66**(3), 836—844, doi: 10.1190/1.1444973.

Landrø, M., H. H. Veire, K. Duffaut, and N. Najjar, 2003, Discrimination between pressure and fluid saturation changes from marine multicomponent time-lapse seismic data: *Geophysics*, **68**(5), 1592—1599, doi: 10.1190/1.1620633.

Lavergne, M., 1986, *Méthodes sismiques* : Editions TECHNIP, 116-117, isbn : 2.7108-0514-6.

Lee, D. S., V. M. Stevenson, P. F. Johnston, and C. E. Mullen, 1995, Time-lapse cross-well seismic tomography to characterize flow structure in the reservoir during the thermal stimulation: *Geophysics*, **60**, SPECIAL ISSUE, 660—666, doi: 10.1190/1.1443805.

Lefeuvre, F., Y. Kerdraon, J. Peliganga, S. Medina, P. Charrier, R. L'Houtellier and D. Dubucq, 2003, Improved Reservoir Understanding Through Rapid And Effective 4D: Girassol Field, Angola, West Africa, SEG Technical Program Expanded Abstracts: pp. 1334-1337, doi: 10.1190/1.1817533

Levin, X. A., 2003: Fast, effective curved ray moveout corrections for Kirchhoff time migration, 2003 SEG Annual Meeting, Society of Exploration Geophysicists.

Lin, J., L. Teng, and F. Muir, 1993: Comparison of different interpolation methods for Stolt migration: SEP-79, 255–260.

Lopez, J. L., P. B. Wills, J. R. La Follett, T. B. Barker, Y. Xue, J. K. Przybysz-Jarnut, J. H. H. M. Potters, M. van Lokven, D. R. Brouwer, and C. Berron, 2015, Real-time seismic surveillance of thermal EOR at Peace River: Proceedings of the Canada Heavy Oil Technical Conference, Society of Petroleum Engineers, doi: 10.2118/174459-MS.

Lumley, D. E., 2001, Time-lapse seismic reservoir monitoring: *Geophysics*, **66**, 50—53, doi: 10.1190/1.1444921.

Mari, J. L., F. Huguet, J. Meunier and M. Becquey, 2011, Natural Gas Storage Seismic Monitoring. *Oil & Gas Science and Technology—Revue d'IFP Energies nouvelles*, **66**(1), 9-20.

Mateeva, A., J. Lopez, H. Potters, J. Mestayer, B. Cox, D. Kiyashchenko, P. Wills, S. Grandi, K. Hornman, B. Kuvshinov, W. Berlang, Z. Yang, and R. Detomo, 2014, Distributed acoustic sensing for reservoir monitoring with vertical seismic profiling: *Geophysical Prospecting*, **62**(4), 679–692, doi: 10.1111/1365-2478.12116.

Mateeva, A., J.C. Hornman, P. Hatchell, H. Potters and J. Lopez, 2015, Frequent Seismic Monitoring for Pro-Active Reservoir Management: SEG Technical Program Expanded Abstracts 2015: pp. 4817-4821. doi: 10.1190/segam2015-5899850.1

Mathisen, M. E., A. A. Vasiliou, P. Cunningham, J. Shaw, J. H. Justice, and N. J. Guinzy, 1995, Time-lapse cross-well seismic tomogram interpretation: Implications for heavy oil reservoir characterization, thermal recovery process monitoring, and tomographic imaging technology: *Geophysics*, **60**(3), 631–650, doi: 10.1190/1.1443803.

Meunier, J., Huguet, F., & Meynier, P. (2001). Reservoir monitoring using permanent sources and vertical receiver antennae: The Céré-la-Ronde case study. *The Leading Edge*, **20**(6), 622-629.

Meunier, J. and Herculin, S., 2003, Positioning Accuracy and 4D Seismic Sensitivity in Land Acquisition: 65th EAGE Conference.

Meunier, J., 2004, U.S. Patent No. 6,714,867. Washington, DC: U.S. Patent and Trademark Office.

Meunier, J., T. Bianchi, J. Postel and R. Taylor, 2008: The future of VibroSeis for high-density wide-azimuth land acquisition, *First Break*, **26**(2).

Michou, L., Y. Lafet, T. Coleou & J. Przybysz-Jarnut, 2013, 4D seismic inversion on continuous land seismic reservoir monitoring of thermal EOR, 75th EAGE Conference & Exhibition incorporating SPE EUROPEC 2013, doi: 10.3997/2214-4609.20130427.

Monk, D. J, 1990, Wavefield separation of twin streamer data, *First Break*, **8**(3).

Mordret, A., M. Landès, N. Shapiro, S. Singh, P. Roux, and O. Barkved, 2013, Near-surface study at the Valhall oil field from ambient noise surface wave tomography, *Geophys. J. Int.*, **193**(3), 1627–1643.

Munoz, P. A., J. Uribe, L. Rodriguez, R. Parrado, N. Sanabria, M. Polanco and D. Berguer, 2015: Survey Design and Data Acquisition Using Nodal Systems in the Sub Andean Basins, 77th EAGE Conference and Exhibition 2015, doi 0.3997/2214-4609.201413124.

Nakstad, H., J. Langhammer and M. Eriksrud, 2011, Permanent reservoir monitoring technology breakthrough in the North Sea, 73rd EAGE Conference & Exhibition Extended Abstracts, I044.

Oliveira R. M, D. Bampi, R. C. Sansonowski, N. M. Ribeiro, P. R. Johann, M. S. Santos, and D. Ferreira, 2007, Marlim Field: Incorporating 4D seismic in the geological model and application in the reservoir management decisions: Presented at X LACPEC, SPE 108062

Osdal, B., & T. Alsos, 2010, Norne 4D and reservoir management – the keys to success, 72nd EAGE Conference and Exhibition incorporating SPE EUROPEC 2010.

Parrack, A. L., 1976, Method of marine reflection-type seismic exploration, U.S. Patent 3 952 281, 1976.

Pecholcs, P. I., S.K. Lafon, T. Al-Ghamdi, H. Al-Shammery, P.G. Kelamis, S.X. Huo, O. Winter, J-B. Kerboul and T. Klein, 2010, Over 40,000 vibrator points per day with real-time quality control: Opportunities and challenges, SEG Technical Program Expanded Abstracts, 111-115, doi: 10.1190/1.3513041.

Pevzner, R., V. Shulakova, A. Kepic, and M. Urosevic, 2011, Repeatability analysis of land time-lapse seismic data: CO2CRC Otway pilot project case study: Geophysical Prospecting, **59**, no. 1, 66–77, doi: 10.1111/j.1365-2478.2010.00907.x.

Popovici, A. M., P. Blondel and F. Muir, 1993: Interpolation in Stolt migration: SEP–79, 261–264.

Posthumus, B. J., 1993, Deghosting using a twin streamer configuration, Geophysical Prospecting, **41**(3), 267-286.

Prats, M., 1969, The heat efficiency of thermal recovery processes: *Journal of Petroleum Technology*, **21**(03), pp.323-332.

Reasnor, M., G. Beaudoin, M. Pfister, I. Ahmed, S. Davis, M. Roberts, J. Howie, G. Openshaw and A. Longo, 2010, Atlantis time-lapse ocean bottom node survey: A project team's journey from acquisition through processing: 80th Annual International Meeting, SEG, Expanded Abstracts, 4155–4159.

Rennie, J., R. Alexandre S. and Ronen, 1997, Sensitivity of repeat 3-D seismic surveys to geometry variations - A controlled experiment: 67th Ann. Internat. Mtg., Soc. Expl.Geophys., Expanded Abstracts, 91–95, doi: 10.1190/1.1886168.

Ribeiro N. M., D. Steagall, R. Oliveira, L. Formiga, P. Kerber, M. Jarger, 2005, Challenges of the 4D seismic in the reservoir management of the Marlim Field: Presented at IX LACPEC, SPE 94905.

Roach, L. A. N., D. J. White, and B. Roberts, 2015, Assessment of 4D seismic repeatability and CO2 detection limits using a sparse permanent land array at the Aquistore CO2 storage site: *Geophysics*, **80**(2), WA1—WA13, doi: 10.1190/geo2014-0201.1.

Roberts, M., T. Dy, S. Ji, M. Reasnor, and D. Shepherd, 2011, Improving Atlantis TTI model building: OBN + NATS, prism waves & 3D RTM angle gathers: 81st Annual International Meeting, SEG, Expanded Abstracts, 3238–3242.

Robertsson, J. O. A., J. E. Kragh and J. E. Martin, 2004, Method and system for reducing effects of sea surface ghost contamination in seismic data, U.S. Patent No. 6775618, Washington, DC: U.S. Patent and Trademark Office.

Sablon, R., T. Payen, H. Tonchia, R. Siliqi, X. Labarre, N. Salaun, and Y. L. Men, 2013, Ghost-free imaging combining synchronized multi-level source and variable-depth streamer, SEG Technical Program Expanded Abstracts 2013, Society of Exploration Geophysicists, pp. 72-76.

Sansonowski, R. C., R. M. de Oliveira, N. M. S. Ribeiro Jr., D. Bampi, and L. F. Camarão, Jr., 2007, 4D seismic interpretation in the Marlim field, Campos Basin, offshore Brazil. SEG Technical Program Expanded Abstracts, 2872-2877, doi: 10.1190/1.2793063

Schinelli, M. C., U. R. A. Lino, O. F. Keller and S. S. Sacramento, 2006, Time Lapse Monitoring of Steam Injection Using High Resolution Seismic. 68th EAGE Conference and Exhibition incorporating SPE EUROPEC 2006, doi: 10.3997/2214-4609.201402277.

Schisselé, E., E. Forgues, J. Echappé, J. Meunier, O. De Pellegars, and C. Hubans, 2009, Seismic Repeatability–Is There a Limit?. In 71st EAGE Conference and Exhibition incorporating SPE EUROPEC 2009. Extended Abstracts, V021.

Shabrawi, A., A. Smart, B. Anderson, G. Rached and A. El-Emam, 2005, How single-sensor seismic improved image of Kuwait's Minagish Field, *First Break*, **23**(2).

Sharma, R., M. Prasad, M. Batzle and S. Vega, 2013, Sensitivity of flow and elastic properties to fabric heterogeneity in carbonates. *Geophysical Prospecting*, **61**(2), 270-286, doi: 10.1111/1365-2478.12030

Sheriff, R. E., and L. P. Geldart, 1995, *Exploration seismology*: Cambridge University Press, 128-130, isbn: 9780521462822.

Shragge, J., and D. Lumley, 2013, Time-lapse wave-equation migration velocity analysis: *Geophysics*, **78**(2), S69—S79, doi: 10.1190/geo2012-0182.1.

Shulakova, V., R. Pevzner, J. C. Dupuis, M. Urosevic, K. Tertyshnikov, D. E. Lumley and B. Gurevich, 2015, Burying receivers for improved time-lapse seismic repeatability: CO2CRC Otway field experiment, *Geophysical Prospecting*, **63**(1), 55-69.

Simm, R. and M. Bacon, 2014, *Seismic Amplitude: an interpreter's hand book*: Cambridge University press, 102 -104, isbn: 1139915940, 9781139915946

Smit, F., M. Ligtenag, P. Wills & R. Calvert, 2006, Toward affordable permanent seismic reservoir monitoring using the sparse OBC concept. *The Leading Edge*, **25**(4), 454-459.

Soroka, W. L., P. Melville, E. Kleiss, M. Al-Jenaibi, A. B. Al-Jeelani, H. H. Hafez, and A. Modavi, 2005, Successful pilot onshore Abu Dhabi shows that 4D can monitor fluid changes in a giant Middle East carbonate field. *SEG Technical Program Expanded Abstracts*, pp. 2430-2433, Society of Exploration Geophysicists, doi: 10.1190/1.2148212.

Sønneland, L., L. E. Berg, P. Eidsvig, A. Haugen, B. Fotland and J. Vestby, 1986, 2-D deghosting using vertical receiver arrays. *SEG Technical Program Expanded Abstracts 1986*, Society of Exploration Geophysicists, pp. 516-519.

Soubaras, R. and R. Dowle, 2010, Variable depth streamer: a broadband marine solution, first break, **28**(12).

Stolt, R. H., 1978, Migration by Fourier transform, *Geophysics*, **43**(1), 23-48.

Stopin, A., P. J. Hatchell, C. Corcoran, E. Beal, C. Gutierrez and G. Soto, 2011, First OBS to OBS time lapse results in the Mars basin, *SEG Technical Program Expanded Abstracts 2011*, 4114-4118.

Strohmenger, C. J., L. J. Weber, K. A. M. Ahmed Ghani, O. Al-Jeelani, A. Al-Mansoori, T. Al-Dayyani, ... and J. C. Mitchell, 2006, High-resolution sequence stratigraphy and reservoir characterization of Upper Thamama (Lower Cretaceous) reservoirs of a giant Abu Dhabi oil field, United Arab Emirates, doi: 10.1306/1215876M883271.

Sun, Y. F., K. Berteussen, S. Vega, G. P. Eberli, G. T. Baechle, R. J Weger and P. D. Wagner, 2006, Effects of pore structure on 4D seismic signals in carbonate reservoirs. *SEG Technical Program Expanded Abstracts* pp. 3260-3264. Society of Exploration Geophysicists, doi: 10.1190/1.2370208.

Tarantola, A., 1986, A strategy for nonlinear elastic inversion of seismic reflection data: *Geophysics*, **51**(10), 1893—1903, doi: 10.1190/1.1442046.

Trad, D., 2009, Five-dimensional interpolation: Recovering from acquisition constraints. *Geophysics*, **74**(6), V123-V132.

Valenciano, A. A., M. Brown, A. Guitton and M. D. Sacchi, 2004, Interval Velocity Estimation Using Edge-preserving Regularization: SEG Technical Program Expanded Abstracts, 2431-2434. doi: 10.1190/1.1845232

Van Gestel, J.-P., J. H. Kommedal, O. I. Barkved, I. Mundal, R. Bakke, and K. D. Best, 2008, Continuous seismic surveillance of Valhall Field, *Leading Edge*, **27**(12), 1616–1621, doi:10.1190/1.3036964.

Van Gestel, J., M. Roberts, S. Davis and P. Ariston, 2013, Atlantis ocean bottom nodes time-lapse observations. SEG Technical Program Expanded Abstracts 2013, 4954-4959.

Vasco, D. W., 2004, Seismic imaging of reservoir flow properties: Time-lapse pressure changes: *Geophysics*, **69**(2), 511—521, doi: 10.1190/1.1707071.

Vasco, D. W., A. Bakulin, H. Baek, and L. R. Johnson, 2015, Reservoir characterization based upon the onset of time-lapse amplitude changes: *Geophysics*, **80**(1), M1—M14, doi: 10.1190/geo2014-0076.1.

Vega, S., K. Berteussen, Y. F. Sun and A. A. Sultan, 2007, Is Gassmann the best model for fluid substitution in heterogeneous carbonates ?. SEG Technical Program Expanded Abstracts, pp. 1575-1578. Society of Exploration Geophysicists, doi: 10.1190/1.2792796.

Wang, K. & P. Hatchell, 2013, Effects of receiver density and mispositioning on time-lapse OBN data, SEG Technical Program Expanded Abstracts 2013, Society of Exploration Geophysicists, 4890-4894

Waters, K. H., 1987, Reflection Seismology: A tool for energy resource exploration.

White, D. J., L. A. N. Roach, and B. Roberts, 2015, Time-lapse seismic performance of a sparse permanent array: Experience from the Aquistore CO2 storage site: *Geophysics*, **80**(2), WA35—WA48, doi: 10.1190/geo2014-0239.1.

Willis, M. E., D. R. Burns, R. Lu, M. N. Toksoz, and N. J. House, 2007, Fracture quality from integrating time-lapse VSP and microseismic data: *The Leading Edge*, **26**(9), 1198–1202, doi: 10.1190/1.2780791.

Witsker, S. O. S., M. Landrø, and P. Avseth, 2014, Using a pseudo-steady-state flow equation and 4D seismic travel time shifts for estimation of pressure and saturation changes: *Geophysics*, **79**(3), M11—M24, doi: 10.1190/geo2013-0247.1

Zwartjes, P., Barker, T., Hornman, J., Przybysz-Jarnut, J. 2015. Quantitative Interpretation of Nine Months of Daily SeisMovie™ Data to Monitor Steam Injection at Schoonebeek. Expanded abstracts, 77th EAGE Conference and Exhibition.



# List of figures

<p><b>Figure 1:</b> A well-known illustration of a 4D study conducted in Gannet C field, North sea central grabben. The Gannet C has a ring-shaped closure around a central salt dome. There is a 120-mthick oil rim under a gas cap. 1993 Baseline (a), 1998 monitor (b) and the differences (c). Illustration from Koster et al., (2000). .....</p>	18
<p><b>Figure 2:</b> Data quality and repeatability comparison in different domain. The data without any ghost removal (top) and ghost attenuation (bottom). We display a stacked sections (left) as well as the calendar evolution of the stack section's center bin (middle). The selected centre bin is at the position of the injection well. The middle panel consists of one trace per day. The right panel is obtained by subtracting a reference to each daily records. The residue is then multiplied by a factor 5. The reference is obtained by averaging the first month of the acquisition. ....</p>	20
<p><b>Figure 3:</b> Acoustic impedance variation maps (left) and interval velocity variation (right) for a) August, b) October and c) December. The injection well is in blue and the two producers are in red. ....</p>	21
<p><b>Figure 4:</b> Reduction of the repeatable overlap area in the case of streamers feathering between the baseline and a monitor survey (a). Monitor over-specification (b) using 10 streamers instead of 6 increases the repeatable overlap area. Illustration from Johnston et al., (2013). ....</p>	28
<p><b>Figure 5:</b> Illustration of cable control with birds (a). Acoustic transceivers are spread along the streamer and eventually on air gun sub-array, head buoys and tail buoys (b). Illustration courtesy of Sercel. ....</p>	29
<p><b>Figure 6:</b> Draugen field location and extension. ....</p>	29
<p><b>Figure 7:</b> Section trough Draugen monitor volume (a) and trough the difference volume (b). Amplitude map extracted from the difference volume (c) showing the major faults (in black) and the interpreted extend of the original oil water contact OOWC (in red). From Koster et al. (2000). ....</p>	30
<p><b>Figure 8:</b> Location map of the Gullfaks field (a), courtesy of petroleumreports.com. Time-lapse seismic data obtained in 1985 and in 1996 (b) show the reduction of the oil water contact. From El Ouair and Strønen, 2006. ....</p>	31
<p><b>Figure 9:</b> Map of the Angolan offshore (a), with location of the exploration blocks. The southwest of the block 17 has been covered by three HR seismic surveys: one baseline in 1999 on Girassol, Jasmin and Dali fields: one seismic monitor in 2002 on Girassol and one seismic monitor in 2004 on Girassol and Jasmin (b). The fields consist of several channel-levee and sheet complexes, separated by mud turbidites, on a turtleback structure (c). The reservoir driving mechanism is water and gas injection. From Gonzales-Carballo et al., (2006). ....</p>	32

**Figure 10:** Marlim location map, from Bruhn et al. (2008), modified. .... 33

**Figure 11:** Amplitude map of Marlim 1997 data (a) with the polygon of the acquisitions of 1986 (green), 1997 (dashed black) and 2005 (dashed red). Azimuth map differences (b) higher and lower than 20 degrees during the acquisition of the 2005 dataset. From Sansonowski et al., (2007), modified..... 33

**Figure 12:** Ocean Bottom Cable seismic operation with the Sercel SeaRay 428. The SeaRay encompasses three orthogonally oriented, digital accelerometers and a hydrophone to form a single four component (4C) receiver. Courtesy of Sercel. .... 35

**Figure 13:** Overview of the Valhall Field showing the layout of the geophone array at the sea floor (red lines), the top of the reservoir, the outline of the field (dark blue) line and the wells (thin blue lines). From Van Gestel et al., (2008)..... 38

**Figure 14:** The acoustic impedance difference responses (thickness of amplitudes) for LoFS surveys 6, 8, and 10, all related back to LoFS survey 1. The figure shows the response of the water injector (in blue) and the nearby producer (in red). LoFS 6 was the last survey before injection started so no response is observed around the injection well. From van Gestel et al., (2008)..... 38

**Figure 15:** Seismic cable network installed at Ekofisk and overlaid with the map of the city of Paris. From Eiksrud et al. (2014)..... 39

**Figure 16:** NRMS map (Left) computed on final stacks (from the second and third Ekofisk survey) in a 2500 – 3500 m/s window. The two surveys were acquired 4.5 months apart. The black area in the centre of the map corresponds to the seismic obscured area (SOA), which is due to an overburden gas cloud. Top reservoir time-shift map (right) computed on final stacks (from the second and third Ekofisk survey). From Buizard et al., (2013)..... 40

**Figure 17:** The evolution of deep-water nodes. Three deep-water ocean bottom nodes displayed to scale which have decreased in size over time, directly affecting ROV deployment efficiency. From Bunting and Moses, (2016). .... 41

**Figure 18:** Map of the Atlantis field (top). An average time shift map (bottom) above the reservoir. Brown faults and depth structure of top reservoir are overlain. Yellow arrows indicate the area dominated by multiple. From Van Gestel et al., (2013). .... 42

**Figure 19:** The Mars field location map (a). Node positions (b) for the 2007 and 2010 surveys respectively depicted by black and pink squares. The black polygon outlines the common node positions area. Amplitude map of the reservoir for the 2010 dataset (c) and amplitude differences (d) between 2010 and 2007. From Stopin et al., (2011). .... 43

**Figure 20:** CDP fold distribution of the seismic surveys. Each CDP bin covers a 3 by 3 meters area. From Greaves and Fulp, (1987). ..... 46

**Figure 21:** The evolution of the seismic response: pre-burn stage (top), mid-burn stage (middle) and post-burn stage (bottom). A color scale representing the envelope amplitude overlies the reflection wiggle traces. A bright spot was created at the top of the Holt sandstone at the mid-burn stage. From Greaves and Fulp, (1987). ..... 46

**Figure 22:** Acoustic impedance (bottom) compared with the saturation changes in the simulation model (top), showing some example of good agreement. From Al-Jenaibi et al., (2006). ... 47

**Figure 23:** Group of records from the base (above) and monitor (below) surveys. Notice the difference in the signal-to-noise ratio, ground roll and energy. From Schinelli et al., (2006). ..... 48

**Figure 24:** Average, seismically derived temperature maps in the upper sand interval reservoir for the base (left) and for the monitor (right). From El-Emam et al., (2018). ..... 49

**Figure 25:** SeisMovie piezoelectric sources (left). A schematic SeisMovie installation for a SAGD heavy oil production operation (right). Buried piezo-electric sources are shown in yellow along with a network of buried receiver arrays. The autonomous system works 24 hrs a day, recording and pre-processing data on site before transmitting it back to the office for analysis. (Courtesy of CGG).. 51

**Figure 26:** Location of Peace River (top). Weekly 4D time-shifts below the reservoir (bottom). The steam is injected in the northern well. From Forgues et al., (2011). ..... 52

**Figure 27:** Schoonebeek location (left). Map showing the equipment procured for both the initial 2010 2D survey and added in 2012 to enable 3D monitoring (right). The coloured dots represent the imaging bins with the associated fold. From Cotton et al., (2013). ..... 53

**Figure 28:** Comparison of travel time variations and pressure measured at both observation wells O1391 on the west (top graph) and O1392 on the west (bottom graph). From Cotton et al. (2013). ..... 54

**Figure 29:** Calendar time line of reservoir production in Peace River 31. From Berron et al. (2015). ..... 55

**Figure 30:** Time shift variations at reservoir level over seven months. Snapshots are taken every 12 days. Baseline is sliding and is taken 12 days before monitor. From Berron et al., (2015). .... 56

**Figure 31:** Comparison of 4D amplitudes on sparse and high-fold data, highlighting relative amplitude differences (a). Comparison of 4D time shifts (b) on sparse and high-density data, after three and seven months of production. The dashed lines in the top figures correspond to the areal extent of the sparse data set. From Smit et al., (2006). ..... 57

**Figure 32:** Normalized differential RMS maps calculated using different datasets. From Wang and Hatchell, (2013). ..... 58

**Figure 33:** The concept of i4D. From Hatchell et al., (2013). ..... 58

**Figure 34:** 4D data acquired over a water injection well using a sparse acquisition system using 16 OBN and 8 shot lines (a). 4D data acquired over the same water injection well using the full-fold OBN surveys acquired 3 years apart (b). From Hatchell et al., (2013). ..... 59

**Figure 35:** Decimation tests conduct on the Schoonebeek project. The original monitoring survey design (a) with the time-shift and amplitude variations maps. A first decimation test with 2 times less sources and ~3 times less sensors (b). A second decimation test with 2 times less sources and ~5 times less sensors (c). A third decimation test with only 8 sources and 63 sensors (d). ..... 60

**Figure 36:** Asymmetric expansions of the steam chest due to the small fault throw. From Hornman et al., (2012). ..... 68

**Figure 37:** Permanent seismic monitoring time schedule covering the transition period between cold production and steam injection. Black triangles represent the system installation period. The monitoring includes an initial 2D phase that was then extended to 3D. .... 68

**Figure 38:** Aerial photos of the monitoring area. Top: Trenches during installation. Bottom: Four months later during continuous monitoring. .... 69

**Figure 39:** A SeisMovie shot point recorded by 3 sensor lines: hydrophones at 6 m and 9 m depth (left and middle) and geophones at 9 m depth (right). The S-wave (red) is visible on the near offset. The chalk reflection (green) appears at 0.4 s. The reservoir (yellow) is around 0.65 s. S-P converted waves (blue) are visible on the hydrophones only. Geophones are noisier than hydrophones in this application. .... 70

**Figure 40:** Map showing the equipment used for both the initial 2010 2D survey and its extension in 2012 to enable 3D monitoring. The coloured dots represent the imaging bins with associated fold. Blue line: injector well; Red line: production wells and Green line: observation wells. We have dual depth hydrophones (6 and 9 m) in any sensor positions. Geophones are collocated with hydrophones at 9 m only for the centre receiver line. A 3 level source vertical array (yellow triangle) is located in the southeast of the spread. .... 71

**Figure 41:** Ghost waves in continuous seismic monitoring: source ghost (red), receiver ghost (blue) and S-P converted ghost (orange). All varying ghosts interfere with the primary waves (green). ..... 72

**Figure 42:** S-P converted ghost fluctuation over calendar time. Top: ambient surface temperature, middle: S-P converted wavelet over the calendar time. Bottom left cross plot between S-

P ghost time shifts and temperature. Bottom right: cross plot between and S-P ghost amplitude variation..... 74

**Figure 43:** The reduction of the S-P ghost wave. Top: input data before S-P ghost wave attenuation. Bottom: After S-P ghost wave attenuation using a HR Radon filter. Left: Shot point with NMO applied. Middle: repeated record over calendar time (1 trace par day over several months). Right: Calendar variation obtain by subtracting the stack of the first 7 traces (1 week) to each daily trace. The obtained differences are multiplied by a factor 5..... 75

**Figure 44:** The full deghosting workflow applied in continuous seismic monitoring. .... 76

**Figure 45:** Illustration of the receiver ghost and primary separation. The input seismic records at the 2 levels of sensor (a). The subsequent application of the primary alignment and stack (b). Black arrows figure out the ghost residues. The application of the deghosting (c) as expressed in Equation 13 and the estimated ghost (d) as expressed in Equation 9. .... 80

**Figure 46:** illustration of the cross deghosting on daily synthetic dataset (b) with a perfect ghost and primary separation and its comparison with the subsequent time alignment and stack method showing high primary and ghost leakage (a). The velocity error effect on the cross deghosting (c and d) and the random noise addition effect (e). .... 81

**Figure 47:** Effect of the S-P converted ghost and receiver ghost attenuation on the CMP stack (top) and on the repeatability metrics (bottom). The subsequent reduction of the S-P converted ghost (middle) and receiver ghost (right) improves significantly the repeatability of the data. .... 82

**Figure 48:** Illustration of the cross deghosting at the vertical array of sources. On the input records (top), we observe upgoing and downgoing primaries and ghost (top, left). In the calendar time (top, right), The primary (green window) is constant whereas the ghost (red window) varies with the weathering layer changes. After cross deghosting (middle and bottom), the primaries and the ghost are isolated. .... 83

**Figure 49:** Illustration of the time-lapse wave separation. The process applied to the synthetic dataset without noise (a) and with noise (b). The process applied with some bias introduced in the ghost model (c and d). .... 85

**Figure 50:** Application of the time-lapse wave separation on several sources located in different places over the survey (a to f) as showed in the map (g). Before processing (top) and after processing (bottom). The reduction of the source ghost further improves the repeatability as seen on the calendar variations (right). .... 86

**Figure 51:** Data quality and repeatability comparison in different domain. The data without any ghost removal (top) and with the S-P converted ghost attenuation (bottom). We display a stacked sections (left) as well as the calendar evolution of the stack section’s center bin (middle). The selected

centre bin is right at the position of the injection well. The middle panel consists of one trace per day and its relative calendar variations (right). The right panel is obtained by subtracting a reference to each daily records. The residue is then multiplied by a factor 5. The reference is obtained by averaging the first month of the acquisition. .... 87

**Figure 52:** Same as for Figure 51 but for the receiver ghost attenuation using the cross-deghosting (top) and with the attenuation of the source ghost using the time-lapse wave separation (bottom). .... 88

**Figure 53:** At the injection well (a), the steam injection rate (blue) is correlated with the seismic travel time shift below the reservoir (red curve) and with amplitude measured in the reservoir (green curve). Above the reservoir, the time shift and the amplitude variations (light red and light green) are very stable. Comparison between the travel time variations and pressure measured at both observation wells (b) and (c). The well O1391 is located on the east and the well O1392 is located on the west. .... 90

**Figure 54 :** Travel time variations below the reservoir (Left) and amplitude variations in the reservoir (Right) at different dates. The east part of the reservoir is clearly not swept by the steam. ... 91

**Figure 55:** Evolution of the 7% iso amplitude volume over calendar time. .... 92

**Figure 56:** Interpretation and conclusions made by SHELL. Courtesy of SHELL ..... 92

**Figure 57:** Moveout corrected gathers and the illustration of the differences between the NMO and the M-NMO on a simple 2D synthetic data set. Left: NMO correction in  $v(0)$  on the base line; top: NMO corrections for different velocity perturbations applied to the monitor line; bottom: same as for top, but with the M-NMO correction. The M-NMO corrects simultaneously the event curvature and the time-shifts. .... 102

**Figure 58:** Exact (solid line) and estimated (dotted line) interval velocity perturbations for each horizon (a and d), theoretical beta values (b and e), and one compare to the other (c and f). The images (a-c) correspond to random perturbations above the reservoir, while the images (d-f) to biased deviations between the monitor and the base. All estimated values are contained within the 10% error range indicated by dotted lines (c and f). .... 103

**Figure 59:** Elastic parameters used to generate the synthetic data set a)  $V_p$ , b)  $V_s$  and c) density models. The 4D variations are localized within the 20 m-thick reservoir. .... 104

**Figure 60:** Synthetic data sets (left: base, middle: monitor, right: differences) associated to macro bins ( $48 \times 48 \text{ m}^2$ , top) and to standard bins ( $8 \times 8 \text{ m}^2$ ) In practice, b and c are not available and a is obtained by locally averaging the input data set. .... 105

**Figure 61:** Workflows to determine  $v(0)$  (left) and  $v(c)$  with the moveout analysis (middle) and with the M-NMO (or M-PSTM) and cross-correlation approach (right). ..... 106

**Figure 62:** Comparison between the conventional approach based on maximizing the stack (b-d) and the M-NMO and cross-correlation approach (e-g). The gather (a) is obtained by applying a NMO correction in  $v(0)$ . For (b), the NMO correction is designed in  $v(c)$ . The optimal velocity model (d) is the one maximizing the stack. In both cases (red and blue lines, c), the stack are almost superimposed due to limited offset. The M-NMO gather (e) looks similar, but the cross-correlation is able to detect subtle velocity variations (g). The time shifts corresponding to the maximum value of the cross-correlation are reduced in  $v(c)$  (black and purple curves, f). ..... 107

**Figure 63:** Interval velocity models (blue: reference, red: perturbation) for a) the exact model, b) and c) the inverted interval velocity models, for thicknesses equal to 14 ms and 42 ms, respectively. .... 108

**Figure 64:** Illustration of the macro-binning (NMO corrected gathers): a 48x48 m<sup>2</sup> macro bin (a) and a 8x8 m<sup>2</sup> nominal size bin (b). The two arrows indicate the base (BR) and top (TR) reservoir 109

**Figure 65:** Calendar differences with the baseline (stack of May) at the injection well a) without updating the velocity model and b) with a velocity model update using the M-PSTM approach. .... 111

**Figure 66:** Top: Northern section differences (15th April 2012 and 28th July 2012) without updating the velocity model (a), with updating the velocity model by stack optimization (b) and with velocity updating using the M-PSTM approach (c). Bottom: the velocity variations: no variation (d), variations obtained by stack optimization (e) and variations obtained with the proposed 4D M-PSTM approach (f). .... 112

**Figure 67:** a) Migrated image section in the southern part (background grey scale) for 15th April 2012 and the RMS velocities model; b) the variation percentages (15th April to 28th July) with the horizons and c), the location map. .... 113

**Figure 68:** Same as Figure 67, but for the interval velocity models. .... 114

**Figure 69:** a) 4D interval velocities (in red, with blocky aspect) compared to  $V_p$  given at the observation well in blue. b) 4D interval velocities at the injection well and c) the corresponding variations. .... 115

**Figure 70:** Seismic trace at the observation well a) after calibration to fit the impedance log values in purple. b), the low-frequency part of the log (< 10 Hz). c) Estimation of the impedance. .... 116

**Figure 71:** a) Acoustic impedance section obtained by combining well data and seismic section for the 15th of April 2012 and b) impedance variations between the 15th of April and the 28th

of July 2012 (b). In (b), the arrows show the well positions (blue: injector, red: producers). c) Location map..... 117

**Figure 72:** Acoustic impedance variation maps for a) June, b) August, c) October and d) December. The injection well is in blue and the two producers are in red. .... 119

**Figure 73:** Same as for Figure 72, but for the interval velocity variations. .... 120

**Figure 74:** a) and b): cumulated and steam injection, c) the interval velocity variations, and d) the impedance variations at the steam injection well. .... 121

**Figure 75:** The harbour experiment showing a diffraction hyperbola. From Claerbout (1985), modified. (illustration done for a TeraMig lecture given to field QC geophysicist at CGG-University) ..... 128

**Figure 76:** Diffraction in a seismic experiment. (illustration done for a TeraMig lecture given to field QC geophysicist at CGG-University)..... 128

**Figure 77:** Illustration of the double square root equation that define the direct Kirchhoff migration. (illustration done for a TeraMig lecture given to field QC geophysicist at CGG-University) ..... 129

**Figure 78:** Cheops' pyramid illustrating the diffraction surface in 3D seismic (yellow: zero-offset diffraction; green: common-offset diffraction; Black: common-midpoint at the scatter point location; red: common-midpoint away from the scatter). (Courtesy of CGG-University) ..... 130

**Figure 79:** source-to-image and receiver-to-image computation ..... 131

**Figure 80:** Representation of the TeraMig indexes and of the spatial discretization: 250 m that is never used in practice (left), 50 m (middle) and 10 m (right). ..... 132

**Figure 81:** Illustration of the tile selection in TeraMig. Each tile comprises numerous imaging positions. .... 132

**Figure 82:** Comparison between a reference PSTM algorithm (TIKIM) in Geovation™ (top) and TeraMig (bottom). Each panel represents a common offset migration from 25 m (left) to 5025 m (right). The results are very close validating the TeraMig algorithm for field QC PSTM. .... 133

**Figure 83:** Illustration of the noise reduction in the image domain after migration. Before migration (top), we show synthetic input data without noise (a) and with an increasing noise level (b and c). The reflections becomes somewhere hidden by the noise (c). After migration (bottom), the noise level is significantly attenuated. Even for the noisier synthetic input record (c), the reflections appears clearly after migration (f). .... 134

**Figure 84:** The acquisition cycles and the maximum time-slots for TeraMig processing. A conventional acquisition with a single vibrator (a). A more advanced productivity using the slip-sweep method (b). The TeraMig time slots are reduced. .... 135

**Figure 85:** Comparison of the computational efforts between real-time field PSTM and post-acquisition PSTM. Computational effort is represented by the surface of the coloured rectangles that is equal to computing time multiplied by number of CPUs. .... 136

**Figure 86:** Real-time Field PSTM network: « TeraMig Everywhere » ..... 137

**Figure 87:** The TeraMig workflow..... 138

**Figure 88:** Operational results as of 13 November (extract of the automated daily reports). .. 139

**Figure 89:** Comparison of the seismic images obtained during the acquisition: automated real-time field PSTM (a) and field stack (b)..... 140

**Figure 90:** Real-time field PSTM, (a) and (c), and the post-stack time migration, (b) and (d). Inline sections are displayed in (a) and (b). Time-slices at 2 seconds are shown in (c) and (d). ..... 141

**Figure 91:** The PSTM cube advancement: 21/12/2015 ..... 143

**Figure 92:** The PSTM cube advancement: 03/01/2015 ..... 144

**Figure 93:** The PSTM cube advancement: 21/01/2015 ..... 145

**Figure 94:** The PSTM Cube advancement: 04/02/2015 ..... 146



# Appendix 1

Simultaneous active and passive seismic monitoring of steam-assisted heavy oil production

Forgues, E., E. Schisselé and J. Cotton, 2011.



## Simultaneous active and passive seismic monitoring of steam-assisted heavy oil production

E. FORGUES, E. SCHISSELÉ, and J. COTTON, CGGVeritas

The world-class heavy oil reserves of Canada represent a significant resource for North America which is free from the geopolitical uncertainty currently affecting conventional oil supplies in some parts of the world. Energy security and the current sustained oil prices make heavy oil extraction an attractive proposition.

Time-lapse seismic is playing an increasingly important role in reservoir monitoring. Used in conjunction with well data, it can improve understanding of reservoir behavior and optimize hydrocarbon recovery. Typical oil and gas reservoirs have a lifespan of many years and evolve slowly over their productive life, so repeat surveys on an annual basis are appropriate for 4D seismic monitoring of conventional reservoirs. The majority of heavy oil reservoirs in Canada will be produced using in-situ enhanced recovery techniques (rather than mining), with steam-assisted production being the most popular method. The state of the reservoir can vary significantly over the course of weeks so it is important to monitor production effects on a frequent basis.

To have a seismic crew on call to perform weekly or monthly surveys is unrealistic. In addition, the extensive surface infrastructure around heavy oil fields would interfere with seismic acquisition, both in terms of surface coverage and high levels of background noise. Steam-assisted production effects may be rapid but they can also be small, requiring highly sensitive acquisition in this noisy environment.

As well as the rapid changes in the reservoir, there is good reason to choose continuous seismic monitoring as there are also some risks involved in steam-assisted production. Steam generation is expensive, so it is important to optimize the injection program and avoid waste to ensure economic recovery of the heavy oil. This requires appraising the volume of reservoir swept or stimulated on a weekly basis and making real-time production decisions. Time-lapse 4D seismic is a good choice for this application, but at an interval that is not economically viable for conventional seismic crews.

High-pressure steam injection can also have some physical risks which include cap-rock failure and subsequent steam escape and compromising the casing in the injection wells, particularly for cyclic-steam injection methods where the well is subjected to repeated cycles of steam injection followed by periods of production. Passive seismic monitoring provides an excellent opportunity to mitigate this kind of risk with real-time results providing early warning by revealing changes in stress in and around the reservoir.

### Continuous seismic reservoir monitoring using buried arrays

CGGVeritas together with Gaz de France (now GDF Suez) and Institut Français du Pétrole (IFP) developed a solution for high-resolution continuous seismic monitoring over a five-year period from 1998 to 2003, initially for the appli-

cation of gas-storage monitoring (Meunier et al., 2001). The design criteria demanded an economic, reliable solution to accurately assess gas saturation and the extent of the gas bubble in a reservoir formation. To fulfil these criteria, it was decided to design a completely autonomous system utilizing buried receiver arrays and a novel piezoelectric vibrator source.

Using a permanent buried installation ensures excellent 4D repeatability and coupling. By going a step further and placing the source and sensors below the weathering layer, near-surface



**Figure 1.** SeisMovie sources laid out prior to installation. The piezoelectric stack is mounted in a “cage” about 2 m long and cemented into the borehole at a depth of 80 m.

variations are eliminated to further improve repeatability over extended periods. Schisselé et al. (2009) demonstrated time and amplitude variations of just 6  $\mu$ s and 0.5%, respectively, during a test period of 13 days.

The piezoelectric source has some unique characteristics which are critical to the system. First, it is maintenance-free and reliable, which suits permanent installation. Secondly, it has a stable signature which contributes further to the excellent repeatability of the system. Several sources can be distributed around the field and, by using a patented discrete frequency sweep, they can operate simultaneously.

There is flexibility in the design and specification of the receiver array which means a variety of configurations and sensors can be used to achieve different monitoring objectives. For areal coverage over a large target, long arrays or grids of buried geophones can be installed. To increase the vertical sensitivity of the system, arrays of sensors (two-, three-, or four-component) can be installed vertically in boreholes to provide VSP-style data sets.

A permanent system such as this has economic benefits for long-term monitoring and a minimal environmental footprint. After initial installation, the operation is fully autonomous and can be controlled remotely. This includes data acquisition, on-site preprocessing, and remote data transfer, which eliminates the need for onsite personnel. The maintenance-free buried equipment is protected from vehicles, animals, and the weather, reducing the chance of damage to the system or the environment. Consequently onsite intervention, and therefore, ongoing operational costs should be minimal.

The combination of passive and active seismic techniques for long-term and continuous 4D monitoring opens up new opportunities for reducing the operational risks while optimizing production. In this article, we present the main seismic and microseismic monitoring results obtained during a three-month steam injection/oil production period on a heavy oil project.

### Combined active and passive seismic monitoring: A case study

A system was deployed for Shell on an existing heavy oil field in Alberta, Canada with the aim to evaluate its suitability for combined active seismic reflection and passive seismic monitoring of steam-assisted production.

The system comprised nine piezoelectric mini-vibrator sources (Figure 1) that were cemented into dedicated boreholes at a depth of 80 m and a variety of both surface and buried sensors (Forgues and Schisselé, 2010). This article deals only with analysis of data from vertical geophones buried at a depth of 12 m and located above horizontal injector/producer wells as described in Figure 2. During 84 days of data acquisition, the nine sources vibrated simultaneously and continuously using a patented technique (IFP, GDF, CGG, US patent 6714867-B2) of swept monofrequency emissions which eliminate crosstalk interference noise.

With the use of low-energy sources, it is necessary to sum the shot records over 24-hour periods using optimized noise-attenuation weighting to achieve an adequate signal-to-noise ratio. The resulting data quality can be seen in Figure 3 with the frequency content extending to 160 Hz at the reservoir reflection

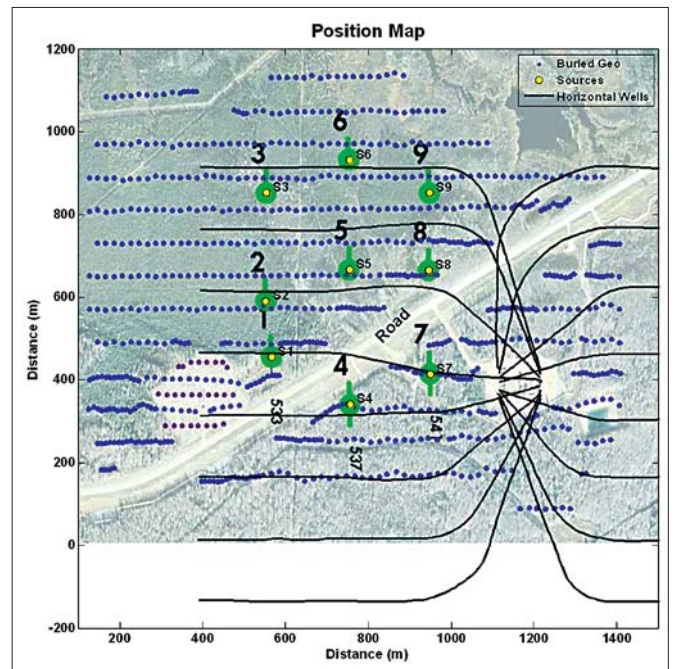


**Figure 2.** Survey acquisition map over the horizontal steam-injector/oil-producer wells. Sensors and sources are buried below the weathering zone.

at 440 ms. Shear-wave (S-wave) energy generated by the source obscures the compressional (P-wave) reflections on near offsets. Low-frequency noise coming from pump production can be seen on the east side of the lines (right side of the record).

The signal processing applied on the data to extract the 4D attributes involved only a few basic steps:

- 90-Hz low-cut filter to remove the S-waves generated by the source. This filter is applied only in the S-wave noise cone.
- 40-Hz low-cut filter for traces strongly contaminated by pump noise (east side of the line).
- High-resolution 3D Radon least-squares shotpoint decomposition to attenuate slow waves (free-surface multiples, guided waves, etc.) interfering with the P-reflections. Velocities lower than 1500 m/s were removed.

Burying sources and sensors greatly increases the signal repeatability (Schisselé et al., 2009). Nevertheless, source and sensor ghosts are still transmitted through the weathering layer and may affect the repeatability. This is an issue we have to pay particular attention to. It is site-dependent as the near-surface velocity and attenuation can vary considerably from one region to the other. One way to address this problem is to increase the depth of sources and receivers from the 80-m source depth and 12-m receiver depth used here.

### Active seismic monitoring results

After signal processing, two time windows were selected. The first one above the reservoir and the second one around the reservoir located at 440 ms. For each trace and each day, a cross-correlation is computed with a reference (the first day of acquisition). The maxima of these daily cross-correlations are picked

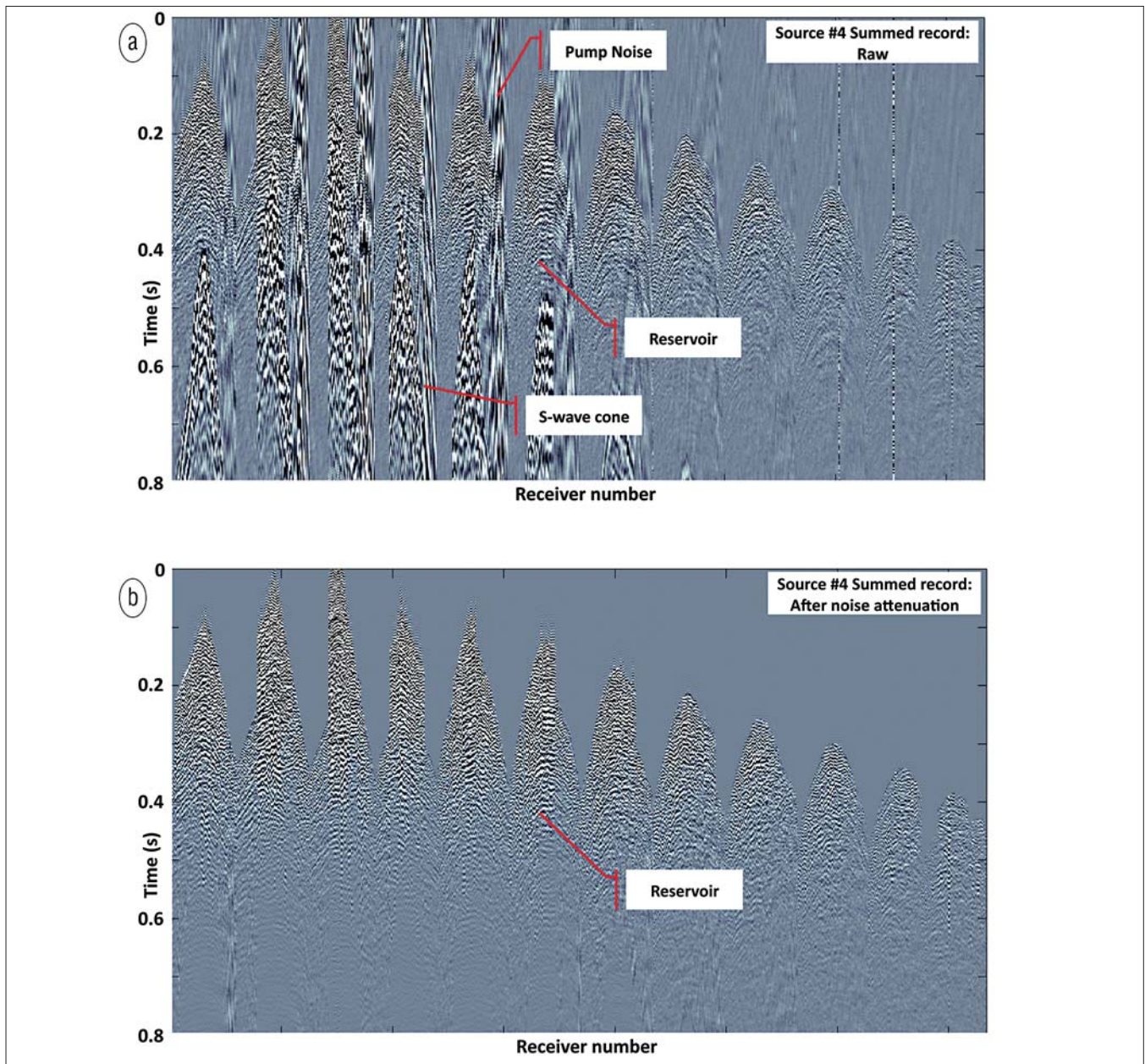


**Figure 3.** Summed 24-hour record for source 4. (a) Strong low-frequency noise coming from well pumps is visible on the east side (right) of the lines, along with a cone of source-generated shear waves in the center of the lines. Reflectors at the reservoir level are clearly visible. (b) Data after signal processing to remove the source-generated shear waves and the low-frequency environmental/pump noise. In both plots, a geometrical spreading compensation is applied for display.

to produce time and amplitude variations in the top and bottom windows. The traveltim variations are computed as the differences between the bottom and top windows.

An average by week is plotted in map form in Figures 4 and 5 for time shifts and amplitude variations, respectively. The maximum range of variations after three months is about 0.2–0.3 ms for the traveltimes in the north where the steam is injected and up to 10% for the amplitudes in the south, which may be due to production effects. These results match the cycle of steam injection-production with steam injection starting in the northern horizontal well in week 7.

Steam injection causes increased reservoir pressure which

induces a decrease in the rock velocity within the reservoir. The strong increase in velocity (negative time shift) in the south-east could be an artifact caused by the remaining low-frequency pump noise. Amplitude variations follow a different pattern. They are generally stable at the beginning of the acquisition, but then amplitude starts to decrease in week 9 in the south at a rate of approximately 2% per week.

When we compared our results with those obtained by dynamite refraction data recorded on the same spread (Hansteen et al., 2010), we obtained the same general map of traveltim variations, albeit with a magnitude three times smaller due to the different sampling of the near surface.

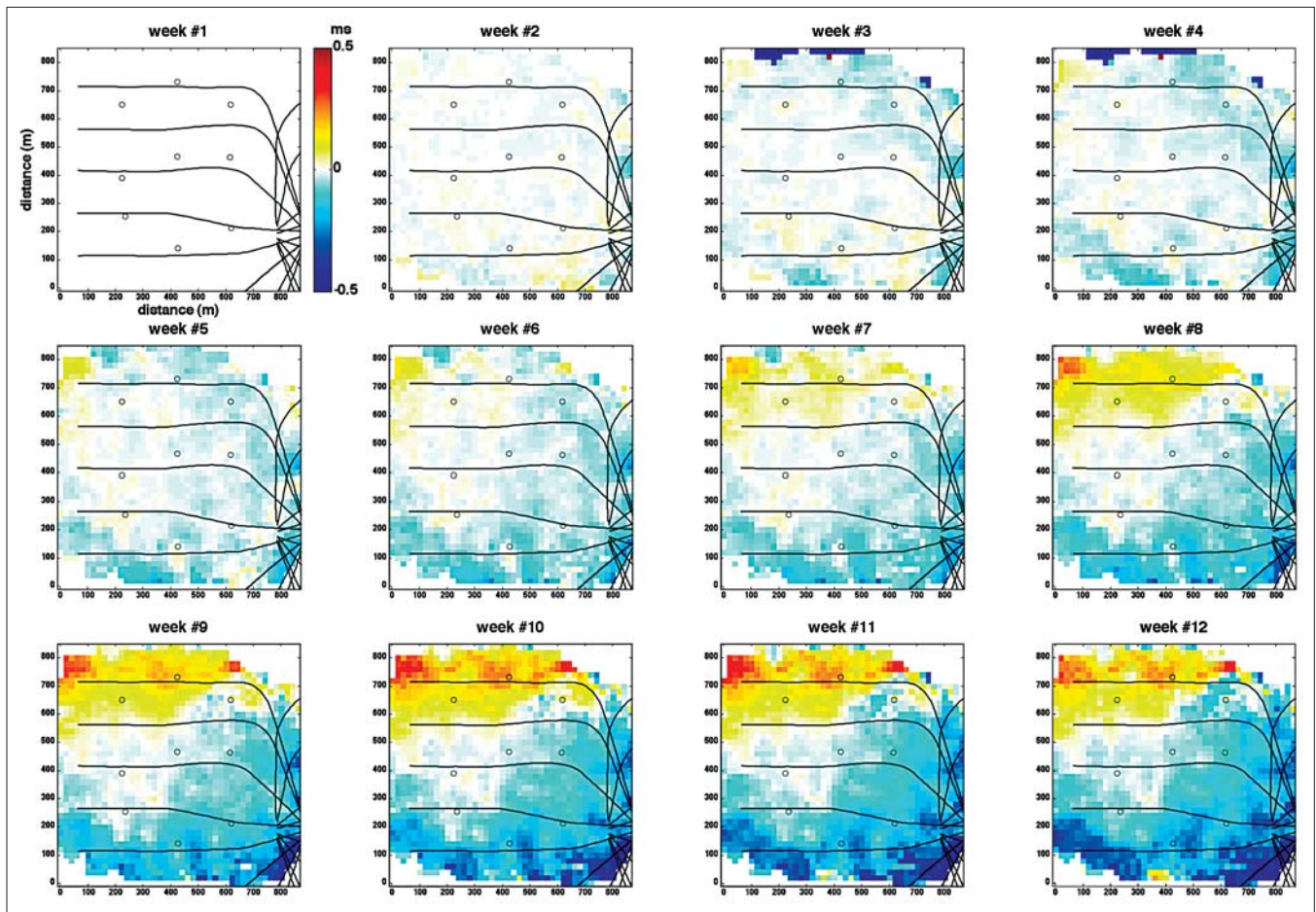


**Figure 4.** Weekly traveltimes through the reservoir. The steam was being injected in the northern horizontal well. A positive time difference corresponds to a decrease in the reservoir velocity.

### Simultaneous microseismic analysis

The permanent reservoir monitoring system allows continuous recording of seismic signals which can be separated in two parts: active and passive. The active part is the signal emitted by the nine buried sources. The passive part is the microseismic events induced by the injection/production process (located in the reservoir) plus ambient noise, mainly due to industrial and human activity such as traffic noise on roads or pump jacks. As the active signal from the sources is highly repeatable, it can be precisely estimated by summing the data over different periods of the source sweep. This estimated active part can therefore be removed from the continuously recorded signal in order to extract the passive part (IFP, GDF, CGG-patented technique, US patent 7388811-B2).

Analysis of the passive seismic signals in the data comprises four steps. The first step is the analysis of a reference shot (perforation shot or string shot). This shot is used firstly to estimate the velocity and static fields and secondly as the correlation operator in the detection step.

The second step is the detection of potential microseismic events. The incoming records are continuously correlated with the reference shot in real time and averaged over the sensors to obtain the detection curve. This curve represents the ampli-

tude contrast between the mean microseismic signal and the mean noise level. When it exceeds a given threshold, an event is detected. Figure 6 shows an example of a strong microseismic event visible across the whole receiver array which has been extracted from the raw seismic records. The active part of the raw record has been filtered out (i.e., the part consisting of the discrete source frequency sweep signals and associated reflection energy).

The third step is the localization of this detected event. A semblance cube is calculated for each event and the spatial position of a microseismic event is found where the semblance reaches a maximum which corresponds to the most constructive signal summation. Figure 7 summarizes the results for a typical event where we see the three orthogonal sections through the maximum of the semblance cube. This particular microseismic event is at the northeast border of the seismic array, at a depth of 600 m along the northern well of the right-hand pad.

This localization procedure was applied to each detected event. The last step of our procedure is still essentially manual. An experienced operator evaluates the semblance maps calculated for all detected events and validates or rejects them. More than 800 events were detected in the field during the last three

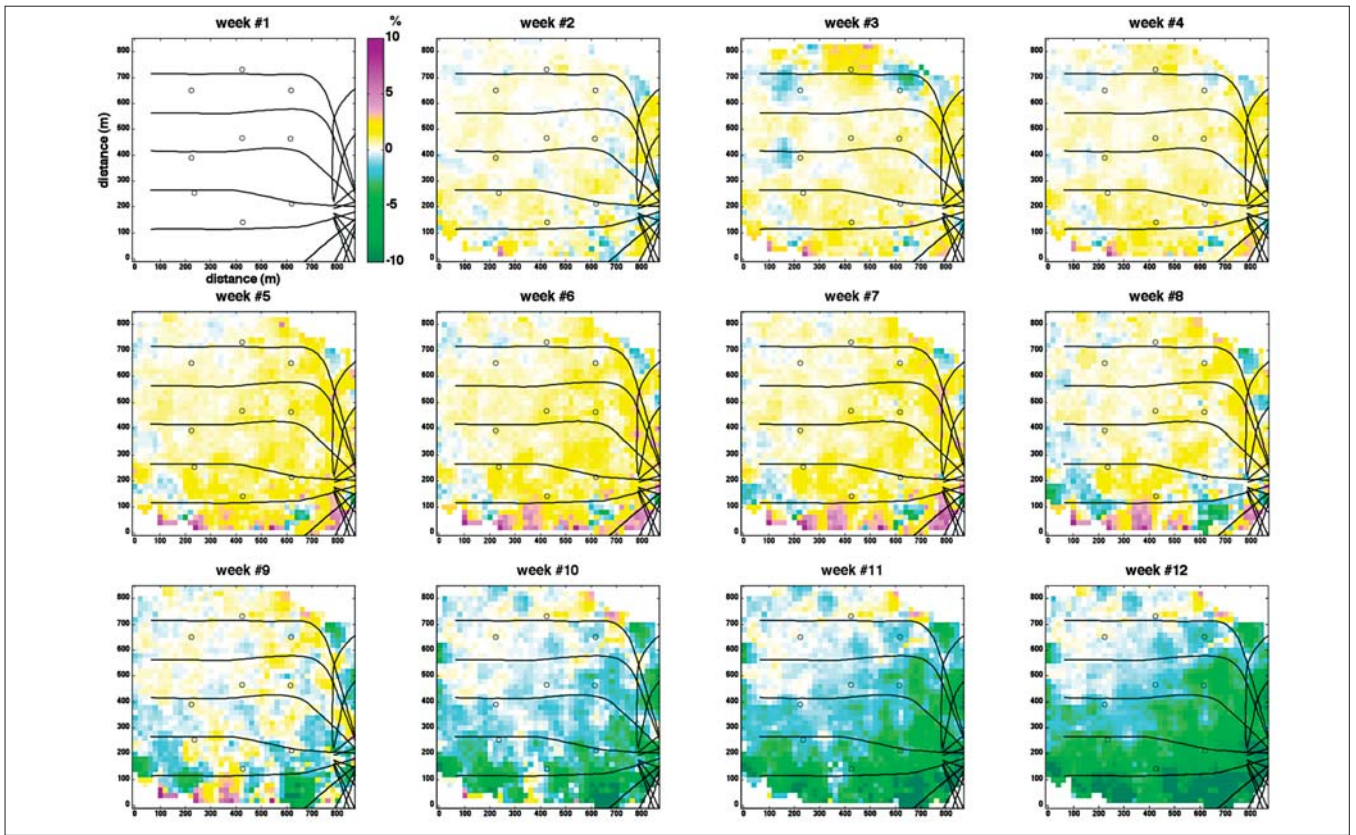


Figure 5. Weekly seismic amplitude variation through the reservoir. The main variations are visible in the southern area and may be associated with production.

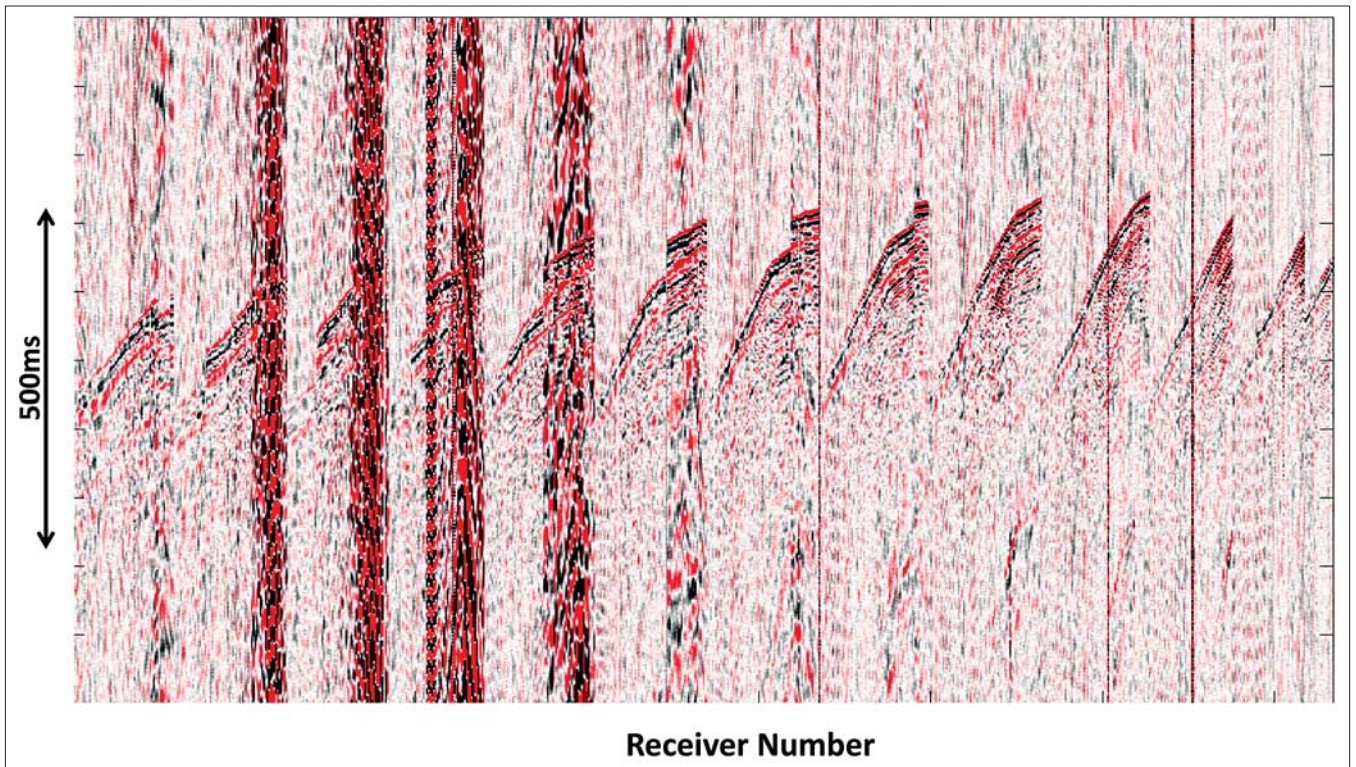
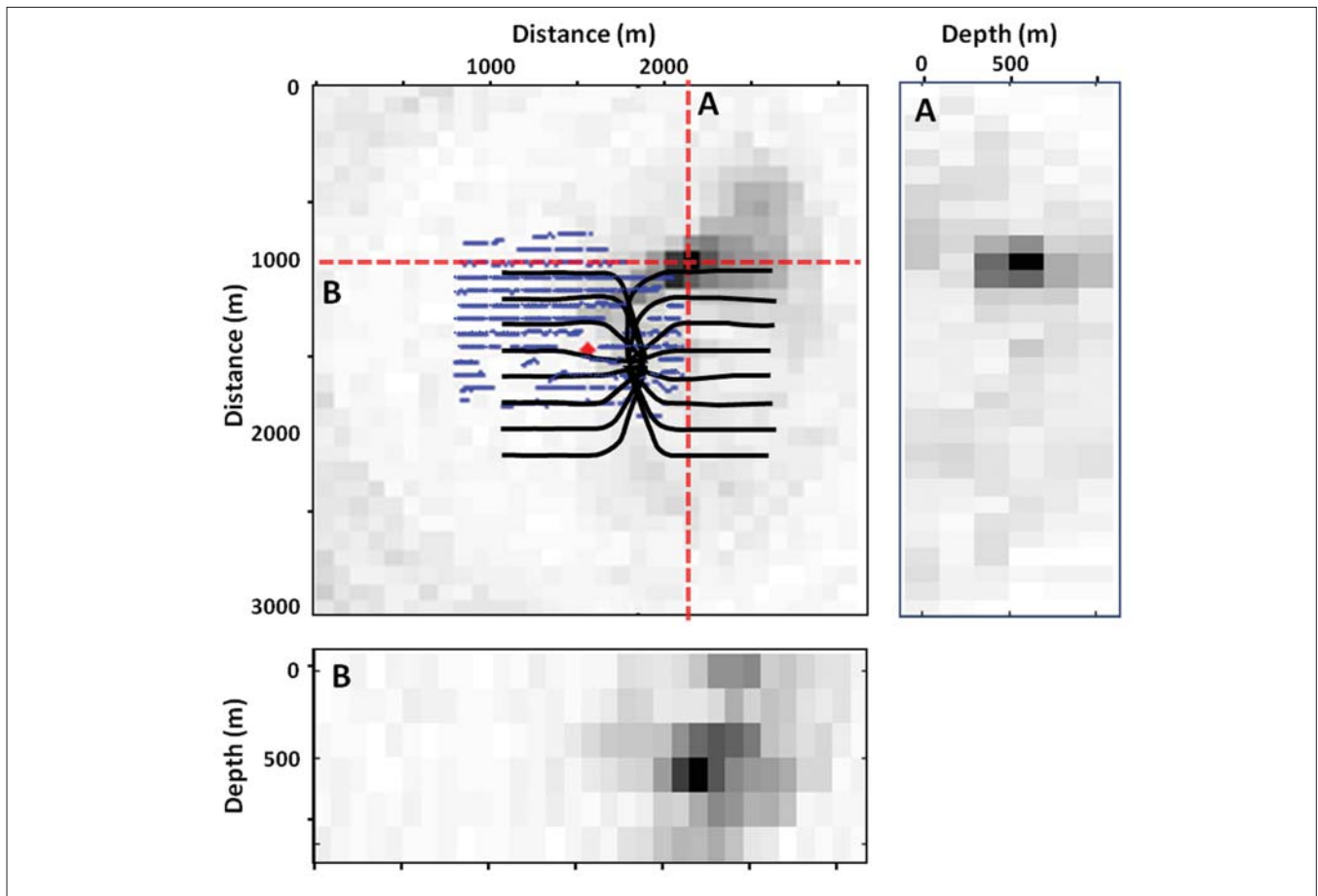


Figure 6. Microseismic event detection. A large-magnitude microseismic event is clearly visible across the whole receiver array in this part of a record. The “active” part of these downhole vibrator records has been filtered out, leaving just the “passive” part, containing some environmental noise and the microseismic events.



**Figure 7.** Microseismic event localization. The displays show orthogonal sections extracted through the maximum of the semblance cube (the maximum being shown in black). The map view also includes the location of the receiver array. The event is at a depth of 600 m along the northern well of the right-hand pad.

weeks of the experiment. Only a portion of them comes from the reservoir. The others are either false detections or events located at the surface.

### Conclusions

The design of this unique onshore life-of-field reservoir monitoring system allows the continuous and simultaneous recording of both active time-lapse seismic reflection data and passive microseismic events. This experiment on a steam-assisted heavy oil production field showed a high level of repeatability in the typically noisy environment of producing fields. Transit-time and amplitude variations through the reservoir could be assessed on a weekly or even daily basis. The time variations were observed where steam was injected while the amplitude variations may be linked to production effects. Additionally, we were able to simultaneously detect and localize microseismic events from the reservoir zone. Further work needs to be done to link the observed 4D attribute variations and detected microseismic events with fluid, pressure, temperature and geo-mechanical effects induced by steam injection and oil production. **TLE**

### References

- Forgues, E. and E. Schisselé, 2010, Benefits of hydrophones for land seismic monitoring: 72nd EAGE Conference and Exhibition, paper B034.
- Hansteen, F., P. B. Wills, J. C. Hornman, L. Jin, and S. J. Bourne, 2010, Time-lapse refraction seismic monitoring: 72nd EAGE Conference and Exhibition, paper B033.
- Meunier, J., F. Huguet, and P. Meynier, 2001, Reservoir monitoring using permanent sources and vertical receiver antennae: The Céré-la-Ronde case study: *The Leading Edge*, **20**, no. 6, 622–629, doi:10.1190/1.1439008.
- Schisselé, E., E. Forgues, J. Echappé, J. Meunier, O. de Pellegars, and C. Hubans, 2009, Seismic repeatability: Is there a limit?: 71st EAGE Conference and Exhibition, paper V021.

*Acknowledgments:* We thank the managements of Shell and CGGVeritas for their kind permission to present this work.

*Corresponding author:* eric.forgues@cggveritas.com

# Appendix 2

## Continuous Land Seismic Monitoring of Thermal EOR in the Netherlands

Cotton, J., L. Michou and E. Forgues, 2013.



## Continuous Land Seismic Reservoir Monitoring of Thermal EOR in the Netherlands

Julien Cotton\*, Laurene Michou and Eric Forgues, CGGVeritas.

### Summary

A continuous reservoir monitoring system has been installed for Shell, on a medium heavy-oil onshore field situated in the northeast of the Netherlands, to re-develop oil production by Gravity-Assisted Steam Drive. The challenge was to continuously monitor using seismic reflection the lateral and vertical expansion of the steam chest injected in the reservoir during production over more than a year.

The main problems for onshore time-lapse seismic are caused by near-surface variations between base and monitor surveys which affect the seismic signal coming from the reservoir. In our system, a set of permanent shallow buried sources and sensors has been installed below the weathering layer to both mitigate the near-surface variations and minimize the environmental footprint.

The very high sensitivity of our buried acquisition system allows us to track very small variations of the reservoir physical properties in both the spatial and calendar domains.

The 4D reservoir attributes obtained from seismic monitoring fit the measurements made at observation, production, and injector wells (pressure, temperature, and oil/water production). A daily 4D movie of the reservoir property changes allows us to propose a scenario that explains the unexpected behavior of the production and confirms that the steam does not follow the expected path to the producer wells but rather a more complicated 3D path within the reservoir.

## Introduction

The Schoonebeek field with a STOIPP of 1 bln bbls is situated in the northeast of the Netherlands. The medium heavy-oil reservoir is about 20 m thick and located at 650 m depth with an average porosity of 30%. Between 1948 and 1996, the oil (160 cP at 40°C, 25 API, 19% wax) was produced with thermal EOR in vertical wells. The oil is currently produced by Gravity-Assisted Steam Drive using horizontal injectors and producers.

A permanent seismic system (2D then 3D) was installed to monitor the reservoir evolution during the steam injection (Figure 1). The monitoring lasted two years. During this time, we tracked the steam plume propagation injected into a horizontal well located between two horizontal producer wells to understand the 4D behavior of the steam and update the dynamic reservoir model accordingly.

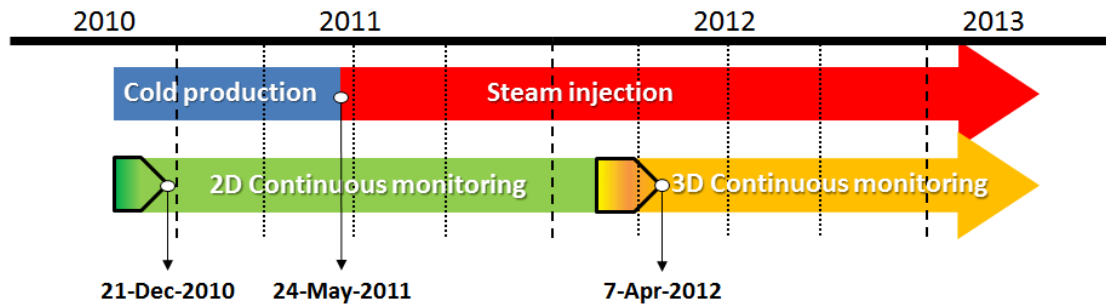


Figure 1: Permanent seismic monitoring time schedule covering the transition period between cold production and steam injection. Black triangles represent the system installation period.

## Gravity-Assisted Steam Drive

Reservoir engineers are interested in knowing how the steam spreads from the injector to the neighboring producers. The pump rate could then be adjusted to optimize reservoir production.

The steam, injected at low pressure, is expected to rise to the top of the reservoir, spread horizontally, and finally condense. Hot water then descends through the reservoir, heating the oil and improving its mobility. According to Hornman *et al.*, 2012, a 3-m sub-seismic fault may delay the steam expansion by three years as shown in Figure 2 by an example of asymmetrical steam chest development.

A feasibility study was conducted by modeling the acoustic response of the pressure during cold production and steam injection. During the early steam injection phase, pressure, temperature, and steam zone thickness should change, but each in a different way:

- 1) The pressure changes should propagate quickly over the reservoir and be nearly the same over the vertical dimension of the reservoir.
- 2) The steam zone should initially be thin and then propagate horizontally along the top of the reservoir.
- 3) The associated temperature increase should first occur near the top of the reservoir and then increase vertically below the steam zone.

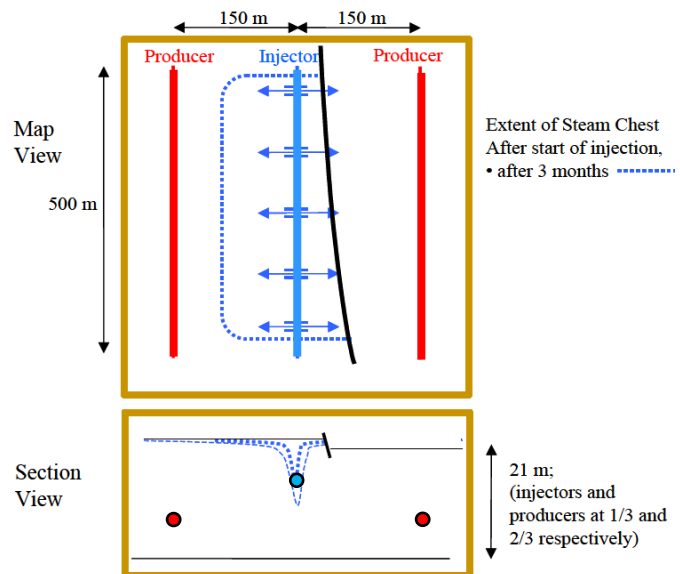


Figure 2: Asymmetric expansions of the steam chest due to the small fault throw.

## 2D and 3D Seismic Monitoring

A permanent buried installation ensures excellent seismic repeatability, as well as having a minimum impact on farming activities and the environment (Figure 3). In December 2010, a 2D pilot survey was carried out (see Cotton et al 2012 for a detailed description). In April 2012, the permanent seismic acquisition geometry was extended to 3D.



Figure 3: Aerial photos of the monitoring area.  
Top: Trenches during installation.  
Bottom: Four months later during continuous monitoring.



Figure 4: A SeisMovie™ piezoelectric source ready to be cemented in the downhole.

The 3D system consists of 36 piezoelectric mini-vibrators (Figure 4) placed in cemented boreholes at a 25-m depth. The signal was recorded by a set of five lines, each composed of 69 dual-depth buried hydrophones at 6 and 9-m depths. As illustrated in Figure 5, the equipment is located above one horizontal injector and two horizontal producers. There are also two deviated observation wells measuring the temperature and pressure inside the reservoir. The sources vibrated simultaneously and continuously during the two year acquisition period using a patented technique (IFP, GDF, CGG, US patent 6714867-B2) of mono-frequency emissions covering a 5-186 Hz band over six hours. The 3D acquisition covers a subsurface imaging area of 800 by 120 m.

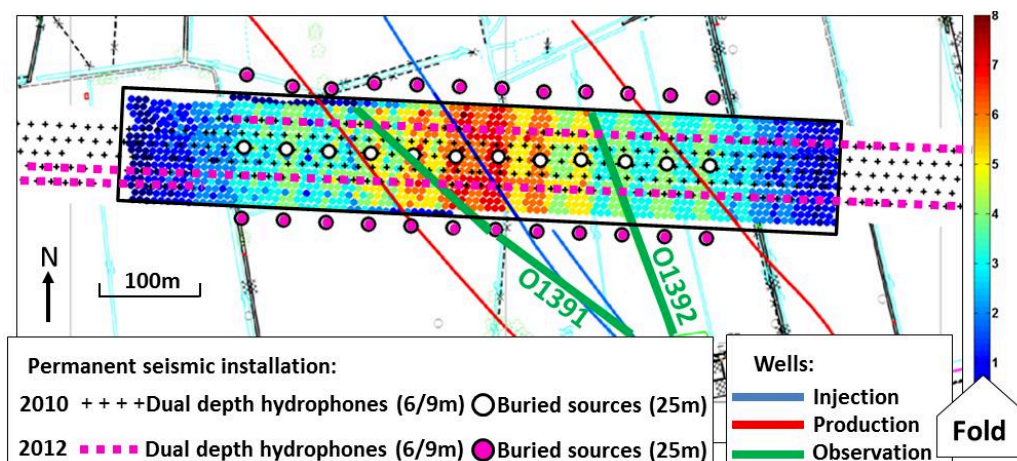


Figure 5: Map showing the equipment used for both the initial 2010 2D survey and that added in 2012 to enable 3D monitoring. The colored dots represent the imaging bins with associated the fold. Blue line: injector well; Red line: production wells; and Green line: observation wells.

A daily summed shotpoint is shown in Figure 6. The zero-offset reservoir reflection arrives at 625 ms. The energetic S-wave cone generated by the source hides the near offsets and was consequently muted. At the reservoir level, the contributing offset extends only from 250 to 800 m and the stacking fold ranges from 4 to 8 in the useful part of the spread covering the injection and the production wells. This very low fold is counterbalanced by favorable data quality and high repeatability provided by the buried sources and receivers under the weathering layer.

Unfortunately, there are five other types of unwanted waves interfering with the reservoir reflections: i) the source ghosts ii) the receiver ghosts, iii) the S-P wave converted at the surface, iv) surface multiple, and v) the ambient noise producing Rayleigh waves. The minimization of these unwanted waves is necessary to ensure an accurate recovery of the seismic monitoring results.

The processing sequence described in Cotton and Fergues, 2012 has been automatically executed on a daily basis to provide migrated seismic cubes and 4D attributes (traveltime and amplitude variations). The processing has two main objectives: firstly, the mitigation of surface reflected waves interfering with the reflections around the reservoir (ghost and near-surface converted waves); and secondly, the collapse of the diffractions to map amplitude changes in the reservoir. The processing workflow consists of:

1. receiver ghost reduction by dual-depth hydrophone-combinations
2. source ghost separation in the calendar domain
3. S-P converted wave mitigation by separation in the calendar domain (Bianchi *et al.*, 2004), plus a high resolution 3D radon filter to remove residual linear waves
4. weekly sliding median filter in the calendar domain to remove remaining ambient noise
5. post-stack migration with a constant velocity to focalize the diffracted events
6. daily 4D attribute computation: amplitude and traveltime variations are obtained using cross-correlation with a reference

The repeatability improvement brought by the processing can be represented as the reduction of both amplitude and traveltime variations above the reservoir, as shown in Figure 7. (A perfect repeatability would produce dots at the origin of both axes.) Both the source and receiver de-ghosting dramatically improve the repeatability. The de-ghosting clearly enhances the repeatability but does not particularly improve the general visual aspect of the stack section shown in Figure 8. On the contrary, the migration only slightly improves the repeatability while enhancing the general image quality by reducing the noise level and focusing the signal.

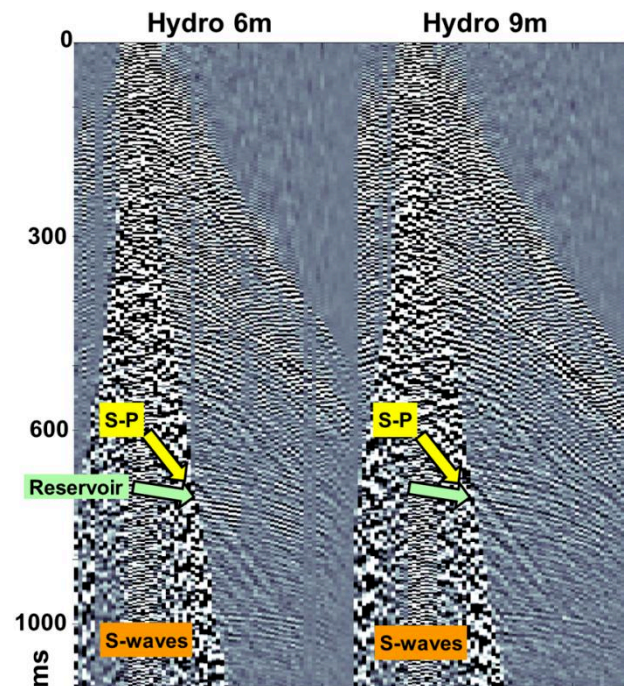


Figure 6: Typical shotpoint recorded daily for one buried source and a line of dual-depth hydrophones buried at 6 and 9-m depths.

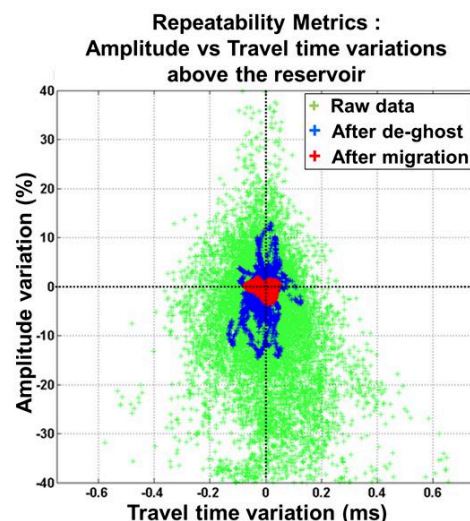


Figure 7: Crossplot of amplitude and traveltime variations computed by cross-correlation above the reservoir in the time windows shown in Figure 8.

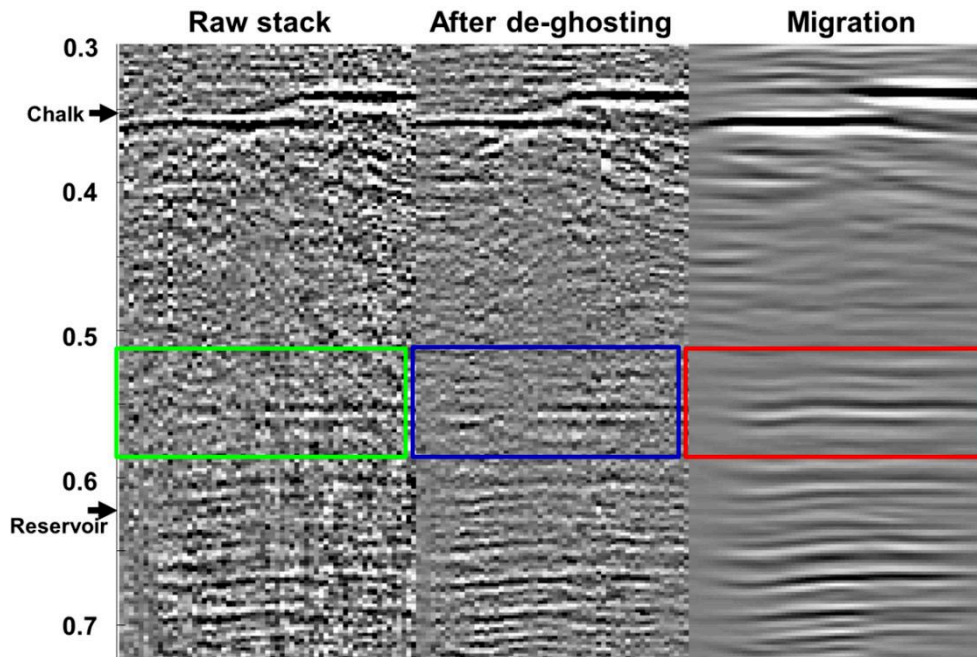


Figure 8: Seismic stack section from the 3D cube for the raw data and after the two main processing stages i) de-ghosting and ii) post-stack migration. The colored time windows above the reservoir are used to compute the crossplots in Figure 7.

#### 4D Monitoring Results

In Figure 9, the difference between two migrated sections at two different dates is a way to appreciate the seismic signal variation within the reservoir. We clearly observe a 4D seismic effect in the vicinity of the injector. The difference (multiplied by 5) is here represented at the early stage of the injection during the 2D phase (one month before the start of the injection on April 24, 2011 and one month after on June 24, 2011).

For both the 2D and 3D seismic monitoring, the daily 4D attributes are obtained using a trace-by-trace cross-correlation with a reference dataset. The lengths of the correlation windows are 100 and 20 ms for the traveltimes and amplitudes, respectively.

The 4D attributes are then compared to the actual well information. Refer to Cotton *et al.*, 2012 for a detailed description of the 2D phase.

At the injector, the seismic attributes are compared to the steam injection rate (Figure 10). The steam injection started on May 9, 2011, and the full injection started around May 24, 2011. This graphical comparison highlights that the steam injection and interruptions are detected almost instantaneously on the time shift curve (red line) and with some delay on the amplitude curve (green line). The time shifts very rapidly follow the steam

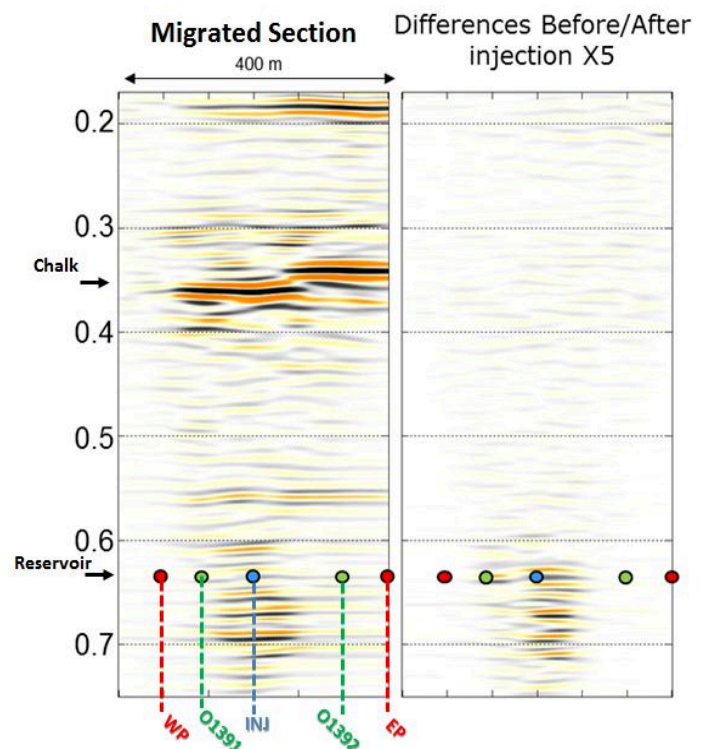


Figure 9: On the left: Stack section with localization of the wells (extracted from the seismic of the 2D phase). On the right: differences multiplied by 5 between sections one month before start of injection and one month after.

injection rate. Three months after the start of steam injection, the maximum observed cumulative variation of amplitude and time shift near the injector are 10% and 0.4 ms, respectively. During the same period, the average calculated daily time shift variations are about 6 microseconds and the daily amplitude variations are about 0.1%.

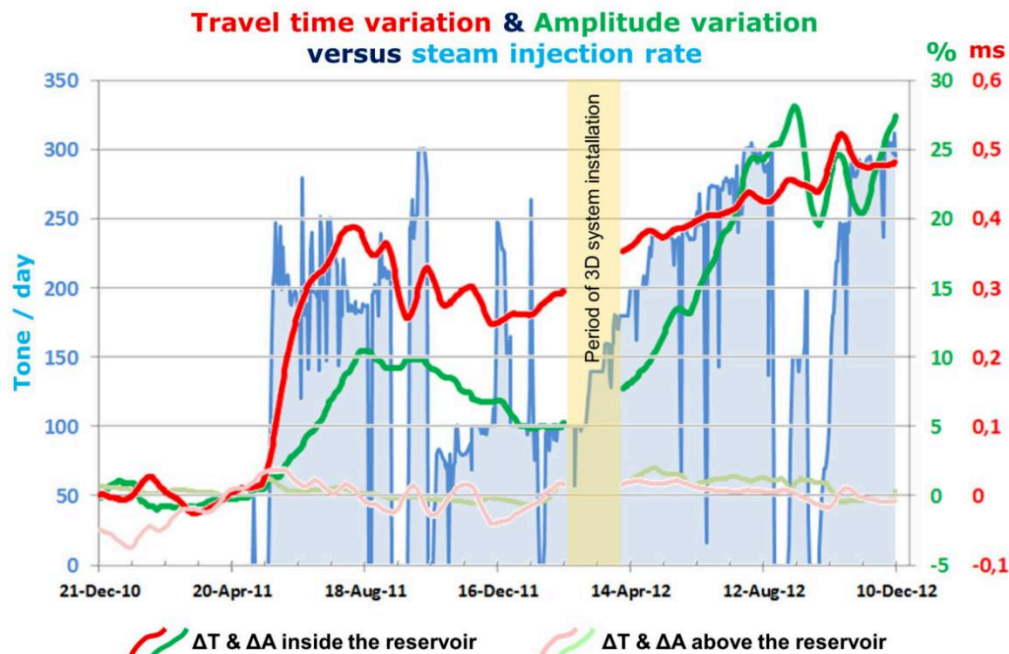


Figure 10: At the injection well, the steam injection rate (blue) is correlated with the seismic travelttime shift below the reservoir (red) and amplitude measured in the reservoir (green). Above the reservoir, the time shift and the amplitude variations (light red and light green) are very stable around zero.

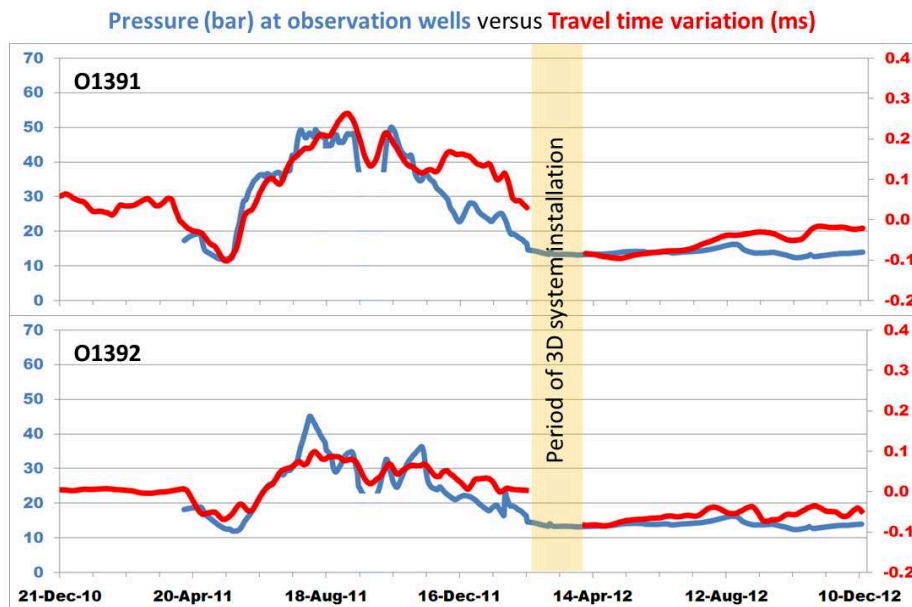


Figure 11: Comparison of travelttime variations and pressure measured at both observation wells O1391 on the west (top graph) and O1392 on the west (bottom graph).

In Figure 11, we see a good correlation between the travelttime variation and the pressure measured at the two observation wells. Between April and December 2011, pressure effects were detected on both observation wells O1391 and O1392 for which the distance from the injector is 80 and 160 m, respectively. Between April and December 2012, almost no pressure effects and travelttime variation were detected at the observation wells, while at the injector the steam injection rate and the travelttime variation were both rising (Figure 10).

The 3D monitoring system is required to understand and map the complex path of the steam propagation. To visualize the daily evolution of the amplitude variations, a 4D movie was produced. Figure 12 shows four maps at different dates. The traveltimes variations were measured 50 ms below the reservoir and the amplitude variations were measured in the reservoir at 625 ms. On the amplitude variation maps (right column), we see that the steam propagates from the injector well (blue) to the western production well (red) passing north of the western observation well O1391 (green). No significant variations are observed on the east side of the injector well. We observe discontinuities on the time seismic horizon situated at the base of the reservoir Figures 13. This horizon map was obtained from a former large scale 3D surface seismic survey.

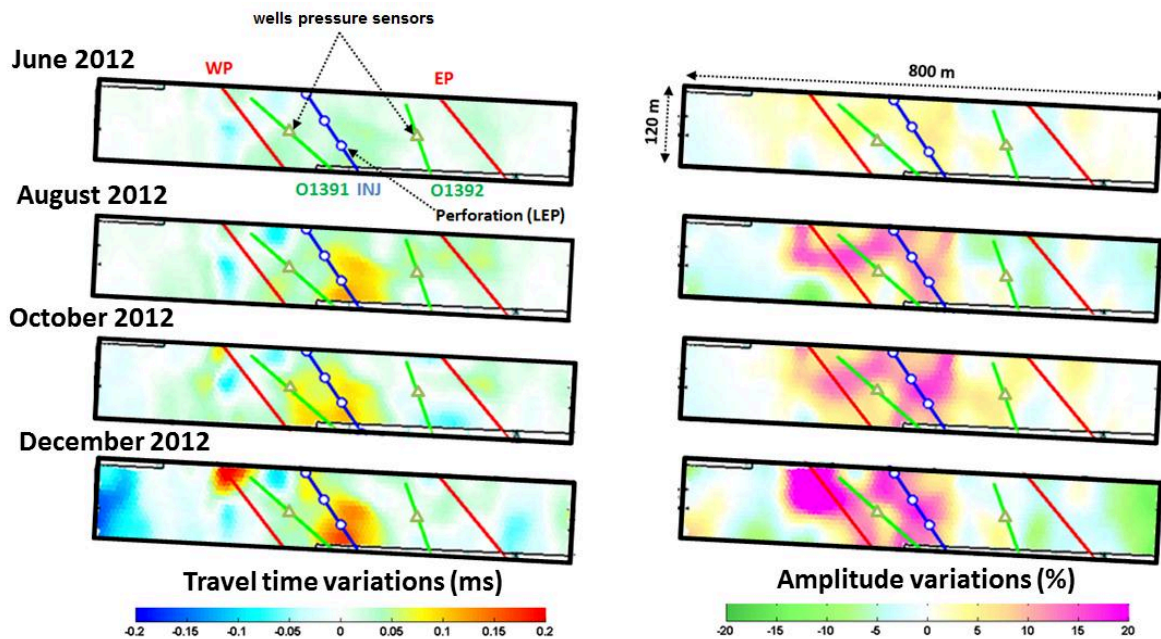


Figure 12: Traveltimes variations below the reservoir (Left) and amplitude variations in the reservoir (Right) at different dates. The east part of the reservoir is clearly not swept by the steam.

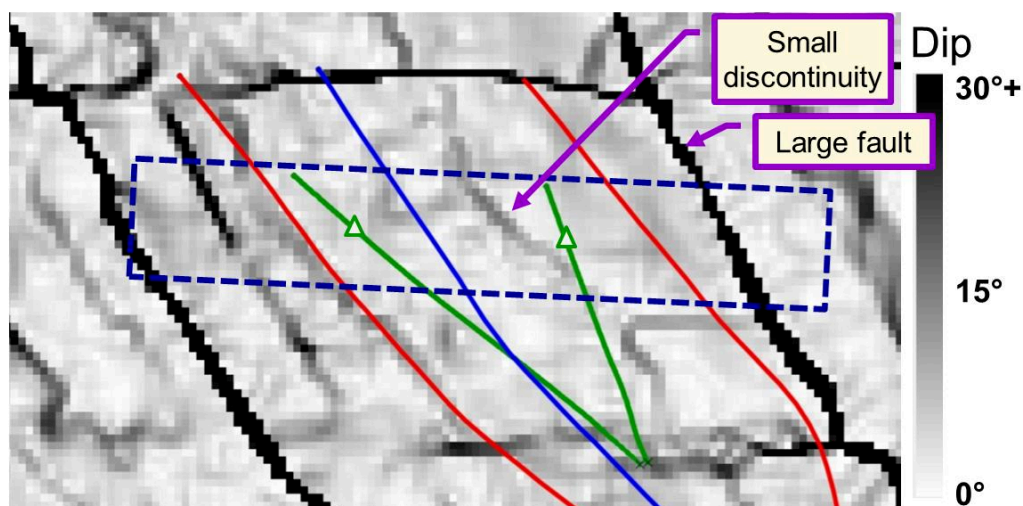


Figure 13: Map of the dips at the base of the reservoir computed using an existing 3D surface dataset acquired in 2005 (Courtesy of NAM). The permanent monitoring area is represented by the dashed rectangle.

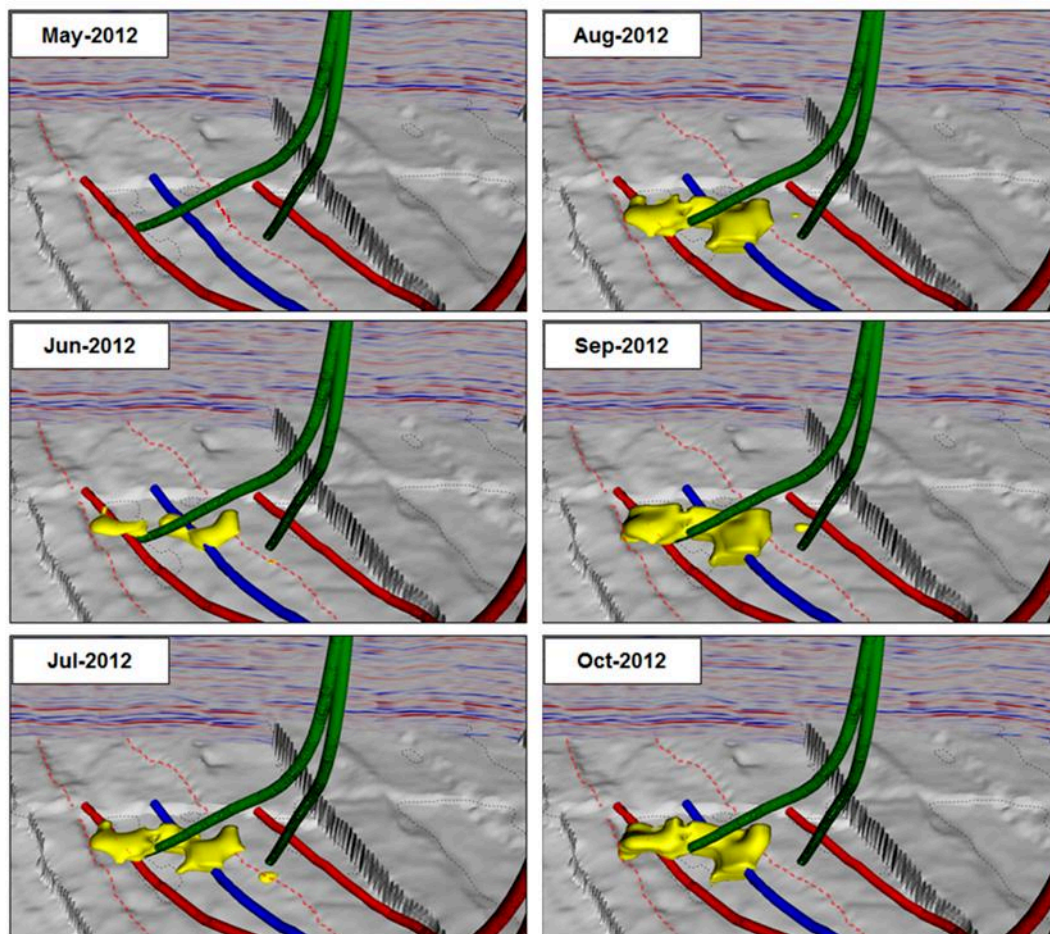


Figure 14: The 3D volumes of the iso 7% amplitude variations (in yellow) shows the evolution of the steam chamber in the reservoir. The steam propagation is asymmetric and delayed on the east side of the injector. The bottom reservoir horizon (shown as the grey surface) was obtained from the conventional 2005 3D seismic (Courtesy of NAM).

Figure 14 shows snapshots of the 4D movie computed during the injection. The 3D yellow blob is the 7% iso amplitude variation as compared to May 2012. It represents the spatial and calendar amplitude spreading due to steam injection.

The amplitude variations obtained by cross-correlation give a cumulative effect of the steam over the whole reservoir thickness but do not allow us to distinguish the 4D effects between the top and the base of the reservoir. To investigate what happens inside the reservoir, a 4D acoustic inversion has been carried out on a monthly basis. The stratigraphic inversion allows a better vertical resolution as shown in Figure 15. Figure 15b shows a 2-ms layer resolution with a total 4-ms impedance variation at the top of the reservoir. In Figure 15c, the amplitude variations are less focused when computed with cross-correlation on a sliding 20-ms time window.

The quantification of 4D effects in term of P-impedance variations (-8%) were in agreement with the Petro-Elastic Model.

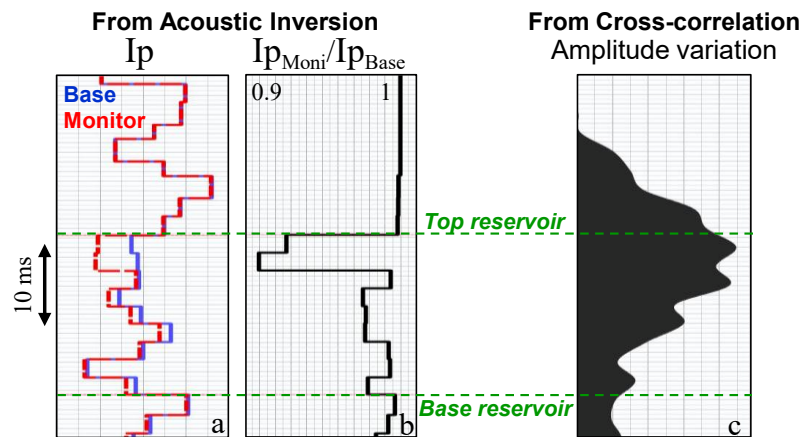


Figure 15: 4D inversion results at the injection well in July 2011: (a) P-impedance for base (blue), monitor (red), (b) monitor over base impedance ratio, (c) base/monitor amplitude variations obtained from cross-correlation.

## Conclusion

The precision and stability of our permanent and continuous buried acquisition system allowed us to detect both small traveltimes and amplitude variations over two years. The accuracy of these values is confirmed by measurements made at the observation wells.

The deployment of the 3D survey enabled us to investigate the complex path of the steam from the injector to the producer, providing valuable information for building more accurate dynamic models that allow our client to make better reservoir management decisions.

The benefit of the 4D acoustic inversion trial conducted on this dataset is the vertical resolution that is used to differentiate  $I_p$  variations between the top and base of the reservoir. These good results encourage us to pursue the analysis of this inspiring dataset.

A next step would be to differentiate pressure, saturation, and temperature effects using additional constraints from the Petro-Elastic Model and taking advantage of the high resolution in the calendar domain. This differentiation would be possible as these effects do not vary in the same ways over calendar time.

## Acknowledgements

First and foremost, we express gratitude to Kees Hornman from Shell for his fertile contribution to this work and his general strong interest in and support for this project. We are grateful to Julien Meunier, Yves Lafet, and Thierry Coleou for their fruitful discussions. We also thank Shell Global Solutions International and NAM for their permission to present this work.

## References

- T. Bianchi, E. Forgues, J. Meunier, F. Huguet, and J. Bruneau, 2004, Acquisition and processing challenges in continuous active reservoir monitoring: 74th Annual International Meeting, SEG, Expanded Abstracts, 2263.
- J. Cotton, E. Forgues, 2012, Dual-Depth Hydrophones for Ghost Reduction in 4D Land Monitoring: 82th Annual International Meeting, SEG, Expanded Abstracts number 667.
- J. Cotton, E. Forgues and J.C. Hornman, 2012, Land Seismic Reservoir Monitoring: Where is the steam going? : 82th Annual International Meeting, SEG, Expanded Abstracts number 1539.
- J.C. Hornman, J. Van Popta, C. Didraga, and H. Dijkerman, 2012, Continuous monitoring of thermal EOR at Schoonebeek for intelligent reservoir management: International Intelligent Energy Conference, SPE, 150215.



## Appendix 3

Permanent, continuous & unmanned 4D seismic monitoring: Peace River case study

Berron, C., L. Michou, B. De Cacqueray, F. Duret, J. Cotton and E. Forgues, 2015.



## Permanent, continuous & unmanned 4D seismic monitoring: Peace River case study

Cécile Berron, Laurene Michou, Benoit De Cacqueray, Florian Duret, Julien Cotton and Eric Forgues; CGG

### Summary

The seismic monitoring solution presented here is a permanently buried, fully automatic, and continuous seismic acquisition and processing system. It ensures remarkably repeatable daily seismic.

Our specific calendar oriented 4D processing flow is described and applied on a monitoring system installed for Shell on their Peace River project to provide daily monitoring of a heavy oil production pad.

The main observation is that 4D attributes vary a lot even when looking at very short calendar periods. This continuous monitoring information gives significant insights into reservoir activities and offers new opportunities to better understand the short term dynamics of the reservoir.

### Introduction

One of the most common *in situ* methods to enhance heavy oil recovery is steam assisted production. As steam generation is expensive, it is important to optimize steam injection programs and avoid waste. This requires appraising the volume of reservoir stimulated on a frequent calendar basis.

In conventional 4D seismic and especially onshore, positioning errors, ambient noise and lack of acquisition repeatability drastically decrease the chance of success to observe small reservoir changes due to production.

In order to provide very frequent seismic acquisition for land reservoir monitoring, CGG has developed an autonomous unmanned permanent seismic monitoring system, known as SeisMovie™. This repeatable technology enables to detect or image daily reservoir variations.

Such a system has been installed on a production pad of the Peace River heavy oil reservoir in Alberta, Canada for Shell (Lopez et al., 2015). The seismic monitoring has been ongoing since May 2014. We present the 4D processing flow driven by the specificities of this unique seismic monitoring acquisition.

### Permanent, buried, repeatable, unmanned, and continuous

Our 4D seismic acquisition system differs from conventional 4D time-lapse seismic methods through six main characteristics:

Permanent, buried sources and receivers ensure perfect positional repeatability and improve both 4D signal to noise ratio and signal repeatability, thanks to the insulation from

surface noise and near surface variations (Cotton & Forgues, 2012).

Reliable piezoelectric seismic sources ensure the repeatability of the emission system as shown by Schisselé et al., 2010.

Once installed the seismic acquisition system is fully unmanned. There is no crew onsite, and therefore zero HSE exposure. As such, the total cost of monitoring becomes virtually independent of the number of repeated acquisitions and is amortized over time. Continuous monitoring of reservoir activity is made possible: daily 3D seismic data are acquired and processed. These specific acquisition characteristics drive the 4D processing flow.

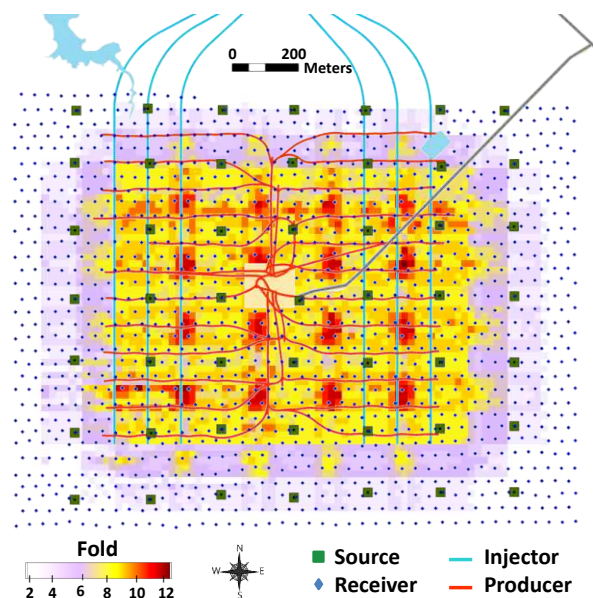


Figure 1: Peace River seismic acquisition system of permanent buried sources (squares) and buried receivers (blue dots) for continuous reservoir monitoring of horizontal well injectors (blue) and producers (red). The background color is the acquisition fold.

### Peace River Monitoring

Figure 1 presents the acquisition geometry installed on a production pad at Peace River: 1490 hydrophones are buried at 20 m depth and 49 sources at 25 m depth. The source grid is 200 m by 220 m and the receivers are 40 m spaced. The monitored area is 1.8 km by 1.6 km.

The survey is sparse: the average fold is 8 on a 20 m bin size (background color of Figure 1).

The system monitors the reservoir activity of 24 East-West horizontal producers and 6 North-South horizontal injector wells (Figure 1).

## Permanent, continuous & unmanned 4D seismic monitoring: Peace River case study

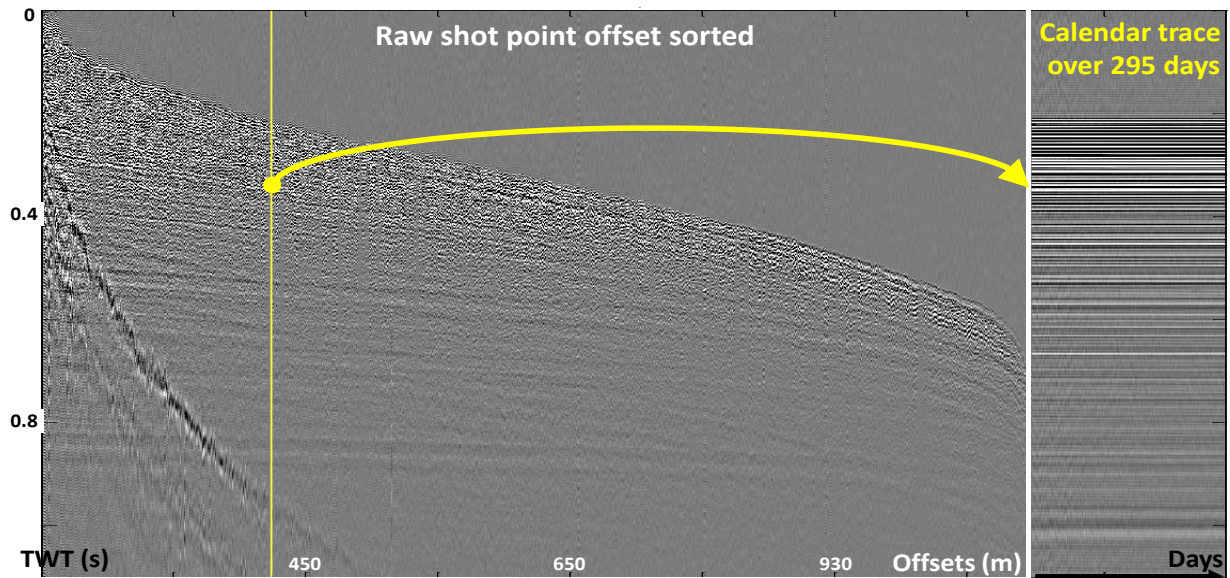


Figure 2: Left: Daily raw shot point sorted by offsets for the 1490 hydrophones. Right: one raw daily response of a single hydrophone channel over the first 295 days. The stability of the calendar trace highlights the repeatability of the acquisition.

### Calendar oriented 4D processing flow

The aim of the current processing sequence is to provide: daily Pre-Stack Time Migrated (PSTM) seismic cubes, 4D seismic attributes and QC. Processing flow was delivered two months after the first day of monitoring. The automatic processing workflow is described below.

**First step:** We keep the same number of traces over days. If for any reason the acquisition is interrupted, the missing data is replaced by the latest available records (“copy & paste”). In practice, since May 2014 and after 300 days of acquisition, only 0.35% of the traces have been replaced and none since November. There has been no failure for all the buried equipment. Figure 2 shows a daily raw shot point and one raw calendar trace of the input data. It represents the daily response of a single hydrophone channel. The stability of the calendar trace highlights the repeatability of the acquisition.

**Second step:** In order to homogenize spatial sensors sensitivity differences, a spatial amplitude compensation is applied. The coefficients are kept constant for the entire monitoring period.

**Third step:** To correct residual variations, data are stabilized by a scalar in the calendar domain. A Root Mean Square (RMS) stabilization calculated above the reservoir is applied per source and per receiver. It is the only

processing step that tends to compensate for remaining unwanted calendar changes.

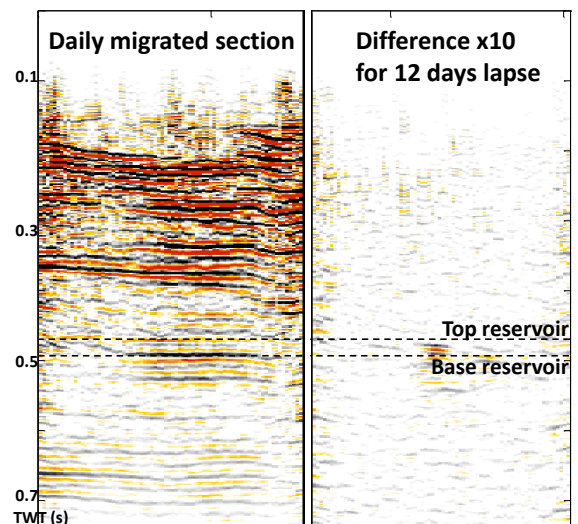


Figure 3: Migrated inline of a daily acquisition (left section) and the difference multiplied by 10 between this vintage and a baseline taken 12 days before (right section). This East-West inline is taken along a producer well during the steam injection period.

**Fourth step:** The data are Pre-Stack Time Migrated with a 3D velocity model kept constant over days. Figure 3 illustrates a migrated section of a daily acquisition and the differences over 12 days. As observed, at reservoir level the

## Permanent, continuous & unmanned 4D seismic monitoring: Peace River case study

reflectivity appears weaker on the western side which highlights the reservoir heterogeneities.

Clear 4D seismic variations are observed at reservoir level. Furthermore, no significant variation is observed above the reservoir, which is a first illustration of the repeatability and quality of the processed seismic data. The frequency content of the 4D migrated seismic data covers a [30-150] Hz band pass.

On certain areas short term variations of free surface reflections (ghosts) had a significant impact on the measured 4D attributes, and thus needed to be removed through dedicated calendar deghosting step (Cotton & Forgues, 2012). In the particular context of the Peace River project though, measured 4D attributes are well correlated with reservoir activity (Figure 4). No major footprint of near surface variations on the 12 days monitoring scale is observed; currently no specific deghosting process is implemented.

### 4D attributes

On a daily basis, several 4D attributes are automatically computed on the migrated cubes. Some attributes are used to quantify the repeatability of the monitoring to provide a confidence map of the observed variations. Other attributes, such as time shift variations, give significant insight into reservoir activity.

Figure 4 illustrates sixteen snapshots of time shift variation maps at reservoir level between September 2014 and March 2015. Snapshots are taken every 12 days. Time shift variations are computed against a sliding baseline 12 days behind of the current monitor in order to enhance short term variations. They are computed using trace-by-trace cross correlation with a sliding window of 60 ms on the migrated seismic data. The time line shown above the maps contextualizes the snapshots during the reservoir production. The first six maps, “a” to “f”, are computed during a blow-down period (i.e. a production period to reduce the reservoir pressure). Maps “g” to “p” are calculated during the steam injection period.

A first observation is that in some areas time shifts vary a lot even when looking at very short calendar periods. This unprecedented dense calendar information offers new opportunities to better understand the short term dynamics of the reservoir.

During the blow-down period, a velocity slowdown (*i.e.* decrease of time shift according to the calculation convention taken) is observed along one East-West horizontal producer.

Steam injection was initiated in mid-November, via the six North South injectors. It was followed by the clear observation of time shifts along the two eastern injectors.

No significant variation is measured on the western injectors.

About 45 days after the start of steam injection, a velocity increase is suddenly observed where the velocity slowdown was measured during the blown-down period (blue spot on maps “j” to “l”).

As the baseline is sliding, no time shift variation means that travel times are kept constant compared to the previous period, as for example snapshots “e” and “n”.

Time shift maps provide a significant overview of the reservoir activity not only on areas where variations are measured but also where no change is observed. The supplementary areal information provided by seismic monitoring should be closely linked with well measurements for further interpretation.

### Conclusion

The continuous monitoring of steam assisted production on the Peace River site is achieved by a fully unmanned, permanently buried seismic monitoring system with an automatic acquisition and processing workflow. The 4D processing workflow is driven by the main characteristics of this onshore continuous seismic monitoring. Daily 3D seismic data are automatically processed to provide daily 4D time lapse attributes.

The monitoring gives significant insights into the reservoir activity and highlights short term calendar variations that would be missed by conventional time lapse 4D seismic. Linked with well information, the continuous seismic monitoring could help optimize production and enhance heavy oil recovery.

### Acknowledgments

The authors would like to thank Shell for their kind permission to present this work

### References

- Cotton, J., Forgues, E., 2012, Dual-Depth Hydrophones for Ghost Reduction in 4D Land Monitoring: 82th Annual International Meeting, SEG, Expanded Abstracts, 667.
- Lopez, J.L., Wills, P.B., La Follett, J.R., Barker, T.B., Xue, Y., Przybysz-Jarnut, J.K., Van Lokven, M., Brouwer, R.R., Berron, C., 2015, Real-Time Seismic Surveillance of Thermal EOR at Peace River: SPE Canada Heavy Oil Technical Conference, SPE-174459-M.
- Schissel , E., Forgues, E., Echapp , J., Meunier, J., de Pellegars, O., Hubans, C., 2010, Seismic Repeatability - Is There a Limit?: 72nd Conference and Exhibition, EAGE, Extended Abstracts, V021.

Permanent, continuous & unmanned 4D seismic monitoring: Peace River case study

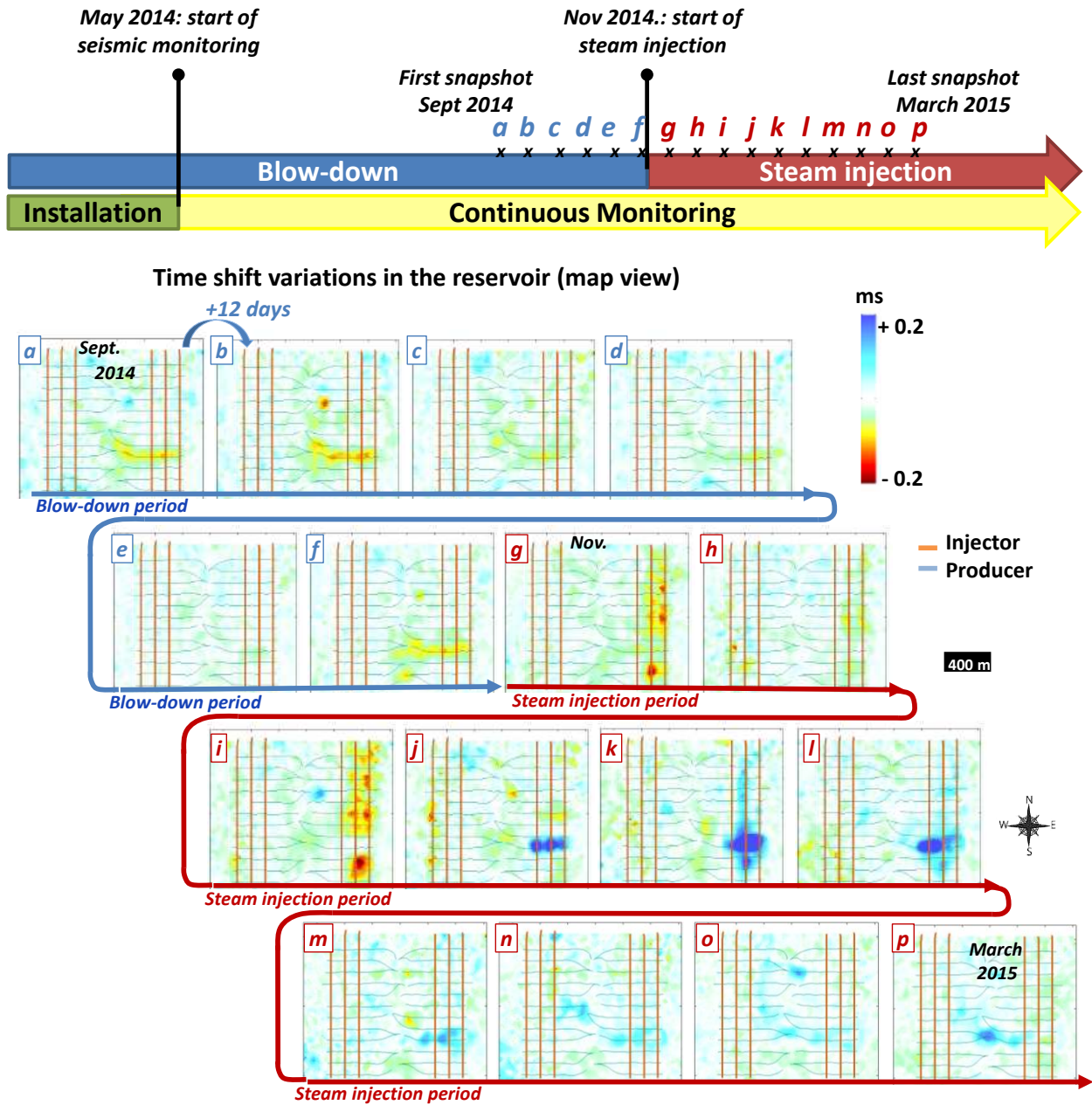


Figure 4: Top: Calendar time line of reservoir production. Bottom: time shift variations at reservoir level over seven months. Snapshots are taken every 12 days. Baseline is sliding and is taken 12 days before monitor

# Appendix 4

## An optimal source for continuous monitoring

Cotton, J., 2019.



# An optimal source for continuous monitoring

Cotton Julien (CGG)

## 1. Introduction

A permanent buried installation below the near-surface weathering layer ensures minimum impact on surface activities as well as excellent repeatability avoiding positioning issues and coupling variations from a seismic campaign to the next. Onshore, repeating a seismic experiment may be difficult using conventional seismic sources for a least three reasons.

- 1) A mechanical source requires redundant maintenance,
- 2) A long term continuous emission may damage the source components leading to its deterioration,
- 3) Energetic sources may lead to settlement, subsidence, ground instability and erosion.

The seismic experiment represented in Figure 1 may illustrates a very poor 4D acquisition. Note that the experiment was simply a mechanical maintenance test, without any 4D expectations.

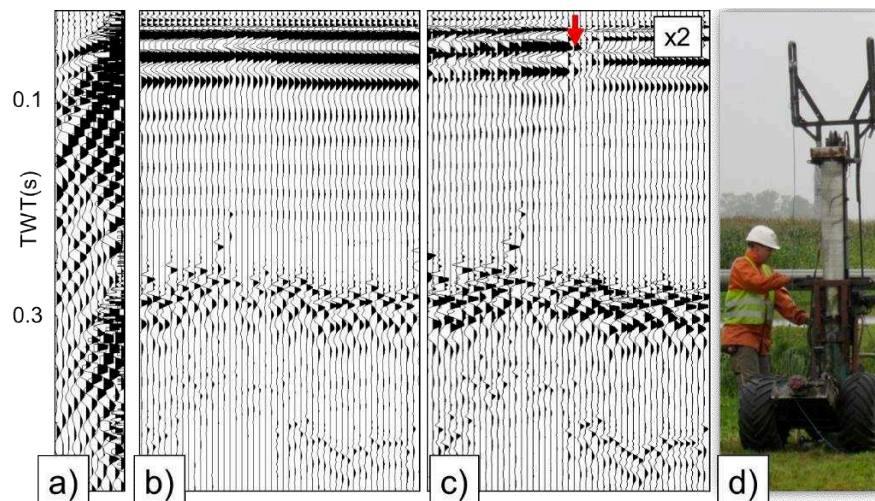


Figure 1: Shot repetition using a weight drop vackimpack. The fluctuating weight rebound is clearly visible at 0.3 s. The compaction of the surface as well. Channels sorted in decreasing offset (a). Repeated seismic (b) and variations (c). Image of the vackimpack (d) operating in the field.

## 2. The SeisMovie source: a piezo-actuator

CGG has developed, in collaboration with Gaz de France (now ENGIE) and Institut Français du Pétrole (now IFPEN), a solution based on sparse and permanent piezo-actuator sources and buried receivers: SeisMovie (Meunier and Huguet, 1998; Meunier et al., 2000). The SeisMovie system was initially designed for geological gas-storage applications (Mari et al., 2011). The repeatability of the system is excellent and is enhanced using buried sources (Figure 2).

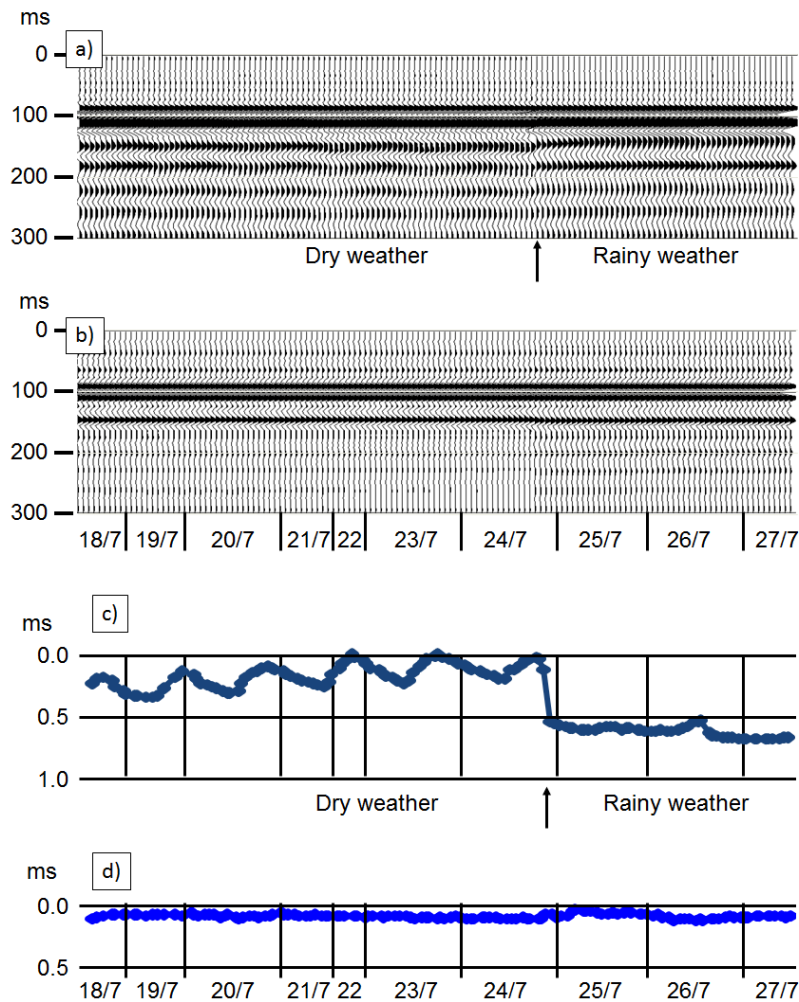


Figure 2: Repeated seismic traces using the SeisMovie source at the surface (a) and using a buried source (b). The travel time variation computed by cross-correlation for both the surface (c) and the buried (d) experiments. From Meunier et al., (2000).

Piezo-actuators like stacks, benders, tubes, rings make use of the deformation of electro-active PZT ceramics (PZT: lead (Pb) zirconia (Zr) Titanate (Ti)), when they are exposed to electrical fields. The deformation is used to produce motions and / or forces. The produced effect is the complementary effect to piezoelectricity, where electrical charges are produced upon application of mechanical stress to the ceramics. As an analogy, the term “piezo-mechanics” was introduced in the early 80’s of the past century to describe the conversion of electricity into a mechanical reaction by a piezo-material. A PZT monolayer structure acts as a capacitive element defined by two thin conductive electrodes enclosing the piezo-ceramic as dielectric.

The driving element of the piezo-actuator seismic source pillar consists of a stack of PZT ceramics interposed between control electrodes. Under the action of an electrical voltage applied to the electrodes, the thickness of the ceramics increases. A sinusoidal AC voltage applied to the electrodes causes a sinusoidal variation in the length of the pillar. When this “piezo-capacitor” is charged by applying a voltage, a deformation is created (Figure 3).

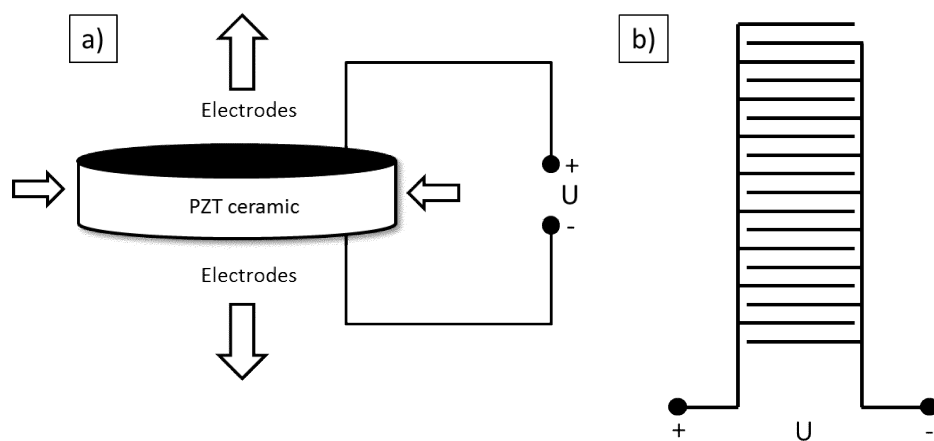


Figure 3: Scheme of the piezo-actuator and the associated deformation created by applying a voltage (a). The electronic scheme (b).

Piezo stack actuators make use of the increase of the ceramic thickness in direction of the applied electrical field. Stacking of several layers towards a multilayer structure increases equivalently the total stroke. Similar to normal elastic deformation of a solid-state body, the thickness expansion of a PZT layer induces an in-plane shrinking being complementary in motion.

The pillar part of the source (ceramics and electrodes) is protected from the external environment by a flexible polyurethane covering. A typical pillar has a cylindrical shape with a radius of 5 cm and a length of 95 cm (Figure 4).



Figure 4: A typical piezo-actuator seismic source pillar without the polyurethane (left) and with the polyurethane envelope (right).

This pillar consists of 120 PZT ceramics, known under the commercial name NAVY type I (the military standard MIL-STD-1376B defines the performance properties of Navy Type piezoelectric ceramics). Each ceramic have a ring shape with 20 mm internal diameter, 40 mm external diameter and 4 mm thickness. The maximum length expansion obtainable for this pillar in the absence of constraints is 120  $\mu\text{m}$ , corresponding to a volume change of about 1000  $\text{mm}^3$ . Power amplifiers supply the electric signal (92500 Volt, 2 Ampere, 5-300 Hertz) to the pillar. A high-security cable connects the source and the amplifier. The voltage and current must be controlled; otherwise, this would result in bad repeatability therefore, significant engineering efforts were conducted to optimize the amplifier design. In a continuous monitoring project, the amplifiers are placed in surface bungalows as illustrated in Figure 5.

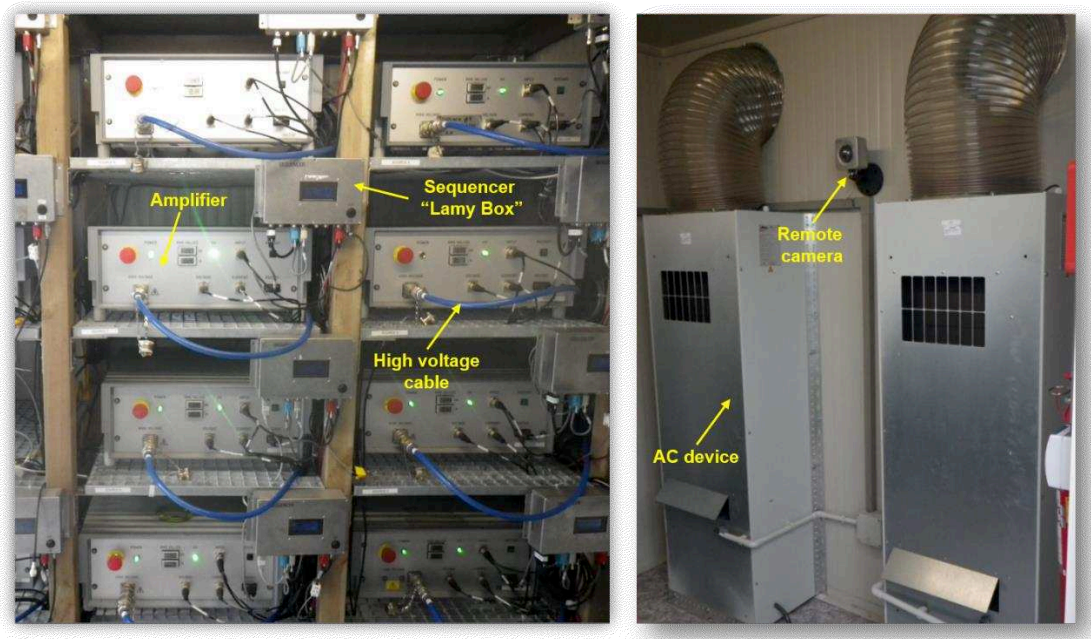


Figure 5: Inside a surface bungalow. The amplifier and the sequencer (left) and the AC devices (right).

The stabilization of the temperature inside the amplifier bungalow was key to ensure the high repeatability in continuous seismic monitoring as illustrated in Figure 6.

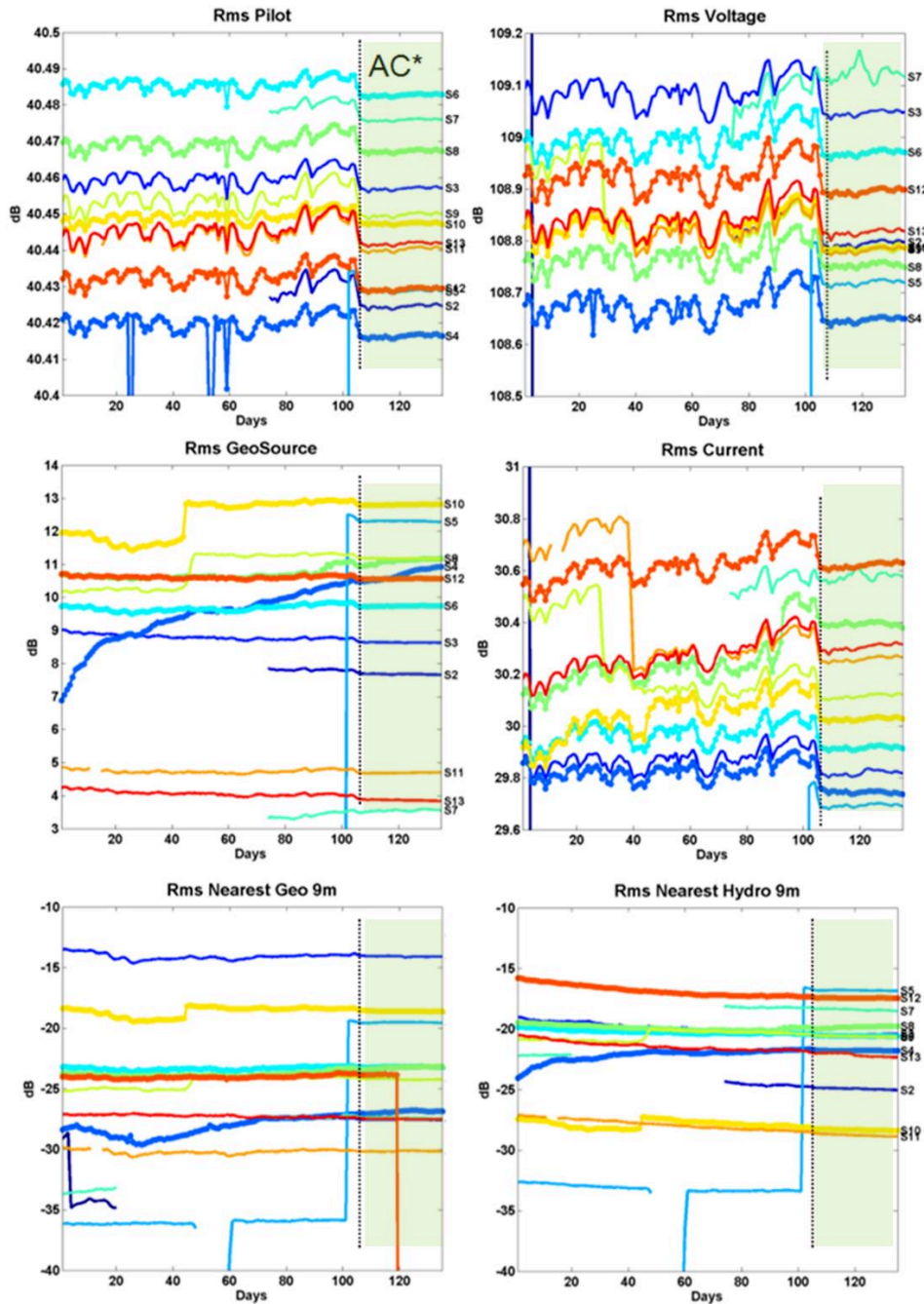


Figure 6: Different control points showing the improvement brought by the use of the AC devices in the amplifier bungalows. Different colors are used for each source.

### 3. Energy of the SeisMovie source

Figure 7 compares the data recorded using a piezo-actuators seismic source pillar with the data obtained using a conventional seismic source (a M22 vibrator

truck). The piezo-actuators seismic source pillar is a low energy source but an equivalent signal to noise ratio can be obtained by increasing the length of the emission.

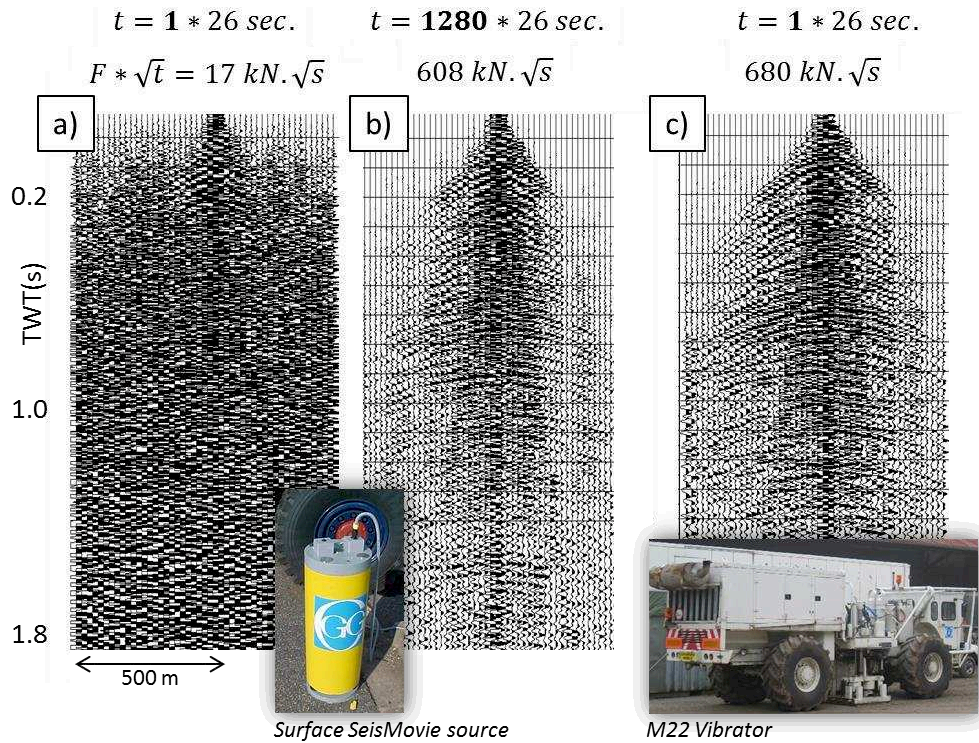


Figure 7: Energy of the surface SeisMovie source (a) and( b) compared to a vibrator truck (c)

The piezoelectric technology is well suited in the context of seismic monitoring. The installed sources are reliable and stable over time; however, some engineering points can easily be improved to increase the source energy in order to achieve deeper objectives such as deep oil reservoirs. In the case of a buried SeisMovie source, two coaxial forces of equal intensities and opposite directions are generated at the coupling surfaces (top and bottom plates). White, (1983) gives the far-field radiation from a buried seismic source:

$$d = \frac{G * \cos^2 \theta * h}{4 * \pi * \rho * v_p^3 * r} * g \left( t - \frac{r}{v_p} \right). \quad (1)$$

In the previous equation,  $d$  is the generated displacement,  $G$  is the amplitude of the force. The distance between the top and bottom plate is noted  $h$ . The polar coordinates

of the receiver as a function of the source center are noted  $r$  and  $\theta$ . The compressional wave velocity and density are respectively noted  $v_p$  and  $\rho$ . Among other solutions (essentially ceramic designs including forms, characteristics, and quantity), the overall increase of the signal emitted by the source can be achieved by playing on the distance  $h$  between the points of application of the forces. To emphasize the signal gain provided by increasing the distance between application points of the forces, we compared two sources equipped with the same ceramic pillar (pillar of 120 PZT ceramics). The distance between the plates is increased by using two metallic spacer plates placed at the ends of the pillar (Figure 8).

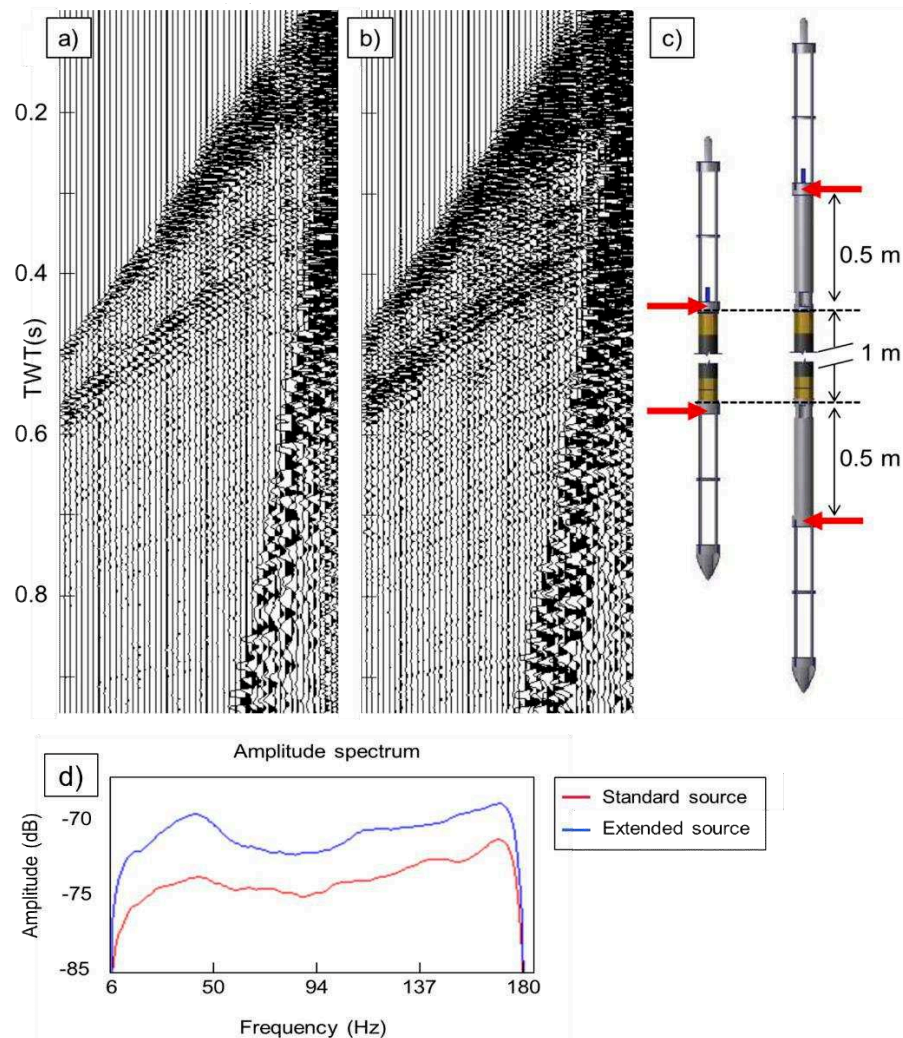


Figure 8: Comparison between a standard SeisMovie source (a) and an extended one (b). A scheme showing the metallic extensions (c). The extensions enable to increase the emitted signal by 6 dB for all the frequencies (d).

## 4. Radiation pattern of the SeisMovie source

The piezo-actuator seismic pillar generates a combination of compressional (P-waves) and shear waves (S-waves). The directivity of such a source is showed in the radiation pattern depicted in Figure 9a. P and S-waves carry different information regarding the subsurface and are both useful for characterizing the subsurface. However, emitting simultaneously a combination of P and S-waves has at least two disadvantages:

- 1) Blended P and S-waves interferences appear on short source-receiver offset records. This generates a noisy time-offset cone on the data.
- 2) S-waves appears spatially aliased when recorded by horizontal arrays designed for P-waves.

The P and S-wave separation remains highly challenging. In practice, the near-offset noisy cone is simply muted. This causes a significant decrease of the fold at the target level. A way to mitigate this would be to use a volumetric monopole source. A volumetric monopole piezoelectric source uses a spherical transducer (2 hemispheres) whereas a piezo-actuator seismic pillar uses a ring stack. The volumetric monopole source offers in theory a broadband, omnidirectional “pure” P-wave transmitting and receiving response (Forgues et al., 2014) (Figure 9b).

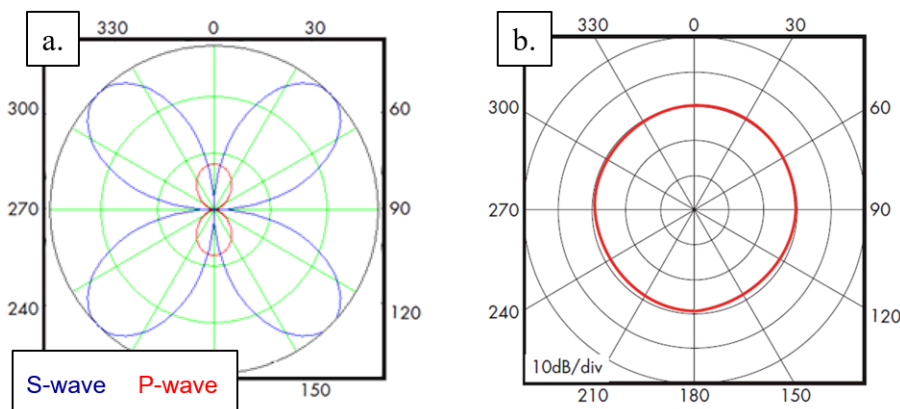


Figure 9: Radiation pattern of a buried SeisMovie source (a). The radiation pattern of a volumetric, monopole piezoelectric source (b).

The volumetric monopole source offers a way to recover usable near offset data that is interesting for the estimation of the intercept in AVO analysis, for the fold

increase and for the penetration depth. Figure compares a standard seismic source to a volumetric one. The volumetric monopole source gives promising results showing less P and S-waves interferences on the near offsets.

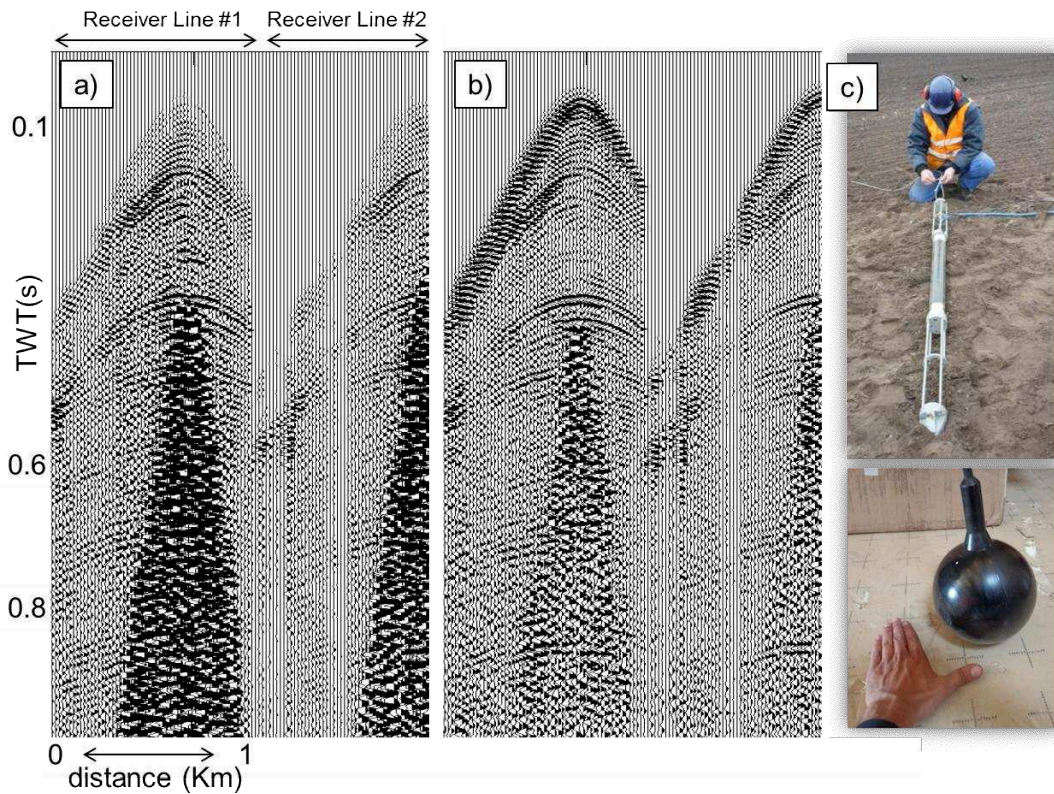


Figure 10: Comparison between a standard SeisMovie source (a) and the volumetric monopole one (b). Pictures showing the two sources (c) with the standard SeisMovie source (top) and the volumetric one (bottom).

The volumetric monopole piezoelectric source was also tested in recording mode exactly as if it was a sensor (Figure 11). In Figure 11b, a volumetric monopole source (used as a sensor) records the signal emitted by several standard SeisMovie sources.

Contrary to piezo-actuator seismic source pillars, needing one vertical drill per source to form a source line, spherical sources (or likes) would need only one horizontal drill per line (Cotton and Grésillon, 2018) (Figure 12). Using the volumetric monopole source alternatively as a source or as a receiver may lead to significant increase of the fold (Figure 13) and therefore, its development is key for continuous reservoir monitoring.

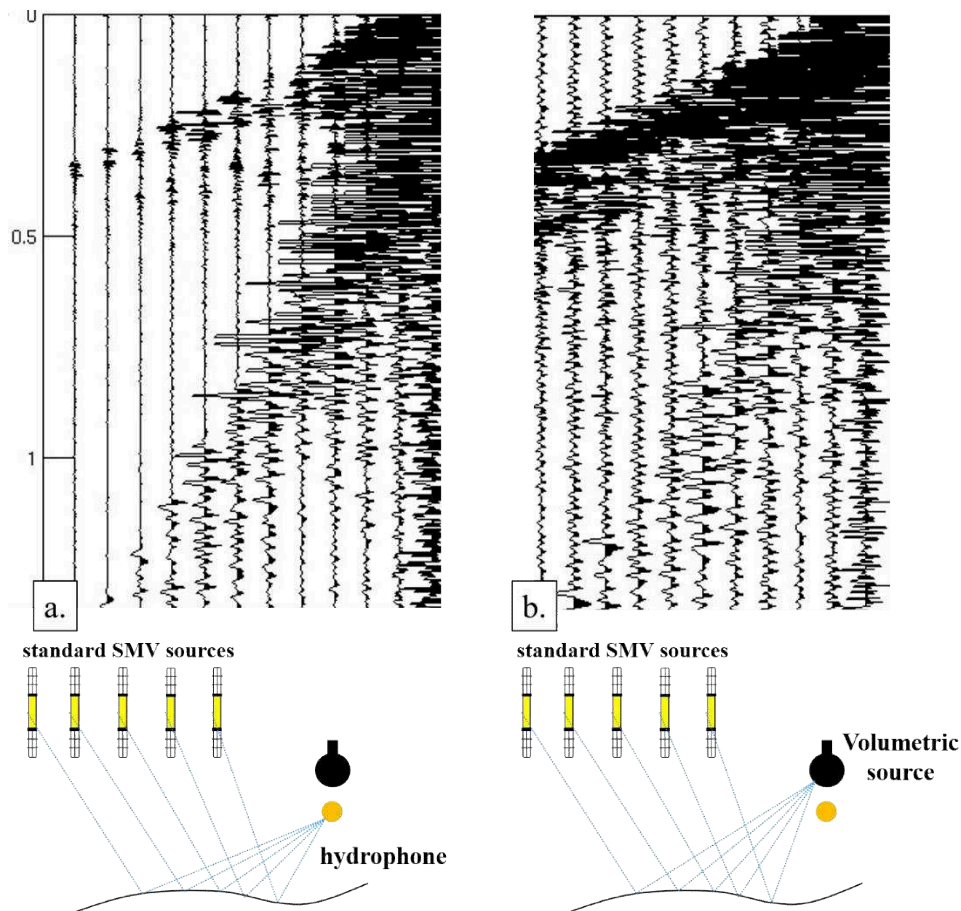


Figure 11: Several standard SeisMovie sources data recorded using hydrophones (left) and using a volumetric source as a sensor in a recording mode (right).

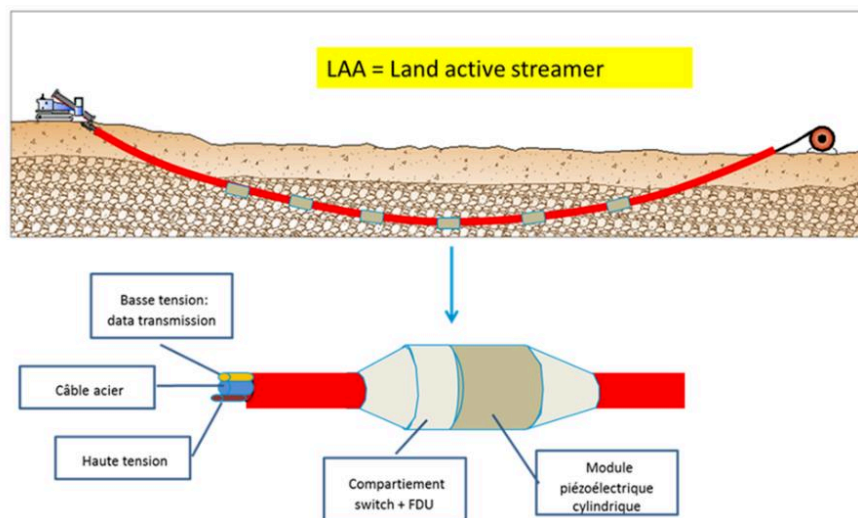


Figure 12: The Land Active Streamer (LAS) installation (top). The LAS uses piezo-electric units, alternatively as seismic sources or as seismic receivers to image the geological layers. From Cotton and Grésillon, (2018).

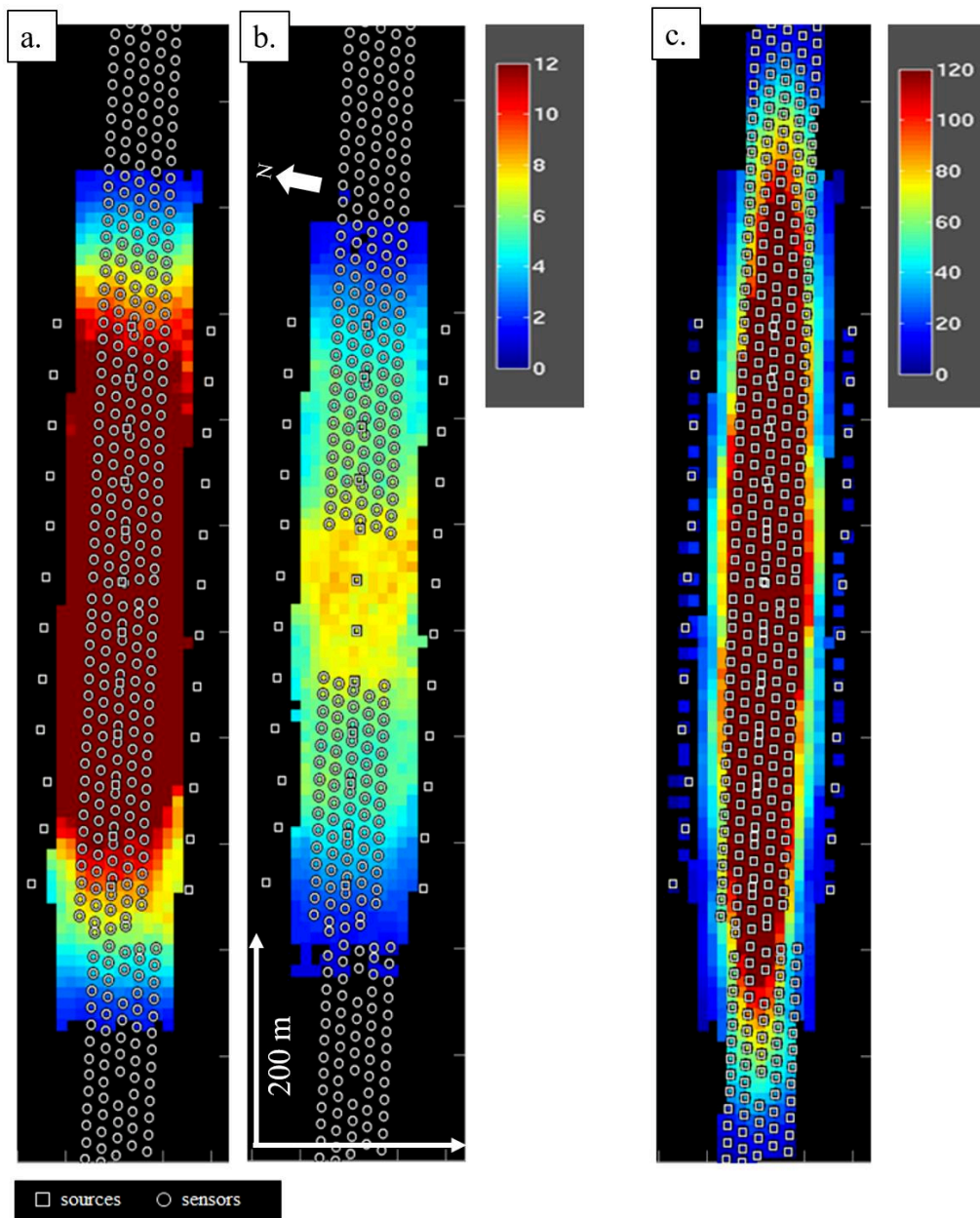


Figure 13: Fold map taking into account all offset that is only possible with the volumetric monopole source (a). The fold map with the inner mute on the S-wave cone (b). Theoretical fold obtained with devices alternatively used either as sensors, either as sources as in the LAS scheme presented previously (c).

## 5. Conclusion

Onshore, repeating an accurate seismic experiment may be difficult using conventional seismic sources that is why CGG, GDF (now ENGIE) and IFP developed the SeisMovie source. The source is highly repeatable and can be operating during long periods without any maintenance.

If the source design is key, we cannot forget that it is the ultimate link of a complete emission chain comprising a controller device and a power amplifier unit. Temperature has undeniably an effect on any electrical components; therefore, it must be controlled; otherwise, the continuous monitoring repeatability may not be sufficient. Air-conditioning devices are thus recommended inside the amplifier bungalows.

The SeisMovie source energy is very low compared to other conventional sources like explosive, weight-drop or vibrator trucks. It is a key advantage, as the SeisMovie source would not damage the medium to which it is coupled. However, in some cases, it could be too weak to reach a sufficient signal to noise ratio. A simple and low cost solution to gain 6 dB at the emission has been proposed. It consists of stiff metallic extension that increases the coaxial force application distance.

The piezo-actuator seismic pillar generates a combination of compressional (P-waves) and shear waves (S-waves). This results in noisy P and S-waves interferences on the short offset records. To mitigate this effect, we successfully tested a new volumetric monopole piezoelectric source. Compared to the SeisMovie pillar, the volumetric source has three advantages. First, it can image deep targets as the near offsets are clean; second, it can be placed into horizontal drills to form a source line; third, the volumetric source could be used alternatively as a source or as a sensor that would have a positive impact on the fold. We foresee the development of this source a key for the future of continuous seismic monitoring.

Mari, J. L., F. Huguet, J. Meunier and M. Becquey, 2011, Natural Gas Storage Seismic Monitoring. Oil & Gas Science and Technology–Revue d'IFP Energies nouvelles, **66**(1), 9-20.

Meunier, J. and F. Huguet, 1998, Céré-la-Ronde: A laboratory for time-lapse seismic monitoring in the Paris Basin. The Leading Edge, **17**(10), 1388-1394.

Meunier, J., F. Huguet and P. Meynier, 2000, Reservoir monitoring using permanent sources and vertical receiver antennae, SEG Technical Program Expanded Abstracts 2000, Society of Exploration Geophysicists, pp. 1619-1622.

Cotton, J., & Grésillon, F. X. (2018). U.S. Patent No. 9,869,789. Washington, DC: U.S. Patent and Trademark Office.

Forgues, E., Grésillon, F. X., & Cotton, J. (2014). U.S. Patent Application No. 14/103,177.

White, J.E. (1983) Underground Sound, Application of Seismic Waves. Elsevier Science Publishing Company Inc, Amsterdam.

# Appendix 5

Method for time-lapse wave separation

Cotton, J. & T. Bianchi, 2013.

United States patent application publication





US 20130258809A1

(19) **United States**

(12) **Patent Application Publication**  
**COTTON et al.**

(10) **Pub. No.: US 2013/0258809 A1**

(43) **Pub. Date: Oct. 3, 2013**

(54) **METHOD FOR TIME-LAPSE WAVE SEPARATION**

**Publication Classification**

(71) Applicant: **CGGVERITAS SERVICES SA**, Massy Cedex (FR)

(51) **Int. Cl.**  
**G01V 1/30** (2006.01)

(72) Inventors: **Julien COTTON**, Paris (FR); **Thomas BIANCHI**, Paris (FR)

(52) **U.S. Cl.**  
CPC ..... **G01V 1/308** (2013.01)  
USPC ..... **367/38**

(73) Assignee: **CGGVERITAS SERVICES SA**, Massy Cedex (FR)

(57) **ABSTRACT**

(21) Appl. No.: **13/766,213**

A method for processing seismic data acquired using the same seismic survey setup over long periods of time includes acquiring sets of seismic data using the same seismic survey setup over multiple days, the sets being gathered as repeated seismic data. The method further includes estimating a time-variable wavelet corresponding to unwanted waves, and determining a propagation of the time-variable wavelet, which propagation is assumed to be constant in time, by solving an inverse problem using the repeated seismic data and the estimated time-variable wavelet. The method also includes extracting signal data by subtracting a convolution of the estimated time-variable wavelet and the propagation from the repeated seismic data.

(22) Filed: **Feb. 13, 2013**

**Related U.S. Application Data**

(60) Provisional application No. 61/617,918, filed on Mar. 30, 2012.

600

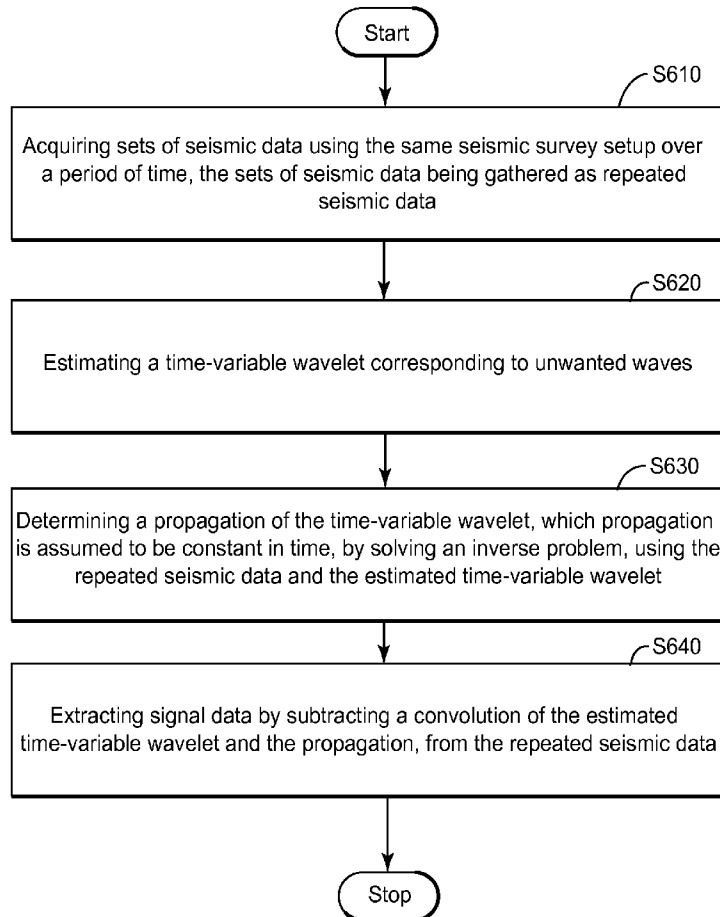


Figure 1  
(Background Art)

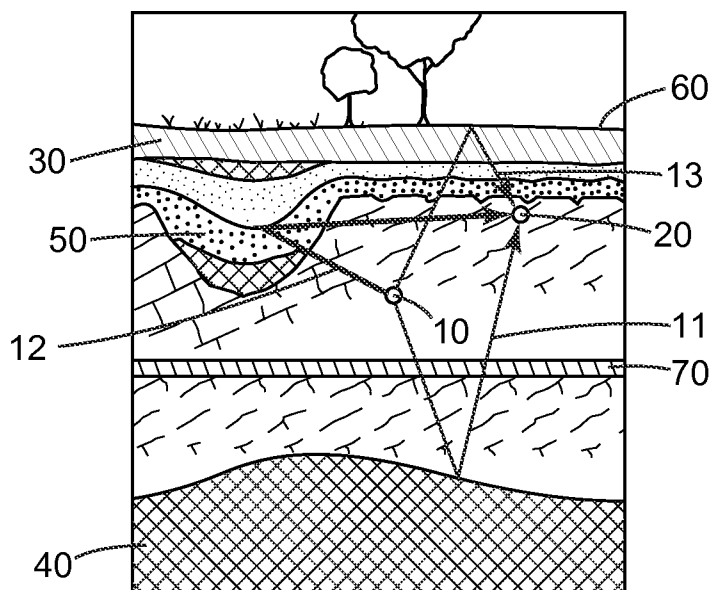


Figure 2  
(Background Art)

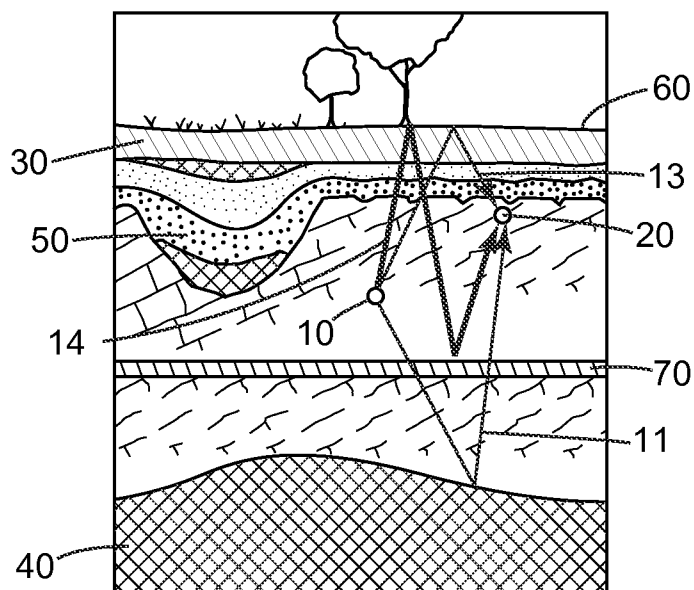


Figure 3  
(Background Art)

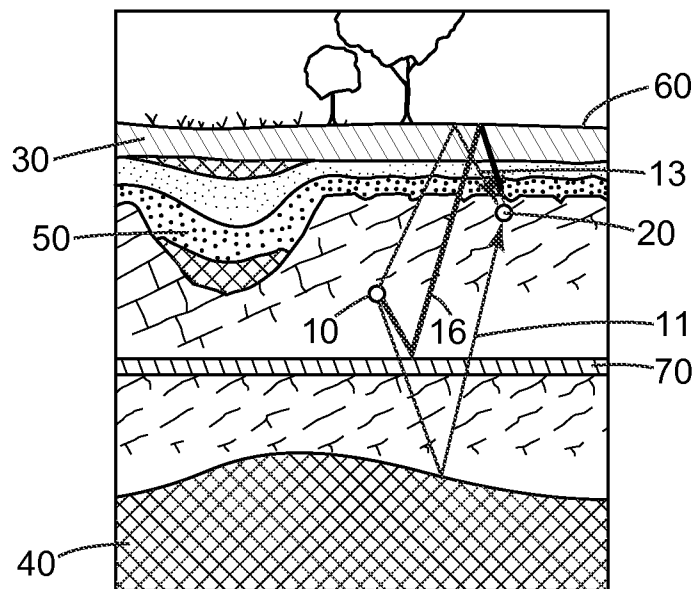


Figure 4A

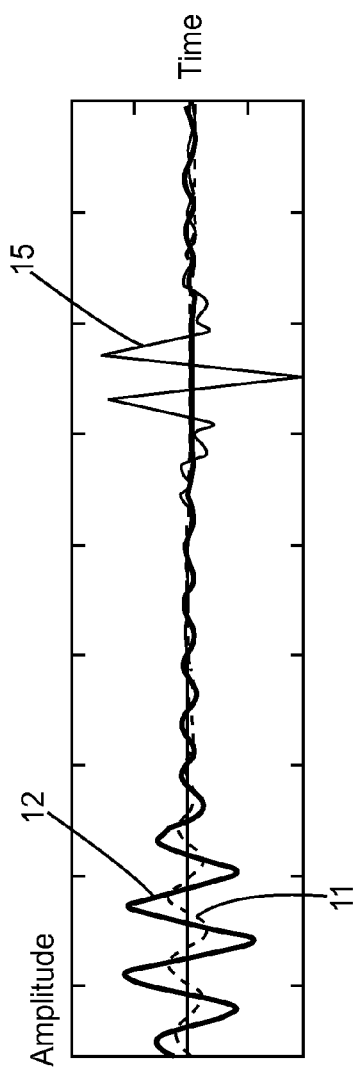


Figure 4B

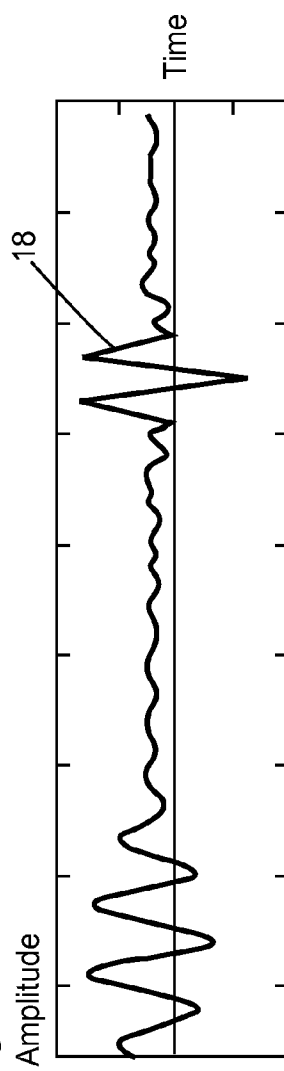


Figure 5

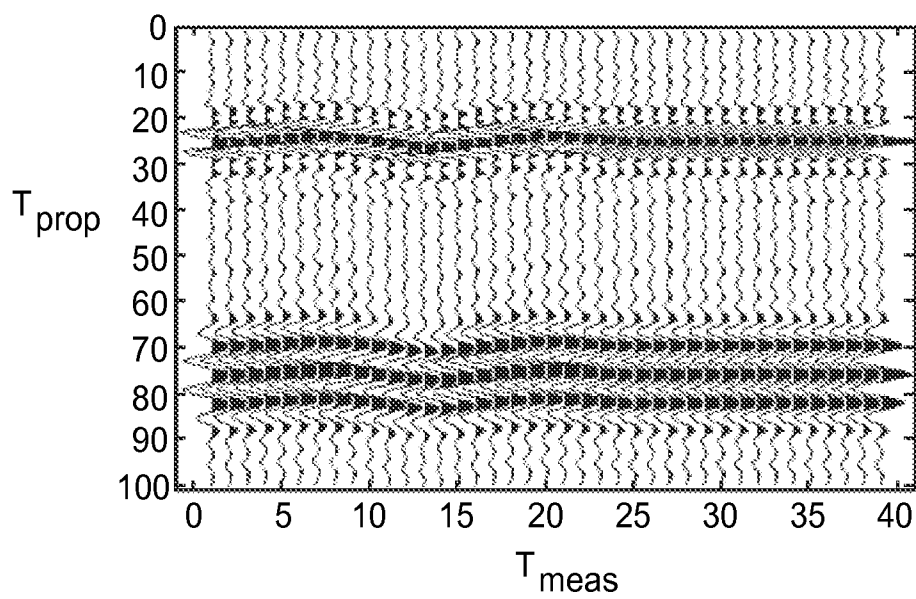


Figure 6

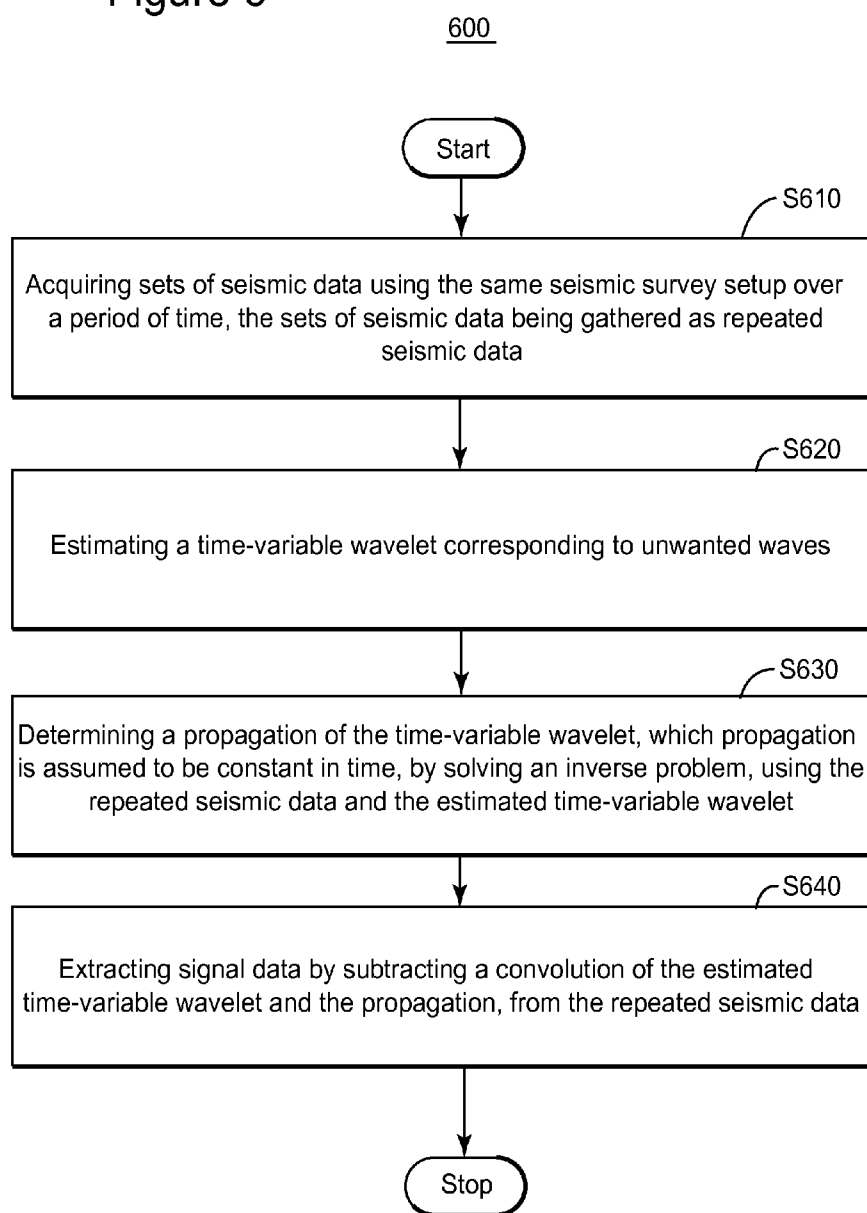


Figure 7

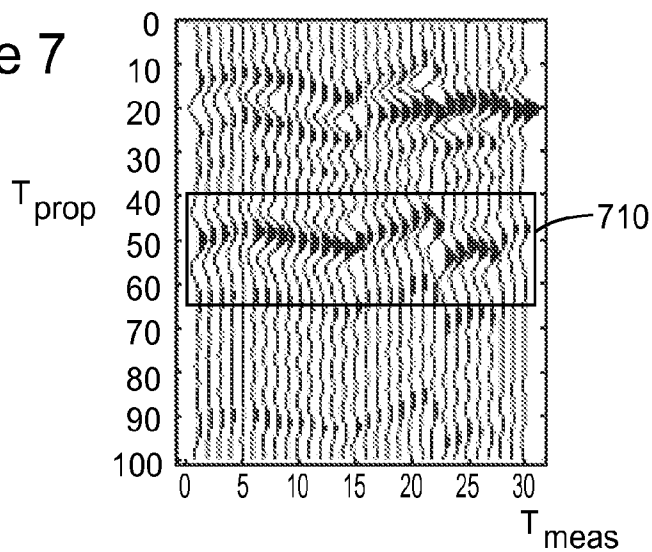


Figure 8

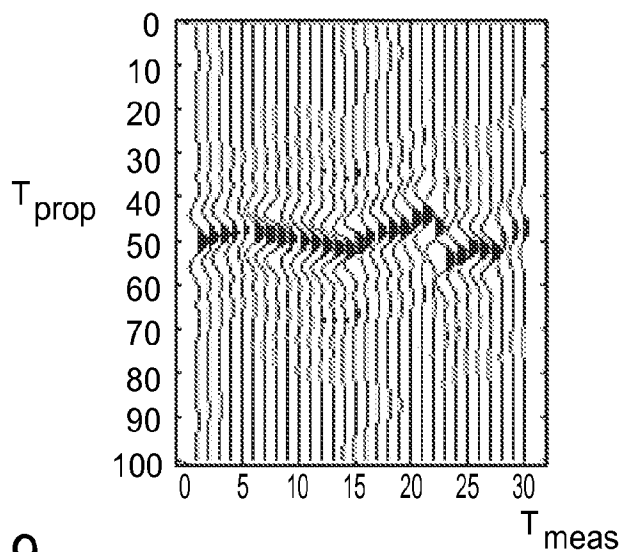
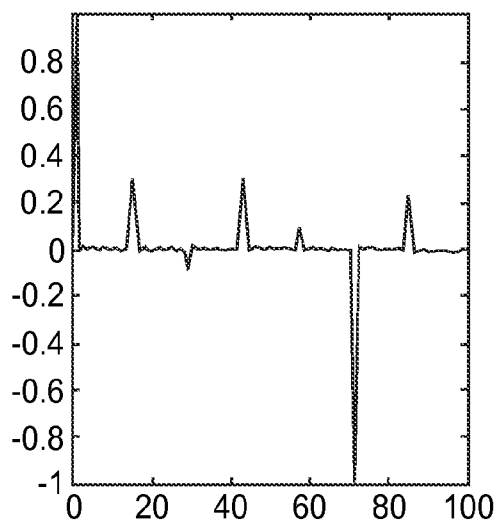


Figure 9



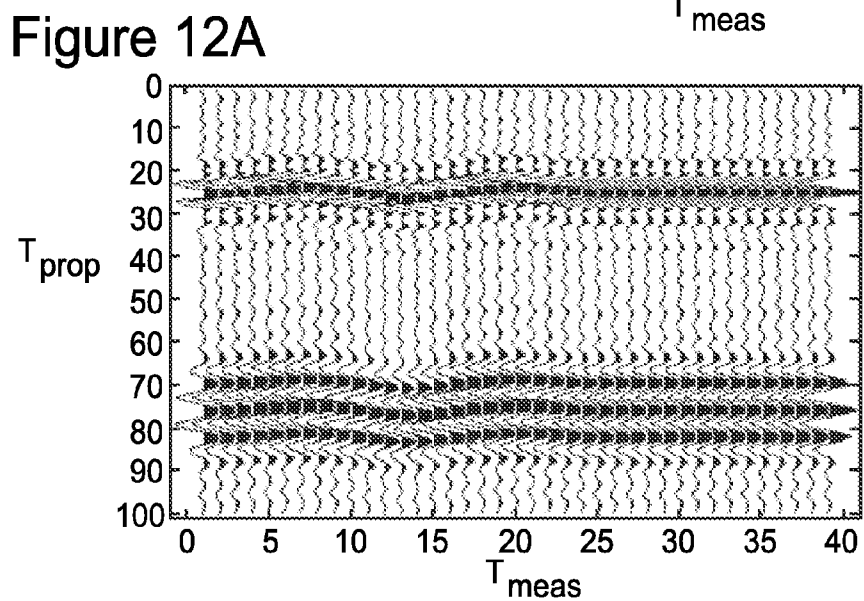
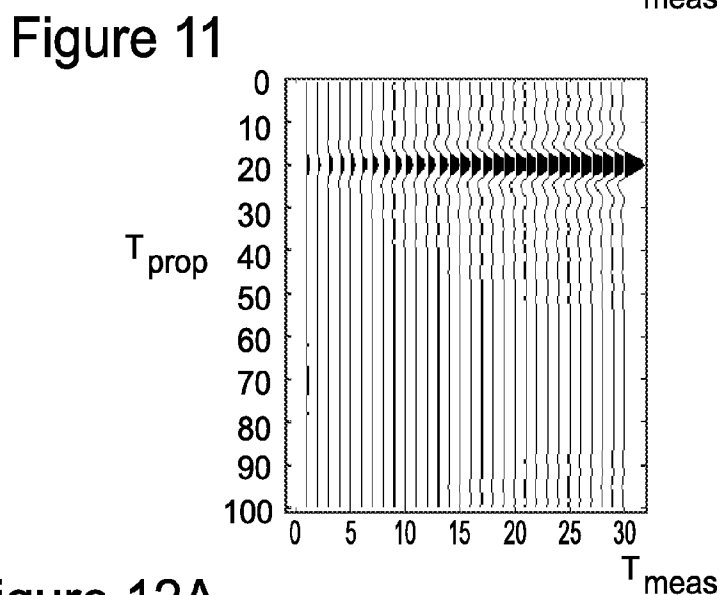
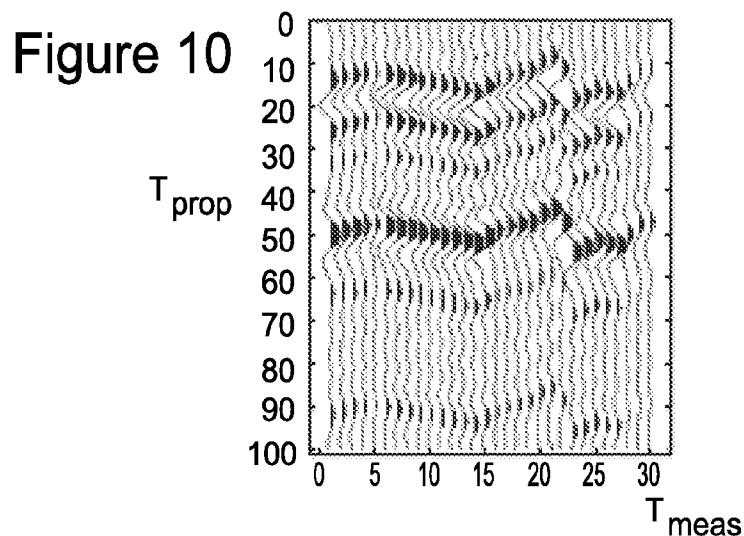


Figure 12B

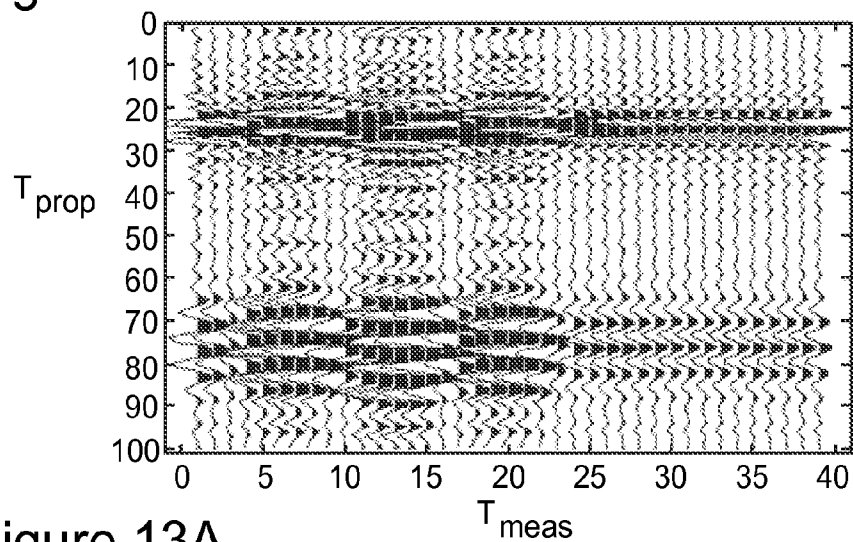


Figure 13A

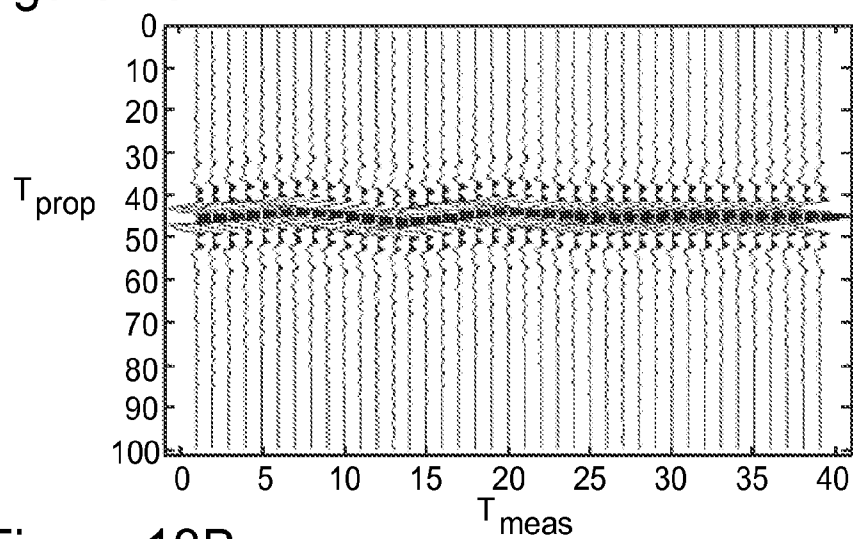


Figure 13B

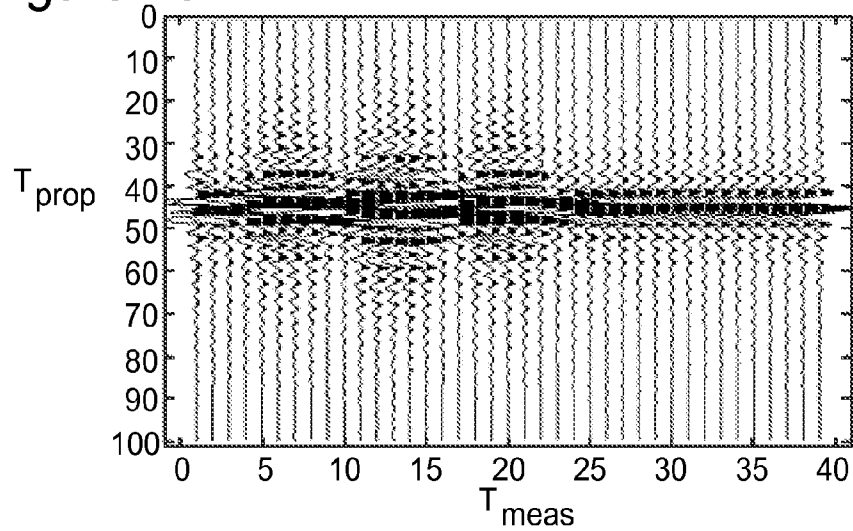


Figure 14A

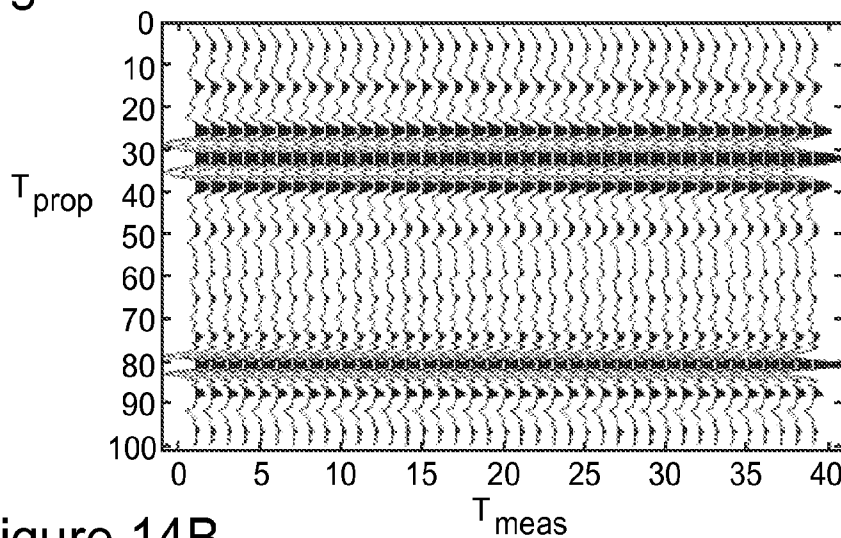


Figure 14B

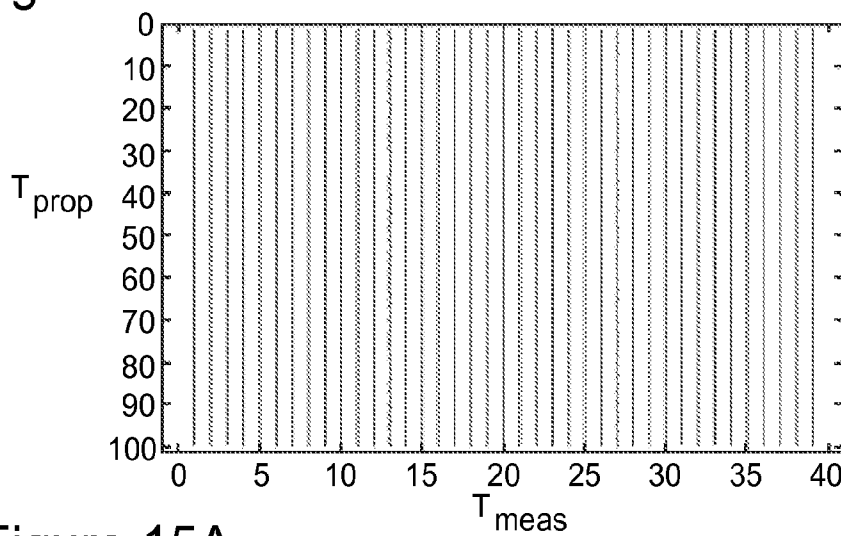


Figure 15A

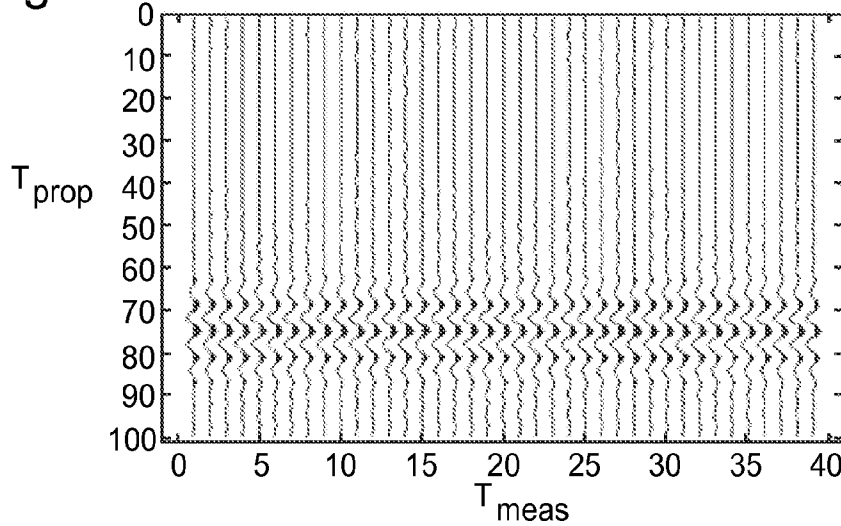


Figure 15B

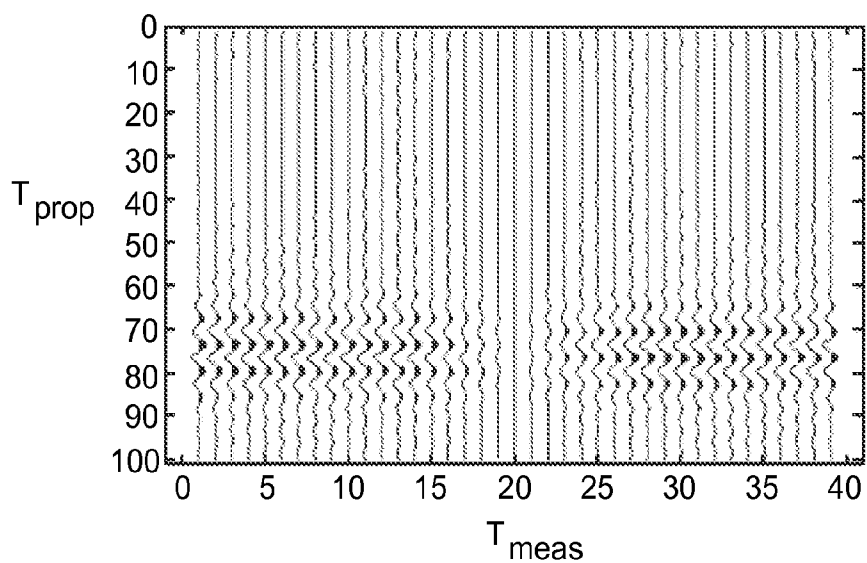
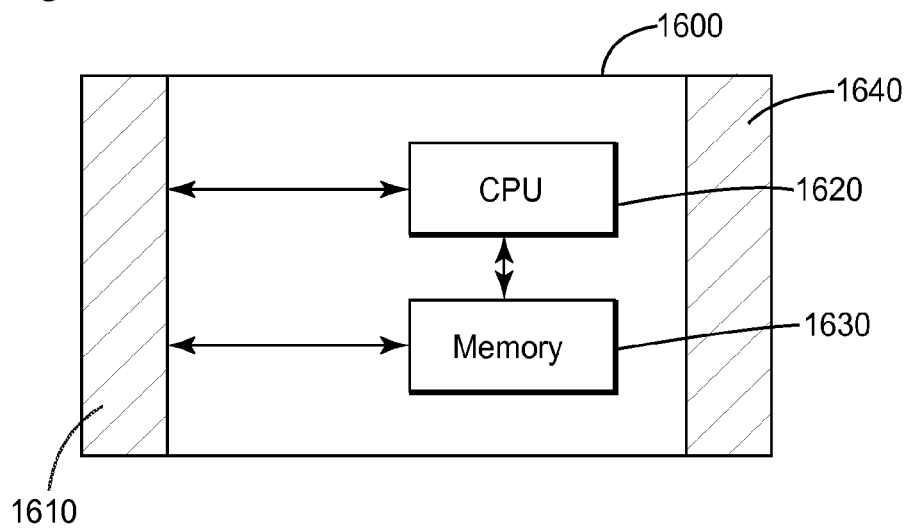


Figure 16



## METHOD FOR TIME-LAPSE WAVE SEPARATION

### CROSS REFERENCE TO RELATED APPLICATIONS

[0001] This application claims priority and benefit from U.S. Provisional Application No. 61/617,918, filed on Mar. 30, 2012, for “Time-Lapse Wave Separation,” the entire content of which is incorporated herein by reference.

### BACKGROUND

[0002] 1. Technical Field

[0003] Embodiments of the subject matter disclosed herein generally relate to methods for processing repeated seismic data acquired using the same seismic survey setup and, more particularly, to mechanisms and techniques for separating seismic waves having different behaviors over the time-lapse domain also called calendar time domain referring to repeated seismic acquisition. To separate waves in this particular domain, the convolution between a constant propagation operator (constant over the calendar time, yet unknown) and a time-lapse variable estimated wave is subtracted from the repeated seismic data. The constant propagation operator that is obtained by solving an inverse problem using the repeated seismic data.

[0004] 2. Discussion of the Background

[0005] A widely-used technique for monitoring oil or gas reservoirs is the seismic imaging of subsurface geophysical structures. The term “seismic imaging” refers to acquiring and analyzing data related to reflected seismic waves after generating seismic waves toward the subsurface structure. The time-lapse wave separation is well suited for processing continuous 4D seismic (repeated seismic) data.

[0006] As illustrated in FIGS. 1-3, a continuous 4D seismic survey setup includes at least one source 10 and a sensor 20 buried below weathering layers 30 (so that the source and sensor and, thus, the target reflections, are not affected by any climatic changes). The source 10 produces seismic waves (i.e., a signal) that propagate through the subsurface structure and are reflected at the interfaces between layers in which the wave propagation velocity differs. Thus, part of the seismic wave energy produced by the source 10 is reflected and detected by the sensor 20. Although the seismic survey target is the reservoir 40, the detected wave is an overlap of target waves 11 and other unwanted waves.

[0007] For example, as illustrated in FIG. 1, unwanted waves include a reflection 12 from a filled ditch or karst 50 connected with the weathering zone and a reflection 13 from the air-earth interface 60. In another example illustrated in FIG. 2, unwanted waves include a reflection 14 which is reflected twice before reaching the sensor 20: the first time by the air-earth interface 60, and the second time by a layer 70 located above the reservoir 40. In yet another example in FIG. 3, the unwanted waves include a reflection 16 which is also reflected twice before reaching the sensor 20: the first time by the layer 70 and the second time by the air-earth interface 60. Unwanted waves that travel through the weathering layers are affected by climatic changes (arrival time at the sensor and this amplitude change depending on temperature and moisture in the weathering layers). The unwanted waves degrade the quality of the final image.

[0008] FIG. 4A is a graph in which the y-axis represents amplitudes as detected by sensor 20, and the x-axis represents

two-way times (from the source 10 to the sensor 20 via at least one reflection point). The detected amplitude includes a wave 11 corresponding to the target reflection, and unwanted reflections 12 and 15. Some of the unwanted waves come at the same time (and overlap) with the target waves, but some other unwanted waves may be separate in time. The longer a wave travels, the more it is attenuated, and the lower the detected amplitude.

[0009] The sensor 20 is unable to distinguish between waves as differently marked in FIG. 4A. The detected amplitude versus time 18 illustrated in FIG. 4B which is called a seismogram is an overlap of the target wave and the unwanted waves. Although FIGS. 1-3, 4A and 4B refer to a pair source-sensor, it should be understood that a seismic survey setup usually includes plural sensors and may also include plural sources at known positions relative to one another.

[0010] In order to monitor an oil and/or gas reservoir evolution during production, seismic measurements are repeated at time intervals that are large relative to the duration of the seismic measurement. Conventionally, seismic measurements are repeated each year or decade. However, to monitor a reservoir during production, a “continuous” 4D data acquisition means that seismic measurements are performed 4 to 6 times a day, allowing an oil and gas company to make rapid decisions and adjust the production plan.

[0011] The data acquired during different measurements is gathered in 4D data sets, the four dimensions being (1) amplitude versus (2) time while data is acquired, (3) distance between the source and the sensor, and then, (4) time as to when the measurement was performed. These 4D data sets are known as repeated seismic data. A subset of repeated seismic data is illustrated in FIG. 5, where each wavy up-down line is a seismogram (i.e., amplitude versus time graph) acquired in one measurement. The y-axis is propagation time  $T_{prop}$  from the source to the sensor, in seconds. The x-axis represents a time ( $T_m$ ) when the measurement was performed, for example, daily. Note that the values on x-axis are not expressed in time unite, but a first measurement a second measurement, etc.

[0012] Accordingly, it would be desirable to provide reliable methods (and devices performing these methods), to accurately extract the target wave (i.e., reflected by the monitored reservoir) from the detected signal that also includes unwanted waves, in order to be able to monitor the target based on repeated seismic data.

### SUMMARY

[0013] According to one exemplary embodiment, there is a method for processing seismic data acquired with the same seismic survey setup over long periods of time. The method includes acquiring sets of seismic data using the same seismic survey setup over multiple days, the sets being gathered as repeated seismic data. The method further includes estimating a time-variable wavelet corresponding to unwanted waves, and determining a propagation of the time-variable wavelet, which propagation is assumed to be constant in time, by solving an inverse problem using the repeated seismic data and the estimated time-variable wavelet. The method also includes extracting signal data by subtracting a convolution of the estimated time-variable wavelet and the propagation from the repeated seismic data.

[0014] According to another exemplary embodiment, there is a computer-readable storage medium non-transitory storing executable codes which, when executed on a computer,

make the computer process repeated seismic data gathered from sets of seismic data acquired using the same seismic survey setup over multiple days. The method includes estimating a time-variable wavelet corresponding to unwanted waves, and determining a propagation of the time-variable wavelet, which propagation is assumed to be constant in time, by solving an inverse problem using the repeated seismic data and the estimated time-variable wavelet. The method further includes extracting signal data by subtracting a convolution of the estimated time-variable wavelet and the propagation from the repeated seismic data.

[0015] According to another embodiment there is a seismic data processing device including an interface configured to receive repeated seismic data gathered using the same seismic survey setup over multiple days, and a data processing unit connected to the interface. The data processing unit is configured to process the repeated seismic data by (1) estimating a time-variable wavelet corresponding to unwanted waves, (2) determining a propagation that is constant in time by solving an inverse problem using the gathered repeated seismic data and the estimated time variable wavelet, and (3) extracting signal data by subtracting a convolution of the estimated time-variable wavelet and the propagation from the repeated seismic data.

#### BRIEF DESCRIPTION OF THE DRAWINGS

[0016] The accompanying drawings, which are incorporated in and constitute a part of the specification, illustrate one or more embodiments and, together with the description, explain these embodiments. In the drawings:

[0017] FIG. 1 is a schematic diagram of a seismic source and a seismic sensor pair;

[0018] FIG. 2 is a schematic diagram of another seismic source and a seismic sensor pair;

[0019] FIG. 3 is a schematic diagram of another seismic source and a seismic sensor pair;

[0020] FIG. 4A is a graph illustrating different reflected waves reaching the sensor;

[0021] FIG. 4B is a graph illustrating a seismogram;

[0022] FIG. 5 illustrates repeated seismic data for one sensor;

[0023] FIG. 6 is a flowchart of a method for processing seismic data acquired in the same seismic survey setup over long periods of time, according to an exemplary embodiment;

[0024] FIG. 7 is a graph illustrating one manner of estimating the time-variable wavelet according to an exemplary embodiment;

[0025] FIG. 8 is a graph illustrating an estimated time-variable wavelet;

[0026] FIG. 9 is a graph illustrating a propagation obtained using a method according to one exemplary embodiment;

[0027] FIG. 10 is a graph illustrating the convolution of a time-variable wavelet and a propagation thereof, obtained using a method according to one exemplary embodiment;

[0028] FIG. 11 is a graph illustrating signal data obtained using a method according to one exemplary embodiment;

[0029] FIG. 12A is a graph illustrating repeated seismic data;

[0030] FIG. 12B is a graph illustrating variation of the repeated seismic data in FIG. 12A;

[0031] FIG. 13A is a graph illustrating an estimate of the time-variable wavelet obtained using a method according to another exemplary embodiment;

[0032] FIG. 13B is a graph illustrating variation of the data in FIG. 13A;

[0033] FIG. 14A is a graph illustrating the propagation of the time-variable wavelet obtained using a method according to another exemplary embodiment;

[0034] FIG. 14B is a graph illustrating variation of the data in FIG. 14A;

[0035] FIG. 15A is a graph illustrating the signal data obtained using a method according to another exemplary embodiment;

[0036] FIG. 15B is a graph illustrating variation of the signal data in FIG. 15A; and

[0037] FIG. 16 is a block diagram of a seismic data processing device according to an exemplary embodiment.

#### DETAILED DESCRIPTION

[0038] The following description of the exemplary embodiments refers to the accompanying drawings. The same reference numbers in different drawings identify the same or similar elements. The following detailed description does not limit the invention. Instead, the scope of the invention is defined by the appended claims. The following embodiments are discussed, for simplicity, with regard to the terminology and structure of data processing for seismic survey data. However, the embodiments to be discussed next are not limited to this type of data being useable for 4D data acquired using other methods or for processing similar type of data acquired in similar circumstances.

[0039] Reference throughout the specification to “one embodiment” or “an embodiment” means that a particular feature, structure or characteristic described in connection with an embodiment is included in at least one embodiment of the subject matter disclosed. Thus, the appearance of the phrases “in one embodiment” or “in an embodiment” in various places throughout the specification is not necessarily referring to the same embodiment. Further, the particular features, structures or characteristics may be combined in any suitable manner in one or more embodiments.

[0040] In order to monitor the evolution of a reservoir (i.e., the target), signal data representing seismic waves reflected from the target need to be extracted from the recorded seismic data.

[0041] Thus, in an exemplary embodiment illustrated in FIG. 6, a method 600 for processing seismic data acquired with the same seismic survey setup over long periods of time includes acquiring sets of seismic data using the same seismic survey setup over a period of time (e.g., multiple days), at S610. These sets are gathered as repeated seismic data (e.g., as illustrated in FIG. 5). The repeated seismic data may represent an amplitude versus a propagation time as recorded by each sensor, for each instance of data-gathering during the multiple days.

[0042] The seismic survey setup may include one or more sources and plural sensors buried below a weathering layer of a surveyed formation. The seismic survey setup may be placed above an oil reservoir, and the data is then used to monitor the evolution of the reservoir.

[0043] Further, the method 600 includes estimating a time-variable wavelet corresponding to unwanted waves, at S620. The unwanted waves include noise and other wave reflections due to reflection at other locations than the subsurface. These unwanted waves may be represented as a convolution of a wavelet and a propagation operator none of which is known. Both the wavelet and the propagation operator may be vari-

able in time. However, one can use a reasonable assumption that the wavelet varies in time while the propagator is constant in time.

[0044] The time-variable wavelet may be estimated by identifying unwanted waves that do not interfere with the target waves. For example, in FIG. 7, a window 710 corresponding only to unwanted waves based on the propagation time range may be selected in the repeated seismic data graph. This window 710 may be used to estimate the time-variable wavelet, because in the window 710 the unwanted waves do not overlap the target waves. The resulting time-variable wavelet estimate is illustrated in FIG. 8.

[0045] However, in another example discussed below, the time-variable wavelet may be estimated using seismic data detected in another sensor receiving substantially the same unwanted waves as the first sensor, but (due to its location) the unwanted waves detected by the other sensor do not interfere with the target waves.

[0046] The method 600 also includes determining a propagation of the time-variable wavelet, at S630. This propagation is assumed to be constant over the calendar time (i.e., over all the measurements), and is determined by solving an inverse problem using the repeated seismic data and the estimated time-variable wavelet. For example, if  $rsr$  is the repeated seismic data of  $m$  measurements, each measurement having  $n$  samples as illustrated in FIG. 5,  $RSR$  is a Fourier transform of  $rsr$ ,  $Y=RSR^T$ ,  $pwu$  is pure unwanted wave as illustrated in FIG. 8,  $PWU$  is a Fourier transform of  $pwu$ ,  $G=PWU^T$ , then, in the frequency domain, a Fourier transform  $X$  of the propagation  $p$  is  $X=(G^T G)^{-1} \cdot G^T Y$ . The resulting propagation vector  $X$  having amplitudes corresponding to  $n$  frequencies is illustrated in FIG. 9.

[0047] Finally, the method 600 includes extracting signal data (i.e., corresponding to waves reflected by the target) by subtracting a convolution of the estimated time-variable wavelet and the propagation from the repeated seismic data, at S640. For example, following the notation described above and  $tr$  being the signal data in time domain, while  $TR$  being the Fourier transform of  $tr$ ,  $TR=RSR-(PUW \cdot X)$ . The inverse Fourier transform of  $PUW \cdot X$  is illustrated in FIG. 10 and the resulting  $tr$  (i.e. the inverse Fourier transform of  $TR$ ) is illustrated in FIG. 11.

[0048] Steps S630 and S640 may be performed in frequency domain or in time domain as illustrated relative to another embodiment in FIGS. 12-15. FIG. 12A illustrates repeated seismic data other than the repeated seismic data in FIGS. 5 and 7. FIG. 12B is the variation of the repeated seismic data. Variations are defined as a subtraction of the mean or median trace over the whole period from each of the repeated traces of the input.

[0049] FIG. 13A illustrates an estimate of the time-variable wavelet corresponding to the unwanted waves obtained from data recorded by another sensor. FIG. 13B is a variation of the estimated time-variable wavelet in FIG. 13A. Further, FIG. 14A is the propagation of the time-variable wavelet determined by solving an inverse problem using the repeated seismic data and the estimated time-variable wavelet in time domain. The propagation is assumed to be constant in time which results in a zero variation as shown in FIG. 14B.

[0050] The signal data is then extracted by subtracting a convolution of the estimated time-variable wavelet and the propagation from the repeated seismic data, is illustrated in FIG. 15A. The variation of the subtracted signal data is illustrated in FIG. 15B.

[0051] By comparing FIGS. 12B, 13B and 15B, it becomes apparent that the method of extracting the signal data from the recorded seismic data is reasonably accurate, since the signal data variation is small compared to the signal data, and substantially smaller than the variation of the recorded seismic data. The variation of the unwanted waves that may travel through the weathering layer is (as expected) substantially larger than the variation in the signal data.

[0052] Method 600 and other similar embodiments may be performed by a seismic data processing device 1600 as illustrated in FIG. 16. The seismic data processing device 1600 may have an interface 1610 configured to receive repeated seismic data gathered using the same seismic survey setup over multiple days. The seismic data processing device 1600 may also have a data processing unit 1620 connected to the interface and configured to process the repeated seismic data by: (1) estimating a time-variable wavelet corresponding to unwanted waves, (2) determining a propagation that is constant in time by solving an inverse problem using the gathered repeated seismic data and the estimated time variable wavelet, and (3) extracting signal data by subtracting a convolution of the estimated time-variable wavelet and the propagation from the repeated seismic data.

[0053] The data processing unit 1620 may further be configured to estimate the time-variable wavelet by selecting a subset of the seismic data corresponding to a propagation time range for the multiple days.

[0054] The data processing unit 1620 may be configured to determine the propagation by (A) applying a Fourier transformation to the estimated wavelet to obtain a Fourier transform of the estimated wavelet, (B) calculating an inverse matrix of a product of a transposed of the Fourier transform of the estimated wavelet and the Fourier transform of the estimated wavelet, (C) applying a Fourier transformation to the repeated seismic records to obtain a Fourier transform of the repeated seismic records, (D) calculating a product of the transposed of the Fourier transform of the estimated wavelet and the Fourier transform of the repeated seismic records, and (E) determining a Fourier transform of the propagation as a convolution of the inverse matrix and the product.

[0055] The seismic data processing device 1600 may also include a memory 1630 configured to non-transitory storing executable codes which when executed on the data processing unit 1620, and the interface 1610 makes the seismic data processing device 1600 process repeated seismic data gathered from sets of seismic data acquired using the same seismic survey setup over multiple days, according to a method including: (i) estimating a time-variable wavelet corresponding to unwanted waves, (ii) determining a propagation of the time-variable wavelet, which propagation is assumed to be constant in time, by solving an inverse problem in a frequency domain using the repeated seismic data and the estimated time-variable wavelet, and (iii) extracting signal data by subtracting a convolution of the estimated time-variable wavelet and a Fourier transform of the propagation from the repeated seismic data.

[0056] The step of estimating the time-variable wavelet (i.e., step i above) may include selecting a subset of the repeated seismic data corresponding to a propagation time range for the multiple days.

[0057] The step of determining the propagation (step ii above) may include (A) applying a Fourier transformation to the estimated time-variable wavelet to obtain a Fourier transform of the estimated time-variable wavelet, (B) calculating

an inverse matrix of a product of a transposed of the Fourier transform of the estimated time-variable wavelet and the Fourier transform of the estimated time-variable wavelet, (C) applying a Fourier transformation to the repeated seismic records to obtain a Fourier transform of the repeated seismic records, (D) calculating a product of the transposed of the Fourier transform of the estimated wavelet and the Fourier transform of the repeated seismic records, and (E) determining a Fourier transform of the propagation as a convolution of the inverse matrix and the product.

**[0058]** The signal wave may include target waves due to a monitored underground reservoir, and the unwanted waves may include noise and other wave reflections due to reflection sources other than the monitored underground reservoir.

**[0059]** The memory **1630** may be configured to store the repeated seismic data.

**[0060]** The seismic data processing device **1600** may also include a display **1640** configured to display images of an underground formation generated by the data processing unit **1620** using the signal data.

**[0061]** Although the features and elements of the present exemplary embodiments are described in the embodiments in particular combinations, each feature or element can be used alone without the other features and elements of the embodiments or in various combinations with or without other features and elements disclosed herein. The methods or flowcharts provided in the present application may be implemented in a computer program, software or firmware tangibly embodied in a computer-readable storage medium for execution by a specifically programmed computer or processor.

**[0062]** The disclosed exemplary embodiments provide methods and devices for processing seismic data gathered during multiple days. It should be understood that this description is not intended to limit the invention. On the contrary, the exemplary embodiments are intended to cover alternatives, modifications and equivalents, which are included in the spirit and scope of the invention as defined by the appended claims. Further, in the detailed description of the exemplary embodiments, numerous specific details are set forth in order to provide a comprehensive understanding of the claimed invention. However, one skilled in the art would understand that various embodiments may be practiced without such specific details.

**[0063]** Although the features and elements of the present exemplary embodiments are described in the embodiments in particular combinations, each feature or element can be used alone without the other features and elements of the embodiments or in various combinations with or without other features and elements disclosed herein.

**[0064]** This written description uses examples of the subject matter disclosed to enable any person skilled in the art to practice the same, including making and using any devices or systems and performing any incorporated methods. The patentable scope of the subject matter is defined by the claims, and may include other examples that occur to those skilled in the art. Such other examples are intended to be within the scope of the claims.

What is claimed is:

**1.** A method for processing seismic data acquired with the same seismic survey setup over long periods of time, the method comprising:

acquiring sets of seismic data using the same seismic survey setup over multiple days, the sets being gathered as repeated seismic data;

estimating a time-variable wavelet corresponding to unwanted waves;

determining a propagation of the time-variable wavelet, which propagation is assumed to be constant in time, by solving an inverse problem using the repeated seismic data and the estimated time-variable wavelet; and extracting signal data by subtracting a convolution of the estimated time-variable wavelet and the propagation from the repeated seismic data.

**2.** The method of claim **1**, wherein the estimating of the time-variable wavelet includes selecting a subset of the repeated seismic data corresponding to a propagation time range for the multiple days.

**3.** The method of claim **1**, wherein the determining of the propagation includes:

applying a Fourier transformation to the estimated time-variable wavelet to obtain a Fourier transform of the estimated time-variable wavelet;

calculating an inverse matrix of a product of a transposed of the Fourier transform of the estimated time-variable wavelet and the Fourier transform of the estimated time-variable wavelet;

applying a Fourier transformation to the repeated seismic records to obtain a Fourier transform of the repeated seismic records;

calculating a product of the transposed of the Fourier transform of the estimated wavelet and the Fourier transform of the repeated seismic records; and

determining a Fourier transform of the propagation as a convolution of the inverse matrix and the product.

**4.** The method of claim **1**, wherein the seismic survey setup includes one or more sources and plural sensors buried below a weathering layer corresponding to a surveyed formation.

**5.** The method of claim **1**, wherein the repeated seismic data represent amplitude versus a propagation time as recorded by each sensor, for each instance of data gathering during the multiple days.

**6.** The method of claim **1**, wherein the seismic survey setup is placed above an oil reservoir, the signal data being used to monitor an evolution of the reservoir.

**7.** The method of claim **1**, wherein the signal data includes target waves and the unwanted waves include noise and other wave reflections due to other reflection sources than the target waves.

**8.** A computer readable storage medium non-transitory storing executable codes which, when executed on a computer, make the computer to process repeated seismic data that are gathered from sets of seismic data acquired using the same seismic survey setup over multiple days, according to a method comprising:

estimating a time-variable wavelet corresponding to unwanted waves;

determining a propagation of the time-variable wavelet, which propagation is assumed to be constant in time, by solving an inverse problem using the repeated seismic data and the estimated time-variable wavelet; and

extracting signal data by subtracting a convolution of the estimated time-variable wavelet and the propagation from the repeated seismic data.

**9.** The computer readable storage medium of claim **8**, wherein the estimating of the time-variable wavelet includes

selecting a subset of the repeated seismic data corresponding to a propagation time range for the multiple days.

**10.** The computer readable storage medium of claim **8**, wherein the determining of the propagation includes:

applying a Fourier transformation to the estimated time-variable wavelet to obtain a Fourier transform of the estimated time-variable wavelet;

calculating an inverse matrix of a product of a transposed of the Fourier transform of the estimated time-variable wavelet and the Fourier transform of the estimated time-variable wavelet;

applying a Fourier transformation to the repeated seismic records to obtain a Fourier transform of the repeated seismic records;

calculating a product of the transposed of the Fourier transform of the estimated wavelet and the Fourier transform of the repeated seismic records; and

determining a Fourier transform of the propagation as a convolution of the inverse matrix and the product.

**11.** The computer readable storage medium of claim **8**, wherein the signal data includes target waves due to a monitored underground reservoir and the unwanted waves include noise and other wave reflections due to other reflection sources than the monitored underground reservoir.

**12.** A seismic data processing device, comprising:

an interface configured to receive repeated seismic data gathered using the same seismic survey setup over multiple days; and

a data processing unit connected to the interface and configured to process the repeated seismic data by

(1) estimating a time-variable wavelet corresponding to unwanted waves;

(2) determining a propagation that is constant in time, by solving an inverse problem using the gathered repeated seismic data and the estimated time variable wavelet; and

(3) extracting signal data by subtracting a convolution of the estimated time-variable wavelet and the propagation from the repeated seismic data.

**13.** The seismic data processing device of claim **12**, wherein the data processing unit is configured to estimate the time-variable wavelet by selecting subset of the seismic data corresponding to a propagation time range for the multiple days.

**14.** The seismic data processing device of claim **12**, wherein the data processing unit is configured to determine the propagation by:

applying a Fourier transformation to the estimated wavelet to obtain a Fourier transform of the estimated wavelet;

calculating an inverse matrix of a product of a transposed of the Fourier transform of the estimated wavelet and the Fourier transform of the estimated wavelet;

applying a Fourier transformation to the repeated seismic records to obtain a Fourier transform of the repeated seismic records;

calculating a product of the transposed of the Fourier transform of the estimated wavelet and the Fourier transform of the repeated seismic records;

determining a Fourier transform of the propagation as a convolution of the inverse matrix and the product.

**15.** The seismic data processing device of claim **12**, wherein the seismic survey setup includes one or more sources and plural sensors buried below a weathering layer of a surveyed formation.

**16.** The seismic data processing device of claim **15**, wherein the repeated seismic data represent amplitude versus a propagation time as recorded by each sensor, for each instance of data gathering during the multiple days.

**17.** The seismic data processing device of claim **12**, wherein the seismic survey setup is placed above an oil reservoir, the signal data being used to monitor evolution of the reservoir.

**18.** The seismic data processing device of claim **12**, wherein the signal data includes target waves and the unwanted waves include noise and other unwanted wave reflections.

**19.** The seismic data processing unit of claim **12**, further comprising:

a data storage device configured to store the repeated seismic data.

**20.** The seismic data processing unit of claim **12**, further comprising:

a display configured to display images of an underground formation generated by the data processing unit using the signal data.

\* \* \* \* \*

# Appendix 6

Plural depth seismic deghosting method and system

Cotton, J. 2015

United States patent application publication





US 20150032380A1

(19) **United States**

(12) **Patent Application Publication**  
**COTTON**

(10) **Pub. No.: US 2015/0032380 A1**

(43) **Pub. Date: Jan. 29, 2015**

(54) **PLURAL DEPTH SEISMIC DE-GHOSTING METHOD AND SYSTEM**

(52) **U.S. Cl.**

CPC *G01V 1/36* (2013.01); *G01V 1/364* (2013.01);  
*G01V 2210/6122* (2013.01); *G01V 2210/56* (2013.01)

(71) Applicant: **CGG SERVICES SA**, Massy Cedex (FR)

USPC ..... **702/17**

(72) Inventor: **Julien COTTON**, Paris (FR)

(21) Appl. No.: **14/338,696**

(57) **ABSTRACT**

(22) Filed: **Jul. 23, 2014**

**Related U.S. Application Data**

(63) Continuation-in-part of application No. 14/054,505, filed on Oct. 15, 2013.

(60) Provisional application No. 61/858,234, filed on Jul. 25, 2013.

**Publication Classification**

(51) **Int. Cl.**  
*G01V 1/36* (2006.01)

A method for de-ghosting seismic data includes receiving seismic data corresponding to plural depth sources or plural depth receivers located at a first depth and a second depth below a geophysical surface, wherein the second depth is below the first depth, where the plural depth sources or plural depth receivers comprise a first seismic receiver located at the first depth and a second seismic receiver located at the second depth, or, a first seismic source located at the first depth and a second seismic source located at the second depth. The method also includes aligning primary reflections within the seismic data to provide improved seismic data. A corresponding system is also disclosed herein.

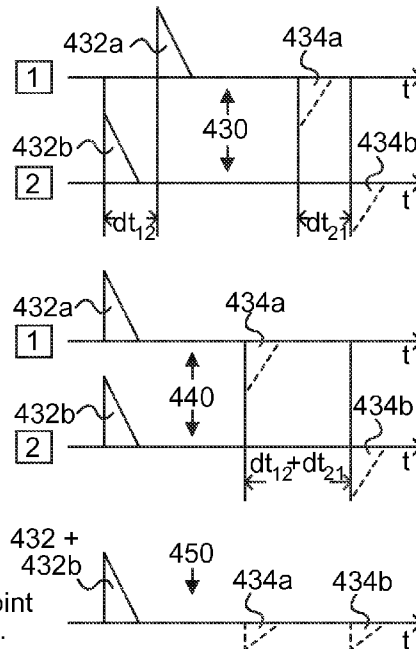
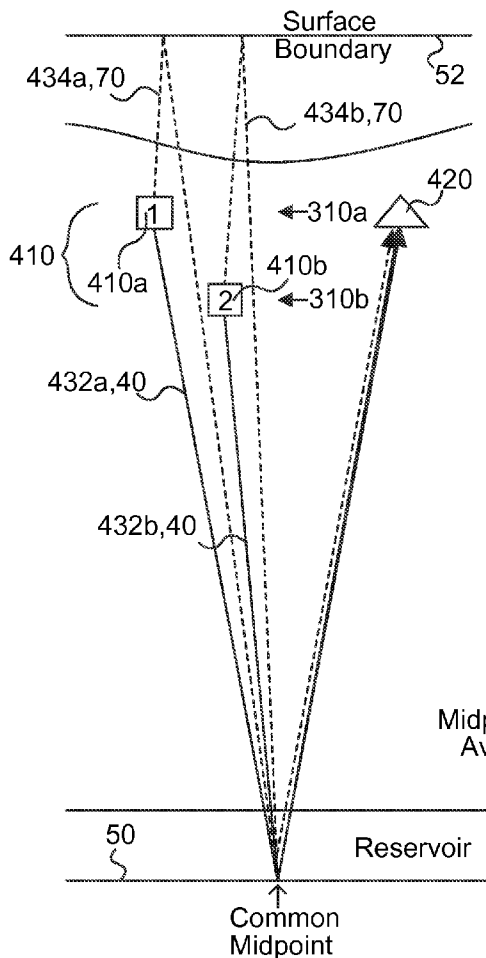
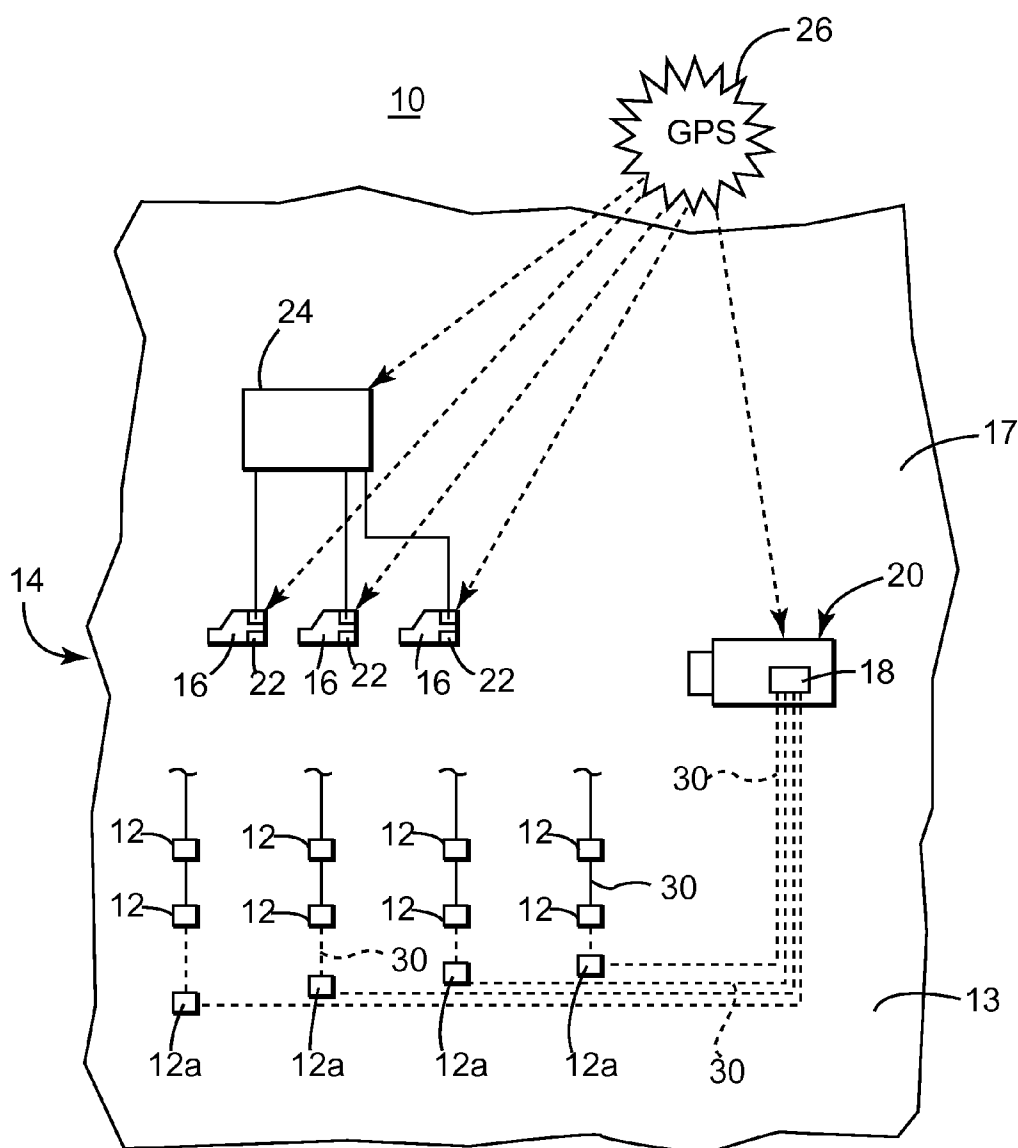


FIG. 1  
(Background art)



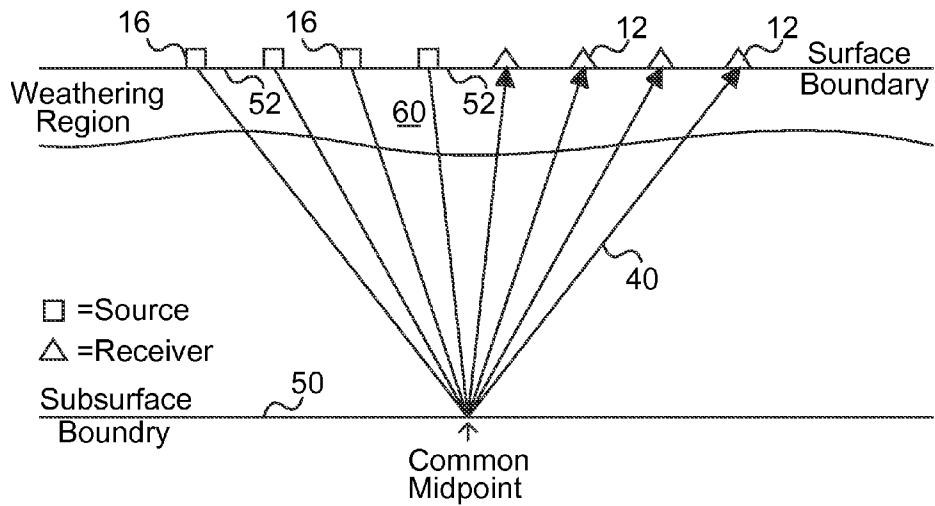


Figure 2a  
(Background Art)

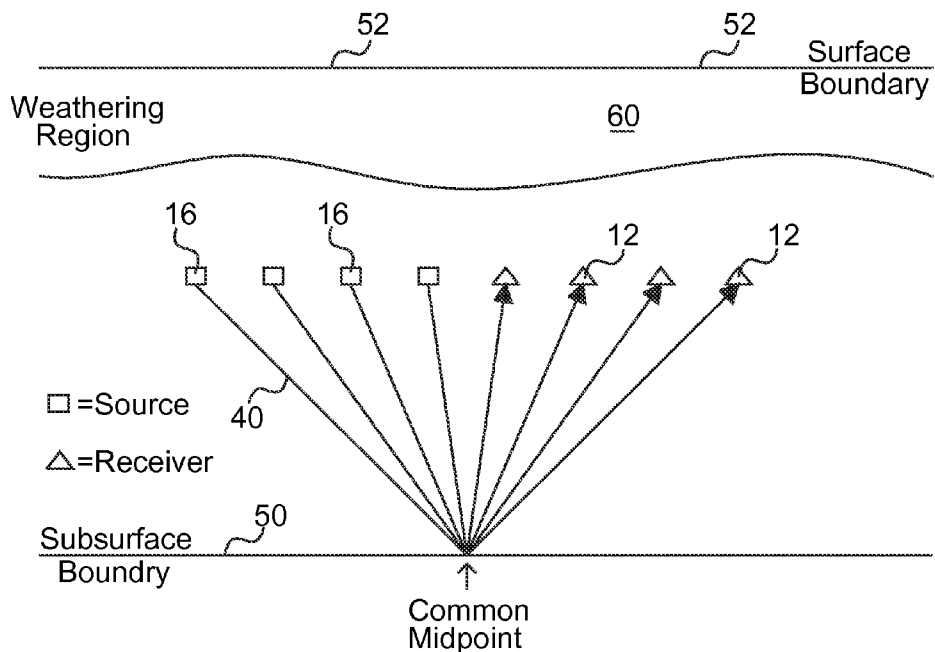


Figure 2b  
(Background Art)

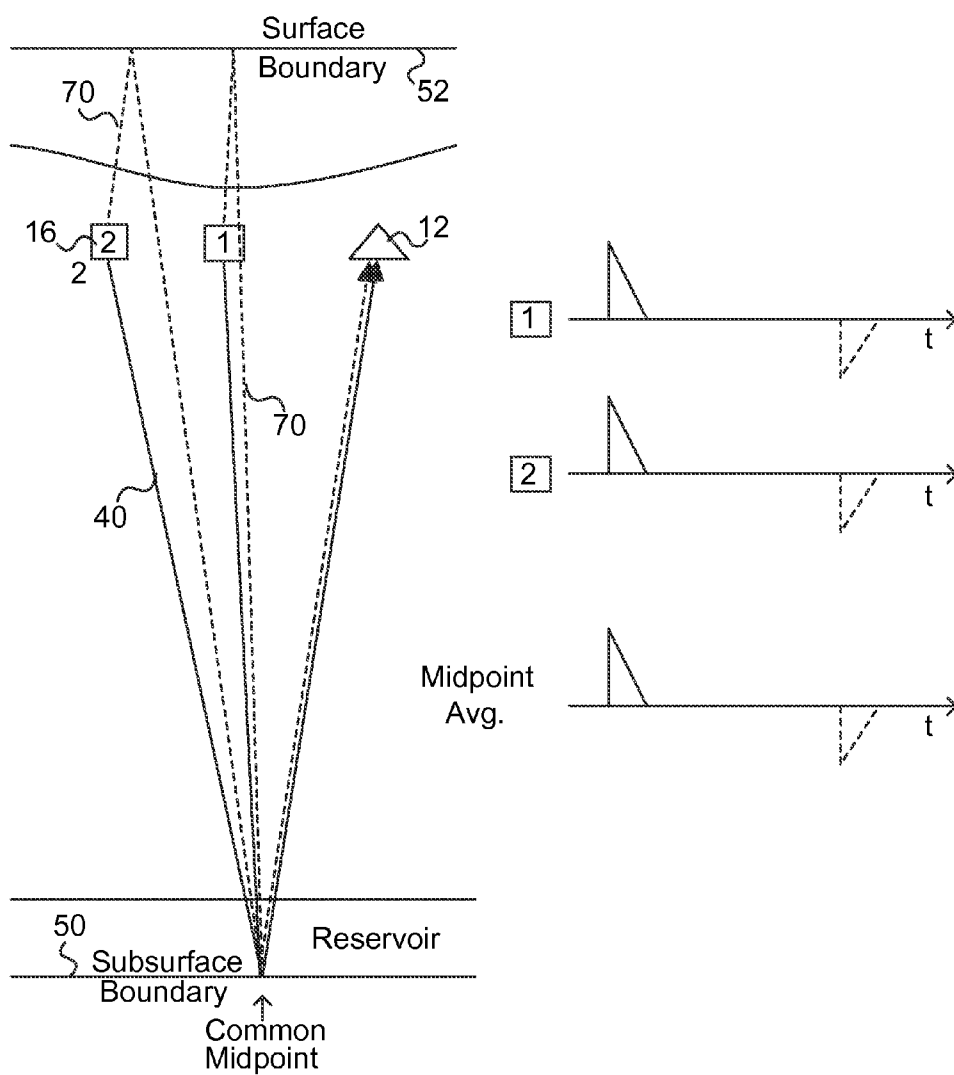


Figure 2c  
(Background Art)

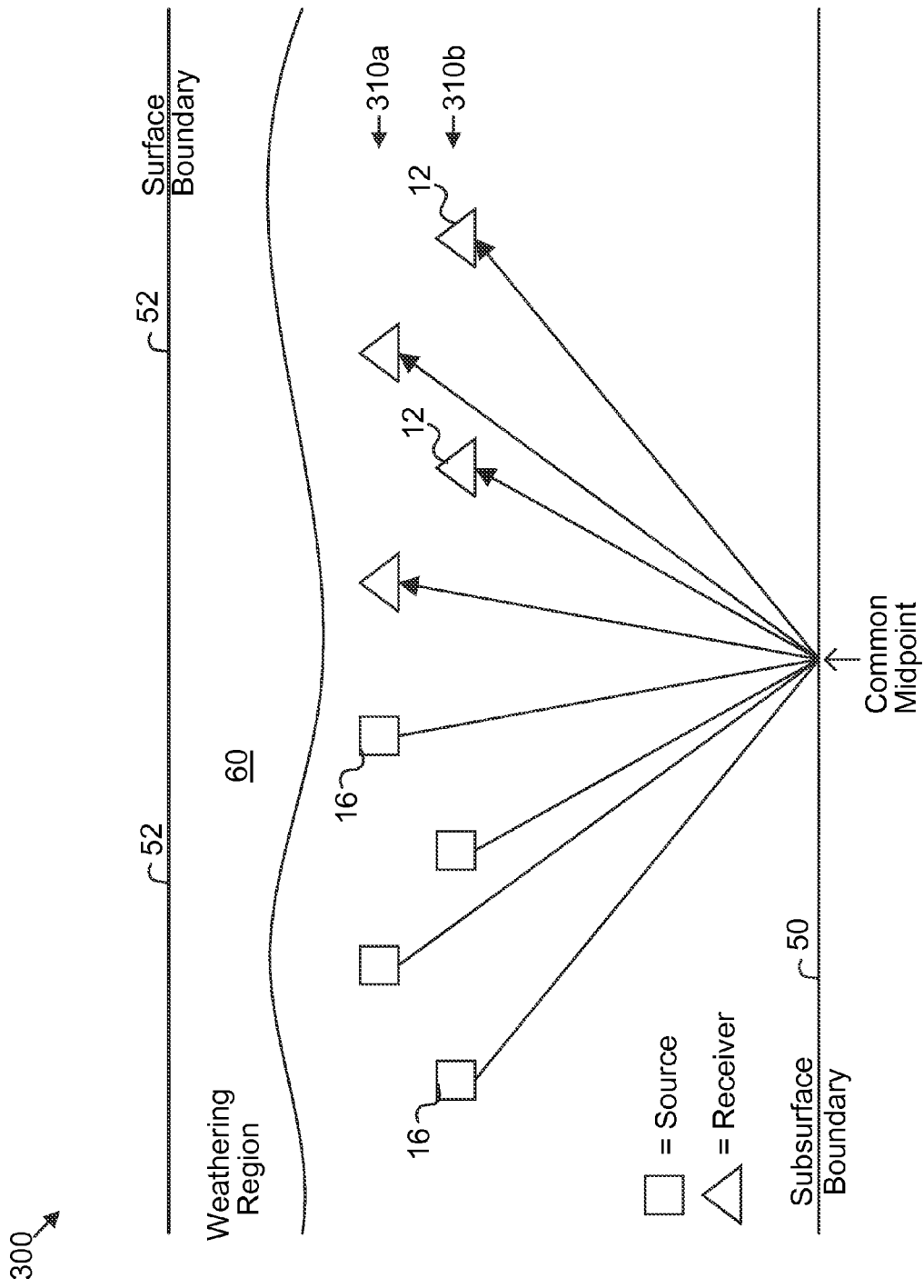


Figure 3

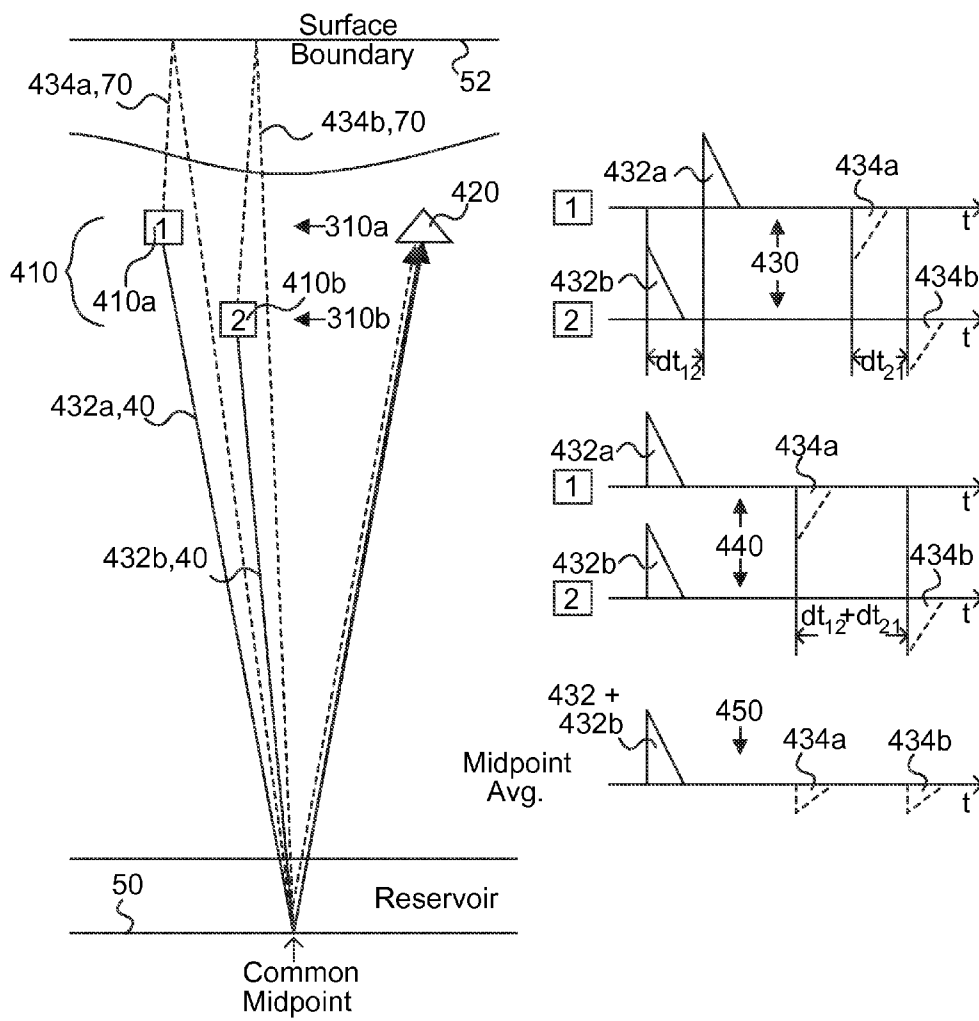


Figure 4

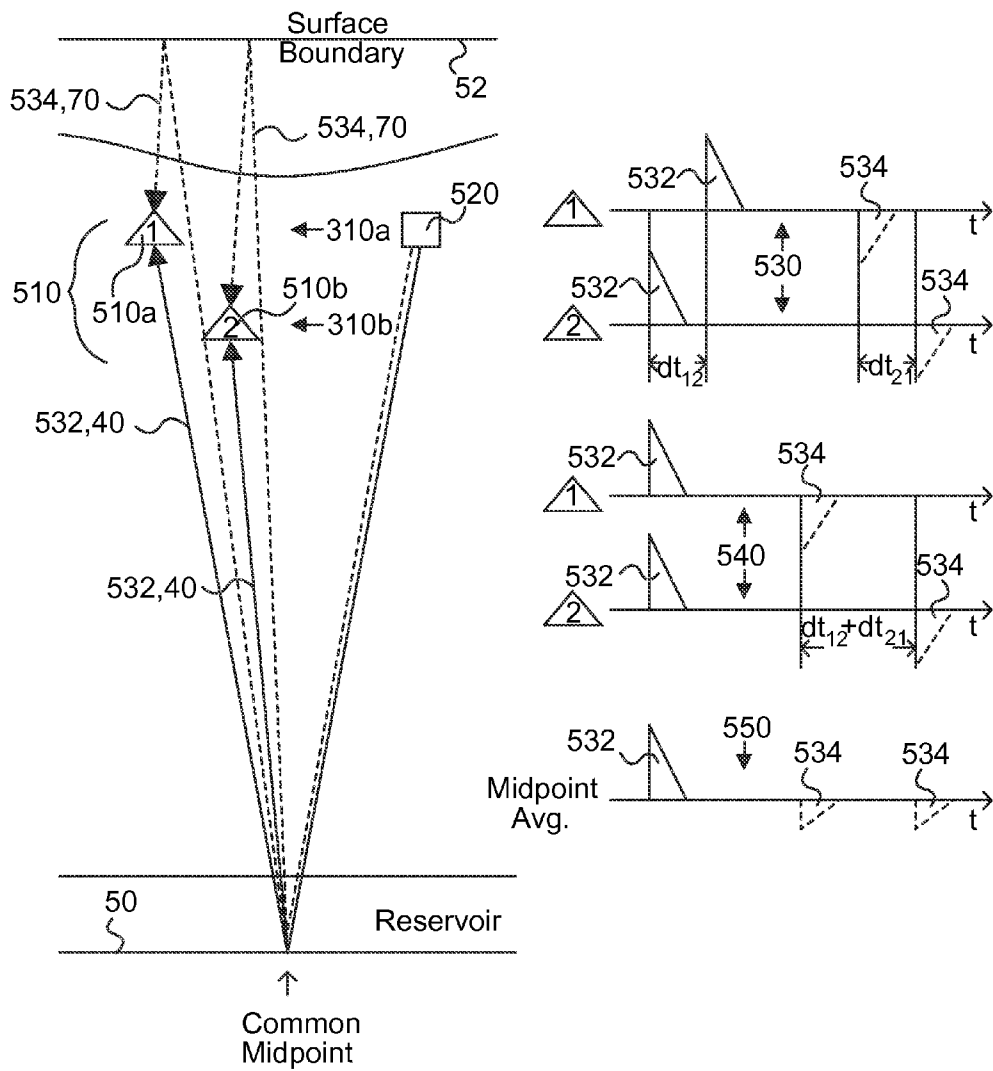


Figure 5a

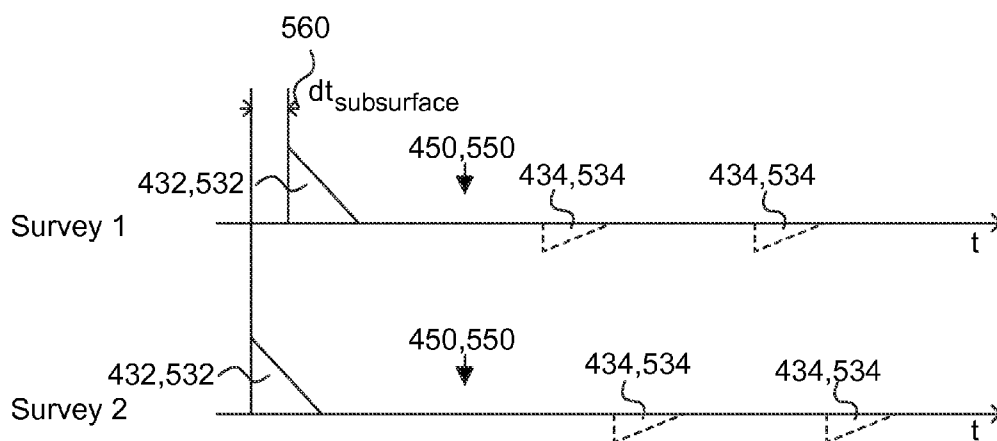
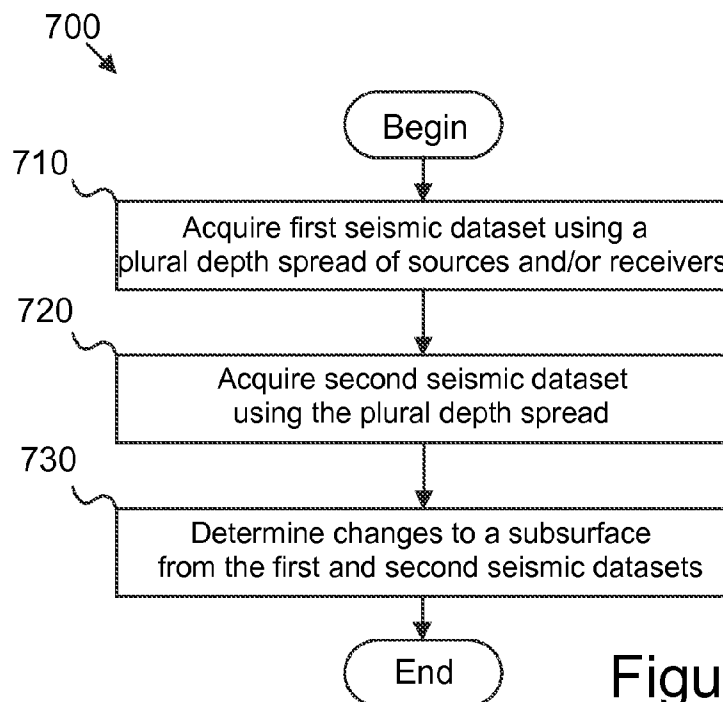
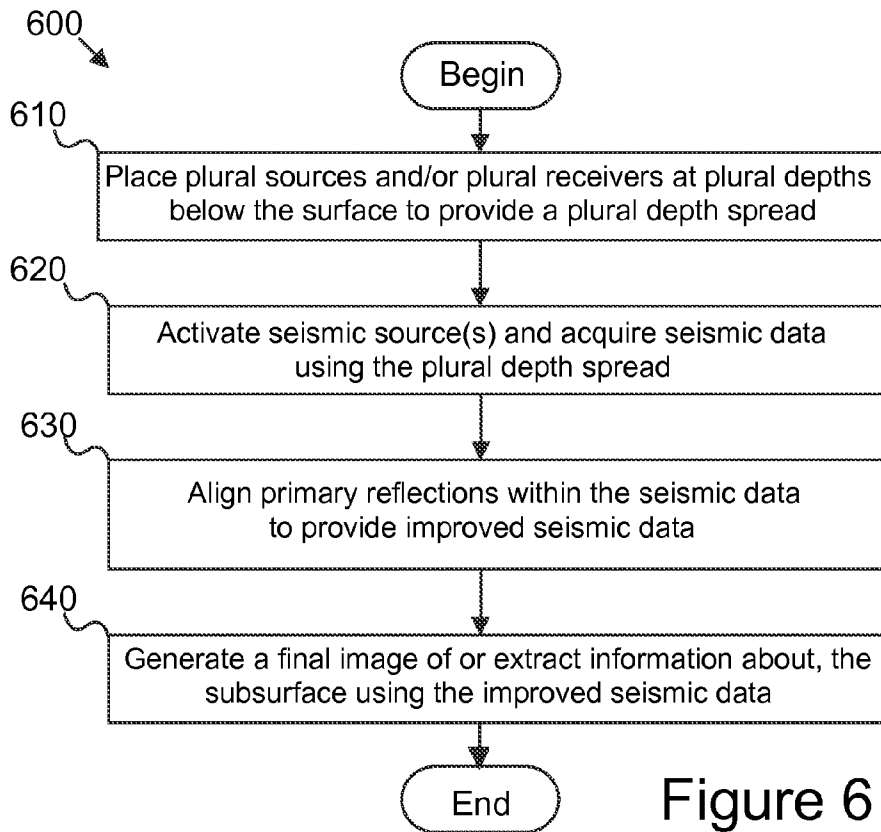


Figure 5b



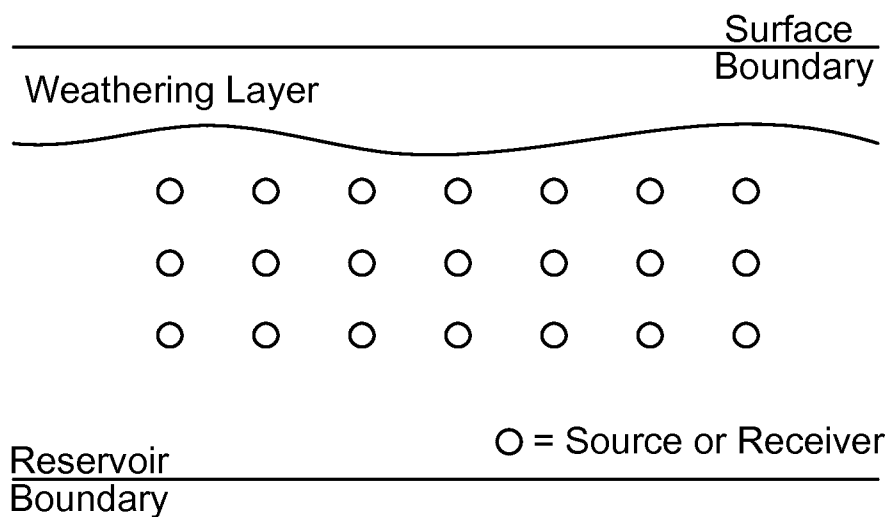


Figure 8a

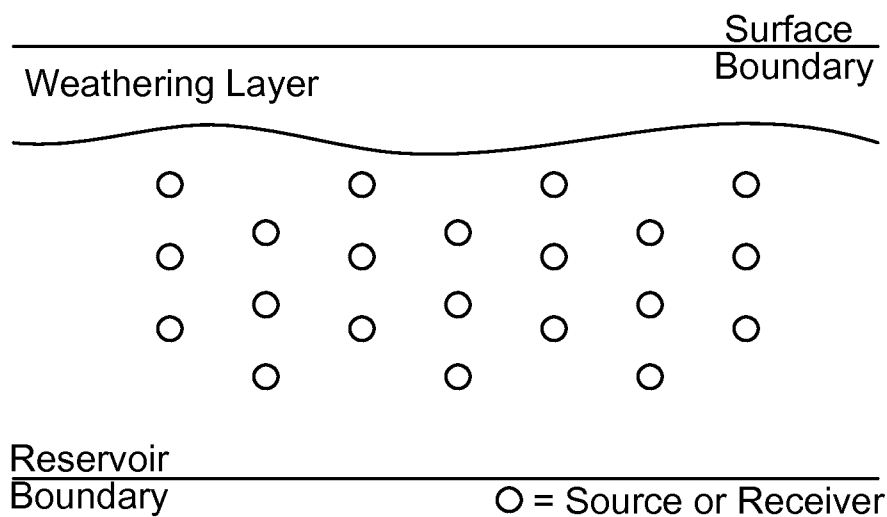


Figure 8b

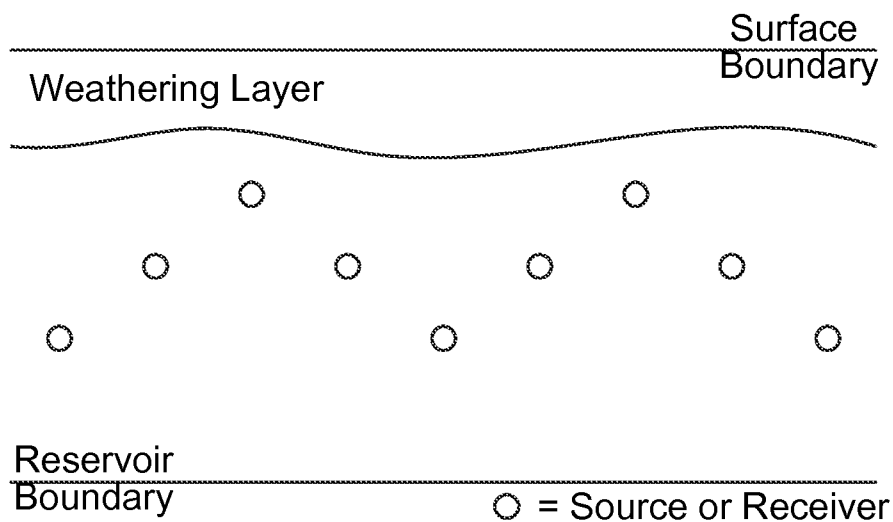


Figure 8c

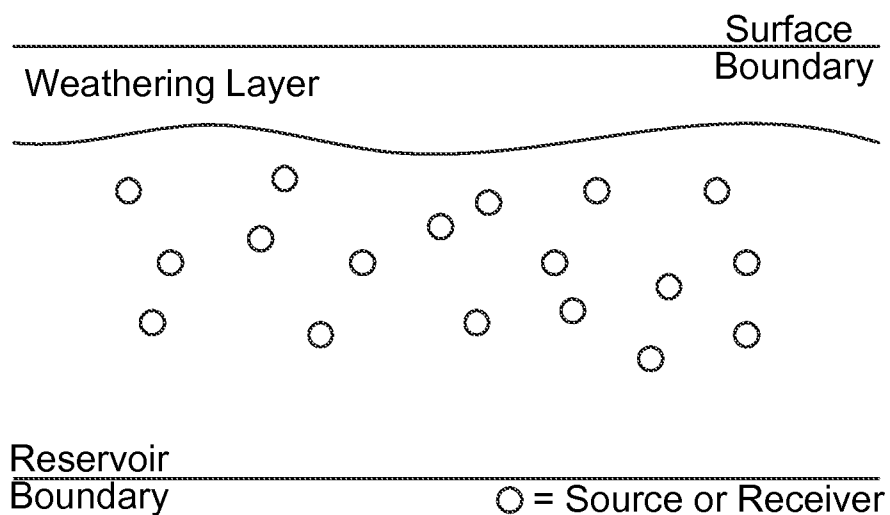


Figure 8d

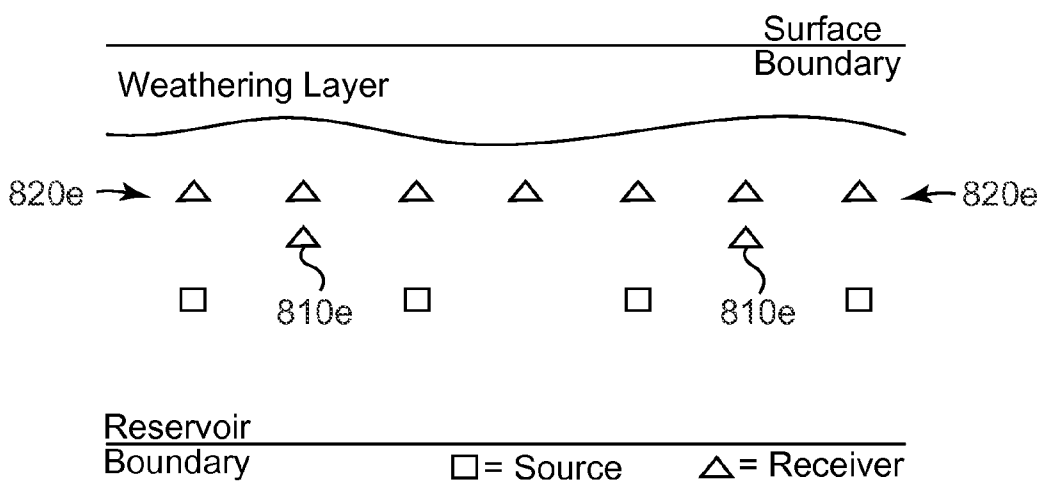


Figure 8e

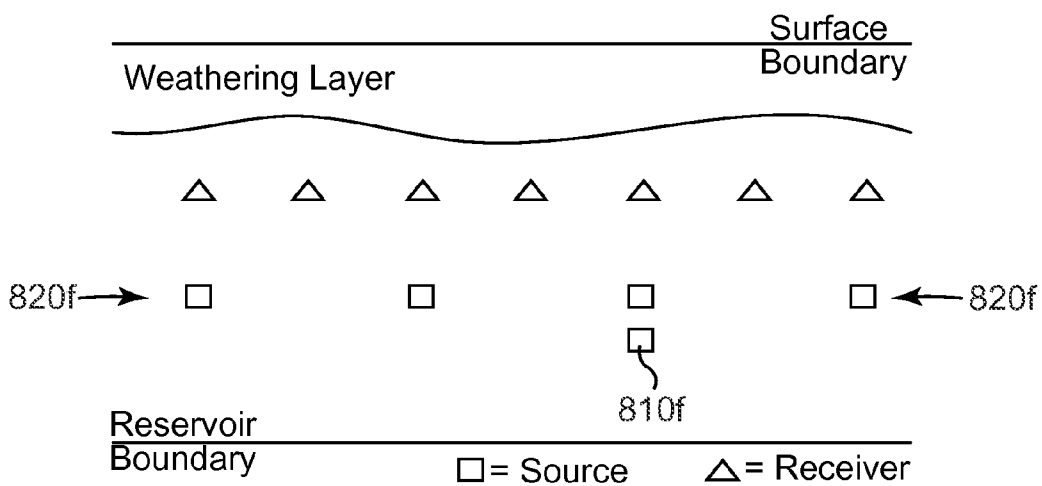


Figure 8f

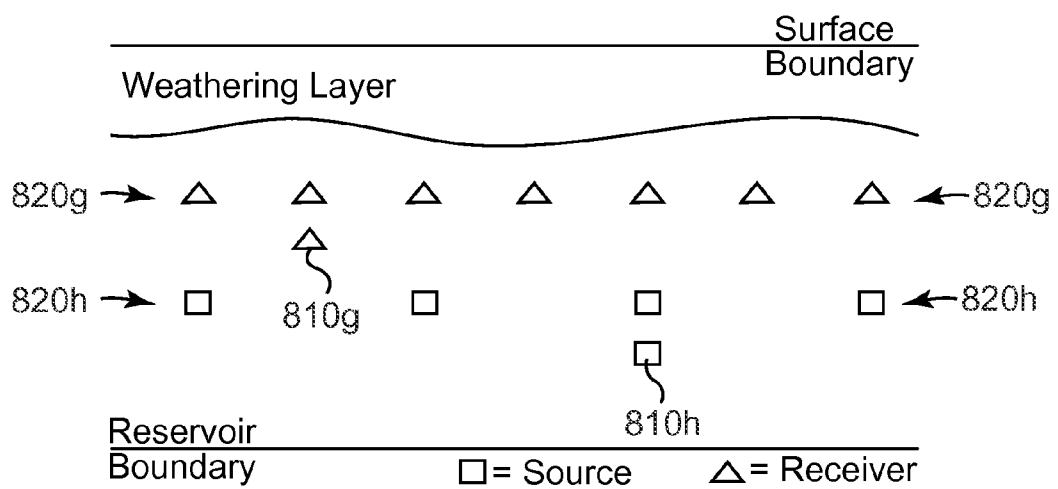


Figure 8g

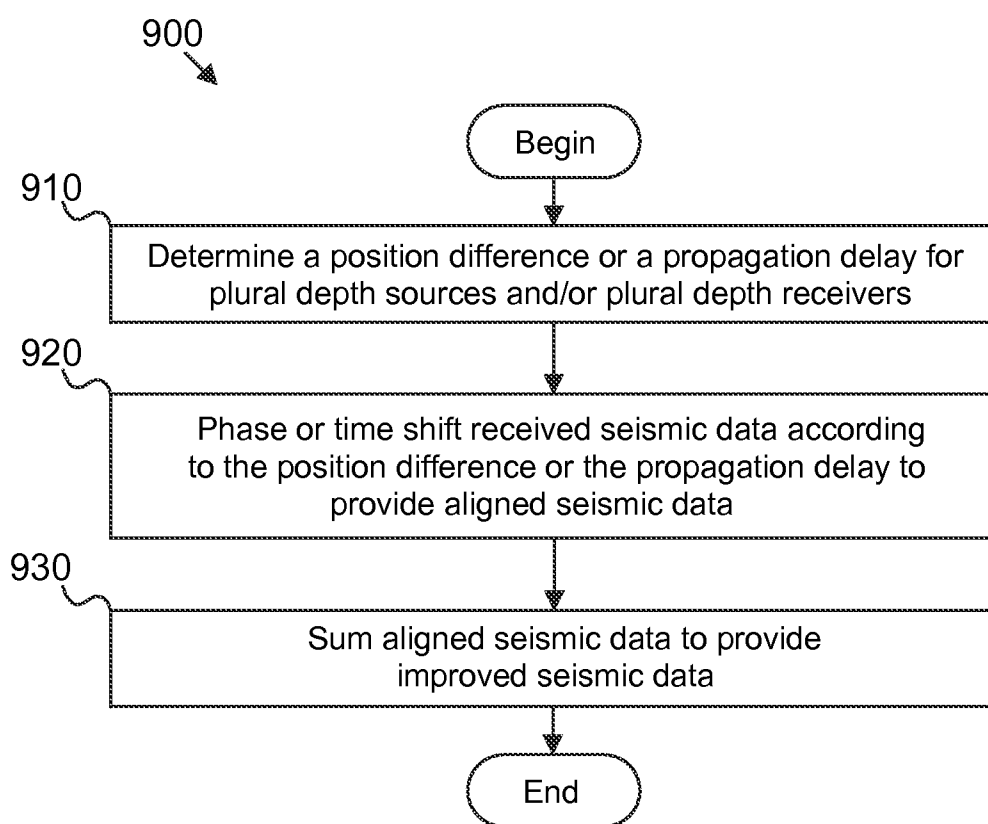
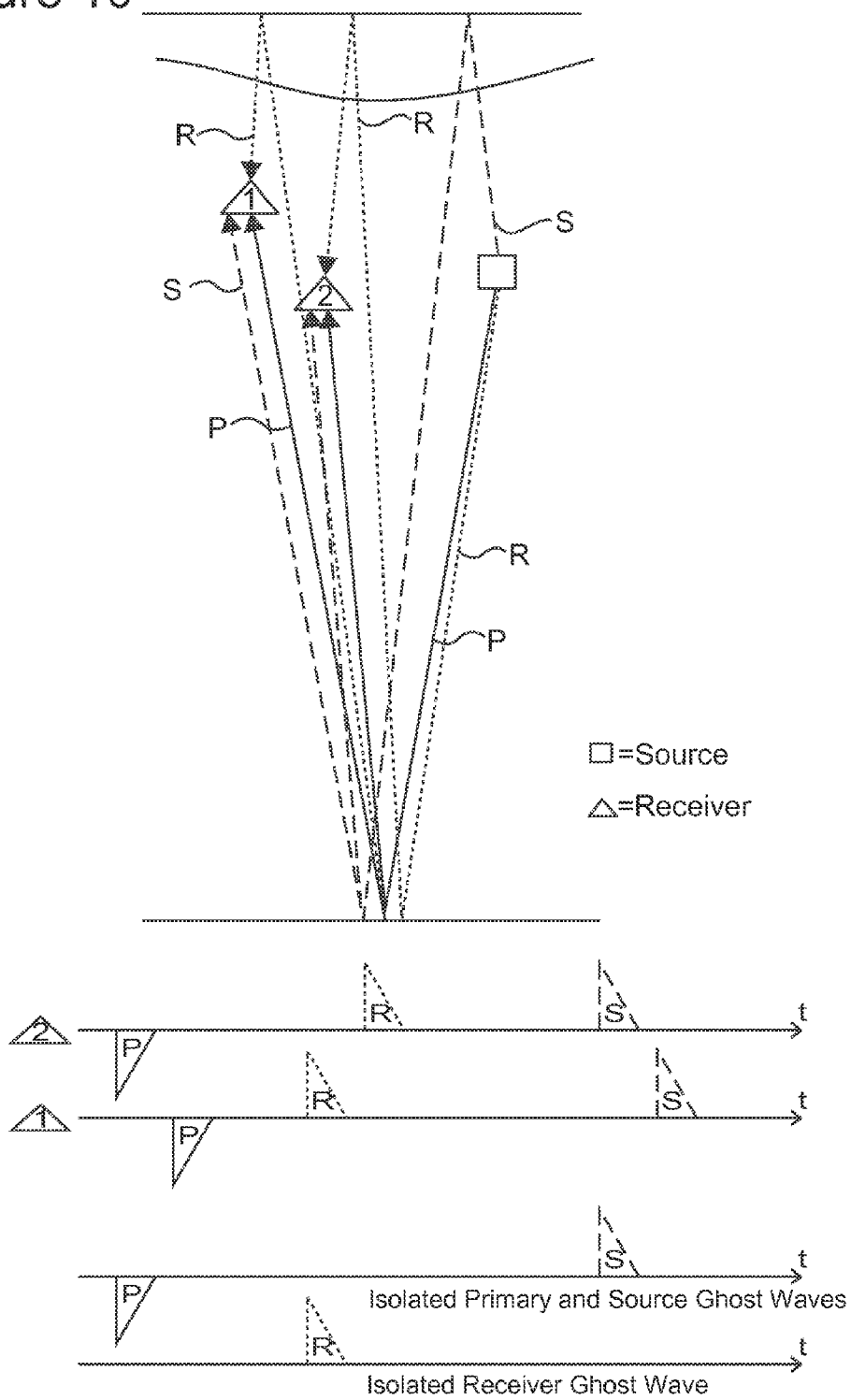
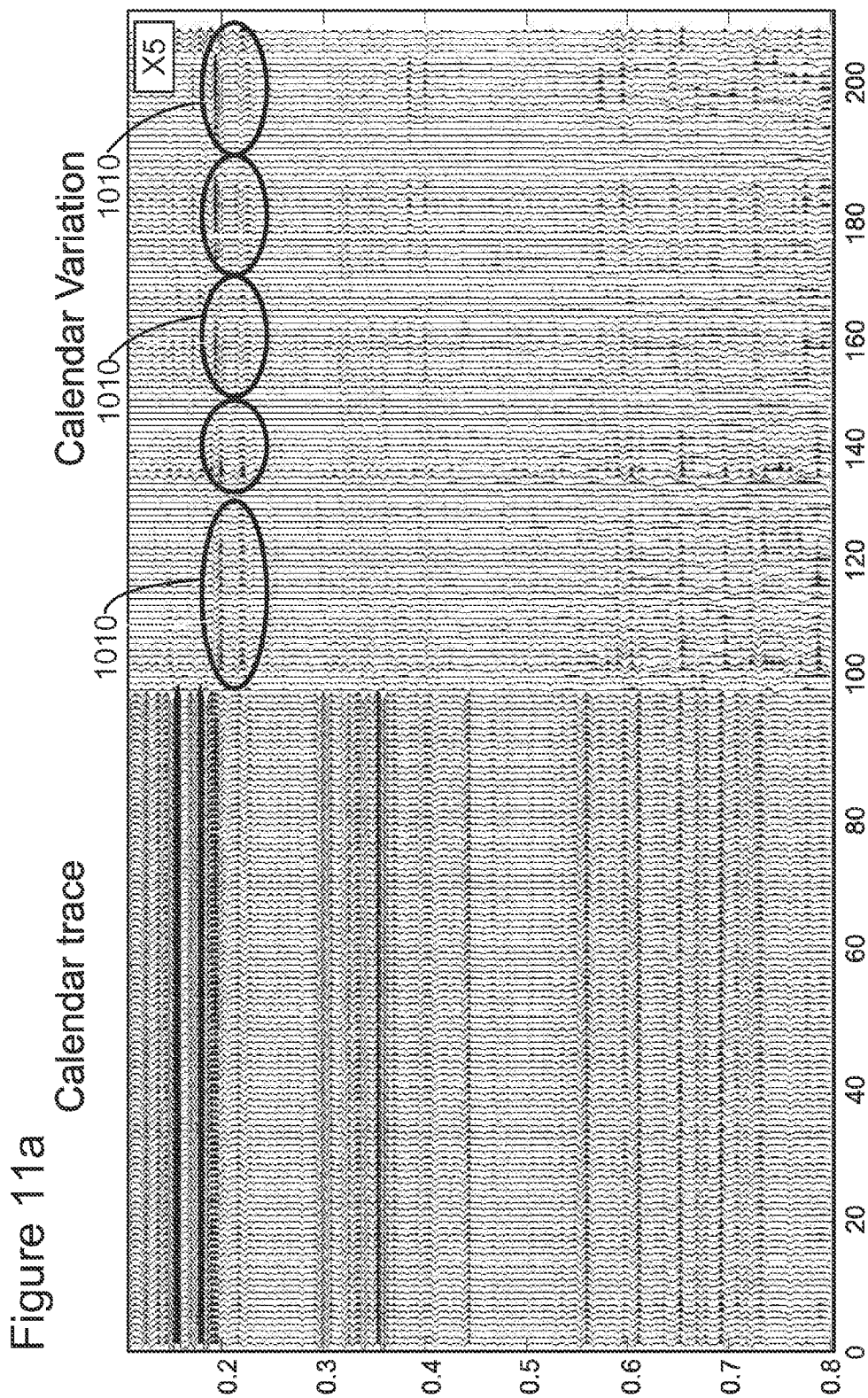


Figure 9

Figure 10





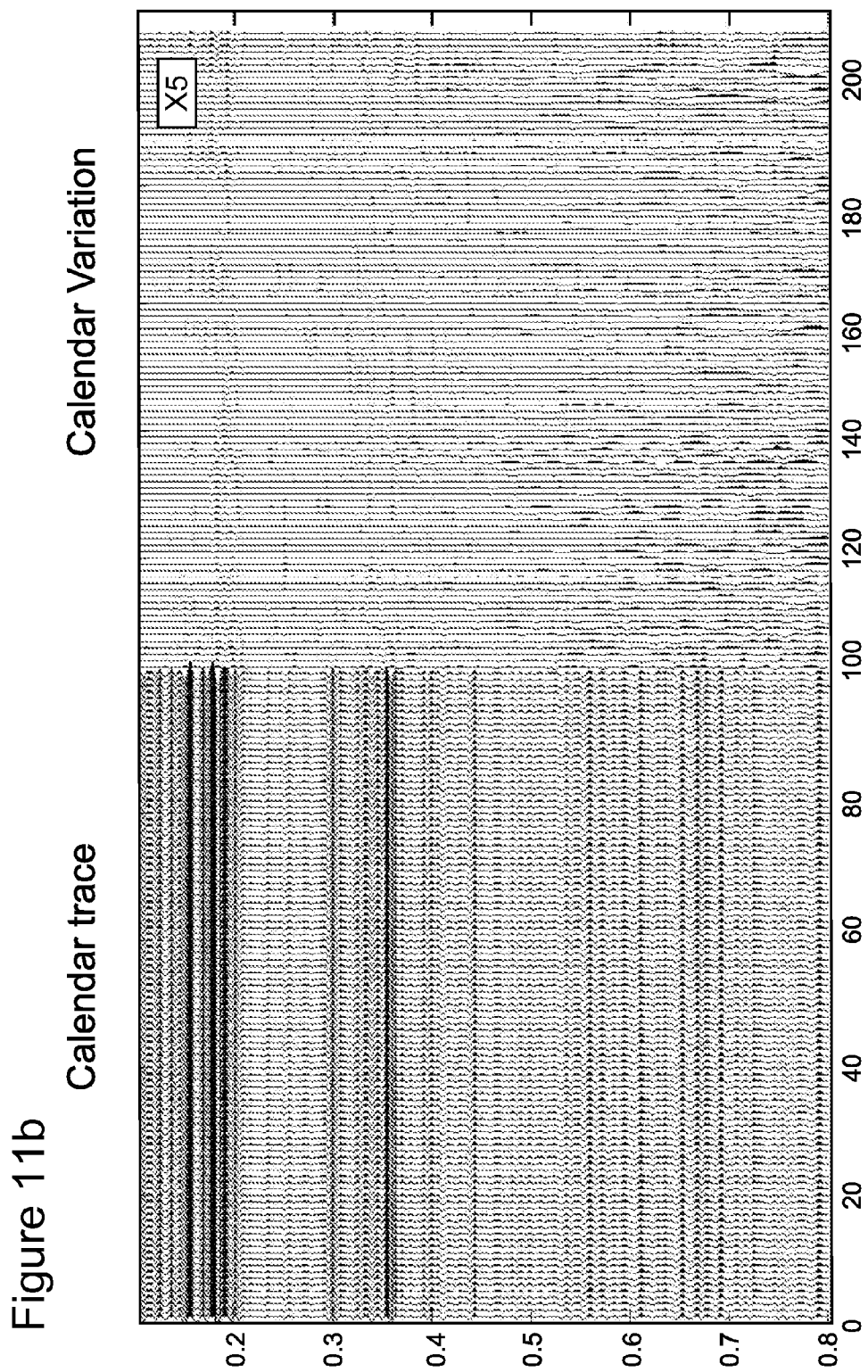
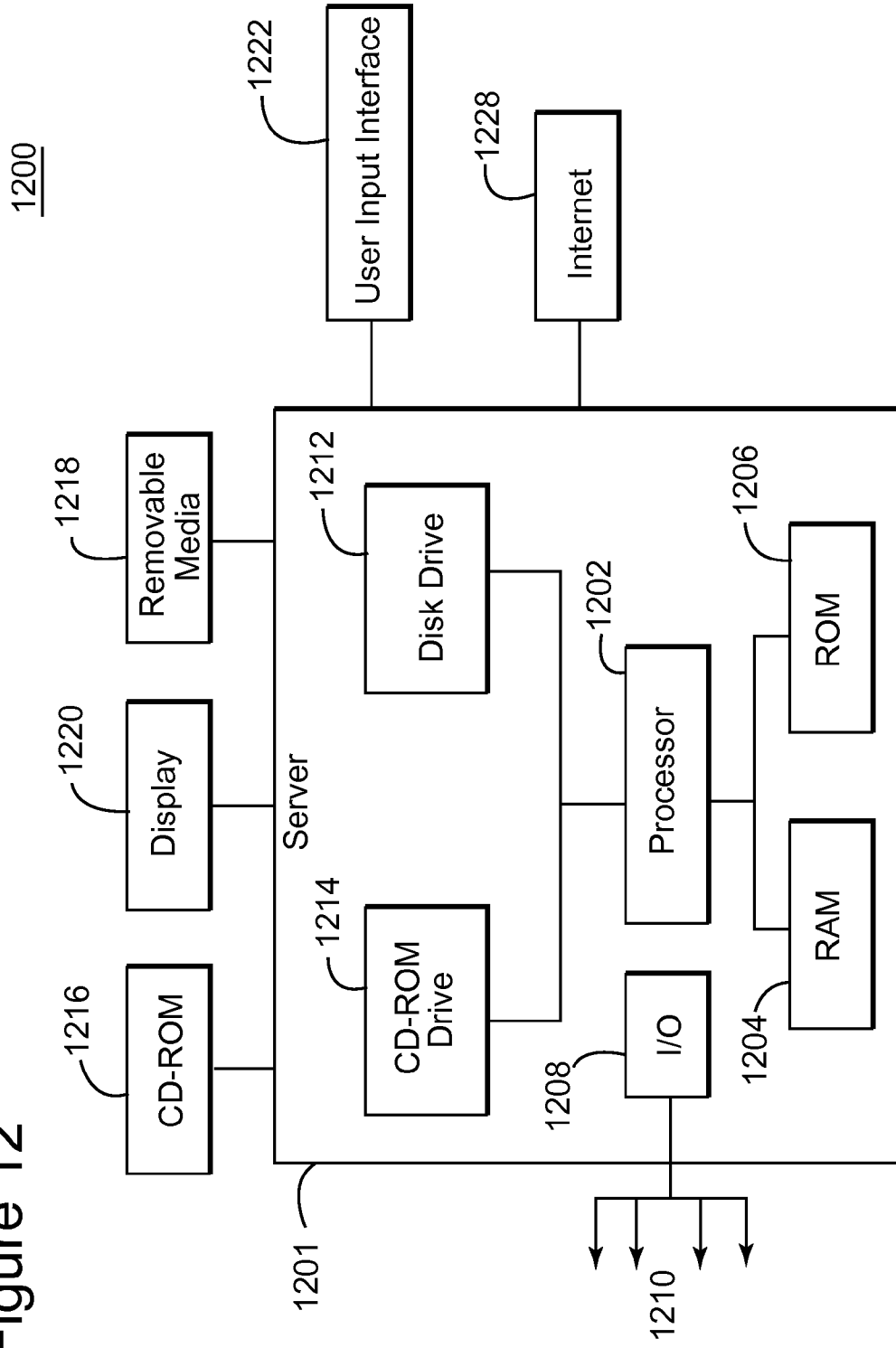


Figure 12



## PLURAL DEPTH SEISMIC DE-GHOSTING METHOD AND SYSTEM

### CROSS-REFERENCE TO RELATED APPLICATIONS

[0001] This application is a Continuation-in-Part of co-pending application Ser. No. 14/054,505 filed on Oct. 15, 2013, and entitled "PLURAL DEPTH SEISMIC SOURCE SPREAD METHOD AND SYSTEM" and for which priority is claimed under 35 U.S.C. §120. This application also claims priority to Provisional Application No. 61/858,234, filed on Jul. 25, 2013, and entitled "DE-GHOSTING PROCESSING METHOD FOR PLURAL DEPTH BURIED SOURCES AND/OR PLURAL DEPTH BURIED SENSORS IN 4D SEISMIC ACQUISITION" and for which priority is claimed under 35 U.S.C. §119. The entire content of each of these applications is incorporated herein by reference.

### BACKGROUND

[0002] 1. Technical Field

[0003] Embodiments of the subject matter disclosed herein relate generally to the field of geophysical data acquisition and processing. In particular, the embodiments disclosed herein relate to methods and systems for acquiring and processing seismic data from plural depth buried sources and receivers.

[0004] 2. Discussion of the Background

[0005] Geophysical data is useful for a variety of applications, reservoir monitoring, subsoil imaging, environmental monitoring, mining, and seismology. As the economic benefits of such data have been proven, and additional applications for geophysical data have been discovered and developed, the demand for localized, high-resolution, and cost-effective geophysical data has greatly increased. This trend is expected to continue.

[0006] For example, seismic data acquisition and processing may be used to generate a profile (image) of the geophysical structure under the ground (either on land or seabed). While this profile does not provide an exact location for oil and gas reservoirs, it suggests, to those trained in the field, the presence or absence of such reservoirs. Thus, providing a high-resolution image of the subsurface of the earth is important, for example, to those who need to determine where oil and gas reservoirs are located.

[0007] Traditionally, a land seismic survey system 10 capable of providing a high-resolution image of the subsurface of the earth is generally configured as illustrated in FIG. 1 (although many other configurations are used). System 10 includes plural receivers 12 and acquisition units 12a positioned over an area 13 of a subsurface to be explored and in contact with the surface 14 of the ground. A number of seismic sources 16 are also placed on surface 14 in an area 17, in a vicinity of area 13 of receivers 12. The area 13 corresponding to the receivers 16 and the area 17 corresponding to the sources 16 may, or may not be, overlapping areas on the surface 14. A recording device 18 is connected to a plurality of receivers 12 and placed, for example, in a station-truck 20. Each source 16 may be composed of a variable number of vibrators or explosive devices, and may include a local controller 22. A central controller 24 may be present to coordinate the shooting times of the sources 16. A GPS system 26 may be used to time-correlate sources 16 and receivers 12 and/or acquisition units 12a.

[0008] With this configuration, the sources 16 are controlled to generate seismic waves, and the receivers 12 record the waves reflected by the subsurface. The receivers 12 and acquisition units 12a may be connected to each other and the recording devices with cables 30. Alternately, the receivers 12 and acquisition units 12a can be paired as autonomous nodes that do not need the cables 30. While the depicted seismic survey system 10 is a land seismic survey, an ocean bottom survey system may have similar components.

[0009] The purpose of seismic imaging is to generate high-resolution images of the subsurface from acoustic reflection measurements made by the receivers 12. Conventionally, as shown in FIG. 2a, the seismic sources 16 and receivers 12 are distributed on the ground surface at a distance from each other. The sources 16 are activated to produce seismic waves that travel through the subsoil. These seismic waves undergo deviations as they propagate. They are refracted, reflected, and diffracted at the geological interfaces of the subsoil. For example, waves 40 that travel through the subsoil and are reflected from a subsurface 50 may be detected by the seismic receivers 12. The reflected waves may be recorded as a function of time in the form of signals (called traces).

[0010] The seismic sources 16 may be placed at a variety of source locations and the receivers 12 may be placed at a variety of receiving locations on the surface 52. The source locations and the receiving locations may be selected to provide a sufficient number of traces to capture the features of the subsurface with high fidelity.

[0011] In many seismic survey applications, known as 4D seismic surveys, it is desirable to detect changes in the subsurface 50 over time. However, with the configuration shown in FIG. 2a, variations in the surface 52 and the weathering region 60 may be subject to significant changes that make it difficult to detect changes in the subsurface 50. For example, the moisture content of the weathering region 60 may change dramatically and alter the velocity of the waves 40. The surface 52 may also be subject to erosion or soil deposition that alters the position of the sources 16 and receivers 12 relative to the subsurface 50.

[0012] To mitigate the changing conditions of the surface 52 and the weathering region 60, the sources 16 and receivers 12 may be buried below the weathering region 60 and placed in a region of greater stability as is shown in FIG. 2b. However, as shown in FIG. 2c, ghost reflections 70 of the waves 40 from the weathering region 60 and the surface 52 contribute to the signal received by the receivers 12 resulting in additional 4D noise and reduced accuracy.

[0013] Due to the foregoing, there is a need for seismic data acquisition and processing systems and methods that are able to reduce noise from ghost reflections

### SUMMARY

[0014] As detailed herein, a method for de-ghosting seismic data includes receiving seismic data corresponding to plural depth sources or plural depth receivers located at a first depth and a second depth below a geophysical surface, wherein the second depth is below the first depth, where the plural depth sources or plural depth receivers comprise a first seismic receiver located at the first depth and a second seismic receiver located at the second depth, or, a first seismic source located at the first depth and a second seismic source located at the second depth. The method also includes aligning pri-

mary reflections within the seismic data to provide improved seismic data. A corresponding system is also disclosed herein.

#### BRIEF DESCRIPTION OF THE DRAWINGS

[0015] The accompanying drawings, which are incorporated in and constitute a part of the specification, illustrate one or more embodiments and, together with the description, explain these embodiments. In the drawings:

[0016] FIG. 1 is a schematic diagram depicting a traditional land seismic survey system;

[0017] FIG. 2a is a schematic diagram depicting selected portions of a traditional 4D reservoir monitoring system with sources and receivers placed proximate to a geophysical surface;

[0018] FIG. 2b is a schematic diagram depicting selected portions of a traditional 4D reservoir monitoring system with single depth sources and receivers;

[0019] FIG. 2c is a schematic diagram depicting ghost reflections associated with traditional 4D reservoir monitoring systems;

[0020] FIG. 3 is a schematic diagram depicting selected portions of a 4D monitoring system with buried plural depth sources and receivers;

[0021] FIG. 4 is a schematic diagram depicting reduced ghost reflections associated with a plural depth source spread;

[0022] FIG. 5a is a schematic diagram depicting reduced ghost reflections associated with a plural depth receiver spread;

[0023] FIG. 5b is a timing diagram depicting shifted reflections associated with a shifting subsurface in a 4D seismic survey that leverages a plural depth source or a plural depth receiver spread;

[0024] FIG. 6 is a flowchart diagram depicting one embodiment of a plural depth seismic processing method;

[0025] FIG. 7 is a flowchart diagram depicting one embodiment of a 4D plural depth seismic processing method;

[0026] FIGS. 8a-8g are schematic diagrams depicting various placement configurations for plural depth source and/or receiver spreads;

[0027] FIG. 9 is a flowchart diagram depicting one embodiment of a plural depth processing method;

[0028] FIG. 10 is a timing and schematic diagram illustrating how a receiver ghost signal can be isolated from a primary signal and a source ghost signal via dual-depth sensors;

[0029] FIG. 11a is a plot of seismic data processed from single depth seismic sources and FIG. 11b is a plot of seismic data processed from plural depth seismic sources; and

[0030] FIG. 12 is a block diagram of a computing device for processing seismic data.

#### DETAILED DESCRIPTION

[0031] The following description of the exemplary embodiments refers to the accompanying drawings. The same reference numbers in different drawings identify the same or similar elements. The following detailed description does not limit the invention. Instead, the scope of the invention is defined by the appended claims.

[0032] Reference throughout the specification to “one embodiment” or “an embodiment” means that a particular feature, structure, or characteristic described in connection with an embodiment is included in at least one embodiment of the subject matter disclosed. Thus, the appearance of the

phrases “in one embodiment” or “in an embodiment” in various places throughout the specification is not necessarily referring to the same embodiment. Further, the particular features, structures, or characteristics may be combined in any suitable manner in one or more embodiments.

[0033] A system and method for acquiring and improving seismic data is presented herein. Applicants have observed that the data precision and stability obtained with disclosed system and method enables subsurface change detection with shorter elapsed times and smaller amplitude variations than attainable with conventional systems and methods. For example, amplitude variations associated with steam injection into a reservoir are detectable with the disclosed system and method.

[0034] FIG. 3 is a schematic diagram depicting selected portions of a 4D monitoring system 300 with buried plural depth sources and/or receivers. The 4D monitoring system 300 includes one or more sources 16 and one or more receivers 12 that are placed at plural depths 310 below a geophysical surface such as the surface of the earth, a seabed, a river bed or the like. In the depicted arrangement, the plural depths 310 include a first depth 310a and a second depth 310b. The use of plural depths reduces ghost reflections and improves 4D (both continuous and time-lapse) seismic repeatability as will be shown in subsequent figures.

[0035] FIG. 4 is a schematic diagram depicting one example of reduced ghost reflections that may occur for a plural depth source spread 410. The depicted source spread 410 includes a source 410a at a first depth 310a and a source 410b at a second depth 310b. For the purpose of clarity, a simplified scenario, where the reflection angles are assumed to be substantially vertical (i.e., the cosine of the propagation angle relative to vertical is substantially equal to 1.0), demonstrates how the source spread 410 reduces ghost reflections and improves 4D seismic repeatability.

[0036] A seismic source wave such as an impulse may be generated by each source in the source spread 410 at a distinct time. In response thereto, a trace corresponding to each source may be recorded by a receiver 420. As shown on the right side of FIG. 4, the traces may be time-aligned relative to the firing of the sources 410a and 410b to provide synchronized traces 430. In one embodiment, time alignment is enabled by synchronized clocks on the sources 410 and the receiver 420.

[0037] Due to the difference in depths between the source 410a and the source 410b, a primary (i.e., subsurface) reflection 432b from the source 410b arrives at the receiver 420 earlier (e.g., by time difference  $dt_{12}$ ) relative to the source event than a primary reflection 432a from the source 410a. The difference in depths between the source 410a and the source 410b also results in a ghost reflection 434b from the source 410b arriving at the receiver 420 earlier (e.g., by time difference  $dt_{21}$ ) relative to the source event than a ghost reflection 434a from the source 410a. The time difference  $dt_{12}$  may be substantially equal to  $dt_{21}$  despite a difference in the direction of wave propagation between the source 410a and the source 410b for the primary reflections 432 and the ghost reflections 434.

[0038] During processing, one of the traces 430 may be phase-shifted or time-shifted to provide aligned traces 440 where the primary reflections 432a and 432b are aligned and the ghost reflections 434a and 434b are further misaligned. Subsequently, the traces may be summed or averaged to pro-

vide a common midpoint trace **450** with reduced ghost reflections **434a** and **434b** relative to the primary reflections **432a** and **432b**.

[0039] FIG. **5a** is a schematic diagram depicting one example of reduced ghost reflections that may occur for a plural depth receiver spread **510**. The depicted receiver spread **510** includes a source **510a** at a first depth **310a** and a source **510b** at a second depth **310b**. For the purpose of clarity, a simplified scenario, where the reflection angles are assumed to be substantially vertical (i.e., the cosine of the propagation angle relative to vertical is substantially equal to 1.0), demonstrates how the receiver spread **510** reduces ghost reflections and improves 4D seismic repeatability.

[0040] A seismic source wave such as an impulse may be generated by the source **520** at a distinct time. In response thereto, a trace corresponding to each source may be recorded by each receiver in the receiver spread **510**. As shown on the right side of FIG. **5**, the traces may be time-aligned relative to the firing of the source **520** to provide synchronized traces **530**. In one embodiment, time alignment is enabled by synchronized clocks on the source **520** and each receiver of the receiver spread **510**.

[0041] Due to the difference in depths between the receiver **510a** and the receiver **510b**, a primary (i.e., subsurface) reflection **532** from the source **520** arrives at the receiver **510b** earlier (e.g., by time difference  $dt_{21}$ ) relative to the source event than the primary reflection **532** arrives at the receiver **510a**. The difference in depths between the receiver **510a** and the receiver **510b** also results in a ghost reflection **534** from the source **520** arriving at the receiver **510a** earlier (e.g., by time difference  $dt_{12}$ ) relative to the source event than the ghost reflection **534** arrives at the receiver **510b**. The time difference  $dt_{12}$  may be substantially equal to  $dt_{21}$  despite a difference in the direction of wave propagation between the receiver **510a** and the receiver **510b** for the primary reflection **532** and the ghost reflection **534**.

[0042] During processing, one of the traces **530** may be phase-shifted or time-shifted to provide aligned traces **540** where the primary reflections **532** are aligned and the ghost reflections **534** are further misaligned. Subsequently, the traces **540** may be summed or averaged to provide a common midpoint trace **550** with reduced ghost reflections **534** relative to the summed or averaged primary reflection **532**.

[0043] The simplicity of the above scenarios demonstrates the value of using a plural depth source spread and/or a plural depth receiver spread. As shown in FIGS. **4** and **5a**, and in comparison to the prior art (see, for example, FIG. **2c**) ghost reflections may be significantly reduced and result in improved seismic data. Furthermore (optional) explicit deghosting operations may be conducted on the improved seismic data (e.g., seismic data filtering or generating a model of the primary reflections using matrix inversion) in order to further reduce ghost reflections.

[0044] Mathematically, the seismic data corresponding to a plural depth source or receiver spread may be represented in the frequency domain as:

$$S_1(f) = P_1(f) + G_1(f) \quad (1)$$

$$S_2(f) = P_2(f) + G_2(f) \quad (2)$$

where  $f$  is a selected frequency,  $S_1$  and  $S_2$  represent signals corresponding to sources or receivers at two distinct depths (namely  $z_1$  and  $z_2$ ),  $P_1$  and  $P_2$  represent up-going (i.e., primary) waves that occur at those depths, and  $G_1$  and  $G_2$  represent down-going (i.e., ghost) waves. The relationship

between up-going waves  $P$  and down-going waves  $G$  at the two depths may be represented as:

$$\tau = e^{-i2\pi(dt)} \quad (3)$$

$$dt = \Delta z / V \quad (4)$$

where  $f$  is the frequency component of the signal,  $\tau$  is a phase term corresponding to the arrival time difference  $dt$  between the two levels of sources or receivers separated by the depth difference  $\Delta z$ , and  $V$  is the propagation velocity between the two levels of sources or receivers.

[0045] Assuming that there is no absorption between the two levels, which is a reasonable assumption in a consolidated media, and that  $\Delta z$  is in the order of a few meters, the relationship between up-going wave  $P$  and the down-going waves  $G$  at the two levels can be written as:

$$G_2(f) = G_1(f) / \tau \quad (5)$$

$$P_2(f) = \tau P_1(f) \quad (6)$$

$$P_1(f) = [S_1(f) - S_2(f)\tau] / [1 - (1/\tau)^2] \quad (7)$$

$$G_1(f) = [S_1(f) - \tau S_2(f)] / [1 - \tau^2] \quad (8)$$

[0046] In equation (7) and (8), we have a zero denominator when  $\tau = 1$ , which occurs in several situations including when:

$$f = n / (2\tau) \quad (9)$$

[0047] The condition defined in equation (9) corresponds to a set of spurious frequencies (i.e., harmonics) that may not be separated by aligning the primary reflections  $P$ . However, an appropriate choice of the depth difference  $\Delta z$  places the first spurious frequency ( $n=1$ ) at the upper edge of a selected useful (processing) bandwidth as demonstrated in the following table 1:

TABLE 1

	$V = 1000$ m/s	$V = 1500$ m/s	$V = 2500$ m/s
$\Delta z = 3$ m	$f = 166.67$ Hz	$f = 250$ Hz	$f = 416.67$ Hz
$\Delta z = 6$ m	$f = 83.33$ Hz	$f = 125$ Hz	$f = 208.33$ Hz

[0048] One of skill in the art will appreciate the advantages of being able to place the spurious (potentially non-separable) frequency at the upper edge of the processing bandwidth by controlling the depth difference for the plural depth sources or receivers. In addition to the above, a pre-whitening signal  $w$  may be used during processing to reduce the effect of the spurious frequencies. For example, a whitening signal  $w$  may be leveraged according to the following equations to reduce the effect of the spurious frequencies and improve the quality of the seismic image:

$$w > |1 - (1/\tau)^2| \quad (10)$$

$$P_1(f) = [S_1(f) - S_2(f)\tau] / w \quad (11)$$

$$G_1(f) = [S_1(f) - \tau S_2(f)] / w \quad (12)$$

[0049] FIG. **5b** is a timing diagram depicting shifted primary and ghost reflections associated with a shifting subsurface in a 4D seismic survey that leverages a plural depth source or a plural depth receiver spread. As is shown, reduced ghost reflections **434** or **534** may enable better detection of subsurface changes by enabling improved detection of a timing shift for the primary reflections **432** or **532** over single

depth surveys. The timing shift **560** may be used to determine a corresponding subsurface shift (not shown).

[0050] FIG. 6 is a flowchart diagram depicting one embodiment of a plural depth seismic processing method **600**. As depicted, the method **600** includes, placing (**610**) plural sources and/or plural receivers at plural depths to provide a plural depth spread, activating one or more seismic sources and acquiring (**620**) seismic data using the plural depth spread, aligning (**630**) primary reflections within the seismic data, and generating a final image of, or extracting information about, the subsurface (**640**).

[0051] Placing (**610**) plural sources and/or plural receivers at plural depths may include boring holes into the ground (on land or underwater) into which multiple sources and/or receivers are placed. In some embodiments, two or more sources and/or receivers may be placed into the same hole at different depths. The placed sources and receivers may provide a plural depth spread **410** and/or a plural depth spread **510**.

[0052] Activating one or more seismic sources and acquiring (**620**) seismic data using the plural depth spread may include leveraging the seismic survey system **10** configured as shown in FIG. 3 or using a similar system and configuration. The sources within the system may be fired in a manner that facilitates separation, i.e., impulsive sources may be separated in time while vibratory sources may be separated in time and/or frequency. Frequency separated vibratory sources may be single frequency sources, multi-frequency sources, or chirped sources.

[0053] Aligning (**630**) primary reflections within the seismic data may include determining a depth or position difference between the plural depth sources and/or receivers and using the depth or position difference to align the primary reflections within the seismic data. The depth or position difference may be determined from GPS data for the sources and receivers or from data collected when the sources or receivers were placed by a field crew.

[0054] Generating a final image of, or extracting information about, the subsurface (**640**) may include conducting operations familiar to those of skill in the art such as a common image point (i.e., midpoint) gather, common receiver gather, common source gather, common offset gather, cross-spread gather, and the like. The final image of the subsurface or the extracted information may communicate specific details about the subsurface including layer boundaries, velocity parameters, saturation, porosity, permeability, amplitude variation with offset or azimuth, or the like.

[0055] FIG. 7 is a flowchart diagram depicting one embodiment of a 4D plural depth seismic processing method **700**. As depicted, the method **700** includes acquiring (**710**) a first seismic dataset using a plural depth spread, acquiring (**720**) a second seismic dataset using the plural depth spread, and determining (**730**) changes to a subsurface.

[0056] The acquiring operations **710** and **720** may be conducted according to the plural depth seismic processing method **600** described above or a similar method. The operation **710** may be conducted on a first seismic dataset collected during a first survey and the operation **720** may be conducted on a second seismic dataset collected during a second survey.

[0057] Determining (**730**) changes to a subsurface from the first and second seismic datasets may include aligning primary reflections within the first and second datasets and conducting various operations including cross-correlation, reservoir inversion, differencing, NRMS, and change prediction.

[0058] FIGS. **8a-8g** are schematic diagrams depicting various placement configurations for plural depth source and/or receiver spreads. The depicted configurations are intended to be illustrative rather than definitive. For example, FIGS. **8a-8g** show two-dimensional configurations while actual deployed configurations may be three-dimensional.

[0059] FIGS. **8a** and **8b** depict a grid configuration and an offset grid configuration, respectively. FIG. **8c** shows a sawtooth configuration and FIG. **8d** shows a random configuration. Selection of a configuration may be application and/or objective dependent. For example, the position of the sources and/or receivers may be selected to minimize aliasing, reduce cost, or a combination thereof.

[0060] FIGS. **8e-8g** show various examples of plural depth configurations that benefit from having a sparse array **810** that is at a different depth than a primary array **820**. A sparse array pertains to an arrangement of plural depths of receivers and/or sources are located below the weathering layer at predefined depth levels. For example, FIG. **8e** shows a sparse receiver array **810e** at a different depth than the primary receiver array **820e**. The sparse receiver **810e** is placed at a different depth than the primary array of receivers **820e**. The source array is placed at a depth below the sparse array. The number of receivers in the sparse array depends on the area under monitoring. For example, one sparse array may be used for an area of 1 km<sup>2</sup>. However, any number of sparse arrays may be used. Similarly, FIG. **8f** shows a sparse source array **810f** at a different depth than the primary source array **820f**. Here the receivers are placed at a depth less than the primary source array **820f**. The sparse source array **810f** may be placed at a greater depth than the primary source array **820f**. FIG. **8g** shows both a sparse receiver array **810g** and a sparse source array **810h** that are at different depths than a primary receiver array **820g** and a primary source array **820h**, respectively. By using the methods disclosed herein, or similar methods, each source or receiver within the sparse arrays **810** may be used to de-ghost sources or receivers within the primary arrays **820** that are proximate to the particular source or receiver within the sparse arrays **810**. For example, in some embodiments, primary and ghost waves are separated using a sparse array (e.g., the sparse receiver array **810e** shown in FIG. **8e**) on a repeated basis in order to determine ghost variation. Subsequently, the ghost variation may be leveraged according to the methods described in the commonly assigned U.S. patent application Ser. No. 13/766,213, which is incorporated herein by reference, to deghost other sources or receivers (e.g., the receiver array **820e** shown in FIG. **8e**).

[0061] FIG. 9 is a flowchart diagram depicting one embodiment of a plural depth processing method **900**. As depicted, the method **900** includes determining **910** a position difference or a propagation delay for plural depth sources and/or plural depth receivers, phase or time shifting **920** received seismic data according to the position difference or propagation delay to provide aligned seismic data, and summing **930** the aligned seismic data to provide improved seismic data. The improved seismic data provided by the method **900** may enable improved subsurface imaging and change detection.

[0062] Determining **910** a position difference or a propagation delay for plural depth sources and/or plural depth receivers may include accessing GPS data for the plural depth sources and/or receivers. In some embodiments, the propagation delay is computed directly from synchronized seismic traces. In some situations, the position difference may be substantially identical to a depth difference.

[0063] Phase or time shifting 920 received seismic data according to the position difference or propagation delay may include determining an average velocity within the spread and converting the position difference to a phase or time difference. In another embodiment, the phase or time difference is computed directly from the seismic traces. A time difference may be converted to a specific phase by knowing the frequency content of the source. Phase or time shifting the seismic data according to the position difference or the propagation delay may align the primary reflections within the seismic data and thereby provide aligned seismic data.

[0064] Summing 930 the aligned seismic data may include summing traces that have their primary reflections aligned with one another. One of skill in the art may recognize that operations 920 and 930 may be accomplished with a digital filter that includes one or more taps corresponding to phase shift terms.

[0065] FIG. 10 is a timing and schematic diagram illustrating how a receiver ghost signal can be isolated from a primary signal and a source ghost signal via dual-depth sensors and substantially completely removed from the seismic data. The configuration illustrated in the FIG. 10 represents a representative step of multiple acquisition scenarios explained in FIG. 8. The configuration illustrated in FIG. 10 assumes upgoing and downgoing waves that are essentially vertical and planar. Onshore, such an assumption is acceptable as a velocity gradient is often observed in the shallow subsoil resulting in highly vertical propagation. By reciprocity, a source ghost could be separated at a plural depth source array with one receiver using a similar scheme. We consider first any receiver location on the acquisition spread. The seismic data recorded by a receiver can be expressed as:

$$Z_{(s,r,f,c)} = P_{(s,r,f,c)} + R_{(s,r,f,c)} + S_{(s,r,f,c)} + N_{(r,f,c)} \quad (13)$$

where the recorded seismic data  $Z$  comprises primary waves  $P$ , receiver ghost waves  $R$ , source ghost waves  $S$ , and noise signal  $N$ . In this example, waves  $P$ ,  $R$ ,  $S$  have four dimensions, namely  $s$  corresponding to the considered source,  $r$  corresponding to the considered receiver,  $f$  corresponding to the selected frequency and  $c$  corresponding to the calendar time. Consequently,  $Z$  may be referred to as a calendar trace gather, namely the seismic record between one source and one receiver over calendar time. Note that the noise  $N$  has only three dimensions as it is independent of the considered active seismic source. Let us consider the waves recorded at the two levels of sensors as shown in FIG. 10. We can write:

$$Z_{(1,1,f,c)} = P_{(1,1,f,c)} + R_{(1,1,f,c)} + S_{(1,1,f,c)} + N_{(1,f,c)} \quad (14)$$

$$Z_{(1,2,f,c)} = P_{(1,2,f,c)} + R_{(1,2,f,c)} + S_{(1,2,f,c)} + N_{(2,f,c)} \quad (15)$$

[0066] Normally it is convenient to assume no absorption between two levels of sources or receivers since the depth difference is of an order of a few meters in a consolidated media. The equations (14) and (15) may be written in simplified notion below as equation (16) and (17) respectively, assuming noise is negligible relative to the primary and ghost signals

$$Z1 = P1 + R1 + S1 \quad (16)$$

$$Z2 = P2 + R2 + S2 \quad (17)$$

[0067] However, if there is any absorption between the two levels of sources, absorption compensation may be applied to the two comparable traces and the equations 16 and 17 may be

written with absorption or amplitude compensation as equation 16 (i) and equation 17(i) respectively

$$aZ1 = aP1 + aR1 + aS1 \quad (16(i))$$

$$bZ2 = bP2 + bR2 + bS2 \quad (17(i))$$

wherein,  $a$  and  $b$  in equation (16(i)) and (17(i)), respectively are the absorption compensation/amplitude compensation factors.

[0068] Now proceeding with the assumption that there is no absorption between the two levels of sources, the relationship between the primary waves and the ghost waves at the two levels can be written (similar to equations (7) and (8)) as:

$$P2 + S2 = \frac{Z2 - \frac{Z1}{\tau}}{1 - \frac{1}{\tau^2}} \quad (18)$$

$$R2 = \frac{Z2 - \tau Z1}{1 - \tau^2} \quad (19)$$

wherein,  $\tau$  is a phase term that describes arrival time delay between the primary wave and the ghost wave. Value of  $\tau$  may be determined as:

$$\tau = e^{-2\pi f(dt)}; \quad dt = \Delta z/V \quad (20)$$

wherein,  $V$  is the propagation velocity between the two levels of sources or the two levels of receivers separated by a depth distance  $\Delta z$ .

[0069] In equation (18) & (19), we can separate the receiver ghost from the primary wave and the source ghost, however we have a zero denominator for certain values of  $\tau$ :

$$\text{For example, } \tau = 1, \tau = 0, f = 0, f = \frac{K}{2\tau}; \quad (21)$$

These values corresponds to a set of spurious frequencies that may not be separated by aligning the primary reflections  $P$ . However, appropriate choice of depth difference places the first spurious frequency ( $n=1$ ) at the upper edge of a selected useful (processing) bandwidth as shown previously in Table 1.

[0070] Further, a pre-whitening signal  $w$  may be used to remove the effect of the spurious frequencies wherein

$$\left| 1 - \frac{1}{\tau^2} \right| < w \quad (22)$$

When the conditions described in the equation (21) are met, the equation (18) and equation (19) can be written as

$$P2 + S2 = \frac{Z2 - \frac{Z1}{\tau}}{w}$$

$$R2 = \frac{Z2 - \tau Z1}{w}$$

[0071] The receiver ghost ( $R2$ ) calculated as a part of dual depth sensor array processing may be used to separate either

any source ghost for any receiver ghost using high redundancy calendar time for a time lapse or 4D data.

**[0072]** Now if the monitoring is performed using the sparse acquisition or plural depth acquisition as mentioned in the FIG. 8(e)-8(g) additional processing steps are needed to obtain deghosted seismic data. Consider FIG. 10 as an incident in a continuous monitoring scenario. So the seismic trace recorded at one of the receiver can be expressed as described in equation (13)

$$Z_{(s,r,f,c)} = P_{(s,r,f,c)} + R_{(s,r,f,c)} + S_{(s,r,f,c)} + N_{(r,f,c)} \quad (23)$$

For a source-receiver couple (i.e. a seismic trace over the calendartime) for a given frequency the equation (23) becomes

$$Zn(c) = Pn(c) + Rn(c) + Sn(c) + Nn(c) \quad (24)$$

Now the variation of the calendar trace  $Zn'$  is obtained as below

$$Zn'(c) = Zn(c) - \left( \frac{1}{c} \sum Zn(c) \right) = Pn'(c) + Sn'(c) + Rn'(c) + Nn'(c) \quad (25)$$

wherein,

$$Pn'(c) = Pn(c) - \left( \frac{1}{c} \sum Pn(c) \right)$$

$$Sn'(c) = Sn(c) - \left( \frac{1}{c} \sum Sn(c) \right)$$

$$Rn'(c) = Rn(c) - \left( \frac{1}{c} \sum Rn(c) \right)$$

$$Nn'(c) = Nn(c) - \left( \frac{1}{c} \sum Nn(c) \right)$$

**[0073]** Assuming variations in the reservoir during the time lapse survey is minimum thus primary variations induced by reservoir changes may be considered negligible compared to the ghost variations,

$$Pn'(c) = Pn(c) - \left( \frac{1}{c} \sum Pn(c) \right) \approx 0$$

Now the equation (25) becomes:

$$Zn'(c) = Sn'(c) + Rn'(c) + Nn'(c)$$

**[0074]** Similarly, the variation in the receiver ghost  $R2'$  corresponding to the receiver ghost  $R2$  identified at the plural depth array of sensor may be determined as

$$R2' = \begin{bmatrix} R1'(k) \\ \vdots \\ R1'(x) \end{bmatrix}; R2 = \begin{bmatrix} R1(k) \\ \vdots \\ R1(x) \end{bmatrix};$$

$$Zn' = \begin{bmatrix} Sn'(k) + Rn'(k) + Nn'(k) \\ \vdots \\ Sn'(x) + Rn'(x) + Nn'(x) \end{bmatrix}$$

-continued

$$Zn = \begin{bmatrix} Pn(k) + Sn(k) + Rn(k) + Nn(k) \\ \vdots \\ Pn(x) + Sn(x) + Rn(x) + Nn(x) \end{bmatrix}$$

**[0075]** If the variation of the ghost  $R1'$  are comparable to the variations of the plural source and receiver ghosts covered in  $Zn'$ , a matching operator  $\alpha$  can be derived by resolving a simple least squares problem for a given frequency:

$$R2' = \alpha Zn' \quad (26)$$

**[0076]** For a given frequency, the matching operator  $\alpha$  can be derived by

$$\alpha = \frac{R2'^T Zn'}{R2'^T R2'} \quad (27)$$

The matching operator remains constant over the calendar time for a given frequency. Also, the value of the matching operator can be determined by selecting plural short periods. During the selection of the calculated receiver ghost ( $R1'$ ) and the variation of the calendar trace ( $Zn'$ ) may be composed of suitable non-consecutive records; however the resulting matrix should be of same size.

Finally the calendarwave separation that gives a deghosted calendar seismic record can be written as:

$$Sn' + Rn' = R2'^* \alpha;$$

$$Sn + Rn = R2^* \alpha;$$

$$Zn \text{Deg} = Zn - R2^* \alpha$$

wherein,  $Zn \text{Deg}$  is calendar trace after deghosting,  $Zn$  is calendar trace before deghosting. Similar process may be used to remove the source ghosts.

**[0077]** FIGS. 11a and 11b show one specific example of the improvements that may be attained with plural depth sources and receivers over conventional configurations using the methods described herein. FIG. 11a is a plot of seismic data processed from conventional single depth seismic sources and receivers and FIG. 11b is a plot of seismic data processed from plural depth seismic sources at depths of 25, 28, and 35 meters and plural depth receivers at depths of 6 and 9 meters. FIGS. 11a and 11b were generated from real seismic data collected for the same region. FIG. 11a was processed using conventional techniques while FIG. 11b was processed using the methods described herein.

**[0078]** As mentioned above, Applicants have observed that the data precision and stability obtained with the systems and methods disclosed herein enable subsurface change detection with shorter elapsed times and for smaller amplitude variations than previously possible. FIGS. 11a and 11b are evidence of that observed improvement. While FIG. 11a shows significant residual noise 1010 (highlighted with oval annotations), the residual noise is substantially eliminated in FIG. 11b.

**[0079]** In addition to shorter elapsed times and detection of smaller amplitude variations, the systems and methods disclosed herein may increase the signal-to-noise ratio of seismic data, improve 4D seismic repeatability, increase frequency content, reduce positioning error between acquisitions, subdue industrial noise, and enable Strati-

graphic Inversion. Applicants assert that improvement in the aforementioned metrics and attributes may be seen with depth variations of less than 0.3 meters (corresponding to a propagation delay of less than 0.25 milliseconds).

**[0080]** The above-discussed procedures and methods may be implemented partially or wholly in the computing device illustrated in FIG. 12. Hardware, firmware, software, or a combination thereof may be used to perform the various steps and operations described herein. The computing device **1200** of FIG. 12 is an exemplary computing structure that may be used in connection with such a system.

**[0081]** The computing device **1200** may include a server **1201**. Such a server **1201** may include a central processor (CPU) **1202** coupled to a random access memory (RAM) **1204** and to a read only memory (ROM) **1206**. The ROM **1206** may also be other types of storage media to store programs, such as programmable ROM (PROM), erasable PROM (EPROM), etc. The processor **1202** may communicate with other internal and external components through input/output (I/O) circuitry **1208** and bussing **1210**, to provide control signals and the like. The processor **1202** carries out a variety of functions as are known in the art, as dictated by software and/or firmware instructions.

**[0082]** The server **1201** may also include one or more data storage devices, including disk drives **1212**, CDDROM drives **1214**, and other hardware capable of reading and/or storing information such as DVD, etc. In one embodiment, software for carrying out the above-discussed steps may be stored and distributed on a CDDROM or DVD **1216**, a USB storage device **1218** or other form of media capable of portably storing information. These storage media may be inserted into, and read by, devices such as the CDDROM drive **1214**, the disk drive **1212**, etc. The server **1201** may be coupled to a display **1220**, which may be any type of known display or presentation screen, such as LCD displays, plasma display, cathode ray tubes (CRT), etc. A user input interface **1222** is provided, including one or more user interface mechanisms such as a mouse, keyboard, microphone, touchpad, touch screen, voice-recognition system, etc.

**[0083]** The server **1201** may be coupled to other devices, such as sources, detectors, etc. The server may be part of a larger network configuration as in a global area network (GAN) such as the Internet **1228**, which allows ultimate connection to the various landline and/or mobile computing devices.

**[0084]** The disclosed exemplary embodiments provide a computing device, a method for acquiring and de-ghosting seismic data, and systems corresponding thereto. For example, the disclosed computing device and method could be integrated into a variety of seismic survey and processing systems including land, ocean bottom, and transitional zone systems with either cabled or autonomous data acquisition nodes. It should be understood that this description is not intended to limit the invention. On the contrary, the exemplary embodiments are intended to cover alternatives, modifications, and equivalents, which are included in the spirit and scope of the invention as defined by the appended claims. Further, in the detailed description of the exemplary embodiments, numerous specific details are set forth in order to provide a comprehensive understanding of the claimed invention. However, one skilled in the art would understand that various embodiments may be practiced without such specific details.

**[0085]** Although the features and elements of the present exemplary embodiments are described in the embodiments in particular combinations, each feature or element can be used alone without the other features and elements of the embodiments or in various combinations and sequences with or without other features and elements disclosed herein.

**[0086]** This written description uses examples of the subject matter disclosed to enable any person skilled in the art to practice the same, including making and using any devices or systems and performing any incorporated methods. The patentable scope of the subject matter is defined by the claims, and may include other examples that occur to those skilled in the art. Such other examples are intended to be within the scope of the claims.

What is claimed is:

1. A method for de-ghosting seismic data, the method comprising:
  - receiving seismic data corresponding to plural depth sources or plural depth receivers located at a first depth and a second depth below a geophysical surface, wherein the second depth is below the first depth;
  - the plural depth sources or plural depth receivers comprising a first seismic receiver located at the first depth and a second seismic receiver located at the second depth, or, a first seismic source located at the first depth and a second seismic source located at the second depth; and
  - aligning primary reflections within the seismic data to provide improved seismic data.
2. The method of claim 1, wherein aligning the primary reflections misaligns ghost reflections within the seismic data that correspond to regions above the first depth.
3. The method of claim 1, wherein the primary reflections correspond to regions below the second depth.
4. The method of claim 3, further comprising determining changes to the regions below the second depth.
5. The method of claim 4, wherein determining changes to the regions below the second depth comprises comparing the improved seismic data corresponding to a first acquisition event with the improved seismic data corresponding to a second acquisition event.
6. The method of claim 1, further comprising phase-shifting or time-shifting a portion of the seismic data.
7. The method of claim 6, wherein an amount of phase-shifting or time-shifting corresponds to a propagation delay between the first seismic source and the second seismic source or the first seismic receiver and the second seismic receiver.
8. The method of claim 1, further comprising acquiring seismic data with another seismic receiver.
9. A system for de-ghosting seismic data, the system comprising:
  - plural depth sources or plural depth receivers comprising a first seismic receiver located at a first depth and a second seismic receiver located at a second depth, or, a first seismic source located at the first depth and a second seismic source located at the second depth;
  - wherein the second depth is below the first depth; and
  - a processor configured to aligning primary reflections within the seismic data to provide improved seismic data.
10. The system of claim 9, wherein aligning the primary reflections misaligns ghost reflections within the seismic data that correspond to regions above the first depth.

**11.** The system of claim **9**, wherein the primary reflections correspond to regions below the second depth.

**12.** The system of claim **11**, wherein the processor is configured to determine changes to the regions below the second depth.

**13.** The system of claim **11**, wherein the processor determines the changes to the regions below the second depth by comparing the improved seismic data corresponding to a first acquisition event with the improved seismic data corresponding to a second acquisition event.

**14.** The system of claim **9**, wherein the processor is configured to phase-shift or time-shift a portion of the seismic data.

**15.** The system of claim **14**, wherein an amount of phase-shift or time-shift corresponds to a propagation delay between the first seismic source and the second seismic source or the first seismic receiver and the second seismic receiver.

**16.** A method for de-ghosting seismic data, the method comprising:

receiving seismic data corresponding to plural depth sources or plural depth receivers located at a first depth and a second depth below a geophysical surface, wherein the second depth is below the first depth;

the plural depth sources or plural depth receivers comprising a first seismic receiver located at the first depth and a second seismic receiver located at the second depth, or, a first seismic source located at the first depth and a second seismic source located at the second depth; determining a position difference or a propagation delay corresponding to the plural depth sources or the plural depth receivers; and providing improved seismic data from the seismic data by using the position difference or the propagation delay to align primary reflections within the seismic data.

**17.** The method of claim **16**, wherein aligning the primary reflections misaligns ghost reflections within the seismic data that correspond to regions above the first depth.

**18.** The method of claim **16**, wherein the primary reflections correspond to regions below the second depth.

**19.** The method of claim **18**, further comprising determining changes to the regions below the second depth.

**20.** The method of claim **19**, wherein determining changes to the regions below the second depth comprises comparing the improved seismic data corresponding to a first acquisition event with improved seismic data corresponding to a second acquisition event.

\* \* \* \* \*

# Appendix 7

Volumetric and non-volumetric sources-based seismic survey and method

Forgues, E., F-X. Grésillon and J. Cotton, 2014

United States patent application publication





US 20140177386A1

(19) **United States**

(12) **Patent Application Publication**  
**FORGUES et al.**

(10) **Pub. No.: US 2014/0177386 A1**

(43) **Pub. Date: Jun. 26, 2014**

(54) **VOLUMETRIC AND NON-VOLUMETRIC SOURCES-BASED SEISMIC SURVEY AND METHOD**

**Publication Classification**

(71) Applicant: **CGG SERVICES SA**, Massy Cedex (FR)

(51) **Int. Cl.**  
**G01V 1/04** (2006.01)  
**G01V 1/34** (2006.01)

(72) Inventors: **Eric FORGUES**, Bures-sur-Yvette (FR); **Francois-Xavier GRESILLON**, Rully (FR); **Julien COTTON**, Paris (FR)

(52) **U.S. Cl.**  
CPC ... **G01V 1/04** (2013.01); **G01V 1/34** (2013.01)  
USPC ..... **367/7**; 367/75; 702/16

(73) Assignee: **CGG SERVICES SA**, Massy Cedex (FR)

(57) **ABSTRACT**

(21) Appl. No.: **14/103,177**

(22) Filed: **Dec. 11, 2013**

A seismic survey system for surveying a subsurface. The system includes a volumetric land source buried underground for generating P-waves; a non-volumetric land source buried underground for generating P- and S-waves; plural receivers distributed about the volumetric and non-volumetric land sources and configured to record seismic signals corresponding to the P- and S-waves; and a controller connected to the volumetric land source and the non-volumetric land source and configured to shot them in a given pattern.

**Related U.S. Application Data**

(60) Provisional application No. 61/740,915, filed on Dec. 21, 2012.

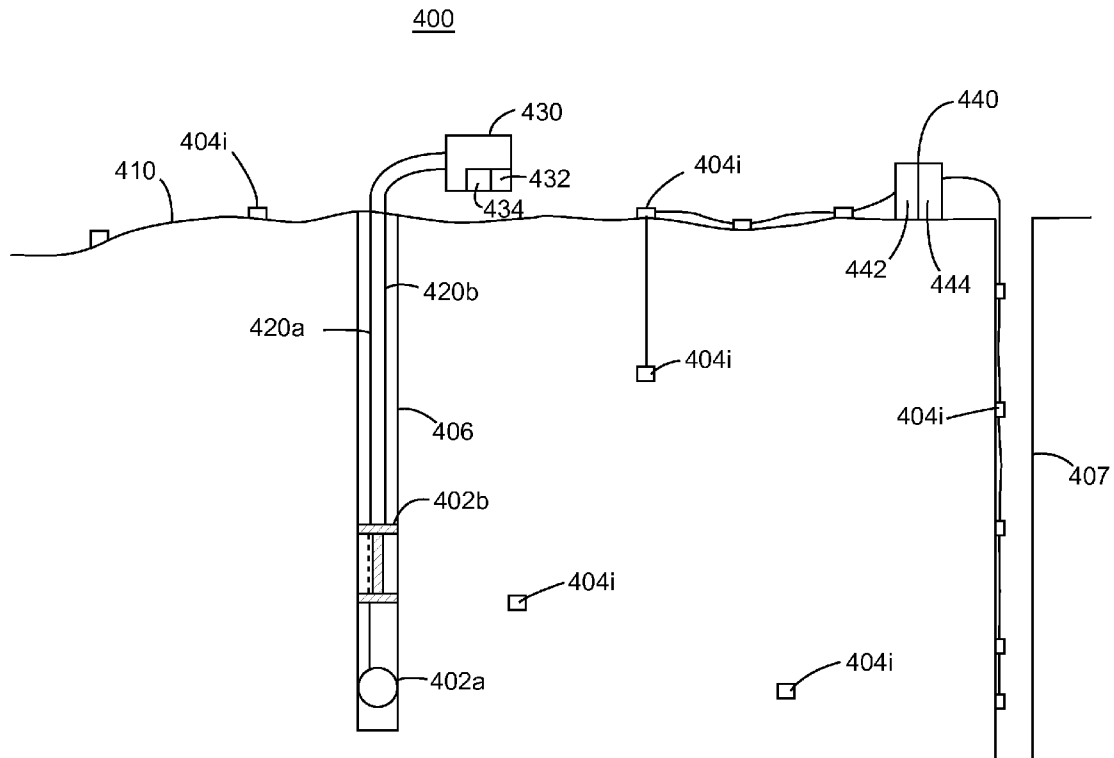


Figure 1B

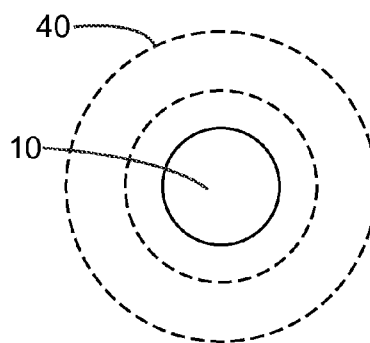


Figure 1A

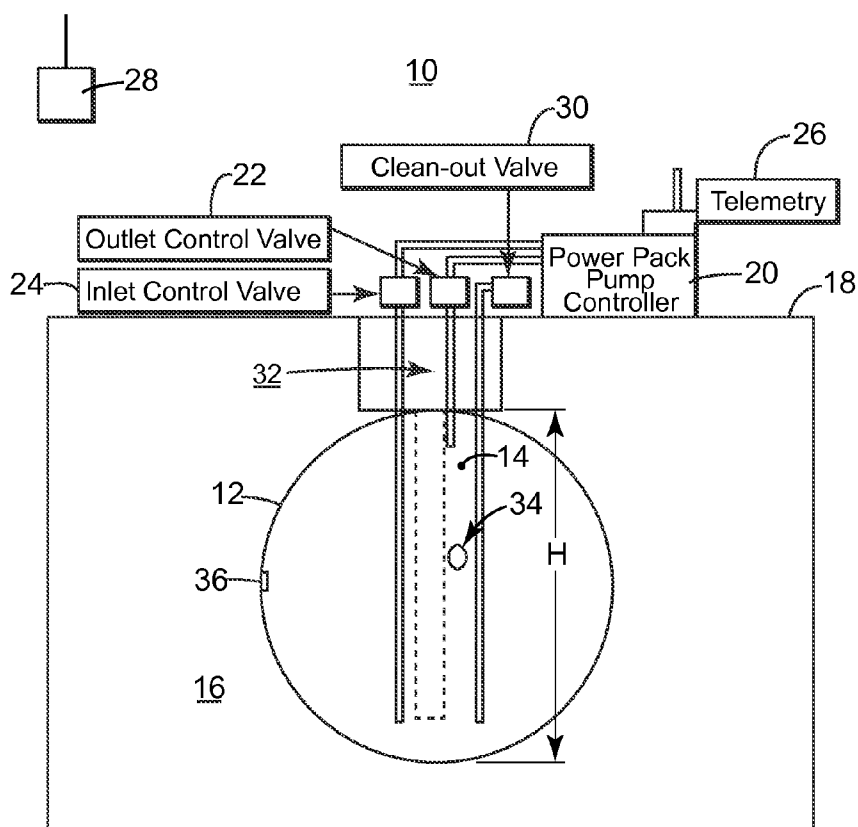
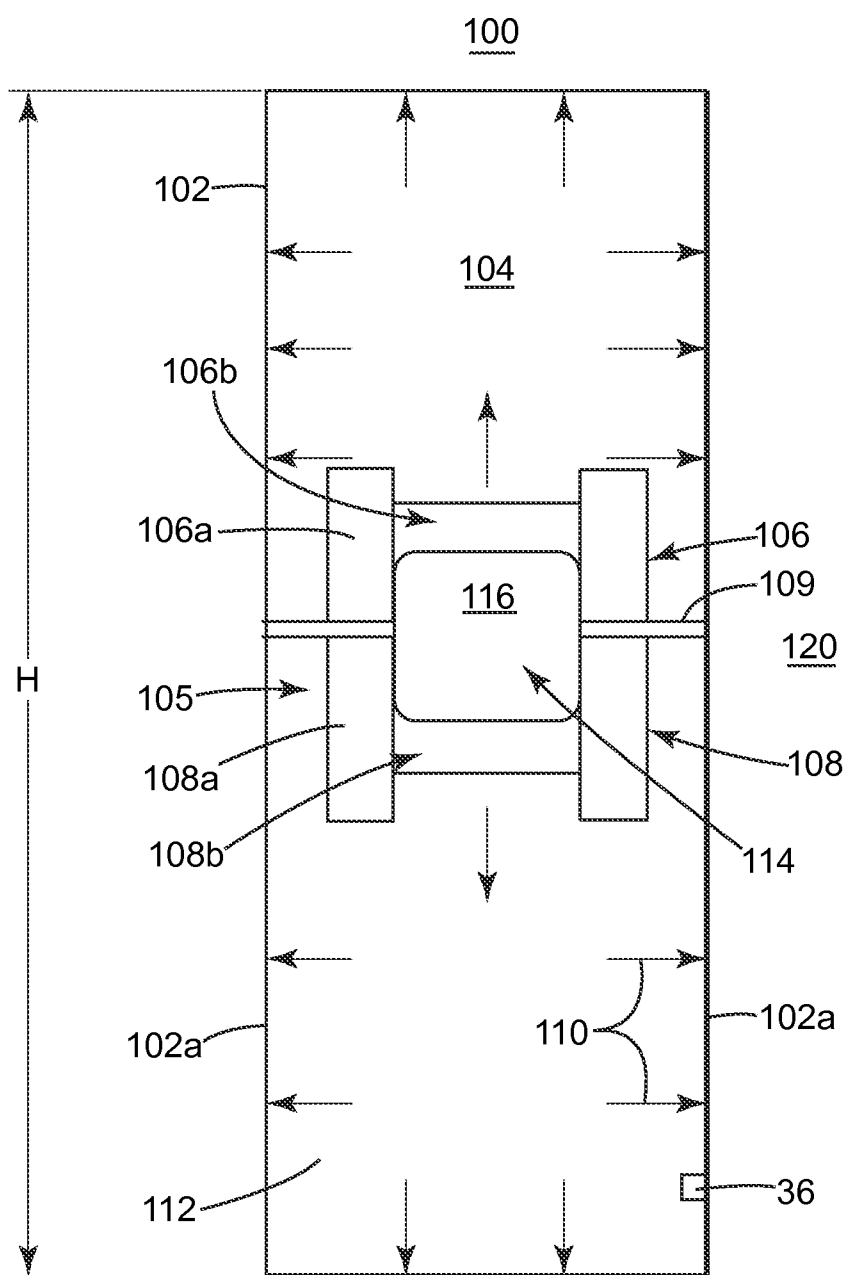


Figure 2



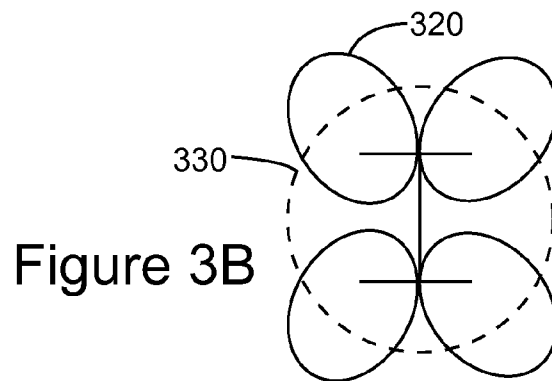
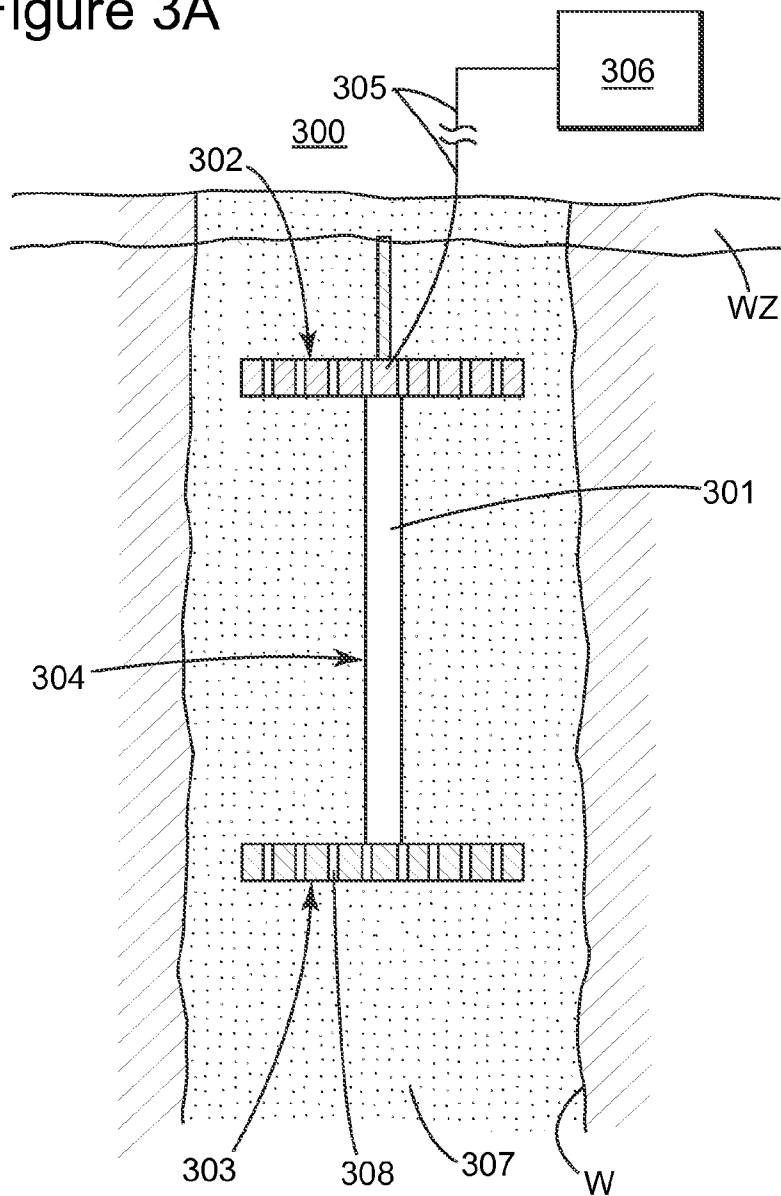


Figure 3A



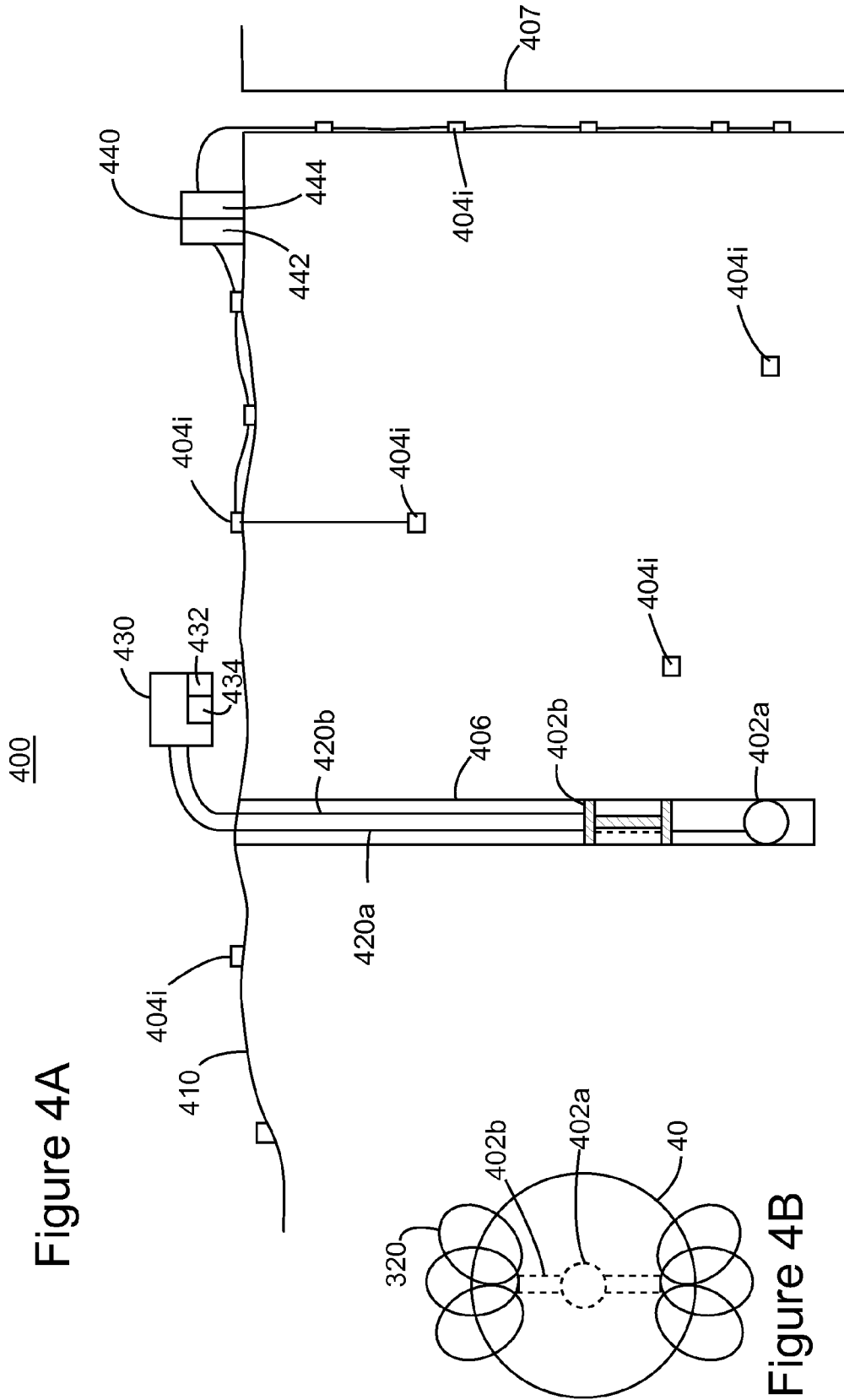


Figure 4A

Figure 4B

Figure 5

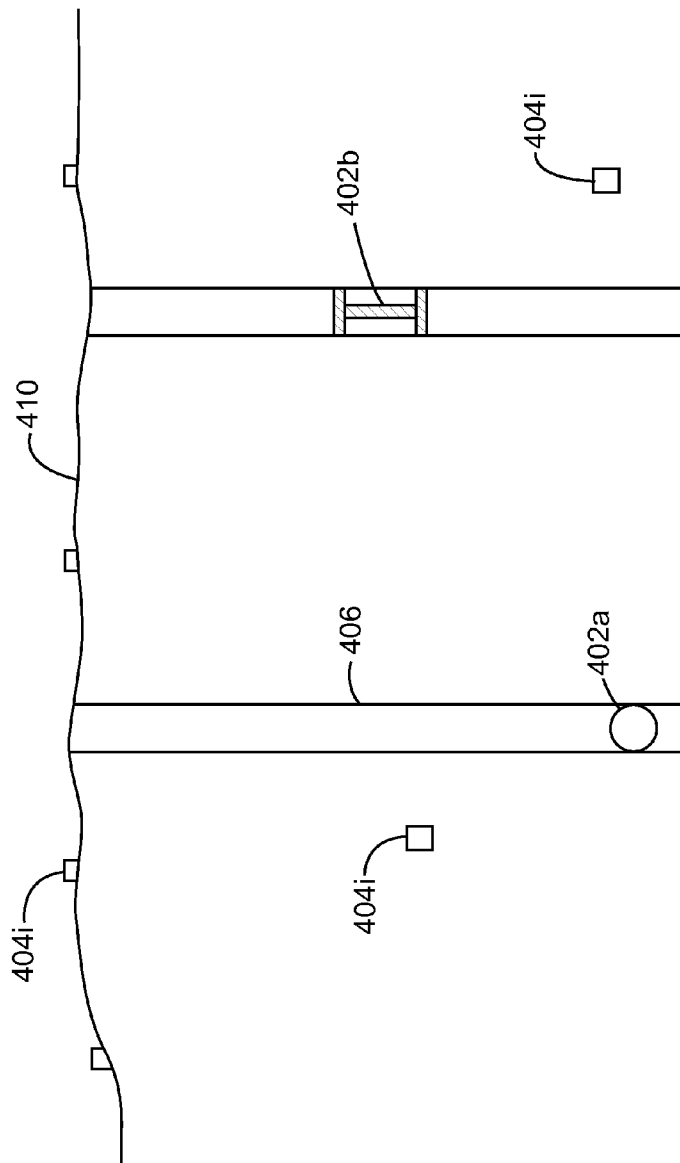


Figure 6

600

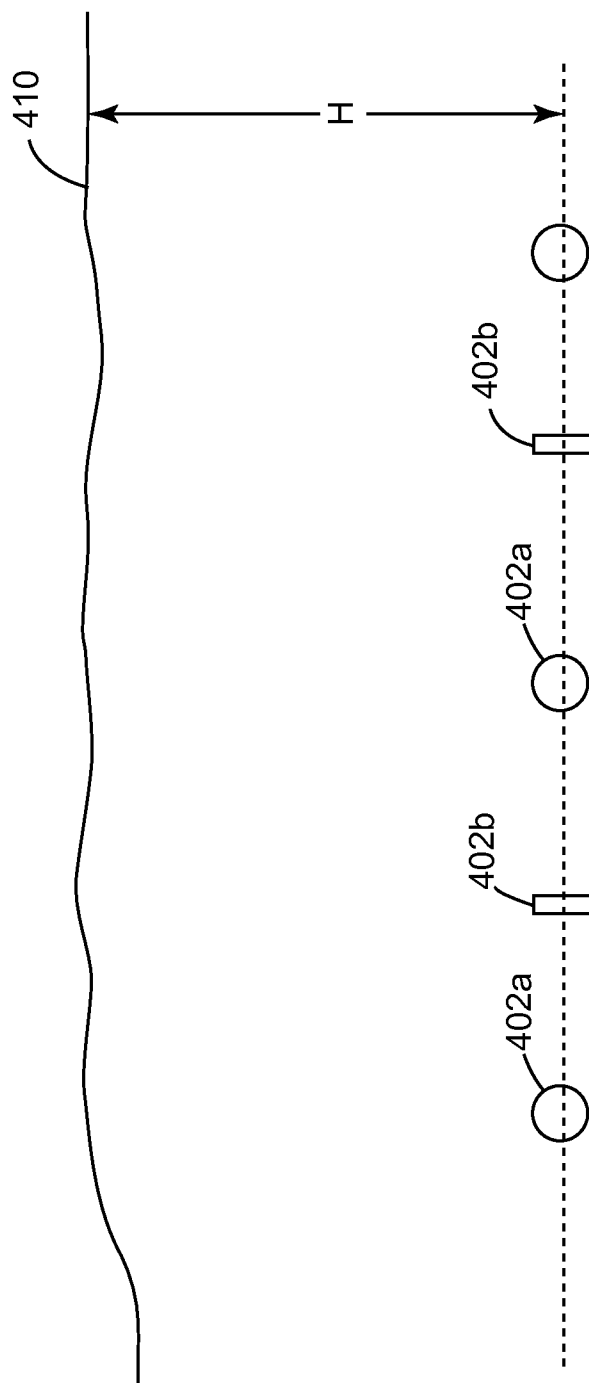
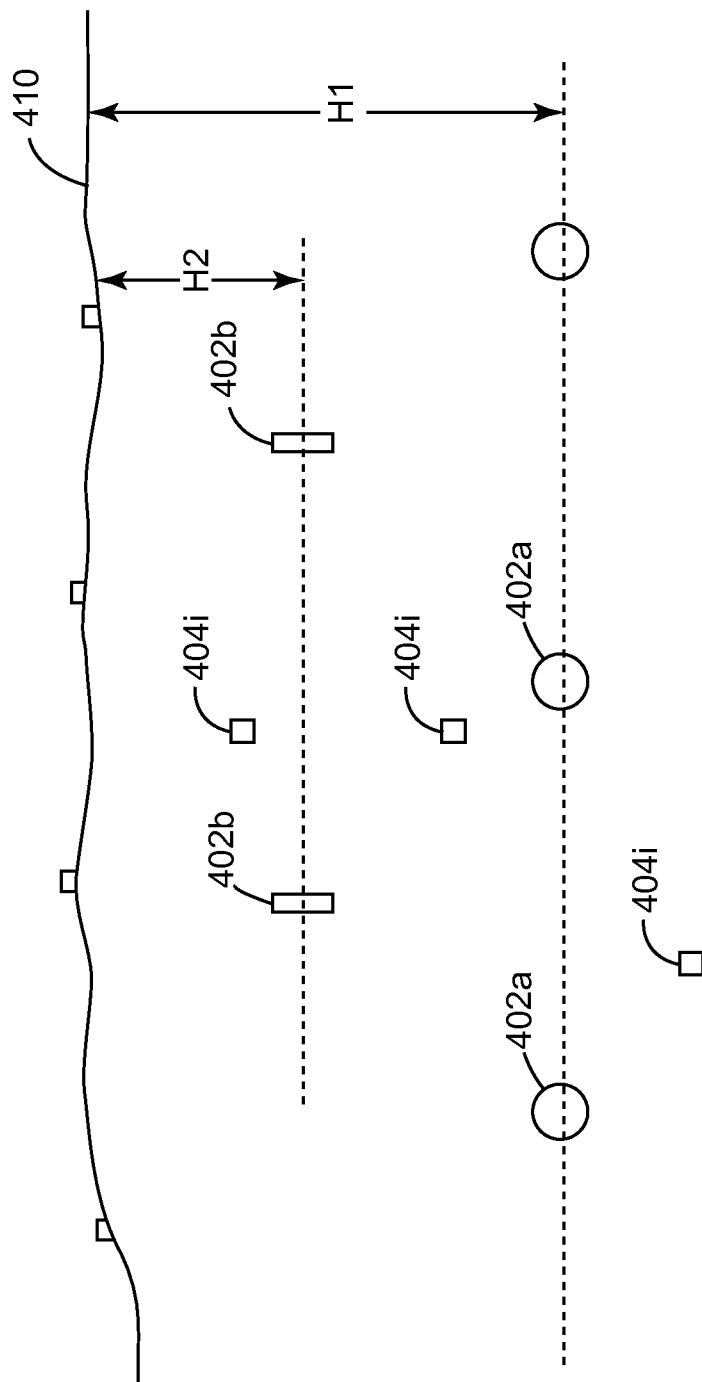
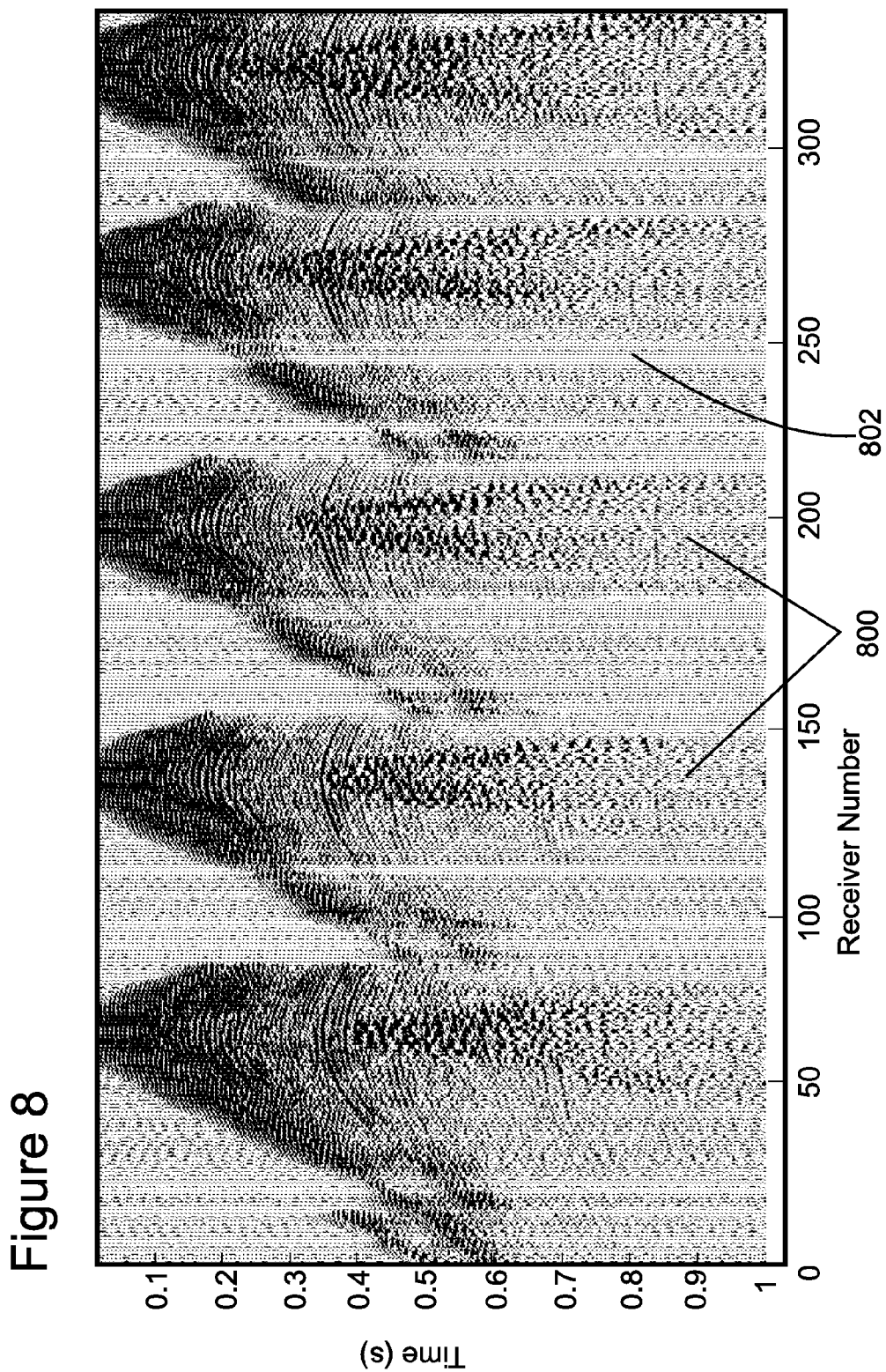
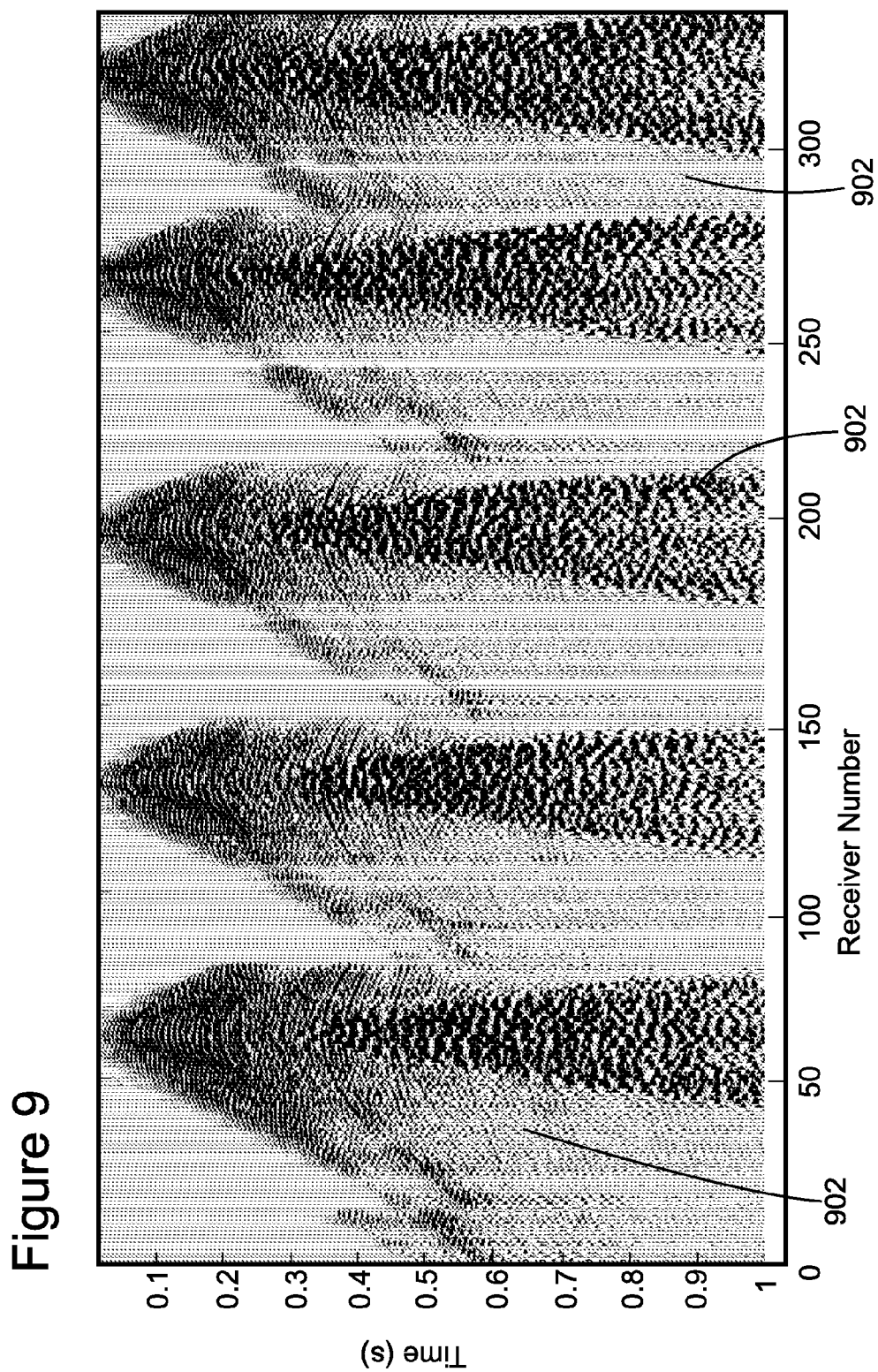


Figure 7







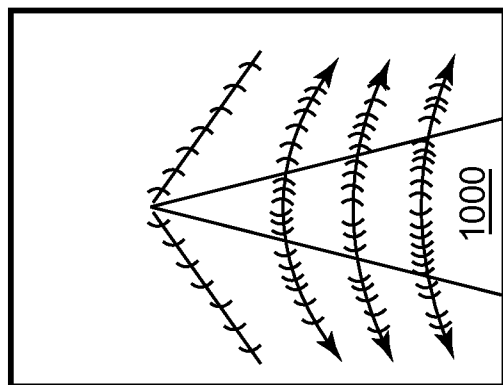


Figure 10C

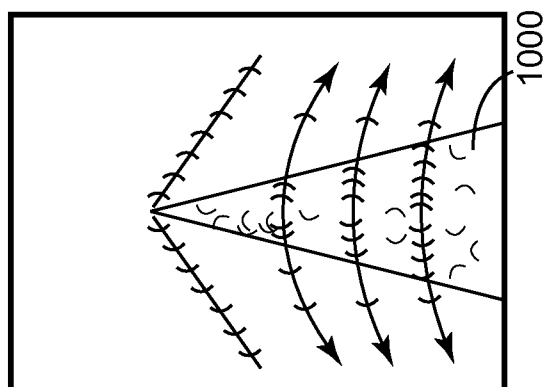


Figure 10B

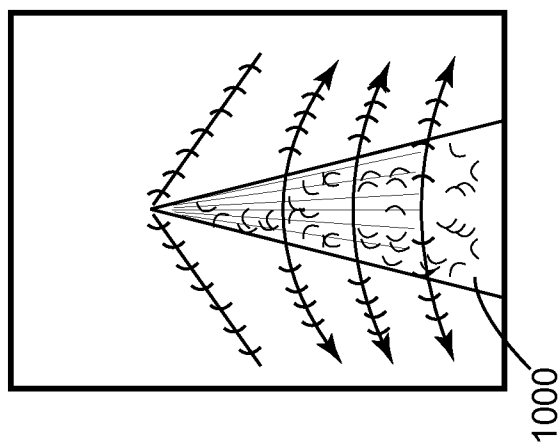


Figure 10A

Figure 11

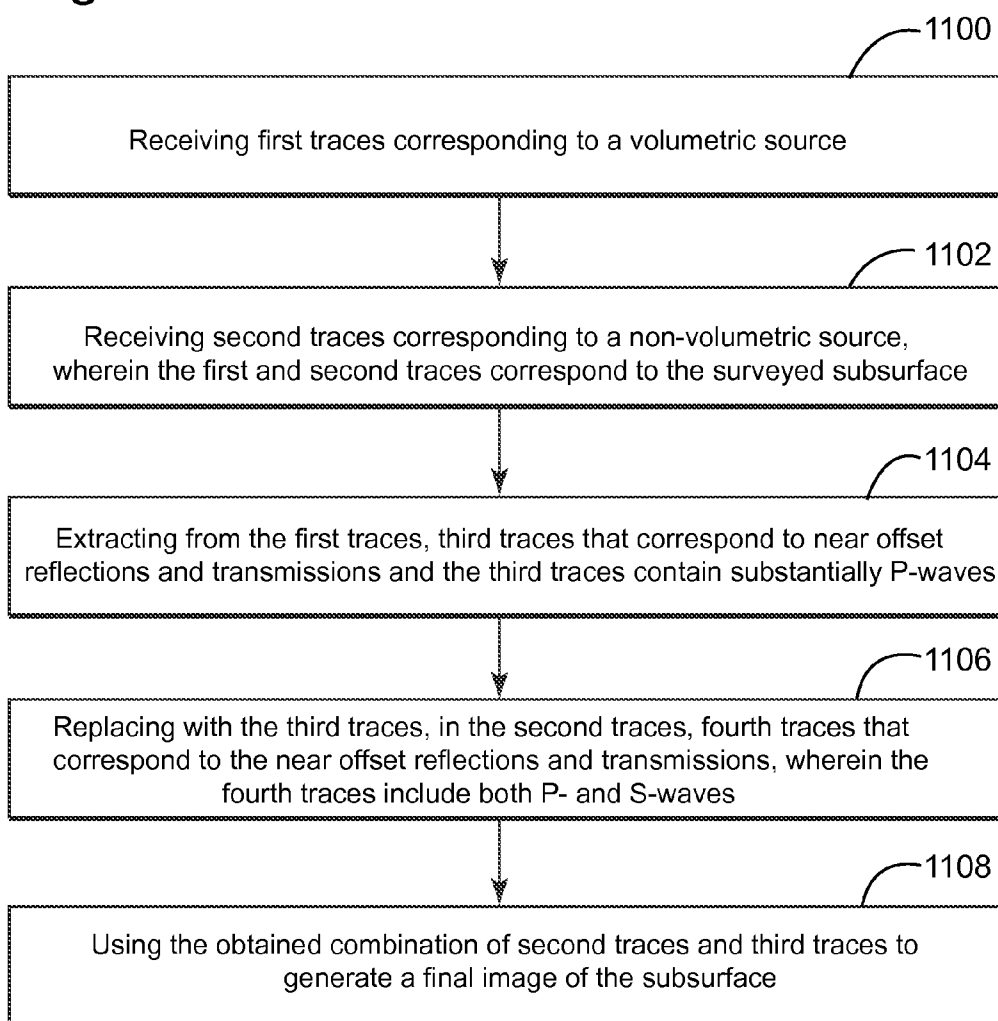
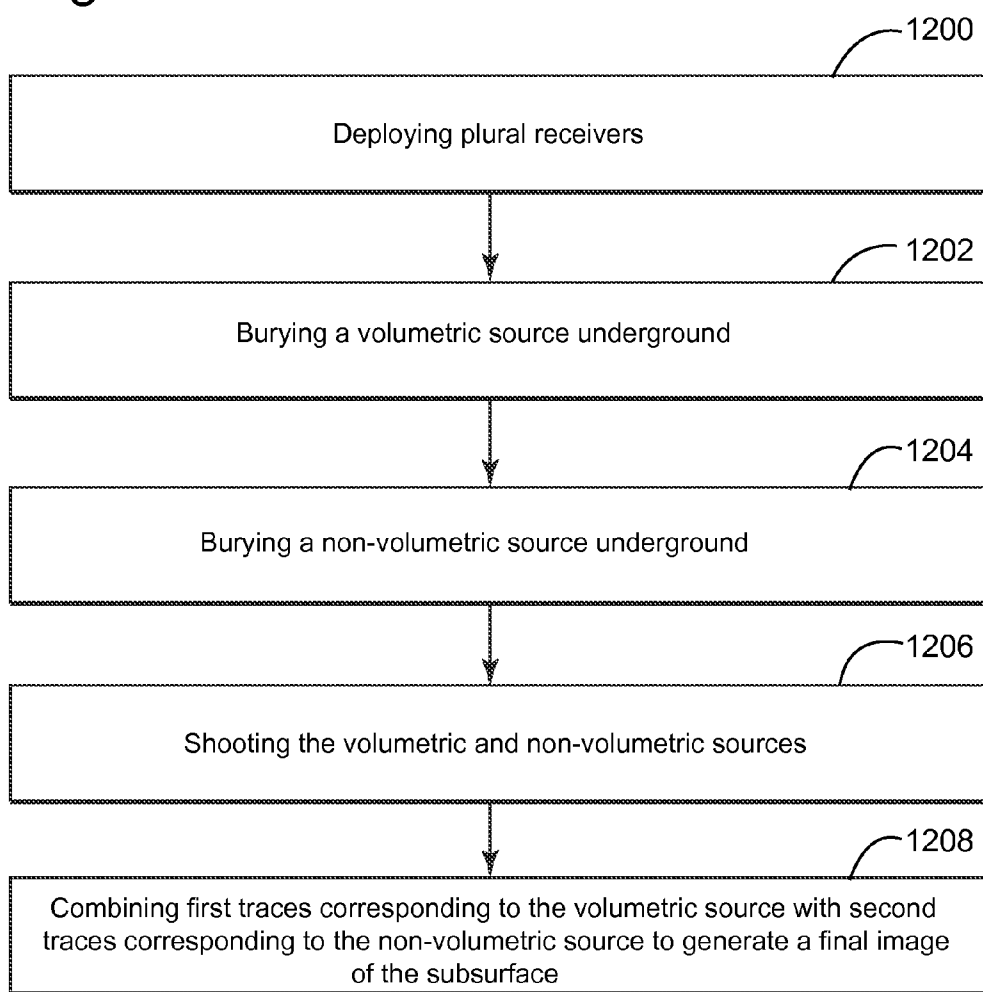


Figure 12



## VOLUMETRIC AND NON-VOLUMETRIC SOURCES-BASED SEISMIC SURVEY AND METHOD

### BACKGROUND

#### [0001] 1. Technical Field

[0002] Embodiments of the subject matter disclosed herein generally relate to devices and methods for generating seismic waves underground and, more particularly, to mechanisms and techniques for generating seismic waves with volumetric and non-volumetric seismic sources.

#### [0003] 2. Discussion of the Background

[0004] Land seismic sources may be used to generate seismic waves in underground formations for investigating geological structures. A seismic source may be located on the ground or it may be buried in the ground. The seismic source, when activated, imparts energy into the ground. Part of that energy travels downward and interacts with the various underground layers. At each interface between these layers, part of the energy is reflected and part of the energy is transmitted to deeper layers. The reflected energy travels toward the surface of the earth, where it is recorded by seismic sensors. Based on the recorded seismic data (traces), images of the underground layers may be generated. Those skilled in the art of seismic image interpretation are then able to estimate whether oil and/or gas reservoirs are present underground. A seismic survey investigating underground structures may be performed on land or water.

[0005] Current land seismic sources generate a mixture of P-waves and S-waves. A P-wave (or primary wave or longitudinal wave) is a wave that propagates through the medium using a compression mechanism, i.e., a particle of the medium moves parallel to a propagation direction of the wave and transmits its movement to a next particle of the medium. This mechanism is capable of transmitting energy both in a solid medium (e.g., earth) and in a fluid medium (e.g., water). An S-wave, different from a P-wave, propagates through the medium using a shearing mechanism, i.e., a particle of the medium moves perpendicular to the propagation direction of the wave and shears the medium. This particle makes the neighboring particle also move perpendicular to the wave's propagation direction. This mechanism is incapable of transmitting energy in a fluid medium, such as water, because there is not a strong bond between neighboring water particles. Thus, S-waves propagate only in a solid medium, i.e., earth.

[0006] The two kinds of waves propagate with different speeds, with P-waves being faster than S-waves. They may carry different information regarding the subsurface and, thus, both are useful for generating a subsurface image. However, when both of them are recorded with the same receiver, the strong S-wave content may obscure the P-wave content in certain portions, rendering the final image inaccurate.

[0007] Thus, there is a need to record both types of waves, with the ability to separate, at the emission stage, the two kinds of waves as needed. However, current use of land seismic sources does not offer this possibility. Currently, P- and S-waves generated by a land seismic source are simultaneously recorded by plural receivers, and during the processing stage, various strategies are employed for separating the two. However, this process may be time-intensive and inaccurate.

### BRIEF SUMMARY OF THE INVENTION

[0008] According to an exemplary embodiment, there is a seismic survey system for surveying a subsurface. The system includes a volumetric land source buried underground for generating P-waves; a non-volumetric land source buried underground for generating P- and S-waves; plural receivers distributed about the volumetric and non-volumetric land sources and configured to record seismic signals corresponding to the P- and S-waves; and a controller connected to the volumetric land source and the non-volumetric land source and configured to shot them in a given pattern.

[0009] According to another exemplary embodiment, there is a method for combining traces related to a surveyed subsurface for enhancing clarity of the subsurface. The method includes receiving first traces corresponding to a volumetric source; receiving second traces corresponding to a non-volumetric source, wherein the first and second traces correspond to the surveyed subsurface; extracting from the first traces, third traces that correspond to near offset reflections and transmissions and the third traces contain substantially P-waves; replacing with the third traces, in the second traces, fourth traces that correspond to the near offset reflections and transmissions, wherein the fourth traces include both P- and S-waves; and using the obtained combination of second traces and third traces to generate a final image of the subsurface.

[0010] According to still another exemplary embodiment, there is a method for conducting a surveying a subsurface. The method includes deploying plural receivers above and/or below land; burying a volumetric source underground; burying a non-volumetric source underground; shooting the volumetric and non-volumetric sources; and combining first traces corresponding to the volumetric source with second traces corresponding to the non-volumetric source to generate a final image of the subsurface.

### BRIEF DESCRIPTION OF THE DRAWINGS

[0011] For a more complete understanding of the present invention, reference is now made to the following descriptions taken in conjunction with the accompanying drawings, in which:

[0012] FIG. 1A is a schematic diagram of a volumetric seismic source;

[0013] FIG. 1B is a schematic illustration of the waves produced by a volumetric source;

[0014] FIG. 2 is a schematic diagram of another volumetric seismic source;

[0015] FIG. 3A is a schematic diagram of a non-volumetric seismic source;

[0016] FIG. 3B is a schematic illustration of the waves produced by a non-volumetric source;

[0017] FIG. 4A is a schematic diagram of a surveying system using a combination of volumetric and non-volumetric sources according to an embodiment;

[0018] FIG. 4B is a schematic illustration of the waves produced by a combined volumetric and non-volumetric source according to an embodiment;

[0019] FIG. 5 is a schematic diagram of a surveying system using a combination of volumetric and non-volumetric sources buried in different wells according to an embodiment;

[0020] FIG. 6 is a schematic diagram of a surveying system using a combination of volumetric and non-volumetric sources buried at a same depth according to an embodiment;

[0021] FIG. 7 is a schematic diagram of a surveying system using a combination of volumetric and non-volumetric sources buried at different levels according to an embodiment;

[0022] FIG. 8 is a graphic illustrating recorded traces generated by a volumetric source according to an embodiment;

[0023] FIG. 9 is a graphic illustrating recorded traces generated by a non-volumetric source according to an embodiment;

[0024] FIGS. 10A-C schematically illustrate how the traces from volumetric and non-volumetric sources are to be combined according to an embodiment;

[0025] FIG. 11 is a flowchart of a method for processing traces from volumetric and non-volumetric sources according to an embodiment; and

[0026] FIG. 12 is a flowchart of a method for performing a land seismic survey using simultaneously or sequentially volumetric and non-volumetric seismic sources according to an embodiment.

#### DETAILED DESCRIPTION OF THE INVENTION

[0027] The following description of the exemplary embodiments refers to the accompanying drawings. The same reference numbers in different drawings identify the same or similar elements. The following detailed description does not limit the invention. Instead, the scope of the invention is defined by the appended claims. The following embodiments are discussed, for simplicity, with regard to the terminology and structure of a land seismic source used to perform a seismic survey to evaluate the structure of a solid formation. However, the embodiments are not limited to this structure, but they may be used for reservoir characterization, e.g., 4-dimensional surveying.

[0028] Reference throughout the specification to “one embodiment” or “an embodiment” means that a particular feature, structure or characteristic described in connection with an embodiment is included in at least one embodiment of the subject matter disclosed. Thus, the appearance of the phrases “in one embodiment” or “in an embodiment” in various places throughout the specification is not necessarily referring to the same embodiment. Further, the particular features, structures or characteristics may be combined in any suitable manner in one or more embodiments.

[0029] According to an exemplary embodiment, a combination of a volumetric source and a non-volumetric source is used to perform a seismic survey. The two different land seismic sources may be shot sequentially or simultaneously to generate both P- and S-waves. The reflected waves are recorded by plural receivers. While the non-volumetric source produces strong S-waves for near offset reflections and transmission (i.e., the waves that travel directly from the source to the receivers) and they hide the reflected and transmitted waves for long offsets, the volumetric source produces, essentially, only P-waves, which do not hide the near offset reflections and transmissions. Thus, by recording P-waves generated by the volumetric source and also P- and S-waves generated by the non-volumetric source over a same subsurface, it is now possible to separate the S-waves from the P-waves for near offset reflections and transmissions as discussed next.

[0030] Some examples of volumetric sources are now presented. A first volumetric source may be driven in an impulsive mode or in a vibratory mode. For example, FIG. 1A illustrates a seismic source 10 configured to operate in an

impulsive mode. The seismic source 10 includes a spherical tank 12 filled with fluid 14 (e.g., mineral oil or water) buried underground 16 and in close contact with the ground. At the surface 18, a pump 20 is used to feed fluid into the tank 12, and valves 22 and 24 are used to control the out-flow and in-flow of the fluid between the tank 12 and the pump 20. The pump 20 may include a power pack and controllers. With these controls, which may be operated remotely via telemetry unit 26 from a central control and recording station 28, it is possible to build up pressure in the tank that will expand its volume and then quickly release it, causing a pressure pulse and generating P-wave seismic energy.

[0031] Although the tank 12 is illustrated in FIG. 1A as being spherical, it may have a cylindrical shape. Note that a spherical shape minimizes S-wave production because a spherical shape source 10 is acting like a monopole, i.e., generating only spherical waves 40, as schematically illustrated in FIG. 1B. However, even a cylindrical tank having a length comparable to the cylinder's diameter can be considered a volumetric source. From this point of view, a source is considered to be volumetric when most of the generated energy is carried by P-waves and not S-waves. Thus, although an ideal volumetric source is considered to generate no S-waves, in practice, a volumetric source also generates some S-waves.

[0032] Optionally, a clean-out line equipped with valve 30 may be used to drain the fluid from the tank 12. A cement plug 32 may be provided on top of the tank 12 for burying the source, and a seismic sensor 34 (e.g., hydrophone) may be placed in the tank 12 for measuring the seismic waves produced. Also, a pressure transducer 36 may be provided inside the tank 12 for measuring the fluid pressure acting on the walls in contact with the earth. This configuration is best suited when the tank 12 is buried at a shallow depth, because if the inlet and outlet lines are too long, the high frequency output of the system may be compromised due to the fluid inertance imposed by long passageways. The fluid inertance will tend to limit the rate at which pressure can change.

[0033] Alternatively, the seismic source may be vibratory as illustrated in FIG. 2. The source 100 has a tank 102 that includes a cavity 104. The same considerations discussed above regarding the shape of the tank 12 apply to tank 102. An actuation mechanism (e.g., piston arrangement) 105 is provided inside the cavity 104 and may include two back-to-back actuators 106 and 108, which may be electromagnetic. The actuation mechanism may be fixed relative to the tank 102 with a support element 109, which may be a bracket. In one application, one or more than two electromagnetic actuators are used. Each actuator may include a coil 106a or 108a configured to electromagnetically displace a corresponding piston 106b or 108b. Alternatively, the piston may be driven by a motor and cam system at a frequency geared to the motor speed.

[0034] The piston motion causes an increase and decrease in the pressure 110 of a working fluid 112 inside the tank 102, causing an increase and decrease in pressure on the ground 120. These pressure changes cause a seismic P-wave signal to propagate from the source into the ground. The frequency of the generated P-wave may be controlled by controlling the movement of the pistons 106b and 108b. Note that electromagnetic actuators have a larger displacement than conventional piezoelectric units.

[0035] To transform the displacement of the pistons 106b and 108b from a low force into a large force with smaller

displacements, as desired for the present volumetric source, a fluid may be used for coupling, as discussed next. The volumetric source 100, as already noted above, is configured to change one or more dimensions and, thus, its volume when actuated. However, because the tank 102 is made of steel or other similar material, the source 100 cannot accommodate overly large dimensional changes. Thus, it is desirable that displacement of the pistons with low force be transformed into a small displacement with high force to act on the walls 102a of the tank 102.

[0036] According to the exemplary embodiment illustrated in FIG. 2, the piston arrangement 105 is immersed in the working fluid 112 so that the working fluid 112 couples the pistons 106b and 108b to the walls 102a of the tank 102. At the same time, the working fluid also cools the coils 106a and 108a. The back sides of the pistons 106b and 108b form an inner cavity 114. This inner cavity 114 may be configured to trap another fluid 116 (e.g., air). Thus, the back sides of the pistons 106b and 108b work against the fluid 116. In this case, the fluid 116 works to counteract the hydrostatic pressure in the first fluid 112. In other words, the fluid 116 works as a spring. Other volumetric sources exist but are not discussed herein.

[0037] An example of a non-volumetric source is discussed next. FIG. 3A illustrates a non-volumetric source 300 (a similar source is described, for example, in U.S. Pat. No. 7,420, 879 to Meynier et al., the entire content of which is incorporated herein by reference) that includes plural vibrators (electromechanical, electromagnetic, hydraulic, piezoelectric, magnetostrictive, etc.) forming a pillar 301 in contact with plates 302 and 303. A force is applied to the pillar 301 to displace the plates 302 and 303, thereby generating a seismic wave. Because the ground around the source is displaced unsymmetrically, strong S-waves are generated. FIG. 3B schematically illustrates lobes 320 representing the S-waves and waves 330 representing the P-waves. Note that a volume of the source does not necessarily increase when the plates 302 and 303 move apart, contrary to a volumetric source, because the ground between these two plates may move toward the pillar 301.

[0038] Pillar 301, which may be covered with a deformable membrane 304, is connected by a cable 305 to a signal generator 306. Source 300 is placed in a cavity or well W, for example, of 5 to 30 cm in diameter, at a desired depth under the weather zone layer WZ, for example, between 5 and 1000 m. A coupling material 307, such as cement or concrete, is injected into the well to be in direct contact with pillar 301 over the total length thereof and with plates 302 and 303. To allow the coupling material 307 to be homogeneously distributed in the space between plates 302 and 303, the plates may have perforations 308. The diameter of plates 302 and 303 substantially corresponds to the diameter of the cavity or well W so as to achieve maximum coupling surface area.

[0039] The signal generator 306 generates an excitation signal in a frequency sweep or a single frequency, causing elements forming the pillar 301 to expand or contract temporarily along the pillar's longitudinal axis. Metal plates 302 and 303 are mounted on the pillar ends to improve the coupling of pillar 301 with coupling material 307. Coupling material 307 intermediates the coupling between the source and the formation. For example, plates 302 and 303 have a thickness of 10 cm and a diameter of 10 cm. Pillar 301 may have a length exceeding 80 cm. The membrane 304 may be made of polyurethane and surround pillar 301 to decouple it

from the coupling material (cement) 307. Thus, only the end portions of pillar 301 and plates 302 and 303 are coupled with the coupling material (cement) 307. Upon receiving an excitation (electrical signal) from the signal generator 306, source 300 generates forces along the pillar's longitudinal axis. This conventional source provides good repeatability and high reliability, once a good coupling is accomplished.

[0040] A typical pillar has a cylindrical shape with a radius of 5 cm and a length of 95 cm. This pillar may consist of 120 ceramics made, for example, of lead-zirconate-titanate (PZT) known under the commercial name NAVY type I. Each ceramic may have a ring shape with 20 mm internal diameter, 40 mm external diameter and 4 mm thickness. The maximum length expansion obtainable for this pillar in the absence of constraints is 120  $\mu\text{m}$ , corresponding to a volume change of about 1000  $\text{mm}^3$ . The electrical signals fed to the pillars have 5-300 Hz, 2500 V peak maximum and 2 A peak maximum. The numbers presented above are exemplary and those skilled in the art would recognize that various sources have different characteristics. Other non-volumetric sources exist but are not presented herein.

[0041] However, the novel embodiments discussed next apply to any kind of volumetric and non-volumetric sources. According to an exemplary embodiment illustrated in FIG. 4A, a land seismic surveying system 400 includes sources 402a-b and receivers 404i. Sources 402a-b may be located inside a well 406, underground. Source 402a may be volumetric and source 402b may be non-volumetric, as discussed above. In another embodiment, the non-volumetric source is at a greater depth than the volumetric source, i.e., opposite what is shown in FIG. 4A. This arrangement has the advantage that a single well accommodates both sources. FIG. 4B schematically illustrates the P- and S-waves generated by a combination of volumetric and non-volumetric sources 402a-b.

[0042] However, as illustrated in FIG. 5, multiple wells may be dug to accommodate individual sources 402a-b. Receivers 404i are distributed at the surface 410 and/or below the surface. In one exemplary embodiment, the receivers are buried in the ground as discussed with regard to FIG. 4A. Also, the depths of the various sources may change with the survey. In one application, all the sources are buried at the same depth H as illustrated in FIG. 6. In another exemplary embodiment, the volumetric sources 402a are located at a first depth H1, and the non-volumetric sources 402b are located at a second depth H2, different from H1. FIG. 7 illustrates the case when H1 is greater than H2. Note that the sources may be located in a well as shown in FIG. 4A or completely buried underground.

[0043] Returning to FIG. 4A, each source is linked to a corresponding cable 420a and 420b that connects the sources to one or more controllers 430, a controller including a processor 432 and a storage device 434. The processor 432 may be programmed to shoot the sources simultaneously, sequentially, using the slip-sweep technique, or any other known technique. Receivers 404i may be distributed according to various configurations. For example, the receivers may be located above or below the ground. If below ground, they may be located vertically above the sources, between the volumetric and non-volumetric sources, below the sources or based on a combination of these arrangements. In one application, receivers 404i are distributed in another well 407. The depth distribution of the receivers inside this additional well may be similar to that used when the receivers are not placed in the

well. Receivers 404*i* may be linked to a controller 440 that includes a processor 442 and a storage device 444. When in use, the receivers may send the seismic data, through a wireless or wired interface, to the storage device 444 and the processor 442 may be configured to process the data as discussed later. The controller may be located in the field or at a remote location, for example, in a processing center.

[0044] With this mixed arrangement of land seismic sources, an actual seismic survey has been performed and the following results have been obtained. FIG. 8 illustrates traces recorded by the plural receivers using only volumetric sources 402*a*. The number of receivers is represented on the X axis, and the time in seconds is represented on the Y axis. Note that good signals are obtained for the near offset reflections and transmissions 800, but not-so-good signals are obtained for the far offset reflections and transmissions 802. A near offset reflection means a reflected signal recorded by a receiver that is close (near) to the source while a far offset reflection is a trace recorded by a receiver that is far from the source. A near offset transmission means a signal that is transmitted directly from the source to a close by receiver while a far offset transmission is a signal that is transmitted directly from the source to a faraway receiver.

[0045] FIG. 9 illustrates traces recorded with the plural receivers when non-volumetric sources are used. Note that the traces 900 corresponding to the near offset reflections and transmissions are very difficult to separate and process because of the strong S-waves, while the traces 902 corresponding to the far offset reflections and transmissions have better quality than the corresponding traces 802. The traces shown in FIGS. 8 and 9 may be obtained by sequentially shooting volumetric sources and non-volumetric sources. Alternatively, the volumetric and non-volumetric sources may be shot simultaneously in time, but with different frequencies, e.g., using sinusoids to drive the sources. In another embodiment, the sources may be fired simultaneously based on orthogonal signals.

[0046] Thus, according to an exemplary embodiment, traces 800 corresponding to the near offset reflections and transmissions may be extracted from the recordings corresponding to the volumetric source (P-waves) and then subtracted from traces 900 corresponding to the near offset reflections and transmissions corresponding to the non-volumetric source (P- and S-waves). In this way, for the near offset reflections and transmissions (not for the far offset reflections and transmissions), the traces corresponding to the S-waves may be separated. These traces can then be subtracted from traces 900 shown in FIG. 9 to remove the S-waves contribution for the near offset reflections and transmissions, but not for the far offset reflections and transmissions.

[0047] In other words, as schematically illustrated in FIG. 10A, traces recorded with non-volumetric source have good quality (many wiggle lines) for the far offset reflections and transmissions (outside triangle 1000) and low quality (few wiggle lines) for the near offset reflections and transmissions (inside the triangle 1000). The traces recorded with the volumetric source, as illustrated in FIG. 10B, have poor quality for the far offset reflections and transmissions (outside triangle 1000) and good quality for the near offset reflections and transmissions (inside the triangle 1000). Thus, the volumetric data inside the triangle 1000 in FIG. 10B is used to substitute the non-volumetric data inside the triangle 1000 in FIG. 10A and, thus, as illustrated in FIG. 100, good quality traces are obtained for both the near offset reflections and transmissions

(from the volumetric source) and the far offset reflections and transmissions (from the non-volumetric source). Note that far offset reflections and transmissions from both volumetric and non-volumetric data may be added together to enhance this portion of data as illustrated in FIG. 100.

[0048] Thus, as illustrated in FIG. 11, a method for combining traces related to a surveyed subsurface for enhancing clarity of the subsurface includes a step 1100 of receiving first traces corresponding to a volumetric source; a step 1102 of receiving second traces corresponding to a non-volumetric source, wherein the first and second traces correspond to the surveyed subsurface; a step 1104 of extracting from the first traces, third traces that correspond to near offset reflections and transmissions and the third traces contain substantially P-waves; a step 1106 of replacing with the third traces, in the second traces, fourth traces that correspond to the near offset reflections and transmissions, wherein the fourth traces include both P- and S-waves; and a step 1108 of using the obtained combination of second traces and third traces to generate a final image of the subsurface.

[0049] According to another exemplary embodiment illustrated in FIG. 12, there is a method for conducting a surveying a subsurface. The method includes a step 1200 of deploying plural receivers; a step 1202 of burying a volumetric source underground; a step 1204 of burying a non-volumetric source underground; a step 1206 of shooting the volumetric and non-volumetric sources; and a step 1208 of combining first traces corresponding to the volumetric source with second traces corresponding to the non-volumetric source to generate a final image of the subsurface. The step 1208 may include a step 1210 of extracting first traces corresponding to the volumetric source; a step 1212 of extracting second traces corresponding to the non-volumetric source, wherein the first and second traces correspond to the surveyed subsurface; a step 1214 of extracting from the first traces, third traces that correspond to near offset reflections and transmissions and the third traces contain substantially P-waves; and a step 1216 of replacing with the third traces, in the second traces, fourth traces that correspond to the near offset reflections and transmissions, wherein the fourth traces include both P- and S-waves.

[0050] The disclosed exemplary embodiments provide volumetric and non-volumetric seismic sources and related methods for generating seismic waves in a formation. It should be understood that this description is not intended to limit the invention. On the contrary, the exemplary embodiments are intended to cover alternatives, modifications and equivalents, which are included in the spirit and scope of the invention as defined by the appended claims. Further, in the detailed description of the exemplary embodiments, numerous specific details are set forth in order to provide a comprehensive understanding of the claimed invention. However, one skilled in the art would understand that various embodiments may be practiced without such specific details.

[0051] Although the features and elements of the present exemplary embodiments are described in the embodiments in particular combinations, each feature or element can be used alone without the other features and elements of the embodiments or in various combinations with or without other features and elements disclosed herein.

[0052] This written description uses examples of the subject matter disclosed to enable any person skilled in the art to practice the same, including making and using any devices or systems and performing any incorporated methods. The pat-

entable scope of the subject matter is defined by the claims, and may include other examples that occur to those skilled in the art. Such other examples are intended to be within the scope of the claims.

What is claimed is:

1. A seismic survey system for surveying a subsurface, the system comprising:

a volumetric land source buried underground for generating P-waves;

a non-volumetric land source buried underground for generating P- and S-waves;

plural receivers distributed about the volumetric and non-volumetric land sources and configured to record seismic signals corresponding to the P- and S-waves; and  
a controller connected to the volumetric land source and the non-volumetric land source and configured to shot them in a given pattern.

2. The system of claim 1, wherein the volumetric land source is spherical.

3. The system of claim 1, wherein the volumetric land source is buried in a well below the non-volumetric land source.

4. The system of claim 1, wherein the volumetric land source includes plural individual volumetric sources and the non-volumetric land source includes plural individual non-volumetric sources.

5. The system of claim 4, wherein the plural individual volumetric sources are buried a first depth H1 and the plural individual non-volumetric sources are buried at a second depth H2.

6. The system of claim 5, wherein the first depth H1 is larger than the second depth H2.

7. The system of claim 5, wherein the first depth H1 is smaller than the second depth H2.

8. The system of claim 5, wherein the first depth H1 is equal to the second depth H2.

9. The system of claim 1, wherein the given pattern includes shooting the volumetric and the non-volumetric sources sequentially or simultaneously.

10. The system of claim 9, further comprising:

a memory device for storing traces recorded by the plural receivers; and

a processor connected to the memory device and configured to combine traces corresponding to the volumetric source with traces corresponding to the non-volumetric source.

11. The system of claim 10, wherein the processor is further configured to:

separate first traces corresponding to the volumetric source from second traces corresponding to the non-volumetric source;

extracting from the first traces third traces that correspond to near offset reflections and transmissions and contain substantially P-waves;

replacing with the third traces, in the second traces, fourth traces that correspond to the near offset reflections and transmissions; and

using the obtained combination of second traces and third traces to generate a final image of the subsurface.

12. A method for combining traces related to a surveyed subsurface for enhancing clarity of the subsurface, the method comprising:

receiving first traces corresponding to a volumetric source; receiving second traces corresponding to a non-volumetric source, wherein the first and second traces correspond to the surveyed subsurface;

extracting from the first traces, third traces that correspond to near offset reflections and transmissions and the third traces contain substantially P-waves;

replacing with the third traces, in the second traces, fourth traces that correspond to the near offset reflections and transmissions, wherein the fourth traces include both P- and S-waves; and

using the obtained combination of second traces and third traces to generate a final image of the subsurface.

13. The method of claim 12, wherein the first traces have better signal quality for the near offset reflections and transmissions than for the far offset reflections and transmissions.

14. The method of claim 12, wherein the second traces have better signal quality for the far offset reflections than for the near offset reflections.

15. The method of claim 12, wherein the volumetric source generates substantially all energy as P-waves while the non-volumetric source generates both P- and S-waves.

16. A method for conducting a surveying of a subsurface, the method comprising:

deploying plural receivers;

burying a volumetric source underground;

burying a non-volumetric source underground;

shooting the volumetric and non-volumetric sources; and combining first traces corresponding to the volumetric source with second traces corresponding to the non-volumetric source to generate a final image of the subsurface.

17. The method of claim 16, wherein the volumetric source generates substantially all energy as P-waves while the non-volumetric source generates both P- and S-waves.

18. The method of claim 16, wherein the step of shooting comprises:

shooting the volumetric and non-volumetric sources sequentially.

19. The method of claim 16, wherein the step of shooting comprises:

shooting the volumetric and non-volumetric sources simultaneously but with different frequencies or with orthogonal signals.

20. The method of claim 16, wherein the step of combining comprises:

extracting first traces corresponding to the volumetric source;

extracting second traces corresponding to the non-volumetric source, wherein the first and second traces correspond to the surveyed subsurface;

extracting from the first traces, third traces that correspond to near offset reflections and transmissions and the third traces contain substantially P-waves; and

replacing with the third traces, in the second traces, fourth traces that correspond to the near offset reflections and transmissions, wherein the fourth traces include both P- and S-waves.

# Appendix 8

Methods and systems for monitoring a subsurface formation with a land active streamer

Cotton, J. and F-X. Grésillon, 2017

United States patent application publication





US 20170075016A1

(19) **United States**

(12) **Patent Application Publication**  
**COTTON et al.**

(10) **Pub. No.: US 2017/0075016 A1**  
(43) **Pub. Date: Mar. 16, 2017**

(54) **METHODS AND SYSTEMS FOR MONITORING A SUBSURFACE FORMATION WITH A LAND ACTIVE STREAMER**

**Publication Classification**

(71) Applicant: **CGG SERVICES SA, MASSY (FR)**

(51) **Int. Cl.**  
**G01V 1/52** (2006.01)  
**G01V 1/02** (2006.01)

(72) Inventors: **Julien COTTON, Paris (FR); François-Xavier GRÉSILLON, Rully (FR)**

(52) **U.S. Cl.**  
CPC ..... **G01V 1/52** (2013.01); **G01V 1/159** (2013.01)

(73) Assignee: **CGG Services SA, Massy (FR)**

(21) Appl. No.: **15/120,205**

(57) **ABSTRACT**

(22) PCT Filed: **Feb. 23, 2015**

(86) PCT No.: **PCT/IB2015/000491**

§ 371 (c)(1),

(2) Date: **Aug. 19, 2016**

**Related U.S. Application Data**

(60) Provisional application No. 61/943,890, filed on Feb. 24, 2014.

The present disclosure includes a method for monitoring a subsurface formation including disposing an antenna in a horizontal wellbore, the antenna including a plurality of piezoelectric modules. A voltage signal is applied to at least one of the piezoelectric modules to cause the at least one piezoelectric modules to emit seismic energy into the subsurface formation. A resulting signal is received at a receiver. A property of the subsurface formation is determined based, at least in part, on the resulting signal.

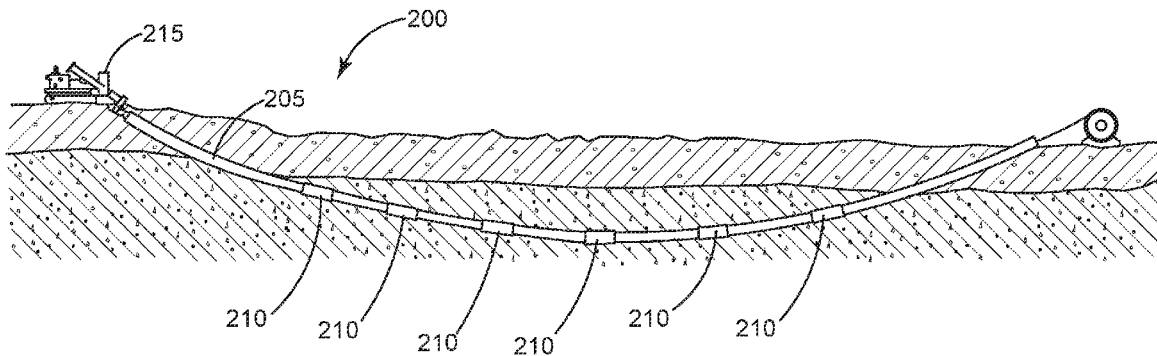


FIG. 1

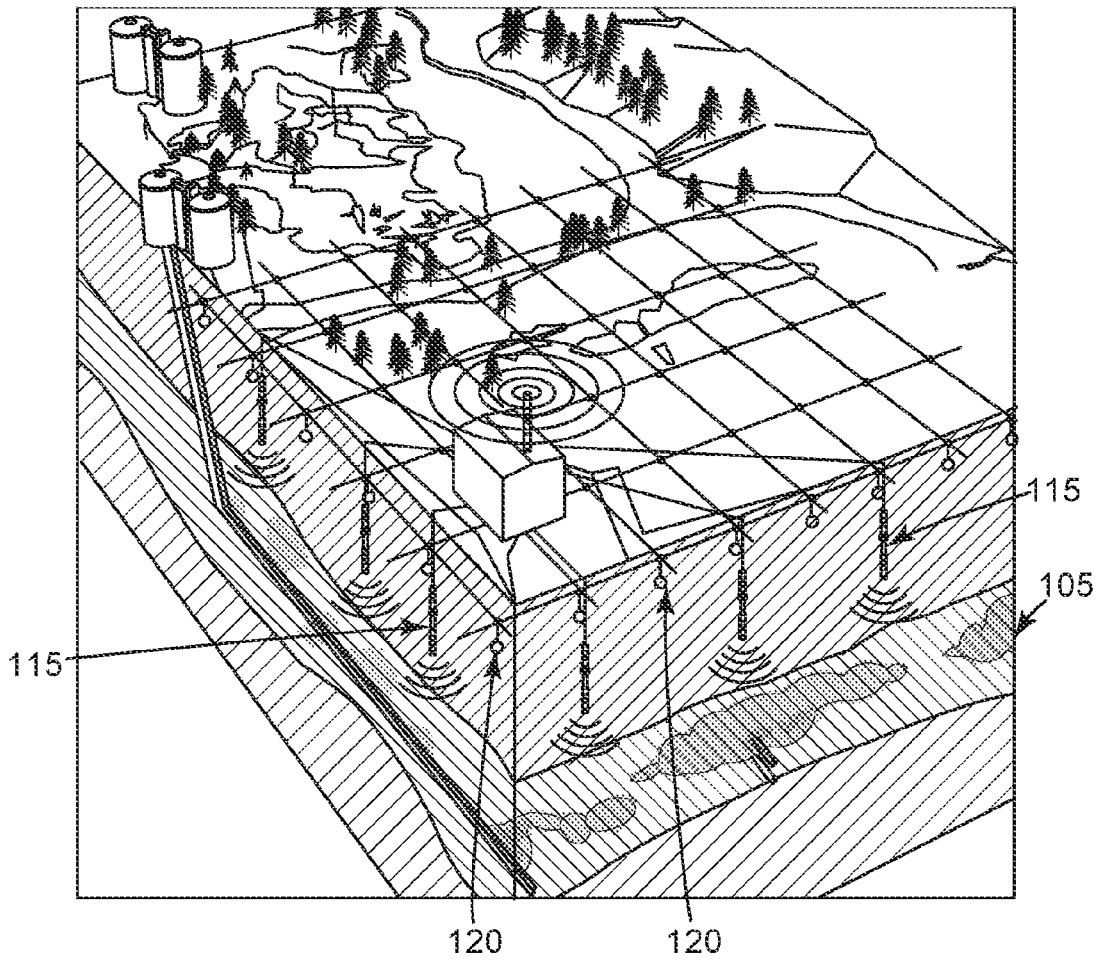


FIG. 2

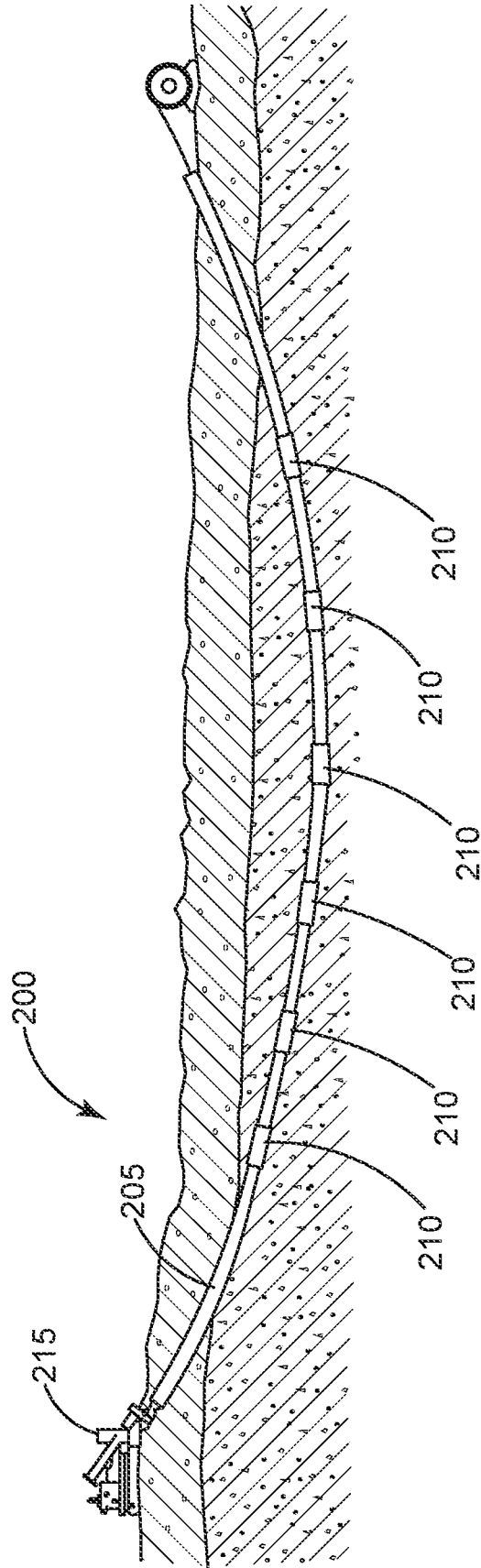


FIG. 3

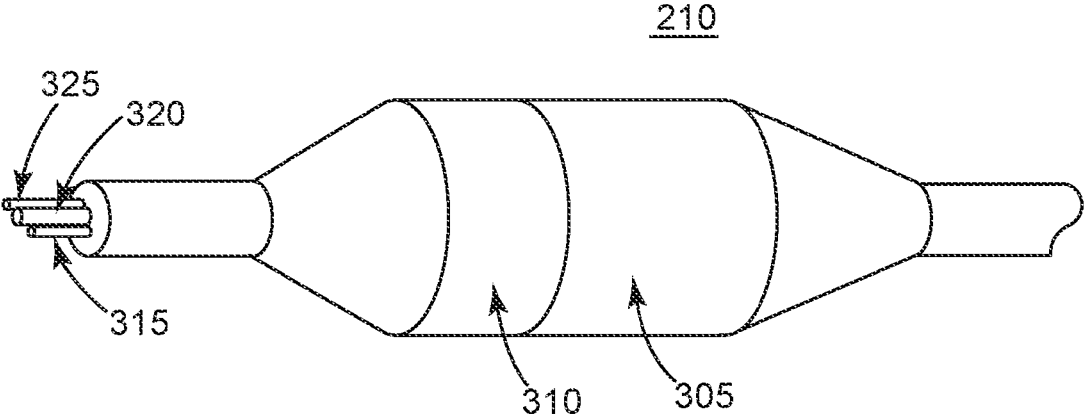


FIG. 4

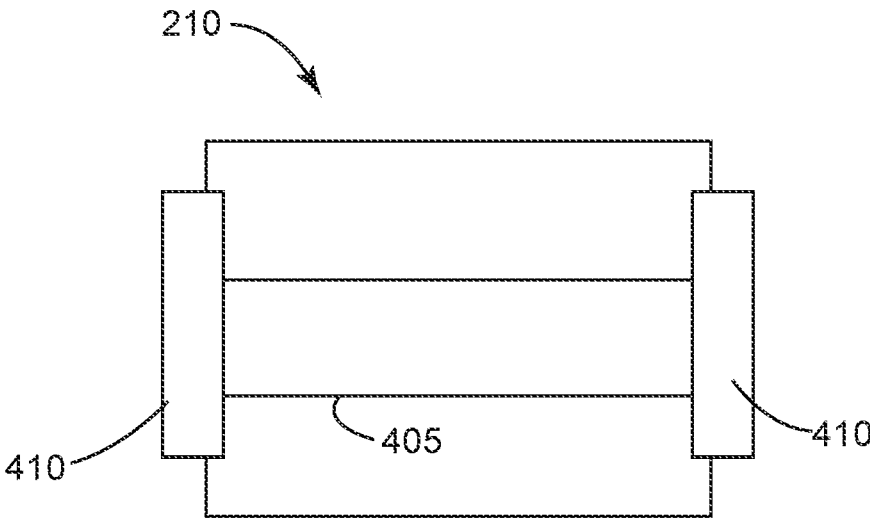
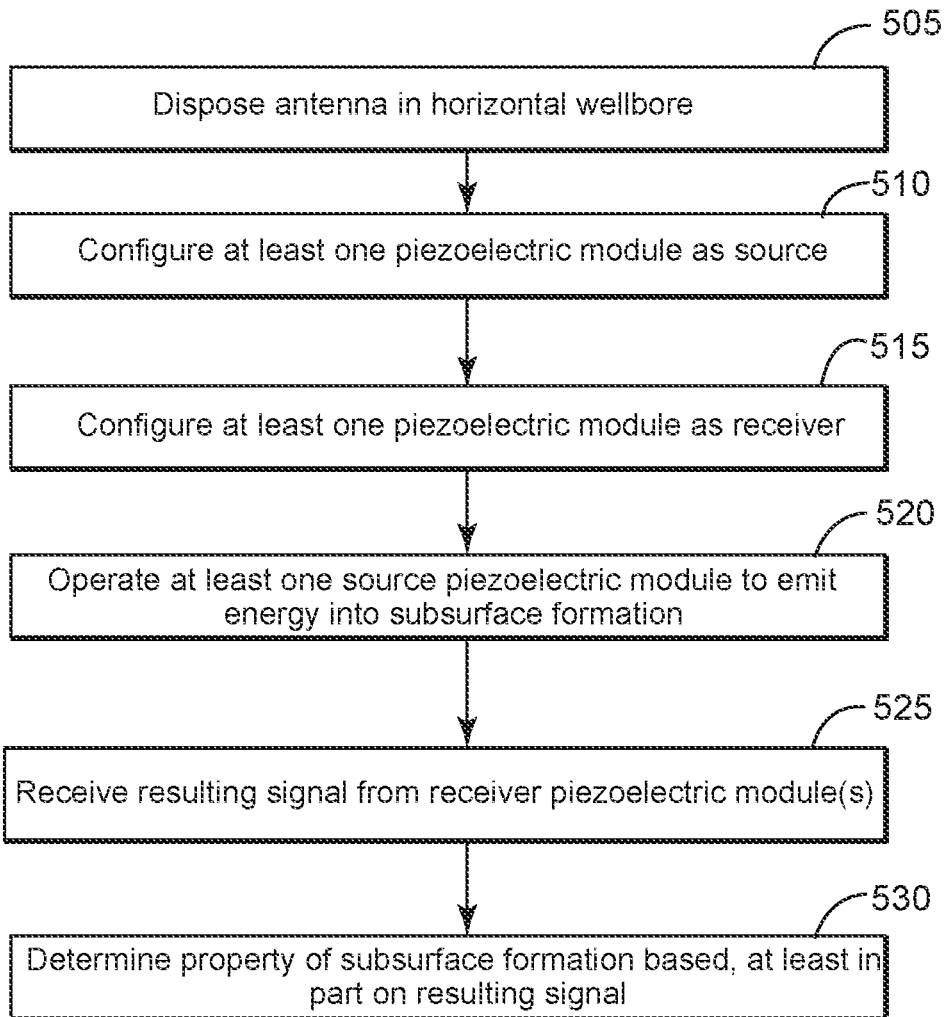


FIG. 5



## METHODS AND SYSTEMS FOR MONITORING A SUBSURFACE FORMATION WITH A LAND ACTIVE STREAMER

### CROSS-REFERENCE TO RELATED APPLICATION

[0001] The present application claims the benefit of priority under 35 U.S.C. §119 from U.S. Provisional Patent Application Ser. No. 61/943,890, filed on Feb. 24, 2014, which is incorporated by reference in its entirety for all purposes.

### TECHNICAL FIELD OF THE DISCLOSURE

[0002] This disclosure relates generally to monitoring subsurface formations, and in particular, to methods and systems of piezoelectric modules disposed in horizontal wells for monitoring subsurface formations.

### BACKGROUND

[0003] Land-based seismic data acquisition and processing techniques are used to generate an image of a geological structure in a subsurface formation. FIG. 1 shows a conventional system for monitoring characteristics of a subsurface formation 105. Conventional systems and methods for monitoring characteristics of a subsurface formation 105 typically include drilling multiple vertical wells 110. Seismic sources 115 are placed into one or more of the vertical wells 110 and seismic receivers 120 are placed into one or more of the vertical wells 110. Wells 110 that contain seismic sources 115 may be referred to as source wells. Wells 110 that contain seismic receivers 120 may be referred to as monitoring wells. Typically, seismic sources 115 and seismic receivers 120 are installed near the surface to reduce installation costs.

[0004] Conventional monitoring systems including a network of buried sensors in vertical wells 110 have been used to monitor steam injection in shallow reservoirs, typically between 200 to 1000 meters. Conventional monitoring systems have proven less useful for deeper reservoirs. For example, a deeper reservoir may be located at a depth of around 2,000 meters. Conventional monitoring systems may be hampered by hard formations, which mitigate the seismic response. Likewise, conventional systems that are near surface are less efficient for complex geology. For example, very hard lithographic layers (e.g., anhydrite-type lithography) or inhomogeneous layers diffract seismic energy before it can reach a reservoir being monitored.

[0005] Another limitation of conventional monitoring systems is the cost and environmental impact of drilling multiple vertical wells 110. For example, the installation of equipment (such as seismic sources 115 and seismic receiver 120) in tens, hundreds, or more vertical wells 110 can generate permitting issues or, such installation may be forbidden in environmentally fragile areas or in urban areas. What is needed therefore are methods and systems for locating seismic sources and seismic receivers closer to the reservoir and/or decreasing the numbers of holes. What is further needed is a high density of these seismic sources and seismic receivers near the area of interest.

### SUMMARY

[0006] In one embodiment, the present disclosure may include a method for monitoring a subsurface formation

including disposing an antenna in a horizontal wellbore. The antenna includes a plurality of piezoelectric modules. The method further includes applying a voltage signal to at least one of the piezoelectric modules to cause the at least one piezoelectric modules to emit seismic energy into the subsurface formation. The method further includes receiving a resulting signal at one or more seismic receivers. The method further includes determining a property of the subsurface formation based, at least in part, on the resulting signal.

[0007] In another embodiment, the present disclosure may include a system for monitoring a subsurface formation. The system includes an antenna configured to be disposed in a horizontal wellbore, the antenna including a plurality of piezoelectric modules. At least one of the piezoelectric modules is selectively configurable as a seismic source and one or more of the piezoelectric modules are selectively configurable as seismic receivers.

[0008] In another embodiment, the present disclosure may include a system for monitoring a subsurface formation. The system includes an antenna in a horizontal wellbore, the antenna including a plurality of piezoelectric modules. The system includes at least one processor and a memory including non-transitory computer-readable executable instructions. The executable instructions cause the at least one processor to cause at least one of the piezoelectric modules to selective emit seismic energy into the subsurface formation. The executable instructions cause the at least one processor to receive a resulting signal at one or more seismic receivers. The executable instructions cause the at least one processor to determine a property of the subsurface formation based, at least in part, on the resulting signal.

### BRIEF DESCRIPTION OF THE DRAWINGS

[0009] For a more complete understanding of the present disclosure and its features, reference is now made to the following description, taken in conjunction with the accompanying drawings, in which like reference numbers indicate like features and wherein:

[0010] FIG. 1 illustrates an example land-based system for monitoring a subsurface formation;

[0011] FIG. 2 illustrates an example land-based system with equipment installed in horizontal boreholes for monitoring a subsurface formation;

[0012] FIG. 3 illustrates an example piezoelectric module;

[0013] FIG. 4 is an example piezoelectric module in accordance with some embodiments of the present disclosure; and

[0014] FIG. 5 is a flow chart of an example method of monitoring a subsurface formation, in accordance with some embodiments of the present disclosure.

### DETAILED DESCRIPTION

[0015] FIG. 2 shows an example land-based system for monitoring a subsurface formation according to the present disclosure. An antenna according to the present disclosure is shown generally at 200. Although described herein as land-based, the systems and methods of the present disclosure are equally applicable to use at the floor of a body of water. The antenna 200 is disposed in a horizontal wellbore. The wellbore may be located above or near a subsurface formation of interest. In one example embodiment, the antenna 200 is disposed in a horizontal wellbore above one or more

portions of a reservoir for monitoring. In some example embodiments, the horizontal wellbore is drilled to a depth that is deeper than typical vertical wells. In other example embodiments, the horizontal wellbore is drilled to a depth that is shallower than a typical vertical well. In some example embodiments, the horizontal well is placed close to the subsurface that is being monitored. The example antenna 200 includes cabling 205 to draw the antenna into the horizontal wellbore. In some example embodiments, the cable 205 includes a cable that is used to place the antenna into the borehole. In certain example embodiments, the cable 205 includes a steel cable. In other example embodiments, the cable 205 includes a chain. In certain example embodiments, the cable 205 includes a cable or rope made from a material that has a high tensile strength. Example materials include steel, Kevlar, or aramid fibers. In some example implementations, cabling 205 includes at least one high-voltage lines to pilot the piezoelectric modules. The example antenna 200 may further include low voltage cables to operate switches for the piezoelectric modules 210. The following description of the exemplary embodiments refers to the accompanying drawings. The same reference numbers in different drawings identify the same or similar elements. The following detailed description does not limit the invention. Instead, the scope of the invention is defined by the appended claims. Some of the following embodiments are discussed, for simplicity, with regard to the terminology and structure of sensors including a plurality of piezoelectric modules that are disposed in a horizontal well. The embodiments, however, are not limited to these configurations, and may be extended to other arrangements.

**[0016]** Reference throughout the specification to “one embodiment” or “an embodiment” means that a particular feature, structure or characteristic described in connection with an embodiment is included in at least one embodiment of the subject matter disclosed. Thus, the appearance of the phrases “in one embodiment” or “in an embodiment” in various places throughout the specification is not necessarily referring to the same embodiment. Further, the particular features, structures or characteristics may be combined in any suitable manner in one or more embodiments.

**[0017]** As used herein, a horizontal wellbore is not limited to a wellbore that runs parallel to the surface of the earth. Instead, a horizontal wellbore is one that includes a segment that deviates from vertical. Example horizontal wellbores according to the present disclosure include two or more segments with different deviations from vertical. Example horizontal wellbores according to the present disclosure include a vertical segment that is connected to a deviated segment of wellbore.

**[0018]** The antenna 200 may comprise a plurality of piezoelectric modules 210. In certain example embodiments, one or more piezoelectric modules 210 are configured as acoustic sensors. In certain example embodiments, one or more piezoelectric modules 210 are configured as acoustic sources. In one example embodiment, a single piezoelectric module 210 is configured as an acoustic source and the remaining piezoelectric modules 210 are configured as acoustic sensors. In one example embodiment, two piezoelectric modules 210 are configured as an acoustic source and the remaining piezoelectric modules 210 are configured as acoustic sensors. In one example embodiment, all of the piezoelectric modules 210 are configured as acoustic sources. In one example embodiment, all of the piezoelectric

modules 210 are configured as acoustic receivers. In certain example embodiments, one or more piezoelectric modules 210 are used as seismic sources in a system with one or more conventional seismic receivers, such as geophones, hydrophones, or accelerometers. In certain example embodiments one or more the piezoelectric modules 210 further include switches to change the module of the piezoelectric modules 210 between active (e.g., mode where the piezoelectric module 210 acts as a source) to passive (e.g., mode where the piezoelectric module 210 acts as a receiver). In certain example embodiments, the piezoelectric modules 210 are selectively reconfigurable to act as a source or a receiver. In certain example embodiments, the piezoelectric modules 210 have a solid structure and are not fluid-filled. An antenna 200 with solid piezoelectric modules 210 may be used in a borehole that is not fluid-filled.

**[0019]** In some example embodiments, the antenna 200 is connected with a control system 215. In some example embodiments, the control system 215 controls the operation of antenna 200. In some example embodiments, the control system 215 receives data from the antenna 200 to monitor the subsurface formation.

**[0020]** FIG. 3 shows an example piezoelectric module 210. The piezoelectric module 210 includes a ceramic piezoelectric module 305. The module 305 shown in FIG. 3 is shown as a cylinder. Other example embodiments include a spherical or nearly-spherical piezoelectric module 305. Other example piezoelectric modules 305 include a pillar, which may be formed by a stack of ceramic rings. In certain example embodiments, other piezoelectric modules 305 are a pillar with plates on either end that may be connected to each other. The piezoelectric modules 305 may include piezoelectric materials configured as segmented rings, as a striped cylinder, as a slotted cylinder, or as a bender-type of piezoelectric element.

**[0021]** Certain example piezoelectric modules 305 are configured to produce a seismic signal when voltage signal is applied to the piezoelectric module 305. Other example piezoelectric modules 305 are configured to produce an electric signal in response to the presence of an acoustic wave. In certain example embodiments, one or more others piezoelectric modules 305 are configured to receive acoustic waves. In certain example embodiments, one or more others piezoelectric modules 305 are configured to transmit acoustic waves.

**[0022]** In certain example implementations, the size and shape of the ceramic piezoelectric module 305 are based on the dimensions of the wellbore where the antenna 200 will be placed. In some example implementations, the geometry of the ceramic piezoelectric module 305 is optimized for the borehole. In some implementations, the size of the piezoelectric modules 305 is based on a desired sensitivity of a receiver or desired power of a source. In general, larger piezoelectric modules 305 are more sensitive than smaller piezoelectric modules 305.

**[0023]** In certain example embodiments, the system may include one or more seismic receivers other than piezoelectric modules 305 that are configured as seismic receiver. Example systems include one or more hydrophones, geophones, accelerometers, or other seismic receivers. Seismic receivers may be located on, buried beneath, or proximate to surface of the earth within an exploration area. In general, seismic receivers may be any type of instrument that is operable to transform seismic energy or vibrations into a

signal compatible with the data acquisition system, for example a voltage signal, a current signal, or an optical signal. For example, seismic receivers may be a vertical, horizontal, or multicomponent geophone, accelerometers, or optical fiber or distributed acoustic sensor (DAS) with wire or wireless data transmission, such as a three component (3C) geophone, a 3C accelerometer, hydrophone, or a 3C Digital Sensor Unit (DSU). Multiple seismic receivers may be utilized within an exploration or monitoring area to provide data related to multiple locations and distances from seismic sources. In certain example embodiments, the seismic receivers include one or more disturbed acoustic sensors. In other example embodiments, the seismic receivers include one or more optical fiber sensors. Seismic receivers may be positioned in multiple configurations, such as linear, grid, array, or any other suitable configuration. In some embodiments, seismic receivers are positioned along one or more strings.

[0024] Example piezoelectric modules 210 may further include an electronics module 310. Example electronics modules 310 include a digitizer to convert an analog signal from the piezoelectric module 305 to a digital signal for transmission to the control system 215. Example electronics modules 310 include one or more processors and memory for performing one or more signal processing operations or storing measurements. Example electronics modules 310 include a transmitter or other networking capability to communicate with the control system 215 at the surface or with one or more other piezoelectric modules 210. Example electronics modules 310 include a switching element to selectively configure the piezoelectric module 305 either as a source or as a sensor. Example switching elements are controlled by, for example, the control system 215. Other example switching elements are automated according to a programmed pattern. In some example embodiments, the mode of the piezoelectric modules 210 may be switched before the piezoelectric modules 210 are disposed in the borehole. In other example embodiments, the mode of the piezoelectric modules 210 may be switched after piezoelectric modules 210 are disposed in the borehole.

[0025] The piezoelectric modules 210 are connected with one or more high voltage cables 315 for controlling the operation of active piezoelectric modules 210. In certain embodiments, the high voltage cables 315 allows for control of active piezoelectric modules 210 at the surface, for example, by a control system 215. The piezoelectric modules 210 are connected with a communications cable 320 for transmitting and receiving data. Example communications cables are copper or optical fiber. The piezoelectric modules 210 are attached to a cable 325 to permit recovery of the antenna 200. One example cable 325 is a steel cable.

[0026] In certain example embodiments, two or more piezoelectric modules 210 are configured as sources to perform multi-source acquisition. In certain example embodiments, one piezoelectric module 210 is configured as a source to perform single-source acquisition. In certain example implementations, for piezoelectric modules 210 that are configured as sources, a series of signals are applied to the piezoelectric modules 210 to cause the piezoelectric modules 210 to output multi-source emissions. Example multi-source emissions may include one or more monofrequency emissions or one or more frequency sweeps. In some example implementations, the frequency sweep is controlled by the control system 215. The output from the control

system 215 is amplified by an amplifier before being output by the piezoelectric modules 210 that have been configured as sources. In other example implementations, the frequency sweep is controlled by one or more electronics modules. In some example embodiments, two or more of the piezoelectric modules 210 are operated as sources to filter or focus a resulting signal.

[0027] In addition to antenna 200, some example implementations also use one or more geophones located on the Earth or in subsurface formations as part of the monitoring of the subsurface formation. Signals from the geophones may be sent to the control system 215. In addition to antenna 210, some example implementations also use one or more accelerometers located on the Earth or in subsurface formations as part of the monitoring of the subsurface formation. Signals from the accelerometers may be sent to the control system 215. Some example implementations also use one or more hydrophones located on the Earth or in subsurface formations as part of the monitoring of the subsurface formation. Signals from the hydrophones may be sent to the control system 215.

[0028] One or more seismic receivers, such as one or more piezoelectric modules 305 that are configured as receivers, transmit seismic data from reflected seismic energy via a network to control system 215. In certain embodiments, the transmission from the seismic receivers to the control system 215 is by a network. The control system 215 may perform seismic data processing on the seismic data to prepare the data for interpretation. For example, control system 215 may perform the data processing techniques described in FIG. 5. Control system 215 may include any equipment or combination of equipment operable to compute, classify, process, transmit, receive, store, display, record, or utilize any form of information, intelligence, or data. Control system 215 may include one or more personal computers, storage devices, servers, or any other suitable device and may vary in size, shape, performance, functionality, and price. Example embodiments of control system 215 include random access memory (RAM), one or more processing resources, such as a central processing unit (CPU) or hardware or software control logic, or other types of volatile or non-volatile memory. Additional components of control system 215 include one or more disk drives, one or more network ports for communicating with external devices, and one or more input/output (I/O) devices, such as a keyboard, a mouse, or a video display. Control system 215 may be located in a station truck or any other suitable enclosure.

[0029] Example control systems 215 may include one or more amplifiers to provide a signal to seismic sources, such as one or more piezoelectric modules 210 that are configured to be seismic sources. Example control systems 215 may include one or more digitizers to convert signals from seismic receivers to corresponding values for further analysis by the control systems 215.

[0030] As shown in FIG. 4, an example piezoelectric module 210 includes a pillar source 405, which may be formed by the stacking of ceramic rings and plates 410 on either end of the pillar source. In some example implementations, the plates 410 are connected.

[0031] FIG. 5 is a flow chart of an example method of the present disclosure. Example embodiments may omit one or more of blocks 505-530. Other example embodiments include additional steps. Other example embodiments per-

form one or more of block 505-304 in an alternative order. In block 505, the antenna 200 is disposed in a horizontal wellbore. In some example embodiments, the wellbore is drilled in the Earth along a path for monitoring of a subsurface formation of interest. In block 510, at least one of the piezoelectric modules 210 is configured as a seismic source. In some example embodiments, this configuration is done at the surface before the antenna 200 is disposed in the wellbore. In other example embodiments, the configuration is performed by the control system 215 sending a signal to electronics modules 310 in one or more piezoelectric modules 210 to selectively configure the piezoelectric module 210 as a source.

[0032] In block 515, at least one of the piezoelectric modules 210 is configured as a receiver. In some example embodiments, this configuration is done at the surface before the antenna 200 is disposed in the wellbore. In other example embodiments, the configuration is performed by the control system 215 sending a signal to electronics modules 310 in one or more piezoelectric modules 210 to selectively configure the piezoelectric module 210 as a receiver.

[0033] In block 520, a high voltage signal is applied to piezoelectric modules 210 that are configured as sources causing acoustic energy to be emitted into the subsurface formation. In block 525, the resulting signal is received at piezoelectric modules 210 that are configured as receivers. In other example embodiments, the resulting signal is received by one or more geophones, hydrophones, or other receivers. In block 430, the control system 215 determines at least one property of the subsurface formation based, at least in part, on the received resulting signal. For example, the control system 215 may determine the depletion of a reservoir. In other embodiments, the control system 215 determines the progression of a work-over operation. In other embodiments, the control system 215 monitors steam injection into a subsurface formation.

[0034] Herein, “or” is inclusive and not exclusive, unless expressly indicated otherwise or indicated otherwise by context. Therefore, herein, “A or B” means “A, B, or both,” unless expressly indicated otherwise or indicated otherwise by context. Moreover, “and” is both joint and several, unless expressly indicated otherwise or indicated otherwise by context. Therefore, herein, “A and B” means “A and B, jointly or severally,” unless expressly indicated otherwise or indicated otherwise by context.

[0035] This disclosure encompasses all changes, substitutions, variations, alterations, and modifications to the example embodiments herein that a person having ordinary skill in the art would comprehend. Similarly, where appropriate, the appended claims encompass all changes, substitutions, variations, alterations, and modifications to the example embodiments herein that a person having ordinary skill in the art would comprehend. Moreover, reference in the appended claims to an apparatus or system or a component of an apparatus or system being adapted to, arranged to, capable of, configured to, enabled to, operable to, or operative to perform a particular function encompasses that apparatus, system, component, whether or not it or that particular function is activated, turned on, or unlocked, as long as that apparatus, system, or component is so adapted, arranged, capable, configured, enabled, operable, or operative.

[0036] Any of the steps, operations, or processes described herein may be performed or implemented with one or more hardware or software modules, alone or in combination with other devices. In one embodiment, a software module is implemented with a computer program product comprising a computer-readable medium containing computer program code, which can be executed by a computer processor for performing any or all of the steps, operations, or processes described.

[0037] Embodiments of the invention may also relate to an apparatus for performing the operations herein. This apparatus may be specially constructed for the required purposes, and/or it may comprise a general-purpose computing device selectively activated or reconfigured by a computer program stored in the computer. Such a computer program may be stored in a tangible computer readable storage medium or any type of media suitable for storing electronic instructions, and coupled to a computer system bus. Furthermore, any computing systems referred to in the specification may include a single processor or may be architectures employing multiple processor designs for increased computing capability.

[0038] Although the present invention has been described with several embodiments, a myriad of changes, variations, alterations, transformations, and modifications may be suggested to one skilled in the art, and it is intended that the present invention encompass such changes, variations, alterations, transformations, and modifications as fall within the scope of the appended claims. Moreover, while the present disclosure has been described with respect to various embodiments, it is fully expected that the teachings of the present disclosure may be combined in a single embodiment as appropriate.

1. A method for monitoring a subsurface formation comprising:

- disposing an antenna in a horizontal wellbore, the antenna including a plurality of piezoelectric modules;
- applying a voltage signal to at least one of the piezoelectric modules to cause the at least one piezoelectric modules to emit seismic energy into the subsurface formation;
- receiving a resulting signal at one or more seismic receivers; and
- determining a property of the subsurface formation based, at least in part, on the resulting signal.

2. The method of claim 1, wherein at least one of the piezoelectric modules is configured as a source and one or more of the piezoelectric modules are configured as receivers.

3. The method of claim 1, wherein the one or more receivers include one or more other piezoelectric modules that are selective configured as seismic receivers.

4. The method of claim 1, wherein the one or more receivers include one or more one or more geophones, one or more accelerometers, or one or more hydrophones.

5. The method of claim 1, wherein one or more of the piezoelectric modules are solid.

6. The method of claim 1, wherein one or more piezoelectric modules includes a piezoelectric ceramic pillar.

7. The method of claim 1, wherein one or more piezoelectric modules further includes a digitizer to convert a received resulting signal to a digital signal for transmission to a computer system.

8. The method of claim 1, wherein one or more piezoelectric modules further includes a switching module to selectively configure the piezoelectric module as a seismic source or as a seismic receiver.

9. The method of claim 1, wherein at least two of the piezoelectric modules are configured as a seismic sources and one or more of the piezoelectric modules are configured as seismic receivers.

10. The method of claim 1, wherein the piezoelectric modules are configured as seismic sources.

11. The method of claim 1, wherein one or more of the one of the piezoelectric modules include a switch for selective configuring the piezoelectric module as a seismic source or a seismic receiver.

12. A system for monitoring a subsurface formation comprising:

an antenna configured to be disposed in a horizontal wellbore, the antenna including a plurality of piezoelectric modules;

wherein at least one of the piezoelectric modules is selectively configurable as a seismic source and one or more of the piezoelectric modules are selectively configurable as seismic receivers.

13. The system of claim 12, wherein one or more piezoelectric modules further comprises a digitizer to convert a received resulting signal to a digital signal for transmission to a computer system.

14. The system of claim 12, further comprising:  
an amplifier to amplify a signal from a control system to at least one of the piezoelectric modules.

15. The system of claim 12, further comprising:  
a control system, comprising a memory and at least one processor, the memory including non-transitory executable instruction that, when executed, cause the least one processor to determine a property of the subsurface formation based, at least in part, on the resulting signal.

16. A system for monitoring a subsurface formation:  
an antenna in a horizontal wellbore, the antenna including a plurality of piezoelectric modules;  
at least one processor; and  
a memory including non-transitory computer-readable executable instructions, wherein the executable instructions cause the at least one processor to:

cause at least one of the piezoelectric modules to selective emit seismic energy into the subsurface formation;

receive a resulting signal at one or more seismic receivers; and

determine a property of the subsurface formation based, at least in part, on the resulting signal.

17. The system of claim 16, wherein the executable instructions further cause the at least one processor to:

cause at least one of the piezoelectric modules to selectively receive the resulting seismic signal.

18. The system of claim 16, wherein the seismic receivers include one or more piezoelectric modules that are selectively configured as seismic receivers.

19. The system of claim 16, wherein the seismic receivers include one or more hydrophones, one or more geophones, and one or more accelerometers.

20. The system of claim 16, wherein one or more of the piezoelectric modules are solid.

\* \* \* \* \*



# Appendix 9

Seismic migration using an indexed matrix

Cotton, J. and E. Forgues, 2017

United States patent application publication





US 20170242141A1

(19) **United States**

(12) **Patent Application Publication**  
**COTTON et al.**

(10) **Pub. No.: US 2017/0242141 A1**

(43) **Pub. Date: Aug. 24, 2017**

(54) **SEISMIC MIGRATION USING AN INDEXED MATRIX**

**Publication Classification**

(71) Applicant: **CGG SERVICES SAS**, Massy Cedex (FR)

(51) **Int. Cl.**  
**G01V 1/30** (2006.01)  
**G01V 1/28** (2006.01)  
**G01V 1/36** (2006.01)

(72) Inventors: **Julien COTTON**, Paris (FR); **Eric FORGUES**, Bures-sur-Yvette (FR)

(52) **U.S. Cl.**  
CPC ..... **G01V 1/30** (2013.01); **G01V 1/36** (2013.01); **G01V 1/282** (2013.01); **G01V 2210/51** (2013.01)

(21) Appl. No.: **15/503,773**

(57) **ABSTRACT**

(22) PCT Filed: **Sep. 8, 2015**

Systems and methods for performing seismic migration using an indexed matrix are disclosed. The method includes receiving a seismic trace from a receiver, determining a discretized position of the receiver, and determining a discretized position of a seismic source. The method also includes determining a set of migration indexes based on a matrix, the discretized position of the receiver, and the discretized position of the seismic source, and determining a set of amplitude weights based on the matrix, the discretized position of the receiver, and the discretized position of the seismic source. The method further includes migrating the seismic trace based on the set of migration indexes and the set of amplitude weights.

(86) PCT No.: **PCT/IB2015/002011**

§ 371 (c)(1),

(2) Date: **Feb. 14, 2017**

**Related U.S. Application Data**

(60) Provisional application No. 62/047,072, filed on Sep. 8, 2014.

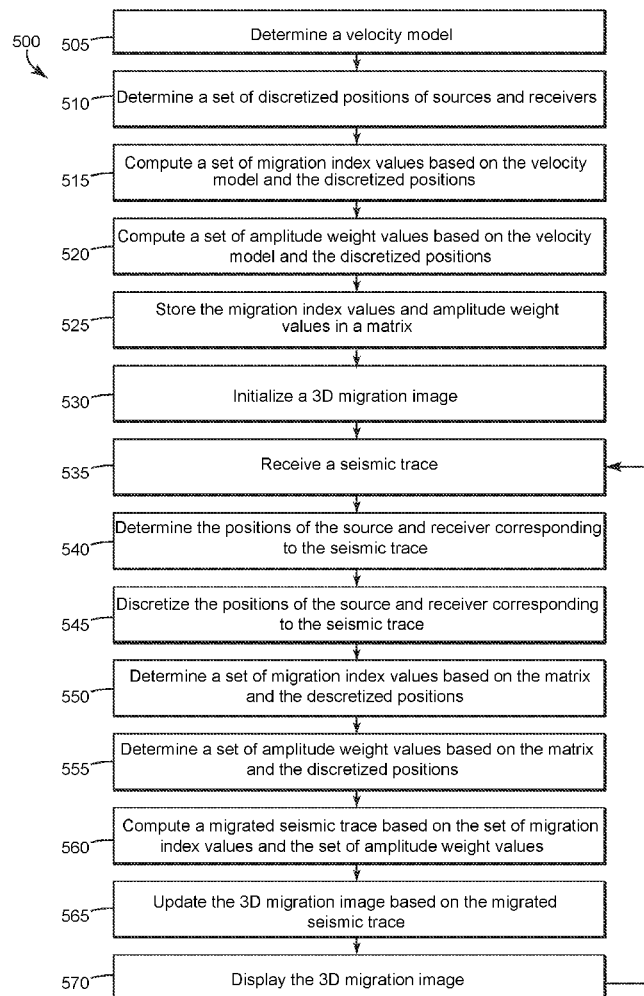


FIG. 1

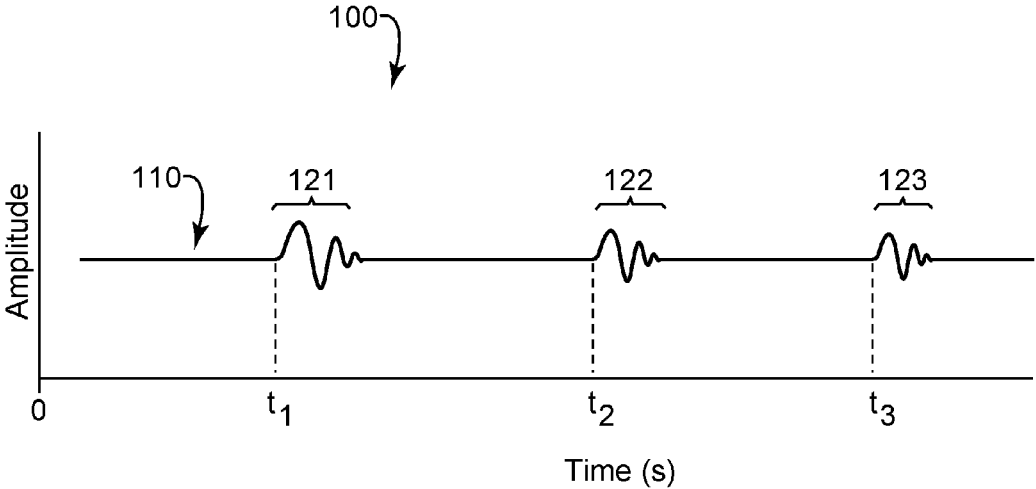


FIG. 2

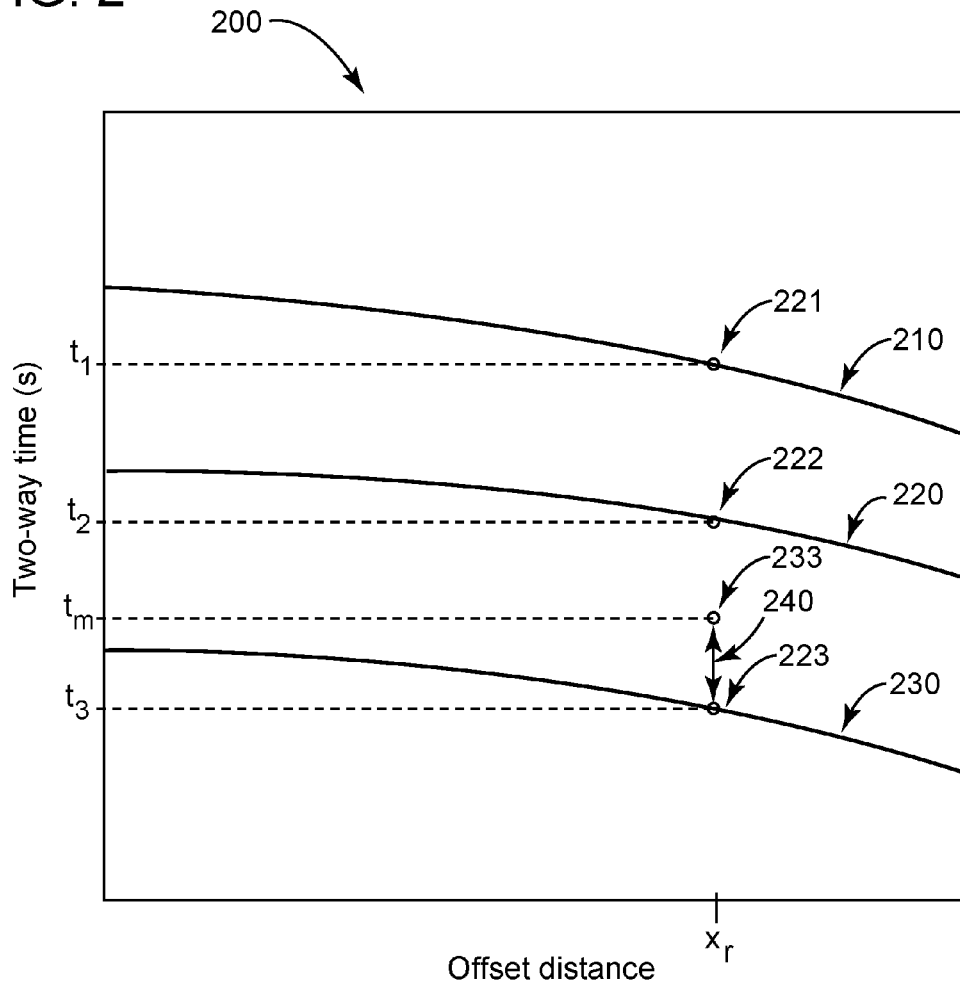


FIG. 3

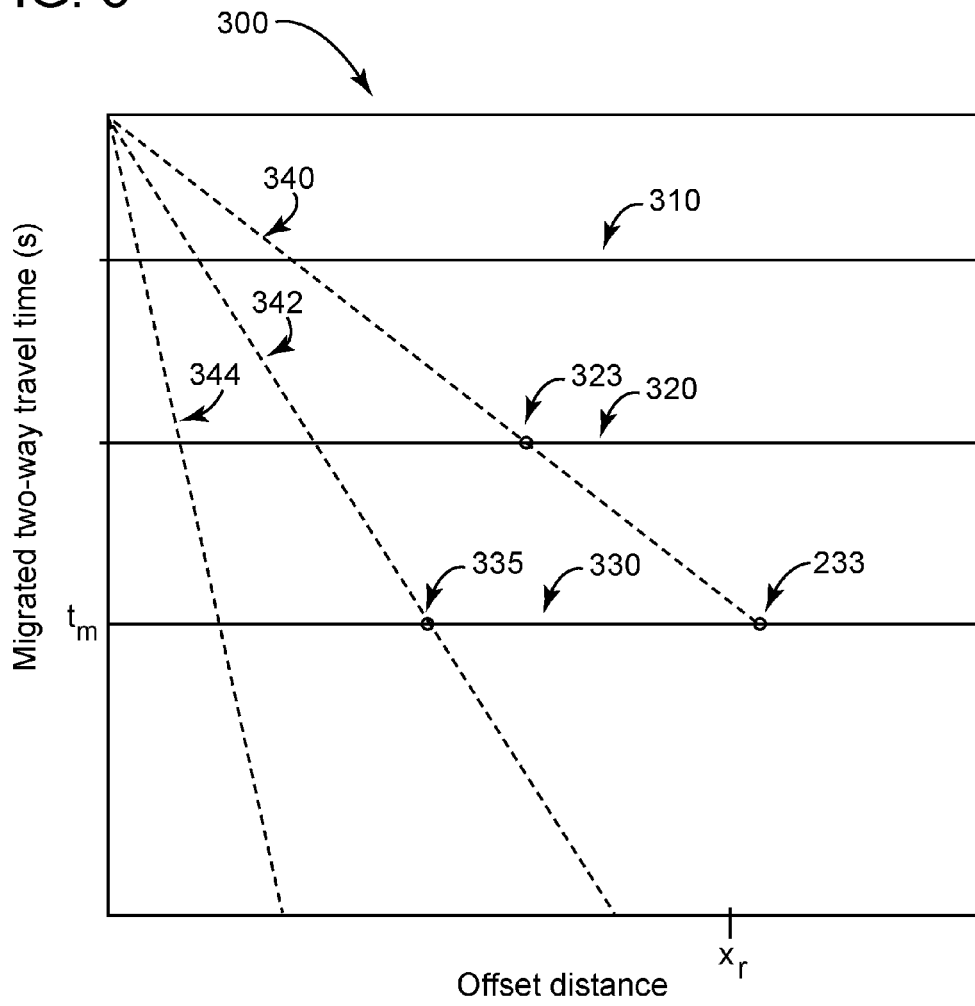


FIG. 4

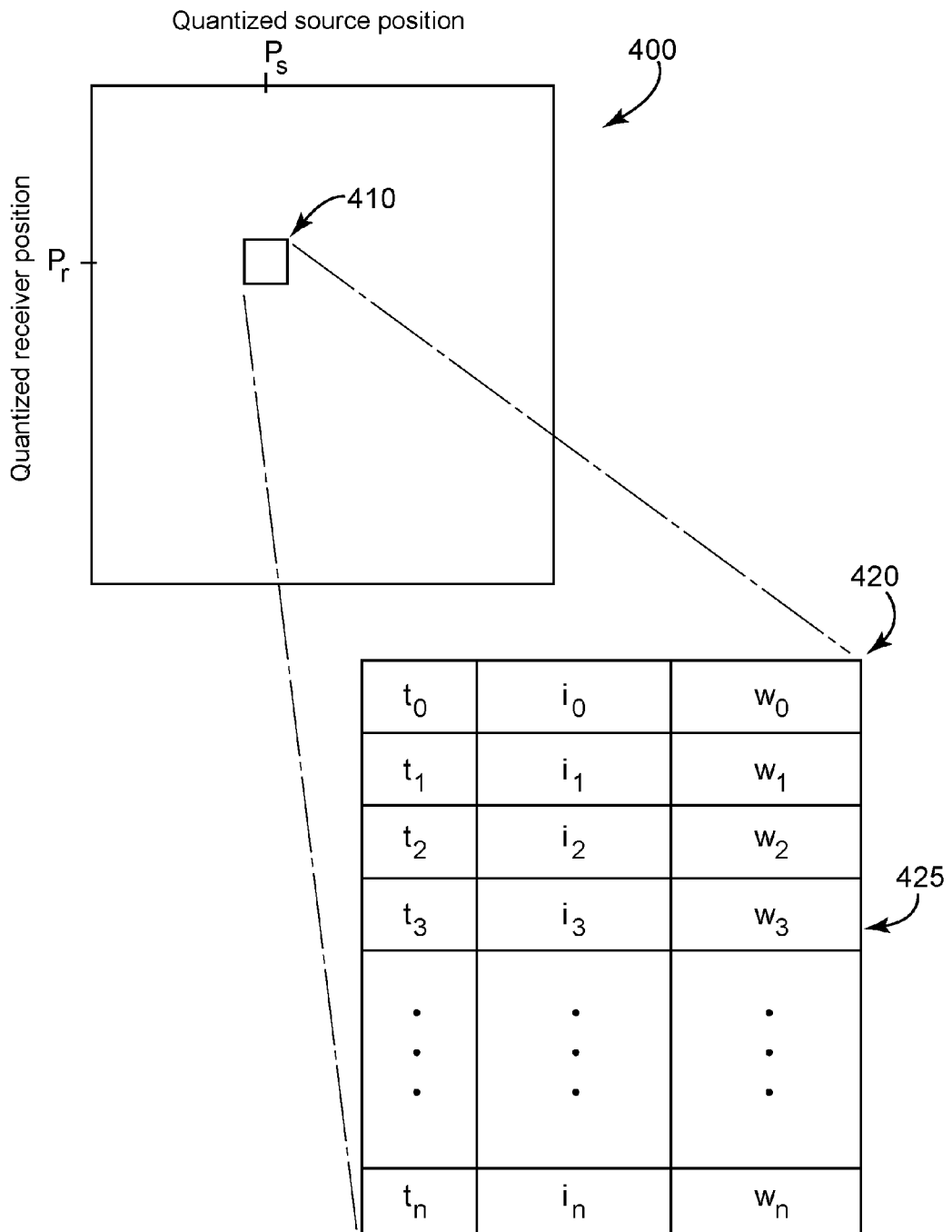
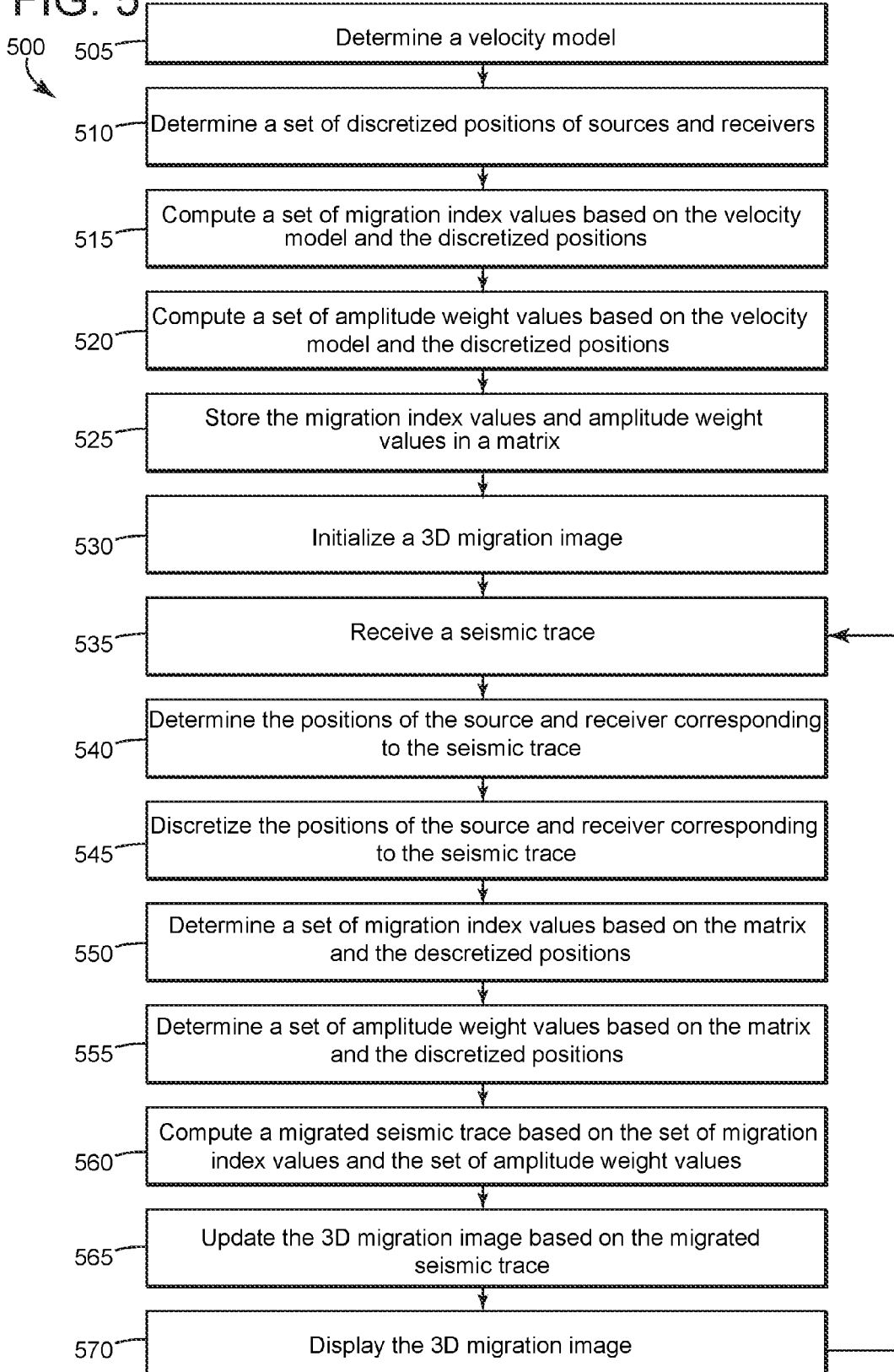
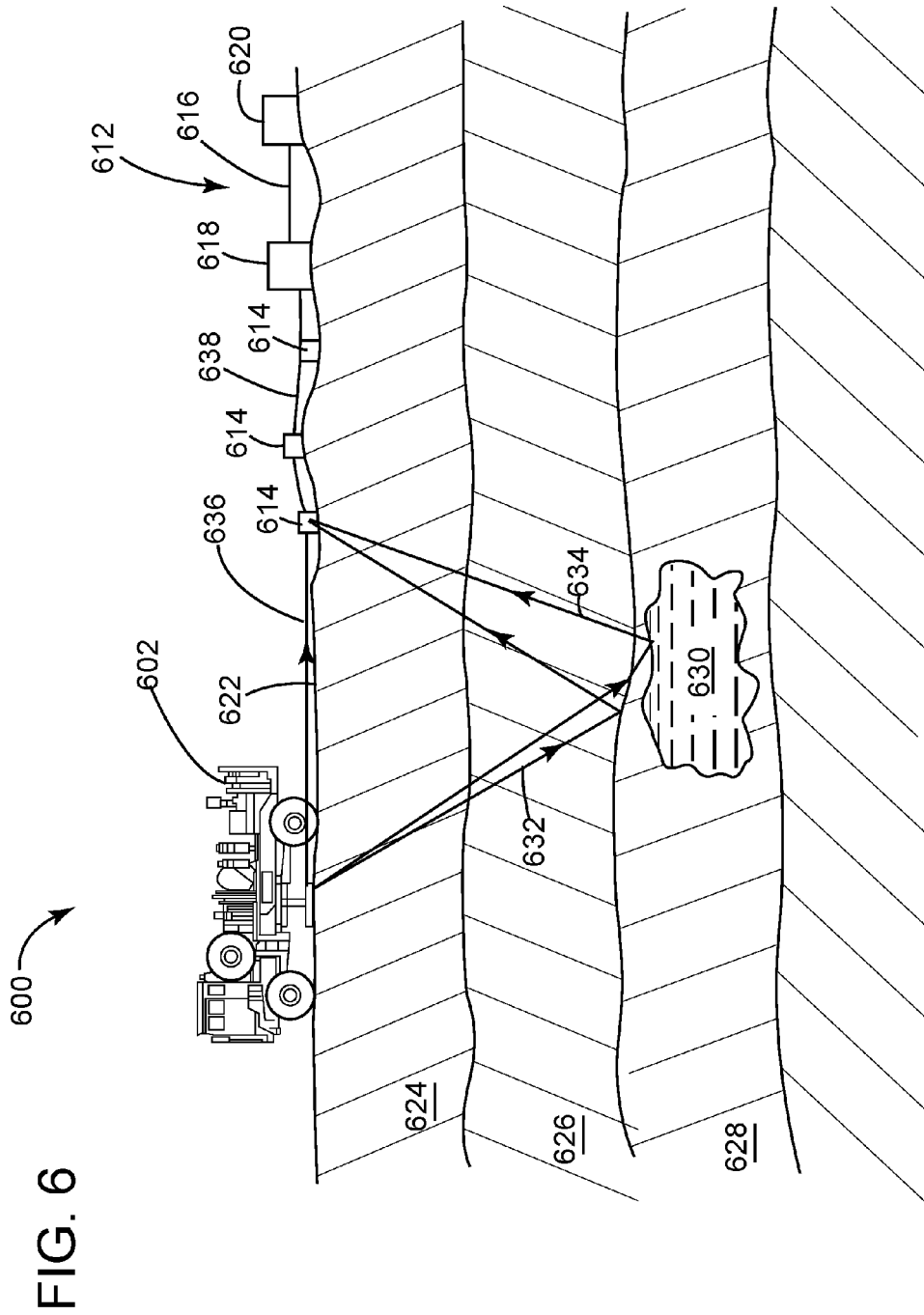


FIG. 5





## SEISMIC MIGRATION USING AN INDEXED MATRIX

### CROSS-REFERENCE TO RELATED APPLICATION

**[0001]** This application claims the benefit of U.S. Provisional Application Ser. No. 62/047,072 filed on Sep. 8, 2014, which is incorporated by reference in its entirety for all purposes.

### TECHNICAL FIELD

**[0002]** The present disclosure relates generally to seismic exploration and, more particularly, to seismic migration using an indexed matrix.

### BACKGROUND

**[0003]** In the oil and gas industry, seismic exploration techniques are commonly used to aid in locating subsurface deposits of oil, gas, and other useful minerals. Because drilling involves high costs and high risks, seismic surveys are used to produce an image of subsurface geological structures. While the image may not directly show the location of oil or gas, those trained in the field can use such images to more accurately predict the location of oil and gas and thus reduce the chance of drilling a non-productive well.

**[0004]** Seismic exploration, whether on land or at sea, is a method of detecting geologic structures below the surface of the earth by analyzing seismic energy that has interacted with the geologic structures. Generally, a seismic energy source imparts a force at or near the surface of the earth. The resulting mechanical stress propagates according to the elastic properties of the subsurface, and is at least partially reflected by subsurface seismic reflectors (interfaces between geologic structures that have different acoustic impedances). Seismic receivers, placed at or near the earth's surface, within bodies of water, or below the earth's surface in wellbores, record the ground motion or fluid pressure resulting from the reflection. The recordings are processed to generate information about the location and physical properties of the subsurface geologic structures that reflected the seismic energy. For example, recordings may be processed to generate a 2D or 3D image of the subsurface seismic reflectors.

**[0005]** In many survey areas, the speed at which seismic energy moves through the subsurface, known as the seismic velocity, varies with location and/or depth below the surface. In addition, in many survey areas, seismic reflectors are not positioned horizontally, but at a variety of dip angles. Such variable seismic velocities and dipping seismic reflectors cause images produced from raw seismic data to show seismic reflectors at incorrect locations. Such images may also show reflected seismic energy from a seismic reflector smeared across a surface such as a hyperbolic diffraction curve, rather than at a single point. As a result, during processing, some form of seismic migration is applied to the recorded data to focus energy spread out through the raw seismic data and to accurately position the subsurface seismic reflectors at the correct subsurface positions. For example, seismic migration may compute a weighted sum of the energy along a diffraction curve and apply a time correction to shift the summed energy in time.

**[0006]** Seismic migration may be applied before or after normal moveout (NMO) and stacking of the seismic traces.

For example, in many survey operations, the source and receiver are not positioned in the same location, but are offset by some distance. During processing, seismic traces that share a common midpoint between the seismic source and the seismic receiver, known as a common-midpoint gather, are combined to form a stacked data trace that simulates a zero-offset seismic trace at the common midpoint. In post-stack migration, a migration technique is applied to the stacked data. In pre-stack migration, a migration technique is applied to each individual seismic trace and the migrated results are then stacked with the other migrated traces. Pre-stack migration often produces more accurate results than post-stack migration. However, pre-stack migration is more computationally expensive than post-stack migration.

**[0007]** In traditional survey operations, seismic migration is applied to the entire data set for the survey operation. Typically, this post-survey seismic migration is performed at a data-processing facility after the entire data set for the survey operation has been gathered in the field. Acquiring the entire data set and processing it may take several months. In some survey operations, fast-track processing is applied in the field after a block of seismic data is collected. However, acquiring a block of seismic data may take several weeks, and processing the data may take up to a week, even when post-stack migration techniques are used. As a result, there is a substantial time delay between acquiring raw seismic data in the field and producing analyses or images using migrated seismic data. Thus, such analyses and images are not available in the field for use in detecting failures of survey equipment or other errors in data acquisition.

**[0008]** Accordingly, there is a need for systems and methods that can perform seismic migration in real time or near real time in the field.

### SUMMARY

**[0009]** In accordance with one or more embodiments of the present disclosure, a method for performing seismic migration using an indexed matrix includes receiving a seismic trace from a receiver, determining a discretized position of the receiver, and determining a discretized position of a seismic source. The method also includes determining a set of migration indexes based on a matrix, the discretized position of the receiver, and the discretized position of the seismic source, and determining a set of amplitude weights based on the matrix, the discretized position of the receiver, and the discretized position of the seismic source. The method further includes migrating the seismic trace based on the set of migration indexes and the set of amplitude weights.

**[0010]** In accordance with another embodiment of the present disclosure, a seismic data acquisition system includes a processor, a memory communicatively coupled to the processor, a receiver configured to transform seismic signals into seismic signal data, and a seismic source. The system also includes a matrix stored in the memory and instructions stored in the memory that, when executed by the processor, cause the processor to receive a seismic trace from a receiver, determine a discretized position of the receiver, determine a discretized position of a seismic source, determine a set of migration indexes based on a matrix, the discretized position of the receiver, and the discretized position of the seismic source, determine a set of amplitude weights based on the matrix, the discretized

position of the receiver, and the discretized position of the seismic source, and migrate the seismic trace based on the set of migration indexes and the set of amplitude weights.

[0011] In accordance with another embodiment of the present disclosure, a non-transitory computer-readable medium includes instructions that, when executed by a processor, cause the processor to receive a seismic trace from a receiver, determine a discretized position of the receiver, determine a discretized position of a seismic source, determine a set of migration indexes based on a matrix, the discretized position of the receiver, and the discretized position of the seismic source, determine a set of amplitude weights based on the matrix, the discretized position of the receiver, and the discretized position of the seismic source, and migrate the seismic trace based on the set of migration indexes and the set of amplitude weights.

#### BRIEF DESCRIPTION OF THE DRAWINGS

[0012] For a more complete understanding of the present disclosure and its features and advantages, reference is now made to the following description, taken in conjunction with the accompanying drawings, which may include drawings that are not to scale and wherein like reference numbers indicate like features, in which:

[0013] FIG. 1 illustrates a graph of an example seismic trace in accordance with some embodiments of the present disclosure;

[0014] FIG. 2 illustrates a graph of two-way travel times to sample reflectors for a shot gather, in accordance with some embodiments of the present disclosure;

[0015] FIG. 3 illustrates a graph of migrated two-way travel times to sample reflectors for a shot gather, in accordance with some embodiments of the present disclosure;

[0016] FIG. 4 illustrates an example indexed matrix **400** used to accelerate a migration computation in accordance with some embodiments of the present disclosure;

[0017] FIG. 5 illustrates a flow chart of an example method **500** for performing seismic migration using an indexed matrix in accordance with some embodiments of the present disclosure; and

[0018] FIG. 6 illustrates an elevation view of an example seismic exploration system **600** configured to perform seismic migration using an indexed matrix in accordance with some embodiments of the present disclosure.

#### DETAILED DESCRIPTION

[0019] The present disclosure is directed to seismic migration using an indexed matrix. As discussed above, seismic migration is used to focus energy spread out through the raw seismic data and to accurately position the subsurface seismic reflectors at the correct subsurface positions. In conventional pre-stack time migration, a set of time corrections (migration indexes) and amplitude weights is calculated based on the exact positions of the source and receiver for each seismic trace and a velocity model of the survey area, and applied to the seismic trace recorded by the receiver prior to stacking traces. This calculation requires significant time and substantial computing power to accomplish, and often dominates the seismic migration process. In embodiments of the present disclosure, seismic migration is accelerated using a precomputed matrix of indexes and amplitude weights for a set of predefined discrete source and receiver positions. A seismic migration process may discretize the

source and receiver position for a particular seismic trace, then look up the corresponding indices and amplitude weights in the precomputed matrix and apply them to the seismic trace in real time or near real time in the field.

[0020] The migrated seismic trace may be used to build and display a 2D or 3D image of the subsurface during the survey operation. For example, at the beginning of a survey, a 3D subsurface image may be initialized to all zero values. As each seismic trace is received, the samples constituting the trace may be migrated and added to the 3D subsurface image. The 3D subsurface image that results may be displayed to operators of the survey for use in field-quality control of the survey operation.

[0021] FIG. 1 illustrates a graph **100** of an example seismic trace in accordance with some embodiments of the present disclosure. Graph **100** represents the amplitude of seismic trace **110** received by a particular receiver as a function of time. For example, seismic trace **110** may represent a trace received by a receiver at a distance  $x_r$  to the north of a seismic source. Seismic trace **110** may include portion **121** that begins at time  $t_1$ . Portion **121** may represent a reflection of the seismic signal generated by the seismic source from a first subsurface reflector, in which case  $t_1$  represents the two-way travel time of the seismic signal from the seismic source to the first subsurface reflector and from the first subsurface reflector to the receiver. Similarly, seismic trace **110** may include portion **122** that begins at time  $t_2$ . Portion **122** may represent a reflection of the seismic signal generated by the seismic source from a second subsurface reflector, in which case  $t_2$  represents the two-way travel time of the seismic signal from the seismic source to the second subsurface reflector and from the second subsurface reflector to the receiver. Seismic trace **110** may also include portion **123** that begins at time  $t_3$ . Portion **123** may represent a reflection of the seismic signal generated by the seismic source from a third subsurface reflector, in which case  $t_3$  represents the two-way travel time of the seismic signal from the seismic source to the third subsurface reflector and from the third subsurface reflector to the receiver.

[0022] FIG. 2 illustrates a graph **200** of two-way travel times to sample reflectors for a shot gather, in accordance with some embodiments of the present disclosure. For example, graph **200** may include one or more reflection or diffraction curves (hereinafter referred to as reflection curves) representing the two-way travel time from a seismic source to a subsurface reflector or diffracting point (hereinafter referred to as a subsurface reflector) and from the subsurface reflector to a receiver as a function of the offset distance between the seismic source and the receiver. For example, graph **200** may include reflection curve **210** representing the two-way travel time from a seismic source to the first subsurface reflector and from the first subsurface reflector to a receiver as a function of the offset distance between the seismic source and the receiver. As an example, point **221** on reflection curve **210** may correspond to time  $t_1$  in graph **100**, where the seismic source and receiver were separated by an offset distance  $x_r$ . Similarly, graph **200** may include reflection curve **220** representing the two-way travel time from a seismic source to a second subsurface reflector and from the second subsurface reflector to a receiver as a function of the offset distance between the seismic source and the receiver. Point **222** on reflection curve **220** may correspond to time  $t_2$  in graph **100**. Graph **200** may also

include reflection curve **230** representing the two-way travel time from a seismic source to a third subsurface reflector and from the third subsurface reflector to a receiver as a function of the offset distance between the seismic source and the receiver. Point **223** on reflection curve **230** may correspond to time  $t_3$  in graph **100**.

**[0023]** In practice, seismic traces contain noise that may interfere with identification and visualization of the subsurface reflectors. Multiple seismic traces may be combined into a single stacked trace with a higher signal-to-noise ratio. However, because the points on reflection curves **210**, **220**, and **230**, each of which corresponds to reflections from a single subsurface reflector, do not fall at the same time in each trace, simply summing the samples taken at the same point in time from each raw seismic trace in a shot gather fails to fully combine the energy reflected by each subsurface reflector. Seismic migration corrects the times of each sample in each seismic trace to position the points corresponding to reflections from a single subsurface reflector at the proper time. Once the trace samples have been migrated in time, a weighted sum of the samples at each migrated time is performed to create a set of migrated data traces that can be incorporated into the 2D or 3D subsurface image. The value of the proper time correction and the proper weighting value used in the weighted sum are determined in part by the velocity of seismic signals through the subsurface in the survey area. Because the exact velocity may not be known at all locations, in some embodiments, the velocity at which seismic signals propagate through the subsurface in the survey area may be estimated using a velocity model. The velocity model may include a single predicted velocity for all locations. In some embodiments, the velocity model may be smooth or may vary as a function of depth below the surface. Such a velocity model may represent a series of horizontal layers within the entire survey area. In some embodiments, the velocity model may also vary based on one or more factors such as surface location, direction of propagation, or other suitable factors. A velocity model may be defined by the survey operators, estimated based on previous surveys of the survey area, or calculated in any other suitable manner.

**[0024]** During processing, a set of time corrections for a seismic trace may be estimated based on the velocity model, the locations of the seismic source and the receiver, and the two-way time between the source, the reflector, and the receiver. For example, the two-way travel time from a source at location S to a subsurface reflector and then to a receiver at location R may be modeled according to the following equation:

$$t = \sqrt{t_0^2 + \frac{(A-S)^2}{V_{rms}^2}} + \sqrt{t_0^2 + \frac{(A-R)^2}{V_{rms}^2}} \quad (1)$$

where

**[0025]**  $t$ =the total travel time from the source to a subsurface reflector and back to a receiver;

**[0026]**  $t_0$ =the one-way travel time from the surface location of the subsurface reflector to the subsurface reflector and back (i.e., the point being imaged);

**[0027]** A=the surface location directly above the subsurface reflector;

**[0028]** S=the location of the source;

**[0029]** R=location of the receiver; and

**[0030]**  $V_{rms}$ =the root-mean-square velocity at the subsurface reflector according to the velocity model.

The modeled two-way travel time  $t$  and the two-way travel time to point A provides the time correction to be applied. Such a time correction is known as a migration index. For example, migration index **240** may be calculated based on the velocity model, the locations of the sources and receivers of the seismic traces represented by graph **200**, the offset  $x_r$  between the seismic source and the receiver for seismic trace **110**, discussed with reference to FIG. 1, and the time  $t_3$ . During processing, the sample contained in seismic trace **110** at time  $t_3$  is shifted to time  $t_m$  as a result of applying migration index **240**.

**[0031]** In some embodiments, every sample of each recorded trace is migrated. In some embodiments, only samples needed to compute a particular image are migrated. For example, an operator may desire to view a particular inline or crossline section of the 3D subsurface image. As a result, the migration process may migrate only those traces that would contribute samples to the portions of the 3D subsurface image appearing on the desired section.

**[0032]** In some surveys, calculating and applying a migration index to each sample in each seismic trace of a shot gather improves the time alignment of the seismic energy in each seismic trace in the gather, as illustrated in FIG. 3. FIG. 3 illustrates a graph **300** of migrated two-way travel times to sample reflectors for a shot gather, in accordance with some embodiments of the present disclosure. For example, graph **300** may represent the result of calculating and applying a migration index to each sample of the seismic traces represented by FIG. 2. As a result, FIG. 3 represents the migrated two-way travel times from a seismic source to three subsurface reflectors and from the three subsurface reflectors to a receiver as a function of the offset distance between the seismic source and the receiver. For example, line **310** may represent the migrated two-way travel times corresponding to reflection curve **210**, discussed with reference to FIG. 2. Line **320** may represent the migrated two-way travel times corresponding to reflection curve **220**, discussed with reference to FIG. 2. Line **330** may represent the migrated two-way travel times corresponding to reflection curve **230**, discussed with reference to FIG. 2. In some embodiments, lines **310**, **320**, and **330** may be straight horizontal lines, as depicted in FIG. 3. However, in operation, lines **310**, **320**, and **330** may be curved or irregular, and may be oriented non-horizontally, based on the accuracy of the velocity model, the accuracy of the positions of the seismic source and receiver, or other factors.

**[0033]** In operation, the migrated samples in each seismic trace in a shot gather are “stacked” to produce a stacked data trace that simulates a zero-offset seismic trace at the common midpoint. The combination of the traces may use a weighted sum of the samples from each trace by multiplying each sample by a weighting factor. For example, after migration, all the samples corresponding to migrated time  $t_m$ , including the sample at point **233**, may be combined in a weighted sum. The weighting factor for each sample is known as an amplitude weight.

**[0034]** The amplitude weight of each sample reflects the fact that more energy is reflected at the apex of a reflection curve (e.g., where the offset distance is small) than on the sides. The amplitude weight of each sample may also reflect the fact that the attenuation of the reflected energy from a

subsurface reflector may depend on the angle at which the energy encounters the reflector. As a result, the amplitude weight is a function of at least the time of the sample, the offset distance between the seismic source and the receiver, and the velocity model. For example, lines 340, 342, and 344 may represent contours along which the amplitude weight is constant. Points 233 and 323, which lie along contour 323, may be assigned the same weight  $w_3$ . Point 335, which lies along contour 342, may be assigned a different weight. Although contours 340, 342, and 344 are illustrated as substantially straight lines in FIG. 3, any suitable amplitude weight function may be used.

[0035] In conventional seismic migration, the migration index and amplitude weight for each point in a seismic trace is calculated at the time the migration calculation is performed. Furthermore, the migration index and amplitude weight for each point is based on the exact position of the source and receiver for that seismic trace. For example, the position of each source and receiver may be determined using GPS at the time the trace is recorded. In some embodiments, the calculations required to determine the migration index and amplitude weight for each point in a seismic trace represent a significant fraction of the total time required to perform the migration.

[0036] FIG. 4 illustrates an example indexed matrix 400 used to accelerate a migration computation in accordance with some embodiments of the present disclosure. Matrix 400 may be indexed by discretized positions of the source and the receiver. For example, cell 410 of matrix 400 may correspond to a seismic source position  $P_s$  and a receiver position  $P_r$ . Discretized positions are selected in advance of computing matrix 400, and may correspond to expected or typical locations of sources or receivers during the survey operation. For example, in a land-based survey, the seismic sources and receivers may be positioned on a grid spaced approximately 8 meters apart. In such a survey, the discretized positions used to index matrix 400 may be approximately 8 meters apart, aligned with the grid, and covering the surface of the survey area. In a marine survey, the seismic sources may be positioned at a fixed distance behind the survey vessel, and the receivers may be positioned on streamers behind the survey vessel spaced approximately 25 meters apart. Because the course of the survey vessel and the time of each shot of the seismic source are known, the positions of the seismic sources and receivers may thus be predicted. In such a survey the discretized positions used to index matrix 400 may be approximately 25 meters apart, aligned to the expected positions of the sources and receivers, and covering the surface of the water in the survey area. Although the present disclosure discusses specific values of the spacing between discretized positions of the seismic source and receiver, any suitable spacing may be used.

[0037] Each cell of matrix 400 may contain a list of migration indexes and amplitude weights used to migrate a seismic trace. For example, cell 410 may include list 420, in which each row corresponds to a particular sample time. For example, row 425 may correspond to time  $t_3$  at which the sample of point 233, discussed with reference to FIG. 2, was recorded. List 420 may include, for each sample time, a precomputed migration index and a precomputed amplitude weight. In some embodiments, the precomputed migration index and the precomputed amplitude weight are based on the sample time, the midpoint between source position  $P_s$  and receiver position  $P_r$ , the offset between source position

$P_s$  and receiver position  $P_r$ , and the velocity model, as discussed in connection with FIGS. 2 and 3. For example, row 425 may include migration index  $i_3$ , for example migration index 240 as discussed with reference to FIG. 2. Row 425 may also include amplitude weight  $w_3$ , discussed with reference to FIG. 3.

[0038] The contents of matrix 400 may be precomputed prior to performing a migration computation. In some embodiments, the contents of matrix 400 may be computed before the survey begins. In some embodiments, the contents of matrix 400 may be computed during the survey process.

[0039] In operation, matrix 400 may be used to construct a 3D migration image from the seismic traces as they are received. In some embodiments, the 3D migration image may be initialized to all zero values at the beginning of the survey operation. During the survey, matrix 400 may be used to migrate the samples of each seismic trace as it is received from the seismic receiver. For example, when trace 100, discussed with reference to FIG. 1, is received, the position of the seismic source that corresponds to trace 100 may be position  $P_s$ , and the position of the receiver that corresponds to trace 100 may be position  $P_r$ . In such an example, matrix cell 410 may be selected and list 420 retrieved. The migration indexes and amplitude weights stored in list 420 may be used to migrate the samples of trace 100. For example, the sample of trace 100 taken at time  $t_3$  may be shifted in time by migration index  $i_3$  (stored in row 425 of list 420) and weighted by amplitude weight  $w_3$  (stored in row 425 of list 420). The migrated sample may then be added to the 3D migration image.

[0040] In some embodiments, upon receipt of a seismic trace, the positions of the seismic source and seismic receiver corresponding to the trace may differ from the discretized positions used to index matrix 400. In such an embodiment, matrix 400 may be referenced using a discretized source position that approximates the actual source position and a discretized receiver position that approximates the actual receiver position. For example, the closest discretized position may be selected. However, any suitable method of quantizing the source and receiver positions may be used.

[0041] Although the present disclosure discusses using an indexed matrix for pre-stack time migration of seismic traces, an indexed matrix may also be used to migrate stacked traces after stacking is complete. In addition, other corrections and adjustments to seismic traces can also be accelerated in a similar fashion. For example, in some embodiments, a normal moveout correction may be applied to a seismic trace prior to stacking. In such embodiments, the normal moveout correction values may be stored in matrix 400. For example, the normal moveout correction for seismic source position  $P_s$  and receiver position  $P_r$  may be calculated using the velocity model and stored in another column of list 420. During operation, the seismic source position and receiver position for each trace may be discretized as described above. The normal moveout correction values in the cell of matrix 420 corresponding to those discretized positions may then be retrieved and applied to the seismic trace before it is added to the stack.

[0042] FIG. 5 illustrates a flow chart of an example method 500 for performing seismic migration using an indexed matrix in accordance with some embodiments of the present disclosure. The steps of method 500 can be per-

formed by a user, electronic or optical circuits, various computer programs, models, or any combination thereof, configured to perform seismic migration using an indexed matrix. The programs and models may include instructions stored on a non-transitory computer-readable medium and operable to perform, when executed, one or more of the steps described below. The computer-readable media can include any system, apparatus, or device configured to store and retrieve programs or instructions such as a hard disk drive, a compact disc, flash memory, or any other suitable device. The programs and models may be configured to direct a processor or other suitable unit to retrieve and execute the instructions from the computer readable media. Collectively, the user, circuits, or computer programs and models used to perform seismic migration using an indexed matrix may be referred to as a "processing tool." For example, the processing tool may be a computer located on a survey ship.

**[0043]** At step **505**, the processing tool determines a velocity model. For example, the velocity model may represent the velocity at which seismic signals propagate through the subsurface at various points in the survey area, as discussed in connection with FIG. 1. The velocity model may vary as a function of depth below the surface, surface location, direction of propagation, or other suitable factors. In addition, the velocity model may be defined by the survey operators, estimated based on previous surveys of the survey area, or calculated in any other suitable manner. Although specific velocity models are discussed in the present disclosure, any suitable velocity model may be used.

**[0044]** At step **510**, the processing tool determines a set of discretized positions of sources and receivers used to index a matrix. For example, in a land-based survey, the processing tool may determine a set of positions in a grid spaced approximately 8 meters apart and covering the surface of the survey area, as discussed in connection with FIG. 4. As another example, in a marine survey, the processing tool may determine a set of discretized positions in a grid spaced approximately 25 meters apart and covering the surface of water in the survey area, as discussed in connection with FIG. 4.

**[0045]** At step **515**, the processing tool computes a set of migration index values. For example, the processing tool may calculate a set of migration index values for each time  $t$  in seismic trace **200**, discussed with reference to FIG. 2, based on the velocity model, the location of the shot point of the seismic traces represented by graph **200**, and the offset  $x_s$  between the seismic source and the receiver for seismic trace **110**, discussed with reference to FIG. 1, and the time  $t$ . For example, the processing tool may compute the set of migration index values  $i_0, \dots, i_n$  stored in row **425** of list **420** in matrix **400**, discussed with reference to FIG. 4. In some embodiments, the processing tool may calculate a set of migration index values for each pair of discretized source and receiver positions used to index matrix **400**. In some embodiments, one or more migration index values may be computed before the survey begins. In some embodiments, one or more migration index values may be computed during the survey process.

**[0046]** At step **520**, the processing tool computes a set of amplitude weight values. For example, the processing tool may calculate a set of amplitude weight values for each time  $t$  in seismic trace **200**, discussed with reference to FIG. 2, based on the velocity model, the offset  $x_s$  between the

seismic source and the receiver for seismic trace **110**, discussed with reference to FIG. 1, and the time  $t$ . For example, the processing tool may compute the set of amplitude weight values  $w_0, \dots, w_n$  stored in row **425** of list **420** in matrix **400**, discussed with reference to FIG. 4. In some embodiments, the processing tool may calculate a set of amplitude weight values for each pair of discretized source and receiver positions used to index matrix **400**. In some embodiments, one or more amplitude weight values may be computed before the survey begins. In some embodiments, one or more amplitude weight values may be computed during the survey process.

**[0047]** At step **525**, the processing tool stores the migration index values and the amplitude weight values in the matrix. For example, the processing tool may store the set of migration index values  $i_0, \dots, i_n$  and the set of amplitude weight values  $w_0, \dots, w_n$  in row **425** of list **420** in matrix **400**, discussed with reference to FIG. 4. Furthermore, to increase processing speed, the processing tool may store matrix **400** on a solid-state hard-drive or in RAM. However, the processing tool may use any suitable storage medium to store matrix **400**.

**[0048]** At step **530**, the processing tool initializes a 3D migration image. For example, the processing tool may initialize all values in a 3D migration image to zero.

**[0049]** At step **535**, the processing tool receives a seismic trace. For example, the processing tool may receive seismic trace **100**, discussed with reference to FIG. 1.

**[0050]** At step **540**, the processing tool determines the positions of the source and receiver corresponding to the seismic trace. For example, the position of the source and receiver corresponding to seismic trace **100** may be determined using GPS at the time seismic trace **100** is recorded.

**[0051]** At step **545**, the processing tool discretizes the positions of the sources and receivers corresponding to the seismic trace. For example, as discussed with reference to FIG. 4, the processing tool may select discretized source position  $P_s$  because it is the closest discretized source position to the position of the source that corresponds to seismic trace **100**. Similarly, the processing tool may select discretized receiver position  $P_r$  because it is the closest discretized receiver position to the position of the source that corresponds to seismic trace **100**.

**[0052]** At step **550**, the processing tool determines a set of migration index values based on the index matrix and the discretized positions of the sources and receivers corresponding to the seismic trace. For example, the processing tool may retrieve list **420** from cell **410** of matrix **400**, discussed with reference to FIG. 4. The processing tool may then retrieve migration index values  $i_0, \dots, i_n$  stored in row **425** of list **420**.

**[0053]** At step **555**, the processing tool determines a set of amplitude weight values based on the amplitude weight matrix and the discretized positions of the sources and receivers corresponding to the seismic data. For example, the processing tool may retrieve amplitude weight values  $w_0, \dots, w_n$  stored in row **425** of list **420**.

**[0054]** At step **560**, the processing tool computes a migrated seismic trace based on the set of migration index values, the set of amplitude weight values, and the seismic data. For example, the processing tool may shift each sample in time using the corresponding migration index stored in row **425** of list **420**. For example, the processing tool may shift the sample at point **223**, discussed with reference to

FIG. 2, from time  $t_3$  to time  $t_m$  based on migration index  $i_3$ . The processing tool may multiply each sample in the seismic trace by the corresponding amplitude weight stored in row 425 of list 420. For example, the processing tool may multiply the sample at migrated point 233 (corresponding to time  $t_m$ ) by amplitude weight  $w_3$ .

[0055] At step 565, the processing tool updates the 3D migration image. For example, the processing tool may add the migrated seismic trace to the 3D migration image. For example, the processing tool may add each migrated sample computed in step 560 to the 3D migration image at a point determined by the source and receiver positions of the seismic trace and the time of the sample. In some embodiments, the processing tool updates only a portion of the 3D migration image. For example, the processing tool may update only the portion of the 3D migration image corresponding to a crossline section that the operation desires to view.

[0056] At step 570, the processing tool displays the 3D migration image. For example, the processing tool may render a portion of the 3D migration image on a computer display. In some embodiments, the portion of the 3D migration image rendered includes one or more of a time slice of the 3D migration image, an inline vertical slice of the 3D migration image, and a cross-line vertical slice of the 3D migration image. However, any suitable portion of the 3D migration image may be displayed. The processing tool then returns to step 535.

[0057] Modifications, additions, or omissions may be made to method 500 without departing from the scope of the present disclosure. For example, the steps may be performed in a different order than that described and some steps may be performed at the same time. Further, more steps may be added or steps may be removed without departing from the scope of the disclosure.

[0058] FIG. 6 illustrates an elevation view of an example seismic exploration system 600 configured to perform seismic migration using an indexed matrix in accordance with some embodiments of the present disclosure. The images produced by system 600 allow for the evaluation of subsurface geology. Seismic data is acquired and processed to produce images of subsurface formations. System 600 includes one or more seismic energy sources 602 and one or more receivers 614 which are located within a pre-determined area selected for seismic survey or exploration. Survey of the exploration area includes the activation of seismic energy source 602 that applies a force which in turn generates elastic waves that propagate through the earth. The seismic energy is then partially reflected, refracted, diffracted, and otherwise returned by one or more subsurface formations such as rock layers beneath the earth's surface, producing a motion recorded by receivers 614.

[0059] System 600 includes one or more seismic energy sources 602. In some embodiments, source 602 is located on or proximate to surface 622 of the earth within an exploration area. A particular source 602 may be spaced apart from other adjacent sources 602. Further, a positioning system, such as a global positioning system (GPS), may be utilized to locate sources 602 and receivers 614 and time-stamp their recordings.

[0060] Source 602 is any type of seismic device that generates controlled seismic energy used to perform reflec-

tion seismic surveys, such as a land-based or marine seismic vibrator, dynamite, an air gun, or any other suitable seismic energy source.

[0061] Seismic exploration system 600 includes one or more monitoring devices 612 that operate to record reflected seismic energy 632, 634, and 636. In some embodiments, monitoring device 612 includes one or more receivers 614, network 616, recording unit 618, and processing unit 620. Monitoring device 612 may be located remotely from source 602.

[0062] In some embodiments, receiver 614 is located on or proximate to surface 622 of the earth within an exploration area. Receiver 614 is any type of instrument that is operable to transform seismic energy or vibrations into a measurable signal. For example, receiver 614 may be a geophone configured to detect and record seismic velocity displacement reflected from subsurface formations and convert the motions into electrical energy, such as electric voltages. Receiver 614 may include a vertical, horizontal, or multi-component geophone such as a three component (3C) geophone. Receiver 614 may include a 3C Digital Sensor Unit (DSU), an optical fiber sensor, or a distributed acoustic sensor (DAS). As another example, receiver 614 may include a hydrophone configured to detect and record pressure variations. In some embodiments, multiple receivers 614 are utilized within an exploration area to provide data related to multiple locations and distances from sources 602. For example, system 600 may utilize two thousand receivers (or geophones) 614. Receivers 614 may be positioned in multiple configurations, such as linear, grid, array, or any other suitable configuration. In some embodiments, receivers 614 are positioned along one or more strings 638. Each receiver 614 is typically spaced apart from adjacent receivers 614 in the string 138. Spacing between receivers 614 in string 138 may be approximately the same preselected distance, or span, or the spacing may vary depending on a particular application, exploration area topology, or any other suitable parameter. For example, spacing between receivers 614 may be approximately ten meters.

[0063] In some embodiments, one or more receivers 614 transmit raw seismic data from reflected seismic energy via network 616 to recording unit 618. Recording unit 618 transmits raw seismic data to processing unit 620 via network 616. Processing unit 620 performs seismic migration on the raw seismic data to prepare the data for interpretation. For example, processing unit 620 may be configured to perform one or more steps of method 500 and may include a processing tool as discussed in connection with FIG. 5. Processing unit 620 may also display the resulting 3D migration image to operators of the seismic survey for use in real time or near-real time quality control of the survey operation. Although discussed separately, recording unit 618, and processing unit 620 may be configured as separate units or as a single unit. Recording unit 618 or processing unit 620 may include any instrumentality or aggregation of instrumentalities operable to compute, classify, process, transmit, receive, store, display, record, or utilize any form of information, intelligence, or data. For example, recording unit 618 and processing unit 620 may include one or more personal computers, storage devices, servers, or any other suitable device and may vary in size, shape, performance, functionality, and price. Recording unit 618 and processing unit 620 may include random access memory (RAM), one or more processing resources, such as a central processing unit

(CPU) or hardware or software control logic, or other types of volatile or non-volatile memory. Additional components of recording unit **618** and processing unit **620** may include one or more disk drives, one or more solid-state disk drives, one or more network ports for communicating with external devices, and one or more input/output (I/O) devices, such as a keyboard, a mouse, or a video display. Recording unit **618** or processing unit **620** may be located in a station truck or any other suitable enclosure.

**[0064]** Network **616** communicatively couples one or more components of monitoring device **612** with any other component of monitoring device **612**. For example, network **616** communicatively couples receivers **614** with recording unit **618** and processing unit **620**. Furthermore, network **638** communicatively couples a particular receiver **614** with other receivers **614**. Although discussed separately, network **616**, network **638**, and network **616** may be configured as separate networks or as a single network. Network **616**, network **638**, and network **616** may be any type of network that provides communication. For example, network **616** may include one or more of a wireless network, a local area network (LAN), or a wide area network (WAN), such as the Internet.

**[0065]** In some embodiments, sources **602** are controlled to generate energy and receivers **614** record seismic energy traveling along paths **632** and **634** and reflected by interfaces between subsurface layers **624**, **626**, and **628**, oil and gas reservoirs, such as target reservoir **630**, or other subsurface formations. Subsurface layers **624**, **626**, and **628** may have various densities, thicknesses, or other characteristics. Target reservoir **630** may be separated from surface **622** by multiple layers **624**, **626**, and **628**. Because the embodiment depicted in FIG. **6** is exemplary only, there may be more or fewer layers **624**, **626**, or **628** or target reservoirs **630**.

**[0066]** The seismic survey may be repeated at various time intervals to determine changes in target reservoir **630**. The time intervals may be months or years apart. Data may be collected and organized based on offset distances, such as the distance between a particular source **602** and a particular receiver **614** and the amount of time it takes for seismic energy traveling along paths **632** and **634** from source **602** to a particular receiver **614**. The amount of time seismic energy takes to reach a receiver is known as the travel time. Data collected during a survey by receivers **614** is reflected in traces that may be gathered, processed, and utilized to generate a model of the subsurface formations.

**[0067]** Although discussed with reference to a land implementation, embodiments of the present disclosure are also useful in marine applications. In a marine application, monitoring device **612** may include hydrophones contained inside buoyant streamers, which may be towed behind a vessel. Seismic energy source **602** and monitoring device **612** may be towed behind the same or a different vessel. Similarly, in a marine application, recording unit **618** and processing unit **620** may include one or more computers aboard the vessel.

**[0068]** Although the present disclosure discusses seismic migration in the context of a survey operation, embodiments of the present disclosure may be used in permanent or continuous monitoring operations without departing from the scope of the present disclosure.

**[0069]** Any of the steps, operations, or processes described herein may be performed or implemented with one or more hardware or software modules, alone or in combination with

other devices. In some embodiments, a software module is implemented with a computer program product comprising a computer-readable medium containing computer program code, which can be executed by a computer processor for performing any or all of the steps, operations, or processes described.

**[0070]** Embodiments of the disclosure may also relate to an apparatus for performing the operations herein. This apparatus may be specially constructed for the required purposes, and/or it may comprise a general-purpose computing device selectively activated or reconfigured by a computer program stored in the computer. Such a computer program may be stored in a tangible computer readable storage medium or any type of media suitable for storing electronic instructions, and coupled to a computer system bus. Furthermore, any computing systems referred to in the specification may include a single processor or may be architectures employing multiple processor designs for increased computing capability. For example, the processing tool described in method **500** with respect to FIG. **5** may be stored in tangible computer readable storage media.

**[0071]** Although the present disclosure has been described with several embodiments, changes, variations, alterations, transformations, and modifications may be suggested to one skilled in the art, and it is intended that the present disclosure encompass such changes, variations, alterations, transformations, and modifications as fall within the scope of the appended claims. Moreover, while the present disclosure has been described with respect to various embodiments, it is fully expected that the teachings of the present disclosure may be combined in a single embodiment as appropriate. Instead, the scope of the disclosure is defined by the appended claims.

What is claimed is:

1. A method comprising:
  - receiving a seismic trace from a receiver;
  - determining a discretized position of the receiver;
  - determining a discretized position of a seismic source;
  - determining a set of migration indexes based on a matrix, the discretized position of the receiver, and the discretized position of the seismic source;
  - determining a set of amplitude weights based on the matrix, the discretized position of the receiver, and the discretized position of the seismic source; and
  - migrate the seismic trace based on the set of migration indexes and the set of amplitude weights.
2. The method of claim **1**, wherein determining the set of migration indexes comprises retrieving the set of migration indexes from the matrix.
3. The method of claim **1**, further comprising
  - determining a set of discretized source positions;
  - determining a set of discretized receiver positions;
  - computing a set of migration indexes based on the discretized source positions and the set of discretized receiver positions;
  - computing a set of amplitude weights based on the discretized source positions and the set of discretized receiver positions; and
  - storing the migration indexes and the amplitude weights in the matrix.
4. The method of claim **3**, wherein computing the set of migration indexes is further based on a velocity model.

5. The method of claim 3, wherein determining the discretized position of the receiver comprises selecting a closest position from the set of discretized receiver positions.

6. The method of claim 1, further comprising updating a 3D migration image based on the migrated seismic trace.

7. The method of claim 6, further comprising displaying the 3D migration image.

8. A seismic data acquisition system comprising:

a processor;

a memory communicatively coupled to the processor;

a receiver configured to transform seismic signals into seismic traces;

a seismic source;

a matrix stored in the memory; and

instructions stored in the memory that, when executed by the processor, cause the processor to:

receive a seismic trace from the receiver;

determine a discretized position of the receiver;

determine a discretized position of the seismic source;

determine a set of migration indexes based on the matrix, the discretized position of the receiver, and the discretized position of the seismic source;

determine a set of amplitude weights based on the matrix, the discretized position of the receiver, and the discretized position of the seismic source; and migrate the seismic trace based on the set of migration indexes and the set of amplitude weights.

9. The seismic data acquisition system of claim 8, wherein determining the set of migration indexes comprises retrieving the set of migration indexes from the matrix.

10. The seismic data acquisition system of claim 8, the instructions further causing the processor to:

determine a set of discretized source positions;

determine a set of discretized receiver positions;

compute a set of migration indexes based on the discretized source positions and the set of discretized receiver positions;

compute a set of amplitude weights based on the discretized source positions and the set of discretized receiver positions; and

store the migration indexes and the amplitude weights in the matrix.

11. The seismic data acquisition system of claim 3, wherein computing the set of migration indexes is further based on a velocity model.

12. The seismic data acquisition system of claim 3, wherein determining the discretized position of the receiver comprises selecting a closest position from the set of discretized receiver positions.

13. The seismic data acquisition system of claim 8, the instructions further causing the processor to update a 3D migration image based on the migrated seismic trace.

14. The seismic data acquisition system of claim 13, the instructions further causing the processor to display the 3D migration image.

15. A non-transitory computer-readable medium, comprising instructions that, when executed by a processor, cause the processor to:

receive a seismic trace from a receiver;

determine a discretized position of the receiver;

determine a discretized position of a seismic source;

determine a set of migration indexes based on a matrix, the discretized position of the receiver, and the discretized position of the seismic source;

determine a set of amplitude weights based on the matrix, the discretized position of the receiver, and the discretized position of the seismic source; and

migrate the seismic trace based on the set of migration indexes and the set of amplitude weights.

16. The non-transitory computer-readable medium of claim 15, wherein determining the set of migration indexes comprises retrieving the set of migration indexes from the matrix.

17. The non-transitory computer-readable medium of claim 15, the instructions further causing the processor to:

determine a set of discretized source positions;

determine a set of discretized receiver positions;

compute a set of migration indexes based on the discretized source positions and the set of discretized receiver positions;

compute a set of amplitude weights based on the discretized source positions and the set of discretized receiver positions; and

store the migration indexes and the amplitude weights in the matrix.

18. The non-transitory computer-readable medium of claim 17, wherein computing the set of migration indexes is further based on a velocity model.

19. The non-transitory computer-readable medium of claim 17, wherein determining the discretized position of the receiver comprises selecting a closest position from the set of discretized receiver positions.

20. The non-transitory computer-readable medium of claim 15, the instructions further causing the processor to: update a 3D migration image based on the migrated seismic trace; and display the 3D migration image.

\* \* \* \* \*





## RÉSUMÉ

---

La sismique réflexion 3D est largement utilisée dans l'industrie pétrolière. Cette méthode d'auscultation du sous-sol fournit des informations sur les structures géologiques et peut être utilisée pour construire des modèles de réservoir. Cependant, les propriétés dérivées des données sismiques 3D (et 2D) ne sont que statiques: elles ne permettent pas d'évaluer ce qui change avec le temps. L'ajout d'une dimension temporelle aux données 3D est obtenue par la répétition des mesures à plusieurs dates séparées de plusieurs mois voire même de plusieurs années. Ainsi, la sismique 4D (time-lapse) permet d'appréhender les modifications du sous-sol sur le long terme. Depuis les années 90, cette méthode est utilisée dans le monde entier en mer et à terre. Pour réaliser une surveillance beaucoup plus fréquente (quotidienne), voire continue (quelques heures) du sous-sol, CGG a développé, en collaboration avec Gaz de France (désormais ENGIE) et l'Institut Français du Pétrole (maintenant IFPEN), une solution basée sur des sources et des récepteurs enterrés: SeisMovie. SeisMovie a été initialement conçu pour suivre et cartographier en temps-réel le front de gaz lors des opérations de stockage en couche géologique. Il est aussi utilisé pour observer l'injection de vapeur nécessaire à la production d'huile lourde. Dans cette thèse, nous apportons des contributions à trois défis qui apparaissent lors du traitement des données sismiques issues de ce système. Le premier concerne l'atténuation des variations de proche surface causées par les ondes « fantômes » qui interfèrent avec les ondes primaires. Le second concerne la quantification des modifications du sous-sol en termes de variation de vitesse de propagation et d'impédance acoustique. Le troisième concerne le temps-réel : le traitement doit être au moins aussi rapide que le cycle d'acquisition (quelques heures). En effet l'analyse des données doit permettre aux ingénieurs réservoirs de prendre rapidement des décisions (arrêt de l'injection, diminution de la production). Dans un cadre plus général, il existe des similitudes conceptuelles entre la 3D et la 4D. En 4D, ce sont les acquisitions répétées qui sont comparées entre elles (ou avec une référence). En 3D, pendant l'acquisition, les géophysiciens de terrain comparent les points de tir unitaires entre eux afin d'évaluer la qualité des données pour prendre des décisions (reprendre le point de tir, continuer). Dès lors, certains outils 4D temps-réel développés pendant cette thèse peuvent être appliqués. Ainsi une toute nouvelle approche appelée TeraMig pour le contrôle qualité automatisé sur le terrain sera également présentée.

## MOTS CLÉS

---

Géophysique, surveillance, temps réel, SeisMovie, TeraMig, 4D.

## ABSTRACT

---

3D seismic reflection is widely used in the oil industry. This standard subsoil auscultation method provides information on geological structures and can be used to build reservoir models. However, the properties derived from 3D (and 2D) seismic data are only static: 3D does not allow to evaluate the changes with calendar time. The addition of a temporal dimension to 3D data is obtained by repeating the measurements at several dates separated by several months or even several years. Thus, 4D seismic (time-lapse) makes it possible to measure and to analyze the changes of the subsoil in the long term. Since the 90s, this method is used worldwide at sea and on land. To carry out a much more frequent monitoring (daily), even continuous (a few hours) of the subsoil, CGG developed, in collaboration with Gaz de France (now ENGIE) and Institut Français du Pétrole (now IFPEN), a solution based on buried sources and receptors: SeisMovie. SeisMovie was originally designed to monitor and map the gas front in real time during geological disposal operations. It is also used to observe the steam injection required for heavy oil production. In this thesis, we bring contributions to three challenges arising in the processing of seismic data from this system. The first one concerns the attenuation of near-surface variations caused by "ghost" waves that interfere with primary waves. The second one concerns the quantification of subsurface changes in terms of propagation velocity variation and acoustic impedance. The third one concerns real-time: the data processing must be at least as fast as the acquisition cycle (a few hours). In fact, the analysis of the data must enable the reservoir engineers to make quick decisions (stop of the injection, decrease of the production). In a more general context, there are conceptual similarities between 3D and 4D. In 4D, the repeated acquisitions are compared with each other (or with a reference). In 3D, during acquisition, field geophysicists compare unitary shot points with each other to assess the quality of the data for decision-making (reshooting, skipping or continuing). Therefore, some 4D real-time tools developed during this thesis can be applied. A new approach called TeraMig for automated quality control in the field will also be presented.

## KEYWORDS

---

Geophysics, monitoring, real-time, SeisMovie, TeraMig, 4D.